Nikolai Vatin
Svetlana Roshchina
Dmitrijs Serdjuks   *Editors*

Proceedings of MPCPE 2022

Selected Papers

Springer

Lecture Notes in Civil Engineering

Volume 335

Lecture Notes in Civil Engineering (LNCE) publishes the latest developments in Civil Engineering—quickly, informally and in top quality. Though original research reported in proceedings and post-proceedings represents the core of LNCE, edited volumes of exceptionally high quality and interest may also be considered for publication. Volumes published in LNCE embrace all aspects and subfields of, as well as new challenges in, Civil Engineering. Topics in the series include:

- Construction and Structural Mechanics
- Building Materials
- Concrete, Steel and Timber Structures
- Geotechnical Engineering
- Earthquake Engineering
- Coastal Engineering
- Ocean and Offshore Engineering; Ships and Floating Structures
- Hydraulics, Hydrology and Water Resources Engineering
- Environmental Engineering and Sustainability
- Structural Health and Monitoring
- Surveying and Geographical Information Systems
- Indoor Environments
- Transportation and Traffic
- Risk Analysis
- Safety and Security

To submit a proposal or request further information, please contact the appropriate Springer Editor:

- Pierpaolo Riva at pierpaolo.riva@springer.com (Europe and Americas);
- Swati Meherishi at swati.meherishi@springer.com (Asia—except China, Australia, and New Zealand);
- Wayne Hu at wayne.hu@springer.com (China).

All books in the series now indexed by Scopus and EI Compendex database!

Nikolai Vatin · Svetlana Roshchina ·
Dmitrijs Serdjuks
Editors

Proceedings of MPCPE 2022

Selected Papers

Springer

Editors
Nikolai Vatin
Peter the Great St. Petersburg Polytechnic
University
Saint-Petersburg, Russia

Svetlana Roshchina
Department of Building Constructions
Vladimir State University
Vladimir, Russia

Dmitrijs Serdjuks
Faculty of Civil Engineering
Riga Technical University
Riga, Latvia

Preface

Dear colleagues!

III International Conference on Materials Physics, Building Structures and Technologies in Construction, Industrial and Production Engineering (MPCPE 2022) has been held on April 26–28, 2022, at Vladimir, Russian Federation. The conference encompasses key directions of scientific and scientific-practical research in all aspects of industrial and civil construction, including numerical–analytical methods for calculating building structures, buildings, and facilities; the strength and deformability of construction materials and structures; structural and functional materials in the construction industry and other production technologies; design and operation of building structures and engineering systems; the application of achievements in applied physics in construction and related industries, as well as current issues of energy and resource conservation in construction.

The conference was organized by Vladimir State University named after Alexander and Nikolay Stoletovs in partnership with Peter the Great St. Petersburg Polytechnic University (St. Petersburg, Russian Federation) and Research Institute of Building Physics of Russian Academy of Architecture and Construction Sciences (Moscow, Russian Federation). Vladimir State University named after Alexander and Nikolay Stoletovs is renowned in the domestic construction science largely due to its scientific school of reinforced wooden structures, established at the Department of Building Structures. The study and development of such structures have been conducted at the university since the 1970s. The majority of the developed and tested building structures have been implemented in actual construction projects. The accumulated experience in the research and operation of reinforced wooden structures attests to their sufficiently high characteristics and prospects for their application in modern construction. Currently, the scientific team is focused on creating various types of composite structures and is conducting several research projects in this field. In addition to the development of new structures, the university's department of building structures excels in technical inspection and design of buildings and structures, as well as the improvement of existing building constructions.

As editors, we would like to express our sincere gratitude to all participants for their valuable contributions and their keen interest in the conference. The scientific level exhibited in the presented materials was exceptionally high, reflecting the dedication and expertise of the researchers involved. We are truly appreciative of the effort and thought put into each submission. We would also like to extend our gratitude to the members of the Program Committee and the reviewers for their diligent work. Their commitment to conducting a thorough analysis of the submitted materials and engaging in constructive discussions has been instrumental in maintaining the scholarly rigor of the conference. Their expertise and attention to detail have significantly contributed to the quality and coherence of the conference proceedings. The collaborative efforts of all participants, including researchers, reviewers, and committee members, have ensured the success of this academic event. It is through the dedication and professionalism of each individual involved that we have been able to uphold the conference's standards of excellence.

Saint Petersburg, Russia   Nikolai Vatin
                                                                                  Conference Chairman

Contents

Three-Dimensional Stress State of Earth Dams Under Static Loads

Doniyor Juraev , **Paxridin Matkarimov** , **and Mirziyod Mirsaidov**

Abstract The article is devoted to the study of the stress–strain state and strength of various earth dams under the action of static loads. The stress–strain state of the Gissarak, Sokh and Pachkamar earth dams built in Central Asia is studied in a three-dimensional formulation under the action of body forces and hydrostatic water pressure. It was established that under the action of body forces and hydrostatic water pressure, the plane deformed state for some dams is realized in a very narrow range along the length of the dam, and for other dams, this state is realized in a wide range. The equivalent stress for the three-dimensional stress state of the dams under consideration was estimated using the fourth maximum-strain-energy theory, and the results obtained were compared with the allowable stress for the soil material of the dams, which showed sufficient strength of these dams under the action of static loads.

Keywords Earth dam · Three-dimensional problem · Static load · Stress–strain state · Equivalent stress · Maximum-strain-energy theory

1 Introduction

When designing earth dams in seismic regions, there arises the problem of choosing a calculation model for studying their stress–strain state (SSS) and dynamic behavior in general. In most cases, simplified plane design schemes are used in the study of such types of structures.

D. Juraev · M. Mirsaidov (✉)
National Research University -Tashkent Institute of Irrigation and Agricultural Mechanization Engineers, Tashkent, Uzbekistan
e-mail: theormir@mail.ru; diyorbekmuhammadamir@mail.ru

P. Matkarimov
Namangan Institute of Engineering and Technology, Namangan, Uzbekistan

M. Mirsaidov
Institute of Mechanics and Seismic Stability of Structures of the Academy of Sciences of the Republic of Uzbekistan, Tashkent, Uzbekistan

Simplified design schemes are unable to describe many effects of the spatial work of real structures. In this regard, the material of the structures is often used non-rationally. This causes an overrun of the material and the impossibility of providing the required margin of safety and reliability of the structure.

The solution to the above problem, considering the factors listed, can be most fully obtained using numerical methods, for example, the finite element method (FEM) or the finite difference method (FDM) [1–5, 22].

To date, there are a number of scientific publications devoted to the study of the stress–strain state of earth structures, both in a plane or spatial formulation.

The stress–strain state of various earth dams in a plane or spatial formulation is considered in [6–15]; this formulation takes into account the design features of structures, the moisture properties of soil, the interaction of structures with the water environment of the reservoir, and other features of structures.

The study in [16] presents the results of the assessment of the stress–strain state of high earth dams depending on time (consolidation analysis) in a plane formulation. Some results of calculations to determine the effect of water pore pressure on the stress–strain state and subsidence of the dam are analyzed.

In [17], the stress state of earth dams under static and dynamic effects was studied by the finite element method, taking into account the elastic–plastic strain of the soil of the dam. The numerical results obtained were compared with the results of field measurements during the Wenchuan earthquake.

The study in [18] analyzes in detail the use of non-traditional materials (rock and soil mixes) to ensure the stability of the slopes of earth dams.

In [19], scientific achievements and main conclusions are described; i.e. accumulated experience in the construction of high rock-and-earth dams is systematically summarized, and major technical issues are discussed, including control of strains, seepage, slope stability, safety assessments and other issues related to earth dams.

In [20], a review and analysis of the results of studies of the stress–strain state of rockfill dams with a reinforced concrete screen, performed by different authors, were presented. The results of analytical, experimental and numerical studies are considered. The models used to reproduce the non-linear nature of the screen deformation and rockfill in the numerical simulation of the stress–strain state of dams are described.

As the review shows, the stress–strain state and strength of earth dams, taking into account design features and real work in a three-dimensional formulation, were not studied sufficiently, therefore, research in this direction is of great scientific interest. The prediction of the behavior of earth dams should be based on the most complete consideration of all factors affecting their SSS and strength under various types of loads.

Based on the above, this work is devoted to the development of methods for assessing the stress–strain state and strength of the Gissarak, Sokh, and Pachkamar earth dams built in Central Asia in a three-dimensional formulation, taking into account the design features, physical and mechanical properties of building materials. In this article, the finite element method (FEM) is used as a computing tool.

2 Methods

A three-dimensional non-homogeneous deformable system (Fig. 1) is considered here, i.e. a model of an earth dam that occupies volume $V = V_1 + V_2 + V_3$. The area of the base of the system along the bottom is Σ_4'' and the areas of two coastal faces Σ_4', Σ_4'' are rigidly fixed; the surface of the lower slope and crest are stress-free. It is assumed that body forces $\vec{f}$ and hydrostatic water pressure $\vec{p}$ act on surface S_p of the earth dam.

Here: V_1, V_3 are the volumes of the upper and lower prisms, V_2 is the volume of the core.

It is necessary to determine the components of the displacement vectors and the components of the stress tensor in a three-dimensional body (Fig. 1) under the action of force $\vec{f}$, and water pressure $\vec{p}$.

For the mathematical formulation of the problem, the principle of virtual displacements, the generalized Hooke's law, the Cauchy relation for a three-dimensional body [8], and kinematic boundary conditions are used.

Boundary conditions are:

$$\vec{x} \in \Sigma_4' + \Sigma_4'' + \Sigma_4''' : \quad \vec{u} = 0 \tag{1}$$

Here $\vec{u} = \{u_1, u_2, u_3\} = \{u, v, w\}$ are the components of the displacement vector of the point of the body; $\{x\} = \{x_1, x_2, x_3\} = \{x, y, z\}$ are the coordinates of the point of the body; $i, j, k = 1, 2, 3$.

We determine the functions of displacements $\vec{u}(\vec{x})$, strains $\varepsilon_{ij}(\vec{x})$ and stresses $\sigma_{ij}(\vec{x})$ arising under static forces $(\vec{f})$ and pressure $(\vec{p})$ in the body of the system (Fig. 1).
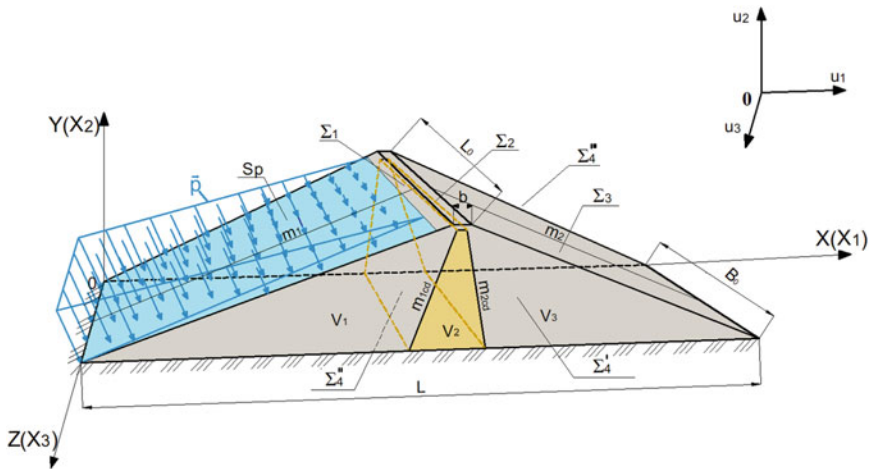
Fig. 1 Calculation scheme of a non-homogeneous three-dimensional system

The finite element method (FEM) is the most appropriate in order to solve this problem for a domain of non-canonical shape (Fig. 1); it allows taking into account both the geometry features and the properties of the material of the system.

Here, the domain occupied by the body is divided into sub-domains with different physical and mechanical characteristics, then the sub-domains are automatically partitioned into finite elements. As a result, a discrete model of the system is created.

When solving this three-dimensional problem, first-order volumetric elements were used in the form of tetrahedra with 12 degrees of freedom. A linear function is used to approximate the displacement field inside a volumetric tetrahedron.

The procedure of the finite element method allows us to reduce the three-dimensional problem under consideration to a system of non-homogeneous high-order algebraic equations, i.e.:

$$[k]\{u\} = \{P\} \tag{2}$$

Here: $[K]$ is the stiffness matrix for the system under consideration (Fig. 1); $\{u\}$ are the sought-for components of the displacement vectors, in the nodes of the finite element; $\{P\}$ are the components of external forces (body and surface ones) acting on the nodes of the finite element.

In the study of specific three-dimensional problems, the partition of given domain V into finite elements is performed considering the design features and physical and mechanical properties of the material of different parts of the dam. When solving this problem, the computer programs developed by the authors, and the standard ABAQUS programs were used. When solving specific problems, the number of unknowns in these equations reached 68,493.

3   Results and Discussion

The stress–strain state (SSS) and the strength of the Gissarak, Sokh, and Pachkamar earth dams are investigated in the article under the action of body forces and hydrostatic water pressure, in a three-dimensional formulation.

Body forces $\vec{f}$ acting on the structure and the hydrostatic pressure of water in the upstream face acting on the upper slope of the dam were taken as external impacts, determined by the following formula

$$\vec{p} = \rho_0 g (h - x_2) \tag{3}$$

here, ρ_0 is the density of water; h is the height of reservoir filling.

The study was performed for the following earth dams built on the territory of the seismic region of Central Asia. The main geometric parameters of these structures, as well as the physical and mechanical characteristics of soil in various sections of the dam, were taken from the design data:

1) **Gissarak dam** (Fig. 2), H = 138.5 m high, built on the Aksu river in the Kashkadarya region of Uzbekistan, with slope coefficients $m_1 = 2.2$, $m_2 = 1.9$. Retaining prisms 1 are laid out of rock mass with the following physical and mechanical parameters E = 3600 MPa, soil specific gravity $\gamma = 1.9$ tf/m^3, Poisson's ratio $\nu = 0.3$ and cohesion coefficient C = 2 kPa. Core 4 is laid from loam with physical and mechanical parameters - E = 2400 MPa, soil specific gravity $\gamma = 1.7$ tf/m^3, Poisson's ratio $\nu = 0.35$ and cohesion coefficient C = 20 kPa. The transition zone is of sandy-gravelly soil. The crest of the dam is b = 16 m wide and L = 660 m long.

2) **Sokh dam,** H = 87.3 m high, was built on the Sokh River in the Fergana region, with slope coefficients $m_1 = 2.5$, $m_2 = 2.2$. Retaining prisms are laid from pebbles with physical and mechanical parameters - E = 3550 MPa, specific gravity of soil $\gamma = 2.1$ tf/m^3, Poisson's ratio $\nu = 0.35$ and cohesion coefficient C = 10.9 kPa. The core is laid from loam with physical and mechanical parameters E = 2400 MPa, soil specific gravity $\gamma = 1.75$ tf/m^3, Poisson's ratio $\nu = 0.35$ and cohesion coefficient C = 30 − 50 kPa. The crest of the dam is b = 10 m wide and L = 487.3 long.

3) **Pachkamar dam,** H = 70 m high, erected in Kashkadarya region, with slope coefficients $m_1 = 2.25$, $m_2 = 2.25$. Retaining prisms are from sand-pebbles with physical and mechanical parameters E = 3600 MPa, soil specific gravity $\gamma = 2.25$ tf/m^3, Poisson's ratio $\nu = 0.3$ and coefficient of cohesion C = 11 kPa. The core is laid from loam with physical and mechanical parameters E = 2400 MPa, soil specific gravity $\gamma = 1.78$ tf/m^3, Poisson's ratio $\nu = 0.35$ and cohesion coefficient C = 30 kPa. The crest of the dam is b = 8 m wide and L = 589 m long.
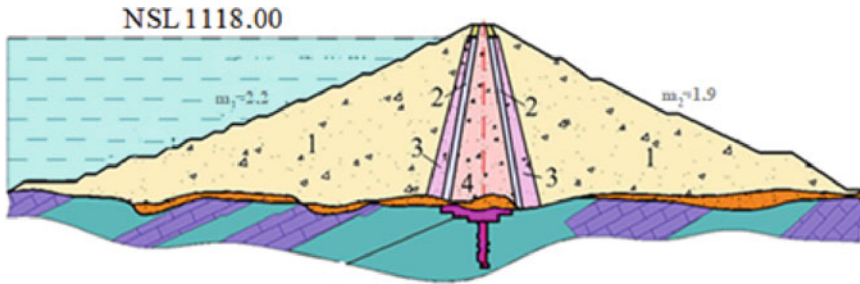
Fig. 2 Cross section of the Gissarak dam 1 - retaining prisms, 2 - I layer of transition zones, 3 - II layer of transition zones, 4 – core

3.1 Evaluation of the Stress–Strain State of Earth Dams

The SSS of earth dams is studied in a three-dimensional formulation. The calculation results are the components of displacement vectors u_1, u_2, u_3, strains ε_{11}, ε_{22}, ε_{33}, ε and stresses σ_{11}, σ_{22}, σ_{33}, σ for all points of the structure (Fig. 1).

To analyze the results in the characteristic transverse and longitudinal sections of the dam, isolines of equal values of the components of displacements, strains, and stresses were constructed.

Figure 3 shows the distribution field of equal values of vertical u_2 - (along the x_2 axis) and longitudinal u_3- (along the x_3 axis) displacements in the middle of the longitudinal section of the Gissarak (a, d), Sokh (b, e), and Pachkamar (c, f) dams obtained in a three-dimensional formulation under the own weight of the structures.

An analysis of the results presented (Fig. 3), shows that in the longitudinal section of the Gissarak dam, there is a sharp change in the distribution pattern of vertical u_2 and longitudinal u_3 displacements of points from the middle part of the dam to the coastal slopes (Fig. 3a). This indicates a significant influence of the left and right banks on the value of vertical and longitudinal displacements of the middle part of the dam.

For this dam (Fig. 3a), a plane deformed stress state is realized in a very narrow range (a section marked in blue) since the geometric dimensions of this dam in three directions are of the same order.

For the Sokh and Pachkamar dams, the area where the plane-deformed stress state is observed is quite large (Fig. 3b, c) since for these structures the influence of coastal slopes on the stress state of the structure is insignificant (a section marked in blue).

The values of longitudinal displacements u_3 in the left and right slopes of all dams increase sharply. This phenomenon can lead to the formation of transverse cracks in the upper part of the dams adjacent to the banks.

Along with this, the value of displacements (i.e., absolute deformation) of the profile points of the dams under consideration depends significantly on considering the level of water filling in the reservoir. In this case, the distribution pattern of displacements in the body of the dam completely changes, the symmetry is broken, and the absolute deformation of the dam significantly depends on the value of water pressure in the upstream face, which is especially evident when calculating the structure for the case of a completely filled reservoir.

Figure 4 shows lines of equal levels of horizontal σ_{11} (a), vertical σ_{22} (b) and shear σ_{12} (c) stresses of the Gissarak dam under its own weight and hydrostatic water pressure when the reservoir is completely filled. Such results were also obtained for the Pachkamar and Sokh earth dams in three-dimensional and spatial formulations at different levels of reservoir filling.

The results obtained also showed that in the central part of the Sokh and Pachkamar dams, the conditions of plane deformation of the theory of elasticity are observed, which are not observed in the Gissarak dam.

a) u_2, m

b) u_2, m

c) u_2, m

d) u_3, m

e) u_3, m

f) u_3, m
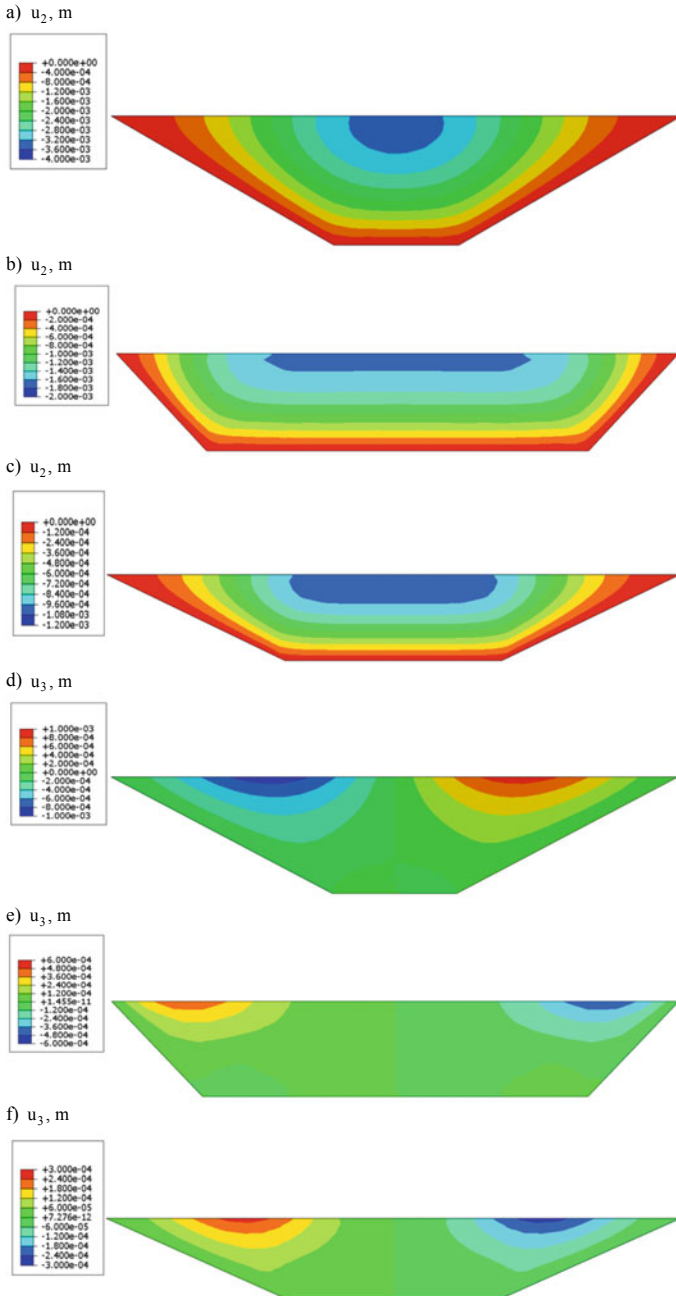
Fig. 3 Distribution field of equal values of vertical u_2 (along the x_2 axis) and longitudinal u_3 (along the x_3 axis) displacements in the middle of the longitudinal section of the Gissarak (a, d), Sokh (b, e) and Pachkamar (c, f) dams in a three-dimensional formulation under the action of their own weight

a) σ_{11}, MPa

S, S11
(Avg: 75%)

+2.869e+03
+0.000e+00
-5.000e+04
-1.000e+05
-1.500e+05
-2.000e+05
-2.500e+05
-3.000e+05
-3.500e+05
-4.000e+05
-4.500e+05
-5.000e+05

b) σ_{22}, MPa

S, S22
(Avg: 75%)

+1.123e+03
+0.000e+00
-1.000e+05
-2.000e+05
-3.000e+05
-4.000e+05
-5.000e+05
-6.000e+05
-7.000e+05
-8.000e+05
-9.000e+05
-1.000e+06
-1.100e+06
-1.200e+06

c) σ_{12}, MPa

S, S12
(Avg: 75%)

+4.000e+05
+3.627e+05
+3.255e+05
+2.882e+05
+2.509e+05
+2.136e+05
+1.764e+05
+1.391e+05
+1.018e+05
+6.455e+04
+2.727e+04
-1.000e+04
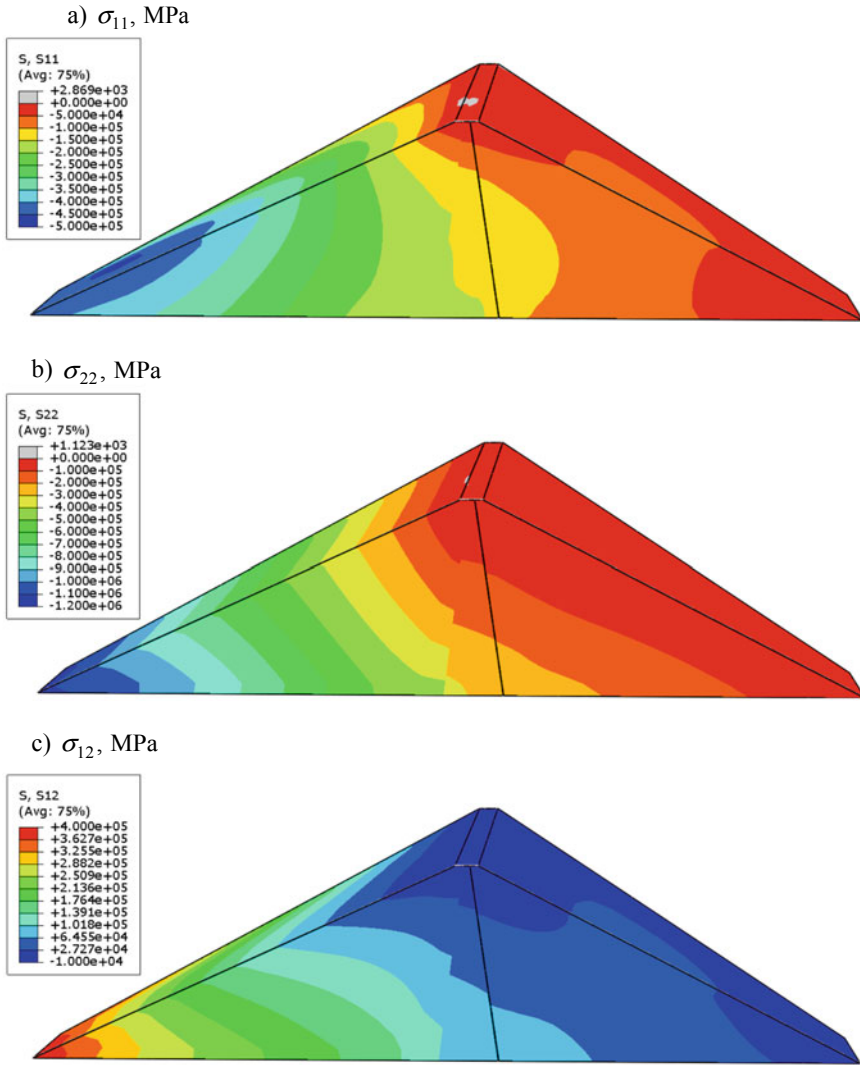
Fig. 4 Isolines of equal values of horizontal σ_{11} **a** vertical σ_{22} **b** and shear σ_{12} **c** stresses for the Gissarak dam in 3D formulation when the reservoir is completely filled

3.2 Strength Assessment of Earth Dams

Using the results obtained in paragraph 3.1 for stresses, the strength of the three dams under consideration was estimated in a three-dimensional formulation using the maximum-strain-energy theory. It is assumed that the potential energy of deformation of the material in the elastic region is the sum of the potential energy of a change in its volume and the potential energy of a change in its shape.
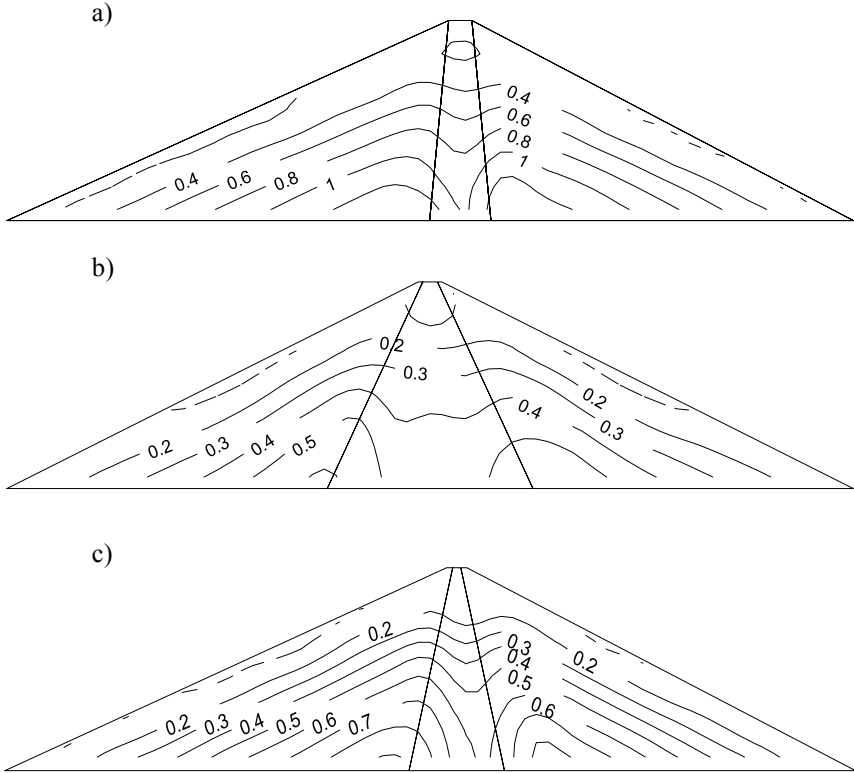
Fig. 5 Isolines of equal values of equivalent stress σ_{equiv} in the body of the Gissarak **a** Sokh **b** and Pachkamar **c** earth dams

In accordance with the requirements of the maximum-strain-energy theory, the following condition must be met at all points of earth dams:

$$\sigma_{equiv}\sqrt{\frac{1}{2}\left[(\sigma_1 - \sigma_2)^2 + (\sigma_1 - \sigma_3)^2 + (\sigma_3 - \sigma_2)^2\right]} \leq [\sigma] \qquad (4)$$

Here $\sigma_1, \sigma_2, \sigma_3$ are the principal stresses, and $[\sigma]$ is the allowable normal stress.

To assess the strength of the Gissarak, Sokh, and Pachkamar earth dams in a three-dimensional formulation under the action of their own weight and hydrostatic water pressure in a completely filled reservoir, the values of equivalent stress σ_{equiv} at all points of the dam body were determined using expression (4). The results obtained, i.e. isolines of equal values of σ_{equiv} for the average cross-section are shown in Fig. 5.

To compare the results of σ_{equiv} with the value of $[\sigma]$, the following estimate can be made: in [21], it was noted that the high strength of individual particles of gravel-pebble soil predetermines the boundary of mass damage at $[\sigma] = 2.0 \pm 0.5$ MPa (the values of $[\sigma]$ were determined experimentally).

An analysis of the distribution pattern of equivalent stress σ_{equiv} in the body of the dams shows that the value of σ_{equiv} in the body of the dams under consideration completely satisfies the condition of the maximum-strain-energy theory of mechanics (4) at all points of these dams. The results obtained show that the required strength of the dams under the action of body forces and hydrostatic water pressure is ensured at completely filled reservoirs.

4 Conclusions

1. The Stress–strain State and Strength of Three Earth Dams of Different Heights in a Three-Dimensional Formulation Under the Action of Body Forces and Hydrostatic Water Pressure Were Studied.
2. It was determined that under the action of body forces and hydrostatic water pressure, the plane deformed state for the Gissarak dam is realized in a very narrow range along the length of the dam, and for other dams, this state is realized in a wide range.
3. Equivalent stress for the three-dimensional stress state for these dams was estimated using the maximum-strain-energy theory and the results obtained were compared with the allowable stress for soil; this showed sufficient strength of these dams under the action of static loads.

References

1. Konstantinov, I.A.: Dynamics of hydro-technical structures. Part **2**, 196, LPI (1976)
2. Mirsaidov, M.M.: Theory and methods for calculating earth structures for strength and seismic resistance. Tashkent: "FAN," 312 (2010)
3. Zaretsky, Y.K., Lombardo, V.N.: Statics and dynamics of earth dams, p. 256, Energoizdat (1983)
4. Krasnikov, N.D.: Seismic resistance of hydro-technical structures made of earth materials, p.240, Energoizdat (1981)
5. Lyakhter, V.M.: I.I.N. Seismic resistance of earth dams, p. 233, Nauka (1986)
6. Sinenko, E.G., Konisheva, O.V.: Kinematics and geometry of misaligned epicyclic mechanisms. J. Irkutsk State Univ. Commun. Modern Technol. **4**(40), 39–43 (2013)
7. Mirsaidov, M.: An account of the foundation in assessment of earth structure dynamics. In: E3S Web of Conferences (2019). https://doi.org/10.1051/e3sconf/20199704015
8. Mirsaidov, M.M., Toshmatov, E.S.: Spatial stress state and dynamic characteristics of earth dams. Mag. Civil Eng. (2019). https://doi.org/10.18720/MCE.89.1
9. Pinyol, N.M., Alonso, E.E.: Earth dam, spatial model, stress-strain state, dynamic characteristic, natural frequency, modes of oscillations. Int. J. Civil Eng. **17**, 501–513 (2019)
10. Mirsaidov, M., Sultanov, T., Yarashov, J., Toshmatov, E.: Assessment of dynamic behaviour of earth dams taking into account large strains. In: E3S Web of Conferences, vol. 97 (2019). https://doi.org/10.1051/e3sconf/20199705019
11. Mirsaidov, M.M., et al.: Mathematical simulation and the methods to assess the strength of earth dams. In: International Conference on Information Science and Communications Technologies:

Applications, Trends and Opportunities, ICISCT 2019, p. 9011818 (2019). https://doi.org/10.1109/ICISCT47635.2019.9011818

12. Urazmukhamedova, Z., Juraev, D., Mirsaidov, M.: Assessment of stress state and dynamic characteristics of plane and spatial structure. J. Phys: Conf. Ser. (2021). https://doi.org/10.1088/1742-6596/2070/1/012156

13. Mirsaidov, M.M., Sultanov, T.Z., Yarashov, J.Y.: Strength of earth dams considering elastic-plastic properties of soil. Maga. Civil Eng. (2021). https://doi.org/10.34910/MCE.108.13.8.pp.10813

14. Fu, Z., Chen, S., Li, G.: Hydrodynamic pressure on concrete face rockfill dams subjected to earthquakes. J. Hydrodyn. **31**, 152–168 (2019)

15. Wang, M., Chen, J., Xiao, W.: Experimental and numerical comparative study on gravity dam-reservoir coupling system. KSCE J. Civil Eng. **22**, 3980–3987 (2018)

16. Germanov, T.: Effect of the pore water pressure on the stress-strain behavior of earth dams. In: GEOTECH YEAR 2000, Developments in Geotechnical Engineering, pp. 429–438 (2000)

17. Kong, X.J., Liu, J.M., Zou, D.G.: Numerical simulation of the separation between concrete face slabs and cushion layer of Zipingpu dam during the Wenchuan earthquake. Sci. China Technol. Sci. (2016). https://doi.org/10.1007/s11431-015-5953-6

18. Alonso, E.E., Cardoso, R.: Behavior of materials for earth and rockfill dams: perspective from unsaturated soil mechanics. Front. Archit. Civil Eng. China (2010). https://doi.org/10.1007/s11709-010-0013-6

19. Ma, H., Chi, F.: Major technologies for safe construction of high earth-rockfill dams. Eng. (2016). https://doi.org/10.1016/J.ENG.2016.04.001

20. Soroka, V.B., Sainov, M.P., Korolev, D.V.: Rockfill dams with reinforced concrete screen: experience of stress-strain state studies. Bull. MGSU Hydraulics. Geotech. Hydraulic Eng. **14**(2), 207–224 (2019)

21. Grishin, M.M.: Hydro-technical structures. Part 1. High School, 615 (1979)

22. Ilichev, V.A., Yuldashev, S.S., Matkarimov, P.J.: Forced vibratins of an inhomogeneous planar system with passive vibratinal insulation. Soil Mech. Found. Eng. **36**, 50–54 (1999). https://doi.org/10.1007/BF02469084

Corrosion of Steel Reinforcement in Hydrophobized Concrete Under the Influence of Aggressive Chloride-Containing Medium

Varvara Rumyantseva ⓘ **, Viktoriya Konovalova** ⓘ **, Boris Narmaniya** ⓘ **, and Mikhail Korinchuk** ⓘ

Abstract The study of the reasons for shortening the period of concrete protection of steel reinforcement and the development of ways to increase its duration are the basis for increasing the durability of reinforced concrete products and structures. To increase the durability of reinforced concrete products, calcium stearate in an amount of 0.7 wt. % was introduced into the cement paste at the preparation stage to ensure volumetric hydrophobization. Corrosion studies of steel reinforcement in cement stone were carried out under the conditions of exposure to a 2% $MgCl_2$ solution. Breaking of the passivity of reinforcement in cement stone without the addition of calcium stearate occurs after about 6 months of exposure to an aggressive environment, in hydrophobized cement stone after 9 months of liquid corrosion. The electrochemical behavior of steel reinforcement in conventional and hydrophobized concrete was evaluated using polarization measurements. The calculated corrosion rates of steel reinforcement in cement stone have small values, but over time aggressive particles will accumulate near the surface of the reinforcement, which will contribute to the intensive development of corrosion processes. Corrosion of reinforcement in cement concrete without the addition of a hydrophobizer proceeds 1.3 times faster than reinforcement in hydrophobized concrete. However, it takes much longer to reach the maximum concentration of chloride ions at the surface of steel reinforcement in concrete with a hydrophobizer, therefore, corrosion processes will begin to develop later.

Keywords Steel Reinforcement · Reinforcement Corrosion · Corrosion Rate · Hydrophobized Concrete · Durability · Corrosion Resistance

V. Rumyantseva · V. Konovalova (✉) · B. Narmaniya · M. Korinchuk
Ivanovo State Polytechnic University, Sheremetevskiy ave., 21, Ivanovo 153000, Russia
e-mail: kotprotiv@yandex.ru

V. Rumyantseva
Ivanovo Fire Rescue Academy of State Firefighting Service of Ministry of Russian Federation for Civil Defense, Emergencies and Elimination of Consequences of Natural Disasters, Stroiteley ave., 33, Ivanovo 153040, Russia

1 Introduction

Due to the physical, chemical and mechanical characteristics, concrete used in various environments is exposed to various aggressive components that reduce its durability. The durability assessment is related to the expected performance characteristics of the product and consists in determining the factors that are crucial for the destruction of the material depending on its composition and properties, determining changes caused by the interaction of the material with external aggressive substances, and measuring damage over time.

Corrosion of reinforced concrete proceeds in two phases and is directly related to corrosion of steel reinforcement (Fig. 1). During the initial phase, the steel reinforcement is protected by a layer of concrete. The duration of this phase is determined by the rate of penetration of aggressive particles through the concrete layer to the reinforcement surface and the corrosion processes occurring in the concrete [1–3]. Due to the provision of good quality and lower permeability of concrete, as well as a greater coating thickness, the period of initiation of corrosion of steel reinforcement in reinforced concrete structures can be increased. The second phase begins after the depassivation of the surface of the steel reinforcement and ends with the processes of destruction of the reinforced concrete structural element due to the accumulation of corrosion products of the reinforcement [4–6]. To increase the service life of reinforced concrete products, it is necessary to study the reasons for the reduction of the first phase and develop methods for the duration of the second phase.

The penetration of water into concrete is the main cause of all major physical and chemical degradation processes in reinforced concrete products [8–12].
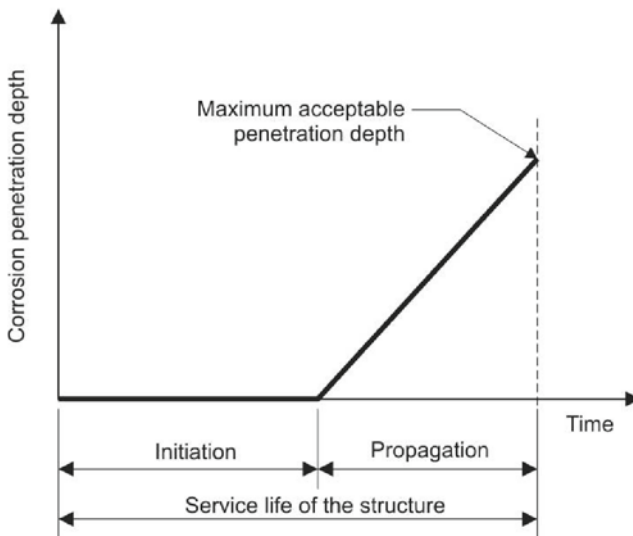
Fig. 1 Periods of the beginning and development of corrosion of reinforced concrete [7]

To prevent the entry of water and aggressive particles dissolved in it deep into the concrete, hydrophobization is resorted to. Due to the decrease in water absorption, the amount of liquid aggressive medium entering the concrete decreases, and, therefore, the degree of its corrosion destruction decreases [13–15]. The introduction of hydrophobic additives into the concrete composition or the treatment of the concrete surface with special penetrating compounds increases the water resistance of concrete, prevents the occurrence of corrosion processes and damage to the concrete structure [16–19]. All this contributes to the durability of concrete and reinforced concrete structures.

The positive effect of concrete hydrophobization usually lies in the fact that this type of treatment prolongs the period before the onset of corrosion. When corrosion begins, the hydrophobicity of the surface of the pores of the cement stone effectively prevents the penetration of the liquid medium and reduces the rate of corrosion. The absence of chloride penetration into hydrophobized concrete was found on the motorway pier after 7 years of operation [20–22].

Corrosion resistance of reinforced concrete with hydrophobic additives requires additional study to determine the regularity of mass transfer. To assess the contribution of hydrophobization to the durability of the structure, it is necessary to know how effectively this treatment method prevents the penetration of various aggressive substances, and how long this efficiency can be maintained.

2 Materials and Methods

The studies were carried out on bars of reinforcement made of rolled steel A500C, filled in a cylindrical shape with Portland cement of the CEM I 42.5N grade with a water-cement ratio W/C = 0.3.

Calcium stearate in the amount of 0.7 wt. % was introduced as a hydrophobic additive at the cement mixing stage. This amount of hydrophobizer is necessary to obtain concrete of the W8 waterproof grade. As a result of volumetric hydrophobization, insoluble calcium stearate is deposited on the surface of the pores of cement stone concrete [23].

After curing for 28 days in air, the samples were placed in containers with a 2% $MgCl_2$ solution as an aggressive medium. The $MgCl_2$ solution concentration of 20 g/l was accepted as highly aggressive towards concrete [24].

The reinforcement potential in the cement stone was measured for 24 months. Determination of the electrode potential of the surface of steel reinforcement in concrete was carried out by a non-destructive method of measuring the potentials of the half-element. The measurement is performed by installing a reference electrode connected to the negative pole of the voltmeter on a concrete surface through a moistened sponge. The positive pole of the voltmeter is connected to the steel reinforcement. The measurement scheme is shown in Fig. 2. The voltmeter readings are taken after the device readings are stabilized. Readings are considered stable if
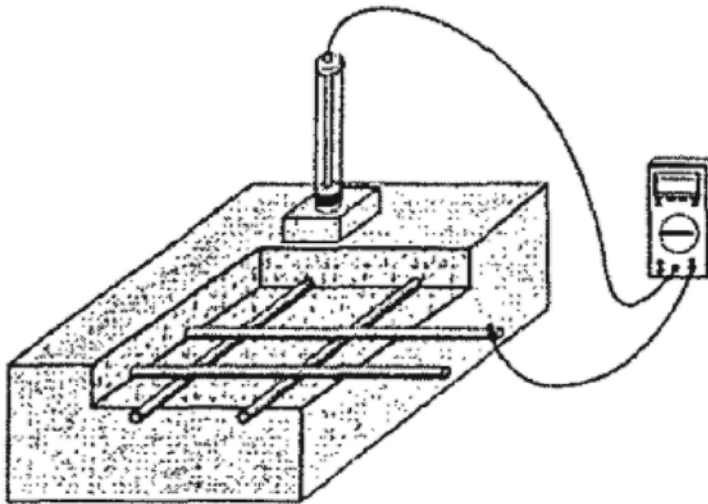
Fig. 2 Scheme for measuring the potential of the reinforcement surface in concrete by the method of half-element potentials with one reference electrode

they remain unchanged for at least 15 s when measured in the operating mode of the device with a discreteness of 1 mV.

To recalculate the potential of steel reinforcement with respect to the hydrogen electrode E_{Me}, it is sufficient to add the potential of the comparison electrode $E_{c.e}$ to the potential of the E_m measured by this method, taken with its own sign.:

$$E_{Me} = E_M + E_{c.e}. \tag{1}$$

The measurement of the polarization resistance was carried out at alternating current in a two-electrode cell, which is a glass with a capacity of 150 ml with a lid in which the electrodes are attached (Fig. 3). The electrodes in the form of rods are made of St3 steel. The working surface is 0.6 cm^2, the non-working part of the electrodes is isolated from the solution by a glass shell. The distance between the working parts of the electrode was 20 mm. The cell was filled with the studied phosphating solution, then it was connected to the measuring device. The resistance of the system under study was recorded initially every 20 s, after 5 min – every 60 s for 30 min at room temperature with one type of solution.

Polarization measurements provided information about the electrochemical behavior of steel reinforcement in cement stone and allowed us to calculate the corrosion rate:

$$K_m^- = \frac{j \cdot A}{z \cdot 26, 8}, \tag{2}$$
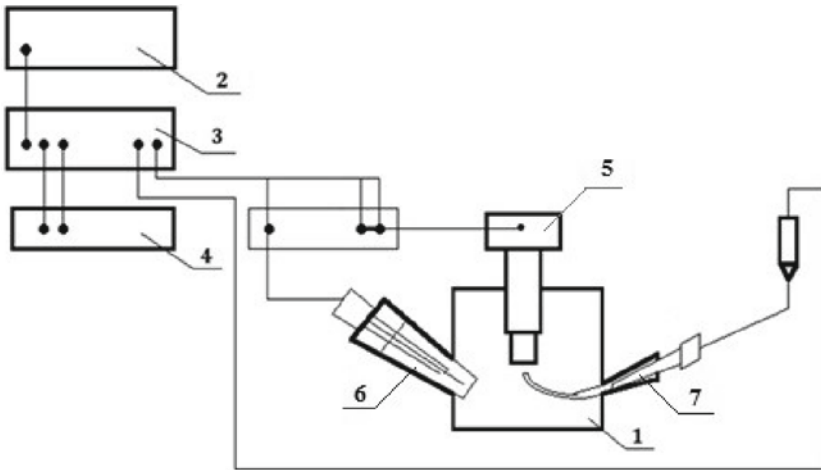
Fig. 3 Diagram of an experimental installation for conducting polarization measurements: 1 – electrochemical cell; 2 – programmer; 3 – potentiostat; 4 – two-coordinate recording device; 5 – working electrode; 6 – auxiliary electrode; 7 – reference electrode

$$K_h = K_m^- \frac{8,76}{\rho_{Me}},\qquad(3)$$

where: K_m^- is negative mass change indicator, g/(m^2 · h); j is corrosion current density, A/m^2; A is atomic mass of metal, g/mol; z is valence of the metal; 26,8 is Faraday 's constant, A·h/mol; K_h is deep corrosion index, mm/year; ρ_{me} is metal density, g/cm^3.

3 Results and Discussion

It can be seen from Fig. 4 that at the initial stage the steel reinforcement changes potential, which is due to the formation of a passive film on its surface. In hydrophobized cement stone, steel reinforcement remains passive for 9 months, then the potential decreases slowly. Breaking of the passivity of reinforcement in cement stone without the addition of calcium stearate occurs after about 6 months of exposure to an aggressive environment. At potential values below -100 mV, steel enters an active state when corrosion processes can begin to develop, but at an extremely low rate [7]. With a further decrease in the potential, the corrosion process of steel becomes more intense and more cathodically controlled.

The polarization curves (Fig. 5) show that the corrosion current density is higher in cement stone without additives, hence the corrosion of steel reinforcement will proceed faster. Anodic dissolution of reinforcement in cement stone without additives begins at a surface potential of about -290 mV and actively continues until the
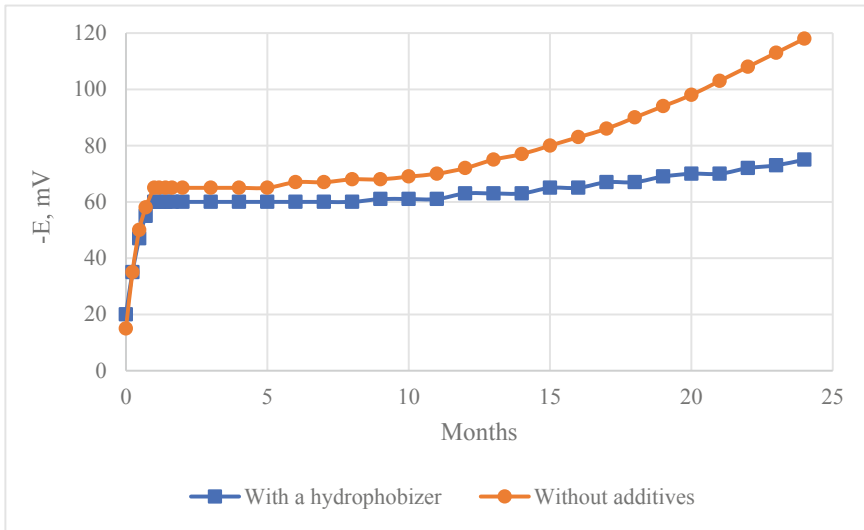
Fig. 4 The change in the potential of reinforcement made of rolled steel A500C in cement stone under conditions of liquid corrosion in a 2% MgCl$_2$ solution

potential increases to 760 mV. The passive state of the metal surface does not last long. Then pitting formation begins on the surface of the steel. In hydrophobized cement stone, anodic dissolution of steel begins at a potential of -255 mV. The active–passive state of the surface occurs at a potential of 340 mV. There is no breaking of the passivity of the steel surface, since the cement stone has a dense structure and prevents the entry of aggressive particles to the metal surface.

Table 1 shows the corrosion rate indicators calculated according to formulas (2) and (3) for the maximum achieved value of the corrosion current.

When aggressive particles accumulate near the surface of steel reinforcement in an amount sufficient to destroy its passivation and the beginning of the development of corrosion processes, corrosion of reinforcement in cement concrete without the addition of a hydrophobizer proceeds 1.3 times faster than reinforcement in hydrophobized concrete. However, it takes much longer to achieve such a concentration of chloride ions at the surface of steel reinforcement in concrete with a hydrophobizer. It has been established [25] that the threshold value of chloride ion concentrates are achieved in concrete grades for water resistance W8 after 3 years. To achieve such a concentration of chloride ions at the surface of the reinforcement in concrete without hydrophobic additives at liquid corrosion in a 2% MgCl$_2$ solution, it will take 174 days.

These calculated data are confirmed by the results of experimental studies of changes in the potential of steel reinforcement in cement samples exposed to 2% MgCl$_2$ solution (Fig. 4).
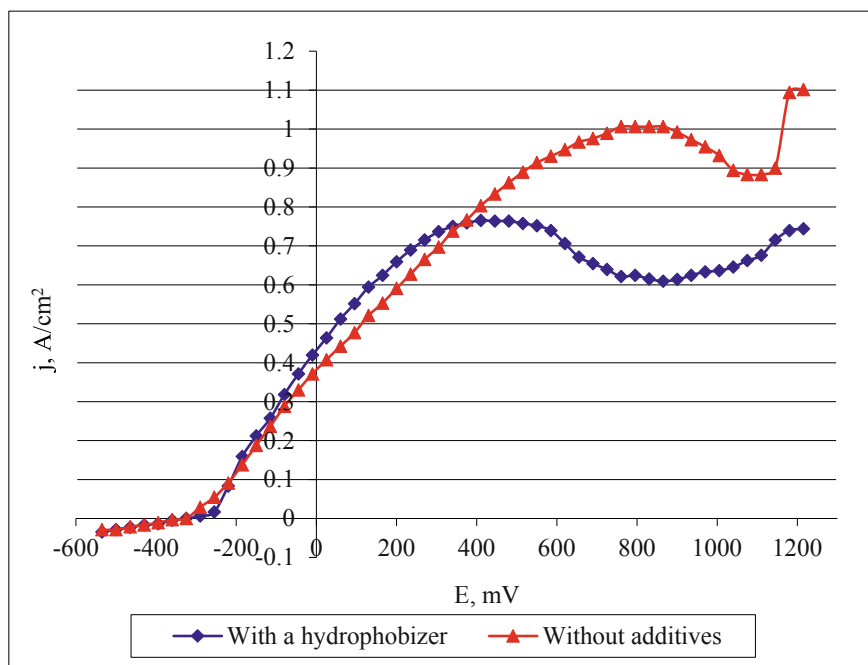
Fig. 5 Polarization curves of reinforcement made of rolled steel A500C in cement stone under conditions of liquid corrosion in a 2% MgCl$_2$ solution

Table 1 Corrosion rates of reinforcement made of rolled steel A500C in cement stone after 24 months of liquid corrosion in 2% MgCl$_2$ solution

Type of cement stone	Mass change indicator K_m^-, , g/(m^2·h)	Deep corrosion index K_h, mm/year
Without additive	1.05·10^{-4}	1.17·10^{-4}
With a hydrophobizer	0.8·10^{-4}	0.894·10^{-4}

4 Conclusion

Volumetric hydrophobization allows to reduce water absorption and increase the density of cement stone, which means to reduce the amount of aggressive medium entering the concrete and reduce the degree of corrosion destruction of steel reinforcement.

It has been experimentally established that the change in the electrode potential of the surface of steel reinforcement in concrete begins after 6 months of samples being in a 2% MgCl$_2$ solution, in the case of corrosion of hydrophobized concrete – after 9 months, however, no significant change in the potential of reinforcement was recorded for 2 years.

The values of the corrosion rate of steel reinforcement in concrete show that the dissolution of the metal surface at the initial stage of operation of a reinforced concrete product in a liquid chloride-containing medium of a high degree of aggressiveness occurs slowly. By introducing calcium stearate into the cement mixture at the stage of concrete production, it is possible to significantly increase the period of preservation of the passive state of the reinforcement steel surface in concrete and reduce the rate of corrosion after the accumulation of a critical concentration of chloride ions at the surface of the reinforcement.

References

1. Alekseev, S.N.: Corrosion and Reinforcement Protection in Concrete. Stroyizdat, Moscow (1968)
2. Moskvin, V.M., Ivanov, F.M., Alekseev, S.N., Guzeev, E.A.: Corrosion of Concrete and Reinforced Concrete, Methods of Their Protection. Stroyizdat, Moscow (1980)
3. Leonovich, S.N., Riachi, J.: 3D-modeling for life cycle of the structure. Sci. Tech. **20**(1), 5–9 (2021)
4. Suvash, C.P., Adewumi, J.B.: A review on reinforcement corrosion mechanism and measurement methods in concrete. Civil Eng. Res. J. **5**(3), 80–90 (2018)
5. Ožbolt, J., Brajković, A., Lin, H.: Modeling corrosion of steel reinforcement in concrete: natural vs. accelerated corrosion. In: Proceedings of 10th International Conference on Fracture Mechanics of Concrete and Concrete Structures, IA-FraMCoS, Bayonne, France, p. 11 (2019)
6. Leonovich, S.N., Shalyi, E.E., Kim, L.V.: Reinforced concrete under the action of carbonization and chloride aggression: a probabilistic model for service life prediction. Sci. Tech. **18**(4), 284–291 (2019)
7. Tuutti, K.: Corrosion of Steel in Concrete. Swedish Cement and Concrete Research Institute, Stockholm (1982)
8. Ahmad, S.: Reinforcement corrosion in concrete structures, its monitoring and service life prediction—a review. Cement Concr. Compos. **25**(4–5), 459–471 (2003)
9. Yoo, J.-H., Lee, H.-S., Ismail, M.A.: An analytical study on the water penetration and diffusion into concrete under water pressure. Constr. Build. Mater. **25**(1), 99–108 (2011)
10. Dobias, D., Pernicova, R., Mandlik, T.: Water transport properties and depth of chloride penetration in ultra high performance concrete. Key Eng. Mater. **711**, 137–142 (2016)
11. Zhang, Y., Li, X., Yu, G.: Chloride transport in undersea concrete tunnel. Adv. Mater. Sci. Eng. **2016**, 1085934 (2016)
12. Zhu, X., Meng, Z., Liu, Y., Xu, L., Chen, Z.: Entire process simulation of corrosion due to the ingress of chloride ions and CO2 in concrete. Adv. Mater. Sci. Eng. **2018**, 9254865 (2018)
13. Patel, R.A., Perko, J., Jacques, D., De Schutter, G., Ye, G., Van Bruegel, K.: Effective diffusivity of cement pastes from virtual microstructures: role of gel Porosity and capillary pore percolation. Constr. Build. Mater. **165**, 833–845 (2018)
14. Bertolini, L., Elsener, B., Pedeferri, P., Redaelli, E., Polder, R.B.: Corrosion of Steel in Concrete: Prevention Repair. Wiley-VCH Verlag GmbH & Co., Diagnosis (2013)
15. Bouteiller, V., Cherrier, J.-F., L'Hostis, V., Rebolledo, N., Andrade, C., Marie-Victoire, E.: Influence of humidity and temperature on the corrosion of reinforced concrete prisms. Eur. J. Environ. Civ. Eng. **16**(3–4), 471–480 (2012)
16. Razak, S.A., Raj, A.: An overview on effects of water repellent concrete protective coatings in the durability of concrete structures. Int. J. Sci. Res. **5**(7), 1565–1572 (2016)
17. Velichko, E., Polkovnikov, N., Sadchikova, Y.: Efficient concrete increased water resistance modified with mineral and polymeric additives. In: E3S Web of Conferences, vol. 97, p. 02017 (2019)

18. Fedosov, S.V., Rumyantseva, V.E., Konovalova, V.S., Evsyakov, A.S.: Pore colmatation in case of liquid corrosion of concrete. In: IOP Conference Series: Materials Science and Engineering, vol. 911, p. 012002 (2020)
19. Sohawon, H., Beushausen, H.: The effect of hydrophobic (silane) treatment on concrete durability characteristics. In: MATEC Web of Conferences, vol. 199, p. 07015 (2018)
20. Basheer, P.A.M., Long, A.E.: Protective qualities of surface treatments for concrete. Proc. Inst. Civil Eng. – Struct. Build. **122**(3), 339–346 (1997)
21. Basheer, P.A.M., Basheer, L., Cleland, D.J., Long, A.E.: Surface treatments for concrete: assessment methods and reported performance. Constr. Build. Mater. **11**(7–8), 413–429 (1997)
22. Basheer, L., Cleland, D.J., Long, A.E.: Protection provided by surface treatment against chloride-induced corrosion. Mater. Struct. **31**, 459–464 (1998)
23. Ramachandran, V.S.: Concrete Admixtures Handbook: Properties, Science and Technology, 2nd edn. William Andrew, Norwich (1996)
24. Konovalova, V.S.: Influence of chloride-containing media on the protective properties of concrete. In: Klyuev, S., Lesovik, V., Vatin, N. (eds.) Innovations and Technologies in Construction. BUILDINTECH BIT 2020. Lecture Notes in Civil Engineering, vol. 95, pp. 260–265. Springer, Cham (2021). https://doi.org/10.1007/978-3-030-54652-6_39
25. Fedosov, S.V., Rumyantseva, V.E., Konovalova, V.S., Evsyakov, A.S.: The role of colmatation in liquid corrosion of hydrophobized concrete. In: IOP Conference Series: Materials Science and Engineering, vol. 896, p. 012096 (2020)

Modular Construction. Modular Ventilated Façade Concept

Irina Leonidovna Kotlyarskaya ⓘ, **Aleksei Sergeevich Sinelnikov** ⓘ,
Nikolai Ivanovich Vatin ⓘ, **Darya Viktorovna Nemova** ⓘ,
Nikita Artemovich Iakovlev ⓘ,
and Rustamkhan Alimkhanovich Abdikarimov ⓘ

Abstract The object of research is a modular ventilated facade. This design was developed based on ventilated façade and modular façade systems. The combination of the two systems will result in a more advanced and modern design. The research methods used in the work are the analysis and review of the literature, the modeling of the structure, and the calculation of the bearing capacity of the facade pillar. The concept of a modular ventilated facade with cassette cladding, as well as using solar panels, is proposed. Thermoprofile TS150-50-2.0 used in the facade concept has a section weakened by notches in the section wall. The bearing capacity of the rack profile of the facade according to the calculation in the SCAD software package is provided.

Keywords Energy-efficient buildings · Ventilated façade · Modular facade · Modular ventilated façade · Enclosing structure · Bearing capacity · Reduced wall thickness

1 Introduction

Modular buildings are made up of prefabricated components and assemblies (called modules) that are transported and assembled on-site to form a building. Since the modules are manufactured under controlled conditions at the factory and are not exposed to different climatic factors during the manufacturing process, they are of the best quality. The demand for this technology is also explained by its advantages in the speed of construction and compliance with sustainable development trends. Examples of such buildings [1]:

I. L. Kotlyarskaya (✉) · A. S. Sinelnikov · N. I. Vatin · D. V. Nemova · N. A. Iakovlev
Peter the Great St. Petersburg Polytechnic University, 195251 St. Petersburg, Russian Federation
e-mail: iravassilek@mail.ru

R. A. Abdikarimov
Tashkent Institute of Architecture and Civil Engineering, Tashkent, Uzbekistan

1) The Collins House building in Melbourne (Australia) is currently the tallest modular building in the world with 60 floors.
2) The Tower T30 and Tower J57 Mini Sky in China are notable for setting the world record for being the fastest building in the world. The T30 tower was completed in just 15 days, while the J57 Mini Sky tower was completed in just 19 days (at a rate of three floors per day).
3) The Clement Canopy Tower (40 floors) is the tallest modular building in Singapore.

In practice, in addition to volumetric modular construction, panel modular construction is also used. It is a construction of flat elements, but with a complete finish [2, 3]. Such an element is a modular facade. Modules are structural elements consisting of individual metal profiles forming a flat frame. It is filled with insulation and lined with decorative materials. There are modular facades with and without a translucent part.

Modular facades can be divided into several groups:

1) Reinforced concrete panels

A reinforced concrete panel is a large-sized flat element of a factory-made structure. It consists of a concrete frame, insulation, and cladding.

2) Sandwich panels

Sandwich panels are a three-layer structure consisting of metal outer and inner linings and a middle part (core), interconnected by an adhesive composition [4–6]. Sandwich panels are also produced on production lines. They are mainly used in prefabricated buildings.

3) Frame-sheathing walls

This kind of wall is a multi-layer non-load-bearing structure, consisting of a frame (usually made of light steel thin-walled structures), filling the cavity of the frame with materials for thermal insulation or sound insulation, wall cladding (external and internal), and external cladding.

4) Translucent modular structures

They are external non-bearing walls, consisting of a frame, fasteners, seals, and translucent and opaque filling. According to the composition, there are varieties of cable-stayed, frameless, combined, two-layer construction. Such structures are installed at a distance from the building frame, in-wall openings, and between floor slabs [7, 8].

5) Ventilated modular walls

They differ from typical ventilated facades in that the facades are assembled at the factory and delivered to the facility ready for installation in the form of large-format facade modules with cladding, which are mounted on pre-installed special brackets.

There is very little scientific literature about the latter type of modular facade. Although the phrase "Modular ventilated facades" is well-established, nothing is found when searching through the scientific database.

The movement of air masses in a ventilated facade allows ventilation of the structure. Thus, mold formation and further destruction of the insulation and the load-bearing wall do not begin inside the system [7, 9–11].

The advantages of a modular facade are its quick installation, reduced load on the foundation, as well as the quality of the modular components of the facade. Facade modules are completely manufactured in the factory. During the manufacturing process, they are not affected by climatic factors. Also, this design leads to a reduction in construction waste (25%) [12].

Both directions are promising and complementary. Based on their combination, it is possible to create a rational and energy-efficient facade design.

Preliminary calculation of the rack of a modular ventilated facade is also subject to consideration. The calculation is necessary to understand at the first stage whether it is possible to use a thermal profile in a structure to improve its thermal properties and lighten the weight of the structure.

The purpose of this study is to determine the potential of the concept of a modular ventilated facade and its prospects in the modular construction of buildings.

To achieve this goal, this study was carried out in several stages:

- to propose, based on the studied literary material, the concept of a modular ventilated facade;
- to determine the reduced wall thickness of the section of the thermoprofile TS150-50-2.0 (rack of a modular ventilated facade).

2   Method

In the first part of the article, the computer simulation method is used. Based on the analysis of existing variants of ventilated and modular facades, new types of facades are proposed. They are executed in the Revit software package.

In the second part of the work, for the proposed version of the facade, the reduced wall thickness of the section of the thermal profile TS150-50-2.0 (modular ventilated facade rack) is determined.

In the European regulations EN 1993-1-1 (3.5) [13–15] and SP 260.1325800.2016 "Cold-formed thin-walled steel profile and galvanized corrugated plate constructions. Design rules" [16], the calculation of thin-walled cold-formed profiles is based on determining the geometry of the "effective" section of the profile. This technique is based on the theory of stability of a compressed rectangular plate with different boundary conditions, developed by Timoshenko S.P. [17]. The standard [16] contains a methodology for determining the effective cross-section [13–15]. The work is based on the normative methodology [16].

Thermoprofile TS150-50-2.0 used in the facade concept has a section weakened by notches in the section wall. In the normative documents considered above, there is no calculation method for considering the perforation area when determining the geometry of the effective section. In engineering practice, there is a simplified method for accounting for a perforated section, based on its exclusion from the wall

of the "effective" section. With this approach, the bearing capacity is determined according to the American AISI standard "North American Specification for the design of cold-formed steel structural members". Accounting for perforation is to reduce the resulting bearing capacity by multiplying by a factor of 0.8 [6].

The classical solution to the problem of accounting for perforation is based on replacing the perforated section of the section with a solid plate with a reduced thickness. The further algorithm for determining the geometry of the "effective" section coincides with [13–15]. The search for the thickness of a solid section wall plate, which is equivalent to a plate with notches, assumes that the critical compressive stresses are equal for both types of plates. This method involves the determination of the stability coefficient K_{perf}. for a compressed square perforated plate supported around the perimeter. It is determined by the finite element method. The stability coefficient for a solid plate K_{gr}. under similar conditions is assumed to be 4. The advantage of the classical approach is its versatility (section perforation can have any regular pattern).

The practical application of a similar approach was proposed in the work of P. Salmi [18]. Instead of stability coefficients, critical values of compressive stresses are determined. The plate thickness reduction factor was determined according to Eq. 1:

$$k_{red} = \sqrt{\frac{\sigma_{cr.perf}}{\sigma_{cr.plaim}}} \tag{1}$$

where $\sigma_{cr.perf}$ is critical compressive stress of the perforated plate and $\sigma_{cr.plain}$ is critical compressive stress of a solid plate.

Equation 1 allows determining the reduction factor for a compressed rectangular plate. It is an important difference from the classical solution. The aspect ratio of the width and length of the compressed plate according to [17] directly affects the actual value of the critical compressive stress and the number of half-waves of the buckling form. For this reason, when using the formula, it is necessary to accurately determine the reduction factor iteratively.

3 Results and Discussion

3.1 The Modular Ventilated Façade Concept

The starting stage in the implementation and production of a building structure is the development of its concept. New ideas must, first of all, meet such requirements as practical significance, simple feasibility, economic rationality, environmental and social public safety, etc. The idea of a modular ventilated façade meets all these requirements. This design is as energy efficient as a ventilated façade. It helps to avoid unnecessary heat loss, which means that fuel resources are saved. Saving fuel

resources leads to a cleaner environment. The modularity of the design reduces the installation time of the façade. Thus, builders work less on the construction site and the risks of accidents on the construction site are reduced. It is a safer mounting method.

The design of the ventilated facade module consists of a frame made of light steel thin-walled structures (pillars and guides). Insulation in the form of plates is placed in the frame. The internal lining will be made of reinforced cement-mineral sheets AQUAPANEL. The outer cladding is composite panels. They are three-dimensional panels with iklies (cassette holders) riveted to the vertical sides, which provide hidden fastening. The outer cladding is fastened based on the U-kon fastening facade system.

A graphical representation of the modular ventilated façade concept is shown in Fig. 1.

The outer cladding can also consist of solar panels (Fig. 2), which have proven themselves as a source of autonomous (independent) energy supply [19–21].

3.2 Determination of the Reduced Wall Thickness of the Section (Thermoprofile TS150-50-2.0)

External enclosing structures, as a rule, are designed from a perforated profile. It is also used in the concept of a modular ventilated facade. The perforated profile in the section wall has a section weakened by notches. Due to the location of the perforation in a checkerboard pattern in the wall of the section, it was possible to reduce the thermal conductivity of the profile, avoiding the formation of a cold bridge [22]. This decision harmed the overall bearing capacity of the thin-walled cold-formed profile.

The solution to the problem was carried out based on the finite element method with a partition step of 3 mm. The thickness of the plates is 1.95 mm. The dimensions of the wall plates were set considering the section thickness, 148×148 mm (Figs. 3, 4).

The boundary conditions were chosen so that the compressed plate was supported along the entire perimeter. The load was set in the form of a uniformly distributed along the line on one of the transverse sides in the plate plane.

The reduced wall thickness of the section is 1.32 mm according to the methodology written above.

The rack profile was calculated for the peak wind load of the II wind region of the Russian Federation. The pitch of the posts of the modular facade is p = 0.6 m. The height of the post is 3 m. The coefficient of redistribution of forces for a continuous two-span beam scheme is n = 1.25 (for example, the area near the window).

The calculated distributed load from the peak wind load on the rack of the modular facade q is 198 kgf/m according to Eq. 2.

$$q = 264 \cdot \text{n} \cdot \text{p} \tag{2}$$
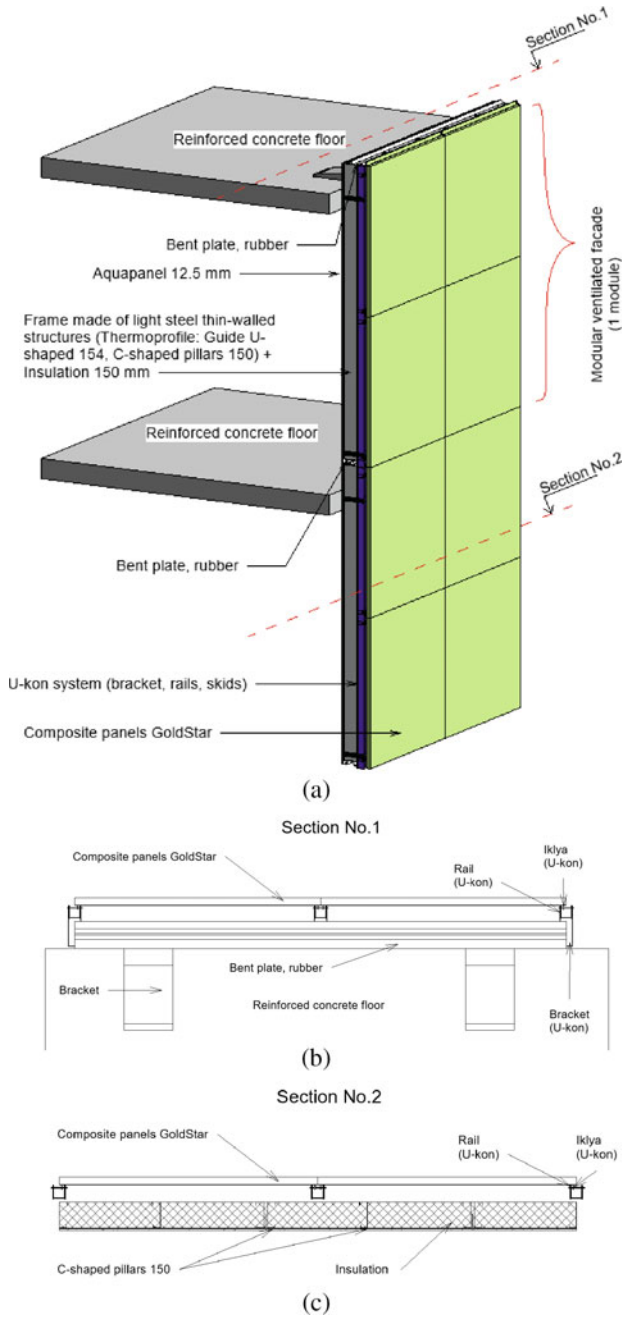
Fig. 1 Modular ventilated facade **a** 3D view **b** section no.1 **c** section no.2
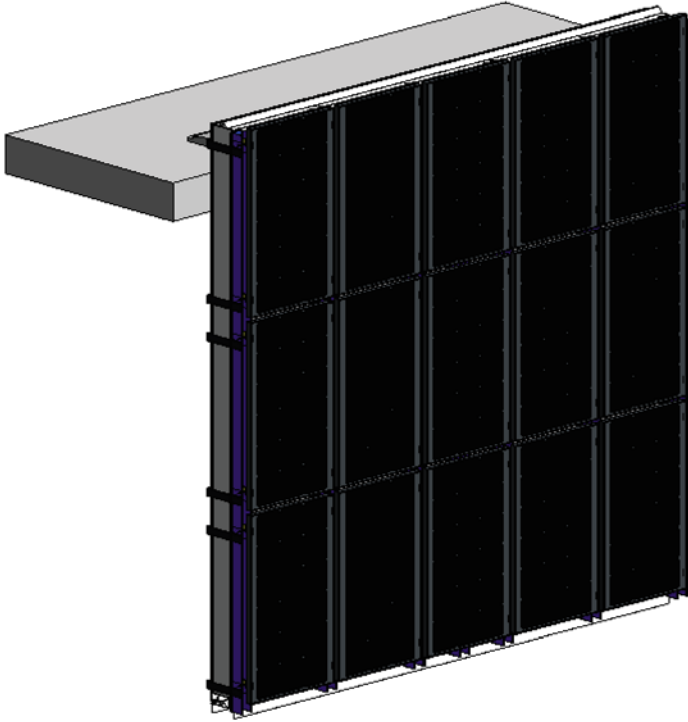
Fig. 2 Modular ventilated facade with solar panels

Fig. 3 Perforated plate
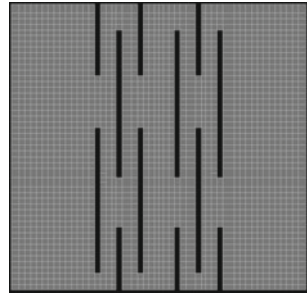
The calculated bending moment in the post of the modular facade M_y is 0.223 tf · m according to Eq. 3.

$$M_y = \frac{q \cdot l^2}{8}$$ (3)
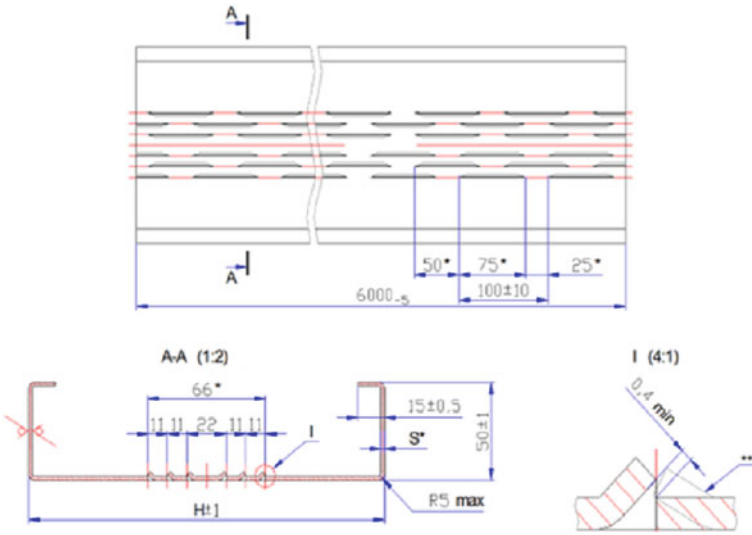
Fig. 4 Perforated thermoprofile

The design shear force in the post of the modular façade Q is 0.297 tf according to Eq. 4.

$$Q = \frac{q \cdot l}{2} \qquad (4)$$

The calculation of the cold-formed profile TS 150-50-2.0 was performed according to [16]. The coefficient of use for strength under the combined action of the longitudinal force N and bending moments M_y and M_z is 0.476 (considering the loss of local stability), which is less than the maximum allowable value is 0.95.

4   Conclusions

1. Based on the studied literature on modular facades and ventilated facades, a combined design is proposed. The modular ventilated façade has the advantages of both façade systems. The facade is both energy-efficient and quickly assembled.

2. The bearing capacity of the profile TS 150-50-2.0 with the given parameters (section step, loads) is ensured.

Accordingly, this design at the initial stage proved to be promising and requires further detailed consideration.

References

1. Thai, H.T., Ngo, T., Uy, B.: A review on modular construction for high-rise buildings. Structures **28**, 1265–1290 (2020)
2. Li, Y., Chen, L.: Investigation of European modular façade system utilizing renewable energy. Int. J. Low-Carbon Technol. **17**, 279–299 (2022)
3. Dan-Adrian, C., Tsavdaridis, K.D.: A comprehensive review and classification of inter-module connections for hot-rolled steel modular building systems. J. Build. Eng. **50**, 104006 (2022)
4. Zhang, C., Liang, L., Yan, L., Sun, X., Zheng, X.: Environmentally friendly bio-inspired folded sandwich panels—fabrication and mechanical behavior. Polymer Compos. **43**(10), 7086–7098 (2022). https://doi.org/10.1002/pc.26770
5. Barbirato, G.H.A., et al.: Sandwich OSB trapezoidal core panel with balsa wood waste. Waste Biomass Valoriz. **13**(4), 2183–2194 (2022)
6. El-Gamal, S., Al-Kalbani, A., Al-Hatmi, O.: Developing and investigating the performance of thermal insulation lightweight sandwich wall panels. In: Proceedings of the Canadian Society of Civil Engineering Annual Conference 2021, pp. 653–666. Springer, Singapore (2023)
7. Tao, Y., Fang, X., Setunge, S., Tu, J., Liu, J., Shi, L.: Naturally ventilated double-skin façade with adjustable louvers. Sol. Energy **225**, 33–43 (2021)
8. Huang, Y., Tao, Y., Shi, L., Liu, Q., Wang, Y., Tu, J., Peng, Q., Cao, C.: Thermal and ventilation performance of a curved double-skin facade model. Energy Build. **268**, 112202 (2022)
9. De Masi, R.F., Festa, V., Gigante, A., Ruggiero, S., Vanoli, G.P.: Experimental analysis of grills configuration for an open joint ventilated facade in summertime. J. Build. Eng. **54**, 104608 (2022)
10. Tina, G.M., Bontempo Scavo, F., Aneli, S., Gagliano, A.: A novel building ventilated façade with integrated bifacial photovoltaic modules: analysis of the electrical and thermal performances. In: 2020 5th International Conference on Smart and Sustainable Technologies, SpliTech 2020. Split, Croatia (2020)
11. Andreeva, D., Nemova, D., Kotov, E.: Multi-skin adaptive ventilated facade: a review. Energies **15**, 3447 (2022)
12. Torres, J., et al.: Plug and play modular façade construction system for renovation for residential buildings. Buildings **11**, 419 (2021)
13. EN 1993-1-1: 2005. Eurocode 3: Design of steel structures. Part 1-1: General rules and rules for buildings (2005)
14. EN 1993-1-3: 2006. Eurocode 3 - Design of steel structures - Part 1-3: General rules - Supplementary rules for cold-formed members and sheeting (2006)
15. EN 1993-1-5: 2006. Eurocode 3 - Design of steel structures - Part 1-5: Plated structural elements (2006)
16. SP 260.1325800.2016 Cold-formed thin-walled steel profile and galvanized corrugated plate constructions. Design rules. https://meganorm.ru/Data2/1/4293748/4293748507.pdf. Accessed 27 June 2022
17. Timoshenko, S.P.: Stability of Rods, Plates and Shells. Science, Moscow (1971)
18. Salmi, P.: Design of web-perforated steel wall studs. In: 4th Finnish Steel Structures R&D Days Lappeenranta, Finland (1998)
19. Pradhan, A., Panda, B., Nanda, L., Jena, C., Sahoo, S.: Analysis of various types of reflectors on the performance of PV panel. In: 2022 International Conference for Advancement in Technology, ICONAT 2022. Goa, India (2022)
20. Kannan, A., Tumuluru, V.K.: Shared investment in PV panels and battery storage for residential building. Energy Ecol. Environ. **7**, 236–249 (2022)
21. Nasser, M., Megahed, T.F., Ookawara, S., Hassan, H.: Performance evaluation of PV panels/ wind turbines hybrid system for green hydrogen generation and storage: Energy, exergy, economic, and enviroeconomic. Energy Convers. Manag. **267**, 115870 (2022)
22. Sergeev, V.V., et al.: The building extension with energy efficiency light-weight building walls. Mag. Civil Eng. **84**, 67–74 (2018)

Thermal Characteristics of a Modular Additive Enclosing Structure

Irina Leonidovna Kotlyarskaya ⓘ, **Nikolai Ivanovich Vatin** ⓘ,
and **Darya Viktorovna Nemova** ⓘ

Abstract The object of the study is a modular wall panel made on a 3D printer. Previously, this sample was tested in climatic chambers. The aim of the study is to assess the energy efficiency potential of the additive structure under study based on a more detailed analysis of the data obtained from the experiment in the climatic chamber and the thermal imaging performed. The work uses numerical and analytical methods. The heat transfer coefficient was calculated based on the data on the distribution of temperature and heat flux over the surface. The heat transfer coefficient U is equal to 0.464 W/m^2 °C. This value is higher than the normative value for Saint-Petersburg, Russia (climate zone according to the Köppen-Geiger climate classification is Dfb). For the comfortable use of these modular additive panels, it is necessary to additionally insulate them. An analysis of thermal imaging of the additive structure showed that the temperature is distributed unevenly over the surface. Under the same conditions, the temperature variation can be more than 10 °C. This factor can significantly affect the overall heat transfer coefficient of the structure.

Keywords Energy-efficient buildings · Modular building · 3D printing · Additive technology · Enclosing structure · Heat transfer coefficient · Thermal imaging

1   Introduction

Prefabrication is a process in which building components (modules) are manufactured in a factory and delivered to a construction site to form a building [1]. There are three classes of prefabricated structures: element 1D, panel 2D, and volumetric 3D systems (Fig. 1) [2].

Panel 2D and 3D bulk buildings are also known as modular buildings. It allows more than 70% of the building to be prefabricated in the factory before it is transported for assembly at the construction site. Factory manufacturing of modular components

I. L. Kotlyarskaya (✉) · N. I. Vatin · D. V. Nemova
Peter the Great St. Petersburg Polytechnic University, 195251 St. Petersburg, Russian Federation
e-mail: iravassilek@mail.ru
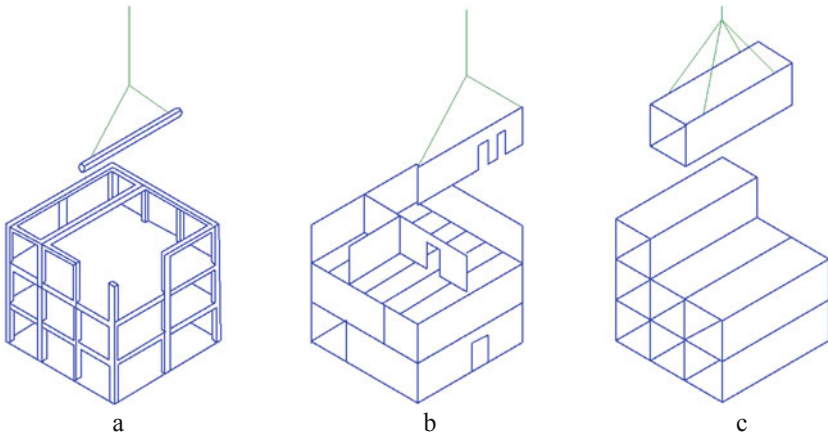
Fig. 1 Modular building systems **(a)** elemental **(b)** panel **(c)** volumetric

varies greatly from static factory floors to conveyor belts and even robotic module production.

Modular construction offers significant advantages over traditional construction:

1) Faster production (by 50%);
2) Better predictability of construction completion time [3–6];
3) Better quality of construction (The materials used in modular buildings are the same as in classical construction but of better quality. The reason is that the components are manufactured under controlled conditions in the factory and are not exposed to long-term climatic factors during the construction process);
4) Waste reduction (Most of the waste on a construction site is generated during the concreting process. This process and related works lead to the formation of more than 80% of all construction waste [7–9]);
5) Reducing the number of visits to the object of delivery vehicles up to 70%;
6) Reducing the noise level by 30–50%;
7) Improving safety at the construction site (Reported accidents are estimated to be reduced by more than 80% compared to intensive conventional construction);
8) Reduced theft on the construction site (Most finishes and expensive exterior elements are installed already at the factory in the module).

The use of prefabricated construction is most relevant for the creation of typical apartment buildings, hotels, schools, hospitals, offices, student dormitories, and other types of buildings, where preference is given to repeating elements [6, 10, 11]. Repetitive units may include building components such as rooms, corridors, and finished plumbing modules [12].

One of the innovative options for creating ready-made building modules is the 3D printing method. 3D concrete printing (3DCP) is also known as Additive Manufacturing AM [13]. 3DCP implies an automated process during which concrete structures are created by extruding concrete layer by layer through a digitally controlled nozzle

[14]. With the use of additive technology, it is possible to manufacture both individual elements of a building and the building itself. Buildings and building elements (wall modules, for example) made by 3D printing can have a complex geometric shape in terms of plan and height. This contributes to the creation of expressive architecture [15]. Theoretically, 3D printing can allow any shape to be printed [16, 17].

3D printing technology is actively developing. Therefore, it becomes important to study the structures made in this way from the point of view of thermal properties and to assess the potential of their energy efficiency.

In the article [18] modeling was carried out for the thermotechnical study of a wall enclosing structure made in an additive way. The article describes modeling in the Ansys software package with different configurations of the internal edges of the structure (internal mesh). The authors considered the temperature distribution and conducted a physical experiment in climatic chambers. After carrying out the cycles of the experiment, the design was examined using a thermal imager for thermal imperfections and irregularities.

Designs made using 3D printing are non-standard. For structures of this type, the existing norms for calculating the resistance to heat transfer are hardly applicable. In article [18] with the help of mathematical modeling, the heat transfer coefficient of one of the options for such wall structures was calculated. The U-value was 1.18 W/m$^2\cdot{}^\circ$C. The purpose of this work is to assess the energy efficiency potential of the modular additive structure under study based on a more detailed analysis of the data obtained in the previous work on the experiment in the climate chamber and the thermal imaging performed.

The object of the study is an additive panel made by a 3D printer (Fig. 2). The size of the completed sample is 390 mm × 680 mm × 310 mm [18]. Now, this panel is a separate module from which a wall can be assembled. Also, the enclosing walls of the building can be initially made according to this principle. They may have an internal configuration that affects thermal inhomogeneity and heat leakage.

Fig. 2 Modular additive wall panel made by a 3D printer
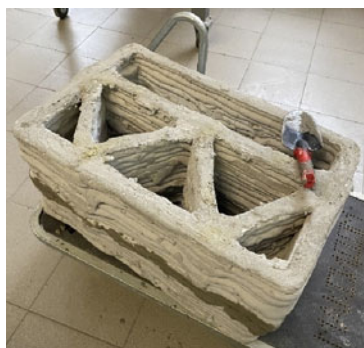
2 Method

The actual heat transfer coefficient U (or heat transfer resistance R) of any enclosing structure, including a modular additive enclosing structure, can be determined by testing it in climatic chambers using a non-destructive method. The data obtained during the laboratory experiment is processed and applied for further calculations. The research method used in this work to calculate the heat transfer coefficient U is numerical.

The study of thermal inhomogeneity is carried out by a non-destructive method using thermal imaging. The Fluke TiS60 + Thermal Imager (Fluke Corporation, USA; Fluke Corporation, USA) was used for this part of the experiment.

3 Results and Discussion

3.1 Calculation of the Heat Transfer Coefficient of the Structure

Three cycles of tests were carried out in the climatic chamber. Temperature and heat flow were recorded every 15 min using special sensors. Based on the data obtained on temperature and heat fluxes in the previous work [18], the total heat transfer coefficient of the enclosing structure is calculated. The temperature on the surface of the structure is unevenly distributed. Taking this fact into account, the heat transfer coefficient is calculated by Eq. 1:

$$U_0^{red} = \frac{\sum F_j \cdot U_{oj}^i}{F} \tag{1}$$

To determine U_0^{red}, thermal sensors were located in the center of thermally homogeneous zones of the building envelope. The layout of the sensors on the thermally homogeneous zones of the panel is shown in Fig. 3:

In Eq. 1: F is the area of the surface through which the flow passes (for the presented model $F = 0.2108$ m^2). F_j is the area of the characteristic isothermal zone (for the presented model, the area of each characteristic zone is 0.0702 m^2). U_{oj}^i is the heat transfer coefficient of the characteristic isothermal zone, W/ m$^2 \cdot °$C. It is calculated by Eq. 2:

$$U_{oj}^i = \frac{q_j^i}{t_{int,j}^i - t_{ext,j}^i} \tag{2}$$

where:

i is the index indicating the number of the experiment;
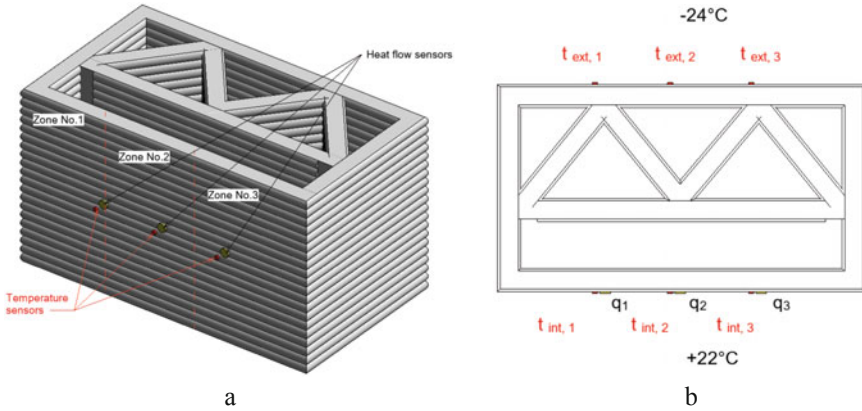
Fig. 3 The layout of the sensors, Revit model:(a) 3D model, (b) Top view

j is the index indicating the number of the isothermal zone;

t_{int} and t_{ext} are average values of measurements of temperatures of internal and external air for the billing period;

q is the measured actual heat flux density averaged over the billing period.

Data were selected at which the temperature on the surface of homogeneous zones did not differ from the average by $\pm$ 0.5 °C. This is a steady-state heat flow.

The final values are presented in Table 1.

In Saint-Petersburg, Russia (climate zone according to the Köppen-Geiger climate classification [19–21] is a humid continental climate with warm summers, Dfb, Fig. 4) the enclosing wall structures must have a heat transfer coefficient U of 0.324 W/ $m^2 \cdot °C$ and a heat transfer resistance R of 3.08 $m^2 \cdot °C/W$. The value of the heat transfer coefficient obtained during the experiment (0.464 W/ $m^2 \cdot °C$) is greater, and the heat transfer resistance (2.15 $m^2 \cdot °C/W$) is less. For comfortable use in practice, the studied wall structures will require additional insulation. Without additional insulation, this design can be used in climatic zones with warmer winters.

Table 1 Summary table with heat transfer coefficients of isothermal zones in three tests

Zone	Test 1, U, W/ $m^2 \bullet °C$	Test 2, U, W/ $m^2 \bullet °C$	Test 3, U, W/ $m^2 \bullet °C$
Zone 1	$U_{01}^1 = 0,481$	$U_{01}^2 = 0,597$	$U_{01}^3 = 0,558$
Zone 2	$U_{02}^1 = 0,371$	$U_{02}^2 = 0,462$	$U_{02}^3 = 0,430$
Zone 3	$U_{03}^1 = 0,379$	$U_{03}^2 = 0,471$	$U_{03}^3 = 0,434$
	$U^1 = 0,409$	$U^2 = 0,509$	$U^3 = 0,474$
Final U	$U = 0,464$		

Fig. 4 Location of the study area on the global climate map
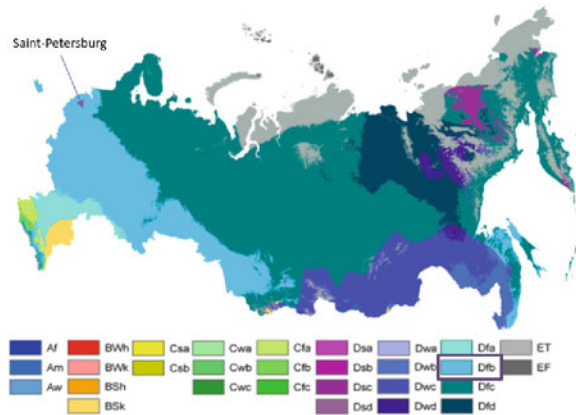
3.2 Study of Thermal Engineering Heterogeneity of the Structure

A thermal imaging study was carried out for a short period after being removed from the climatic chambers (Fig. 5, Fig. 6). The temperature of the outer edges of the structure after being removed from the climatic chambers quickly becomes equal to room temperature. Figure 5 shows a view of the structure from above, which makes it possible to consider the change in temperature along the upper plane.

Line 0 (L0) runs along the solid face of the structure. Line 1 (L1) passes through all the internal ribs of the structure. The character of L0 is smoother than the character of L1. L1 has curves and extrema. Along with L0, the temperature changes smoothly. The temperature of the investigated face in the area of triangular recesses is 17–18 °C. In the area of a rectangular recess, the temperature begins to rise rapidly to 23 °C.

The graph of L1 reflects the temperature distribution along with it and shows all the temperatures that fell into the nearest space near the line L1. Not only the temperatures of the structure are affected, but also what is in the shooting area. The temperature on the back side is 14–15 °C (the back side was in a cold chamber), in the middle part of the structure the temperature is 15.5–17 °C, and on the front side, the temperature is 20–21.5 °C (the front side was in a warm chamber). These temperatures characterize the change in temperature over the upper surface. In triangular recesses, the temperature along the inner walls varies in the range of –4.7 °C to + 8.9 °C. The lowest temperature (−4.7 °C) is observed at the inner corners of the recesses.

The investigated wall structure is made in an additive way. The structure was formed during the layer-by-layer hardening of the building mixture. Thus, the edges of the structure are not smooth surfaces. They have specific irregularities in the form of thinning and broadening. This design is interesting from the point of view of thermal inhomogeneity. Figure 7 and Fig. 8 consider temperature changes along the
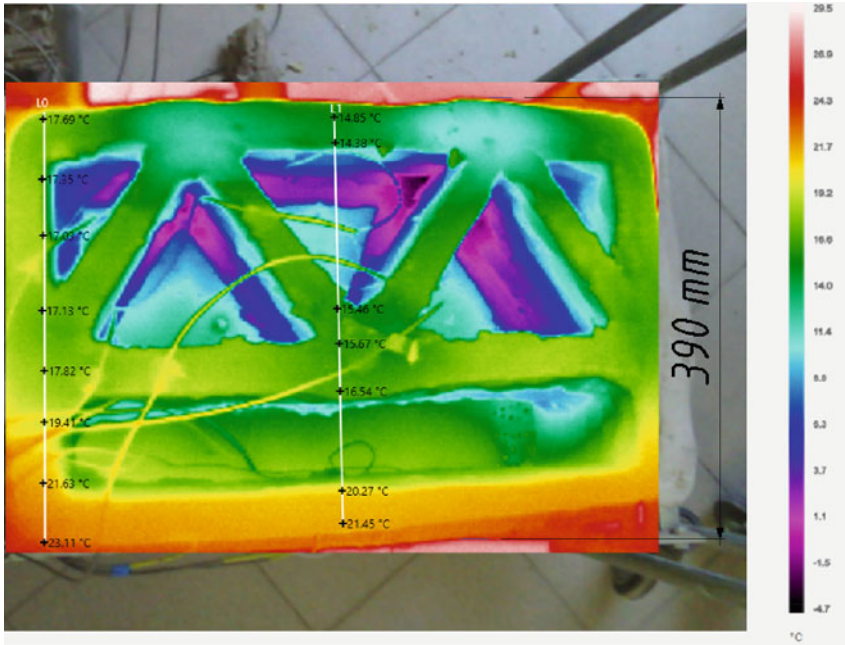
Fig. 5 Thermal image of the investigated additive wall panel. Top view
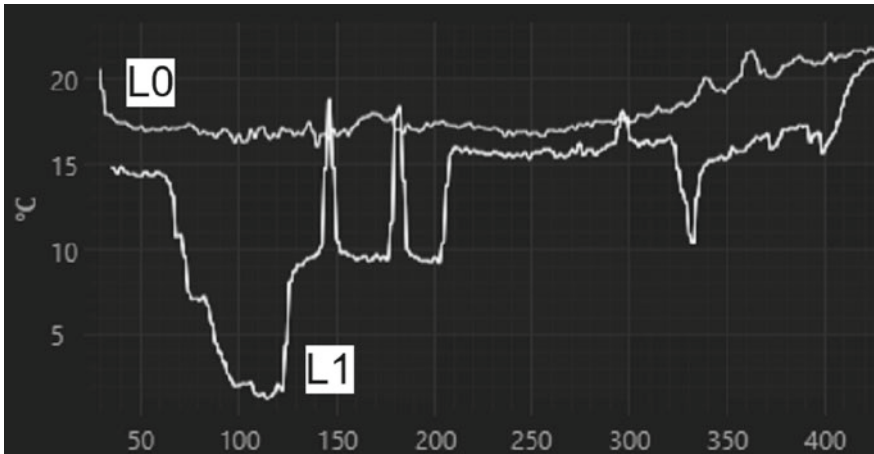
Fig. 6 Y-Profile

characteristic line L0 on the surface of the structure (the back side of the structure under study, which was in the cold chamber).

It can be seen that the design is maximally thermally inhomogeneous. On the additive face, the temperature varies from 4.98 °C to 14.17 °C. To study the heat transfer
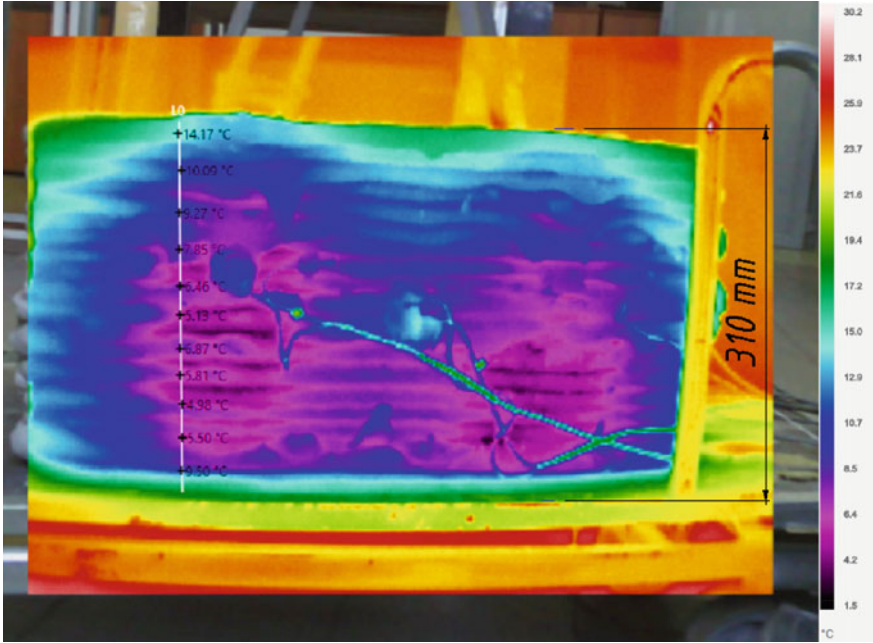
Fig. 7 Thermal image of the investigated additive wall panel
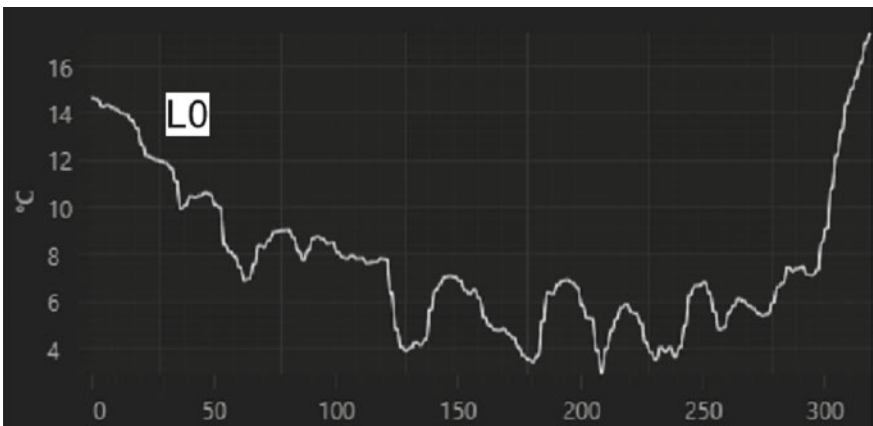
Fig. 8 Y-Profile

coefficient U, as many temperature sensors as possible for this type of structure are required.

4 Conclusions

1. The heat transfer coefficient U of the modular additive wall panel was obtained based on the data on the distribution of temperatures and heat flows from the experiment in the climatic chamber. It amounted to 0.464 W/ m^2·°C. This parameter is higher than allowed in the regulations for Saint- Petersburg, Russia (climate zone according to the Köppen-Geiger climate classification is Dfb). It is not recommended to use the original design. The design requires additional insulation.
2. Analysis of thermal imaging showed that the temperature of the outer edges of the structure after being removed from the climatic chambers quickly becomes equal to room temperature. In the internal recesses of the structure (especially in triangular ones), the temperature remains negative for a long time.
3. The ribbed (wavy) structure of the additive panel significantly affects the temperature distribution over the surface. The temperature variation on the same surface can be 10 °C. This fact significantly affects the final heat transfer coefficient U or resistance to heat transfer R. The most accurate determination of these parameters requires the use of as many sensors as possible in the course of a physical experiment.

5 Funding

References

1. Thai, H.-T., Tuan Ngo B.U.: A review on modular construction for high-rise buildings. Structures **28**, 1265–1290 (2020)
2. Boafo, F.E., Kim, J.-H., Kim, J.-T.: Performance of modular prefabricated architecture: case study-based review and future pathways. Sustainability **8**(6), 558 (2016)
3. Boyd, N., Khalfan, M.M.A., Maqsood, T.: Off-site construction of apartment buildings. J. Archit. Eng. **19**(1), 51–57 (2013)
4. Kasperzyk, C., Kim, M.K., Brilakis, I.: Automated re-prefabrication system for buildings using robotics. Autom. Constr. **83**, 184–195 (2017)
5. Badir, Y.F., Kadir, M.R.A., Hashim, A.H.: Industrialized building systems construction in malaysia. J. Archit. Eng. **8**(1), 19–23 (2002)
6. Annan, C.D., Youssef, M.A., Ei-Naggar, M.H.: Effect of directly welded stringer-to-beam connections on the analysis and design of modular steel building floors. Adv. Struct. Eng. **12**(3), 373–383 (2016)

7. Jin, R., Hong, J., Zuo, J.: Environmental performance of off-site constructed facilities: a critical review. Energy Build. **207**, 109567 (2020)
8. Yu, Y., Chen, Z.: Rigidity of corrugated plate sidewalls and its effect on the modular structural design. Eng. Struct. **175**, 191–200 (2018)
9. Lawson, R.M., Ogden, R.G., Bergin, R.: Application of modular construction in high-rise buildings. J. Archit. Eng. **18**(1), 148–154 (2012)
10. Fifield, L.J., Lomas, K.J., Giridharan, R., Allinson, D.: Hospital wards and modular construction: summertime overheating and energy efficiency. Build. Environ. **141**, 28–44 (2018)
11. Fathieh, A., Mercan, O.: Seismic evaluation of modular steel buildings. Eng. Struct. **122**, 83–92 (2016)
12. Cisse, M., Kosterev, D.A., Vasileva, I.L., Nemova, D.V.: Design of modular structures and use of prefabricated sanitary modules. a review. AlfaBuild **16**, 1602 (2021)
13. Xianggang, W., et al.: Optimization of 3D printing concrete with coarse aggregate via proper mix design and printing process. J. Build. Eng. **56**,104745 (2022)
14. Mohammad, M., Masad, E., Al-Ghamdi, S.G.: 3D concrete printing sustainability: a comparative life cycle assessment of four construction method scenarios. Buildings **10**(12), 1–20 (2020)
15. Panda, B., Tay, Y.W.D., Paul, S.C., Tan, M.J.: Current challenges and future potential of 3D concrete printing. Materwiss Werksttech **49**, 666–673 (2018)
16. Anastasiou, A., Tsirmpas, C., Rompas, A., Giokas, K., Koutsouris, D.: 3D printing: basic concepts mathematics and technologies. In: 13th IEEE International Conference on BioInformatics and BioEngineering, Chania, Greece, pp. 1–4. IEEE (2013)
17. Khajavi, S.H., Tetik, M., Mohite, A., Peltokorpi, A., Li, M., Weng, Y., Holmström, J.: Additive manufacturing in the construction industry: the comparative competitiveness of 3D concrete printing. Appl. Sci. **11**(9), 3865 (2021)
18. Nemova, D., Kotov, E., Andreeva, D., Khorobrov, S., Olshevskiy, V., Vasileva, I., Zaborova, D., Musorina, T.: Experimental study on the thermal performance of 3D-Printed enclosing structures. Energies **15**, 4320 (2022)
19. Peel, M.C., Finlayson, B.L., McMahon, T.A.: Updated world map of the Köppen-Geiger climate classification. Hydrol. Earth Syst. Sci. **11**(5), 1633–1644 (2007)
20. Kottek, M., Grieser, J., Beck, C., Rudolf, B., Rubel, F.: World Map of the Köppen-Geiger climate classification updated. Meteorol. Z. **15**(3), 259–263 (2006)
21. Congedo, P.M., Baglivo, C., Seyhan, A.K., Marchetti, R.: Worldwide dynamic predictive analysis of building performance under long-term climate change conditions. J. Build. Eng. **42**, 103057 (2021)

Stability of the Right-Bank Slope of the Oka River

Igor Gandelsman and **Artem Gandelsman**

Abstract The article analyzes the engineering and geological conditions of the right bank, which is in a state of dynamic equilibrium, of the Oka River in the city of Pavlovo. Calculation schemes have been compiled to perform calculations of the total static stability of the slope for two calculated cases in the existing natural state and taking into account the water saturation of the water-bearing rocks, the boundaries of the landslide zone for various cases have been determined. The article identifies possible risks, analyzes the main models of the behavior of the soil base taking into account negative factors, calculates the stability of soil massifs using various known methods. The geometric scheme of the computational model was built on transverse profiles. The width of the calculated area was chosen in such a way that there were no changes in the stress–strain state of the array due to the introduction of artificial boundary conditions along the edges of the finite element grid. The method of calculating stability based on numerical modeling programs by reducing strength characteristics has a number of advantages over the traditionally used methods of calculating stability based on the equations of limiting equilibrium. Based on the results of calculations, the boundaries of the landslide zone for various cases were determined by the method of circular cylindrical sliding surfaces (SAM). A potential landslide zone has been identified, including residential development. Based on the calculations performed, it is proposed to provide alternative measures to ensure the safety of buildings falling into a landslide zone to ensure reliable fastening and minimal impact on the existing slope.

Keywords Landslide slope · Static stability · Landslide pressure · Geological structure

I. Gandelsman (✉) · A. Gandelsman
Vladimir State University Named After Alexander and Nikolay Stoletovs, Gorky Street, 87, 600000 Vladimir, Russia
e-mail: igvlsu@mail.ru

1 Introduction

During the construction of buildings, land plots located on the banks of rivers and ravines are sometimes used. During the operation of these buildings, atmospheric influences are inevitable, man-made, as well as changes in hydrogeological conditions are possible. Anti-landslide measures for these objects are not always carried out in the proper volume, the volume and structure of green spaces are insufficient.

All this can lead to the loss of stability of slopes, the formation of landslides that threaten existing buildings and people living in them [1–13]. When operating such facilities, it is advisable to monitor the condition of the slope, make dynamic forecasts of its reliable operation when the initial conditions of their operation change.

The theoretical foundations and methods for calculating slopes are described in the works of domestic researchers S.S. Vyalov, Yu.K. Zaretsky, Z.G. Ter Martirosyan [1–3], A.A. Bartolomey, G.V. Postoev [4], A.B. Ponomarev [5], A. Torgoev [6] and foreign scientists A. Bishop [7], N. Morgenstern [8], E. Bromhead [9, 10], G. Gitirana [10], A. Federico [11], A. Malkavi [12], S. Gshvind [13], K. Komamura, D.N. Loops, A.P. Hwang AP [14], A.W Skempton [19], H. Herrmann [22], К.Cha [24], etc. el.

Despite numerous studies, it is still important to ensure the stability of specific slopes in various localities [14–18, 19–21].

The criterion for ensuring the stability of the slope is the condition that the calculated values of the generalized shear forces on the collapse prism do not exceed the forces of the ultimate resistance of the soil mass or the moments of forces tending to turn (overturn) and hold the soil mass. This calculation is allowed to be performed only for the simplest forms of the sliding surface separating the collapse prism from the stationary soil mass (in the form of a straight line segment or a circle). In general, stability calculations are performed for arbitrary shapes of the sliding surface. The slope stability coefficient (slope) is found as the minimum value of k_{st} for all possible test sliding surfaces. The slope stability coefficient (slope) can be found both using traditional methods of the theory of marginal equilibrium (with or without splitting the slide prism into compartments) and elastic–plastic calculations by the finite element method using the method of reducing strength characteristics.

The article considers the issues of the current state of the landslide slope, presents the results of the calculation taking into account various models of the soil base. Based on the results, work is proposed to prevent landslides on this section of the Oka River bank.

2 Methods

The climate of the design area is moderately continental with moderately harsh and snowy winters and moderately warm summers. The wind regime is formed under the influence of physical and geographical features. Cyclonic activity is predominant here for most of the year. The area belongs to the zone of sufficient moisture. The

annual precipitation is 527 mm. The height of snow by the end of winter (the second decade of March) reaches 50 cm.

The geological structure of the site up to the studied depth of 70.0 m involves deposits of quaternary age (Q_{IV}) (soil-vegetation layer (pdQ_{IV}), alluvial sands pulverized (aQ_{IV}), loess loams deluvial-solifluction loams (prQ_{II-III}) and medium-sized sands (dsQ_{II-III}), sediments of the upper Permian system (P_3).

The absolute level of the roof of deposits varies from 70.7 to 124.8 m of the Baltic system. The absolute mark of the sole of the deposits varies from 70.6 to 124.5 m.

The hydrogeological conditions of the site up to a depth of 20.0–70.0 m (January- February 2022) are characterized by the presence of Quaternary and Upper Permian aquifers. The groundwater level is recorded at depths of 0.9–13.7 m, which corresponds to the absolute marks of 69.8–111.1 m of the Baltic system (Table 1).

The aquifer is unpressurized, the water-bearing soils are quaternary sediments. The Upper Permian clays (P_3) serve as a water barrier. The aquifer is fed by infiltration of atmospheric precipitation. The Oka River is an area of both supply and discharge of groundwater. The aquifer has a hydraulic connection with the Oka River.

One of the most important tasks in the practice of construction is to assess the stability of soil slopes. The criterion for ensuring slope stability the dependence for the stability coefficient k_{st} is the condition: $k_{st} = R/F \geq (\gamma_n \cdot \psi)/\gamma_d$. The slope stability coefficient is found as the minimum value of k_{st} for all possible test sliding surfaces. The slope stability coefficient can be found using traditional methods of the theory of ultimate equilibrium, or by elastic–plastic calculations using the finite element method using the method of reducing strength characteristics. In construction practice, to determine the stability of a ground structure or slope, the methods of marginal equilibrium of the following authors are used - Shakhunyants, Maslov, Tertsagi, Bishop, Morgenstern, Spencer and others. Calculation methods are divided

Table 1 Physical and mechanical characteristics of soils

No	Name of the engineering-geological element	standard values				calculated values (α = 0.85)			Calculated values (α = 0.95)		
		ρ, g/sm³	c. кPa	φ, deg	E, MPa	ρ, g/sm³	C, кPa	φ, rdeg	ρ, g/sm³	c. кPa	φ, deg
1	sand dusty, medium density, saturated with water (aQ_IV)	1.95	2	26	11	1.95 ± 0.00	2	26	1.95 ± 0.01	1,3	24
2	clay semi solid, loess, subsidence (prQ_II-III)	1.97	25/15	20/18	11/10	1.97 ± 0.01	22/14	18/7	1.97 ± 0.02	20/12	17/7
3	Clay semi solid (dsQ_II-III)	2.10	41/34(19)	14/11(14)	15	2.10 ± 0.01	37/30(17)	13/10(7)	2.10 ± 0.02	34/27(15)	12/9(5)
4	Sand medium size, medium density (dsQ_II-III)	2.00	1	35	30	2.00 ± 0.00	1	35	2.00 ± 0.01	0,7	32
5	Clay solid (P_3)	2.01	87/64(45)	30/21(17)	21	2.01 ± 0.02	81/58(41)	28/19(14)	2.01 ± 0.03	77/55(39)	26/18(15)
6	Clay of medium strength (P_3)	$R_c = 26.9/31.3$ MPa									

by mechanisms: satisfying the general equilibrium of moments (Fellenius, Bishop), methods of equilibrium of forces (Shaunyants, Kray, Maslov-Berer) and methods of equilibrium of moments and forces (Yanbu, Morgenstein and Price, Spencer). A number of assumptions are made in the computational model [7–9, 15]: the solidified body hypothesis is used; a certain shape of the sliding surface is allowed; stresses are replaced by forces; assumptions about groundwater pressure and seismicity are made. The general sequence of application of limit equilibrium methods is such that they are first set by the sliding surface, after which the position of the critical sliding surface with the minimum value of the stability coefficient is determined by iterations. As follows from the above sequence, the disadvantage of this approach is that the sliding surface is set before the calculation begins. As a rule, the decision on the possible shape of the sliding surface is made on the basis of calculations on circular cylindrical or polygonal (pre-defined) sliding surfaces [19].

The slope stability coefficient (slope) can be found both using traditional methods of the theory of marginal equilibrium (with or without splitting the slide prism into compartments) and elastic–plastic calculations by the finite element method using the method of reducing strength characteristics.

Thus, based on the need to cover as many cases encountered in practice as possible (heterogeneous geological structure, presence of groundwater, seismic impacts, etc.), the methods of marginal equilibrium have many assumptions and simplifications, but at the same time they allow obtaining sufficient results for practice in the case of engineering-geological conditions of moderate complexity.

The method of determining stability, devoid of the described disadvantages, is the method of reducing strength. According to the underlying principle, the sliding surface is determined automatically by the calculation input. From the provisions of soil mechanics, it is known that the stress state at any point of the soil is considered as the limit in the case when a slight additional effect disturbs the equilibrium and leads the soil into an unstable state. The destruction of the soil occurs as a result of overcoming the internal forces of friction and adhesion between the particles on certain sliding surfaces.

In general, the stability of the structure is determined by the safety coefficient, which is the ratio of the maximum possible strength of the soil to the minimum value necessary to ensure the equilibrium of the actions.

The SRM – shear reduction method is implemented in programs based on the finite element and finite difference method (Midas GTS NX, Plaxis, GEO5, Phase2, FLAC). The fracture prediction is carried out by simultaneously lowering both shear strength indicators: $c_r = c/k_{st}$, $\varphi_r = \varphi/k_{st}$.

A significant advantage of the strength reduction method in comparison with the methods of limiting equilibrium is that the sliding surface and the stability coefficient are determined simultaneously during the calculation process.

The analysis of the comparison of stability calculations based on the methods of limiting equilibrium and strength reduction for a large number of parameters of embankments with different configurations showed that such methods as Taylor (calculated by untrained strength cu), Bishop, Morgenstein (strength was given by effective characteristics c' and φ'), which can be considered proven However, they do not have much difference with calculations using the strength reduction method. Discrepancies of several percent are due to the fact that MPR uses exclusively circular cylindrical sliding surfaces, and the method of reducing strength has no restrictions on the geometry of the fracture mechanism [13, 14, 16, 20, 21].

The method of calculating stability based on numerical modeling programs by reducing strength characteristics has a number of advantages over the traditionally used methods of calculating stability based on the equations of limiting equilibrium. For simple cases, all methods give the same result, in other cases, the discrepancies reach up to 20%.

3 Results and Discussion

Calculations of the overall stability of the slope are carried out in a flat formulation. The position of the design section is timed to the most characteristic section of the slope. Stability calculation is performed for the existing terrain of the territory. The calculation scheme (see Fig. 1). The topography and geological structure of the site is taken from the materials of engineering surveys.
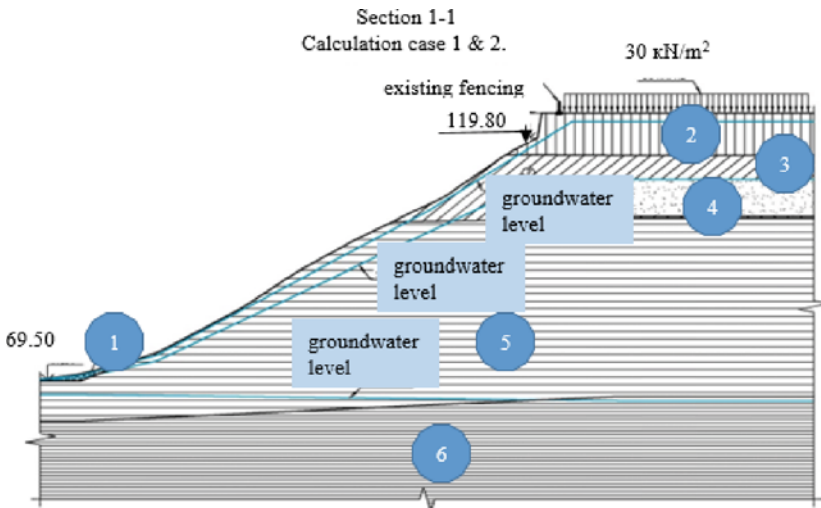
Fig. 1 Calculation scheme of the ground slope

Table 2 Results of slope stability calculations

Section	Calculation result Bush	$\gamma_c \cdot \gamma_n$	Condition
1–1	1.01	1.15	Not being executed
2–2	0.73	1.04	Not being executed

Calculations of the general static stability of the slope in a flat formulation were performed for two design cases: design case No. 1 (main) – the slope is considered in the existing state, the physical and mechanical characteristics of soils in the natural state; design case No. 2 (special) - the slope is considered in the existing state, taking into account the water saturation of the water-bearing rocks.

The load from transport and buildings is 30 kN/m². Seismic loads are not taken into account, since the estimated seismicity is less than 7 points.

The calculation results are shown in Table 2 (see Figs. 2, 3). The boundaries of the landslide zone for potential landslide phenomena for a slope in a natural and water-saturated state are determined by the method of circular cylindrical sliding surfaces. The boundary corresponding to the value of the bush stability coefficient $k_{st} = 1.15$ is determined, beyond which the slope stability is ensured in accordance with regulatory requirements. For a slope in a water-saturated state, a boundary corresponding to the value of the stability coefficient $k_{st} = 1.04$ is determined, beyond which the slope stability is ensured in accordance with regulatory requirements.
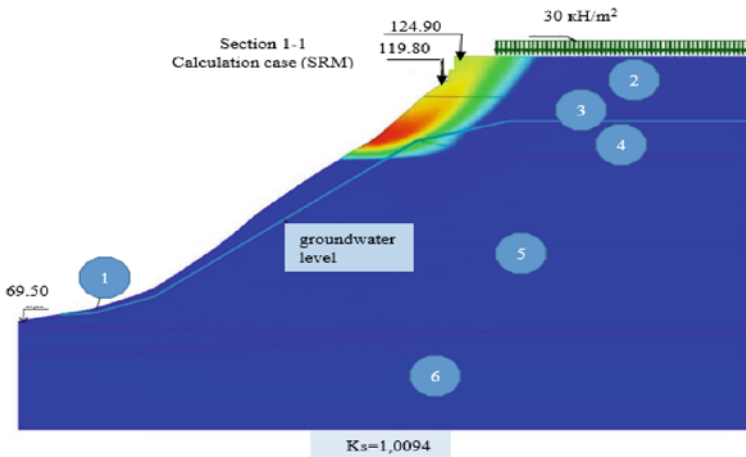
Fig. 2 Calculation results of slope stability in Sect. 1–1
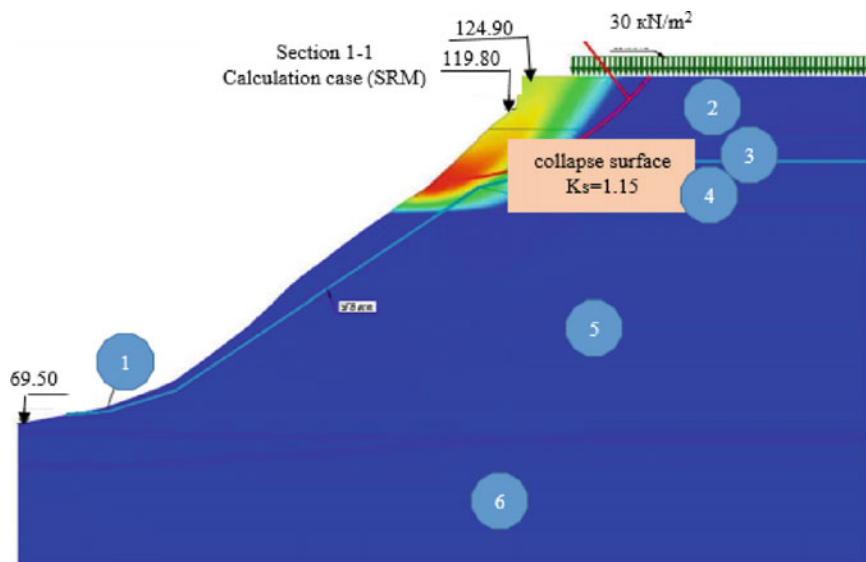
Fig. 3 Results of stability calculation by the method of circular cylindrical sliding surfaces of the slope in Sect. 1–1

Fig. 4 The area of potential landslide phenomena

4   Conclusions

Based on the results of the slope stability studies, taking into account the existing relief, the following conclusions can be drawn:

1. the slope is in the existing state, the physical and mechanical characteristics of the soils are determined in the natural state, the stability coefficient was kst = 1.01;
2. the slope in the existing state, taking into account the water saturation of aquifers, the stability coefficient was kst = 0.73.

The slope is not stable. The stability coefficients obtained as a result of calculations do not meet regulatory requirements.

2. According to the results of calculations by the method of circular cylindrical sliding surfaces, it is clear that existing buildings fall into a potential landslide zone. The boundaries of landslide zones for different cases are shown in Fig. 4.

3. Based on the results of calculations, it was determined the need to take measures to ensure the safety of buildings and structures falling into the landslide zone (removal of buildings from the landslide zone, implementation of anti-landslide measures, etc.). As an alternative, it is possible to use the Titan anchor system designed to solve a wide range of engineering tasks. One of the main areas of its application is anti-landslide fastening and stabilization of slopes, fixing unstable steep sections of the coastal strip. The use of this technology, especially in combination with Geobrugg slope reinforcement systems, avoids the use of bulky support and enclosing structures, allows you to quickly and efficiently carry out work in a confined space without negative destructive effects on nearby objects and ensure reliable operation of the slope for decades.

References

1. Ter-Martirosyan, Z.G., Luzin, I.: The long piles interaction with the surrounding and underlying soils, taking into account the linear and nonlinear rheological properties. IOP Conf. Ser. Mater. Sci. Eng. **698**(2), 1–8 (2019). https://doi.org/10.1088/1757-899X/698/2/022040
2. Ter-Martirosyan, Z., Ter-Martirosyan, A., Ermoshina, L.: Creep of clayey soil with kinematic shear, taking into account internal friction, adhesion and viscous resistance. IOP Conf. Ser. Mater. Sci. Eng. **661**(1), 1–9 (2019). https://doi.org/10.1088/1757-899X/661/1/012095
3. Yuan, R., Wang, Y., Jin, J., et al.: Local structural and geomorphological controls on landsliding at the Leigu restraining bend of the Beichuan-Yingxiu fault system during the 2008. Wenchuan earthquake. Landslides **16**(12), 2485–2498 (2019). https://doi.org/10.1007/s10346-019-01264-x
4. Postoev, G.P.: Mechanism specifics of the landslide-hazardous massif limit state formation and landslide block displacement. Геоэкология. Инженерная геология. Гидрогеология. Геокриология **2**, 13–20 (2019). https://doi.org/10.31857/S0869-78092019213-20
5. Tatiannikov, D., Ponomaryov, A.: Application of variable pitch reinforcement with horizontal geosynthetic elements in pads made from cohesive soils. J. Phys. Conf. Ser. **56**, 371–377 (2020). https://doi.org/10.1088/1742-6596/1928/1/012051

6. Havenith, H.-B., Torgoev, A., Braun, A., Schlögel, R., Micu, M.: A new classification of earthquake-induced landslide event sizes based on seismotectonic, topographic, climatic and geologic factors. Geoenviron. Dis. **3**(1), 1–24 (2016). https://doi.org/10.1186/s40677-016-0041-1

7. Bishop, A.W., Morgenstern, N.R.: Stability coefficient for earth slopes. Geotechnique **10**(4), 129–150 (1960)

8. Morgenstern, N.R., Price, V.E.: The analysis of stability of general slip surfaces. Inst. Civil Eng. **15**, 79–93 (1965). https://doi.org/10.1680/GEOT.1965.15.1.79

9. Bromhead, E., Ibsen, M.: Bedding-controlled coastal landslides in southeast britain between axmouth and the Thames estuary. Landslides **1**(2), 131–141 (2004)

10. Gitirana, G., Santos, M.A., Fredlund, M.D.: Three-dimensional analysis of the Lodalen landslide. GeoCongr. Geosustainab. Geohazard Mitig. (2008).https://doi.org/10.1061/40971(310)23

11. Federico, A., Popescu, M., Elia, G., et al.: Prediction of time to slope failure: a general framework. Environ. Earth Sci. **66**(1), 245–256 (2012)

12. Malkawi, A.I.H., Hassan, W.F., Abdulla, F.A.: Uncertainty and reliability analysis applied to slope stability. Struct. Saf. **22**(2), 161–187 (2000)

13. Gschwind, S., Loew, S., Wolter, A.: Multi-stage structural and kinematic analysis of a retrogressive rock slope instability complex (Preonzo: Switzerland). Eng. Geol. **252**, 27–42 (2019)

14. Hwan, A.P.: A Possible model of a landslide. Constr. Techn. Saf. **15–16**, 55–56 (2006)

15. Janbu, N.: Application of composite slip surfaces for stability analysis. Proc. Eur. Conf. Stabil. Earth Slopes (Stockholm). **3**, 43–49 (1954)

16. Wang, W.D., Qu, X., Liu, P.: Prediction on land slide displacement using a combination model with optimal weight. Nat. Hazards **96**, 1121–1139 (2019)

17. Wu, L.Z., Li, S.H., Huang, R.Q., Xu, Q.: A new grey prediction model and its application to predicting land slide displacement. Appl. Soft Comput. **95**, 257–269 (2020)

18. Griffiths, D., Lane, P.: Slope stability analysis by finite elements. Geotechnique **49**(3), 387–403 (1999)

19. Skempton, A.W.: Residual strengths of clays landslides, folded strata and the laboratory. Geotechnique. **35**(1), 3–18 (1985)

20. Gandelsman, I.A., Gandelsman, A.I.: Forecasting of slope stability at the object redevelopment of the territory mill of Emelyan Bashkirov and his sons. J. Phys: Conf. Ser. **1928**(1), 012016 (2021). https://doi.org/10.3850/978-981-09-5346-1_CE-517

21. Harabinová, S., Kotrasová, K., Kormaníková, E.: Analysis of slope stability. Civil Environ. Eng. **17**(1), 192–199 (2021)

22. Herrmann, H., Bucksch. H.: Slope Stability Analysis, pp. 1251–1251. Springer Berlin Heidelberg (2014)

23. Liao, H., Li, H., Ma, Z.: Slope Stability Analysis, pp. 161–185. World Scientific (2020)

24. Cha, K., Kim, T.: Evaluation of slope stability with topography and slope stability analysis method. KSCE J. Civ. Eng. **15**(2), 251–256 (2011)

Seismic Isolation of NPP Turbine Unit Using Dry Friction Devices

Ibrakhim Mirzaev and **Malikjon Turdiev**

Abstract The possibility of reducing the acceleration of NPP turbine unit during earthquakes with the use of devices working on the principle of dry friction is investigated. A review of works on seismic isolation of structures is given. Problems for calculation of structures with seismic isolation using the principle of dry friction are formulated. A new algorithm for solving seismodynamics problems of structures in the presence of dry friction forces has been proposed. Vibration of a seismically isolated NPP turbine unit has been calculated for four different earthquakes on the basis of seismogram and accelerogram records with intensity 8–10 points on MSK-64 scale. Influence of vertical component of seismic wave on the process of horizontal vibrations of the structure is studied. Displacements and accelerations of the base of the structure and the turbine unit are given in the form of diagrams and tables. The degree of reduction of horizontal acceleration of the turbo-generator when using seismic isolation from 2.4 to 12 times in comparison with the maximum acceleration of the base is shown.

Keywords Seismic waves · Seismic isolation · Fluoroplastic · Dry friction · Seismogram · Slider · Turbine unit

1 Introduction

The object of the study in this paper is the seismic isolation of the turbine unit of a nuclear power plant (NPP) using dry friction devices (flat slider, fluoroplastic) between its foundation and the base.

Turbine unit is the main device of NPP, and its protection from the action of earthquakes is an important task for those regions where it is planned to build NPP [1]. For the Republic of Uzbekistan, this task is relevant, because in Jizzakh region it is planned to build and put into operation NPP by Russian specialists. Uzbekistan

I. Mirzaev (✉) · M. Turdiev
Tashkent State Transport University, Tashkent, Uzbekistan
e-mail: ibrakhim.mir@mail.ru

is a seismic active zone. Seismic isolation of NPP is considered by different models in [1–4].

Seismic isolation devices do not allow the full passage of seismic wave energy from the base to the structure, as a result of which the acceleration of the points of the structure will be several times less than the acceleration of the base. This in particular is confirmed in [5] where the results of laboratory experiment on the model of a rigid building with seismic-isolating sliding belt made of steel and fluoroplastic with friction factor 0.04. The possibility of reducing the building acceleration up to 10 times for an earthquake of intensity 10 points on MSK-64 scale is shown. By results of experiments on harmonic influence with frequency up to 10 Hz and acceleration of platform up to 10 m/s² graph of change of relation between acceleration of structure and acceleration of seismic influence was built.

Various methods of seismic isolation, damping and other structural solutions are used to reduce the impact of earthquakes on buildings and structures [6–14].

In [15, 16] the results of studies of spatial structures of buildings on the action of real earthquakes using the LS-DYNA software package are given. For certain types of buildings, an effective seismic isolation method is a sliding foundation using fluoroplastic [17, 18]. Numerical algorithms for solving dynamic problems for composite structures are considered in [19].

It should be noted that dynamic problems with dry friction are essentially nonlinear problems [20–23]. In [23] the problem of oscillator oscillation in the presence of dry friction force using slip and stick–slip modes was solved. The onset of sliding depends on the acceleration and masses of the rubbing elements, but in [23] this is related to their velocities. However, many researchers oversimplify the problem and actually arrive at a linear problem without justification and assessment of the error of the calculation model. In this work, to estimate the efficiency of seismic isolation of NPP turbine unit by dry friction devices, a numerical algorithm for solving a nonlinear dynamic problem is proposed [20–22].

2 Research Methods

Let the horizontal and vertical motions of the base of the structure be given in the form of a seismogram of a real earthquake. Let us assume that the rooftop is separated by a flat slider [26] or a two-layer fluoroplastic [17, 18]. Sliders have a dry friction coefficient of 0.025 to 0.055 [26], and fluoroplastic provides a sliding coefficient of 0.05 or more [18]. In the horizontal direction, we will take Coulomb's model of dry friction as a model of interaction between the base and the slab; in the vertical direction, we will consider them to be absolutely rigidly connected.

The structure is represented by a one-dimensional shear model with concentrated masses and inertial-free elastic bonds [21]

$$[M] \cdot \left\{\ddot{U}\right\} + [C] \cdot \left\{\dot{U}\right\} + [K] \cdot \{U\} = \{Q(t)\}, \tag{1}$$

$$\{U\} = \{U_{st}\}, \quad \{\dot{U}\} = 0, \quad at \quad t = 0,$$

where $[M]$ – diagonal mass matrix, the masses are located in the floor levels, $[K]$ – stiffness matrix, $[C] = \alpha \cdot [M] + \beta \cdot [K]$ – viscosity matrix, $\{U\} = \{u_0, u_1, ..., u_n, v_0, v_1, ...v_n\}^T$ — displacement vector, u_i, v_i – horizontal and vertical displacements of masses, $\{U_{st}\}$ – vector of displacements at the initial moment of time, the elements corresponding to the shear displacement are equal to zero, and the vertical displacement is determined from the solution of the static problem.

Horizontal mass interaction condition $[M_0]$ of the skeleton with the foundation is [21]

$$u_0 = u_g - u_r, \quad if \quad |F_0| < |F_{fr}|, \quad \text{i.e. under joint motion,} \tag{2}$$

$$F_0 = F_{fr}, \text{under sliding,} \tag{3}$$

$$v_0 = v_g, \tag{4}$$

where u_0, v_0 – of displacement of the beam, u_g, v_g – horizontal and vertical displacements of the base, i.e., approximated spline Hermite functions of the digitized earthquake seismogram, u_r – is the displacement value at the moment of time at the beginning of the current joint movement of the foundation and the dike, i.e. the difference between the values of foundation and dike displacements (at the initial moment of time $u_r = 0$), F_0 – unknown value of the adhesion force between the foundation and the dike, $F_{fr} = sign(\dot{u}_g - \dot{u}_0) \cdot f \cdot P$ – value of the dry friction force, f – coefficient of dry friction, P – the pressure force on the sliding element of the foundation in the dynamic process, if vertical vibrations are not taken into account, then it is the weight of the structure [21]. The linear approximation of the earthquake seismogram gives an error in calculating the velocity and acceleration of the foundation, so its spline approximation is used.

It should be noted that the vertical vibrations do not depend on the horizontal vibrations of the structure, and the horizontal vibrations depend on the vertical vibrations of the structure through the condition (3), since during the vertical vibrations the pressure on the sliding foundation changes [21].

When moving together, the displacement u_0 is determined by equality (2) and the equation of motion of the mass M_1 looks like this [20–22]:

$$M_1\ddot{u}_1 + k_1 u_1 + c_1\dot{u}_1 - k_2(u_2 - u_1) - c_2(\dot{u}_2 - \dot{u}_1) = k_1 u_0 + c_1\dot{u}_0. \tag{5}$$

In this case $Q_1 = k_1 u_0 + c_1\dot{u}_0$, other vector elements $\{Q\}$, corresponding to the horizontal displacements of concentrated masses are equal to zero. The equation of the vertical motion of a mass M_1 has a form similar to Eq. (5), in the right part we add $M_1 g$. Elements of a vector $\{Q\}$, corresponding to the vertical displacements

of concentrated masses are equal to the values of weights of the corresponding concentrated masses [21].

Sliding with dry friction occurs only when condition (3) [21] is satisfied. The considered problem Eqs. (1), (2), (3) is a nonlinear problem and there are no conditions for calculating the unknown function F_0, as well as during the dynamic process the dimensions of the matrices change $[M]$ and $[K]$.

When sliding, the equation for mass $[M_0]$ [21]

$M_0\ddot{u}_0 - k_1(u_1 - u_0) - c_1(\dot{u}_1 - \dot{u}_0) = F_{fr,}$ that said $Q_0 = F_{fr.}$.

To solve the problem as a whole, we use the following algorithm. At each time step we solve the problem in three statements [20]:

1. Solve Eq. (1) with condition (2);
2. Eq. (1) is solved with condition (3), at $F_0 = f \cdot P$;
3. Eq. (1) is solved with condition (3), at $F_0 = -f \cdot P$.

At the same time the matrices $[M]$ and $[K]$ in the first staging have the size of $2n \times 2n$ (here n – floor number), and in the second and third productions $(2n + 1) \times 2n$ [21]. The choice of the true solution among these three solutions is as follows. If the relative velocities $\dot{u}_g - \dot{u}_r$ in the second and third problem statements have different signs, then the true solution is the solution of the problem in the first statement, because the applied dry friction force makes move in different directions and hence the unknown force is less than the limiting value of the dry friction force, i.e. the masses of the lower and upper foundations move together without sliding at this step in time. If relative velocities in the second and third problem statements have the same signs, then the true solution is the solution of the problem in that statement in which the relative velocity by absolute value is the smallest, because the dry friction force is directed against the relative motion [20–22]. All three problems are solved by the Newmark method [24], the digitized earthquake seismogram is approximated by a spline Hermite function. The time step in the Newmark method should be less than the step of the earthquake record.

3   Results and Discussion

Let's discuss the results of calculations on the example of seismic isolation of NPP turbine unit [1]. Let the model of the structure be represented as a three-mass system (Fig. 1.). Let the characteristics of the structure be given, as well as seismograms of the following strong earthquakes [25]:

1. Cairano 3 – 000,319 (16/01/1981, higher 8 according to MSK-64 scale, maximum acceleration – 1.47 m/s^2, maximum displacement – 0.0029 m, digitization step – 0.005 s, duration – 22.175 s);
2. Nocera Umbra 2 – 000,856 (03/04/1998, higher 9 according to MSK-64 scale, maximum acceleration – 3.73 m/s^2, maximum displacement – 0.0054 m, digitization step – 0.005 s, duration – 40.990 s);..
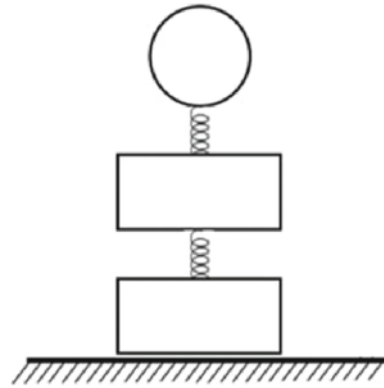
3. Tolmezzo-Diga Ambiesta – 000,055 (06/05/1976, higher 9 according to MSK-64 scale, maximum acceleration – 3.35 m/s^2, maximum displacement – 0.039 m, digitization step – 0.005 s, duration – 46.535 s);
4. Gazli - 000,074 (17/05/1976, higher 10 according to MSK-64 scale, maximum acceleration - 7.23 m/s^2, maximum displacement - 0.1827 m, digitization step - 0.005 s, duration - 28 s).

Turbine unit mass is 2.5·10^6 kg, turbine unit foundation mass is 5.0·10^6 kg. The shear stiffness of the equivalent spring between the turbo unit and the foundation is 1.0·10^8 N/m, and its vertical stiffness is 2.0·10^9 N/m. The horizontal and vertical stiffness of the foundation are 1.0·10^{10} N/m and 2.0·10^{10} N/m respectively. Attenuation coefficients are α = 0.94 s^{-1}, β = 0.00116 s. In calculations, the coefficient of dry friction between the foundation and the foundation was taken in two variants 0.025 and 0.05.

When numerically solving dry friction problems, the time step must be chosen to ensure sufficient accuracy. In our example calculations, the time step was chosen to be 0.001 s.

Figure 2 shows comparison of foundation and turbine unit displacements, and Fig. 3 the corresponding accelerations during the earthquake No.1, 8 point intensity. Dry friction coefficient f = 0.025. There is relatively big displacement of turbo-unit due to foundation sliding, but its accelerations have small values, the maximum value of this acceleration is 6.6 times less than the maximum acceleration of foundation. This shows that the device with dry friction made it possible to reduce the effect of an 8-point earthquake. In case of rigid connection of foundation with foundation the maximum acceleration of turbo-generator is 0.662 m/s^2, and in case of using dry friction device - 0.224 m/s^2, which is 3 times less. The reduction of the turbo unit acceleration is also affected by the spring shock absorbers installed between the foundation and the turbo unit [1].

In Fig. 4 and Fig. 5 shows the same comparisons at the value of dry friction coefficient f = 0.05. Increasing the dry friction coefficient by a factor of two slightly changes the vibration pattern of the structure. The oscillations of the turbo-unit have

Fig. 2 Change of
displacements in time of the
base (a: $u_{max} = 0.00287$ m)
and turbine unit (b: $u_{max} = 0.0112$ m)
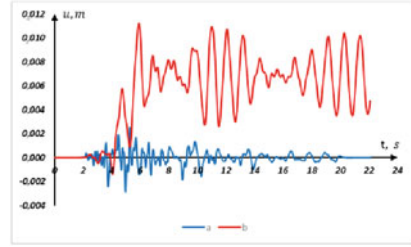
Fig. 3 Changes in
acceleration over time of the
base (a: $w_{max} = 1.47$ m/s^2)
and turbine unit (b: $w_{max} = 0.224$ m/s^2)
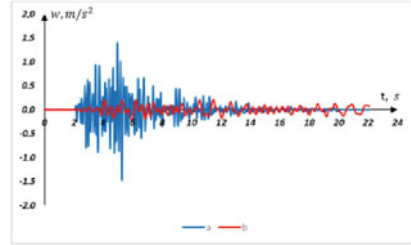
a large amplitude relative to the displaced position, and the maximum value of its acceleration is 4 times less than the maximum acceleration of the base. The process of turbine unit vibration is strongly influenced by the value of the coefficient of dry friction of the seismic isolation device, the less friction, the less the maximum acceleration of the turbine unit. In both cases the run-out process is noticeable.

Fig. 4 Change of
displacements in time of the
base (a: $u_{max} = 0.00287$ m)
and turbine unit (b: $u_{max} = 0.0199$ m)
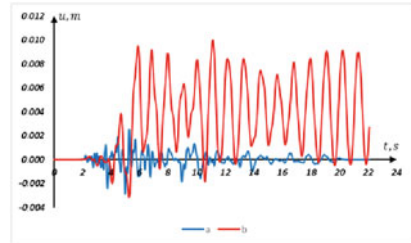
Fig. 5 Changes in
acceleration over time of the
base (a: $w_{max} = 1.47$ m/s^2)
and turbine unit (b: $w_{max} = 0.352$ m/s^2)
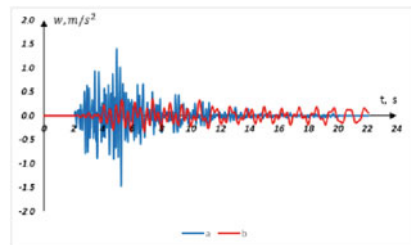
Figure 6 and Fig. 8 compare the displacements of the base and turbo-aggregate, and Fig. 7 and Fig. 9 the corresponding accelerations during earthquake No.2, 9 point intensity. At value of dry friction coefficient f = 0.025, as well as at f = 0.05 as in previous cases residual shear occurs. At that accelerations have small values, maximum value of this acceleration is 12 and 7.7 times less, respectively, than maximum acceleration of foundation. Figures 2, 3,4 5, 6, 7, 8 and 9, shows that the turbine generator oscillates, after the action of tangible acceleration of the base, at its own frequencies.

Figure 10 and Fig. 12 compare displacements of foundation, having maximal value 0.0388 m, and turbo-generator, and in Fig. 11 and Fig. 13 the corresponding accelerations during earthquake No.3, 9-point intensity. Maximum accelerations of turbo-generator at value of dry friction coefficient f = 0.025 and f = 0.05 decrease 3.6 and 2.4 times accordingly in comparison with maximum acceleration of foundation. Apparently, a relatively small decrease in the maximum value of turbine unit acceleration is related to the frequency composition of the earthquake.

Fig. 6 Change of displacements in time of the base (a: u_{max} = 0.00542 m) and turbine unit (b: u_{max} = 0.0141 m)
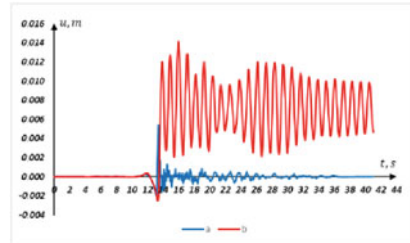
Fig. 7 Changes in acceleration over time of the base (a: w_{max} = 3.05 m/s^2) and turbine unit (b: w_{max} = 0.253 m/s^2)
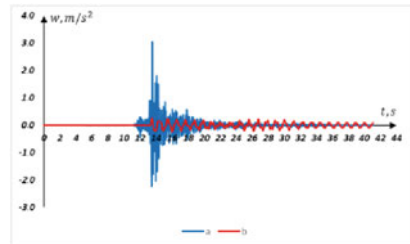
Fig. 8 Change of displacements in time of the base (a: u_{max} = 0.00542 m) and turbine unit (b: u_{max} = 0.0126 m)
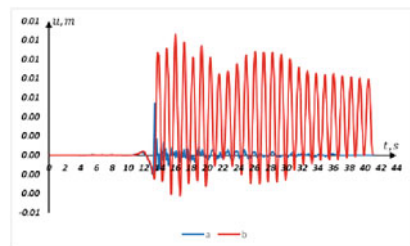
Fig. 9 Changes in acceleration over time of the base (a: $w_{max} = 3.05$ m/s^2) and turbine unit (b: $w_{max} = 0.396$ m/s^2)
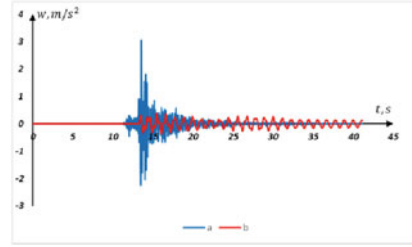
Fig. 10 Change of displacements in time of the base (a: $u_{max} = 0.0388$ m) and turbine unit (b: $u_{max} = 0.0768$ m).
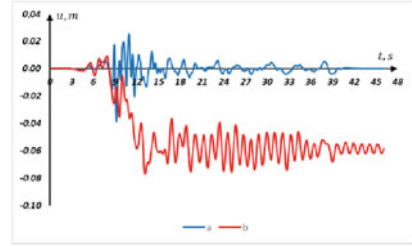
Fig. 11 Changes in acceleration over time of the base (a: $w_{max} = 3.09$ m/s^2) and turbine unit (b: $w_{max} = 0.862$ m/s^2)
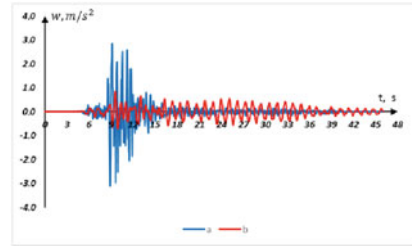
Fig. 12 Change of displacements in time of the base (a: $u_{max} = 0.0388$ m) and turbine unit (b: $u_{max} = 0.075$ m)
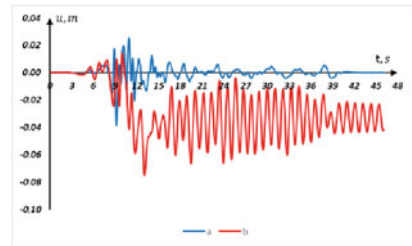
Fig. 13 Changes in acceleration over time of the base (a: $w_{max} = 3.09$ m/s^2) and turbine unit (b: $w_{max} = 1.29$ m/s^2)
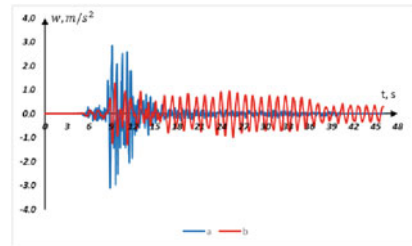
Fig. 14 Change of
displacements in time of the
base (a: $u_{max} = 0.183$ m) and
turbine unit (b: $u_{max} = 0.103$
m)
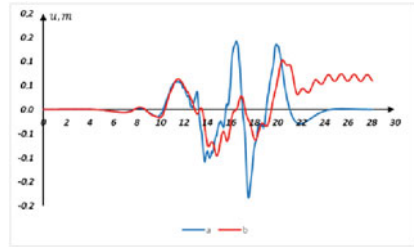
Figure 14 and Fig. 16 compare displacements of the base, having value 0.183 m, and turbine unit, and in Fig. 15 and Fig. 17 corresponding accelerations during earthquake No.4, 10 point intensity. Maximum accelerations of turbine unit at value of dry friction coefficient $f = 0.025$ and $f = 0.05$, respectively, decrease 6.5 and 4.6 times in comparison with the maximum acceleration of the base.

Fig. 15 Changes in
acceleration over time of the
base (a: $w_{max} = 7.23$ m/s^2)
and turbine unit (b: $w_{max} =$
1.12 m/s^2)
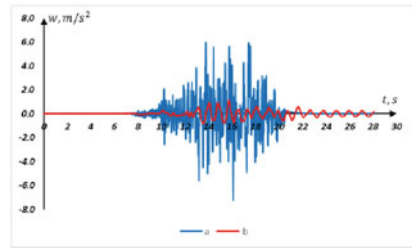
Fig. 16 Change of
displacements in time of the
base (a: $u_{max} = 0.183$ m) and
turbine unit (b: $u_{max} = 0.156$
m)
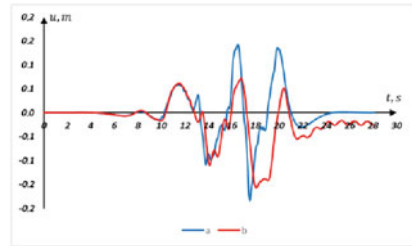
Fig. 17 Changes in
acceleration over time of the
base (a: $w_{max} = 7.23$ m/s^2)
and turbine unit (b: $w_{max} =$
1.57 m/s^2).
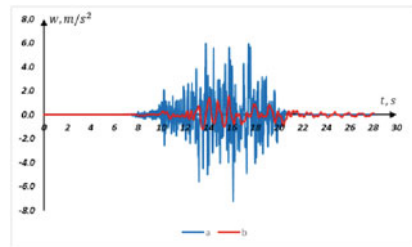
Calculation according to the linear theory, when the friction process is replaced by a weak spring, which does not correspond to the dynamic process of interaction of the structure with the base on the principle of dry friction, gives wrong results.

The following four Tables 1, 2, 3 and 4 show the maximum displacements and accelerations of the base and turbine unit for different earthquakes at different values of the dry friction coefficient.

The vertical component of the seismic wave has an ambiguous effect on the maximum displacements and accelerations of the turbine unit. Depending on the intensity of the earthquake and the spectral composition of its record, as well as on the mechanical characteristics of the structure, the maximum acceleration of the turbine unit may increase or decrease when the vertical component of the seismic

Table 1 Maximum values of horizontal displacement, foundation and turbo-aggregate acceleration without considering vertical component of earthquake (H) and with its vertical component (HV) at earthquake No.1

	$f = 0.025$				$f = 0.05$f $= 0.05$			
	u_{max} (m)		w_{max} (m/s^2)		u_{max} (m)		w_{max} (m/s^2)	
	H	HV	H	HV	H	HV	H	HV
Grounds	0.00287	0.00287	1.47	1.47	0.00287	0.00287	1.47	1.47
Turbine unit	0.0112	0.0109	0.224	0.211	0.00199	0.0126	0.352	0.354

Table 2 Maximum values of horizontal displacement, foundation and turbo-aggregate acceleration without considering vertical component of earthquake (H) and with its vertical component (HV) at earthquake No.2

	$f = 0.025$				$f = 0.05$f $= 0.05$			
	u_{max} (m)		w_{max} (m/s^2)		u_{max} (m)		w_{max} (m/s^2)	
	H	HV	H	HV	H	HV	H	HV
Grounds	0.00542	0.00542	3.05	3.05	0.00542	0.00542	3.05	3.05
Turbine unit	0.0141	0.0149	0.253	0.257	0.0126	0.0135	0.396	0.388

Table 3 Maximum values of horizontal displacement, foundation and turbo-aggregate acceleration without considering vertical component of earthquake (H) and with its vertical component (HV) at earthquake No.3

	$f = 0.025$				$f = 0.05$f $= 0.05$			
	u_{max} (m)		w_{max} (m/s^2)		u_{max} (m)		w_{max} (m/s^2)	
	H	HV	H	HV	H	HV	H	HV
Grounds	0.0388	0.0388	3.09	3.09	0.0388	0.0388	3.09	3.09
Turbine unit	0.0768	0.0782	0.862	1	0.075	0.129	1.29	1.45

Table 4 Maximum values of horizontal displacement, foundation and turbo-aggregate acceleration without considering vertical component of earthquake (H) and with its vertical component (HV) at earthquake No.4

	$f = 0.025$				$f = 0.05$f = 0.05			
	u_{max} (m)		w_{max} (m/s^2)		u_{max} (m)		w_{max} (m/s^2)	
	H	HV	H	HV	H	HV	H	HV
Grounds	0.183	0.183	7.23	7.23	0.183	0.183	7.23	7.23
Turbine unit	0.103	0.421	1.12	2.53	0.156	0.324	1.57	2.84

wave is taken into account. In our example, the greater the intensity of the earthquake, the greater the influence of the vertical component of the seismic wave on the shear accelerations of the turbine unit, i.e., the shear accelerations increase.

4 Conclusions

Flat sliders used for seismic isolation of structures allow the maximum value of acceleration to be reduced several times depending on the mass of the structure, the coefficient of dry friction and the nature of the seismic effect, i.e. the intensity and dominant frequencies.

The vertical component of the seismic wave has an ambiguous effect on the maximum displacements and accelerations of the turbine unit. Depending on the intensity of the earthquake and the spectral composition of its record, as well as on the mechanical characteristics of the structure, the maximum acceleration of the turbine unit may increase or decrease when the vertical component of the seismic wave is taken into account. An increase in earthquake intensity leads to an increase in shear acceleration when the vertical component of the seismic wave is taken into account.

Using a linear interaction model instead of the Coulomb dry friction model in the calculations will lead to erroneous results.

It is necessary to make a conclusion about the efficiency of the used slider on the basis of calculations on sets of earthquake records, on the intensity and spectral composition of frequencies close to the chosen construction site.

References

1. Tarasov, V.A.: Double seismic insulation system of turbine unit foundation construction of unique buildings and structures. Stroitel'stvo Unikal'nyh Zdanij i Sooruzenij. **91**, 9101 (2020). https://doi.org/10.18720/CUBS.91.1

2. Tarasov, V.A., Baranovskii, M.Y., Redkin A.V., Sokolov, E.A., Stepanov, A.S.: Seismic isolation systems. Constr. Unique Build. Struct. **4**(43), 117–140 (2016). URL: https://readera.org/sistemy-sejsmoizoljacii-14322325

3. Tarasov, V.A., et al.: Comparison of the seismic calculation results according to SNiP II-7-81* 1995 and SP 14.13330.2014. Constr. Unique Build. Struct. **1**(28), 52–73 (2015). ISSN 2304-6295

4. Babsky, A.E., Lalin, V.V., Oleinikov, I.I., Tarasov, V.A.: Seismic stability of vibration-insulated turbine foundations depending on the frequency composition of seismic impact. Struct. Mech. Eng. Constr. Build. **17**(1), 30–41 (2021)

5. Apsemetov, M.C., Andashev, A.J.: Calculation of buildings and structures with seismic-insulating sliding belt for seismic effects with intensity over 9 points. Vestnik MIU. **3**(145), 86–91 (2017). https://www.elibrary.ru/item.asp?id=30671944

6. Iurian, C., Ikhouane, F., Rodellar, J., Robert, G.: Identification of a system with dry fiction. Reports de recerca de l'Institut d'Organització i Control de Sistemes Industrials. (2005). https://citeseerx.ist.psu.edu/viewdoc/download?doi=10.1.1.603.5021&rep=rep1&type=pdf

7. Pelekis, I., Madabhushi, G.S.P., DeJong, M.J.: Seismic performance of buildings with structural and foundation rocking in centrifuge testing. Earthq. Eng. Struct. Dynam. **47**(12), 2390–2409 (2018). https://doi.org/10.1002/eqe.3089

8. Vyscrebentseva, M., Le, Q.V.: Methods of seismic and seismic isolation using special devices. Don's Eng. Gazette **1**, 2017–2019. (2019). https://cyberleninka.ru/article/n/metody-seysmogasheniya-i-seysmoizolyatsii-s-primeneniem-spetsialnyh-ustroystv

9. Belash, T.: Dry friction dampers in quake-proof structures of buildings. Proc. Eng. **117**(1), 397–403 (2015). https://doi.org/10.1016/j.proeng.2015.08.184

10. Buckle, I., Constantinou, M., Dicleli, M., Ghasemi, H.: Seismic isolation of highway bridges. University at Buffalo, The State University of New York, 194 p., (2016). ISBN: 9781626239777. https://www.eng.buffalo.edu/mceer-reports/06/06-SP07.pdf

11. Banović, I., Radnić, J., Grgić, N.: Geotechnical seismic isolation system based on sliding mechanism using stone pebble layer: Shake-table experiments. Shock. Vib. (2019). https://doi.org/10.1155/2019/9346232

12. Arutunyan, A.R.: Modern methods of seismic isolation of buildings and structures. Eng. Constr. J. **3**(13), 56–60 (2010). https://doi.org/10.18720/MCE.13.1

13. Ajzenberg, Y.M.: Seismic isolating adaptive foundation systems. Osnovaniya, Fundamenty i Mekhanika Gruntov. **29**, 197–202 (1992). https://doi.org/10.1007/BF02125532

14. Bakre, S.V., Jangid, R.S., Reddy, G.R.: Seismic response of piping systems with isolation devices. In: 13th World Conference on Earthquake Engineering, vol. 2676 (2004). https://www.iitk.ac.in/nicee/wcee/article/13_2676.pdf

15. Mkrtychev, O.V., Mingazova, S.M.: Study of the seismic isolation sliding belt: the case of a monolithic reinforced concrete building. J. Phys. Conf. Ser. **1425**(1), 3–10 (2020). https://doi.org/10.1088/1742-6596/1425/1/012161

16. Mkrtychev, O.V., Mingazova, S.M.: Analysis of the reaction of reinforced concrete buildings with a varying number of stories with a seismic isolation sliding belt to an earthquake. IOP Conf. Ser. Mater. Sci. Eng. **869**(5), 3–12 (2020). https://doi.org/10.1088/1757-899X/869/5/052065

17. Kuznetsov, V., Chen, S.: Sliding girt with fluoroplastic for earthquake-proof building. Eng. Constr. J. **21**(3), 53–58 (2011). https://doi.org/10.18720/MCE.21.8

18. Chen, S.: Seismically isolated building with sliding fluoroplastic belt. Saint Petersburg, 86 p. (2011). https://scadhelp.com/content/downloads/files/2011/Chehn-mag-2011.pdf

19. Mirzaev, I.M.: Reactions of composite structures, with concentrated and distributed parameters, to seismic action (vertical vibrations). Sov. Min. Sci. **12**(3), 296–300 (1976). https://doi.org/10.1007/BF02594874

20. Mirzaev, I., Turdiyev, M.S.: Vibrations of buildings with sliding foundations under real seismic effects. Constr. Unique Build. Struct. **94**, 9407 (2021). https://doi.org/10.4123/CUBS.94.7

21. Mirzaev, I., Yuvmitov, A.S., Turdiev, M.S., Shomurodov, J.F.: Influence of the vertical earthquake component on the shear vibration of buildings on sliding foundations. In: E3S Web of Conferences, vol. 264, p. 02022 (2021). https://doi.org/10.1051/e3sconf/202126402022

22. Mirzaev, I., Turdiyev, M.S.: Vibrations of buildings with a sliding foundation having lateral yielding contact under real seismic impacts. AIP Conf. Proc. **2432**, 030050 (2022). https://doi.org/10.1063/5.0089584
23. Elmer, F.J.: Nonlinear dynamics of dry friction. J. Phys. A: Math. Gen. **30**(97), 6057–6063 (1997). https://doi.org/10.1088/0305-4470/30/17/015
24. Chopra, K.A.: Dynamics of Structures. 4th Edn. Prentice Hall, Upper Saddle River 980 p. (2012). http://faculty.tafreshu.ac.ir/file/download/course/1587566331-dynamic.of.structures.chopra.4th-www.ucivil.ir.pdf. ISBN:0-13-855214-2
25. Ambraseys, N.N., et al.: Internet site for European strong-motion data. Bollettino di Geofisica Teorica ed Applicata. **45**(3), 113–129 (2004). http://www.isesd.hi.is/ESD_local/frameset.htm
26. CURVED SURFACE SLIDERS. https://docplayer.net/133188454-Curved-surface-sliders.html.

Damageability Analysis of Industrial Building Structures

Daria Tupitsyna⬡ **and Albert Baiburin**⬡

Abstract The article is devoted to the study of defects and damages of industrial objects. Reports on inspections of industrial facilities are analyzed. Types and frequency of damages of various building structures are given. According to the results of damage analysis the most significant, statistically justified, damages and defects of building structures have been singled out. The ranking of damage types according to the frequency of their occurrence has been carried out. The obtained results make it possible to expand the information on the types, frequencies and causes of damages of standard structures of industrial buildings, which is important for ensuring their safe operation, substantiating the maintenance and repair plans and increasing the production efficiency.

Keywords Industrial buildings · Defect · Damage · Criticality analysis · Building structures

1 Introduction

The service life of industrial buildings operating under normal conditions must be at least 50 years, the service life of structures exposed to highly aggressive media at least 25 years. These figures are specified in accordance with the recommendations of code of practice SP 255.1325800.2016 [1]. However, the actual service life of a building may be reduced if the structures suffer various damages or defects.

There are many causes of damage to building structures. The following main classes of defects and damages can be identified: manufacturing defects in the factory, construction and installation defects on the construction site, operational damage, repair work defects. Possible operational causes of damage to building structures: atmospheric effects, ageing of materials, foundation settlement, increased

D. Tupitsyna · A. Baiburin (✉)
South Ural State University, 76, Lenin Avenue, Chelyabinsk 454080, Russian Federation
e-mail: baiburinak@susu.ru

loads, effects of workshop aggressive environment, increased humidity and temperature, roof leaks, operation of lifting devices, accidental impacts, cut-outs due to technological needs, etc.

Quantitative analysis of criticality of damages (defects) is a very time-consuming procedure requiring considerable expenses related to accumulation of statistics, mathematical processing of inspection results, and selection of criticality criteria. Classification of defects in construction by significance given in [2] is rather conventional and does not take into account the frequency of observation and probability of detection of defects.

The aim of the work was to analyse the types of damage and defects in industrial buildings on a large body of data from their inspections and industrial safety assessments. Many works of domestic and foreign researchers [3–8] have been devoted to the study of damage to buildings and structures.

According to [9], the following are the most common defects in building structures:

1. Defects in metal structures: cracks in the base metal, welded joints; deviations from the design position, geometric dimensions and non-design cut-outs contributing to weakening of elements and off-centre application of loads; local and general deformation of elements; disorder of bolted and riveted connections; defects of welded connections (undercuts, rough scales etc.); destruction of protective coatings and metal corrosion.
2. Defects in reinforced concrete structures: destruction and spalling of concrete; baring and corrosion of reinforcement; cracks in concrete; damage to reinforcement and embedded parts; bulging of compressed reinforcement; longitudinal cracks and destruction of compressed concrete; rupture or displacement of transverse reinforcement in the area of inclined cracks; deflections and deviations from the design position; oiling, damping and corrosion of concrete.
3. Defects in masonry structures: cracks in the masonry; violation of the geometry of structural elements; delamination of masonry due to failure to tie the rows together; destruction of masonry materials from erosion; bulging, bowing and other deformations.

In order to carry out an objective assessment of the condition of the metal framing elements, according to [10], attention must be paid to the following defects: displacement of columns and supports axes relative to the axis breakdown axes in the support section; columns deviation from vertical; difference in marks of support surfaces of neighbouring columns in a row and span; deflection arrow (curvature) of columns, framework struts, links on columns; cutouts of branches and gratings of through columns; loosening of anchor bolts fastening, etc.

According to [11], the following characteristic damages of concrete and reinforced concrete structures can be identified: cracking in various structures, destruction of the protective layer of concrete, denudation and corrosion of reinforcement, corrosion of concrete. We also gathered statistics on the occurrence of the above damage with an indication of the percentage of defective structures. The most frequently

occurring defects are corrosion of the concrete of the wall cladding, corrosion of the reinforcement of the cover slabs as well as failure of the concrete protection layer.

The following characteristic defects are observed in steelwork [12]: cracks in truss and sub-truss elements, reduced depth of structural support, cracks in welded joints, and general bending of structures.

From the analysed sources it is difficult to draw meaningful conclusions specifically for industrial buildings due to the lack of heterogeneous data, methods of classification and assessment of defects and damages. In order to identify the main damages and defects of industrial building structures and to study their frequency and causes it is necessary to process a large amount of data. Such data was obtained after processing the results of survey of industrial facilities (workshops) of various structural systems.

2   Methods

In order to perform quantitative assessment of defects and damages, inspection and examination reports from more than 100 industrial facilities were analysed. Single-storey industrial buildings from the metallurgical, mechanical engineering, energy and building materials industries were considered as objects of research. Years of commissioning ranged from 1902 to 2016: 1902–1940 - 10 objects; 1941–1970 - 61 objects; 1971–1990 - 21 objects; 1991–2016 - 9 objects.

In terms of structural design, the workshops investigated were divided into frame, wall and frame-wall buildings. In terms of structural design and materials used: full reinforced concrete frame; full metal frame; mixed frame (reinforced concrete and steel); stone bearing walls with different cover options. Practically all surveyed workshops had hoisting equipment in the form of overhead cranes and overhead cranes of capacity from 2 to 280 tons with different modes of operation: from repair to heavy. The degree of aggressiveness of the environment of the investigated productions was defined mainly as non-aggressive or slightly aggressive, less often as moderately and strongly aggressive.

During data collection, the object, operating time, hoisting equipment, aggressive workshop environment, structure, structural element, damage type and location, damage magnitude and frequency as well as the probable cause were recorded. Frequency characteristics for the main types of damage and defects were then plotted. The frequency of damage was defined as the ratio of damaged structures (elements) to their total number at a given facility.

3   Results

The types and frequency of damage to reinforced concrete columns are shown in Fig. 1.

Damage or defect of reinforced concrete columns, %
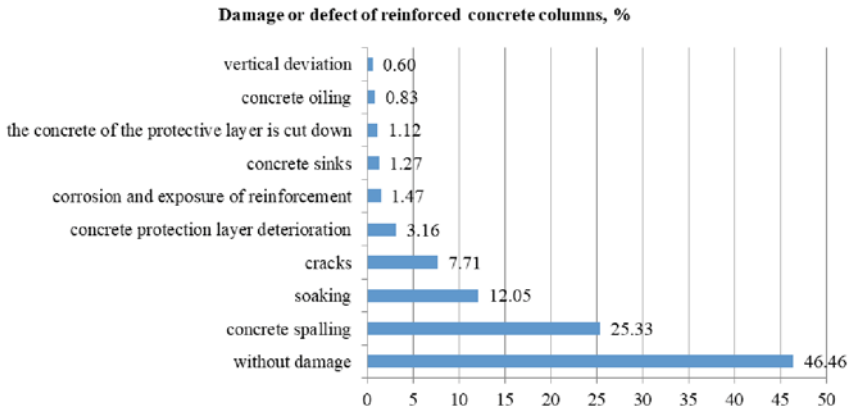
Fig. 1 Damage (defects) to reinforced concrete columns

As can be seen from the presented graph, the most common defect of reinforced concrete columns is spalling of concrete 25.3% and soaking of structures 12.1%. The least common are oiling of concrete and deviation of columns from the vertical.

Types and distribution of damage to metal columns are shown in Fig. 2.

For metal columns, corrosion of 41.8% and local bends of 10.1% can be distinguished as the most common, the least typical defect is the bending of the wall of the I-beam. Such a defect as the vertical deviation is also found in this type of structure, but less often than columns made of reinforced concrete.

The distribution of damage to reinforced concrete trusses is shown in Fig. 3.

As can be seen, for reinforced concrete trusses the number of defects encountered is quite small, which is explained by their massiveness and durability. The most typical defects for this type of structures are minor spalling of concrete 29.6%, and soaking of elements 28.9%.

The list of detected defects and damages of steel trusses are shown in Fig. 4.

Damage or defect of metal columns, %
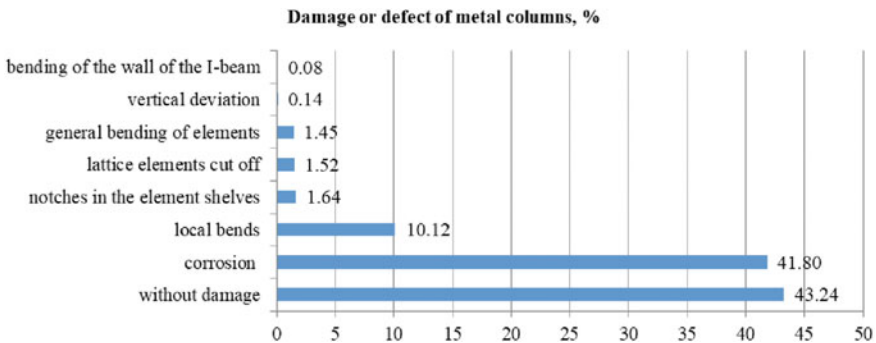
Fig. 2 Damage (defects) to metal columns

Damage or defect of reinforced concrete trusses, %

Fig. 3 Damage (defects) to reinforced concrete trusses
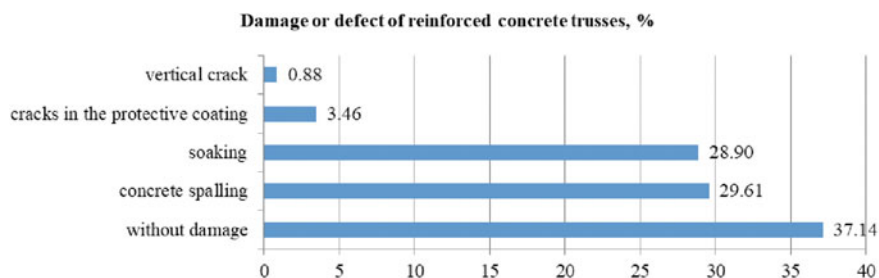
Damage or defect of metal trusses, %
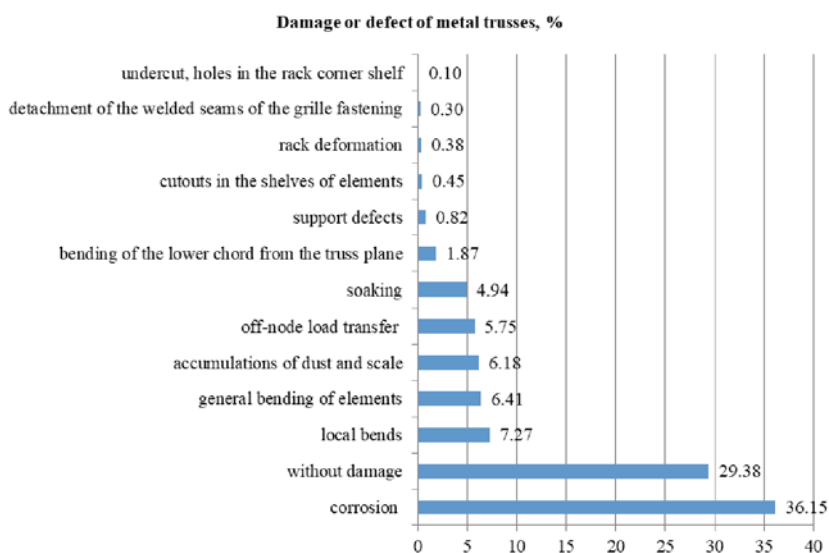
Fig. 4 Damage (defects) to metal trusses

The graph above shows that more than one third of the metal trusses are characterised by corrosion 36.2%. The next highest frequency are local bends 7.3% and general bending of truss components 6.4%. Rare are detachment of the welded seams of the grille fastening as well as various undercuts, holes in the element flanges.

Types and frequency of damage to trusses and columns are shown in Figs. 5, 6.

In the case of linking elements, the list of defects encountered does not depend on whether they are used for columns or trusses. Damage (defects) characteristic of links are as follows: corrosion, cutouts in elements, local bends, absence of communication elements, general bending of elements. However, the incidence of damage (defects) differs depending on the location of the structures. For example, more than half of the truss connections are susceptible to corrosion, but among the column connections this defect occurs in less than 4% of cases. This is due to the location of the ties and roof leaks. The opposite situation is due to mechanical damage to the structures,

Damage or defect in truss connections, %
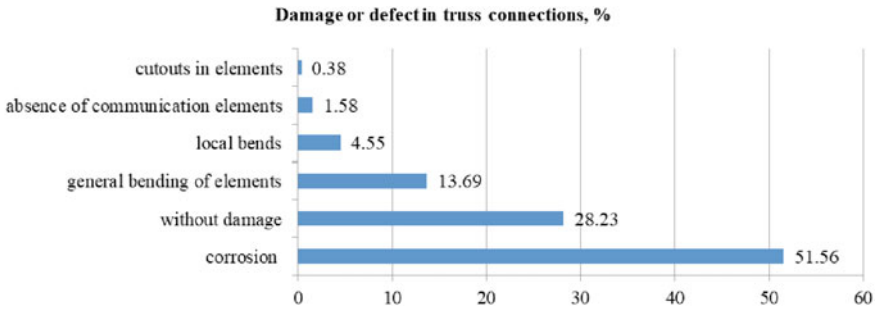
Fig. 5 Damage (defects) to truss connections

Damage or defect of column connections, %
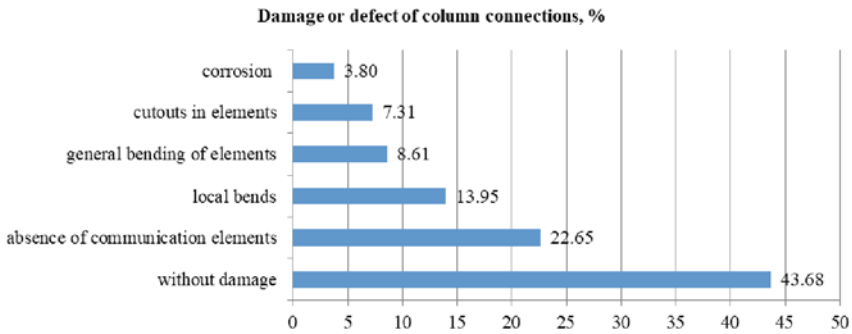
Fig. 6 Damage (defects) to column connections

namely notches in the ties. This damage occurs in 7.3% of column connections and in less than 1% of truss connections. This is due to the positioning of utilities and equipment.

Types and distribution of damage to prefabricated floor and roof slabs are shown in Fig. 7.

Note that more than half of the roof and floor slabs are subject to soaking 57.6%. This defect is the most frequent in this type of construction and is associated with leaks in roofs and gutters. The next most frequent defect is concrete corrosion in 7.7% as a consequence of leaks. Most defects which are not caused by leaks and concrete corrosion occur in no more than 3% of structures. The absence of any damage (defects) is characteristic only for a quarter of the surveyed structures.

The distribution of damage to brick walls is shown in Fig. 8.

The most characteristic damages to brick walls are atmospheric erosion, cracks and soaking. These defects occur in 10–23% of brick walls. Rare ones include spalling, peeling of protective coatings and biological damage to structures.

The types and frequency of damage to steel crane beams are shown in Fig. 9.

As can be seen, the most frequent defect is structural corrosion 29.6%. A fifth of beams (19.2%) have disorder of bolted and riveted joints due to dynamic loads from

Damage or defect of prefabricated floor and roof slabs, %
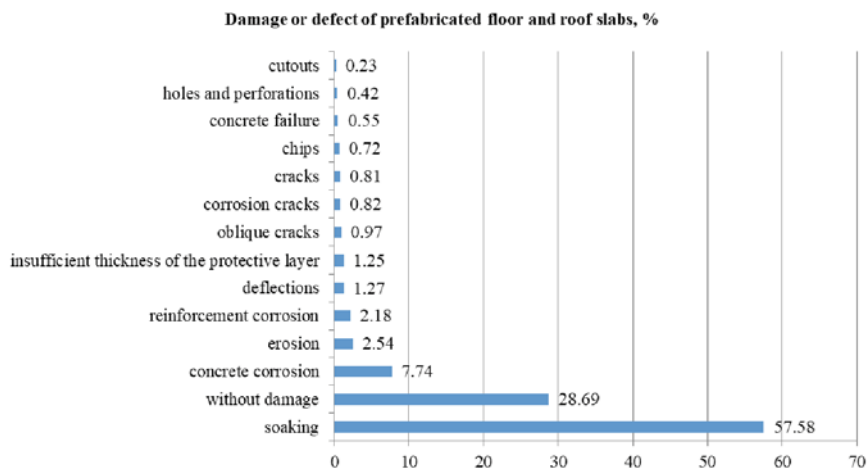
Fig. 7 Damage (defects) to prefabricated floor and roof slabs

Damage or defect in brick walls, %
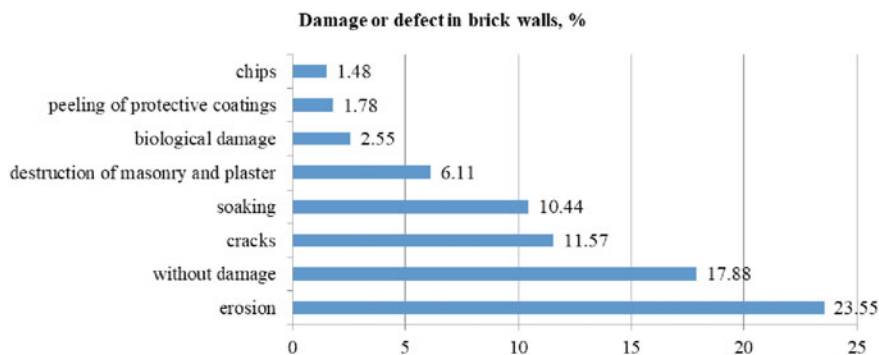
Fig. 8 Damage (defects) to brick walls

Damage or defect of metal crane girders, %
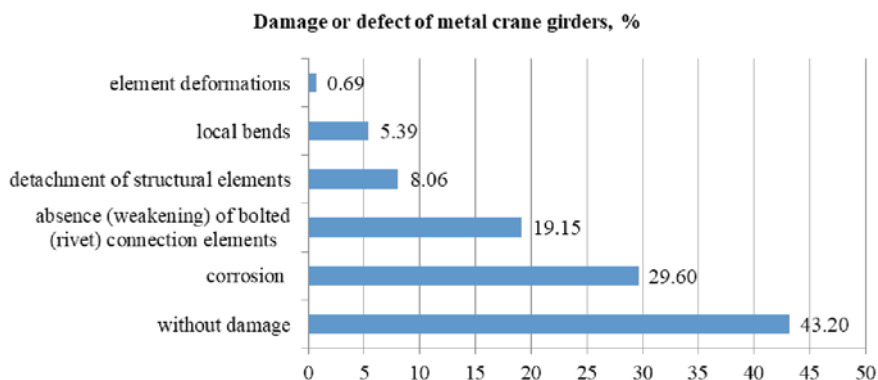
Fig. 9 Damage (defects) to metal crane girders

Damage or defect to the roof, %

without damage	3.14
bloats	4.37
bumps	5.87
clogging elements	8.07
full or partial wear	24.28
absence of roof elements	25.45
abnomalities of adjacencies	28.82
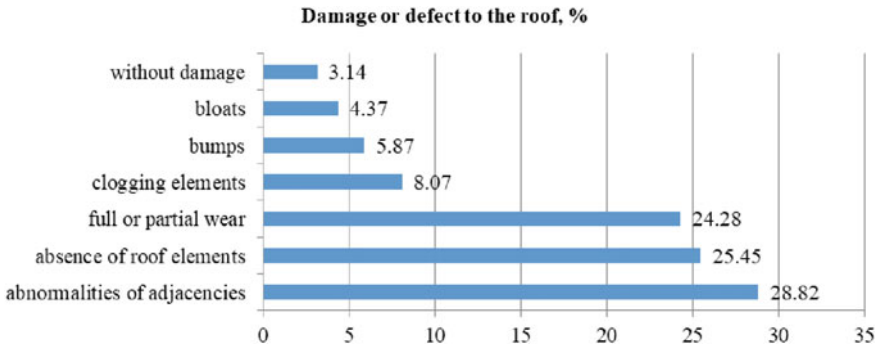
Fig. 10 Damage (defects) to roofs

the hoisting equipment of the workshops. Deformations of elements as well as local bends can be attributed to rare occurrences.

The types and distribution of roof damage are shown in Fig. 10.

As can be seen, the percentage of roofs without damage is quite small at just over 3%. The most characteristic defects in the roof structures are joint failures in 28.8% and missing roofing elements in 25.5% (aprons, parapet protection, expansion joints etc.).

4 Conclusion

Based on the foregoing, the following conclusions can be drawn. The absence of defects is characteristic for about 45% of reinforced concrete and metal columns, while the most significant defect was soaking and spalling of concrete for reinforced concrete columns, corrosion and local bends for metal columns. The proportion of reinforced concrete and metal trusses without damage is approximately 33%. Damage-free linking elements are found in 29% of cover elements and in more than 40% of column connections. The most frequent defect in column connections is a missing connection element in 23%, while corrosion is a characteristic defect in truss connections and is found in more than half of the examined structures. For prefabricated floor and roof slabs, no defects are found in only a quarter of the structures, and the most frequent defect is soaking, which occurs in almost 2/3 of the structures. A large proportion of external brick walls are subject to atmospheric erosion. The proportion of crane beams with damage is 57%. The most common damage to crane girders is corrosion and loose bolted connections. Almost 97% of the roofs have some kind of defects and damage: broken joints, complete or partial wear and tear, missing individual elements as well as clogged gutters, uneven and swollen roof mats. The main causes of damage are impacts during operation: corrosion, deformations from impacts, dynamic loads from cranes, atmospheric erosion.

The results obtained provide more information on the types and frequencies of damage in typical industrial building structures, which is important for ensuring their safe operation and improving the efficiency of production. Further research will focus on the application of neural networks to process damage data for objective assessment and management decision-making in the operation of industrial buildings.

References

1. SP 255.1325800.2016. Buildings and structures. Rules of operation. General provisions. Moscow (2016)
2. Classifier of the main types of defects in the construction and building materials industry. Gosstroi Russia, Moscow (1993)
3. Albrecht, R.: Defects and Damage to Building Structures. Stroyizdat, Moscow (1979)
4. Analysis of the causes of accidents and damage to building structures. Stroyizdat, Moscow (1973)
5. Baiburin, A.K.: Ensuring the Quality and Safety of Constructed Civil Buildings. ASV, Moscow (2015)
6. Grozdov, V.T.: Defects in building structures and their consequences. kN+ Publishing, St. Petersburg (2001)
7. Dobromyslov, A.N.: Diagnosis of Damage to Buildings and Engineering Structures. ASV, Moscow (2008)
8. Yeremin, K.I.: Atlas of faults and damage to building structures in operation. VELD, Magnitogorsk (2010)
9. Narkevich, M.Y.: Visual inspection as the basis for the development of automated systems for remote monitoring and quality assessment of buildings and structures at hazardous industrial facilities. Proceedings of Tula State University. Technical Sciences. 5, 570–575 (2021).
10. Kuzmishkin, A.A.: Classification of defects in the inspection of metal structures. Bull. Grad. School. **12**(39), 95–97 (2014)
11. Solovyov, V.G.: Analysis of defects and damages of reinforced concrete structures, typical for underground structures, by the example of civil defense structures. News Higher Educ. Inst. Invest. Constr. Real Estate. **9**(1), 124–133 (2019)
12. Guseva, K.B.: Peculiarities of the inspection of metal structures. Sci. J. **5**(39), 23–25 (2019)

Concept of the Innovative Model of Architecture Formation of the «Smart» Redistribution of Single-Phased Electric Network

Oleg Vdovin ⓘ**, Sergei Efimenko** ⓘ**, Igor Chernorutsky** ⓘ**,**
Anatolii Smetankin ⓘ**, Sergei Kolesnichenko, and Yliia Cimai**

Abstract The most common emergency situations, processes and phenomena in the electric supply industry are related to the occurrence of short circuits, voltage drops, short-term impulse voltages, current leakage, network overload, phase imbalance, etc. The transition of electrical equipment into pre-emergency or emergency mode of operation is implied by these situations. Consequently, current conducting parts are damaged or destroyed in the emergency mode of operation. Abnormal processes, which are not damage, arise in the pre-emergency mode of operation, but their long duration leads to the occurrence of an accident. The most common causes of pre-emergency mode are short-circuiting currents; the emergency mode is caused by current and voltage overloads and skews. These adverse events call for the implementation of safety controls in the form of design and engineering solutions, as well as engineering and technical measures, aimed at protecting the electrical circuit of the consumer.

Keywords Electric supply industry · Emergency situations · Short circuits · Voltage drop · Short-term impulse voltage · Current leakages · Network overloads · Phase imbalance

1 Current Problems of the Electric Supply Industry and Methods of Their Solution

Nowadays, safety controls that break the electric circuit in emergency situations are used in order to protect electrical equipment from damage and protect people from electric shocks. Such safety controls include circuit breakers (CB), residual current

O. Vdovin · S. Efimenko · I. Chernorutsky · A. Smetankin (✉)
Peter the Great St. Petersburg Polytechnic University, St. Petersburg, Russia
e-mail: smetanckin.anatoly@yandex.ru

S. Kolesnichenko · Y. Cimai
The Admiral Makarov State University of Maritime and Inland Shipping, St. Petersburg, Russia

circuit breakers (RCCB), residual current operated circuit breakers with integral overcurrent protection (RCBO), surge protectors (SP), voltage relays (VR), etc. It is worth mentioning that these safety controls effectively perform in practice, however, their functionality is aimed only at localization of emergency situations in order to prevent possible consequences. Prevention actions that reduce equipment downtime and the number of emergency situations are not provided in such cases [1–3].

Taking into consideration the existing level of obsolescence and physical depreciation of equipment, targeted actions to prevent the occurrence of emergency situations are of particular importance. The demand for the development of design and engineering solutions, as well as engineering and technical measures, which are functionally aimed at early diagnosis of abnormal processes in the circuit pre-fault condition and at finding ways to stabilize its parameters, is determined by the aforementioned facts.

At present, improvement of the reliability of electric networks and power supply systems (ENPS) is carried out in two main directions [4]. On the one hand, there is preservation of the required operational performance under a natural decrease of the level of its technical condition (maintenance, current and overhaul repairs). On the other hand, there is a reservation of elements of the electric network (back-up generators, converters, lines). In one case, maintenance and repair of equipment provides physical restoration of the already obsolete resource, which was originally included in the design that at the moment does not meet the existing demand for consumption. In other cases, reservation reveals the issues of increased cost of the equipment and maintenance of unreasonably increased reserves of the system.

In addition to this, it is worth noting that the existing technological structure in the electric supply industry has reached the limit of its efficiency according to the estimates of the Center of Strategic Research of the Russian Federation (CSR). These circumstances call for a set of design and engineering solutions, as well as engineering and technical measures, aimed not just at upgrading equipment in terms of restoring its technical characteristics, but rather at transforming the network and acquiring new qualitative capabilities. This applies to the active-adaptive properties that allow the emergence of a system with a new appearance – a "smart" energy system [1, 5].

Therefore, this approach forms a relevant request for the development of the ENPS structure based on a new concept called Smart Grid. The ENPS system is considered as a unified energy and information system in the Smart Grid approach. The technological process is controlled automatically, without human involvement, in the unified energy and information system, and it is aimed at improving the efficiency and reliability of the system. Nowadays, there has already been some work done on the implementation of individual elements of the Smart Grid approach, but it is limited only to collection and transmission of power system data by smart metering devices [2, 6]. It is premature to talk about a qualitative leap in the electric supply industry in the absence of the implementation of new control technologies and executive functionality in ENPS systems.

Thus, the necessity to create a new system of views and principles of technological structure for controlling the parameters of the electric network arises.

2 Conceptual Framework

A complex system makes up the foundation of our concept. This system is based on the ternary logic of controlling the parameters of a single-phase / three-phase alternating current network, allowing the analysis of the current network states with the possibility of making operational changes in the circuit arrangement. It can be applied when it is necessary to stabilize the specified characteristics in order to increase the period of uninterrupted power supply to the object [7].

The foundational element of this complex system is an "intelligent" control module [8, 9]. This module is an electrical device in the form of multifunctional control unit (MCU), which analytical functionality is based on the extended (variation) ternary logic. Its structure can be considered as a structure of artificial fuzzy (hybrid) neural network (AFNN) type ANFIC – Adaptive Neural Fuzzy Inference System.

AFNN MCU consists of three layers: input, hidden (logic layer), output.

First Layer: The current electric network parameters are fed to the input, and they are normalized at the expense of the specified values in the input layer, thus, becoming relative values that are in the range (0, 1).

Second Layer: Rules based on input variables and specified criteria implicitly form membership functions in the «IF» sub-layer, and the bilayer neural network of the «TO» sub-layer forms the output of this sub-layer due to weighting coefficients and normalized input parameters.

Third Layer: A strong output signal based on the results obtained in the logic layer is received at the output. Multifunctional control unit (MCU) is an electric device designed to supply industrial and domestic single-phase loads 230 V / 50 (60) Hz from three-phase four-wire (five-wire) network and provide automatic switching of single-phase consumers to the phase of power supply optimal voltage level in order to increase the period of uninterrupted power supply of the object (consumer) [7].

It follows from the definition that three-phase power (L1, L2, L3 and N) is supplied to the input terminals of the MCU, and only the phases, which voltage is the closest to normal, come out. The transfer itself occurs during phase fluctuations, surges, skews, sags, complete failures or loss of power. The power consumption using MCU allows automatic transfer in order to redistribute the load of single-phase consumers in a "smart" way. Moreover, it prevents the occurrence of abnormal and emergency states of network. However, this definition is of generalized form and requires a more detailed consideration of the MCU device [10].

Let's consider the existing electric supply system of 0.4 kV with one power supply source and twelve single-phase consumers with three options in the system V1, V2, V3.

At the same time, V1 and V2 options do not provide for the use of MCU.

Option V3 provides for the use of MCU. Consequently:

– V1 is considered as the design one functioning under the uniform load.
– V2 is considered as the design one functioning in critical modes with uneven
  loads and phase imbalance.
– V3 is considered as an option of "smart" redistribution of the existing load
  eliminating the consequences of suddenly occurring critical modes of V2.

3   Descriptive Examples of Calculations

Electrical circuits, load distribution (connection) diagrams, situational load matrices,
vector diagrams, and graphs of the current network parameters as well as tables of
the results of the calculations are used in the article in order to visually demonstrate
the consideration of the aforementioned options [6, 11].

$$\Delta U = \frac{a_1 M_a}{F} \tag{1}$$

a_1 is a coefficient;
  M_a is a moment of load
  F is a conductor cross-section (mm^2)

$$a_1 = \frac{100}{y U_H^2} \tag{2}$$

γ is a specific conductivity
  $U^2{}_H$ is a rated voltage
  M_a is a moment of load
  (a_1 is 21.9 at 380 V for aluminum)
  (γ is 31.7 m/ohm*mm^2 for aluminum)

$$M_a = P_p \cdot L \tag{3}$$

Pp is power (kW)
  L is line length (km)
  M_a is a moment of load

$$P_p = \sqrt{3U I \cos \varphi} \tag{4}$$

Pp is power (kW)
  U is phase-to-phase voltage
  I is current
  $cos\ \varphi$ is an angle of phase deviation of current to voltage

$$I = \frac{P}{\sqrt{3U} \cos \varphi} \tag{5}$$

4　System's V2 and V3 Options

4.1　V2 Option

It is a system functioning in critical modes with uneven loads and phase imbalance. V1 option for subcritical modes is not considered.

A brief technical description of the V2 option: the rated design solution of the system functioning in critical modes with uneven loads and phase imbalance, where the source of electricity is TP-10/0.4 kV transforming substation with T1 transformer of 100 kW capacity, and with VL-0.4 kV overhead line that has points of connection of loads of outgoing inputs into the consumer building. The Tables 1, 2 and 3 of calculated data of the network parameters for V2 option is presented below [6, 12].

It can be concluded from the obtained data in the table that there are uneven distribution of load and skewed network parameters.

4.2　V3 Option

It is a proposed system with the application of MCU installed at the inputs of the connected loads. It is considered to be the option of "smart" redistribution of the existing load that eliminates the consequences of suddenly occurring critical modes of V2 (Fig. 1).

Situational matrix of "smart" load redistribution for V3 option is presented in the Tables 4, 5 and 6 [6, 13].

It can be considered from the obtained data in the table that the problem of phase imbalance of V2 option is localized due to "smart" phase-by-phase redistribution, and, eventually, the network parameters are normalized [14]. The obtained data was translated into a graphical version using graphs and vector diagrams of the occurring load current parameters in order to make the processes taking place in the proposed options clearer.

This option of events is considered as V1 option under conditions of suddenly occurring critical modes of phase imbalance due to unequal switching of non-normalized consumption load. It is reflected in the parameters of network current:

– Phase "A" is 3.0 kV
– Phase "B" is 22.0 kV
– Phase "C" is 5.0 kV

V2 Option

The vector diagram in Fig. 2 (on the left) shows the unequal magnitude of the vectors in each phase and the presence of a non-symmetric load with the occurrence of a vector of current potential of the ground conductor [15, 19].

The graph (Fig. 2, on the right) shows that the maximum value of the current is 33.3 A in the phase «B», and the minimum value of the current is 7.52 A in the phase

Table 1 Calculated data of network parameters in critical mode B2

Parameters	Control points of network parameters										Σ
	1	2	3	4	5	6	7	8	9	10	
Load capacity	30	28	24	23	22	15	15	14	8	8	30
Phase "A" load		3.5	1.5			0.5			0.5		3.0
Phase "B" load					6,5			5,5			22
Phase "C" load	2.0			1,0			1			1	5.0
Line current of 380	45	42	37	34	33	23	22	21	13	12	45
load current of Phase "A"			7			2			2		13
load current of Phase "B"		16			29			25			99
load current of Phase "C"	13			4			4			4	27

Table 2 Calculated data of the network parameters without taking into account the internal resistance of the source and linear currents in critical mode B2

Parameters	Control points of network parameters										Σ
	1	2	3	4	5	6	7	8	9	10	
Pp – Line	30	28	24	23	22	15	15	14	8	8	30
Pp – Phase "A"			1.5			0.5			0.5		3.0
Pp –Phase "B"		3.5			6,5			5,5			22
Pp –Phase "C"	2.0			1.0			1			1	5.0
Ia – Phase "A"			7			2,			2		13
Ib – Phase "B"		16			29			25			99
Ic – Phase "C"	13			4			4			4	27

Table 3 Calculated data of network parameters without taking into account the reactive component of power in critical mode B2

Parameters	Control points of network parameters										Σ
	1	2	3	4	5	6	7	8	9	10	
Load capacity	30.0	28.0	24.5	23.0	22.0	15.5	15.0	14.0	8.5	8.0	7.0
Phase "A" load			1.5			0.5			0.5		3.0
Phase "B" load		3.5			6.5			5.5			22.0
Phase "C" load	2.0			1.0			1.0			1.0	5.0
Line current of 380	45.5	42.4	37.1	34.8	33.3	23.5	22.7	21.2	12.9	12.1	45.5
load current of Phase "A"			6.81			2.27			2.27		13.6
load current of Phase "B"		15.9			29.5			25.0			99.9
load current of Phase "C"	13.6			4.54			4.54			4.54	27.2
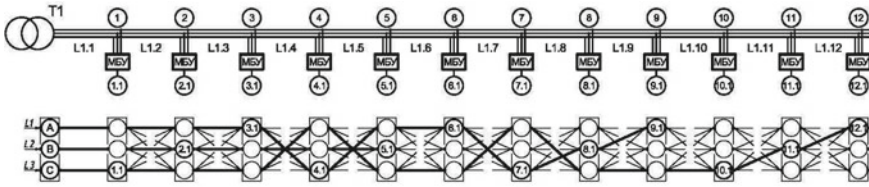
Fig. 1 Connection configuration as a result of automatic load redistribution

«A». However, there is a critical level of current potential that is equal to 27.4 A in the ground conductor [6, 20].

The vector diagram in Fig. 3 (on the left) shows the impact of the occurring event, which is reflected in the voltage values exceeding the established standard of 220 V. This affects the reliability of electric network and the quality of power supply to the consumers, which can have serious consequences:

– Phase «A» is 216.3 V
– Phase «B» is 188.2 V
– Phase «C» is 215.3 V

The graph in Fig. 3 (on the right) demonstrates the unacceptable differences in phase parameters at a critical voltage drop on one of the phases:

– Phase «A» is 1.7%
– Phase «B» is 14.4%
– Phase «C» is 2.1%

V3 Option

This version of events is seen as a result of localization of phase imbalance of V2 option due to «smart» phase by phase load redistribution and eventually normalization of network parameters.

The vector diagram in Fig. 4 (on the left) shows that the vectors in each phase are equal and that there is no current potential in the ground conductor.

The graph in Fig. 4 (on the right) shows that current parameters are the same [6].

The vector diagram of the voltage (Fig. 5, on the left) demonstrates the results of normalization of power supply processes with restoring of the required voltage levels: phase «A» – 206.3 V, phase «B» – 211.9 V, phase «C» – 201,7 V.

The graph of the voltage drop in the line (Fig. 5, on the right) shows some phase difference of parameters, namely: phase «A» – 6.2%, phase «B» – 3.7%, phase «C» – 8.3%.

This data indicates that the voltage parameters, in contrast to load current, have not restored to the required level of system's symmetry. However, the electric network functions normally and remains stable in providing required reliability.

Table 4 Estimated data of network parameters in B3 mode, after normalization of processes

Parameters	Control points of network parameters										Σ
	1	2	3	4	5	6	7	8	9	10	
Load capacity	30	28	24.5	23	22	15.5	15	14	8.5	8	30
Phase «A» load			1.5	1.0		0,5	1.0	5.5	0.5		10.0
Phase «B» load		3.5			6.5						10.0
Phase «C» load	2.0									1.0	10.0
Line current of 380	45.5	42.4	37.1	34.8	33.3	23.5	22.7	21.2	12.9	12.1	45.5
220 load current of Phase «A»			6.81	4.54		2.27	4.54	25.0	2.27		45.6
220 load current of Phase «B»		15.9			29.5						45.6
220 load current of Phase «C»	13.6									4.54	45.6

Table 5 Estimated data of the network parameters without taking into account the reactive component of power after the normalization of processes in B3 mode

| Parameters	Control points of network parameters										Σ
	1	2	3	4	5	6	7	8	9	10	
Load capacity	30	28	24	23	22	15	15	14	8	8	30
Phase «A» load			1	1		0,5	1	5	0,5		10
Phase «B» load		3			6						10
Phase «C» load	2									1	10
Line current of 380	45	42	37	34	33	23	22	21	12	12	45
220 load current of Phase «A»			6	4		2	4	25	2		45
220 load current of Phase «B»		16			29						45
220 load current of Phase «C»	13									4	45

Table 6 Estimated data of the network parameters without taking into account the internal resistance of the source and linear currents after the normalization of processes in mode B3

Parameters	Control points of network parameters										Σ
	1	2	3	4	5	6	7	8	9	10	
Pp - Line	30	28	24	23	22	15	15	14	8	8	30
Pp - Phase «A»			1	1		0,5	1	5	0,5		10
Pp -Phase «B»		3			6						10
Pp -Phase «C»	2									1	10
Ia - Phase «A»			6	4		2	4	25	2		45
Ib - Phase «B»		16			29						45
Ic - Phase «C»	13									4	45

Fig. 2 Vector diagram (on the left) and graph (on the right) of current parameters when phase imbalance occurs
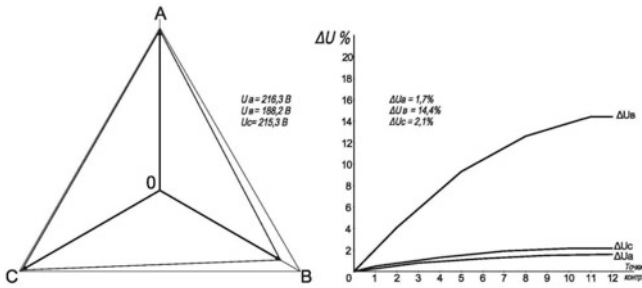
Fig. 3 Vector diagram (on the left) and graph (on the right) of line to ground voltage parameters when phase imbalance occurs
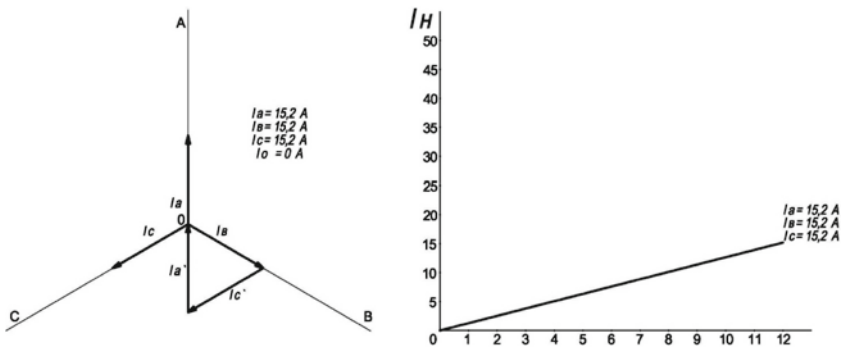
Fig. 4 Vector diagram (on the left) and graph (on the right) of current parameters as a result of automatic phase imbalance localization and restoring of normal operation
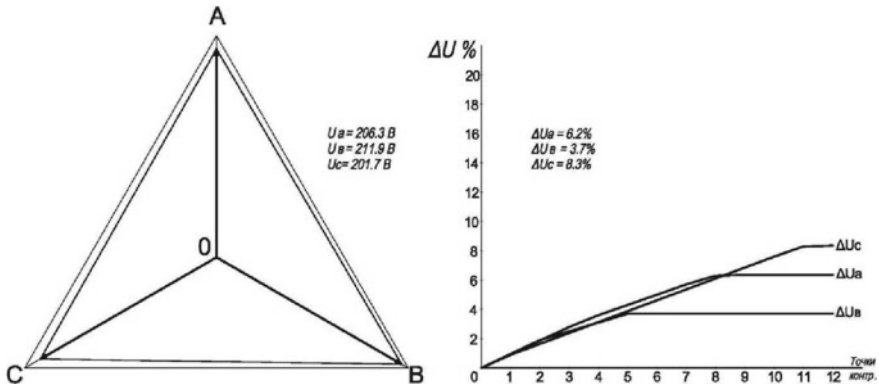
Fig. 5 Vector diagram (on the left) and graph (on the right) of line to ground voltage parameters as a result of restoring of normal operation

5 MCU Device and Its Behavior

The following behaviors can be observed in retrospective view of the occurring processes when the MCU device is installed in a given electric network:

V1 Option: System functions normally, specifically, the load is uniform, current values in all phases are the same and their graphs coincide.

V2 Option: A sudden critical mode occurred, specifically, phase imbalance occurred due to unequal switching of non-normalized consumption load.

Such conditions are sufficient for triggering MCU in order to normalize the network parameters using the method of phase by phase redistribution.

V3 option is the result of problem localization. It is the resultant indicator of «smart» load redistribution and final normalization of the network parameters (Fig. 6).

The graphs visually demonstrate the process of localization of the problem. The sudden critical mode of phase imbalance is localized using «smart» phase by phase load redistribution by means of the MCU. As a result, the network parameters are normalized (Fig. 7).

However, it is worth mentioning that the example is limited to a simple open-ended radial main circuit. Since the example is illustrative, it does not reflect the scale of possibilities in practical application on more branched lines [5]. The application of the proposed electric supply scheme is more convenient in wide implementation [16].

As a result of modernization of equipment based on MCU, this scheme represents the quality of a «smart» energy system (Smart Grid) [17, 18] that has the properties of an artificial fuzzy (hybrid) neural network and consists of:

– Input: TP 10/0.4 kV power source, transforming substation;
– I layer: SG-0.4 kV TP switch gear;
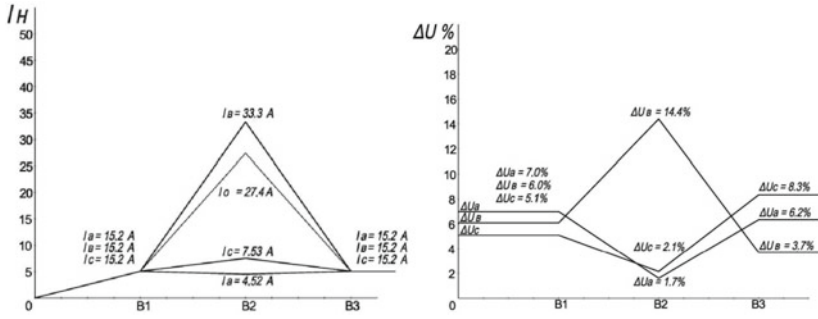
Fig. 6 Diagram of the behavior of the process of automatic restoration of normal operation: the parameters of the voltage drop in the network are on the right; the parameters of load current are on the left
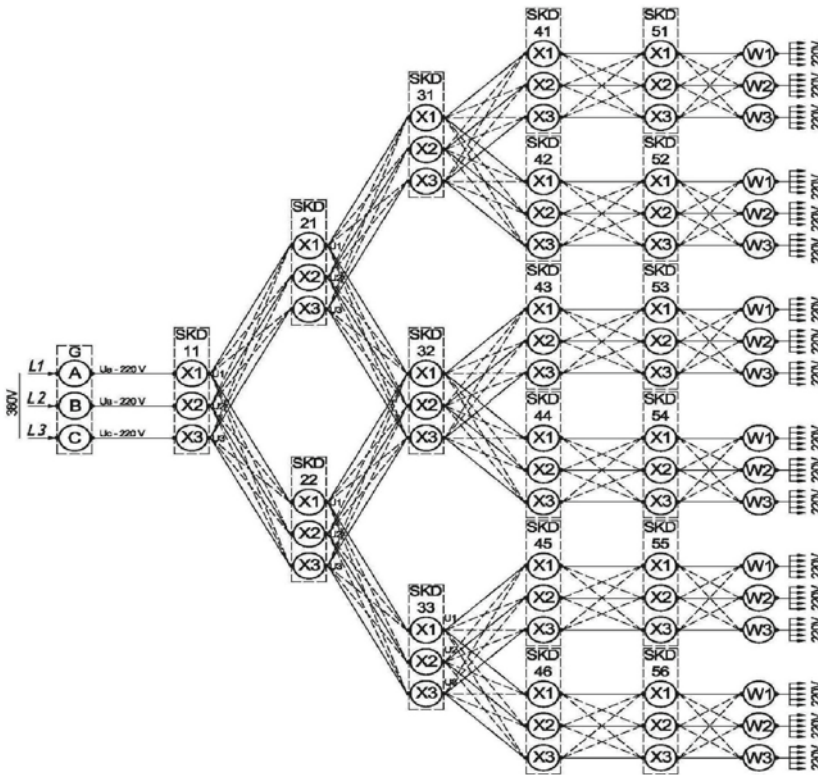
Fig. 7 Principle and architecture of electric network based on MCU

– II layer: CS-0.4 kV cable separator;
– III layer: input CS-0.4 kV cable separator of input of the object;
– IV layer: IDD Input distribution device of the object;
– V layer: LD load distribution cabinet of the object;
– VI layer: PSC power supply cabinet for individual loads;
– VII layer: LDB load distribution board for individual loads.

Notation conventions:
Generator – G
Phases of a line – A, B, C
Phase wires of a line – L1, L2, L3
Consumption load – W
Total load – ΣW
Contact connection – X
Multifunctional Control Unit – MCU

6   Conclusion

It should be recognized that the existing safety controls effectively perform their tasks, but their functionality is aimed only at localization of accidents in order to prevent possible consequences, and it does not provide preventive actions to reduce the emergency downtime of equipment. However, taking into consideration the existing level of obsolescence and physical depreciation of equipment, targeted actions to prevent the occurrence of emergency situations are of particular importance. The demand for the development of design and engineering solutions, as well as engineering and technical measures, which are functionally aimed at early diagnosis of abnormal processes in the circuit pre-fault condition and at finding ways to stabilize its parameters, is determined by the aforementioned facts. The development of the electric network on the basis of integrated implementation of MCU allows creating a network, which architecturally and functionally has some properties of a neural network. The simple scheme of power supply of some number of apartment houses is considered as an example in the article. In fact, this structure contains different levels, i.e. initial level – transforming substation, second level – input switch gear of the house, third level – the floor distribution board, the fours – the consumer. Taking into account the automation of MCU operation, the hidden «smart» multilevel redistribution can be confidently considered.

References

1. Beisenov, K.S.: Problems and prospects of development of the electric power industry in modern conditions. Young Sci. **20**(154), 235–237 (2017)
2. Center for Strategic Research (CSR). https://www.csr.ru/ru. Accessed 08 Feb 2022

3. Aladdin, M., Muhannad, A.: Toward fault tolerant modelling for SCADA based electricity distribution networks machine learning approach. PeerJ Comput. Sci. **7**, 1–17 (2021)
4. Soluyanov, Y., Akhmetshin, A., Soluyanov, V.: Application of digital technologies to analyze the actual electrical loads of multi-apartment residential buildings. In: Proceedings - 2022 International Conference on Industrial Engineering, Applications and Manufacturing, ICIEAM 2022, pp. 153–157 (2022)
5. Code of Regulations for Design and Construction. Design and Installation of Electrical Installations in Residential and Public Buildings. SP 31–110–2003. https://docs.cntd.ru/document/1200035252. Accessed 08 Feb 2022
6. Karpov, F.F., Kozlov, V.N.: Handbook for Calculation of Wires and Cables, 3rd edn., p. 224. Energia Publishing House, Korolyov (1969)
7. Kobets, B.B., Volkov, I.O.: Innovative development of the electric power industry on the basis of the smart grid concept. IAC Energy, 208 (2010)
8. Loskutov, A.B., Zyrin, D.V., Demidova, A.S.: Solid state voltage regulators influence on power flows redistribution in smart grids 6–20 kV. In: 2018 International Multi-Conference on Industrial Engineering and Modern Technologies (2018). 8602520
9. Mousavizadeh, S., Alahyari, A., Bolandi, T., Haghifam, M.-R., Siano, P.: A novel resource allocation model based on the modularity concept for resiliency enhancement in electric distribution networks. Int. J. Energy Res. **45**(9), 13471–13488 (2021)
10. Khan, Z.A., et al.: Efficient short-term electricity load forecasting for effective energy management. Sustain. Energy Technol. Assessments **53**, 102337 (2022)
11. Parizad, A., Hatziadoniu, C.: Deep learning algorithms and parallel distributed computing techniques for high-resolution load forecasting applying hyperparameter optimization. IEEE Syst. J. **15**(3), 3758–3769 (2022)
12. Kulikov, A., Loskutov, A., Loskutov, A., Pelevin, P.: Application of correlation methods for traveling wave fault locating and automation of intelligent electrical networks. In: 2019 International Multi-Conference on Industrial Engineering and Modern Technologies, FarEastCon 2019 (2019). 8934339
13. Klochkova, E., Sadovnikova, N., Darda, E.: Digital transformation in the energy industry: trends and prospects. Adv. Intell. Syst. Comput. **726**, 288–299 (2019)
14. Shurygin, Y.: Intelligent relay protection of electric power systems. In: Proceedings - 2019 1st International Conference on Control Systems, Mathematical Modelling, Automation and Energy Efficiency, pp. 656–660 (2019)
15. Shilin, A.N., Shilin, A.A., Dementiev, S.S.: Smart electromechanical systems in electric power engineering: concept, technical realization, prospects. In: Gorodetskiy, A.E., Tarasova, I.. L. (eds.) Smart Electromechanical Systems, vol. 174, pp. 251–262. Springer, Cham (2019). https://doi.org/10.1007/978-3-319-99759-9_20
16. Kamps, K., Mohrke, F., Zdrallek, M., Awater, P., Schwan, M.: Reliability of decentralized network automation systems and impacts on distribution network reliability. In: 2020 International Conference on Probabilistic Methods Applied to Power Systems (2020)
17. Parol, M., Wasilewski, J., Wojtowicz, T., Arendarski, B., Komarnicki, P.: Reliability analysis of MV electric distribution networks including distributed generation and ICT infrastructure. Energies **15**(14), 5311 (2022)
18. Amiri, S.S., Rahmani, M., McDonald, J.D.: An updated review on distribution management systems within a smart grid structure. In: 2021 11th Smart Grid Conference (2021)
19. Rules for Arrangement of Electrical Installations. Glavgosenergonadzor of Russia Moscow, 606 (1998)
20. Digital Transition in Russia's Electric Power Industry. https://www.csr.ru/ru/publications/tsifrovoj-perehod-v-elektroenergetike-rossii/. Accessed 08 Feb 2022

Thermal Stress State of a Massive Concrete Slab in the Winter Building Period

Polina Tyapkina, **Kirill Semenov**, **Yuri Barabanshchikov**, **and Irina Lebedeva**

Abstract In this paper, a problem of the thermal cracking resistance according to the deformation criterion of a massive concrete foundation slab during the building period in winter was considered. The implementation of tent and thermal insulation has been justified by preventing freezing of an early-age concrete and generation of significant tensile stresses. Optimum time limits for the thermal protection elements removal should be calculated considering the thermal stress state of the slab. The winter concreting of the foundation slab, 2.0 m high and measuring 21.8 m $\times$ 63.8 m in plan, at outside temperatures of $-35\,°C$, $-25\,°C$ and $-15\,°C$, was examined. In this paper, the thermal cracking resistance in this paper was estimated according to the deformation criterion, which means that concrete elongation deformations should not exceed the ultimate concrete elongation. The thermal cracking resistance analysis is based on a calculation of the thermal stressed state of the concrete foundation slab during the hardening period and is carried out in the TERM software taking into account the influence of the curing temperature on the concrete thermophysical and deformation properties. Safe time limits for the thermal insulation and the tent removal have been calculated. A linear dependence of the optimum time limits of the thermal protection elements removal on the outside air temperature has been revealed. The values of cooling rate at the set points located on the top and side surfaces of the slab at various outside air temperatures have been defined.

Keywords Massive concrete and reinforced concrete structures · Building period · Cement setting temperature · Thermal stressed state · Thermal cracking resistance · Cold weather concreting · Thermal protection elements · Thermal insulation

P. Tyapkina (✉) · K. Semenov · Y. Barabanshchikov · I. Lebedeva
Peter the Great St.Petersburg Polytechnic University, 29, Politechnicheskaya St., St. Petersburg 195251, Russia
e-mail: polina.tyapkina@gmail.com

1   Introduction

Imposed loads and actions effect concrete and reinforced concrete structures during the building period. The heat liberation from cement hydration during the concrete hardening process, outside temperature fluctuations, solar exposure, impact on stress state of load-bearing elements. Thermal stresses occurring as a consequence of different technological factors and fire exposure may cause damage to the integrity of concrete structure [1–3]. Concrete deterioration can manifest itself in cracks, peeling of the clear cover and surface spalling of construction [4–6].

Due to technological and manufacturing reasons, it is preferable to concrete massive structures, such as foundation slabs, as a single block of equal height. A concrete hardening is accompanied by exothermic reaction. Heat exchange with the environment lead to the irregular temperature distribution along the block height [7, 8]. As a consequence of this process the dangerous tensile stresses arises first on the surface of the foundation slab and then in its central zone [9, 10]. The alternate freezing and thawing cycles in winter period cause disruptive action within the material of reinforced concrete structures [11, 12].

Sub-zero air temperature slows down the cement hydration process and cause freezing the water included in the concrete. Therefore, the setting and strength development processes in young concrete do not take place if the critical strength has not yet been reached [5, 13]. In other words, freezing of early-age concrete leads to a disturbance of the concrete structure and a reduction of its strength properties.

The calculation of the thermal stress state of concrete structures, as well as the assessment of thermal cracking resistance, are complex engineering tasks. Some researchers solve these problems in a simplified way. In the paper [14] the thermoelastic problem does not take into account the creep deformation of concrete [15]. Most of the current practical calculation methods do not consider the influence of the curing temperature on the deformation characteristics of concrete [16] and its heat dissipation [17].

In order to prevent freezing of an early-age concrete and generation of significant tensile stresses, it is recommended to install thermal insulation on the surface of the concrete block and perform concreting in a tent (an enclosed temporary structure) during the winter period [18, 19]. Early removal of thermal protection elements can lead to the phenomenon of thermal shock: when temperature difference between the core of the structure and the surface increases significantly, resulting in the formation of temperature cracks.

The studies [20, 21] calculate the optimum parameters of thermal protection in winter in a simplified way. Calculations of optimum time limits for the thermal protection elements removal taking into account the influence of the curing temperature on the concrete thermophysical and deformation properties are not available at the present moment.

The purpose of this paper is to evaluate the optimum time limits for removal of the concrete tent and the thermal insulation in winter building period. A research object is a NPP reactor foundation slab, 2.0 m high and measuring 21.8 m × 63.8 m

in plan. The slab must be considered as a technically complex capital construction characterized by a high importance level.

The 2.0 m thick slab is concreted in one block height for technological reason. The subgrade is a soft ground, and a subbase is a 100-mm-thick concrete base made of concrete B12.5. In winter building period the slab can be covered with a thermal insulation, and a tent can be erected. The practical value of this paper consists in determining safe time limits for the thermal insulation and the concrete tent removal, considering thermal cracking resistance of concrete.

2 Materials and Methods

The thermal cracking resistance analysis is based on a calculation of the thermal stressed state of the concrete foundation slab during the hardening period and is carried out in the TERM software developed by the staff on the Graduate School of Civil and Road Construction of the Institute of Civil Engineering at the Peter the Great St. Petersburg Polytechnic University. The program takes into account the influence of temperature and the passage of time on the thermophysical and deformative properties of concrete.

The calculation is carried out using the two-dimensional calculation model shown in Fig. 1. Stress and temperature are functions of two spatial coordinates: X – horizontal and Y – vertical.

The thermal cracking resistance in this paper is assessed according to the deformation criterion. Concrete elongation deformations, determined in view of the concrete creep factor and variable deformation modulus, should not exceed the ultimate concrete elongation. In order to shorten the text of the paper, the results are presented only for the set points, which are located in the centre (core) of the slab as well as on its top and side surfaces and are marked in red in Fig. 1.

Thermal and physical characteristics of the concrete B30 are defined by the concrete thermal conductivity $\lambda = 2.67 \frac{W}{m \cdot K}$ and heat capacity $c = 1.0 \frac{kJ}{kg \cdot K}$. The deformation characteristics of concrete B30 are presented below.
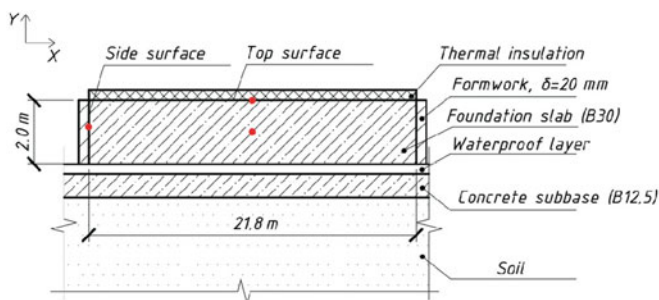
Fig. 1 The structural model of the foundation slab

According to the paper, the instantaneous elastic deformation modulus of concrete is represented by the Eq. (1).

$$E(t) = E_{max}(1 - e^{\alpha t^{\gamma}}) \tag{1}$$

where $E_{max} = 33100 MPa$ the limit value of the concrete deformation, and the slump of the concrete cone higher than 0.08 m and coarse aggregate with 0.04 m grain are used. Functional dependency parameters are $\alpha = -0.37$, $\gamma = 0.72$ and t stands for the current time.

Concrete creep account according to straight line inherited theory of aging using the relaxation function is represented in the Eq. (2).

$$R(t, \tau) = A(1 - e^{-\beta \tau^{\alpha}}) + (B_1 + D_1 e^{-\beta \tau^{\alpha}})e^{-\gamma_1(t-\tau)} + (B_2 + D_2 e^{-\beta \tau^{\alpha}})e^{-\gamma_2(t-\tau)} \tag{2}$$

where functional dependency parameters are as follows $A = 0.7$; $B_1 = 0.2$; $D_1 = 0.4$; $B_2 = 0.1$; $D_2 = 0.3$; $\beta = 3.61 \cdot 10^{-6} sec^{-1}$; $\gamma_1 = 1.17 \cdot 10^{-5} sec^{-1}$; $\gamma_2 = 1.17 \cdot 10^{-5} sec^{-1}$.

The heat dissipation process follows the I.D. Zaporozhets equation, which is stated in the Eq. (3).

$$Q(\tau) = Q_{max}\left[1 - (1 + A_T \tau)^{-\frac{1}{m-1}}\right] \tag{3}$$

where Q_{max} the limit the concrete heat dissipation converges to; A_T is the heat dissipation rate coefficient indicating the heat dissipation rate at a constant temperature T; m is the order of the water hydration reaction that reaches from 1.1 to 2.3 for Portland cement depending on different types of additives.

The heat dissipation process and deformation characteristics depend on the concrete hardening temperature. The temperature effect on heat dissipation is registered by the temperature function, which is given in the Eq. (4).

$$f_T = 2^{\frac{T_1 - T_2}{\varepsilon}} \tag{4}$$

where ε is the characteristic temperature difference. That is, if, for example, $T_1 - T_2 = \varepsilon$ then $f_T = 2$, i.e., in case of the temperature rises by ε degrees, the heat dissipation rate is doubled.

The adjustment time hypothesis is applied in this paper. At moments of equal heat dissipations, i.e., when $Q_1 = Q_2$ with Q_1 and Q_2 being heat dissipation values at respective temperatures T_1 and T_2, the heat dissipation relation and corresponding timelines τ_1 and τ_2 remain constant throughout the process and equal to the temperature function in the Eq. (5).

$$\frac{(\partial Q/\partial \tau)_1}{(\partial Q/\partial \tau)_2} = \frac{\tau_1}{\tau_2} = f_T = const \tag{5}$$

Parameters of the heat dissipation process were determined experimentally. The following results were obtained: the cement heat dissipation is $q = \frac{Q}{C} = 502.8 \frac{kJ}{kg}$; the heat dissipation rate coefficient at 20 C° equals $A_{20} = 6 \cdot 10^{-5} \ sec^{-1}$ he hydration reaction order is $m = 2.2 \ kg$. The weight of cement in the concrete mix is $C = 350 \frac{kg}{m^3}$.

The technological specifications for concrete casting in the tent are included in the calculations as follows.

Temperature of the concrete mix equals 12 °C, air temperature in the tent equals 5 °C.

The insulation made of expanded polystyrene foam with the following characteristics is placed on the top and side surfaces of the foundation slab: the coefficient of the heat dissipation layer is $\beta_{np} = 4.8 \frac{W}{(m^2 \cdot K)}$; thermal conductivity equals $\lambda = 0.045 \frac{W}{m \cdot K}$; the layer thickness is equal to 0.008 m.

The outside winter air temperature is assumed to be -15 °C, -25 °C, -35 °C.

In order to study thermal cracking resistance in the foundation slab, it is necessary to investigate the change of thermal stresses in the centre and on the surfaces of the slab, when the tent is removed. Thus, the zones with the highest stresses are identified.

The concrete thermal cracking resistance is measured in accordance with the deformation criterion. The tensile stresses must be less than some nominal strength, which is defined as the right-hand side of the inequality of the deformation criterion.

Figure 2 shows a graph of the stresses in the slab as a function of time and a curve of the nominal strength of the concrete on the surface, when the thermal insulation remains on the slab and the tent is removed 4 days since the concrete casting. In this example, the outside temperature is assumed to be -25 °C.

The analysis of the results in Fig. 2 shows that thermal cracking resistance is not achieved at the top surface of the slab on the 6th day since the concrete casting. An increase of time limits for the tent removal is required.

The time limits for the thermal protection elements removal are determined by the trial and error approach. The effect of the removal period on the development of tensile stresses on the top surface of the slab at an outside temperature of -25 °C is illustrated in Fig. 3.

In this case, the tent can be removed no earlier than 5 days after concrete casting of the slab. The optimum period for the removal of the tent and thermal insulation at different outdoor temperatures can be determined similarly.

3 Results

Figure 4 presents stress diagrams on the top and side surfaces of the slab at outside temperatures of -35 °C, -25 °C and -15 °C and at various periods of tent removal.

It can be concluded from Fig. 4 that the tent can be removed no sooner than 8, 5 and 4 days after concrete casting at air temperature of -35, -25 and -15 °C, respectively.
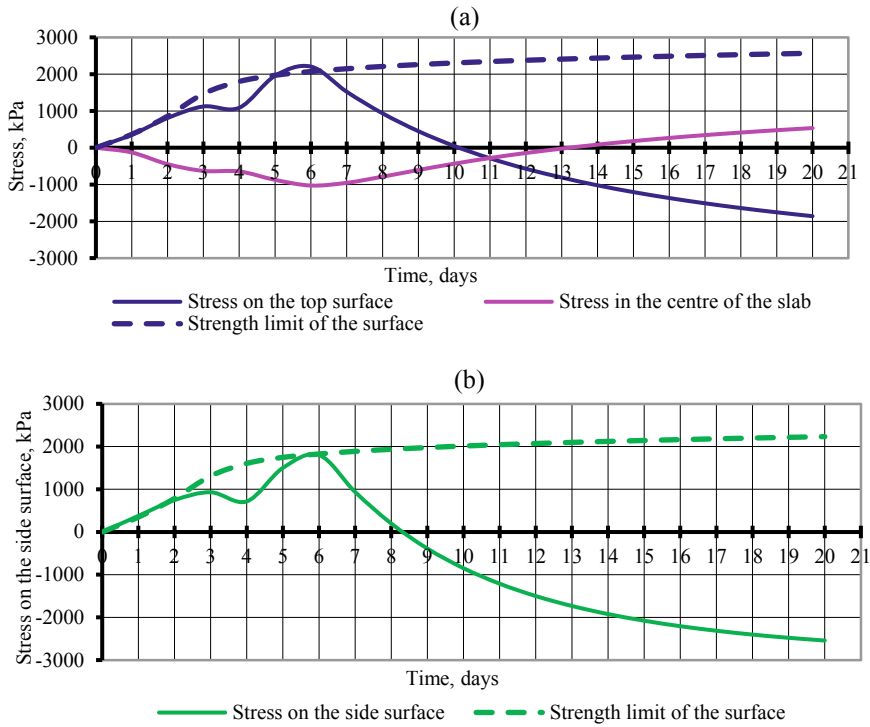
Fig. 2 Thermal stress evolution at T = −25 °C (the tent is removed 4 days since the concrete casting): a) at the centre of the slab and on the top surface; b) on the side surface of the slab
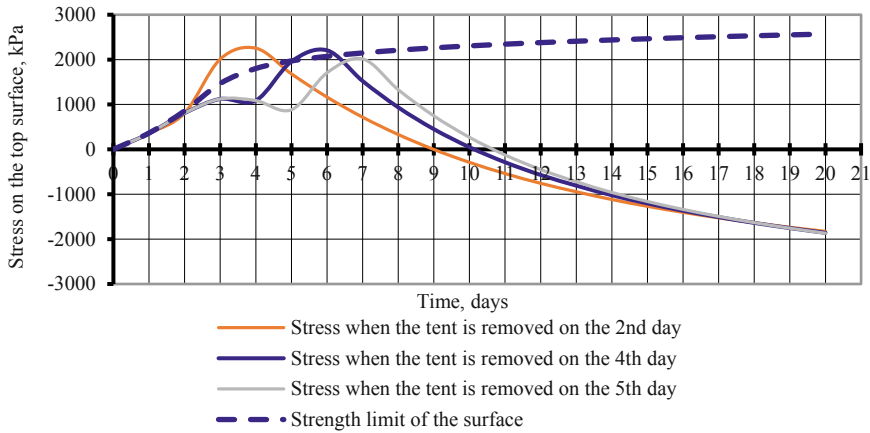
Fig. 3 Evolution of thermal stress on the top surface of the slab at T = −25 °C
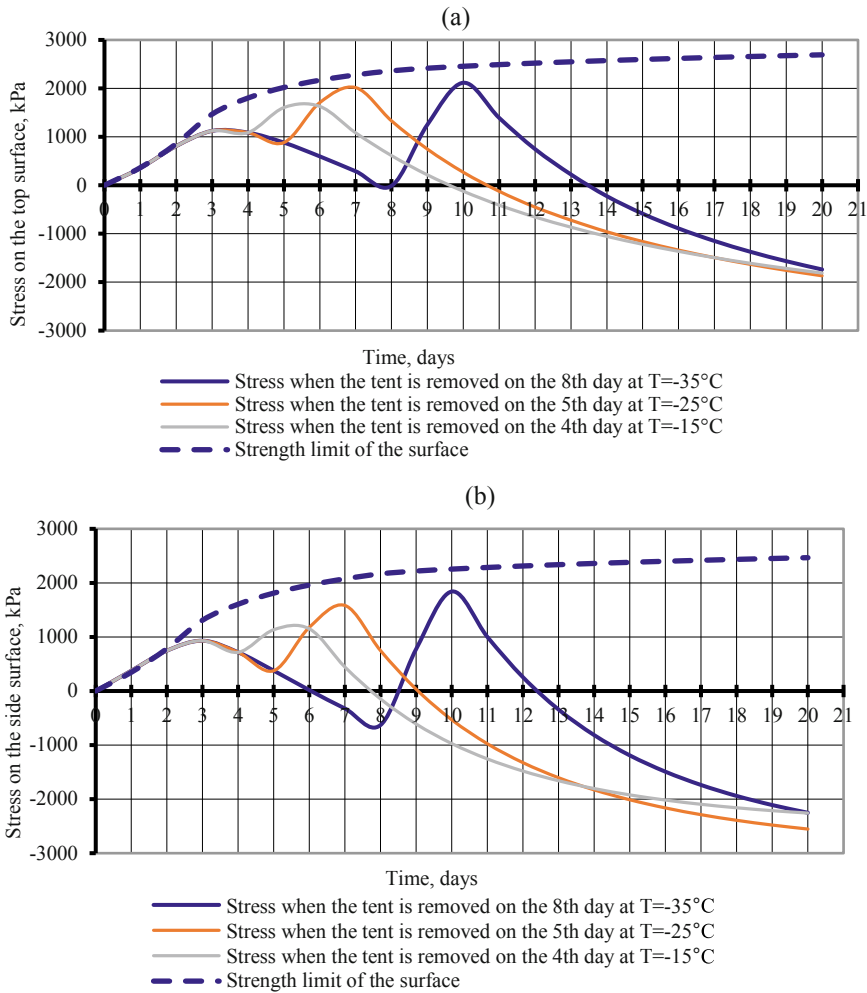
Fig. 4 Evolution of thermal stress when the tent is removed: a) on the top surface of the slab; b) on the side surface of the slab

Once the tent is removed, the thermal insulation must be removed from the concrete slab. The safe removal of the thermal insulation assumes that no cracks will occur. Figure 5 presents the relationship between stresses on the top and side surfaces of the foundation slab and the time of thermal insulation removal at different temperatures:

−35, −25 and −15 °C. Safe time of tent removal was taken as 8, 5 and 4 days, respectively.
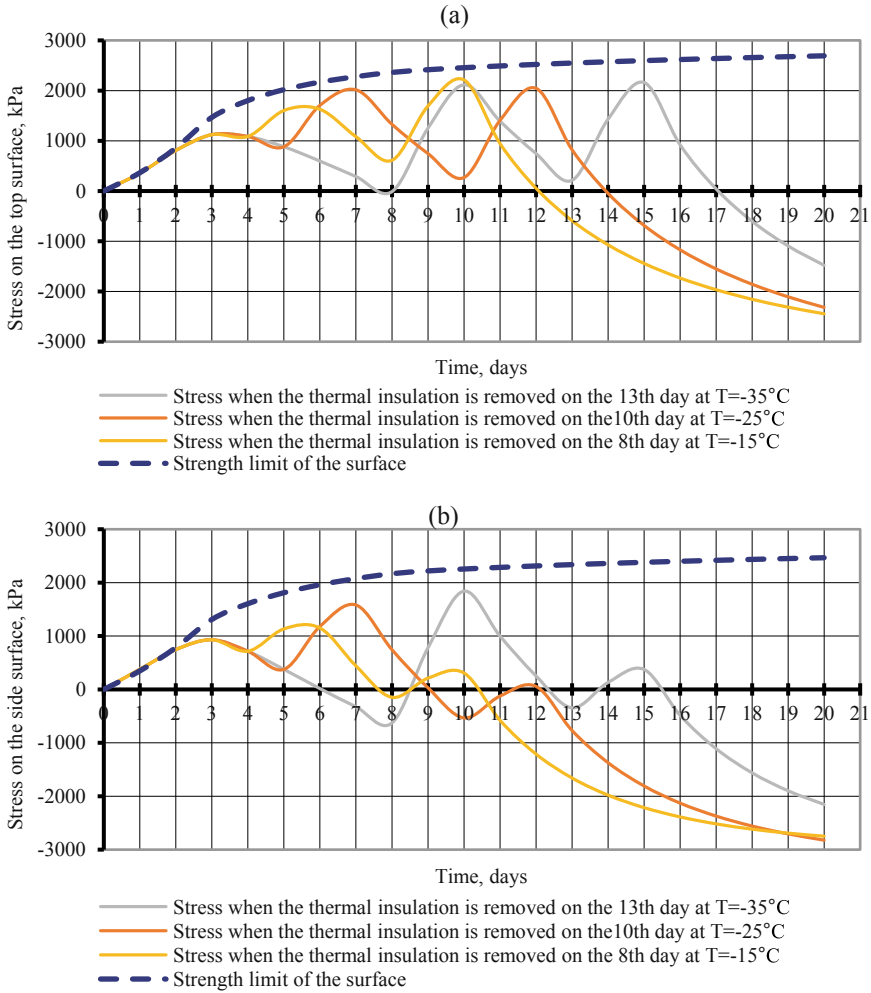
Fig. 5 Evolution of thermal stress when the tent and thermal insulation are removed: a) on the top surface of the slab; b) on the side surface of the slab

It can be concluded from Fig. 5 that the thermal insulation can be removed no sooner than 13, 10 and 8 days after concrete casting at air temperature of −35, −25 and −15 °C, respectively.

Table 1 shows the chronology of the simulated and observed events examined in the analysis. Stress peaks on the 2nd day of both the removal of the tent (I peak) and the removal of the thermal insulation (II peak).

Figure 6 shows relationship between the period of the tent and the thermal insulation removal and the outside air temperature.

Table 1 Time of stress peaks due to removal of the tent and thermal insulation

T_{cp}, °C	Time, days			
	The tent removal	I peak	the thermal insulation removal	II peak
−35	8	10	13	15
−25	5	7	10	12
−15	4	6	8	10
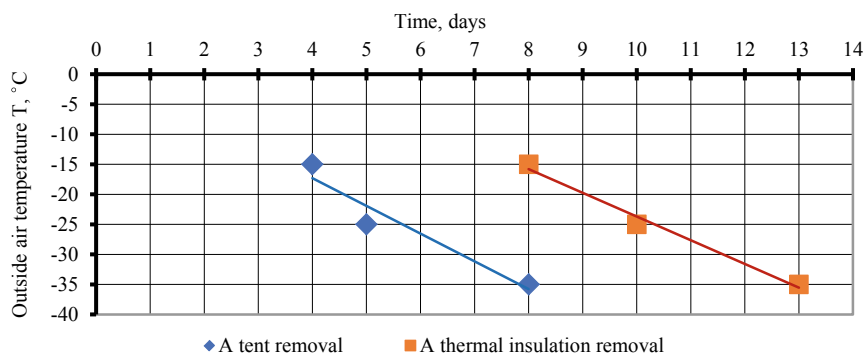
Fig. 6 Evolution of the time limits for the thermal protection elements removal at T = −15 °C, T = −25 °C, T = −35 °C.

The obtained linear dependence of the time limits for the tent removal (in days) is presented in the Eq. (6).

$$t = -0.216 \cdot T + 0.216 \tag{6}$$

where T is an outside air temperature, °C.

The results of determining the cooling rate at the set points located on the top and side surfaces of the slab at various outside air temperatures are presented further in this paper. Figure 7 shows evolution of cooling rate over time, taking into account successive removal of the tent and thermal insulation at outside air temperatures of −35 °C, −25 °C and −15 °C.

It can be concluded from Fig. 7 that the highest cooling rate is achieved on the top surface of the slab after the thermal insulation removal, and on the side surface after the tent removal. The cooling rate of the slab after removal of the tent is maximum at an outside air temperature of −35 °C. After removal of the thermal insulation, the cooling rate of the top surface remains ≈20 °C/day, and the side surface ≈12 °C/day, irrespective of the outside air temperature.

In case of simultaneous removal of the tent and thermal insulation, the cooling rate of the concrete mixture increases significantly, so the safe time limits for the thermal protection elements removal are 37, 18 and 12 days after concrete casting at air temperature of −35, −25 and −15 °C, respectively.
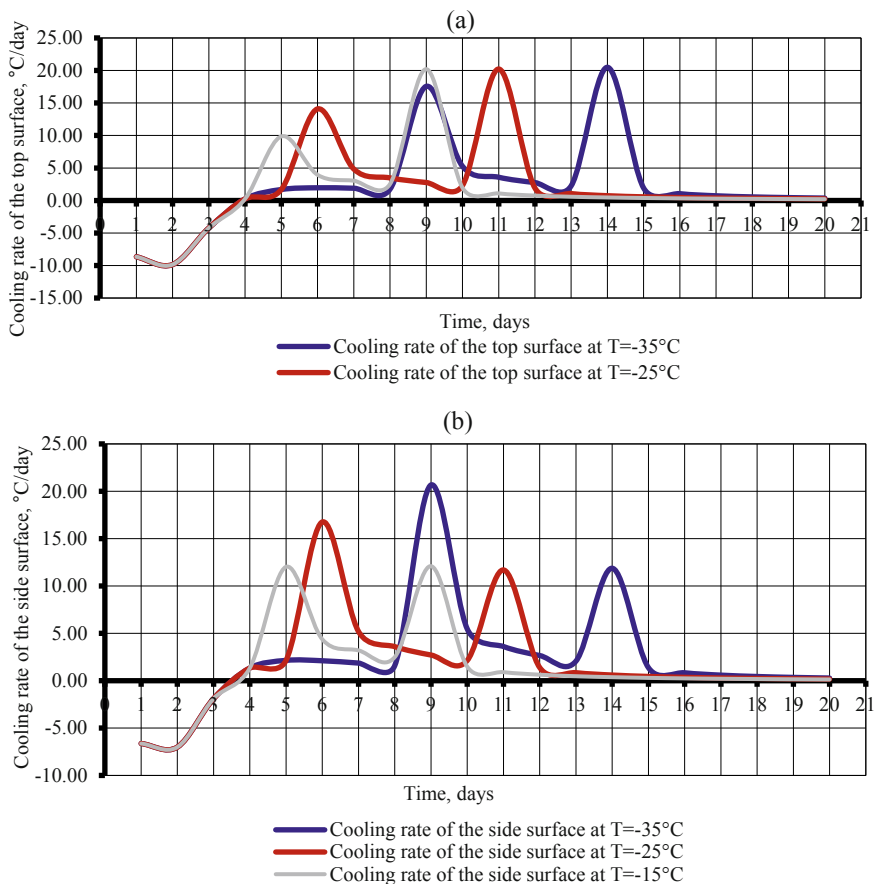
Fig. 7 The cooling rate: а) of the top surface of the slab; б) of the side surface of the slab

4 Discussion and Conclusion

The time of tent removal is linearly dependent on the outside air temperature. While removing the thermal protection elements, it is recommended to remove the tent first, and the surface thermal insulation should be removed 4–5 days later.

After the thermal insulation removal, the cooling rate on the top surface of the slab is 67% higher than the cooling rate on the side surface. As a consequence, the thermal stresses on the top surface of the slab exceed those on the side surface by 22%. Thus, the thermal stresses on the top surface of the plate are critical.

In the case of simultaneous removal of the tent and thermal insulation, the safe time limit of the thermal protection elements removal at −15 °C, −25 °C and −35 °C increases by 150%, 180% and 284% respectively.

The maximum values of thermal stresses are reached in two cases: A) during the maximum exothermic heating of the slab; B) during the occurrence of "core-surface" temperature difference during removal of the tent and thermal insulation due to the increased cooling rate of the concrete mixture. In the first case, the maximum stress of type A is 11 kPa, while in the second case, the maximum stress of type B is no more than 22 kPa and depends on the outside temperature.

Hazardous tensile stresses of type A can be decreased by installing special thermal insulation on the slab surface. Stresses of type B can be reduced by increasing the time limits of thermal protection elements removal. The maximum safe value of the mixture cooling rate equals 0.8 °C/hour and is practically independent of the outside air temperature. In this case the stresses of type B do not exceed the strength limit.

References

1. Lencis, U., Udris, A., Korjakins, A.: Frost influence on the ultrasonic pulse velocity in concrete at early phases of hydration process. Case Stud. Constr. Mater. **15**, e00614 (2021)
2. Korol, E., Kustikova, Y.: Constructive systems, load–bearing and enclosing structures of high–rise buildings. In: E3S Web of Conferences, vol. 33 (2018)
3. Sazonova, S., Nikolenko, S., Akamsina, N.: Consideration of temperature stresses in the calculation of crack formation in concrete massifs of buildings. In: IOP Conference Series: Materials Science and Engineering, vol. 1079 (3) (2021)
4. Shen, L., Ren, Q., Cusatis, G., Cao, M., Xu, L., Yang, Y.: Numerical study on crack thermal resistance effect on thermo–mechanical coupled behavior of concrete structure at room temperature. Int. J. Solids Struct. **182–183**, 141–155 (2020)
5. Shaibakova, A., Semenov, K., Barabanshchikov, Y.: Thermal cracking resistance of stacking concrete blocks. In: MATEC Web of Conferences, vol. 245 (2018)
6. Barabanshchikov, Y., Belkina, T., Semenov, K., Zimin, S., Akimov, S., Vatin N.: Reasons of cracks in floor slab panel. In: IOP Conference Series: Materials Science and Engineering, vol. 896, no. 1 (2020)
7. Xin, J., et al.: Evaluation of early–age thermal cracking resistance of high w/b, high volume fly ash (HVFA) concrete using temperature stress testing machine. Case Stud. Constr. Mater. **16**, e00825 (2022)
8. Ho, N., Nguyen, T., Bui, A., Huynh, T.: Temperature field in mass concrete at early–age: experimental research and numerical simulation. Int. J. Emerg. Technol. **11**(3), 936–941 (2020)
9. Mestnikov, A., Turantaev, G., Fedorov, V.: Mathematical model of the thermodynamic system during winter concreting of bored piles. In: E3S Web of Conferences, vol. 97 (2019)
10. Korablin, S., Nikolenko, S., Sazonova, S.: Modeling of temperature stresses in the foundation slabs of a building. Model. Syst. Process. **13**(1), 54–60 (2020)
11. Aniskin, N.A., et al.: Determination of the temperature field and thermal stress state of the massive of stacked concrete by finite element method. Vestnik MGSU **11**, 1407–1418 (2018)
12. Barabash, M., Romashkina, M., Bashynska, O.: Thermal stress state of reinforced concrete floor slab. Strength Mater. Theory Struct. **0**(103), 43–56 (2019)
13. Shlyakhtina, T.F., Ivankova, E.A., Popov, N.A.: Winter concrete: problems and solutions. In: IOP Conference Series: Earth and Environmental Science, vol. 751, no. 1 (2021)
14. Dugersuren, E., Titov, M.: Winter concreting process design improvement in modern construction. Vestnik Tomskogo gosudarstvennogo arkhitekturno–stroitel'nogo universiteta. J Constr. Archit. **3**, 159–168 (2018)
15. Korotchenko, I., Ivanov, E., Manovitsky, S., Borisova, V., Semenov, K., Barabanshchikov, Y.: Deformation of concrete creep in the thermal stress state calculation of massive concrete and reinforced concrete structures. Mag. Civil Eng. **69**(1), 56–63 (2017)

16. Zalevskii, E., Borisov, N., Abshoff, M., Simankina, T.: Digital model for monitoring temperature distribution during winter concreting. In: Vatin, N., Borodinecs, A., Teltayev, B. (eds.) Proceedings of EECE 2020, vol. 150, pp. 269–280. Springer, Cham (2021). https://doi.org/10.1007/978-3-030-72404-7_27
17. Lim, M.K., Nam, K.Y.: Comparative analysis on the micropore and microstructure characteristics of concrete under insulated formwork. Materials **14**(11), 2862 (2021)
18. Zhuravlyov, E.G.: Review and analysis of winter concreting methods, used on construction sites in Russia. In: IOP Conference Series: Materials Science and Engineering, vol. 880, no. 1 (2020)
19. Van Tang, L., Nguyen, T.C., Bulgakov, B., Pham N.A.: Composition and early–age temperature regime in massive concrete foundation. In: MATEC Web of Conferences, vol. 196 (2018)
20. Xin, J., et al.: Environmental impact and thermal cracking resistance of low heat cement (LHC) and moderate heat cement (MHC) concrete at early ages. J. Build. Eng. **32**, 101668 (2020)
21. Makeeva, A., Amelina, A., Semenov, K., Barabanshchikov, Y.: Temperature action in analysis of thermal stressed state of massive concrete and reinforced concrete structures. In: MATEC Web of Conferences, vol. 245 (2018)

Shear Crack Resistance of I-Shaped Concrete Beams with Basalt FRP Stirrups

Sergey Usanov and **Murat Tamov**

Abstract This paper presents the results of experimental research on the shear crack resistance of I-shaped beams with BFRP transverse reinforcement. The tested specimens had equal sizes and different angles of stirrups inclination, web reinforcement ratio, and shear span-to-depth ratio (a/d). The group with $a/d = 2.5$ and 3.2 also included beams with cold-drawn wire transverse reinforcement. The effect of varied parameters on the load of shear crack formation and the width of the cracks is analyzed. The maximum shear crack width in beams with inclined stirrups was slightly lower than that of beams with vertical stirrups. The corresponding difference in the crack width between twin beams differing only in the angle of stirrups inclination was up to 10% and was more pronounced for beams with $a/d = 3.2$. In most cases, the shear crack width for beams with BFRP transverse reinforcement does not exceed the permissible values established by the codes of different countries. The exceptions mainly comprised beams with the lowest web reinforcement ratio.

Keywords Crack resistance · I-shaped beams · Transverse reinforcement · Shear span · Basalt fiber reinforced polymers (BFRP) · Web-shear cracks

1 Introduction

Fiber-reinforced polymer materials have been used in industrial and civil construction for more than 50 years [1]. For a certain period, there was not much demand for the use of FRP due to the long and costly process of its manufacturing. Now a growing amount of research confirms the feasibility of using FRP [2, 3], and more consumption of FRP in the construction industry is forecast [4, 5]. FRP bars are produced using different fibers such as glass (GFRP), basalt (BFRP), carbon (CFRP), aramid (AFRP), and others placed in a polymer matrix. The matrix is a thermoset compound and usually consists of epoxy or vinyl ester. The advantages of FRP over steel include corrosion resistance, light specific gravity, high tensile strength, non-magnetic properties, etc.

S. Usanov (✉) · M. Tamov
Kuban State Technological University, Krasnodar 350072, Russia
e-mail: svusanov@gmail.com

Among the disadvantages are low modulus of elasticity, anisotropy, and the absence of a yield point [6, 7].

The use of FRP as transverse reinforcement instead of traditional steel reinforcement in flexural members affects their shear strength. The reduced modulus of elasticity of FRP leads to an increase of the width of shear cracks. This leads to a decrease of the aggregate mechanical interlock between the cracks and changes the magnitude of forces in the transverse reinforcement [8]. At the same time, it is known that in reinforced concrete beams the magnitude of the aggregate interlock forces is significant and can lie in the range of 33–50% of the shear capacity of uncracked concrete. Anisotropy, high tensile strength and the absence of a yield point also have an impact on the shear behavior of FRP-reinforced concrete members (FRP-RC members).

Most of the shear design methods implemented in building codes for FRP reinforced elements are similar to those used for steel reinforcement. At the same time, in most cases, codes do not contain methods for calculation of the shear cracking load or width of shear cracks only setting a general limit on the width of cracks in a member.

In the design guidelines of the American Concrete Institute (ACI 440.1R-15) for FRP-RC members the width of inclined cracks is limited by the maximum allowable stresses in the transverse reinforcement $E\varepsilon_{f,lim}$ (E is the modulus of elasticity of the FRP, $\varepsilon_{f,lim} = 0.004$ is maximum strain). A similar provision is adopted in the ACI code for the design of reinforced concrete (RC) structures [9].

Due to the absence, both past and present, in ACI 440 of permitted shear cracks width, researchers (for example, in [10]) take the limit set for flexural cracks width (ca. 0.5 mm) as such limit. This is higher than the maximum allowable crack width for RC elements -0.33 mm [9]. For FRP-RC members, a higher value of the maximum crack width is justified due to the high corrosion resistance of FRP and is set only to meet aesthetic requirements [11]. Shekhata et al. [10] showed that the strains of transverse reinforcement corresponding to the inclined cracks width of 0.5 mm are 0.2% for CFRP bars and 0.35% for GFRP bars. Thus it was suggested that the value of 0.2% ought to be accepted as a limit to control the width of shear cracks.

Russian design code SP 295.1325800.2017 also set the maximum tensile strength of FRP stirrups as $0.004E_f$ (also not exceed $0.5R_f$ or 300 MPa). The Institution of Structural Engineers (IstructE) guidance [11], which is a modification of the British codes BS8110 [12] and BS5400 [13], set the limit $\varepsilon_{f,lim}$ for FRP transverse reinforcement at 0.25% [14].

Possible adjustment to $\varepsilon_{f,lim}$ is still a subject of ongoing discussion. Pilakoutas et al. [15], Valivonis et al. [16], and El-Ghandour et al. [17] based on the results of their own and other researchers' tests suggest increasing $\varepsilon_{f,lim}$ up to 0.45%. Ahmed et al. [18] indicated that the measured maximum value of strains of the transverse reinforcement range from 1 to 2% for GFRP and from 0.8 to 1% for CFRP. Based on the test's results [19] Fiko et al. [8] proposed to set the maximum allowable value of $\varepsilon_{f,lim}$ depending on the type of fibers. For AFRP stirrups $\varepsilon_{f,lim}$ should not be taken more than 0.7%, for CFRP and GFRP stirrups – more than 0.35% and 0.85%, respectively.

Experimental researches of FRP RC members mainly include testing beams with a rectangular cross-section [20–23]. In [16] the author tested 4 twin specimens reinforced with GFRP transverse reinforcement. The longitudinal reinforcement of the beams consisted of steel rebars. The tests were carried out by three-point bending with $a/d = 1.4$. During the tests, shear cracks in all cases occurred later than flexural at loading levels in the range of 23.9–34.6% of the failure load. Said et al. [24] tested 10 beams with cross-sectional dimensions $120 \times 300(h)$ mm and GFRP bars as transverse reinforcement and longitudinal reinforcement of the tension and compression zones.

The stirrups in specimens were set at varying spacing. One of the beams had no transverse reinforcement. Flexural cracks within the zone with the largest bending moment appeared first. Then flexural cracks occurred in the shear span and grew into inclined cracks towards the load with increasing of the latter. The formation of inclined cracks took place within the range of 29.6–50.1% of the shear capacity. Before the failure, the width of the inclined cracks reached 1.5–3.5 mm. The cracking load and the shear capacity of the beams were calculated accurately by FE modeling using ANSYS software package.

Inclined cracks in I-shaped beams generally occur at midheight and subsequently develop towards the flanges. Such cracks are commonly called "web-shear cracks" whereas cracks in rectangular beams developing from tension flange are called "flexure-shear cracks" [25]. The amount of experimental data on the shear crack resistance of I-shaped beams with FRP reinforcement is significantly less than that for rectangular beams. Kurt et al. [26] tested 12 I-shaped beams (24 results for shear spans overall) reinforced with longitudinal and transverse FRP reinforcement. The specimens differed in concrete strength, type, diameter, and spacing of FRP transverse reinforcement. The measurement of the width of the inclined cracks was carried out by a non-contact optical 3D deformation measuring system Aramis and by using crack gauges. The author notes that the cracking pattern in the tested specimens is similar to that observed in RC beams. As the load increased the inclined cracks became flatter. Before the failure, the crack inclination angle ranged from 23 to 40 degrees. The maximum inclined cracks width reached 0.7–3.0 mm and the displacement along the cracks was 0.2–1.7 mm. Other authors [10, 18] carried out tests of T-shaped beams with FRP transverse reinforcement.

This paper studies the shear crack resistance with BFRP transverse reinforcement. To the authors' knowledge, the latter was never previously used for the research of web-shear cracking. In total twenty-eight I-shaped beams were manufactured and tested.
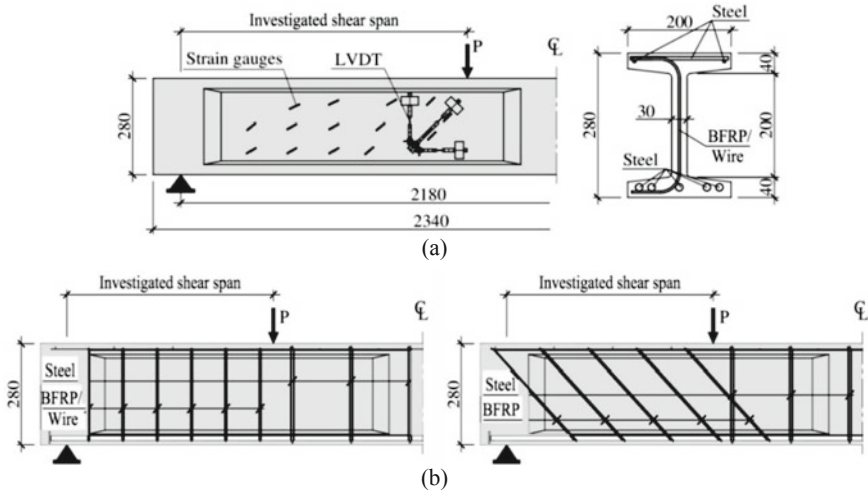
Fig. 1 Details of beams

2 Experimental Program

2.1 Test Specimens

Specimens had the total length 2340 mm (effective span 2180 mm) and total depth h = 280 mm (effective depth d = 260 mm). The flange width of the beams was 200 mm and the web width was 30 mm (Fig. 1a). The shear reinforcement of beams consisted of single bars anchored into the bottom and top flanges. Shear reinforcement was tied to longitudinal bars to form reinforcement cages. The beams differed in the angle of inclination of transverse FRP bars α_{sw} to the longitudinal axis and spacing of shear reinforcement (i.e. shear reinforcement ratio μ_{sw}). The group with shear span ratio a/d = 2.5 and 3.2 also included specimens with cold-drawn wire transverse reinforcement. Longitudinal reinforcement was identical for all beams (Fig. 1b). It consisted of steel bars Grade A500C in the amount sufficient to avoid flexural failure. Beams were tested in four-point bending with an a/d ratio equal to 1.6, 2.5, and 3.2. The list of beams, failure loads, and some parameters of crack resistance of beams are given in Table 1.

2.2 Material Properties

The beams were cast from normal strength concrete made of the M500 Portland cement (JSC "Verkhnebakansky cement plant", Novorossiysk). To ensure the good compaction of concrete for the web with small thickness, coarse aggregate with a

Table 1 Parameters of beams and shear test results

Beam	Type of stirrups	Q_{crc}, kN	α_{crc}, deg.	$\alpha_{crc\ cr}$, deg.	l_s, cm	$a_{crc\ ult}$, mm	Q_{ult}, kN	Mode of failure
B1.6-V-0.4	BFRP	7.7	33–39	39	3.9	0.46	54.9	WC
B1.6-V-0.7		7.5	32–39	35	3.1	0.48	57.6	WC
B1.6-V-1.0		14.7	41–43	41	3.5	0.44	77.4	WC
B1.6-V-1.3		16.4	36–42	36	3.1	0.63	71.5	WC
B1.6-N-0.4		13.6	40–42	40	4.8	0.78	61.7	WC
B1.6-N-0.7		13.1	44–48	45	3.2	0.33	62.1	WC
B1.6-N-1.0		14.5	38–41	38	3.4	0.44	76.2	WC
B1.6-N-1.3		13.4	44–47	44	3.1	0.39	70.5	WC
B2.5-V-0.4	BFRP	14.1	27–58	34	7.9	0.87	42.7	WC
B2.5-V-0.7		15.1	26–46	28	6.2	0.57	47.1	WC
B2.5-V-1.0		13.8	19–43	27	7.0	0.77	51.2	WC
B2.5-V-1.3		13.1	19–43	33	5.5	0.65	57.1	SR
B2.5-N-0.4		10.1	24–42	42	5.9	0.55	48.1	WC
B2.5-N-0.7		13.6	33–48	36	5.6	0.65	50.3	WC
B2.5-N-1.0		4.9	17–54	38	4.5	0.75	44.8	SR
B2.5-N-1.3		8.9	21–57	39	4.1	0.72	55.4	WC
BS2.5–1.0	Wire Vr500	15.6	33–46	35	5.0	0.35	65.1	WC
BS2.5–1.3		20.9	36–54	43	4.2	0.27	74.5	WC
B3.2-V-0.4	BFRP	6.8	24–48	25	4.5	0.98	42.5	SR
B3.2-V-0.7		11.2	28–49	42	3.6	0.60	48.7	WC/SR
B3.2-V-1.0		9.0	17–45	22	6.0	0.87	47.2	SR
B3.2-V-1.3		12.3	25–58	43	4.6	0.55	47.4	SR
B3.2-N-0.4		11.1	26–42	33	5.9	1.18	42.8	WC
B3.2-N-0.7		16.0	20–55	29	3.9	0.57	50.1	SR
B3.2-N-1.0		11.1	21–46	39	6.1	0.60	46.3	WC
B3.2-N-1.3		15.2	29–46	37	4.5	0.37	56.2	WC/SR
BS3.2–1.0		15.6	31–39	39	5.1	0.47	62.5	WC
BS3.2–1.3		19.8	32–45	40	4.1	0.30	70.8	WC

Note: α_{crc} – range of shear cracks angle; $\alpha_{crc\ cr}$ – angle of critical shear crack, l_s – average distance between shear cracks, WC - web crushing, SR – stirrups rupture

size of 3–10 mm was used for a concrete mix. The sand size modulus was 2.3, the content of clay and organic particles did not exceed 1.2%. The compressive strength of concrete was determined by testing prisms with the dimensions of $100 \times 100 \times 400$ mm at the age of 28 days and was in the range of $R_b = 24.1 \div 30.7$ MPa.

Basalt fiber-reinforced polymer bars with a diameter of 4 and 6 mm and cold-drawn wire with a diameter of 4.0 mm were used as transverse reinforcement of

specimens. For BFRP bars standard tensile tests were carried out according to GOST 31,938-2012 with the calculation of the ultimate strength σ_t, the modulus of elasticity E_f, and the elongation at fracture ε_t. Tested samples were straight BFRP bars with steel couplings on their ends designed for clamping these couplings with the grips of the tensile testing machine (Fig. 2). The elongation of the bars was measured with strain gauges. Obtained mechanical characteristics of BFRP bars are summarized in Table 2.

Bending of FRP rebars is possible only during their manufacturing. Precast C-shaped shear BFRP reinforcement with a diameter of 4 and 6 mm for our experiment was provided by LLC "NZK" (Nizhny Novgorod). It is known that a small mandrel diameter of FRP rods can lead to their premature rupture in the bent zones [15].

According to ACI 440.1R-15 [1], the radius of the bend should not be less than 3 diameters d_b of the bar. In Russian building code SP 295.1325800.2017, a similar minimum is set as $6d_b$. Some researchers recommend that the bending radius of the FRP should be at least $4d_b$, but not less than 50 mm [10]. In our research C-shaped BFRP bars (Fig. 3) had a bending radius equal to 35 mm, i.e. not less than the value specified by the aforementioned codes. As a result, the rupture of transverse reinforcement in the bent zone did not happen in any of the tested beams.

Fig. 2 BFRP rods before and after standard tensile tests

Table 2 Mechanical properties of BFRP bars

Bar diameter, mm	Tensile strength σ_t, MPa	Tensile strain ε_t, %, not less than	Modulus of elasticity E_f, MPa
4	1305	1.98	65,916
6	1377	2.07	66,524

Fig. 3 C-shaped BFRP transverse reinforcement

Table 3 Mechanical properties of wire Vr500 bars

Bar diameter, mm	Proof strength $\sigma_{0.2}$, MPa	Tensile strength σ_{vr}, MPa	Elongation per unit length, %, not less than	Var. coeff. of tensile strength ν_{vr}, MPa	Modulus of elasticity E_f, MPa
4.0	664	706	2.6	0.078	$2.01 \cdot 10^5$

Mechanical characteristics of wire Vr500 were determined according to GOST 12,004-81. For testing 15 samples were taken from the same bundle, which meets the requirements of GOST 6727-80. The average values of the mechanical characteristics of wire are given in Table 3.

## 2.3 Instrumentation, Test Setup and Procedure

The beams were tested in a closed load-bearing frame in the structural laboratory of the Department of building structures of Kuban State Technological University. The specimens were placed with compressed flange down which made the control of formation and development of cracks more convenient. The load was provided by a hydraulic jack connected to a pump station. The magnitude of the support reaction was monitored by load cells. Deflections of beams on supports and in the middle of the span were measured by high-sensitivity strain gauge displacement transducers. Concrete strains within the shear span were measured with strain gauges glued along the assumed direction of principal compressive stresses. Three LVDT sensors were attached in the form of a rosette at the expected location of an inclined crack on one side of the beams for measuring strains. Another LVDT sensor on the opposite side of the beam measured the displacement along the shear crack. All measuring devices were connected to the TDS-530 data logger (TML).

3 Results and Discussion

No relationship between the shear force at first cracking Q_{crc} and the angle of inclination α_{sw} of the transverse reinforcement was found (Fig. 4). For both vertical and inclined shear reinforcement (Fig. 4a and 4b), Q_{crc} was about 10–33% of the failure load Q_{ult}. For beams with steel reinforcement (Fig. 4c) Q_{crc} was 15.6–20.9 kN (24–28.1% of Q_{ult}).

Analysis of the test results revealed the following patterns for the Q_{crc} value:

– with an equal value of μ_{sw} inclined cracks in beams with steel transverse reinforcement occurred at higher loads than in FRP RC beams. On average, for beams with steel transverse reinforcement Q_{crc} was 54% larger;
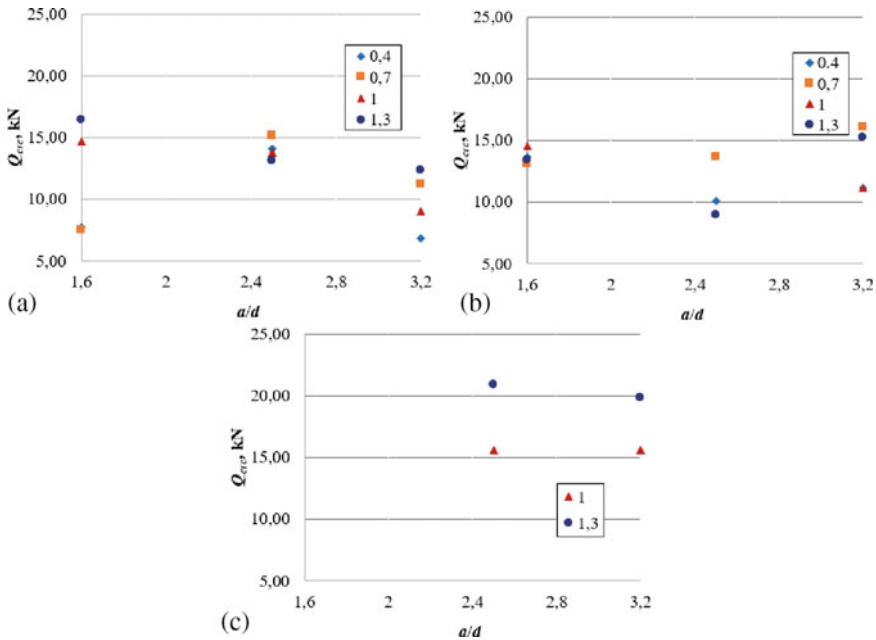
Fig. 4 Shear force at first web cracking for the FRP RC beams with inclined (a) and vertical (b) stirrups and for the RC beams (c)

– with an increase in *a/d* the Q_{crc} decreased. When *a/d* changes from 1.6 to 2.5, the decrease of Q_{crc} is more evident than when in the range of *a/d* from 2.5 to 3.2 for all angles of inclination of the FRP stirrups. In the latter case, for samples with inclined FRP stirrups, there is virtually no decrease of the Q_{crc}.

Cracks in specimens with FRP transverse reinforcement formed mainly at the midheight and propagated to the flanges (web-shear cracks). In most cases, the first shear cracks were located in the middle of the shear span, less often in areas close to the load. As a rule, cracks reached the flanges of the beams several steps after their emergence, but in some cases, they immediately propagated through the entire height of the web. One to three cracks in the shear span initially occurred, the total number of cracks in the shear span in most cases did not exceed 6–8.

During loading with a small shear span (*a/d* = 1.6) cracks occurred parallel to each other, forming 1–2 concrete struts in the direction between the load and the support. In specimens with *a/d* = 2.5 and 3.2 in the areas close to the supports and the loading points, cracks had a fan-shaped pattern, and in the middle of the shear span, the cracks were parallel to each other.

Some crack resistance characteristics of beams are shown in Table 1. The range of values for the maximum shear crack width $a_{crc,ult}$ before the failure was 0.44–0.98 mm for beams with vertical FRP stirrups, 0.33–1.18 mm for inclined FRP stirrups, and 0.27–0.47 mm for specimens with steel stirrups (Fig. 5).
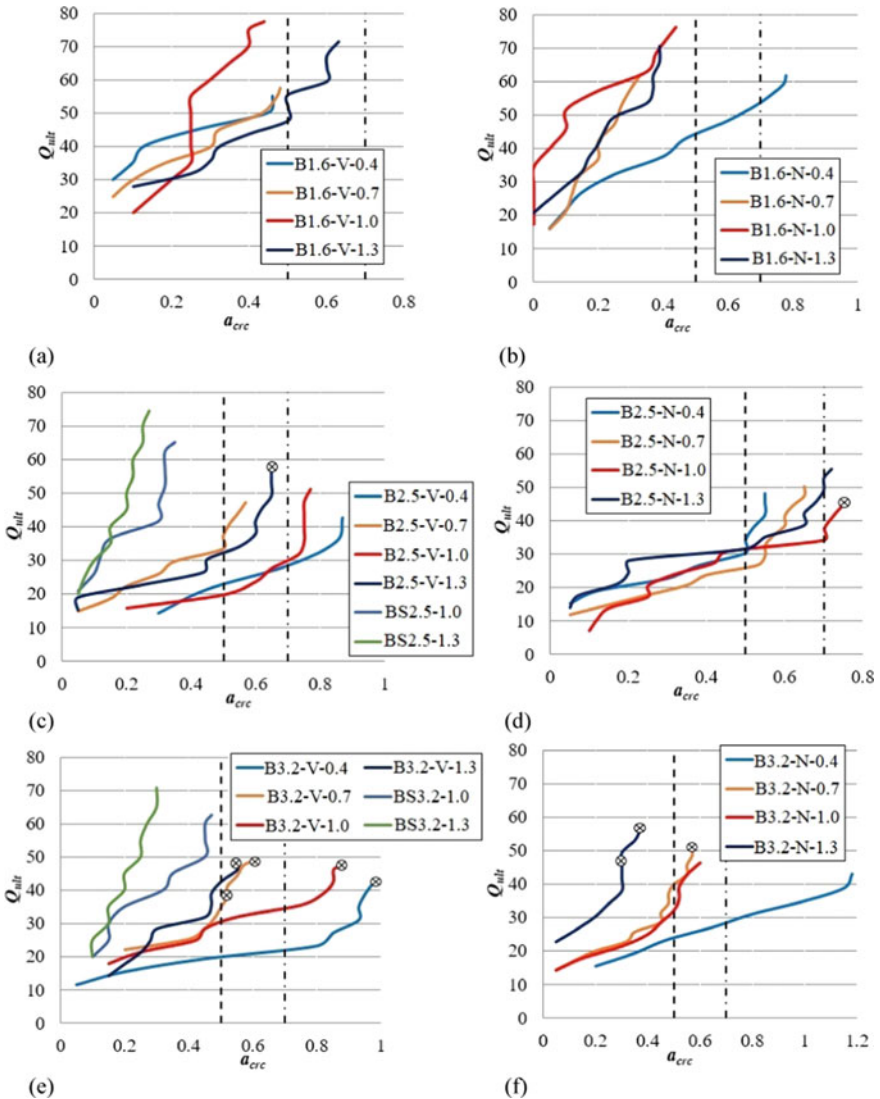
Fig. 5 Shear crack widths of the specimens

The shear crack spacings decreased with an increase in the percentage of transverse reinforcement and ranged from 3.1 to 7.9 cm for FRP RC beams and from 4.1 to 5.1 cm for steel RC members.

As can be seen from Table 1, the angle of the shear cracks' inclination to the longitudinal axis of the FRP RC beams was in the relatively wide range of 17–58 degrees. Critical shear cracks formed at an angle of 22–45 degrees. For specimens with steel transverse reinforcement, these angles were in the range of 31–54 degrees

and 35–43 degrees, respectively. Thus, the angles of inclination of the critical shear cracks correspond to the values provided by the truss analogy adopted in the standards of the American Concrete Institute [1, 9] and Eurocode [27].

The previous research conducted in KubSTU showed that the crack width in I-shaped beams with steel and mesh shear reinforcement increased with increasing the shear span, and the relationship was nonlinear [28]. For our beams, with the change shear span from $1.6d$ to $2.5d$ maximum crack width increased on average 1.47 and 1.84 times for the vertical and inclined FRP transverse reinforcement respectively. With a further increase of shear span up to $3.2d$, the growth of maximum crack width $a_{crc,ult}$ was less noticeable, and in one case, for beam B3.2-N-1.3, the $a_{crc,ult}$ was smaller than for a similar beam tested with a smaller shear span $2.5d$.

The values of $a_{crc,ult}$ in beams with inclined stirrups were slightly lower than those of the specimens with vertical stirrups. The corresponding difference of $a_{crc,ult}$ between twin beams differing only in α_{sw} was up to 10% and was more pronounced for beams with $a/d = 3.2$. This is explained by the fact that with an inclined arrangement of shear reinforcement, its angle with respect to the web cracks approaches 90º, and thus the development of tensile strains is better restrained.

In Fig. 5 it can be seen that the maximum crack width for FRP RC specimens, most times did not exceed 0.8 mm, in some tests reaching a value of 1–1.2 mm. In latter cases, the failure occurred mainly due to the rupture of the stirrups. Beams with wire transverse reinforcement showed a smaller value of the $a_{crc,ult}$, averaging 0.35 mm with a maximum value of about 0.5 mm.

4   Conclusion

There is no unified approach in different building codes for FRP-RC members to assign the allowable crack width. The Russian SP 295.1325800.2017 "Concrete structures reinforced with fiber-reinforced polymer bars. Design rules" establishes the following allowable values of crack width: for short-term opening 0.7 mm, for long-term opening −0.5 mm (shown with vertical lines in Fig. 5). In Japanese [29] and Italian [30] codes, the allowable crack width is set at 0.5 mm. Canadian guidelines [31] the limit is 0.5 mm for structures exposed to harsh conditions and 0.7 mm for other cases. These requirements are mainly aimed at restricting the width of flexural cracks. The values of the maximum web-shear cracks width of the tested I-shaped FRP-RC beams demonstrate that even at high loads $a_{crc,ult}$ in most cases is less than the specified limit values. Significant (up to 30%) exceedance of those limits are cracks in beams with the lowest shear reinforcement ratio. Taking into account also the fact that the crack resistance calculations are made for the service loads, the openings of the inclined cracks observed in our tests can be considered acceptable. Thus, the relatively lower elastic modulus of FRP should not be considered a shortcoming hampering its use as shear reinforcement of I-shaped beams.

References

1. ACI 440.1R-15. Guide for the design and construction of structural concrete reinforced with fiber-reinforced polymer bars. American Concrete Institute, p. 88 (2015)
2. Zhang, T., Oehlers, D.J., Visintin, P.: Shear strength of FRP RC beams and one-way slabs without stirrups. J. Compos. Constr. **18**, 04014007 (2014)
3. Razaqpur, A.G., Spadea, S.: Shear strength of FRP reinforced concrete members with stirrups. J. Compos. Constr. **19**(1), 04014025 (2015)
4. Peng, F., Xue, W., Xue, W.: Database evaluation of shear strength of slender fiber-reinforced polymer-reinforced concrete members. ACI Struct. J. **117**(3), 273–282 (2020)
5. Zaman, A., Gutub, S.A., Wafa, M.A.: A review on FRP composites applications and durability concerns in the construction sector. J. Reinf. Plast. Compos. **32**(24), 1966–1988 (2013)
6. El-Sayed, A.K., Soudki, K.: Evaluation of shear design equations of concrete beams with FRP reinforcement. J. Compos. Constr. **15**, 9–20 (2011)
7. Issa, M.A., Ovitigala, T., Ibrahim, M.: Shear behavior of basalt fiber reinforced concrete beams with and without basalt FRP stirrups. J. Compos. Constr. **20**(4), 1–10 (2016)
8. Fico, R., Prota, A., Manfredi, G.: Assessment of Eurocode-like design equations for the shear capacity of FRP RC members. Compos. B Eng. **39**(5), 792–806 (2008)
9. ACI 318–19. Building code requirements for structural concrete. American Concrete Institute, p. 628 (2019)
10. Shehata, E., Morphy, R., Rizkalla, S.: Fibre reinforced polymer shear reinforcement for concrete members: behaviour and design guidelines. Can. J. Civ. Eng. **27**, 859–872 (2000)
11. IstructE. Institution of structural engineers. interim guidance on the design of reinforced concrete structures using fibre composite reinforcement. SETO Ltd., p. 96 (1999)
12. BS 8110–1: 1997. Structural use of concrete. code of practice for design and construction, Part 1. British Standard Institution, p. 135 (1997)
13. BS 5400–4: 1990. Steel, concrete and composite bridges. Code of practice for design of concrete, Part 4. British Standard Institution, p. 61 (1990)
14. Fib Bulletin No. 40. FRP reinforcement in RC structures. International Federation of Structural Concrete, p. 160 (2007)
15. Pilakoutas, K., Guadagnini, M., Neocleous, K., Matthys, S.: Design guidelines for FRP reinforced concrete structures. P. I. Civil. Eng-Civ. En. **164**, 255–263 (2011)
16. Valivonis, J., Budvytis, M., Atutis, M., Atutis, E., Juknevicius, L.: Study on shear resistance of fiber reinforced polymer–reinforced concrete beams. Adv. Mech. Eng. **7**, 1–17 (2015)
17. El-Ghandour, A.W., Pilakoutas, K., Waldron, P.: Punching shear behavior of FRP RC flat slabs part 1: experimental study. J. Compos. Constr. **7**(3), 258–265 (2003)
18. Ahmed, E.A., El-Salakawy, E.F., Benmokrane, B.: Shear performance of RC bridge girders reinforced with carbon FRP stirrups. J. Bridg. Eng. **15**, 44–54 (2010)
19. Nagasaka, T., Fukuyama, H., Tanigaki, M.: Shear performance of concrete beams reinforced with FRP stirrups. ACI SP **138**, 789–811 (1993)
20. Barris, C., Torres, L., Mias, C., Vilanova, I.: Design of FRP reinforced concrete beams for serviceability requirements. J. Civ. Eng. Manag. **18**(6), 843–857 (2012)

21. Fayyadh, M.M., Razak, H.A.: Analytical and experimental study on repair effectiveness of CFRP sheets for RC beams. J. Civ. Eng. Manag. **20**(1), 21–31 (2014)
22. Tureyen, A.K., Frosch, R.J.: Shear tests of FRP-reinforced concrete beams without stirrups. ACI Struct. J. **99**(4), 427–434 (2002)
23. Oller, E., Mari, A., Bairan, J.M., Cladera, A.: Shear design of reinforced concrete beams with FRP longitudinal and transverse reinforcement. Compos. B **74**, 104–122 (2015)
24. Said, M., Adam, M.A., Mahmoud, A.A., Shanour, A.S.: Experimental and analytical shear evaluation of concrete beams reinforced with glass fiber reinforced polymers bars. Constr. Build. Mater. **102**, 574–591 (2016)
25. Wight, J.K., MacGregor, J.G.: Reinforced Concrete: Mechanics and Design, 6th edn. Pearson Education Inc., Upper Saddle River, New Jersey (2012)
26. Kurth, M., Hegger, J. Experimental and theoretical study on shear capacity of concrete beams with FRP reinforcement. In: 6th International Conference on FRP Composites in Civil Engineering, Italy, pp. 1–2 (2012)
27. Eurocode 2. Design of concrete structures – Part 1–1: general rules and rules for buildings. European Committee for Standardization, p. 230 (2004)
28. Pochinok, V.P., Greshkina, E.V., Tamov, M.M.: Finite element modeling of complexly stressed reinforced concrete structures. In: Vatin, N., Roshchina, S., Serdjuks, D. (eds.) Proceedings of MPCPE 2021. Lecture Notes in Civil Engineering, vol. 182, pp. 161–171. Springer, Cham (2022). https://doi.org/10.1007/978-3-030-85236-8_13
29. JSCE. Recommendation for design and construction of concrete structures using continuous fiber reinforcing materials. Research Committee on Continuous Fiber Reinforcing Materials, Japan Society of Civil Engineers, p. 503 (1997)
30. CNR-DT 203/2006. Guide for the design and construction of concrete structures reinforced with fiber-reinforced polymer bars. National Research Council, p. 35 (2006)
31. CAN/CSA S6–06. Design and construction of building components with fibre-reinforced polymers. Canadian Standards Association, p. 218 (2002)

Control Tests of Long-Span Laminated Timber Structures with Nodes on the Glued-In Rods

Aleksandr Pogoreltsev

Abstract Large-span laminated wooden structures have large dimensions and require the creation of knots and joints to divide the structures into technological elements, convenient for manufacturing and installation. This problem is solved by using both traditional and new types of knot joints.

New types of knots include connections on glued rods. If in Europe there was the way to create knots with rods glued along the fiber of the wood, or along and across the fiber, in Russia the focus was on the knots of laminated wooden structures with reinforcing rods glued at an angle to the fiber of the wood.

Under the leadership of S.B. Turkovsky the systems of knotted connections on glued rods - "CNIISK systems" were developed. Hundreds of objects were built using this system.

Such objects often require control tests. In most cases, the tests are not performed on structures, but on fragments with assemblies in full size. The rationale and purpose of control tests are given.

Examples of control tests during the construction of long-span buildings and structures with glued wood frameworks, carried out by the laboratory of wooden structures of the Kucherenko Central Research Institute of Scientific and Technical Cybernetics under the guidance of V.A. Kucherenko Institute of Wooden Architecture and Construction are given.

Keywords Large-Span Wooden Structure · Control Tests · Glued Reinforcing Bar · Knot

1 Introduction

Glued wood structures combine lightness, strength, aesthetics, corrosion resistance and other positive characteristics. They allow you to implement a variety of architectural forms and gives an expressive visual effect in combination with other

A. Pogoreltsev (✉)
JSC Research Center Construction (Kucherenko TSNIISK), Moscow, Russia

modern building materials. Glued laminated wooden structures are widely used in construction of long-span buildings and constructions.

Elements of large-span laminated wooden constructions can have a great length, which causes difficulties in production and transportation. Especially it concerns bent laminated elements of arches, frames, meridional ribs of domes and other constructions.

There is a necessity to divide long structures into technological elements with implementation of consolidating rigid joints.

A typical solution adopted in Europe is the use of rigid joints with dowels or screws [1], including nodes with steel pads and spacers.

In the second half of the last century the research and practical application of wooden structure joints on glued rods began.

The first application of steel rods glued into the wood along the fibers in the nodes was proposed in the SoyuzDorNII [2]. Later, similar structural solutions were widely investigated abroad [3, 4] and others.

Abroad, the study of knots paid more attention to rods with metric threads along the entire length, glued along the fibers [5–7], and those glued at an angle to the fibers were considered to strengthen wooden constructions [8, 9]. In the USSR and later in Russia, the corrugated reinforcement rods for reinforced concrete structures, glued at an angle to the fibers, were considered first of all for the joints.

The first tests of the rigid beam joint on angled glued rods were carried out by S. B. Turkovsky in 1975. Although the joint was located in the area of maximum bending moment, the failure of the beam occurred outside the joint.

The complex system of node joints of wooden structures on inclined glued rods - CNIISK system - was developed under the supervision of S.B. Turkovskiy [10–18]. A particular case of inclined glued rods were rods glued perpendicular to the fibers.

Hundreds of objects, including large-span ones, have been built using the "TSNIISK system" [19].

2 Control Tests

When designing large-span laminated timber structures with nodes on glued rods, it is sometimes necessary to conduct control tests. The justification for the necessity of testing QDC nodes is as follows:

- structures of unique structures with spans over 100 m, heights over 100 m, with cantilevered structures over 20 m;
- buildings and structures of especially hazardous and technically complex objects, the list or classification of which is established by the national legislation;
- Buildings and constructions with design and construction using brand new design solutions and technologies which have not been tested in construction practice and operation (experimental designs);
- nodes of critical structures in the process of mastering the production;

– large-span structures with manufacturing and (or) assembly defects.

The reasons for the necessity of control tests of glued wood constructions with nodes on the glued rods are often the set of the reasons described above.

Control tests of full-size long-span structures are carried out in rare cases. Usually the bearing capacity of such structures is determined by the bearing capacity of nodes. Therefore, tests are performed on the most loaded or poorly studied nodes. The test objectives are determined depending on the reason for the verification tests:

– Determining the bearing capacity of a structure or assembly in the absence of standard calculation methods;
– assessment of the correctness of the design solutions and calculation assumptions;
– verification of manufacturability of nodes on glued rods;
– quality control of structural fabrication;
– Verification of assemblage ability and quality control during assembly;
– expert evaluation of causes of structural failures.

Often the control tests are complex and include several objectives. When testing by the specialists of V.A. Kucherenko Central Research Institute of Nuclear Power Engineering, there are always additional objectives - issues of research on the operation of knotted joints on glued rods.

3 Examples of Control Tests

Let's consider the experience of the control tests conducted by the staff of the Central Research Institute of Building Research named after V.A. Kucherenko.

3.1 The Main Building of the Country Hotel in the Village of Lipki

The three-story building has a near-circular shape in plan and is blocked by multispan beams set at radii with a 2.8° slope on straight sections. The largest diameter of the building is about 100 m.

All roofing girders were made of unified elements with 140×1100 mm cross-section, up to 20 m long, supplied at the factory with embedded parts of the same type at the ends, which turned these elements into continuous multispan beams by means of welding at assembling (see Fig. 1). Slanted glued rods with a gluing depth greater than the design depth were used to anchor the support plates. This ensured that the glued package was safeguarded against possible delamination and defects in the support areas, and compensated for some weakening of the glue joint during welding.
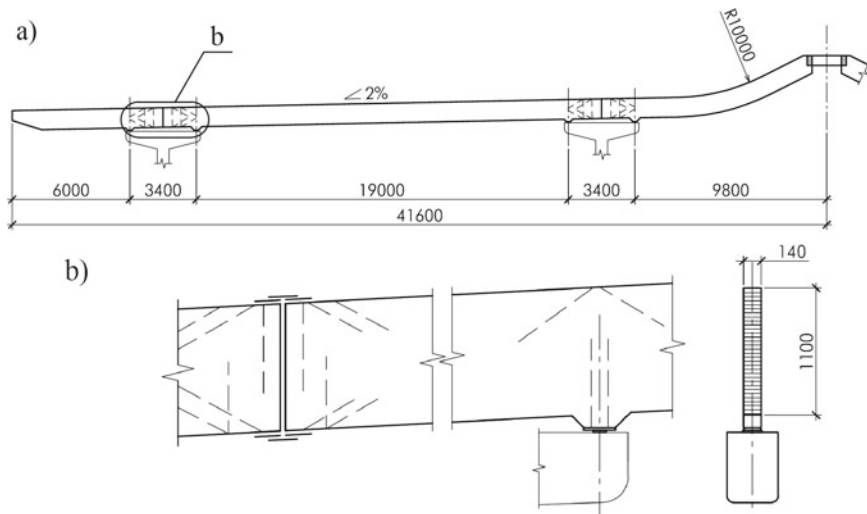
Fig. 1 Covering beams in Lipki: **(a)** scheme of the continuous multispan girder; **(b)** structural scheme of the rigid joint and support node

The most critical in the design of beams were the rigid joints on inclined glued rods, which were first used in the practice of large-span buildings construction. Since beams with joints were experimental designs and the Volokolamsk Factory was mastering the production of joints on inclined glued rods, control tests were conducted until the failure of the full-scale fragment with a rigid joint (see Fig. 2).

The joint failure was caused by the loss of stability of the steel butt-joint lining in the compressed zone with a load of more than 1.6 times higher than the design load, which, taking into account the test time, is more than required.

The general view of the coating at the installation stage is shown in Fig. 3.

3.2 Farms at the Manezh Exhibition Center, Moscow

The historical trusses of the Central Exhibition Hall (CEH) "Manezh" were designed and installed in 1817 by the Russian engineer A. A. Betancourt on the initiative and with the assistance of Emperor Alexander I.

The 48-m span trusses made of 260 × 350 mm beams and up to 10 m long were the finest engineering work of that time and were the first of their kind in the world to be registered with UNESCO as a great engineering achievement. On March 14, 2004, all wooden structures, including the unique trusses, were destroyed by fire.

At a meeting of the Architectural Council of Moscow, held soon after the fire, the task of restoring the Manezh Central Exhibition Hall was set. It took six months to
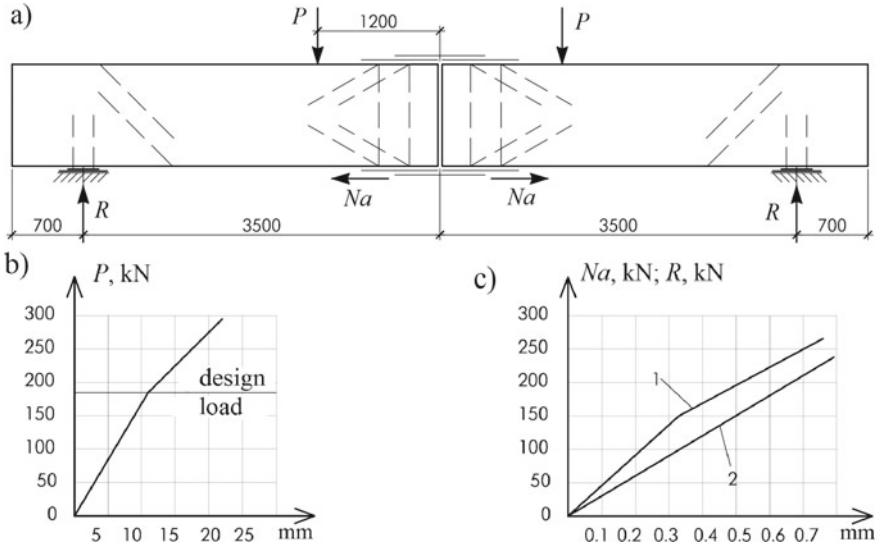
Fig. 2 Testing of a rigid joint: **(a)** an experimental fragment; **(b)** dependence of deflections in the middle of the span on the load P; dependence of the embedded part displacement on the force Na in it (1) and the movement of the support joint relative to the wood on the support reaction R (2)
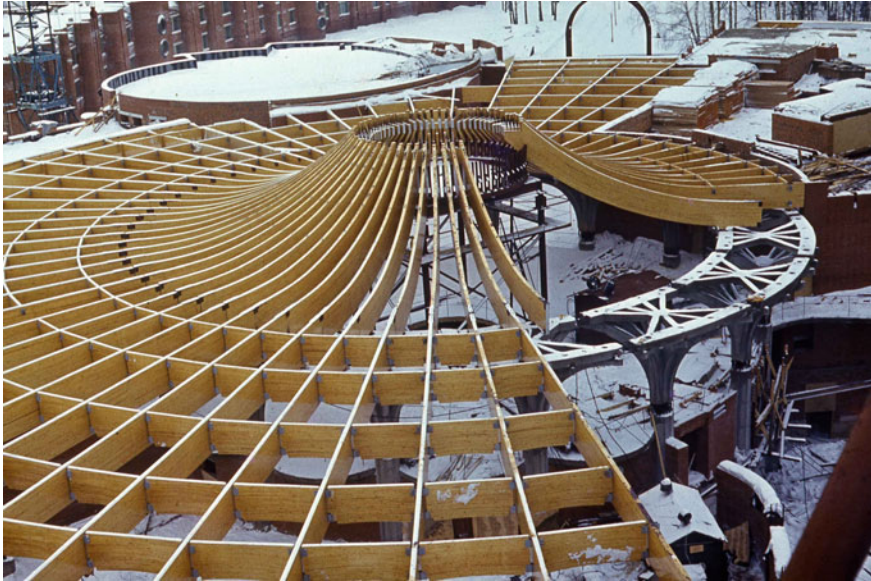
Fig. 3 General view of the coating at the installation stage

design, produce, assemble and install. The frames were to be made of glued wood preserving the structure, geometry and external similarity.

The project design was preceded by the experimental-design works on a variant selection, testing and refinement of manufacturing techniques of the most responsible truss components (supporting, ridge and bottom chord joints).

For the control tests, there was a prototype made in the form of a triangular sill-less truss with a span of about 8 m and the cross-sections and junctions of full-size (see Fig. 4). The support nodes of the model differed from each other in design. One node was made with a steel bottom chord as a stop on the end of the top chord. The other node was made according to "CNIISK system" in the form of a wooden chord with a steel support for the upper chord on V-shaped anchors - rods glued at angles of $+45°$ and $-45°$ to the direction of wood fibers of the lower chord. The ridge knot was also made on glued rods. The bottom chord consisted of two parts - one steel, the other wooden with a rigid joint on glued V-shaped anchors in the middle of the span.

The design load was 820 kN. The loading was carried out up to the collapse in a press equipped with a special traverse (see Fig. 4a).

At the first stage, loading was performed three times to the design load. The test results showed elastic operation of the assemblies.

Further testing was carried out until failure by stepwise increasing load. Failure occurred under 1200 kN load from loss of stability of curvilinear part of compressed, and rupture of tensile bonded rods of V-anchors in the support node stop. In other nodes and in the junction of the lower chord, there were no signs of failure, including in the ridge node, tested by a special method of one-sided load. The sufficient bearing capacity of the main nodes and joints was confirmed by experiment.

When designing the trusses, the support node, by which the collapse occurred, was rejected and the node with emphasis on the end of the upper chord was adopted. In October 2004, the installation of the new roof trusses was completed (see Fig. 5).

3.3 L-shaped Trusses with a Span of 48 m

In the Palace of Sports in Strogino in the covering of the main hall for figure skating the unique for its time (2005) lenticular trusses from laminated wood 48 m long were used (see Figs. 6 and 7).

In static terms, the lenticular trusses are characterized by almost identical forces in all panels of both chords along the length of the span. The forces in the lattice are relatively small. This greatly simplifies their design. But the greatest shear forces between the girders are concentrated in the support nodes, which traditional connections have not been able to absorb before, even for the mid-span trusses. The problem was solved by the use of connections on inclined glued rods.

Supporting rigid units of prefabricated truss liners with spans over 24 m are usually assembled in the factory. Joints of compressed and stretched chords and lattice nodes are assembled. Joints on the glue of the outermost elements of the upper and lower

(a)

(b)   (c)

Fig. 4 Control tests of the experimental sample of the TSVZ "Manezh" truss: **(a)** general view; **(b)** loss of stability of the compressed rod at failure; **(c)** rupture and pulling out of the stretched bar

chords with different directions of wood fibers are performed in the factory, are unreliable. The design assumes that the glue joint is delaminated. Along the joint, glue rods are installed obliquely to replace the glue joint.

When designing, it was taken into account that 48 m is the maximum span of trusses in Russia with wooden upper and lower chords. This caused the necessity of control tests. The purpose of tests were to evaluate the correctness of the taken design solutions and design assumptions, to check the manufacturing quality of glued wooden elements, to evaluate the deformability of tensile joints on inclined glued

Fig. 5 Assembly of the Manezh Central Exhibition Hall trusses

Fig. 6 Figure skating competition hall
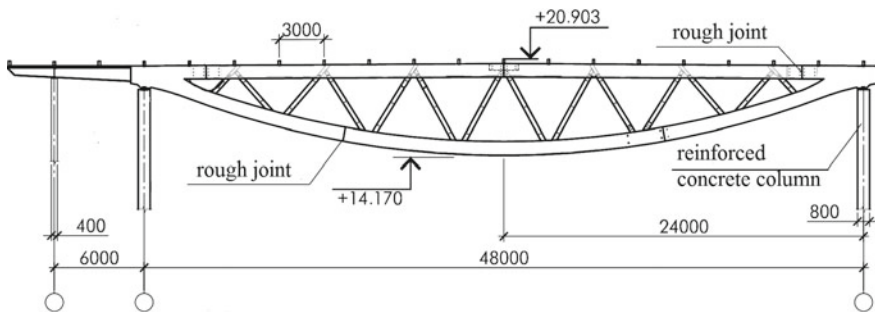
Fig. 7 Design diagram of a lenticular truss with a span of 48 m

rods, to study the stress–strain state of the junction zone of the upper and lower chords.

A block of two trusses taken from a set of fabricated structures having the largest number of manufacturing defects was subjected to the test (see Fig. 8a) [20]. The design load was 1500 kN. The loading mode was adopted as staggered by 20% of design load, which amounted to 300 kN. The loading was carried out by reinforced concrete foundation blocks and piles. At each stage, readings of deflectometers, strain gauges, and load cells glued in the supporting zone were recorded (see Fig. 8b).

When the load reached 1800 kN, or 1.2 of the design load, the welded joints of the bonded reinforcing bars and the steel plate in the support assembly failed. The assembly was strengthened without removing the load.

(a)

(b)   (c)

Fig. 8 Control tests of a block of two lenticular trusses with a span of 48 m: **(a)** general view in the process of loading; **(b)** load cells in the supporting zone; **(c)** pushing through the bars with subsequent crushing on the support

The tests were continued the next day. Failure occurred at a holding step of 2700 kN, or 1.8 of the design load. The cause of the failure was the penetration of the glued rods in the truss support node (Fig. 8c).

The test results showed that all the nodes on the glued rods, except for the support rods, met the load-carrying capacity requirements. Modifications were made to the support assemblies of all subsequent trusses to prevent failure of the welded joints.

4 Conclusion

Joints on glued rods including "CNIISK system" are an effective type of joints for large-span glued wooden constructions.

Conducting control tests of large-span structures and, first of all, control tests of knots make it possible to determine the actual load-bearing capacity, to confirm the correctness of the design decisions and calculation assumptions made, the quality of manufacturing, to assess the causes of structural failure, etc.

Such tests increase the safety of laminated wooden structures of critical buildings and constructions.

References

1. CEN EN 1995-1-1-2004 Eurocode 5: Design of timber structures - Part 1-1: General - Common rules and rules for buildings
2. Pospelov, I.D., Tumas, G.V.: On new glue joints of load-bearing elements of wooden bridge spans, Scientific report. SoyuzDorNII, Moscow 43 (1970)
3. Duchoň, V., et al.: Experimental test of timber connections with glued-in rods in bending. Wood Res. **61**(4), 567–572 (2016)
4. Gaunt, D.: Joints in glulam using groups of epoxy-grouted steel bars. NZ Timber Des. J. **26**(1), 34–38 (1999)
5. Steiger, R., Gehri, E., Widmann, R.: Pull-out strength of axially loaded steel rods bonded in glulam parallel to the grain. Mater. Struct. **40**, 69–78 (2007)
6. Gerold, M.: Verbund von holz und gewindestangen aus stahl. Bautechnik **69**(4), 167–178 (1992)
7. Gustafsson, P.-J, Serrano, E., Aicher, S., Johansson, C.-J.: A strength design equation for glued-in rods. In: International RILEM Symposium on Joints in Timber Structures, pp. 323–332. Stuttgart (2001)
8. Steiger, R., et al.: Strengthening of timber structures with glued-in rods. Constr. Build. Mater. **97**, 90–105 (2015)
9. Jockwer, R., Serrano, E.: Glued-in rods as reinforcement for timber structural elements. In: Branco, J., Dietsch, P., Tannert, T. (eds.) Reinforcement of Timber Elements in Existing Structures: State-of-the-Art Report of the RILEM TC 245-RTE, pp. 29–49. Springer International Publishing, Cham (2021). https://doi.org/10.1007/978-3-030-67794-7_3
10. Turkovsky, S.B.: Designing of glued wood structures joints on glued-in bars. In: Proceedings of CIB-W18 Meeting 22, Berlin, Germany, Paper CIB-W18A/22-7-3 (1989)
11. Turkowsky, S.B., Lukyanov, E.I., Pogoreltsev, A.A.: Use of glued-in bars for reinforcement of wood structures. In: Report for International Timber Engineering Conference, 2–5 September 1991, London, UK, vol. 3, pp. 3212–3217 (1991)

12. Frolov, A.Y., Pranov, B.M., Naichuk, A.Y.: Deformability of joints on glued steel rods working on punching. Izv. Vuzov. Constr. Architect. **8**, 17–20 (1990)
13. Pogoreltsev, A.A.: Calculation of tension joints of laminated wood structures at pasted in bars. Struct. Mech. Anal. Constr. **4**(249), 28–33 (2013)
14. Turkowski, S., Pogorelcev, A.: Złącza konstrukcjidrewnianych na sworznie wklejane. In: Drewno I materiały drewnopochodne w konstrukcjach budowlanych. V konferencja naukowa. Referaty. Szczecin, 17–18 maja 2002 r, pp. 169–176. Politechnika Szczecińska–Szsecin (2002)
15. Naichuk, A., Pogoreltsev, A., Demchuk, I., Ivaniuk, A., Roshchina, S.: Rigid joint of bent glued laminated timber structures using inclined glued-in rods. In: Vatin, N., Roshchina, S., Serdjuks, D. (eds.) Proceedings of MPCPE 2021: Selected Papers, pp. 501–521. Springer International Publishing, Cham (2022). https://doi.org/10.1007/978-3-030-85236-8_45
16. Pogoreltsev, A.: Compressed knots on glued-in rods of wooden structures. In: Vatin, N., Roshchina, S., Serdjuks, D. (eds.) Proceedings of MPCPE 2021: Selected Papers, pp. 337–347. Springer International Publishing, Cham (2022). https://doi.org/10.1007/978-3-030-85236-8_31
17. Pogoreltsev, A.A.: Numerical studies of glued wooden beams with inclined reinforcement. In: Collection of Scientific Works. V.A. Kucherenko Central Research Institute of Construction Materials, pp. 97–100 (1989)
18. Turkowski, S., Pogorelcev, A.: Złącza konstrukcjidrewnianych na sworznie wklejane. In: Drewno I materiały drewnopochodne w konstrukcjach budowlanych. V konferencja naukowa. Referaty. Szczecin, 17–18 maja 2002 r, pp. 169–176. Politechnika Szczecińska. – Szsecin (2002)
19. Turkovsky, S.B., Pogoreltsev, A.A., Preobrazhenskaya, I.P.: Glued Wooden Structures with Knots on Glued-in Rods in Modern Construction (TsNIISK System). RIF Building Materials, Moscow (2013)
20. Gorpinchenko, V.M., Pogorel'tsev, A.A., Ecknadosyan, I.L.: Large-scale tests provided for a block, consisting of two wooden lens-type roof trusses of the sports complex 'Strogino'. Promyshlennoe i Grazhdanskoe Stroitel'stvo **8**, 38–39 (2005)

Conceptual Design a Mobile Agricultural Settlement by Geometric Modeling

Tojiddin Juraev

Abstract The article is devoted to the application of geometric modeling in the design of building structures and engineering systems. The article provides a solution to the problem of developing the concept of a mobile agricultural settlement by justifying the use of geometric modeling methods. The proposed concept is innovative, as it provides a comprehensive solution to socio-economic problems. The analysis of the state of the problem was carried out, as well as the implemented projects and foreign experience over the last 50 years was studied. The Bukhara region of the Republic of Uzbekistan is considered as an example. An agricultural settlement intended for the cultivation of fruit and vegetable products was chosen as the object of modeling. The simulated object as a system is divided into elements and each element is modeled separately and all elements in the aggregate based on intra-system relationships. This approach makes it possible to ensure the mobility of each element and the entire system. In the proposed concept, the living area, the vegetable garden, as well as fences are mobile elements. Therefore, modeling is performed on these elements. The simulation was performed by operating with geometric parameters, namely the shape, position and dimensions of the system elements. Possible variants and various combinations of mobile elements according to geometric parameters are proposed, allowing the effective operation of this system.

Keywords Conceptual design · Geometric modeling · Land plot · Mobility · Geometric parameters

1 Introduction

Construction is one of the most important sectors of the economy, and its role as one of the main components in major projects is invaluable. This is clearly evident in modern Uzbekistan, as a developing country where fundamental reforms require the

Present Address:

T. Juraev (✉)

Bukhara Institute of Natural Resources Management NRU "TIIAME", Bukhara 200108, Uzbekistan

e-mail: tojiddin_1968@mail.ru; tjuraev931@gmail.com; tojiddin1968@tiiamebb.uz

implementation of major socio-economic projects in various sectors of the economy. In such projects, the use of compact building structures and engineering systems is becoming increasingly important. A number of such projects are being implemented in the agricultural sector of the Republic of Uzbekistan, which has been and remains one of the main sectors of the economy [14, 18, 21]. This is justified by the fact that solving the problems of food security, environmental ecology, employment and other global problems of humanity in the modern world are directly related to agriculture [5, 7]. Therefore, the government of the country pays great attention to the development of this sector, which requires the further implementation of large socio-economic projects of the agro-industrial complex, which also include building structures and engineering systems. At the same time, the development of such projects that save material resources and are aimed at solving the above global problems is considered one of the urgent tasks in the design and operation of building structures and engineering systems [3, 4, 16]. It is known that the development of projects implemented in a particular sector of the economy requires an integrated approach, taking into account the links with other sectors. Therefore, it is considered appropriate to implement large projects covering various sectors of the economy on the basis of previously developed concepts. This is also reflected in the successfully implemented socio-economic projects of the Republic of Uzbekistan [14, 18, 21]. Of course, the development and implementation of such projects will be carried out by a group of experts with the involvement of specialists from relevant fields. However, the initial idea, as a concept aimed at solving an existing problem, is first developed by one or more scientists, and then submitted for consideration to an expert group for further development and implementation. The presentation of the concept in many cases is based on the geometric parameters of the project being developed [8–12]. Therefore, this work is devoted specifically to the development of the concept of a "Mobile agricultural village" for the agro-industrial complex and it provides the results of geometric modeling of the elements of this concept.

2 Methods

As you know, the study, research and design of objects, processes and phenomena is carried out by various modeling methods. Geometric modeling, as one of the most common modeling methods, has a number of advantages, its visibility and simplicity of solution and primacy of geometric parameters. At the same time, models of objects, processes or phenomena are developed by operating with geometric parameters. And geometric parameters are divided into three categories: parameters related to size, shape and position in space. Here, the operation of geometric parameters must be understood as changing the parameters of one category in order to change the parameters of other categories. Since these categories are interrelated, a change in the parameters of one category necessarily leads to a change in the parameters of other categories, for example, a quantitative change in dimensional parameters can lead to a qualitative change in the parameters in shape and (or) in position. At the same time, depending on the problem being solved, in some cases one category of

parameters is decisive in relation to the other two categories. Often changing the quantitative values of the dimension, the necessary shape or position is obtained. For example, if parameters related to dimensions are used as defining parameters in the design of building structures and engineering systems, then parameters related to shape and position are used in their geometric modeling. It should also be noted that the parameters in form and position are primary in relation to the parameters in dimension. Consequently, in order to achieve the required results in the design of building structures and engineering systems, as well as any technical object, it is advisable to use geometric modeling in the preliminary design stage, mainly in shape and position [1, 8–12]. Based on this, the proposed concept was developed on the basis of the geometric modeling method. The contours of land plots for agriculture, with residential buildings and adjacent infrastructure that are part of the structure of the agro-industrial complex are considered as modeling objects. And the subject of the study is the layout of these objects by optimal arrangement of their elements. In this problem, the issues of the layout of the elements of the object are solved by operating with geometric parameters, i.e. the choice of optimal shapes, sizes and positions of its elements.

3 Results and Discussions

3.1 Analysis of Problem

As you know, the settled population in the territory of present-day Uzbekistan has been mainly engaged in agriculture for centuries, but its socio-economic situation has always been difficult. Even in Soviet times, when more than half of the country's population was employed in agriculture, the laws of the planned economy did not provide sufficient profit for the rural population. In the years of independence, this problem began to be solved by land reforms, which led to an improvement in the economic and social situation of the rural population. Naturally, the increase in population, the deterioration of the ecological condition of the lands and outdated methods and means of farming did not allow achieving the desired results and led to new socio-economic problems in the agricultural sector of the economy. Of course, the current agrarian reforms that have been carried out have made it possible to solve long-overdue problems and noticeably improve the state of the problem, as a result of which the agricultural sector has finally become profitable and attractive for business [14, 21]. However, we cannot stop there, it is necessary to develop new socio-economic, scientific and technical projects for agriculture, taking into account the current problems and problems of the near future. These projects should have integrated solutions and be more focused on the development of small and medium-sized businesses in the agricultural sector. A comprehensive analysis of the state of this problem in Uzbekistan shows the following: First, recently in Uzbekistan, as in

the whole world, there has been an increasing shortage of land resources for farmland. This, as is well known, is the result of an increase in the world's population, requiring the transfer of part of the land resources for farmland for housing, industrial and communication facilities. In addition, the increase in the world's population has also led to an increase in the need for agricultural products, solutions to which cannot be achieved only by increasing yields, it is also necessary to find ways to expand land resources for farmland. Secondly, as a result of the ongoing socio-demographic changes and technical and economic progress, there is a tendency to increase the number of employment in the production and service sectors than in agriculture, both due to the relocation of the population from rural to urban, and due to changes in farming technologies. Thirdly, the above changes have led to a shortage of jobs and to a decrease in the natural quality of agricultural products, especially fruit and vegetable products. All these circumstances require solving problems comprehensively by organizing attractive jobs in agricultural production [2, 4, 6, 13, 17, 20]. In recent years, a number of fundamental socio-economic reforms and major projects at the state level of both local and international mass staff have been carried out in the agricultural sector of Uzbekistan. For example, according to the Resolutions of the President of the country, such major social projects as "Providing rural population with affordable housing" have been implemented. And as business projects, we can cite the creation of LLC "Bukhara Agro Cluster" by the Decree of the CM of the Republic of Uzbekistan. There are also international projects, for example, the implementation of the agricultural project "BUHARA VARNET" together with the Turkish company "Varnet" specializing in glass greenhouse systems (Glass Greenhouse Systems). Such projects are aimed not only at the construction of production facilities of the agro-industrial complex, but also at the construction of residential buildings and adjacent infrastructure. Although these projects are qualitatively developed, successfully implemented and solve the tasks assigned to them, they require further prospecting work. Such projects should be developed not only as separate social or business projects; they should also comprehensively solve socio-economic problems. They need to be adapted to the peculiarities of the regions, i.e. agro-climatic conditions; the mentality of the population, the economic and ecological state of the region, etc. must be taken into account.

3.2   Land Allocation Projects

Let's consider the state of the problem on the example of the Republic of Uzbekistan. If we consider the periods since the 70 s of the last century, up to *0.16* ha of land have been allocated by the State for families living in rural areas. Naturally, with an increase in the population and the need for agriculture, the area of allocated land began to decrease to *0.12* ha, and subsequently, with the complication of this situation, it was temporarily discontinued. But during the years of independence, due to the difficult economic situation of the country and taking into account the high

housing needs of the population, the allocation of land plots with an area of 0.06 ha was resumed, but with redemption through auctions (Fig. 1).

However, with the improvement of the economic condition of the country since the 2000s, the implementation of social programs to provide the rural population with affordable housing, the area of which was *0.06* ha, was launched. As a result, large-scale work was carried out on the construction of individual housing based on standard projects for rural residents. Only during the period 2009–2016, 69,557 comfortable residential buildings with a total area of 9,573 thousand square meters were built on 1,308 residential areas in the village. Housing conditions have been improved by over 83.5 thousand rural families (Fig. 2).

Taking into account the current socio-economic conditions of the Republic of Uzbekistan, the new leadership of the country has implemented "Affordable Housing" projects on updated projects. The Decree of the President of the Republic of Uzbekistan on the program for the construction of affordable residential buildings on updated standard projects in rural areas for 2017–2021 was adopted. As a result, projects were implemented providing for the provision of residential buildings to the population, located on land plots of *0.04* and *0.02* ha (Fig. 3).

Fig. 1 Land plots with an area of 0.16 ha, 0.12 ha and 0.06 ha in rural areas

Fig. 2 Implementation of the projects "Affordable housing with a backyard garden"
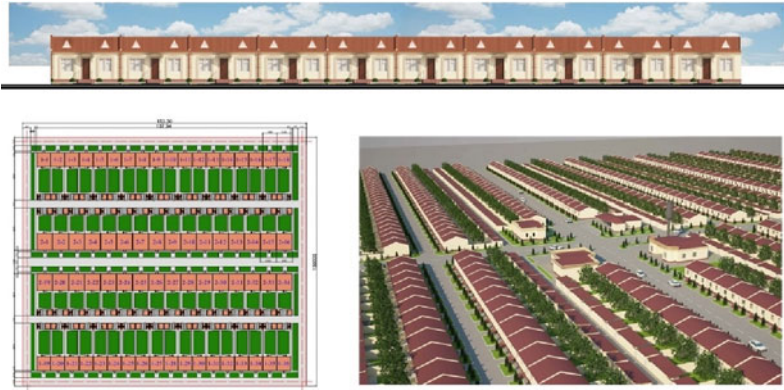
Fig. 3 Updated projects "Affordable housing with a backyard garden"

The practice of developing and implementing projects for the allocation of land plots in the Republic of Uzbekistan shows their social nature, i.e. they are aimed at providing the population of rural areas with housing with a vegetable garden and are not related to agricultural production. And projects related to agricultural production, for example, Bukhara Agro Cluster LLC, as business solutions are not directly related to solving social problems. Therefore, it is advisable to develop projects aimed at simultaneously solving both social and economic problems. Of course, there are such projects, for example, the project "Smart greenhouses with a house" ("Akilli seraevlar") of the Turkish company "Varnet" (Fig. 4). Although this project is very successfully developed, it is more aimed at a business project and it needs to be adapted to local conditions of implementation. Therefore, the main factor of success in the implementation of such projects can be called their mobility, which ensures rapid adaptation.

3.3 Geometric Modeling the "Mobile Agricultural Sattlement"

Modeling Goals and Objectives. Considering projects for the allocation of land plots with a backyard garden, it is possible to identify the following trends based on the above-mentioned well-known reasons: reduction of the total area of land; decrease in the specific area of the garden in relation to the living area, improvement of the layout schemes of the living area. These trends define the task for the development of the concept of "Mobile agricultural sattlement". The tendency to reduce the area of land plots, as noted above, occurred for natural reasons, and is a factor that must be taken into account when solving the problem. The tendency to decrease the specific area of the vegetable garden is a problem that needs to be solved in the task. The tendency to improve the layout schemes is the way to solve the problem. The proposed concept took into account the above-mentioned global and
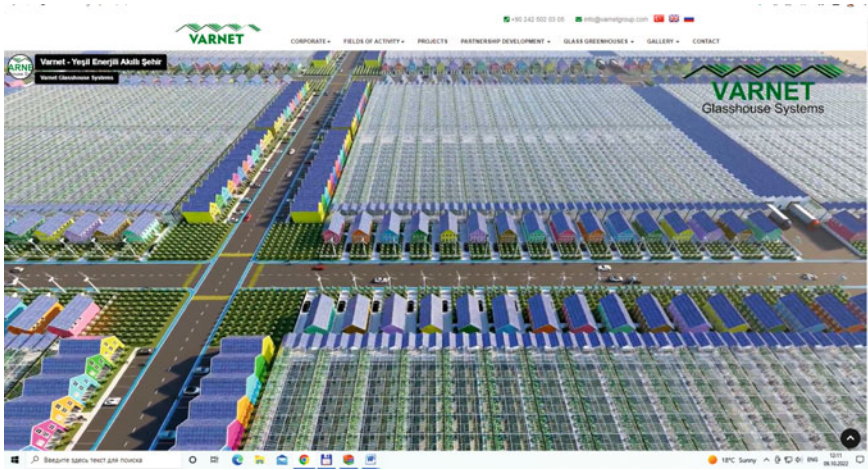
Fig. 4 "Smart greenhouses with a house" ("Akilli seraevlar") of the Turkish company "Varnet"

regional factors. The proposed concept, as a design project, was developed on the basis of geometric modeling. This concept provides for the improvement of housing and working conditions of the rural population, infrastructure facilities and engineering and communication networks of the agro-industrial complex on the basis of modern urban planning requirements, rational use of land resources and the development of rural settlements. The aim of the project is to develop a layout scheme of a typical project of agricultural plots with residential buildings "Mobile agricultural sattlement" for the agro-industrial complex aimed at the rational use of land resources. Currently, a significant part of the rural population, including the population of district centers with land plots, is engaged in agriculture. Agriculture, being the main or additional activity of the rural population, allows partially providing the country's population with employment, agricultural products and income. Therefore, the state supports the population engaged in agriculture in every possible way, and currently a number of projects have been implemented for the construction of standard houses with private plots of land. Of course, as a result of the implementation of these projects, many of the planned tasks were solved. However, the changes taking place in the agricultural sector of the country's economy, related to the current socio-economic conditions and scientific and technological progress, require the development of more modern projects based on the use of innovative agricultural machinery and technologies and aimed at a comprehensive solution to current socio-economic problems. In solving this problem, we will consider the issue of the activity of the population engaged in agriculture in relation to land plots. It can be divided into three categories: 1) Farming in the land plots of your own vegetable garden; 2) Farming in land plots leased from other owners; 3) Farming in land plots as a hired worker to other owners. All categories have their advantages and disadvantages analysis, which allows us to draw the following conclusions: It is necessary to create economic, legal and technical and technological conditions for the use of

land resources in the proposed system. Moreover, these conditions should ensure the mobility of the system, in changing conditions for the terms of use and the volume of use of land resources.

Geometric Model of the Master Plan. As already explained above, the problem will be solved by methods of geometric modeling. Modeling of the elements of the "Mobile Agricultural Settlement" object will begin with the development of a geometric model of its master plan (Fig. 5). At the same time, we will designate the following elements: 1) The outer border of a mobile agricultural settlement is bounded by main roads; 2) Internal roads between pairs of rows of cells, where their number is determined by the number of pairs of rows of cells $R_r = 2N_r\text{-}1$ (Table 1); 3) The adjacent territory with the necessary communication; 4) Production and service and social facilities for a mobile agricultural village with the necessary infrastructure. These objects are proposed to be located on the sides of pairs of rows; 5) Residential buildings of land, i.e. cells of an agricultural settlement; 6) Vegetable gardens of land, i.e. cells of an agricultural settlement; 7) Fencing of land, i.e. cells of an agricultural settlement. The last three elements, i.e. residential buildings, vegetable garden and fences, defining the contour of the cells of land plots, ensures the mobility of the agricultural village. Therefore, these objects are subject to primary geometric modeling.
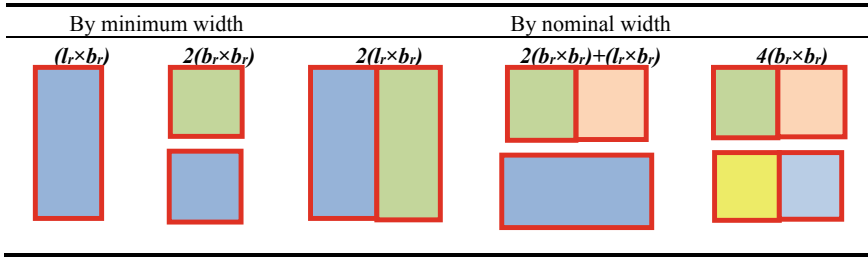
Geometric Modeling the Elements. This problem is solved by geometric modeling of the contour of cells placed in the selected general contour for land plots. Based on the geometric parameters of the contour of the cells as a simulated object, we apply two-dimensional modeling. The shape, position and dimensions of the contour of the cells are considered as geometric parameters. We select the geometric parameters of the contour of the cells of land plots based on the practice of designing and allocating land plots in the Republic of Uzbekistan.

The Shape of the Contour of the Cells. In the practice of designing land plots, traditionally, the splitting of the contour of land plots into various polygons is used,
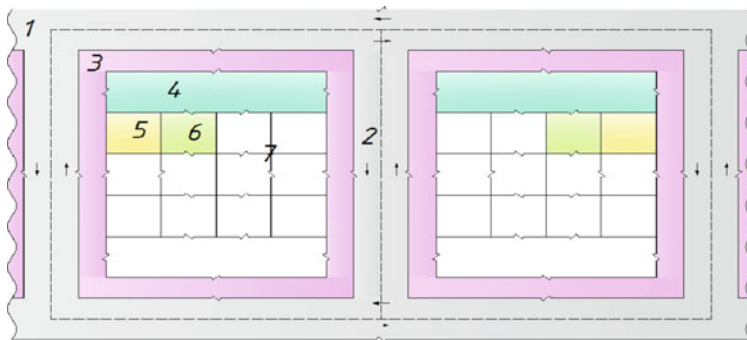
Fig. 5 Geometric model of the master plan "Mobile agricultural settlement": 1-roads along the outer border, 2-internal roads, 3-adjacent territory, 4-infrastructure, 5-living area, 6-vegetable garden, 7-fences

Table 1 Structure of living space premises

By minimum width			By nominal width	
$(l_r \times b_r)$	$2(b_r \times b_r)$	$2(l_r \times b_r)$	$2(b_r \times b_r)+(l_r \times b_r)$	$4(b_r \times b_r)$

and the rectangle is the most optimal. Therefore, for this task, a general contour is selected, divided by a rectangular grid into cells in the form of rectangles with a $S_c = b_c \times l_c$ area. In this case, the contour of the cell includes an area for housing buildings and a vegetable garden for agriculture.

The Positions of the Contour of the Cells. As you know, the positions of the contour of the cells are determined relative to the road and communication, where the front side of the cells, i.e. the width of b_c are located parallel and along the road. Accordingly, the back sides of the cells in width are common to adjacent cells in the adjacent row. And the sides of the cells, i.e. the length of l_c are perpendicular to the road and are common to adjacent cells in a row.

Dimensions of the Sides of the Cells. When choosing the aspect ratio, factors such as the divisibility of the general contour into cells, the cost of fencing along the perimeter length $P_c = (b_c + l_c) \times 2$ cell contours and the construction of roads and communications are taken into account. In the current conditions of the development and implementation of such projects, there are ample opportunities for developers to choose the size of the general contour by divisibility into cells, whereas previous administrative and bureaucratic obstacles limited designers in this. As is known, the smallest length of the perimeter Pc of the rectangle contour for a given area S_c is obtained with a square, i.e. if the sides are equal $l_c = b_c$, where $l_c/b_c = 1$. And the increase in the difference in the lengths of the sides of the contour is directly proportional to the increase in the length of the perimeter of the contour, i.e. $l_c/b_c \rightarrow \infty \leftrightarrow P_c \rightarrow \infty$, within $0 < b_c < l_c$, where $S_c = const$. Reducing the size of b_c allows you to save land resources by reducing the number of internal roads (Fig. 6). Although reducing the size of b_c allows you to save land resources, this will lead to an increase in the lengths of the perimeters of the contour of cells, the relative costs of fencing which in the past had their significance. However, modern building materials and technologies for fences, as well as their price relative to square meters of land plots, make it possible to optimally divide the general contour into cells, choosing the optimal lengths of the sides of the contour of the cell. If we take into account that the reduction in the width of the contour cells is directly proportional to the reduction in the cost of roads and communications along its length, then the task is reduced to determining the minimum value of the width of the land cell. Since the proposed land plots include, in addition to the vegetable garden and the area for
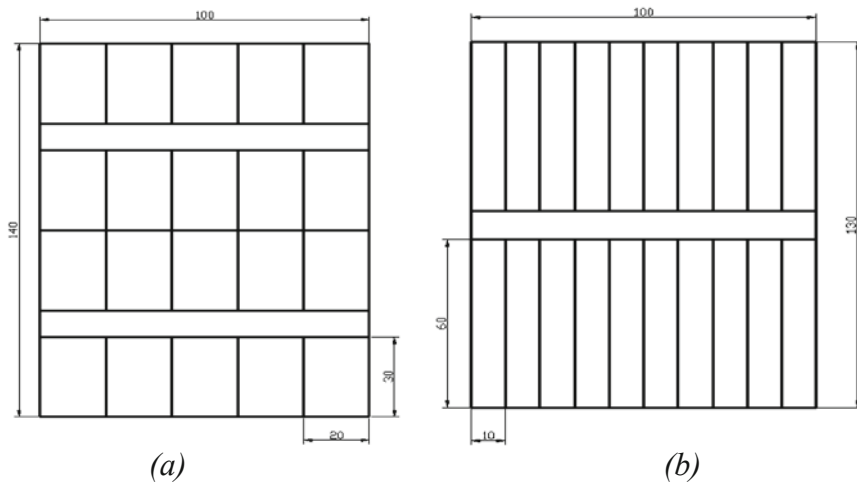
Fig. 6 Increasing the area of the vegetable garden by changing the size of the sides of the cells: *a*)-
the existing breakdown; b)-*the proposed breakdown*

buildings, the minimum value of the width of the b_c cell is determined by the size of
the premises of the living area.

Choosing the Optimal Size of the Living Space. As you know, the living area
consists of various rooms, the volumes of which are determined by the length l_r and
width b_r. According to the well-known rules, we choose the height of h_r premises
equally for all premises. To simplify the task, b_r is equated to h_r, and l_r is multiplied
by h_r, assuming $l_r \times b_r = 2h$ for residential premises and $b_r \times b_r = h_r$ for auxiliary
premises. This will make it possible to develop a universal prefabricated building
structure consisting of l_b beams with a length equal to h_r and ensure the mobility
of residential buildings. In this case, we have the smallest module of rooms with the
dimensions of the h_r cube and the largest module of rooms with the dimensions of
$h_r \times h_r \times 2h$. To specify the task, based on the requirements of the "Building codes
and regulations" for residential buildings, we choose the optimal value $h_r = 3\ m$.
Then we determine the optimal size of the minimum living area of $36\ m^2$, consisting
of such living spaces as a bedroom with a bathroom *(6 × 3)*, a kitchen *(3 × 3)* and
an entrance hall *(3 × 3)*. To reduce the occupied area of residential buildings, we
will place these premises on two floors and get the minimum size of the area for
residential buildings equal to *3 × 6 = 18 m²*. As a result, we get a minimum width
equal to three meters, i.e. $b_r = h_r = 3\ m$ and a nominal width of the cell contour equal
to six meters, i.e. $l_r = 2h = 6\ m$. On the basis of these dimensions, 5 variants of the
structure of the premises of the living area are proposed according to the minimum
and nominal width (Table 1). According to these options, various combinations of
the location of the premises can be made: left/right, front/rear and lower/upper.

Determining the Length of the l_c Cell. The cells are usually placed in rows, the
optimal placement is two adjacent rows, when the front sides of the cells are located

outside along the road communication, and the rear sides are located adjacent from the inside. In existing projects, there are various options for the location of the building in a cell, i.e. partially on the front and back sides and on the sides. For optimal use of the buildings' land area, we place only on the front side of the cell width, and we place the vegetable garden on the back side of the cell width. Through each pair of adjacent rows of the cell we conduct road communication. To set the cell length, various factors must be taken into account. For example, since one of the main goals of the project is the efficient use of land resources for agriculture, we take into account such a factor as irrigation technology, according to which the maximum length of the furrow, depending on the soil structure, should not exceed *200 m*, the average value of which is *100 m*. For the convenience of calculating the area of the general contour for land plots and taking into account the practice of allocating areas for land plots in currently implemented projects, it is proposed to choose the optimal length equal to $l_c = 54\ m$ and divisible by h_r.

"The Total Area of a Mobile Vegetable Garden". Its shape is rectangle and its width is determine along the road communication by the sum of the minimum widths of cells located along the road, i.e. $\Sigma = l_r \times N_r$. And its length is determined by the total length of the vegetable gardens of two adjacent cells located in a pair of adjacent rows, i.e. $2(l_c-l_r) = 2(54-6) = 96\ m$, which also provides the average value of the maximum length of the irrigation furrow. Based on these dimensions, various variants of cell contours are proposed according to the proposed shape, position and dimensions of the sides (Table 2).

Cell Fencing. For this project, fences also have the character of mobility. The fence consists of columns with a height of h_r without taking into account the incoming part in the ground. The columns are arranged in the vertical and horizontal directions of the general contour, the distances between them are equal to l_r. The columns also serve as support posts for precision farming systems operating in both vertical and horizontal directions. It is proposed to use polycarbonate panels and (or) polyethylene film as an enclosing material. Fencing can be carried out in various versions around the perimeter, which ensures its mobility.

Table 2 A variant of the contours of the cells of land plots

Cell's contour	Cell's category	Total area	Garden	Living area
	Minimal - 0,5	3×54=	3×48=	(3×6)×2=
	(0,0162 hectare.)	162 m²	144 m²	36 m²
	Nominal - 1,0	6×54=	6×48=	(6×6)×2=
	(0,0324 hectare)	324 m²	288 m²	72 m²
	Supplemental - 1,5	(6+3)×54=	(6+3)×48=	((3×6)+(6×6))×2=
	(0,0486 hectare)	486 m²	432 m²	108 m²
	Maximal - 2, 0	(6+6)×54=	(6+6)×48=	((6×6)+(6×6))×2=
	(0,0648 hectare)	648 m²	596 m²	144 m²

4 Conclusions

In this context, agricultural land plots are considered as an agricultural production facility with the use of precision farming systems and intensive crop cultivation technologies. This is due to the fact that the land plots of this project provide for the cultivation of agricultural crops intended, in addition to providing for the own needs of the owners of land plots, also for the sale of products, both on the domestic market and for export. The peculiarity of the project is that the land plots qualify as a vegetable garden and they provide for the cultivation of fruit and vegetable crops, which require relatively more labor than technical crops. This allows full or partial employment of the population, an increase in fruit and vegetable production and more efficient use of land resources. In such a village, it is easier to organize careful production, grow naturally pure products and apply precision farming systems. All these issues are urgent tasks not only for Uzbekistan, but also for the global community.

References

1. Agromayor, R., Anand, N., Müller, J., et al.: A Unified Geometry Parameterization Method for Turbomachinery Blades. CAD. https://doi.org/10.1016/j.cad.2020.102987
2. Brenda, B.L., Stacy, M.P., Shalene, J., Heidi, L.: Urban agriculture as a productive green infrastructure for environmental and social well-being. In: , pp.155–179. . https://doi.org/10.1007/978-981-10-4113-6_8
3. Comín, F.A.: Planning the development of urban and rural areas: an integrative approach. In: Leal Filho, W., Marisa Azul, A., Brandli, L., Gökçin Özuyar, P., Wall, T. (eds.) Sustainable Cities and Communities (2020). https://doi.org/10.1007/978-3-319-95717-3_95
4. Dovring, F., Dovring, K.: Agricultural settlement and the layout of land. In: Land and Labor in Europe in the Twentieth Century. Studies in Social Life. Springer, Dordrecht (1965). https://doi.org/10.1007/978-94-017-6137-6_2
5. Food and Agriculture Organization of the United Nations. Homepage. https://www.fao.org/land-water/land. Accessed 30 June 2022
6. Giacomelli, G.: Designing the greenhouse to fit the needs of the plant. https://ceac.arizona.edu/resources/greenhouse-design
7. International Labor Organization. Homepage. https://ilostat.ilo.org/data/country-profiles. Accessed 30 June 2022
8. Juraev, T., Voloshinov, D., Xujakulov, R., Qahharov, A., Ubaydullayeva, D.: Computer simulation the moldboard's surface in SIMPLEX system. In: CONMECHYDRO – 2021. https://doi.org/10.1051/e3sconf/202126401029
9. Juraev, T., Voloshinov, D.: Geometric modeling laboratory as an engineering infrastructure in the digital economy. https://iopscience.iop.org/volume/1757-899X/869
10. Juraev, T.: Computer modeling the moldboards' surface in AutoCAD system. In: Conmechydro–2020, https://iopscience.iop.org/article/, https://doi.org/10.1088/1757-899X/883/1/012156
11. Juraev, T.: Conceptual designing of Mold Board's surface by geometrical modeling. Am. J. Mech. Appl. **5**(4), 28–33 (2017). http://www.ajmechanics.org/archive/621/6210504
12. Juraev, T.: Decision maintenance management problems in agriculture engineering by constructive geometric modeling methods. In: García Márquez, F.P., Papaelias, M. (eds.) Maintenance Management, pp. 23–37. IntechOpen, London (2020). https://doi.org/10.5772/intechopen.79248

13. Lal, R.: Home gardening and urban agriculture for advancing food and nutritional security in response to the COVID-19 pandemic. https://doi.org/10.1007/s12571-020-01058-3
14. National database of legislation of the Republic of Uzbekistan. Homepage. https://lex.uz/en/search. Accessed 30 June 2022
15. Rural & Urban Planning Consultancy. https://www.ruralurbanplanning.co.uk
16. Senitkova, I., Junas, P.: Structural and Building Engineering – An Introduction. https://doi.org/10.1088/1757-899X/1066/1/012001
17. USDA. Urban Agriculture Toolkit. https://www.usda.gov/sites/default/files/documents/urban-agriculture-toolkit.pdf
18. Vanegas, C., Aliaga, D., Beneš, B., Waddell, P.: Interactive Design of Urban Spaces using Geometrical and Behavioral Modeling. ACM Trans. Graphics **28**(5), 1–10 (2009). https://doi.org/10.1145/1661412.1618457
19. Varnet Glass Greenhouse Systems. Homepage. https://www.varnetgroup.com/en/solutions/design. Accessed 30 June 2022
20. Ziadat, F., Bunning, S., Pauw, E.: Land Resource Planning for Sustainable Land Management. Food and Agriculture Organization of the United Nations, Rome (2017)
21. http://kiosk.qishloqqurilishbank.uz/uz/proekt/4xona.php

Reinforced Concrete Structures for the "Harmonica" Resistance Model in Bending with Torsion

Vladimir Kolchunov and **Maxim Protchenko**

Abstract A calculation model of reinforced concrete structure at bending with torsion has been constructed. The deformation effect has been discovered, the physical essence of which is the additional deformation effect when the continuity of concrete and reinforcement discontinuity is broken for an ellipsoid-shaped crack. A special two-cone fracture mechanics element for a single strip is used for the crack. The Saint–Venant principle is fulfilled from the adhesion of the peri-armature zone, where the deformations of the concrete adjacent to the cracks change their sign to compression. In helical, elliptical and harmonic spatial cracks, the crack opening, longitudinal and transverse shifts are determined through the guide cosines. When analyzing the complete picture of crack formation during loading, the levels of spatial cracks are distinguished when comparing the functional or discrete value. Crack opening is the accumulation of relative conditional concentrated mutual displacements of reinforcement and concrete on the sections and banks of the crack. which is calculated using the Thomas-Kolchunov hypothesis. The stiffness of spatial bending cracks with torsion in elastoplastic compressed concrete is obtained by projecting linear and angular deformations (stresses) using tensor diagrams. The stiffness of spatial bending cracks with torsion in elastoplastic compressed concrete is obtained by projecting linear and angular deformations (stresses) using tensor diagrams. Approximation of rectangular cross-sections using small squares in matrix elements for stiffness characteristics with tensile medium working reinforcement is performed.

Keywords Calculation model · Concrete discontinuity effect · Crack opening width · Deplanation · Stiffness · Bending with torsion

V. Kolchunov · M. Protchenko (✉)
South West State University, 50 Let Oktyabrya Street, 94, Kursk 305040, Russian Federation
e-mail: maxBROMmax@yandex.ru

Research Institute of Building Physics, Lokomotiv Avenue 21, Moscow 127238, Russian Federation

1   Introduction

Composite and precast-monolithic reinforced concrete structures in the construction and reconstruction of buildings and structures are characterized by the general resistance of concrete with different properties of strength and deformability [1–5]. This determines a number of specific parameters of calculation and design of composite structures leading to redistribution of internal forces, including at complex resistance.

Relevance. The study of strength, crack resistance and stiffness of reinforced concrete structures in bending with torsion for the first and second group has been conducted in many (theoretical and experimental) works [6–13], where increasing attention is paid to the development of models of deformation of reinforced concrete using and developing the basic provisions of fracture mechanics [1, 8, 9].

2   Working Assumptions of the Deformation Model

In the calculation model of reinforced concrete structures in bending with torsion, the elasticity coefficients of concrete and reinforcement in the cross section I-I ($v_{bi,I}$; $v_{sj,I}$), as well as in the spatial section k-k ($v_{bi,k}$; $v_{sj,k}$) are used. When solving the direct problem between external influences, as a rule, their ratio (Q:M:T) is always given.

The calculation models are based on the following basic assumptions:

A generalized computational model of complex resistance is constructed in the form of a supported block formed by a spatial crack and a compressed zone of concrete closed to it, and a second block between the vertical transverse rectangular sections of reinforced concrete structures under the joint action of bending moment and torsional moment. The bilinear surface of the spiral or x-shaped crack with the spatial patterns of the i-th level cracking due to the detachment perpendicular to the main deformations of the limiting elongation of concrete has been constructed (Figs. 1, 2 and 3).

- Determination of the reaction from the deformation effect of concrete and reinforcement in the crack is performed using the deformation effect of Prof. V.I. Kolchunov and the double-console element (DCE);
- For cross-sections, hypotheses of relative linear and angular deformations during deplanation changes and jump-cracking between the upper and lower fibers of concrete and reinforcement to determine their relationships in distances from the neutral axis using a special geometric figure for the elastic and plastic areas are proposed.
- The first and second functionals are used to determine deformations, and the third and fourth functionals are used to determine bending and torsional moments, respectively.
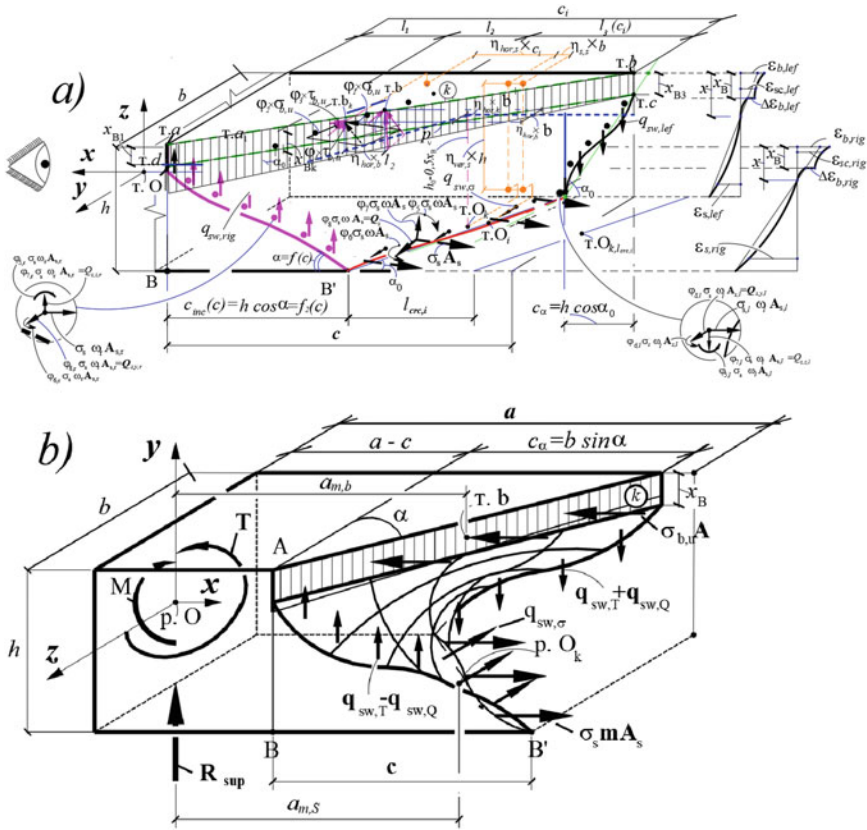
Fig. 1 Calculation model of resistance of reinforced concrete structure under the combined action of bending moment and torsional moment, longitudinal and transverse forces for spiral **a** or x-shaped **b** spatial crack

- Different levels of cracking are distinguished. The tensile strain of the concrete between cracks continues to increase until a new crack appears in this area (Figs. 1 and 2).
- Crack opening is considered as an accumulation of relative conditional concentrated mutual displacements of reinforcement and concrete in the areas located on either side of the crack (Thomas-Kolchunov hypothesis.
- The components of the dowel force as a "triplet" of forces in the working longitudinal and transverse reinforcement crossed by the spatial crack k are taken into account [14, 15].
- Stresses of longitudinal and transverse forces for i-th and j-th elements in the matrix are developed for approximation of any rectangles using their small squares of the design model of reinforced concrete blocks (Figs. 1 and 2). The longitudinal and transverse shifts in helical and icy spatial cracks have been determined using the guide cosines l, m, n (Fig. 3).
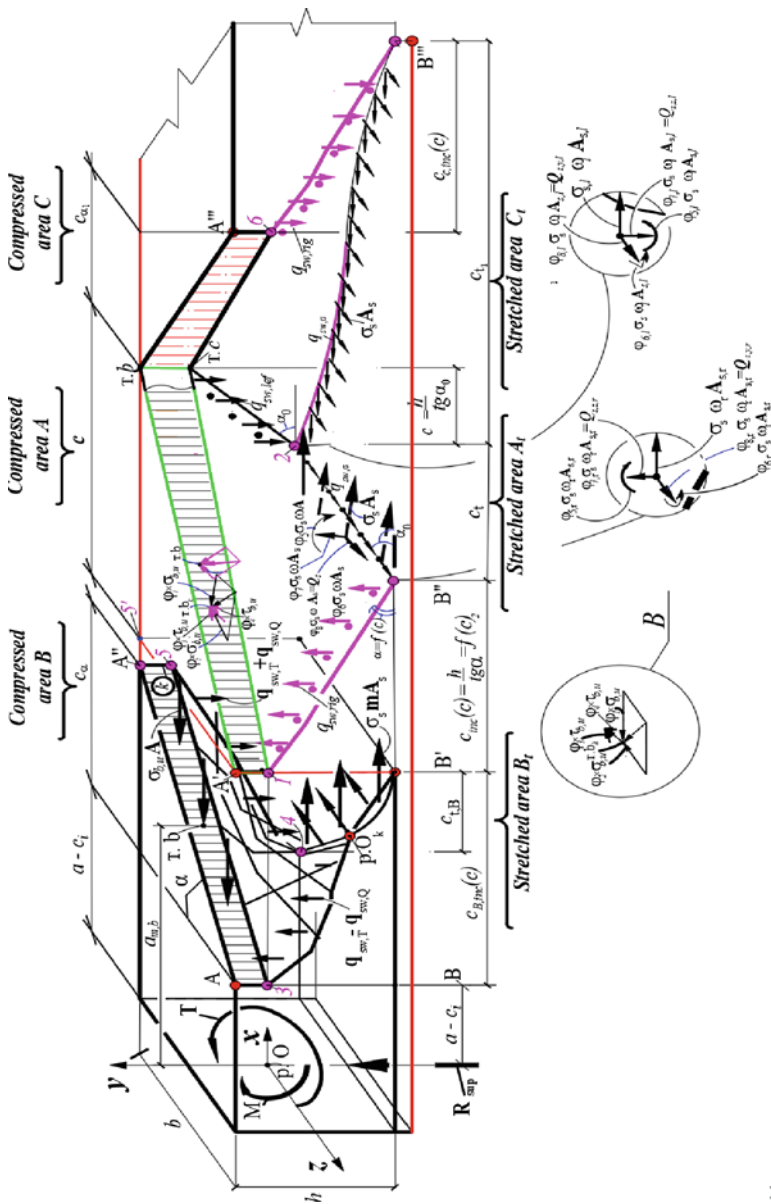
Fig. 2 Reinforced concrete structures for the "harmonica" resistance model, closing the spiral or x-shaped spatial crack in the areas A, B, C (upper compressed) and At, Bt, Ct (lower stretched) in bending with torsion
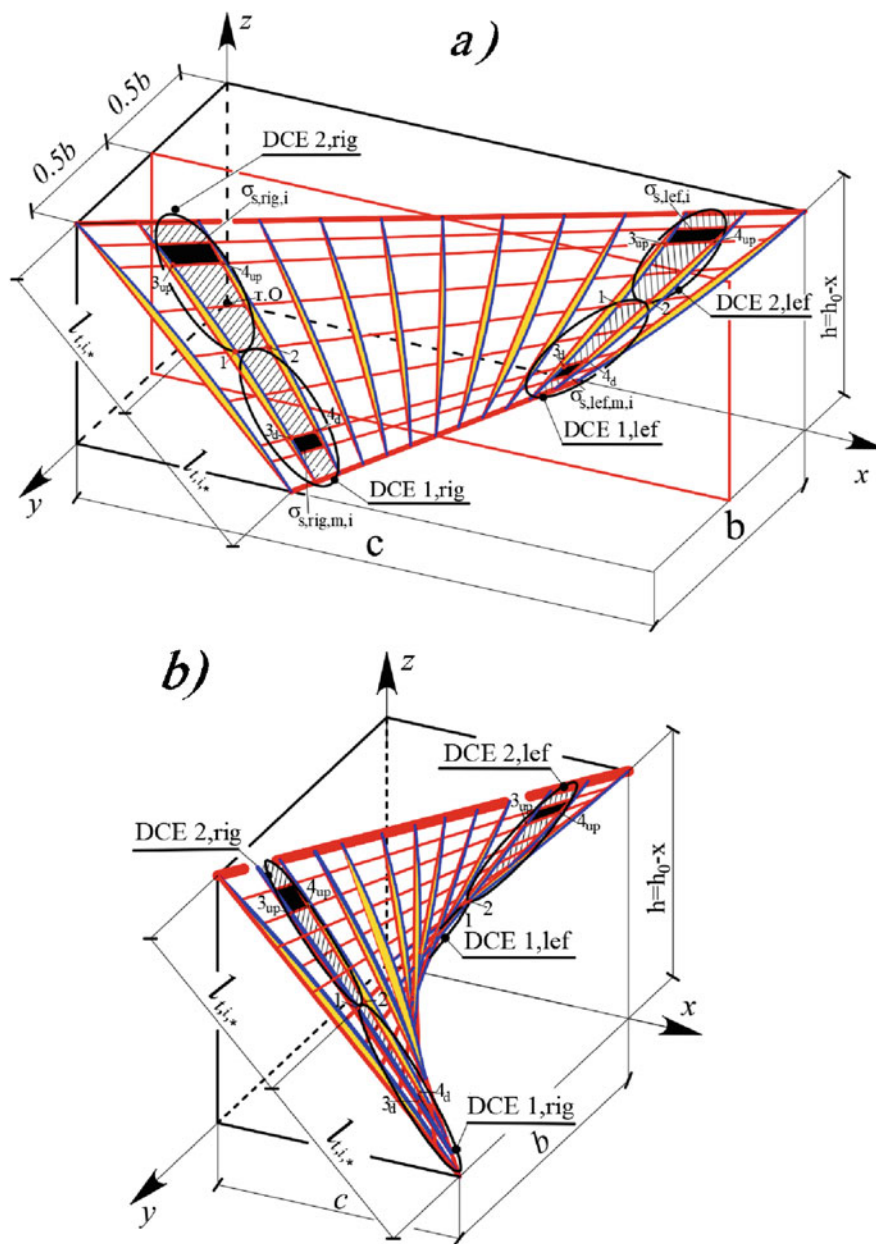
Fig. 3 Double-console element at bending with torsion in model A **a** and model B **b**

3 Solving Equations

By constructing a function of many variables with Lagrange multipliers $F\big(R_{\text{sup}}, x,$
$x_B, \gamma_{Q,t}, \gamma_{T,k}, \sigma_{s,I}, \sigma_{S,k}, q_{sw,rig}, q_{sw,lef}, q_{sw,\sigma}, c, \lambda_1, \lambda_2, \lambda_3, \lambda_4, \lambda_5, \lambda_6, \lambda_7, \lambda_8,$
$\lambda_9\big)$, using equations and equating the partial derivatives of all its variables to zero, we
obtain an additional system of equations.

After appropriate algebraic transformations, we can obtain equations with respect
to the unknown dangerous spatial crack $c_{inc}(c)$:

$$c_{inc}(c) = -a_{15}a_{17}, \tag{1}$$

$$a_{41} \cdot [c_{inc}(c)]^3 + a_{42} \cdot [c_{inc}(c)]^2 + a_{42} \cdot c_{inc}(c) + a_{44} = 0. \tag{2}$$

In this case the constraint from the geometry of the rectangular section applies

$$c_{inc}(c) \le c_u = 2 \cdot h \cdot ctg(\alpha) + b \cdot ctg(\alpha) \approx 2h + b. \tag{3}$$

The coefficients included in the equations include all the design parameters of the
proposed calculation model (see Figs. 1, 2 and 3).

Professor V. Kolchunov discovered the effect of reinforced concrete [2–4, 7, 8,
14–19], the physical essence of which is the additional strain effect of the reaction
of reinforcement and concrete for an ellipsoidal crack at a distance of two diameters
of the working armature from the axis of its rod or its alternate kinematic crack,
associated with a violation of the continuity of concrete. Determination of velocity
in the reduction of potential energy ζ_{bu} and additional work is determined on the
basis of the fracture mechanics functional [19]. In this case, the parameter t_* in
accordance with the Saint–Venant principle and studies of the peri-armature zone
using semi-analytical and numerical methods in the first approximation is equal to
three reinforcement diameters.

As a result, the deformation effect of reinforced concrete for the opening of spatial
cracks in a small individual strip of the left and right double-console element (DCE)
is developed.

For the faces of the structure, displacement and rotation of the axes are performed
for tearing (± 0, $5a_*$); for transverse displacement (± 0, $5b_*$); for longitudinal
displacement (± 0, $5c_*$) in Figs. 3, 4:

$$\begin{cases} x_i = (x_c \pm 0.5a_{*,i}) \cdot (\pm l_i); \\ y_i = (y_c \pm 0.5b_{*,i}) \cdot (\pm m_i); \\ z_i = (z_c \pm 0.5c_{*,i}) \cdot (\pm n_i). \end{cases} \tag{4}$$

The tensile stresses in the selected sections are distributed according to the law of
the square parabola from the neutral axis to the point where the sign of its stresses
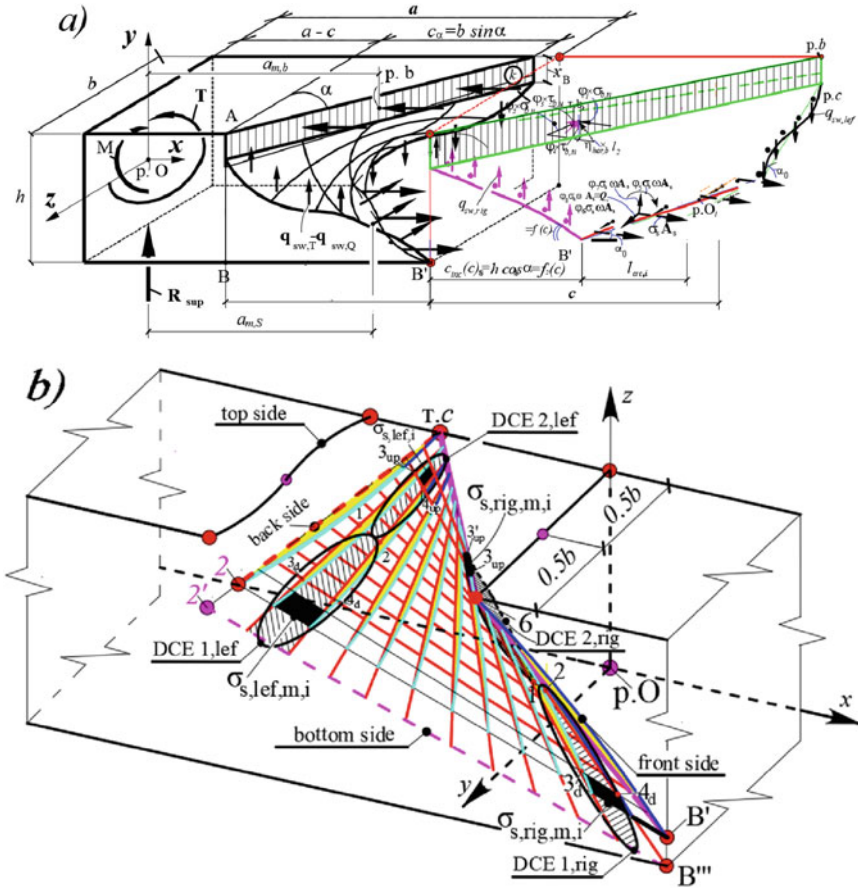changes. Their maximum value is limited by the value R_{bt}.

Fig. 4 Combined computational model and model of duble-console element in bending with torsion for a separate (middle) strip

Performing differentiation after algebraic transformations, we obtain the dependence (function) linking the tangential force near the crack $\Delta T\left(h_{crc},\ \zeta_\tau,\ \varepsilon_{q_1el},\ b,\ t,\ \eta_1,\ \eta_2,\ \eta_5,\ \eta_7,\ \eta_8,\ \eta_{14},\ \eta_{15}\right)$ with the length h_{crc} using the new concrete constant ζ_{bu}. The iterative process is organized by using a two-cone element as a transitional element between the dependencies of fracture mechanics and the equations of reinforced concrete theory.

The distance between spatial cracks $l_{crc,i}$ and the crack opening width a_{crc} are determined from the relative mutual displacements of reinforcement and concrete $\varepsilon_s(x)$ for the differential equation and boundary conditions

$$\frac{d\varepsilon_g(x)}{dx} + B\varepsilon_g(x) = 0 \tag{5}$$

Crack opening is the accumulation of relative concentrated mutual displacements of reinforcement and concrete on the banks of the crack during the development of the Thomas-Kolchunov scientific hypothesis [14–18, 20–23, etc.]:

$$a_{crc} = \varphi_1 \cdot \varphi_2 \cdot \varphi_3 \cdot k_r \cdot \left[-\frac{2\Delta T}{G \cdot t} + \frac{2B_3}{B}(1 - e^{-B \cdot (0.5 l_{crc} - t_*)}) + 2B_2(0.5 l_{crc} - t_*) \right].$$

(6)

Here k_r is coefficient depending on the distance of two diameter of the protective layer of reinforcement to the contact surface with the reinforcement, - deplanation of concrete in the section with a crack; φ_1, φ_2, φ_3 - coefficients from the building codes.

The rigidity of reinforced concrete structures D_{pq} (p, q−1, 2, 3, 4) in bending with torsion has been obtained from the approximation of rectangular cross-sections using small squares in matrix elements a_{ij}. n - the total number of small squares; j - cross sections along the x-axis, j = 1–6. The relative longitudinal deformation $\varepsilon_{b,0,x,j,i}$ of the neutral axis bending fiber (second functional and hypothesis of linear deformations [23, etc.]), the curvature $\frac{1}{r_{x,j,i}}$ of the longitudinal axis in the considered cross section and the twist angle $\varphi_{A,j,i}$ (first functional and hypothesis of angular deformations [23, etc.]) were found for compressed concrete, longitudinal and transverse reinforcement.

The dependencies connecting the relative deformations and stresses of concrete and reinforcement have the form $\varepsilon_{b,j,i} = \varepsilon_{0,b,j,i} + \frac{1}{r_{x,j,i}} \cdot Z_{bx,j,i}$; $\varepsilon_{s,j,i} = \varepsilon_{0,s,j,i} + \frac{1}{r_{x,j,i}} \cdot Z_{sx,j,i}$. Then additionally have found forces and displacements (in the crack), dowel forces, relative angular deformations, torsional rotation angle $\varphi_{A,B,l_2,sum,j,i} \varphi_{b,l_2} + \varphi_{b,l_2,add} = \varphi_{2,A,j}\left(M_{t,i} \cdot l_j \cdot Y_{3,i}(z,y)\right)/\left(M_t \cdot A_{b,,i} \cdot z_{b,t,i}\right) \pm \left(0, 5\Delta_{crc,zx} \pm 0, 5\Delta_{crc,yx}\right) \cdot k_r$, displacement of lateral force of compressed concrete and working reinforcement.

We obtain the elements of the matrix $D_{p,q}$, where the physical meaning through the new functionals using the deformation hypothesis with the stretching of the working reinforcement and the average coefficient $\psi_{s,m}$ and $\psi_{sw,m}$, $\phi = M_t/N + \sum M_{t,i}/N$; $\eta = M_t/M_x + \sum M_{t,i}/M_x$; $x = M_t/Q + M_t/\sum P_i$. In structural mechanics for internal and external forces, for example $M_{sup} = M_{bend} - R_{sup} \cdot a_{m,b} - N \cdot e_x - M_t/\eta$.

4   Conclusion

1. In reinforced concrete the effect of Professor Vladimir Kolchunov is developed, the physical essence of which is the additional deformation impact with the violation of the discontinuity of concrete and reinforcement continuity (at a distance of three diameters of the working reinforcement from the axis of its rod). When determining the width of crack opening, a two-column element for a single strip of composite structures is used. The Saint–Venant principle is used

to bond the near-armature zone, where the deformations of the concrete adjacent to the cracks change its sign.

2. In the spatial crack surface, the strain and stress diagrams are constructed from cutting a special two-column element (for the parameters $\Delta b_{t,i,*,m,rig1}, \Delta b_{t,i,*,m,rig2}, \Delta b_{t,i,*,m,lef1},\ \Delta b_{t,i,*,m,lef2}$) using the i-axes (after displacement and rotation of the axes: $x_i = (x_c \pm 0.5a_{*,i}) \cdot (\pm l_i)$; $y_i = (y_c \pm 0.5b_{*,i}) \cdot (\pm m_i)$; $z_i = (z_c \pm 0.5c_{*,i}) \cdot (\pm n_i)$ and angles $\alpha_i,\ \beta_i,\ \theta_i$) for tearing, transverse and longitudinal shear.

3. Along the longitudinal and transverse reinforcement of reinforced concrete structure in spiral, x-shaped and harmonic-shaped spatial cracks for opening use guide cosines l, m, n. This shows the analysis of determining the full pattern of cracking during loading, different levels of cracking for the distance between adjacent cracks are distinguished. With increasing load the crack opening width increases, and on the other hand, decreases with decreasing distance between cracks.

4. Crack opening is the accumulation of relative displacements $\varepsilon_g(x)$ of reinforcement and concrete located on both sides of the crack in the form of an elliptical crack instead of an alternative kinematic form, - the development of the Thomas-Kolchunov hypothesis. In this case, depending on the distance to the contact surface with the reinforcement (the coefficient k_r at a distance of three diameters or the protective layer of the reinforcement), the deplanation of the concrete in the section with the crack is taken into account.

5. The stiffness and opening of spatial cracks of reinforced concrete structures under bending with torsion in elastoplastic compressed concrete, as well as coefficients $\varphi_{i,j}$, $\nu(\lambda)$ for projecting linear and angular deformations (stresses) using the tensors of the compressed concrete diagram have been obtained. The approximation of rectangular cross-sections using the small-square 4×4 matrix for stiffness characteristics from D_{11} to D_{44}, as well as the inverse transition where known $\frac{1}{r_x}, \varphi, \varepsilon_0$ and Δ_Q or unknown M_x, M_t, N, Q are performed. To determine the tensile strength of the average working reinforcement, the basic parameters $\psi_{s,m}$ and $\psi_{sw,m}$ are applied for the convolute expressions and in the full form.

References

1. Karpenko, N.I.: General Models of Reinforced Concrete Mechanics. Stroyizdat, Moscow (1976)
2. Golyshev, A.B., Kolchunov, Vl.I.: Resistance of Reinforced Concrete. Osnova, Kiev (2009)
3. Bondarenko, V.M., Kolchunov, Vl.I.: Calculation Models of Force Resistance Of Reinforced Concrete. ACB, Moscow (2004)
4. Veryuzhsky, Yu.V., Kolchunov, Vl.I.: Reinforced Concrete Mechanics Methods. NAU, Kiev (2005)
5. Veryuzhsky, Yu.V., et al.: Structural Mechanics Reference Manual. Volume II. ACB, Moscow (2014)

6. Kolchunov, Vl.I., Fedorov, V.S.: Conceptual hierarchy of models in the theory of resistance of building structures. Indust. Civ. Eng. **8**, 16–23 (2020). https://doi.org/10.33622/0869-7019.2020.08.16-23

7. Golyshev, A.B., Kolchunov, V.I., Yakovenko, I.A.: Resistance of Reinforced Concrete Structures, Buildings and Structures Erected in Complex Engineering and Geological Conditions. Talkom, Kiev (2015)

8. Fedorov, V.S., Kolchunov, V.I., Pokusaev, A.A., Naumov, N.V.: Calculation models of deformation of reinforced concrete constructions with spatial cracks. Russ. J. Build. Constr. Architect. **3**(47). 6–26 (2020). https://doi.org/10.36622/VSTU.2020.47.3.001

9. Karpenko, N.I., Kolchunov, Vl.I., Travush, V.I.: Calculation model of a complex stress reinforced concrete element of a boxed section during torsion with bending. Russ. J. Build. Constr. Archit. **3**(51), 7–26 (2021). https://doi.org/10.36622/VSTU.2021.51.3.001

10. Kim, C., Kim, S., Kim, K.-H., Shin, D., Haroon, M., Lee, J.-Y.: Torsional Behavior of Reinforced Concrete Beams with High-Strength Steel Bars. ACI Struct. J. **116**, 251–233 (2019). https://doi.org/10.14359/51718014

11. Bernardo, L.: Modeling the full behavior of reinforced concrete flanged beams under torsion. Appl. Sci. **9**, 2730 (2019). https://doi.org/10.3390/app9132730

12. Lin, W.: Experimental investigation on composite beams under combined negative bending and torsional moments. Adv. Struct. Eng. **24**(6), 1456–1465 (2021). https://doi.org/10.1177/1369433220981660

13. Travush, V.I., Karpenko, N.I., Kolchunov, V.I., Kaprielov, S.S., Dem'Yanov, A.I., Konorev, A.V.: The results of experimental studies of structures square and box sections in torsion with bending. Build. Reconstr. **6,** 32–43 (2018)

14. Kolchunov, V., Dem'yanov, A., Naumov, N.: Analysis of the "nagel effect" in reinforced concrete structures under torsion with bending. IOP Conf. Ser. Mater. Sci. Eng. **953**, 012052 (2020). https://doi.org/10.1088/1757-899X/953/1/012052

15. Kolchunov, V., Smirnov, B., Naumov, N.: Physical essence of the "nagel effect" for main reinforcement in an inclined crack of reinforced concrete structures. IOP Conf. Ser. Mater. Sci. Eng. **896**, 012055 (2020). https://doi.org/10.1088/1757-899X/896/1/012055

16. Kolchunov, V.I., Dem'yanov, A.I., Naumov, N.V, Mikhaylov, M.M.: Calculation of the stiffness of reinforced concrete structures under the action of torsion and bending. J. Phys. Conf. Ser. **1425**, 012077 (2019). https://doi.org/10.1088/1742-6596/1425/1/012077

17. Kolchunov, V.I., Dem'yanov, A.I., Naumov, N.V: The second stage of the stress-strain state of reinforced concrete constructions under the action of torsion with bending (theory). IOP Conf. Ser. Mater. Sci. Eng. **753**, 032056 (2020). https://doi.org/10.1088/1757-899X/753/3/032056

18. Kolchunov, Vl.I., Demyanov, A.I.: The modeling method of discrete cracks and rigidity in reinforced concrete. Mag. Civil Eng. **4**(88), 60–69 (2019)

19. Kolchunov, V.I., Yakovenko, I.A.: About the violation solid effect of reinforced concrete in reconstruction design of textile industry enterprises. In: Proc. Higher Educ. Inst. Technol. Text. Indust. **3**(363). 258–264 (2016)

20. Kolchunov, Vl.I., Dem'yanov, A.I.: The modeling method of discrete cracks in reinforced concrete under the torsion with bending. Mag. Civil Eng. **5**(81), 160–173 (2018)

21. Kolchunov, V.I., Demyanov, A.I., Mikhailov, M.M.: Static-dynamic deformation of compressed concrete in an undetectable reinforced concrete frame under torsional bending Izvestia of higher educational institutions. Construction **4**(736), 5–21 (2020)

22. Kolchunov, V.I., Kolchunov, Vl.I., Fedorova N.V.: Deformation models of reinforced concrete under special impacts. Promyshlennoe i grazhdanskoe Stroit. Industrial Civ. Eng. **8**, 54–60 (2018)

23. Kolchunov, V.I., Demyanov, A.I., Protchenko, M.V.: Moments in reinforced concrete structures under bending with torsion. Build. Reconstr. **95**, 27–46 (2021). https://doi.org/10.33979/2073-7416-2021-95-3-27-46

Improvement of Methods of Inspection of Steel Structures of Overhead Power Line

Nikolai Senkin

Abstract The purpose of this publication is to develop proposals for updating and improving the methodology of technical inspection of steel structures of overhead power lines and assessment of technical condition. It is noted that there is a high proportion of damage to steel supports associated with aging of elements and corrosion wear. Considering the protective layer of corrosion products, there is a decrease in the aggressive effect of the atmosphere on the speed of the corrosion process. A method for determining the thickness of corrosion wear for the future with known wear for a known time of operation of the overhead line is proposed. This technique is confirmed by control measurements of the thickness of the corrosion layer in 1987 and in 2022 on steel supports of a 35 kV overhead line commissioned in 1972. An overhead power transmission line consists of a large number of transmission line supports, therefore, an integral assessment of the technical condition in points is more convenient for drawing up promising works on the reconstruction of overhead lines and repair of damaged structures.

Keywords Steel Structures · Overhead Power Lines · Technical Inspection · Corrosion · Damages · Repairs

1 Introduction

Damages, including emergency, and corrosion wear of the steel structure (SS) are considered as mandatory attributes of its actual operation, which lead to loss of bearing capacity and disruption of the functioning of the structure. Back in 1952, Professor G. A. Shapiro wrote in the book "The actual work of steel structures of industrial workshops" that "when investigating an operational structure, it is advisable to perform the following complex of works: inspection, testing, calculation and reinforcement of structures… A complete survey should be carried out at the

N. Senkin (✉)
Saint-Petersburg State University of Architecture and Civil Engineering, 4 Vtoraya Krasnoarmeiskaya, 190005 Saint-Petersburg, Russia
e-mail: senkin1952@yandex.ru

first stage, drawing up dimensional drawings and studying the operating conditions (operating modes, loads, atmosphere, soils …), the characteristics of steel structures and concrete foundations, the condition of elements, assemblies, and parts, welded and bolted joints, as well as identifying metal corrosion losses and the most damaged weaknesses in the structure" [1]. In the classic textbook "Metal structures" by Professor Yu. I. Kudishin emphasizes that during the examination it is necessary to identify both defects in the design or imperfections of structures that manifest themselves in the process of design, manufacture, and installation, as well as damage that occurs during operation. At the same time, the necessity of anticorrosive protection of overhead power transmission lines (overhead lines) operating in the open air is emphasized [2].

The relevance of the article is due to the high consumption of steel and the significant length of overhead power transmission lines of voltage classes 0.4–750 kV in Russia. Thus, since 2014, the scale of activity of the Russian Electric Power Company Rosseti has grown significantly: the length of transmission lines has increased by more than 150 thousand km—up to 2440 thousand km as of 2022 [3].

In practice, the loss of anticorrosive protection of overhead line steel structures during operation, for example, a layer of hot-dip galvanizing, indicates the presence of a significant impact of aggressive components of the atmospheric environment on the structure, leading to a decrease in the durability of the IC. Nevertheless, despite the loss of anticorrosive coating, steel structures of metal and reinforced concrete overhead line supports continue long-term trouble-free operation in different climatic conditions, while the technical service life of the T often significantly exceeds the economic one (Te = 50 years) and reaches 100 years or more.

The purpose of this publication is to develop proposals for updating and improving the methodology of technical inspection of steel structures of overhead lines and assessment of technical condition.

2 Technical Inspections to Improve the Reliability of Overhead Lines

There are numerous documented cases of emergency damage to steel structures with a voltage of 35–750 kV [4, 5]. So, for 11 years of observation (1997–2007) on 110–750 kV overhead lines, 283 out of 9.5 thousand cases of technological violations were caused by damage to steel supports with the fall of 121 supports. At the same time, the 7.5% share is associated only with aging and corrosion, mainly atmospheric, and the greatest damage to the SS with a 26.2% share is associated with theft of wire and elements of steel supports [5]. First of all, struts, braces, belt corners, steel support diaphragms located near the earth's surface are subject to corrosion wear, therefore, the topic of control and protection against corrosion of SS overhead lines is very relevant. Thus, according to the results of periodic inspections of the overhead line, including checking the condition of the metal structure and the anticorrosive

Fig. 1 A unique hyperboloidnsupport for the 110 kV overhead line crossing over the river. Oka 128 m high, erected in 1927–29 on the left bank 12 km from Dzerzhinsk, Nizhny Novgorod region (photo by the author, 2014)

coating, the need for a specialized technical inspection of the operated overhead line is determined [6, 7]. It is a timely inspection of the technical condition of steel structures of overhead power lines that allows us to identify both unfavorable environmental factors in which the overhead line support is operated, and to determine the critical elements of the SC that have the greatest damage, including corrosion wear.

For example, for a long time from the 1920s to the 1990s, there was a unique special 110 kV overhead line crossing over the river. The eye is based on eight hyperboloid mesh supports up to 128 m high developed by the great Russian engineer V. G. Shukhov [8]. And when there was a threat of destruction of the last highest support, due to the vandal theft of almost a third of the steel struts of the lower tier in the "zero" years, the transfer of this technical object as a monument of cultural heritage was carried out under the patronage of the Branch of Center and Volga Region - Nizhnovenergo, which performed the inspection and restoration of the damaged unique design (Fig. 1).

3   Method for Determining the Corrosion Wear of Steel Structures of Overhead Lines

It is known from experience that it is almost impossible to completely get rid of corrosion losses, so it is rational to allow corrosion of steel elements, but considering the controlled wear of overhead line support structures and the state of corrosion protection.

At the same time, it is necessary to consider the positive nature of the corrosion products formed on an unprotected surface, on which, under conditions of open exposure, protective solid layers of iron corrosion products are formed from colloids,

and in places with shade and high humidity, loose layers with a corroding surface of steel are formed [9]. Approximation of the results of 11-year studies of the Institute of Physical Chemistry of the USSR Academy of Sciences, obtained in the 1970s, shows a significant increase in corrosion wear for unprotected low-carbon steel at the beginning of exposure with its attenuation by the end of 11-year observation [9]. A significant influence of aggressive air conditions on the rate of the corrosion process is noted when considering the protective layer of corrosion products. On this basis, GOST 9.040–74 (2021) [10] provides a formula for determining the expected corrosion losses of the mass of M_t over a long period of operation with a coefficient n, considering the effect of corrosion products on the speed of the corrosion process. This formula Eq. (1) is transformed in the author's article [11] and allows, with a known thickness of the corrosion layer δ_1 in mm during the time τ_1 that has passed since commissioning, to obtain the desired thickness of corrosion wear δ_τ at the time τ:

$$\delta_\tau = \delta_1 (\tau/\tau_1)^n \tag{1}$$

where n is a dimensionless coefficient that considers the effect of corrosion products on the rate of the corrosion process, assumed to be 0.2–0.4 for a rural area, 0.5–0.6 for an industrial area.

Consequently, with known δ_1 in mm during the time of τ_1 obtained because of the survey, it is convenient to obtain the required thickness δ_τ at the time of τ, and this is confirmed by the results of measurements made by the author in June 2022 (Fig. 2).

The corrosion rate of steel elements is significantly influenced by the angle of inclination of the elements to the horizontal, which proceeds twice as fast on horizontal elements than on vertical ones [12]. In addition, the corrosion process is significantly affected by the height of the element location, so it is most intense up to a height of 1–1.5 m from the ground surface [13, 14].

The application of a zinc coating with a thickness of at least 80 μm (microns) using hot-dip galvanizing is the main way to ensure anticorrosive protection of elements of steel overhead line supports. The service life of such a coating in a mildly aggressive environment with a corrosion rate of 1–5 μm per year is at least 4–20 years [15].

In 1982–1990, the Department of Industrial and Civil Engineering of the Ukhta Industrial Institute, under the guidance of the author, carried out studies of corrosion wear of steel supports of 35–110 kV overhead lines of the Komienergo Company in the Komi Republic [11]. In 1987, corrosion wear was measured on steel supports of a 35 kV double-chain overhead line, commissioned in 1972 and running along Cosmonauts Avenue in the city of Ukhta. And in June 2022, a control check of wear after 50 years of operation of this line took place (Figs. 2 and 3), the results of which confirmed the high reliability of the proposed "Methodology for determining the corrosion wear of steel structures of overhead lines".

However, in the proposed formula (1), it is advisable to assign the following coefficients n to the safety margin, taken to be 0.6 for a mildly aggressive environment, 0.8 for a medium aggressive environment and 1.0 for an aggressive environment, like
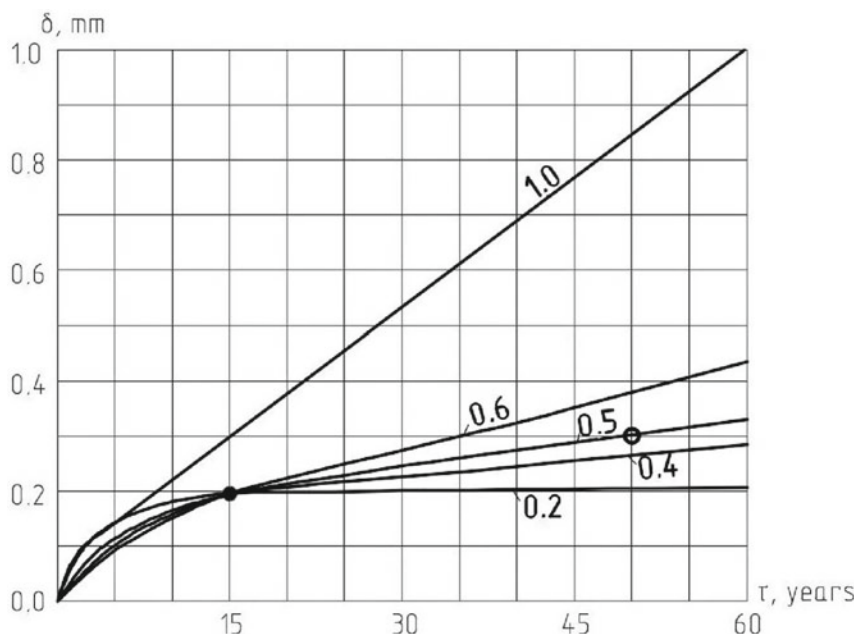
Fig. 2 Forecasting charts corrosion wear δ of unprotected steel, calculated according to the recommended method, considering attenuation corrosion rates in time τ depending on the degree of aggressiveness of the air environment (coefficient $n = 0.2…1.0$ proportional to the degree of aggressiveness)

those adopted in the Standard "Methodological guidelines for assessing the technical condition of overhead lines and the residual life of overhead line components" [16]. At the same time, for structures with protective anticorrosive coatings, the duration of operation is calculated after the destruction of such coatings. Criteria for assigning parameters of aggressiveness of the air environment are determined in accordance with the requirements of the Code of Rules of SP 28.13330.2017 "Protection of building structures from corrosionǁ" [17].

4   Methodology of Inspection of Steel Structures of Overhead Line Supports

Technical inspection of overhead line metal structures is carried out in accordance with the requirements of interstate standards GOST 31,937-2011 "Buildings and structures. Rules of inspection and monitoring of technical condition" [18], GOST 27,751 "Reliability for constructions and foundations. General principles" [19], SP 13-102-2003 "Rules for the inspection of load-bearing building structures of buildings and structures" [20], the industry standard of the organization of PJSC FGC
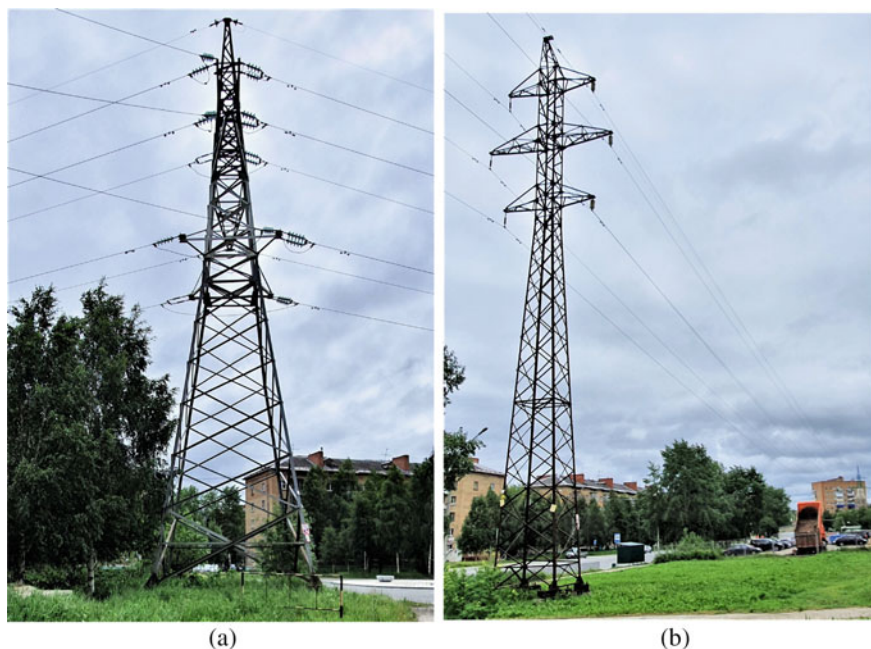
Fig. 3 Anchor-angular **a** and intermediate **b** supports of a 35 kV double-chain overhead line, on the lower struts and braces of which corrosion wear was measured (photo by the author, June 2022)

UES STO 56,947,007–29.240.55.111-2011 "Guidelines for assessing the technical condition of overhead lines and the residual life of overhead line components" [16] and Standard Operating Instructions for overhead power lines with a voltage of 35–800 kV (RD 34.20.504-94) [21]. In accordance with these Rules, the survey is a set of measures to determine and evaluate the actual values of the controlled parameters that characterize the operational condition, suitability, and operability of the objects of study and determine the possibility of their further operation or the need for restoration and strengthening.

The method of inspection of construction structures with an assessment of the technical condition of structures overhead line supports, is based on numerous studies and tests since the beginning of the twentieth century, primarily under the guidance of outstanding Russian scientists and engineers N. N. Aistov, V. A. Trull, K. P. Kryukov, A. A. Zevin, E. V. Gorokhov, L. V. Yakovleva, V. M. Gerasimova, V. V. Alekseeva, C. V. Krylova, L. V. Timashova, P. I. Romanova, L. I. Kachanovskaya, R. S. Kaverina, G. A. Suchkova, etc. and has a long, never-ending period of positive development.

In 2007–2008, the author was the head of several works carried out by the Center for Overhead Line Engineering of JSC "Firm ORGRES" (Moscow), to survey the technical condition of 110–500 kV overhead lines for the purpose of their reconstruction and extension of operational life in various regions of Russia. It should be noted the special methodological approach of ORGRES, which was used in the

comprehensive examination of overhead lines. Then a Program, a Calendar plan and a "Methodology for conducting a survey of overhead lines" were attached to the work contract, in which qualitative quantitative criteria for assessing the technical condition of structures were assigned (in the form of a table).

This Technique was developed by an outstanding researcher Leonid Vasilyevich Yakovlev (1932–2007), who for a long time successfully led the full-scale testing of elements as part of the Civil Engineering laboratory of JSC "Firm ORGRES" in Hotkovo, Moscow region. Even now, this Technique represents a higher and differentiated level of assessment of the technical condition of an energy facility, combining qualitative and quantitative evaluation criteria that are directly related to the reliability characteristics of overhead line structures in comparison with the current industry standard of the organization of PJSC FGC UES STO 56,947,007–29.240.55.111-2011 "Guidelines for assessing the technical condition of overhead lines and residual resource of overhead line components" [16].

The Table 1 presents quantitative and qualitative indicators as criteria for assessing the technical condition of steel structures of overhead lines, proposed in the form of reliability coefficients according to the Method of L. V. Yakovlev (column 1) and a point score (column 2).

For example, in 2007, a technical survey of 220 kV overhead lines in Khakassia was carried out, as a result, the technical condition of this line was recognized as limited-operable with an integral reliability coefficient of the surveyed sections with reinforced concrete (32 pcs.) and steel (33 pcs.) supports: $K = (0{,}80 \cdot 32 + 0{,}88 \cdot 33)/(32 + 33) = 0{,}84 < 0{,}9$, where 0.80 and 0.88 are the average values of the reliability coefficients in accordance with the table (column 1) [22]. The quantitative integral relative estimate proposed by the author (column 2) is $K_a = (2{,}30 \cdot 32 + 2{,}90 \cdot 33)/(32 + 33) = 2{,}60$ points < 3 consequently, the technical condition is limited and workable, which requires the organization of planned repairs or reconstruction of the line within 5 years.

The overhead power line is made up of a large number of transmission line supports, so an integral assessment of the technical condition in points is more convenient for concluding promising works.

Table 1 Criteria for assessing the technical condition of the overhead line structure

Quantitative indicators of the condition of the structure condition Reliability coefficient K	Score in points	Qualitative indicators of the technical of the structure (GOST 31,937–2011) [18]
≥1	4	The state is normative, corresponding to the normative and technical documentation
1–0.9	3	Working condition
0.9–0.7	2	The condition is limited-operable
0.7–0.5	1	The condition is unacceptable, emergency

5 Conclusions and Suggestions

Proposals have been developed to update and improve the methodology of technical inspection of overhead line steel structures, including the Methodology for determining the degree of corrosion wear and assessing the technical condition.

References

1. Shapiro, G.A.: Actual work of steel structures of industrial workshops. Gosstroyizdat, Moskow-Leningrad (1952)
2. Kudishin, Yu.I.: Metal Structures: Textbook. Academy, Moskow (2011)
3. Ryumin, A.: Head of PJSC Rosseti. Achieve complete independence. https://lenta.ru/articles/2022/04/14/zameshchenie/. Accessed 28 June 2022
4. Belyaev, B.I., Kornienko, V.S.: Causes of Accidents of Steel Structures and Ways to Eliminate Them. Stroyizdat. M. (1968)
5. Efimov, E.N., Timashova, L.V., Yasinskaya, N.V.: The causes and nature of damage to components of overhead power transmission lines with a voltage of 110–750 kV in 1997–2007. Energy Unified Grid **2**, 32–41 (2012)
6. Ovchinnikov, I.G., Petrov, V.V.: Determination of durability of structural elements interacting with an aggressive environment. Constr. Mech. Calcul. Struct. **2**(140), 13–18 (1982)
7. Krylov, S.V.: Technical condition of overhead lines 35 kV and above: methods of examination. News Electr. Eng. **1**(37), 35–41 (2006)
8. Shukhov, V.G.: (1953–1939) The art of construction: Trans. from it./Edited by R. Grefe, M. Gapoeva, O. Perchi. Mir. M. (1995)
9. Berukshtis, G.K., Clark, G.B.: Corrosion Resistance of Metals and Metal Coatings in Atmospheric Conditions. USSR Academy of Sciences. In-t phys. chemistry. Nauka. M. (1971)
10. GOST 9.040-2021. Unified system of protection against corrosion and aging. Metals and alloys. Computational and experimental method for accelerated determination of corrosion losses in atmospheric conditions. Russian Institute of Standardization. Moscow (2022)
11. Senkin, N.A.: On the periodicity of painting of steel elements of electric grid structures during operation. (Informenergo, No. 2530-EN-87). Ukhta Industrial Institute. Ukhta (1986)
12. Projector, E.G., Anastasiev, P.I., Kolyada, A.V.: Protection of Cable and Overhead Power Transmission Lines from Corrosion. Energia. Moscow (1974)
13. Romanov, P.I., Kachanovskaya, L.I., Chernova, T.V.: On the issue of increasing the corrosion resistance of overhead line supports. Progressive solutions in power grid construction: collection of scientific tr. in-ta Energosetproekt., pp. 146–152 (1988)
14. Romanov, P.I., Kachanovskaya, L.I., Chernova T.V.: Control of corrosion defects of metal elements of overhead line supports. Progressive solutions in power grid construction: sb. tr. in-ta Energosetproekt., pp. 40–48 (1986)
15. Gorokhov, E.V., Shapovalov, S.M., Udod, E.I. et al.: Improving the Reliability and Durability of Electric Grid Structures/Ed. by Gorokhov, E.V. Technika. Kiev (1997)
16. Standard of PJSC FGC UES STO 56947007-29.240.55.111-2011: Guidelines for assessing the technical condition of overhead lines and the residual life of overhead line components. https://www.fsk-ees.ru/upload/docs/sto_56947007-29.240.55.111-2011.pdf. Accessed 28 June 2022
17. Code of Rules of the Joint Venture SP 28.13330.2017. Protection of building structures from corrosion. Protection against corrosion of construction https://docs.cntd.ru/document/456069587. Accessed 28 June 2022
18. GOST 31937-2011. Buildings and structures. Rules of inspection and monitoring of technical condition

19. GOST 27751. Reliability for constructions and foundations. General principles. Moscow (2021)
20. SP 13-102-2003. Rules for the inspection of load-bearing building structures of buildings and structures. Moscow (2003)
21. Standard Operating Instructions for overhead power lines with a voltage of 35-800 kV (RD 34.20.50494). Moscow (1994)
22. Senkin, N.A.: Actual tasks in the design and construction of the ENES overhead line: an example of a survey. Energoexpert **5**(40). 90–94 (2013)

Square-Section Tube-Concrete Structures Studying Under Axial Compression Both with Spiral Reinforcement of the Concrete Core and Without Reinforcement

Vladimir Rimshin , **Anatoly Krishan** , **Elena Korol** ,
**Svetlana Roshchina** , **and Igor Shubin**

Abstract The article contains a research methodology and the experiments results on samples of square-section tube-concrete structures, both with spiral reinforcement of the concrete core, and without reinforcement, which perceive a short-term compressive load. The aim was studying the strength and features of the stress–strain state of square-section tube-concrete structures samples, made of concrete of classes B40 and B80, taking into account their flexibility. The experimental part of the work was carried out using modern equipment and devices certified and metrologically certified. Probabilistic-statistical calculation methods were used to process the array of experimental data obtained. According to the requirements of the current regulatory documents, before the tests, the measurement error assessment by the tensoresistive method was carried out. The features of force resistance revealed in experiments testify to the operation of a concrete core and a steel tube under conditions of a volumetric stress state. The deformation nature of the steel tube suggests that its walls experience not only compression in the axial direction. Stretching and bending of the walls from the lateral pressure of the concrete core is also observed. Thus, the tube contribution to the perception of the force $N_u{}^{exp}$ is significantly less

V. Rimshin (✉) · E. Korol
Moscow State University of Civil Engineering (MGSU), Yaroslavskoye Shosse, 129337, 26, Moscow, Russia
e-mail: v.rimshin@niisf.ru

V. Rimshin · I. Shubin
Research Institute of Building Physics of the Russian Academy of Architecture and Building Sciences, 21, Locomotive Passage, 127238 Moscow, Russia

A. Krishan (✉)
Nosov Magnitogorsk State Technical University, 455000, 38, Lenin Avenue, Magnitogorsk, Russia
e-mail: kris_al@mail.ru

S. Roshchina
Vladimir State University Named After A.G. and N.G.Stoletov, 87Gorky Street, 600000 Vladimir, Russia

than it would be in the assumption of its operation in uniaxial compression. It indicates a noticeably greater contribution of concrete to the perception of the force $N_u{}^{exp}$ in comparison with the conditions of uniaxial compression. The main conclusion of the experiments follows from it. It is advisable to increase the strength of square-section tube-concrete structures by using high-strength concrete and providing more effective indirect reinforcement for it. The power resistance features of square-section tube-concrete structures revealed in the experiments must be taken into account when calculating their strength.

Keywords Tube-concrete elements of square cross section · Spiral reinforcement · Axial compression · Tensoresistor method · Force resistance

1   Research Methods

The object of the experimental study were samples of square-section tube-concrete structures, both with spiral reinforcement of the concrete core, and without reinforcement, perceiving a short-term compressive load. The aim was studying the strength and features of the stress–strain state of square-section tube-concrete structures samples, made of concrete of classes B40 and B80, taking into account their flexibility.

Nowadays, square-section tube-concrete structures under axial compression have been investigated. 4 series of prototypes were manufactured with cross-sectional dimensions of 100×100 mm and a height of 520 mm to solve the experimental set. Metal plates 10 mm thick were welded to the specimens ends. Each series was based on 3 twin samples [1–3].

All samples in one series were cut off from one tube and end-faced. One series was additionally supplied with a frame with spiral reinforcement (Figs. 1, 2). The frame was made of longitudinal reinforcement bars ⌀6 A500C (GOST R 52,544-2006) and reinforcing wire ⌀5 Bp 500 (GOST 6727-80), which was wound around the longitudinal bars of the frame in a spiral with a pitch of 30 mm. In order to preserve the design shape of the core, the longitudinal and spiral reinforcements were tied with knitting wire. Yield strength of reinforcing wire is A500C $\sigma_{s,y} = 552$ MPa, Bp500 $\sigma_{s,y} = 548$ MPa. Tensile strength at break, respectively, $\sigma_{s,u} = 735$ MPa and $\sigma_{s,u} = 730$ MPa. The spiral winding diameter in the plan was 82 mm. The main samples parameters of each series were as follows: B-45 series - tube-concrete samples made of heavy concrete of class B45, enclosed in a shaped square tube with dimensions $100 \times 100 \times 4$ mm, height 520 mm, made of steel of class C345; B-80 series - samples similar to the B-45 series, but made of B80 class concrete; series S-80 - specimens similar to series B-80, but made of prestressing concrete of class B80 with a self-stressing value of 2 MPa; SA-80 series - samples similar to the S-80 series, but with a frame with spiral reinforcement.

Fig. 1 Frames with spiral
reinforcement for installation
in square-section
tube-concrete structures
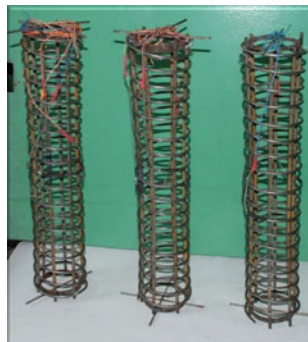
Fig. 2 Frames with spiral
reinforcement for installation
in square-section
tube-concrete structures

The following materials were used as components for prototypes manufacturing: portland cement M500 (GOST 10,178-85); sand from the Magnitogorsk sand quarry with a fraction of 0–5 mm; crushed stone from the Beloretsk granite quarry with a fraction of 5–10 mm; superplasticizer Sika «ViscoCrete» 5-600 SP; Ebelit (multifunctional action modifier) ; electric-welded tubes $\varnothing 219 \times 5$ mm according to GOST 10,705-80; profile steel tubes $140 \times 140 \times 4$ mm according to GOST 30,245-2003; fittings A500C $\varnothing 6$ mm according to GOST R 52,544-2006; fittings Bp500C $\varnothing 5$ mm according to GOST 6727-80; base plates 10 mm thick made of steel grade St3. The concrete mixture compositions for all the studied series are presented in Tables 1, 2, 3 and 4.

Before the prototypes manufacturing, shell tubes segments of the required dimensions were prepared. Billets of the required length were cut from one shell tube and end-faced on a lathe. For the first series, the initial concrete class B45 of increased strength was adopted. Such concretes are recommended for using a shell tube made of steel grade 09G2S. For the other three series, high-strength concrete is adopted, having a class of axial compressive strength B80.

The technology for manufacturing samples of all series was the same. Initially, a concrete mixture was made to form the structure core. Then, the shell tube with a temporarily installed metal plate, which prevents the concrete mixture from flowing out of the tube, was installed on a vibrating table and securely fastened to it with bolts. Then, gradually, in small parts, the concrete mixture was placed into the tube (100 ÷ 150 mm each). Self-compacting concrete mixtures were used. At the end of the molding process, the top of the shell tube was covered with a metal plate, similarly to the lower end, in order to avoid shrinkage deformations in the initial stage of the concrete hardening process. The lower and upper typesetting plates were pulled together with steel bands. The sample was moved for 48 h to the area reserved for storage at a temperature of 20 ± 3 °C [4–8].

After two days, the metal plates were removed from the ends, the element ends were cleaned, and end plates 10 mm thick were welded to the shell tube with a continuous seam. All welds were coated with grease to ensure tightness. These activities created favorable conditions for the hardening of the concrete core. The difference in the samples manufacturing of the SA-80 series was that before installing the sample on the vibrating table, a rod frame and wire reinforcement was installed inside the tube (longitudinal - 6 rods ⌀6 A500C, ring - ⌀5 Bp500). Strain gauges with a base of 5 mm were glued to the longitudinal and spiral frame reinforcement. Control concrete samples in the form of cubes and prisms were made with dimensions of $100 \times 100 \times 100$ mm and $100 \times 100 \times 400$ from one batch, in accordance with GOST 10,180-2012. Prior to their stripping, the samples were stored in wet sawdust, excluding moisture evaporation from them, in a room with an air temperature of (20 ± 5) °C. After stripping, the control concrete cubes and prisms were stored in accordance with GOST 10,180-2012. The self-tension control of self-stressing concrete was carried out in accordance with GOST 32,803-2014. Concrete self-stress was determined using three control samples-prisms $100 \times 100 \times 400$ mm in size, molded and hardened in special dynamometric jigs (Fig. 3).

During the concrete expansion, the conductors create an elastic deformations limitation, equivalent to 1% of the longitudinal reinforcement of the prism specimens. Conductors were measured daily for concrete at the age of 1–7 days and further at the age of 10, 14 and 28 days. Each time the measuring device was checked with a

Fig. 3 Control samples-prisms in conductors

standard (Fig. 4). The measurement results were recorded in the test log for prism specimens in conductors when determining the concrete self-stress. The compressive strength of stress concrete was determined in accordance with the requirements of GOST 10,180-2012. The samples age at the testing time was 30 days. Control samples tests of concrete were performed on an IP-2000 hydraulic press. Electrical strain gauges with a base of 50 mm were used to measure the longitudinal and transverse prisms deformations. The strain gauges readings were recorded using a universal portable multichannel measuring and computing complex MIC-036 (Fig. 5).

The studied samples of square-section tube-concrete structures were tested in a vertical position on a hydraulic press 2PG-500 with a short-term compressive load. The experimental part of the work was carried out using modern equipment and devices certified and metrologically certified. Probabilistic-statistical calculation methods were used to process the array of experimental data obtained. According to the requirements of the current regulatory documents, before the tests, the measurement error assessment by the tensoresistive method was carried out. The features of force resistance revealed in experiments testify to the operation of a concrete core and a steel tube under conditions of a volumetric stress state. Electric strain gauges were used on longitudinal reinforcement with a base of 5 mm and on a shell tube with a base of 20 mm to measure the longitudinal and transverse deformations of

Fig. 4 Checking the measuring device

Fig. 5 Measuring and computing complex MIC-036
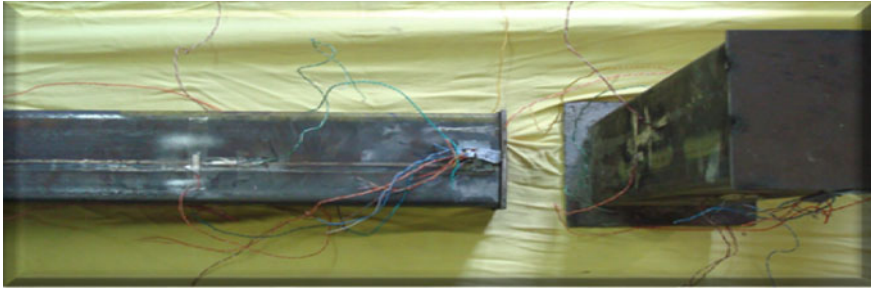
Fig. 6 Electric strain gauges arrangement on a steel tube-sheath

materials during testing (Fig. 6). The readings of strain gauges were recorded using a universal portable multichannel measuring and computing complex MIC-036. On the shell tube, strain measurements were duplicated by Aistov strain gauges with a scale division of 0.001 mm [9–13].

2 The Measurement Error Determination by the Tensoresistive Method

According to the requirements of the current regulatory documents, before the tests, the measurement error assessment by the tensoresistive method was carried out. The error is the difference between the instrument reading and the true measured value:

$$\Delta_\varepsilon = \varepsilon_{pr} - \varepsilon_{or} \tag{1}$$

The error depends on the measured deformation level, the measuring device type and the experiment conditions. The tensoresistive method of measuring deformations makes it possible to exclude errors due to voltage fluctuations in the power supply network of the device and the temperature factor. The influence of intrinsic creep of strain gauges is eliminated due to the strain gauges design and the short experiment duration. In this case, the total limiting error of strain measurement is determined by the error associated with the strain sensitivity coefficients S spread of the strain gauges used and the error φ and φ_o of reading the device and is calculated by the following formulas:

$$\Delta_\varepsilon = \sqrt{D_s^2 + D_f^2 + D_{f0}^2} \tag{2}$$

$$\Delta_\varepsilon = \frac{\Delta_\varepsilon}{\varepsilon} = \frac{1}{\varepsilon}\sqrt{D_s^2 + D_f^2 + D_{f0}^2} \tag{3}$$

$$D_s = \frac{\partial \varepsilon}{\partial S} * \Delta_s = \frac{\Delta_s}{S} * \varepsilon = \overline{\Delta_s} * \varepsilon \tag{4}$$

D_s –partial error due to the spread of the strain gauge factor S, its value is entered as an average value for a batch of strain gauges;

D_f, D_{fo}– partial reading errors φ and φ_o.

It was assumed that random measurement errors are subject to the normal distribution law when determining the error. The error estimation of results statistical processing was carried out according to:

$$\overline{\Delta_s} \le 2\sigma_s \tag{5}$$

where $\sigma_s = \sqrt{\frac{1}{n-1} \sum\limits_{i-1}^{n} \left(S_i + \overline{S}\right)^2}$ – standard deviation S;

n – the number of strain gauges in the evaluated batch;
$\overline{S}$ – arithmetic mean value of quantity S,

$$S = \frac{1}{n} \sum\limits_{i-1}^{n} S_i \tag{6}$$

During testing, eight strain gauges were glued onto the steel tube-shell. The strain sensitivity S of all strain gauges was selected in such a way that it did not differ by more than 0.02 in the selected sensors batch. Then:

$$\sigma_s = \sqrt{\frac{1}{8-1} \left[(2.10 - 2.12)^2 + (2.11 - 2.12)^2 + ... + (2.14 - 2.12)^2\right]} = 0.0214 \tag{7}$$

$$\Delta_s 0.0214 * 2 = 0.0428$$

The partial error D_s at the deformations level 1000×10^{-5} is:

$$D_s = \Delta_s \varepsilon = 0.0427 * 1000 * 10^{-5} = 42.7 * 10^{-5} \tag{8}$$

Total error:

$$\Delta_\varepsilon = \frac{1}{1000 * 10^{-5}} \sqrt{} \tag{9}$$

or ≈4.3%, which provides the required (no more than 6%) measurement accuracy.

The ends support of the samples was assumed to be hinged. The samples were placed on the press in a vertical position and carefully centered. The axial compressive load was applied for a short time. The load was transferred simultaneously to the concrete core and the steel shell. Since the stress concentration usually manifests itself in the upper and lower end zones, before testing, bandages were fixed at the

Fig. 7 Mechanical devices scheme during the test for central compression: 1 - dial gauges; 2 - Aistov strain gauges
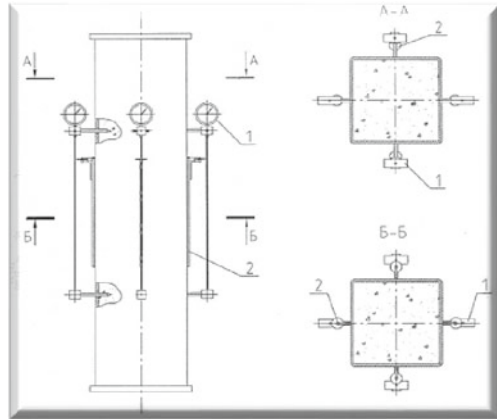
Fig. 8 General view of the sample during testing

ends of the steel shell tubes in height equal to half the external size of the sample cross section. Mechanical devices scheme during the test for central compression is shown in Fig. 7. General view of the sample during testing is shown in Fig. 8.

3 Research Results

In accordance with the requirements of GOST 30,245, GOST 30,432, GOST 32,803, GOST 6727, GOST 52,544 and GOST 10,180, before testing specimens of all columns series, the strength and deformation characteristics of the starting materials were determined. Strips 400×20 mm in size were cut from its to determine the mechanical characteristics of the tube steel in tension walls. The destruction nature of steel strips samples is shown in Fig. 9. The mechanical tests results of steel tubes are shown in Table 5.

Fig. 9 Test result of steel strip samples

Table 1 The concrete mixture composition for samples of the B-45 series

Material name	Quantity per 1 m^3
Cement, kg/m^3	443
Sand, kg/m^3	704
Crushed stone, kg/m^3	945
Embelite, kg/m^3	-
Sika «ViscoCrete», l/m^3	6.65
Water, l/m^3	177
W/C	0.4

Table 2 The concrete mixture composition for samples of the B-80 series

Material name	Quantity per 1 m^3
Cement, kg/m^3	465
Sand, kg/m^3	714
Crushed stone, kg/m^3	936
Embelite, kg/m^3	-
Sika «ViscoCrete», l/m^3	7.0
Water, l/m^3	167
W/C	0.36

Table 3 The concrete mixture composition for samples of the S-80 series

Material name	Quantity per 1 m^3
Cement, kg/m^3	465
Sand, kg/m^3	688
Crushed stone, kg/m^3	912
Embelite, kg/m^3	93
Sika «ViscoCrete», l/m^3	9.0
Water, l/m^3	167
W/C	0.36

Table 4 The concrete mixture composition for samples of the SA-80 series

Material name	Quantity per 1 m^3
Cement, kg/m^3	465
Sand, kg/m^3	688
Crushed stone, kg/m^3	912
Embelite, kg/m^3	93
Sika «ViscoCrete», l/m^3	9.0
Water, l/m^3	167
W/C	0.36

Table 5 The mechanical tests results of steel tubes

Sample type	Quantity, pcs	Yield strength σ_y, MPa	Tensile strength σ_u, MPa	Elasticity modulus E_s, MPa
Steel strip with a section of 20 × 4 mm	5	372	520	2.05×10^5

Table 6 The mechanical tests results of steel tubes

Series	R, MPa	R$_{bu}$, MPa	E$_b$,MPa
B-45	60.1	48,1	38,410
B-80	91.7	82,1	42,545
S-80	94.2	84,5	42,830
SA-80	93.2	83,9	41,750

The test results of concrete control samples are shown in Table 6. The following designations are used here:

R – cubic compressive strength of the original concrete;

R_{bu} – prismatic compressive strength of the original concrete;

E_b –initial modulus of concrete elasticity.

The materials strength characteristics were used to determine the expected breaking load N$_u$ and to assign the load step value of square-section tube-concrete laboratory samples. The samples were loaded in steps of 5–10% from N$_u$ up to 0.7 N$_u$. Further, at N$_u$ more than 0.7 N$_u$, the loads were loaded in steps of 0.05 N$_u$ until the compressive load began to drop. During the 10-min exposure at each stage, the readings of all measuring instruments and sensors were recorded. The main results of testing samples of square-section tube-concrete structures are presented in Table 7. Here, the prism strength values of the initial concrete R and the concrete self-stress values P are given. The average yield strength of steel σ of profile tubes is assumed to be 372 MPa for all samples. Table 7 shows the experimental breaking loads $N_u^{\exp}$ and the forces N_{bp}^{th} equal to the sum of the maximum forces in the concrete (reinforced concrete) core and steel shell assuming their work in uniaxial compression [14–24].

Table 7 The main results of testing samples of square-section tube-concrete structures

Series, sample	R, MPa	P, MPa	$N_u^{\exp}$, kN	N_b^{th}, kN	N_{bp}^{th}, kN	$n_b = \dfrac{N_b^{th}}{N_{bp}^{th}}$	$k = \dfrac{N_u^{\exp}}{N_{bp}^{th}}$
B-45–1	48.1	0	867	372	779	0.48	1.11
B-45–2	48.1	0	867	372	779	0.48	1.11
B-45–3	48.1	0	900	372	779	0.48	1.15
B-80–1	82.1	0	1100	636	1042	0.61	1.05
B-80–2	82.1	0	1150	636	1042	0.61	1.10
B-80–3	82.1	0	1163	636	1042	0.61	1.11
S-80–1	84.5	2	1200	654	1060	0.62	1.13
S-80–2	84.5	2	1220	654	1060	0.62	1.15
S-80–3	84.5	2	1200	654	1060	0.62	1.13
SA-80–1	83.9	2	1450	650	1116	0.58	1.30
SA-80–2	83.9	2	1480	650	1116	0.58	1.33
SA-80–3	83.9	2	1480	650	1116	0.58	1.33
Mean							1.11

The quantitative assessment of indirect reinforcement influence, due to the restraining effect of the steel tube and spiral reinforcement (if any) is made using the coefficient $k = N_u^{\exp} / N_{bp}^{th}$. The results obtained indicate that in all four series there is the indirect reinforcement effect. The samples strength turned out to be noticeably higher than the sum of the maximum forces in the concrete (reinforced concrete) core and steel shell, assuming their work in uniaxial compression. The average value of the coefficient k was:

- 12.3% for samples of the B-45 series;
- 8.7% for samples of the B-80 series;
- 13.3% for samples of the S-80 series;
- 32% for samples of the SA-80 series.

The obtained values of the coefficient k confirm the well-known fact that with an increase in the strength of the original concrete, the effect of indirect reinforcement decreases. At the same time, the positive effect of prestressing concrete precompression in samples of the S-80 series is clearly visible. This circumstance should be taken into account when designing square-section tube-concrete structures. The indirect reinforcement effectiveness was affected by the spiral reinforcement presence to an even greater extent. The coefficient k here turned out to be of the same order as in the centrally compressed tube-concrete elements of a circular cross section. At the same time, it is obvious that in cases of eccentric compression, a square tube can be more efficient than a circular one. According to the measuring results of the sample deformations, the dependencies «n-ε» were constructed, where n is the relative value of the compressive load $n = N / N_u^{\exp}$; ε is the relative deformation of

the sample (positive values are axial shortening deformations, negative values are transverse elongation deformations). Characteristic dependencies «n-ε» are shown in Figs. 10–13. According to these dependencies, it can be seen that the axial deformations of specimens without helical reinforcement already at the loading level n = 0.85 ÷ 0.9 amounted to 0.0038…0.0045. Significant plastic deformations developed with a further increase in the load. The concrete core and the steel tube deformed together. Therefore, it can be concluded that the ultimate deformability of the concrete core is significantly higher compared to the deformability of uniaxially compressed concrete.

In specimens of the SA-80 series with helical reinforcement, axial deformations reached about 1.4–1.5% by the failure time. It was revealed that additional indirect reinforcement in the form of a spiral significantly increases the limiting deformations

Fig. 10 Characteristic dependence «n-ε» for samples of the B-45 series
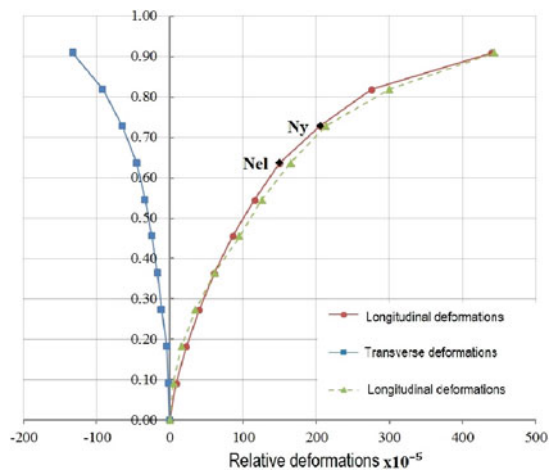
Fig. 11 Characteristic dependence «n-ε» for samples of the B-80 series
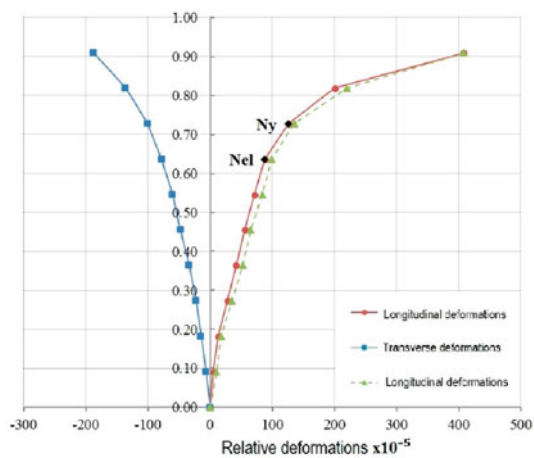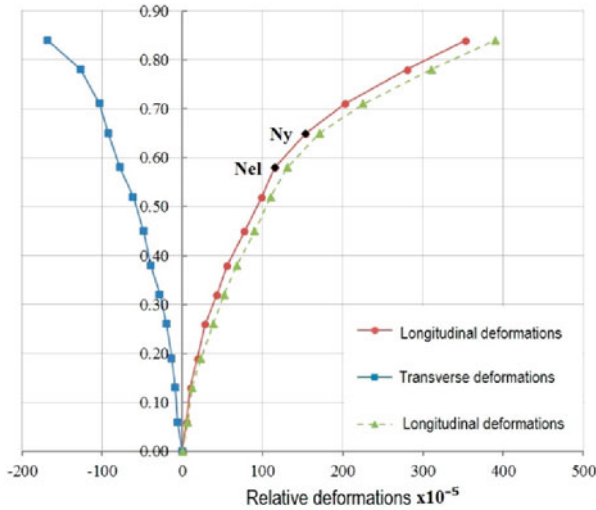
Fig. 12 Characteristic dependence «n-ε» for samples of the S-80 series
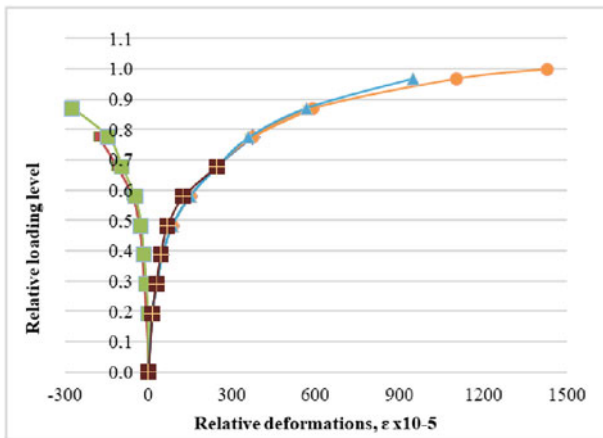
Fig. 13 Characteristic dependence «n-ε» for samples of the SA-80 series

of tube concrete samples. According to these dependences, it can be determined that the elastic work limit of the elements was achieved at loads equal to (0.58 ... 0.65) N_u. For samples made of prestressing concrete, the elastic work limit was slightly higher compared to other samples. At the same time, for all samples, axial shortening deformations were much less than the limiting ones and amounted to the order of $\varepsilon_{el} = 110 \times 10^{-5} ... \varepsilon_{el} = 155 \times 10^{-5}$.

Analyzing the dependencies presented in Figs. 3, 4, 5 and 6 the following features can be noted of the outer steel shell, reinforcing cage and concrete core in the studied

samples. The entire process of power resistance can be conditionally divided into three stages. The first is the quasi-elastic element work. In samples of the SA-80 series, spiral reinforcement is practically not included in the work. The relative elongation strains of the helix did not exceed 64×10^{-5}. The elastic–plastic stage comes next. Here, microcracks begin to form in the concrete core, which contributes to an increase in its volume. The steel tube-shell gradually changes into a fluid state. By the end of this stage, the stresses in the concrete core reach the upper cracking limit. In samples of the SA-80 series, the stresses in the longitudinal reinforcement at this stage do not exceed 60% of the yield strength. Spiral reinforcement is actively included in the work. The presence of indirect reinforcement in the concrete core inhibits the intense microcracks formation. In samples with tension concrete, the the upper and lower boundaries of crack formation become higher. The longitudinal reinforcement of the frame (if any) works practically in conjunction with concrete.

The last work stage is plastic in nature. In the longitudinal and transverse directions, there is a sharp increase in the element deformation. The stresses in the longitudinal reinforcement reach the yield point. In helical reinforcement, the stresses also reach the yield point. A further increase in the load became impossible due to a sharp increase in deformations. Despite the high-strength concrete use in most samples, the destruction nature has always been plastic. At the moment of destruction, folds formed on all side faces of the samples at approximately the same element height. Local buckling of the steel tube was observed, which was more pronounced in the middle zones of the side faces. The concrete was crushed in places where the folds were formed. End plates were removed from some of the samples after testing. Then their steel tube-shell was cut in the vertical direction. The samples destruction nature with a view of the steel tube-shell and the exposed reinforced concrete core are shown in Fig. 14.

The shell tube was difficult to separate from the concrete core. The adhesion was so high that pieces of concrete were removed from the steel shell in elements with

a)   b)

Fig. 14 Samples view of the SA-80 series after destruction: **a** - the formation of a fold on the shell side surface; **b** - spiral rupture

self-stressing concrete and the spiral frame. It turned out that in all the examined samples, the corrugations formed on the steel tube as a result of the loss of local stability were filled with crushed concrete. A rupture of helical reinforcement was found in the places where corrugations are formed and concrete is crushed in a sample of the SA-80 series. The absence or presence of a spiral frame in steel-tube concrete samples significantly affects its behavior in the limit state stage. The limiting axial strains in specimens with helical reinforcement increased by about 2 times compared with specimens strains of other series.

At the same time, the average strength of SA-80 samples series turned out to be 22% higher compared to analogue samples without spiral reinforcement of the S-80 series. This fact is due to an increase in lateral pressure on the concrete core due to additional indirect reinforcement. The SA-80 and B-45 samples strengths comparison indicates that the central compressive strength of the improved design of square-section tube-concrete structures turned out to be 67% higher compared to traditionally used concrete pipe elements.

4 Conclusion

The features of force resistance revealed in experiments testify to the operation of a concrete core and a steel tube under conditions of a volumetric stress state. The deformation nature of the steel tube suggests that its walls experience not only compression in the axial direction. Stretching and bending of the walls from the lateral pressure of the concrete core is also observed. Thus, the tube contribution to the perception of the force $N_u^{\exp}$ is significantly less than it would be in the assumption of its operation in uniaxial compression. It indicates a noticeably greater contribution of concrete to the perception of the force $N_u^{\exp}$ in comparison with the conditions of uniaxial compression. The main conclusion of the experiments follows from it. It is advisable to increase the strength of square-section tube-concrete structures by using high-strength concrete and providing more effective indirect reinforcement for it. The power resistance features of square-section tube-concrete structures revealed in the experiments must be taken into account when calculating their strength.

References

1. Alhatmey, I.A., Ekmekyapar, T., Alrebeh, S.K.: Residual strength capacity of fire-exposed circular concrete-filled steel tube stub columns. Adv. Concrete Constr. **6**(5), 485–507 (2018)
2. Ekmekyapar, T., Alhatmey, I.A.H.: Post-fire resistance of internally ring stiffened high performance concrete filled steel tube columns. Eng. Struct. **183**, 375–388 (2019)
3. Han, L.H., Wei, L., Reidar, B.: Developments and advanced applications of concrete-filled steel tubular (CFST) structures members. J. Constr. Steel Res. **100**, 211–228 (2019)
4. Hassanein, M.F., Patel, V.I., Elchalakani, M., Thai, T.-H.: Finite element analysis of large diameter high strength octagonal CFST short columns. ThinWalled Struct. **123**, 467–482 (2018)

5. Hossain, K.M.A., Chu, K.: Confinement of six different concretes in CFST columns having different shapes and slenderness. Int. J. Adv. Struct. Eng. **11**, 255–270 (2019)
6. Krishan, A., Rimshin, V., Troshkina, E.: Experimental research of the strength of compressed concrete filled steel tube elements. Adv. Intell. Syst. Comput. **1116**, 560–566 (2020)
7. Krishan, A.L., Narkevich, M.Y., Sagadatov, A.I.: Compressed tube-concrete elements with the high-strength compression core and with fibreglass shell. IOP Conf. Ser. Mater. Sci. Eng. **687**(3), 033016 (2019)
8. Krishan, A.L., Narkevich, M.Yu., Sagadatov, A.I., Rimshin, V.I.: The strength of short compressed concrete elements in a fiberglass shell magazine of Civil Eng. **94**(2), 3–10 (2020)
9. Krishan, A.L., Rimshin, V.I., Shubin, I.L., Astafeva, M.A., Stupak, A.A.: Compressed reinforced concrete elements bearing capacity of various flexibility. In: Vatin, N., Roshchina, S., Serdjuks, D. (eds.) Proceedings of MPCPE 2021. LNCE, vol. 182, pp. 283–291. Springer, Cham (2022). https://doi.org/10.1007/978-3-030-85236-8_26
10. Krishan, A.L., Rimshin, V.I., Troshkina, E.A.: Compressed and bending concrete elements with confinement reinforcement meshes. IOP Conf. Ser. Mater. Sci. Eng. **753**(2), 022052 (2020)
11. Martinov, V., Lukin, M., Rimshin, V., Rusak, K., Ivaniuk, A.: 2022 Influence of different types of aggregates on the structural properties of fiber-reinforced concrete. In: Manakov, A., Edigarian, A. (eds.) International Scientific Siberian Transport Forum TransSiberia - 2021 TransSiberia 2021, LNNS, vol. 403, pp. 1467–1476. Springer, Cham (2021). https://doi.org/10.1007/978-3-030-96383-5_164
12. Neverov, A.N., Truntov, P.S., Ketsko, E.S., Rimshin, V.I.: Calculating the strengthening of construction structures before the reconstruction of the building. In: Vatin, N., Roshchina, S., Serdjuks, D. (eds.) Proceedings of MPCPE 2021 Selected Papers, Lecture Notes in Civil Engineering, LNCE, vol. 182, 173–179. Springer, Cham (2022). https://doi.org/10.1007/978-3-030-85236-8_14
13. Rimshin, V.I., Kalaydo, A.V., Semenova, M.N., Bykov, G.S.: Regularities research of radon transfer to underground enclosing buildings structures. IOP Conf. Ser. Mater. Sci. Eng. **953**(1), 012088 (2020)
14. Rimshin, V.I., Roshchina, S.I., Ketsko, E.S., Truntov, P.S., Kuzina, I.S.: Engineering calculations of acidifier retaining walls during water treatment facilities designing. In: Vatin, N., Roshchina, S., Serdjuks, S. (eds.) Proceedings of MPCPE 2021 Selected Papers Lecture Notes in Civil Engineering, LNCE, vol. 182, pp. 55–73. Springer, Cham (2022). https://doi.org/10.1007/978-3-030-85236-8_5
15. Rush, D.I., Bisby, L.A., Jowsey, A., Lane, B.: Residual capacity of fire-exposed concrete-filled steel hollow section columns. Eng. Struct. **100**, 550–563 (2015)
16. Telichenko, V., Rimshin, V., Ketsko, E.: Reinforced concrete structures stress-strain state strengthen with composite materials. IOP Conf. Ser. Mater. Sci. Eng. **869**(5), 052003 (2020)
17. Xu, L., Zhou, P., Chi, Y., Huang, L., Ye, J., Yu, M.: Performance of the high strength self-stressing and self compacting concrete-filled steel tube columns subjected to the uniaxial compression. Int. J. Civil Eng. **16**(9), 1069–1083 (2018)
18. Kuzina, E., Rimshin, V.: Strengthening of concrete beams with the use of carbon fiber. In: Adv. Intell. Syst. Comput. **983**, 911–919 (2019)
19. Varlamov, A.A., Rimshin, V.I., Tverskoi, S.Y.: Planning and management of urban environment using the models of degradation theory. IOP Conf. Ser. Earth Environ. Sci. **177**(1), 012040 (2018)
20. Rimshin, V., Labudin, B., Morozov, V., Kazarian, A., Kazaryan, V.: Calculation of shear stability of conjugation of the main pillars with the foundation in wooden frame buildings. Adv. Intell. Syst. Comput. **983**, 867–876 (2019)
21. Rimshin, V.I., Varlamov, A.A.: Three-dimensional model of elastic behavior of the composite Izvestiya Vysshikh Uchebnykh Zavedenii, Seriya Teknologiya Tekstil'noi Promyshlennosti **375**(3), 63–68 (2018)
22. Varlamov, A., Rimshin, V., Tverskoi, S. A method for assessing the stress-strain state of reinforced concrete structures E3S. Web Conf. **91**, 02046 (2019)

23. Krishan, A.L., Rimshin, V.I., Troshkina, E.A.: Strength of short concrete filled steel tube columns of annular cross section. IOP Conf. Ser. Mater. Sci. Eng. **463**(2), 022062 (2018)
24. Krishan, A.L., Rimshin, V.I., Astafeva, M.A.: Deformability of a volume-compressed concrete. IOP Conf. Ser. Mater. Sci. Eng. **463**(2), 022063 (2018)

Investigation of the Stress–Strain State of Wooden Beams with Rational Reinforcement with Composite Materials

Danila Chibrikin, Usov Alexey, and Anastasia Lukina

Abstract The preservation of retro structures in the monuments of wooden architecture is an important task. During long-term operation (100 years or more), retro wooden structures are exposed to atmospheric and environmental adverse environmental influences. The load-bearing capacity of retro wooden structures can be restored by modifying local destruction zones with polymer compositions. In the proposed technologies for restoring the load–bearing capacity, the peculiarities of changing the stress–strain state of wooden beam retroconstructions with locally destructive sections that have undergone modification have not been sufficiently investigated. Having studied the existing technologies of modification and reinforcement of retro structures, a new method of modification is proposed. The restoration of the bearing capacity of the elements of retro wooden structures with destructive damage to wood is assumed to be modified by the component composition of a polymer composition with a carbon filler under excessive pressure of pulsed action. The developed modification technology according to the results of the study is effective.

Keywords Restored retro wooden beams · Component composition · Polymer composition · Wood modification · Technological mode

1 Introduction

The issue of restoring elements of retro wooden structures when creating technical and technological solutions, because of which the bearing capacity of wooden retro structures is restored without the use of external reinforcement systems, while maintaining the original appearance is an urgent task. In the modern foreign practice of construction in recent years, there are more and more examples of the introduction of wood as a material for load-bearing structures.

D. Chibrikin (✉) · U. Alexey · A. Lukina
Vladimir State University Named after Alexander and Nikolay Stoletovs, Vladimir, Russian Federation
e-mail: dachibrikin@outlook.com

The solution of this issue determined the purpose of the work – the restoration of the bearing capacity of the elements of wooden retroconstructions with destructive damage to wood [1–3].

In Russia, there is a greater number of monuments of wooden architecture that have structural, technical and architectural features, in which wood is the main material. This concept includes manors, temples, engineering and household structures. The most common in the central part of Russia: Suzdal Museum, Vasilevo (Tver region), Kostroma Sloboda, New Jerusalem (Moscow region), Shchelkovsky Farm (Nizhny Novgorod). Also in the Vladimir region there are 161 preserved farmsteads built using wooden elements. Structural elements of wooden monuments, which include floor beams and coverings, wooden piles, wooden log walls, roof truss system, the service life of which exceeds 100 years or more, are defined as retroconstruction. As a result of the environmental impact and the lack of timely repair work of retroconstruction elements, their destruction, loss of strength and destruction occurs. The existing methods of retroconstruction restoration are based on their partial replacement or external reinforcement of elements that lead to a change in the appearance of retroconstructions of the monument of wooden architecture.

A typical retro wooden structure that is used in the monuments of wooden architecture, the manor, is a wooden beam [4–6].

It is established that the change in temperature and humidity conditions has a major impact on the condition of the wooden structure [7–9]. It is worth noting that the supporting parts of wooden beams are the most susceptible to destruction [10–14].

Having studied the existing technologies of modification and reinforcement of retro structures, a new method of modification is proposed [15–19].

The restoration of the bearing capacity of the elements of retro wooden structures with destructive damage to wood is assumed to be modified by the component composition of a polymer composition with a carbon filler under excessive pressure of pulsed action [6, 20–22].

The object of the study is a beam wooden retroconstruction with destructive damage to wood, restored with polymer compositions [23–27].

To achieve this goal the following tasks were set:

1. To analyze retro wooden beam structures with local destruction zones that have undergone modification.
2. To develop a technology for restoring the load-bearing capacity of retro wooden beam structures with modification.
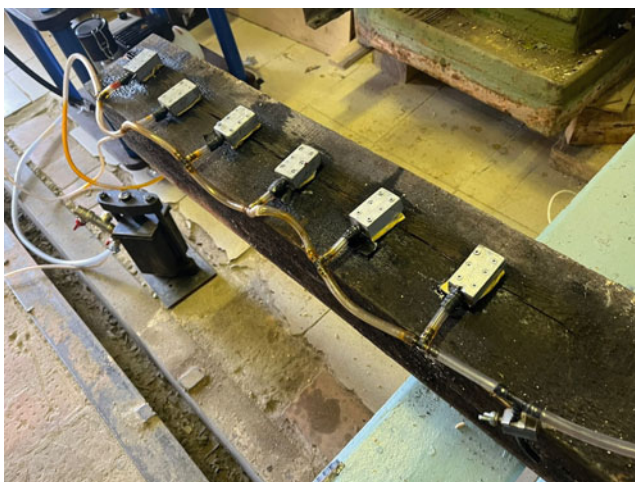
2   Methods

The technological solution for the restoration of retro beams consists in the modification of local destruction zones with a component composition with a carbon filler, the method of overpressure pulse action and consists of the following processes [28, 29]: preparatory, basic, final (Fig. 1, 2).
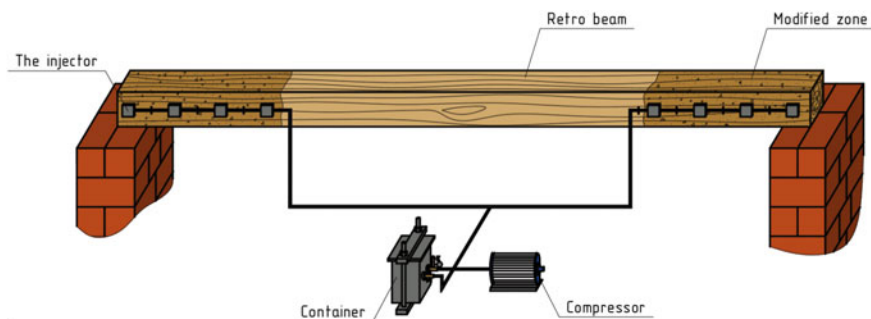
Fig. 1 Visual view of the technological scheme

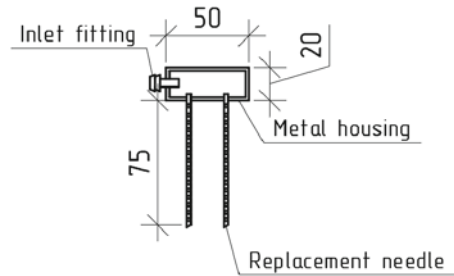**Fig. 2** Retro beam modification process

The preparatory process includes the following types of work:

a) inspection of wooden retroconstructions;
b) setting the required temperature and humidity mode of operation;
c) device of equipment for modification;
d) formwork device for unloading retro beams.

The main process includes the following types of work:

a) modification of zones subject to destruction by the method of overpressure;
b) control of the parameters of the modification equipment.

Fig. 3 The scheme of the wood modification injector

The final process includes the following types of work.

a) inspection of modified zones with destruction of retro forms;
b) dismantling of modification equipment;
c) dismantling of the formwork.

The retro beam modification process consists of the following steps:

a) Definition of the modification zone;
b) Preparation of holes for modification
c) Preparation of component composition with carbon filler;

When retro beams are modified, the surface is divided into zones in which injectors are arranged. The installation of injectors is recorded in the work protocol. The injector is installed in increments of 200 mm, the diameter of the holes is 5 mm. The holes for the installation of injectors are made by drilling perpendicular to the surface. Before the device of the injector, the hole must be cleaned of dust (Fig. 3).

The modification equipment has the following functions:

a) performs modification with the installation of a certain amount of component composition with carbon filler;
b) provides the required flow of the component composition into the wood structure;
c) the ability to quickly clean the injector in case of obstruction.

Modification is carried out under the influence of the technological mode of modification: 10-5-10-5-10 – for 10 min, a wooden retrobalker is injected with a component composition of a polymer composition with a filler, then maintained for 5 min, then the working pressure is repeated for 10 min with alternation. The overpressure is 0.2–0.4 MPa.

3   Results and Discussion

During the tests, three technological modes were investigated:

– 30 min (For 30 min the sample was injected with a polymer composition using the influence of overpressure) (Fig. 4);
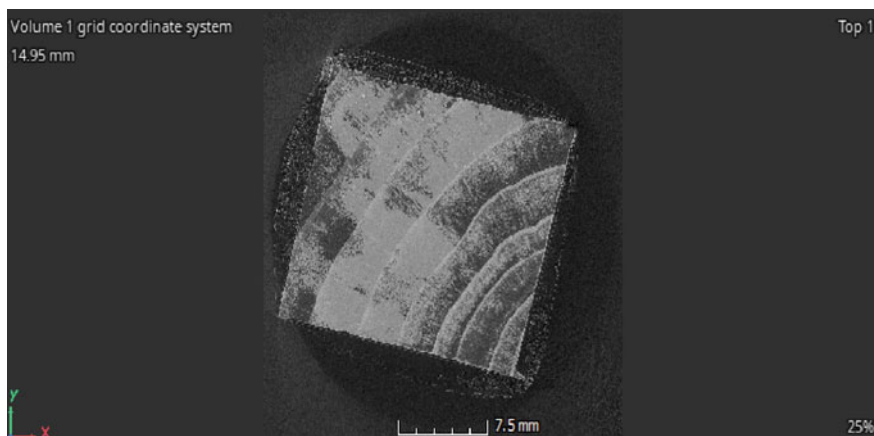
Fig. 4 Technological mode – 30 min

– 15-5-15 min (For 15 min the sample was injected with a polymer composition, then the sample "rested" for 5 min, then the injection of the polymer composition was repeated for 15 min) (Fig. 5);
– 10-5-10-5-10 min (For 10 min the sample was injected with a polymer composition, then the sample "rested" for 5 min, then the injection of the polymer composition was repeated for 10 min, alternating) (Fig. 6).
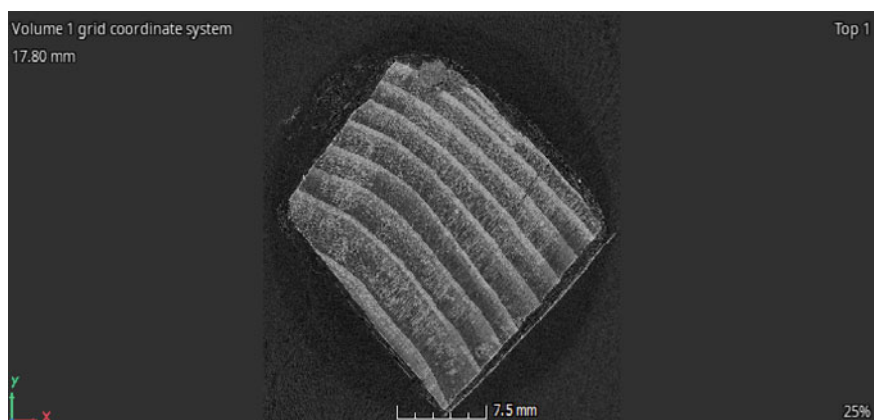
Fig. 5 Technological mode – 15-5-15 min

Volume 1 grid coordinate system
21.77 mm
Top 1
7.5 mm
25%
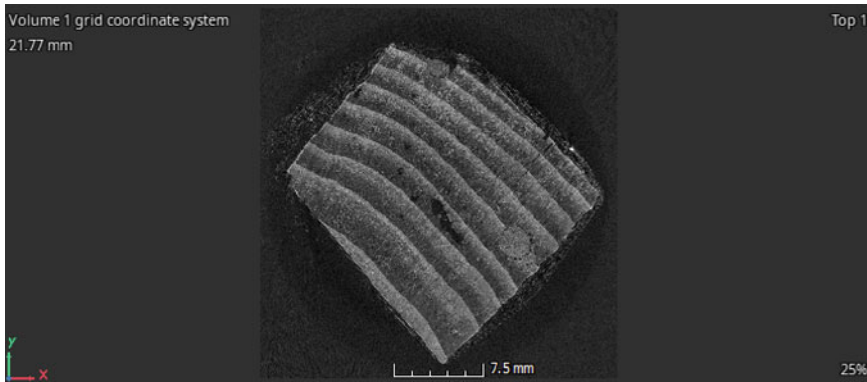
Fig. 6 Technological mode – 10-5-10-5-10 min

4   Conclusions

Based on the results of the research, the following conclusions can be drawn:

1. As a result of the conducted research, the hypothesis about the possibility of restoring the bearing capacity of the elements of wooden retroconstructions with destructed damage has been experimentally proved. The data obtained as a result of the calculation clearly illustrates that the design load on the reinforced beam is 2 times greater than that on the non-reinforced one. For the reinforced beam, the calculated load was 1800 kg/m, for the non-reinforced one 900 kg/m. At the same time, the ultimate strength of the reinforced beam decreased by 40% relative to the non-reinforced one.
2. Technological modes of wood modification with local destruction zones were established to restore the bearing capacity: 10-5-10-5-10 – for 10 min the wooden sample was subjected to injection with a component composition of a polymer composition with a filler, then maintained for 5 min, then the working pressure was repeated for 10 min with alternation.
3. A technical solution is proposed, the task of which is to create a method of local modification of wood in wooden structures without the use of baths, chambers and other large-sized equipment, with minimal consumption of raw materials and energy resources.
4. The developed technology for restoring the load-bearing capacity of retro structures with destructive damage to wood can be used in the restoration work of cultural heritage objects and reinforcement of wooden structures.

References

1. Lisyatnikov, M., Lukina, A., Chibrikin, D., Labudin, B.: Strength of polymer composites reinforced with wood when stretched at an angle to the fibers. Lect. Notes Civ. Eng. **182**, 523–533 (2022). https://doi.org/10.1007/978-3-030-85236-8_46
2. Gribanov, A., Glebova, T., Roschina, S.: Restoration of decaying wood in the support zones of wooden beams. In: Lecture Notes on Civil Engineering (2020). https://doi.org/10.1007/978-3-030-42351-3_14
3. Gribanov, A.S., Roshchina, S.I., Naichuk, A.Yu., Melekhov, V.I.: Wooden beams with local modification of wood. In: IOP Conference Series: Materials Science and Engineering (2020). https://doi.org/10.1088/1757-899X/896/1/012067
4. Lukina, A., Roshchina, S., Lisyatnikov, M., Zdralovich, N., Popova, O.: Technology of restoration of wooden beams by surface repair and local modification. In: Manakov, A., Edigarian, A. (eds.) International Scientific Siberian Transport Forum TransSiberia - 2021. TransSiberia 2021. Lecture Notes in Networks and Systems, LNNS, vol. 403, pp. 1371–1379 Springer, Cham (2021). https://doi.org/10.1007/978-3-030-96383-5_153
5. Lukina, A., Roshchina, S., Lisyatnikov, M., Zdralovic, N., Popova, O.: Technology for the restoration of wooden beams by surface repair and local modification. In: Manakov, A., Edigarian, A. (eds.) International Scientific Siberian Transport Forum TransSiberia - 2021. TransSiberia 2021. LNNS, vol. 403, pp. 1371-1379. Springer, Cham (2022). https://doi.org/10.1007/978-3-030-96383-5_153
6. Lisyatnikov, M.S., Glebova, T.O., Ageev, S.P., Ivanyuk, A.M.: The strength of wood reinforced with polymer composite to crumple across the fibers. In: IOP Conference Series: Materials Science and Engineering (2020). https://doi.org/10.1088/1757-899X/896/1/012062
7. Lukin, M.V., Roshchina, S.I., Gribanov, A.S., Naichuk, A.Yu.: Stress-strain state of wooden beams with external reinforcement. In: IOP Conference Series: Materials Science and Engineering (2020). https://doi.org/10.1088/1757-899X/896/1/012066
8. Preobrazhenskaya, I.P., Pogoreltsev, A.A., Turkovsky, S.B.: Project development and construction of a potassium chloride storage facility with a frame of prefabricated wooden frames measuring 63 m. Builds. Mater. **14–16** (2003)
9. Lukina, A., Roshchina, S., Gribanov, A.: A method for restoring destroyed wooden structures with polymer composites. In: Proceedings of EECE 2020, pp. 464-474 (2021). https://doi.org/10.1007/978-3-030-72404-7_45
10. Roshchina, S.I., Lukina, A.V., Sergeev, M.S., Vlasov, A.V., Gribanov, A.S.: Restoration of wooden structures impregnated with polymer composition on the example of industrial buildings of light and textile industry. Izv. Vss. Educational institutions. Teknol series. Text. Industry (2016)
11. Sergeev, M., Lukina, A., Zdralovich, N., Reva, D.: The stress–strain state of a three-span beam made of glued beams with layered modification. Lecture. Notes Civ. Eng. **182**, 485–491 (2022). https://doi.org/10.1007/978-3-030-85236-8_43
12. Lukin, M., Prusov, E., Roshchina, S., Karelina, M., Vatin, N.: Multi-span wooden beams made of composite materials with rational steel reinforcement. Building **11**, 46 (2021). https://doi.org/10.3390/buildings11020046
13. Roshchina, S.I., Lisyatnikov, M.S., Lukin, M.V., Popova. M.V.: Technology of reinforcement of the support zones of the glued timber structure using nanomodified prepregs. Mater. Scientific Forum. **931**, 226–231 (2018).https://doi.org/10.4028/www.scientific.net/MSF.931.226
14. Gribanov, A.S., Roshchina, S.I., Popova, M.V., Sergeev, M.S.: Layered polymer composites for wooden structures. J. Civ. Eng. (2018). https://doi.org/10.18720/MCE.83.1
15. Roshchina, S., Gribanov, A., Lukin, M., Lisyatnikov, M., Strekalkin, A.: Calculation of wooden beams reinforced with polymer composites with a change in the compression area of wood. In: MATEC Web of Conferences (2018). https://doi.org/10.1051/matecconf/201825104029
16. Roshchina, S., Lukin, M., Lisyatnikov, M.: Compressed-bent reinforced wooden elements with long-term load. In: Anatolijs, B., Nikolai, V., Vitalii, S. (eds.) Proceedings of EECE 2019. EECE

2019. Lecture Notes in Civil Engineering, vol. 70. Springer, Cham (2020). https://doi.org/10.1007/978-3-030-42351-3_7

17. Kosheev, A.A., Roschina, S.I., Alekseevets, V., Labudin, B.V.: Local deformation and strength characteristics of S-shaped reinforcement in wood. In: IOP Conference Series: Materials Science and Engineering (2020). https://doi.org/10.1088/1757-899X/896/1/012060

18. Lisyatnikov, M.S., Shishov, I.I., Sergeev, M.S., Hisham E.: Prefabricated monolithic coating of an industrial building based on beams-slabs of variable height. In: IOP Conference Series: Materials Science and Engineering (2020). https://doi.org/10.1088/1757-899X/896/1/012064

19. Varlamov, A.A., Rimshin, V.I., Tverskoy, S.Yu.: Planning and management of the urban environment using models of the theory of degradation. In: IOP Conference Series: Earth and Environmental Science (2018). https://doi.org/10.1088/1755-1315/177/1/012040

20. Gribanov, A.S., Rimshin, V.I., Roshchina, S.I.: Experimental studies of composite wooden beams with local modification of wood. In: IOP Conference Series: Materials Science and Engineering (2019). https://doi.org/10.1088/1757-899X/687/3/033039

21. Roshchina, S., Sergeev, M., Lukin, M., Strekalkin, A.: Reconstruction of stationary fertilizer warehouses in the Vladimir region. In: IOP Conference Series: Materials Science and Engineering (2018). https://doi.org/10.1088/1757-899X/463/4/042011

22. Byzov, V.E., Melekhov, V.I.: Structural lumber: resource enhancement. J. Civ. Eng. **65**, 67–76 (2016). https://doi.org/10.5862/MCE.65.5

23. Kuzina, E., Rimshin, V., Kurbatov, V.: Reliability of building structures from the effects of energy and environmental degradation. In: IOP Conference Series: Materials Science and Engineering (2018). https://doi.org/10.1088/1757-899X/463/4/042009

24. Djokovic, M., Melovich, B., Vatin, N., Murgul, V.: Modern business strategy of customer relationship management in the field of civil engineering. Appl. Mech. Mater. **678,** 644–647 (2014). https://doi.org/10.4028/www.scientific.net/AMM.678.644

25. Labudin B.V., et al.: Constructive solutions of wood-concrete floors using shear-resistant seams. In: IOP Conference Series: Materials Science and Engineering (2020). https://doi.org/10.1088/1757-899X/896/1/012028

26. Varenik, K.A., Varenik, A.S., Sanzharovsky, R.S., Labudin, B.V.: Accounting for wood moisture in creep equations. In: IOP Conference Series: Materials Science and Engineering (2019). https://doi.org/10.1088/1757-899X/656/1/012054

27. Labudin, B.V., Popov, E.V., Sopilov, V.V.: Stability of compressed shells of wood-composite plate-ribbed structures. In: IOP Conference Series: Materials Science and Engineering (2019). https://doi.org/10.1088/1757-899X/687/3/033041

28. Petrichenko, M., Vatin, N., Nemova, D., Kharkiv, N., Staritsyna, A.: Technology of enhanced oil recovery using a shock wave in a liquid. Appl. Mech. Mater. **627,** 297–303 (2014). https://doi.org/10.4028/www.scientific.net/AMM.627.297

29. Lukin, M., Prusov, E., Roshchina, S., Karelina, M., Vatin, N.: Multi-span wooden beams made of composite materials with rational steel reinforcement. Building **11**, 1–12 (2021). https://doi.org/10.3390/buildings11020046

Strength and Deformability of Butt Joints Made of Wood with Local Modification

Artem Strekalkin ⓘ**, Mikhail Sergeev** ⓘ**, Dmitry Reva** ⓘ**, and Vladimir Rimshin** ⓘ

Abstract The article describes the design and technological solutions for the nodal joints of wooden structures with local wood modification. The results of numerical and experimental studies on the bearing capacity and deformability of such joints are presented. Numerical studies were carried out using the Ansys program. As a modifying composition, a compound based on dimethacrylic polyester with the addition of a hardener and a curing initiator is proposed. Experimental studies were carried out using a modernized hydraulic bench for testing beam structures made of wood. The results obtained allow us to speak about an increase in the bearing capacity of wood in nodal joints due to modification by 29–30%. The possibility of local wood modification has been proved. Design solutions for aluminum connectors are given, which allow modifying wood in production conditions and on the construction site. The setting for the local modification of the wood of the contact zones, consisting of a vacuum pump, a compressor and a container for modification, is considered. Based on the studies carried out, it can be argued that it is important to increase the physical, mechanical and operational characteristics of wood due to local modification. Further research is aimed at improving the technology of modification and design solutions for connections.

Keywords ANSYS · Construction · Dowel · Finite Element · Joint · Simulation · Structure · Timber · Wood · Modification · Buildings

1   Introduction

Structures made of solid and glued wood have always been widely used in Russia and the CIS countries. Its widespread use is due to the absence of corrosion, resistance to aggressive environments, sufficient strength characteristics and the possibility

A. Strekalkin (✉) · M. Sergeev · D. Reva
Vladimir State University Named After Alexander and Nikolay Stoletovs, Vladimir, Russia

V. Rimshin
Research Institute of Building Physics RAASN, Moscow, Russia

191

Fig. 1 SHERPA type
connectors
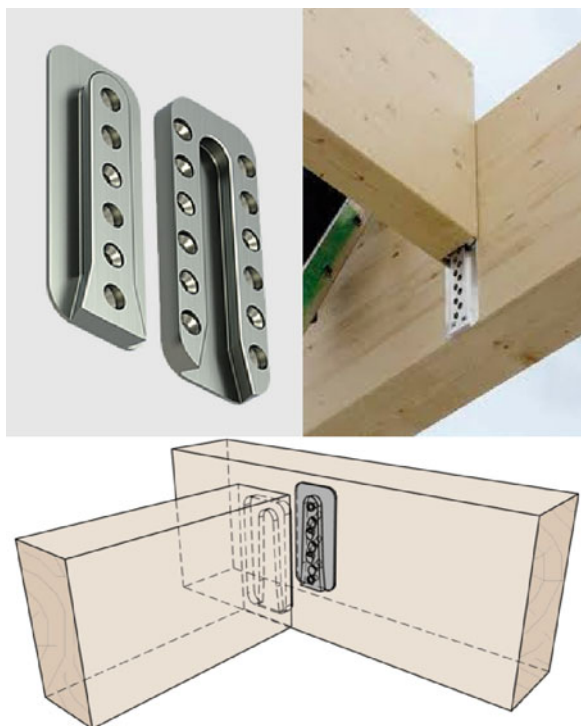
of various modifications and design improvements. In addition, unlike reinforced
concrete and steel, wood is an environmentally friendly and renewable building
material. Extremely relevant in the last few decades is the direction of a multi-storey
wooden structure [1–9]. The use of new design solutions based on the use of wood-
composite structural materials, such as CLT, LVL, OSB, made it possible to increase
the height of buildings made of wooden structures up to 18 floors [10–18]. One
of the ways -to increase the bearing capacity of wood structures is to improve the
connections between the bearing elements [19–26]. Depending on the method of
transmission of forces, the interface of structural elements of wooden and glued
structures are divided into two large groups: glueless joints on mechanical bonds
and adhesive joints. The connection of wooden structures on aluminum connectors
of the SHERPA type is widely used [16, 18–20] (Fig. 1).

2 Methods

To analyze the stress–strain state of the butt joint of wooden structures, several studies
were carried out in the ANSYS Workbench software package. Figure 2 shows the
models of the studied compounds. For the most accurate execution of all elements

of the connection, the simulation of the investigated joint was carried out in the Autodesk Fusion 360 program, followed by the import of the model into ANSYS Workbench.

We have proposed connections on aluminum plates, different from the above-mentioned. The investigated connectors have a unique design that allows for local modification of wood. A general view of the connectors is shown in Fig. 3.
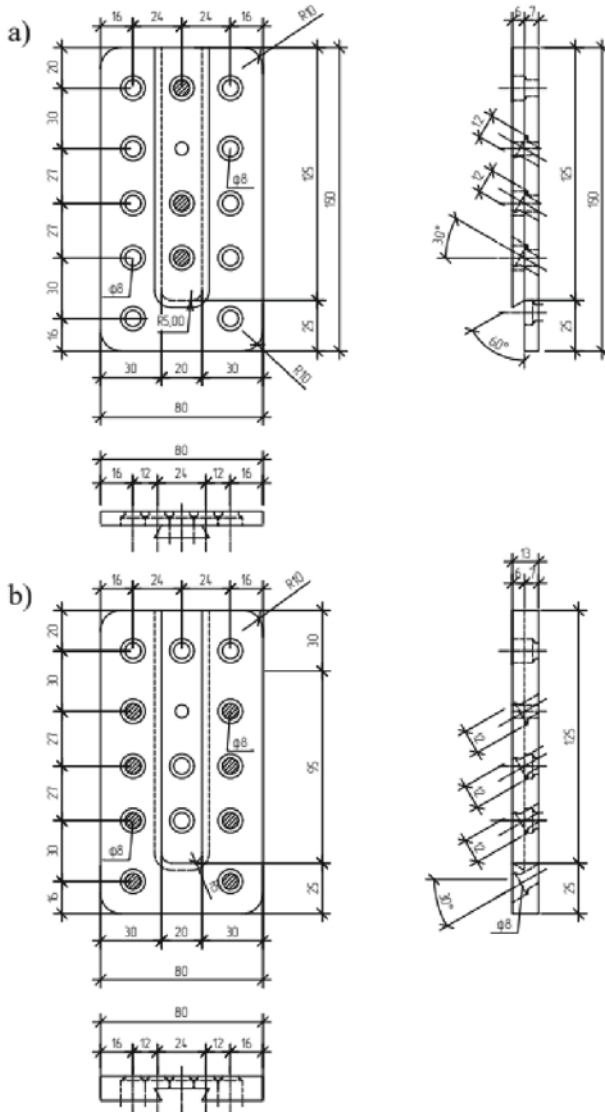
Fig. 2 General view of connectors: a) connector with a protruding part, b) connector with a groove

Fig. 3 Nodal connection of elements of wooden structures, made in the software package Autodesk Fusion 360
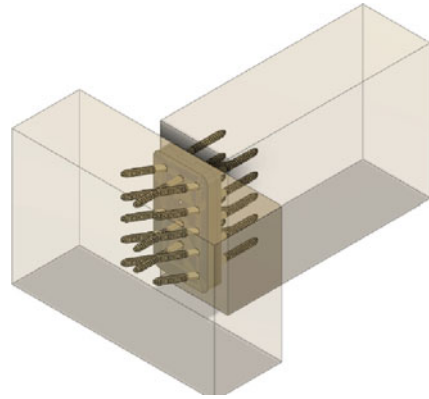
For the engineering calculation of the butt joint, a transtropic model of wood, isotropic models of screws and aluminum connectors were selected.

When modeling the joints under study in the ANSYS Workbench software package, it is necessary to take into account the boundary contact conditions wood-steel, aluminum-aluminum and wood-aluminum. For this, contact pairs of the Frictional type are used, that is, a non-linear contact that takes into account the coefficient of friction. The values of this coefficient for couples in the framework of this study are as follows:

– for a pair of wood - steel $k_{tr} = 0.6$;
– for a pair of wood - aluminum $k_{tr} = 0.5$;
– for a pair of aluminum - aluminum $k_{tr} = 1.25$.

The assignment of the strength characteristics of materials was based on the data obtained during a series of preparatory tests and materials from the ANSYS Workbench library.

Depending on the series of experiments, the load was set differently for comparison with the results of experimental studies.

– to simulate the testing of local samples for pulling out screws from an array of ordinary and modified wood, the increment in the movement of the plate pulling out the bolt was 10 mm per minute;
– to simulate tests of butt joints of elements of wooden structures, the load was applied step by step to one of the wooden elements with a step size of 2 kN.

For simplified identification of samples, the following symbols have been introduced:

– SD - butt connector connection of wood elements;
– SDM - butt connector connection of wood elements with local modification of the contact zones with the composition of dimethacrylic polyester.

To conduct experimental studies, the existing hydraulic bench for testing beam structures was modernized. the modification scheme is shown in Fig. 4.

Wood modification was carried out using a mobile wood modification unit, shown in Fig. 5.
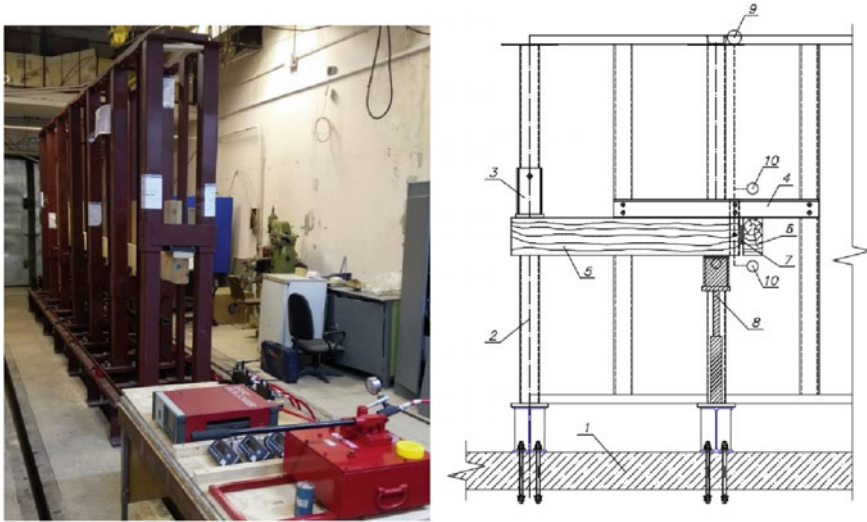
Fig. 4 Experimental setup. modernization for testing nodal connections: 1 - power floor; 2 – stand frame; 3 - support of the secondary beam; 4 - support of the main beam; 5 - secondary beam; 6 - main beam; 7 - connector: 8 - hydraulic jack connected to a dynamometer; 9 – deflection meter PAO 6; 10 - dial indicators

Fig. 5 Mobile wood modification unit
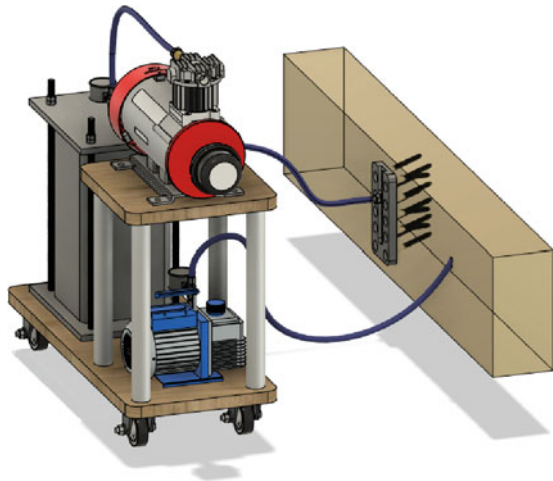
The installation consists of two pumps - a vacuum pump and a compressor, a vacuum bag in which a modified wood element is placed, a container for modification and lines that supply the modifying composition and remove air from the vacuum bag.

3   Results and Discussion

Comparison of theoretical, numerical and experimental studies of the connections of beam elements is given in Table 1.

Figure 6 shows the dependence of displacements on the applied load in numerical and experimental studies.

Table 1 Results of engineering, numerical and experimental studies of compounds of the SD, SDM series

Index	Destruction load, kN	Displacement, mm
Testing of SD series connections		
Engineering calculation	61.06	-
Ansys	62.85	12.32
Experiment	52	11.4
Testing of SDM series connections		
Engineering calculation	82.6	-
Ansys	81.8	9.34
Experiment	72	8.84
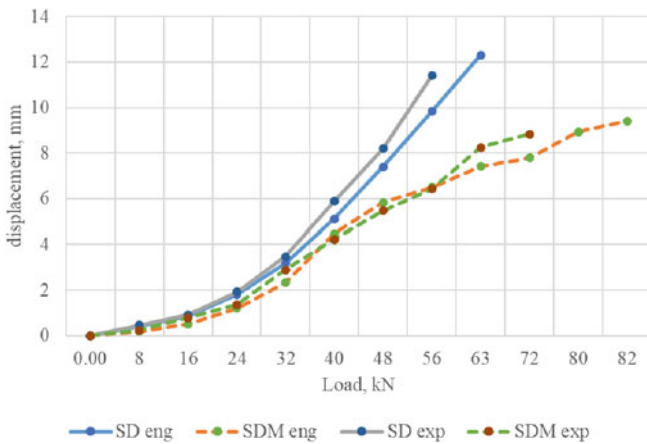
Fig. 6 The dependence of displacements on the applied load in numerical and experimental studies

Based on the experimental studies of butt joints of elements of wooden structures, as well as on the retention of one screw in an array of wood, it seems possible to calculate the coefficients that allow taking into account the physical and mechanical properties of wood when determining the bearing capacity of the screw for pulling out:

$$k_{md} = 72 \text{ kN}/52 \text{ kN} = 1.32 \tag{1}$$

4 Conclusions

According to the results of the experiment on a full-size butt joint of elements of wooden structures with a modification of the contact zones wood - screw showed an increase in the strength of the joint by 38% compared to a butt joint without wood modification. The potential destruction of a series of butt joints of the SD series in a numerical experiment was recorded at values by 16.

In order to take into account, the modification of the wood of the contact zones in the calculation of screw connections, the coefficient $k_{md} = 1.32$ was introduced, which makes it possible to reduce the engineering calculation error to 2–4%.

References

1. Roshchina, S.I., Lukin, M.V., Lukina, A.V., Sergeyev, M.S., Lisyatnikov, M.S.: Experimental research on pressed-bending reinforced timberwork. Int. J. Appl. Eng. Res. **10**, 45307–45312 (2015)
2. Lukin, M. V., Roshchina, S.I., Smirnov, E.A., Shunqi, M.: Strengthening of the operated wooden floor beams with external rigid reinforcement. In: IOP Conference Series: Materials Science and Engineering (2020). https://doi.org/10.1088/1757-899X/896/1/012065.
3. Lisyatnikov, M.S., Glebova, T.O., Ageev, S.P., Ivaniuk, A.M.: Strength of wood reinforced with a polymer composite for crumpling across the fibers. In: IOP Conference Series: Materials Science and Engineering (2020). https://doi.org/10.1088/1757-899X/896/1/012062
4. Buka-Vaivade, K., Serdjuks, D., Goremikins, V., Pakrastins, L., Vatin, N.I.: Suspension structure with cross-laminated timber deck panels. Mag. Civ. Eng. **83**, 126–135 (2018). https://doi.org/10.18720/MCE.83.12
5. Yao, Z., Wu, D., Chen, C., Zhang, M.: Creep behavior of polyurethane nanocomposites with carbon nanotubes. Compos. Part A Appl. Sci. Manuf. **50**, 65–72 (2013). https://doi.org/10.1016/j.compositesa.2013.03.015

6. Yahyaei-Moayyed, M., Taheri, F.: Experimental and computational investigations into creep response of AFRP reinforced timber beams. Compos. Struct. **93**, 616–628 (2011). https://doi.org/10.1016/j.compstruct.2010.08.017

7. Fossetti, M., Minafò, G., Papia, M.: Flexural behaviour of glulam timber beams reinforced with FRP cords. Constr. Build. Mater. **95**, 54–64 (2015). https://doi.org/10.1016/j.conbuildmat.2015.07.116

8. Ruslantsev, A.N., Portnova, Y.M., Tairova, L.P., Dumansky, A.M.: Analysis of mechanical properties anisotropy of nanomodified carbon fibre-reinforced woven composites. In: IOP Conference Series: Materials Science and Engineering. Institute of Physics Publishing (2016). https://doi.org/10.1088/1757-899X/153/1/012003.

9. Sergeev, M.S., Lukin, M.V., Strekalkin, A.A., Roshchina, S.I.: Mathematical modeling of stress-strain state of the nodal joint of wooden beams. J. Phys. Conf. Ser. **2131** (2021). https://doi.org/10.1088/1742-6596/2131/3/032088

10. Rimshin, V.I., Roshchina, S.I., Ketsko, E.S., Truntov, P.S., Kuzina, I.S.: engineering calculations of acidifier retaining walls during water treatment facilities designing. Lect. Notes Civ. Eng. **182**, 55–73 (2022). https://doi.org/10.1007/978-3-030-85236-8_5

11. Strekalkin, A., Koshcheev, A., Roshchina, S., Naichuk, A.: Dowel connections with local wood modification. Lect. Notes Civ. Eng. **182**, 385–392 (2022). https://doi.org/10.1007/978-3-030-85236-8_35

12. Lukin, M., Sergeev, M., Lisyatnikov, M.: Non split wooden beam reinforced with composite reinforcement. In: Proceedings of EECE 2020, pp. 115–123. https://doi.org/10.1007/978-3-030-72404-7_12

13. Roshchina, S., Sergeev, M., Lukin, M., Strekalkin, A.: Reconstruction of Fixed Fertilizer Folders in the Vladimir Region. In: IOP Conference Series: Materials Science and Engineering (2018). https://doi.org/10.1088/1757-899X/463/4/042011

14. Roschina, S., Gribanov, A., Lukin, M., Lisyatnikov, M., Strekalkin, A.: Calculation of wooden beams reinforced with polymeric composites with modification of the wood compression area. In: MATEC Web of Conferences (2018). https://doi.org/10.1051/matecconf/201825104029

15. Lisyatnikov, M., Glebova, T., Rusak, K., Ivaniuk, A.: Strength and deformability of reinforced wooden beams of variable stiffness. Lect. Notes Civ. Eng. **182**, 549–561 (2022). https://doi.org/10.1007/978-3-030-85236-8_48

16. Lukina, A., Roshchina, S., Lisyatnikov, M., Zdralovic, N., Popova, O.: Technology for the restoration of wooden beams by surface repair and local modification. In: Manakov, A., Edigarian, A. (eds.) International Scientific Siberian Transport Forum TransSiberia - 2021. TransSiberia 2021. Lecture Notes in Networks and Systems, LNNS, vol. 403, pp. 1371–1379. Springer, Cham (2022). https://doi.org/10.1007/978-3-030-96383-5_153

17. Popov, E., Ruslanova, A., Sopilov, V., Zdralovic, N., Mamedov, S., Labudin, B.: Contact Interaction of a Claw Washer with Wood at Limiting Shear. Lesn. Zhurnal (Forestry Journal) **4**, 178–189 (2020). https://doi.org/10.37482/0536-1036-2020-4-178-189

18. Khelifa, M., Celzard, A.: Numerical analysis of flexural strengthening of timber beams reinforced with CFRP strips. Compos. Struct. **111**, 393–400 (2014). https://doi.org/10.1016/j.compstruct.2014.01.011

19. D'Ambrisi, A., Focacci, F., Luciano, R.: Experimental investigation on flexural behavior of timber beams repaired with CFRP plates. Compos. Struct. **108**, 720–728 (2014). https://doi.org/10.1016/j.compstruct.2013.10.005

20. Basterra, L.A., Balmori, J.A., Morillas, L., Acuña, L., Casado, M.: Internal reinforcement of laminated duo beams of low-grade timber with GFRP sheets. Constr. Build. Mater. **154**, 914–920 (2017). https://doi.org/10.1016/j.conbuildmat.2017.08.007

21. Kim, Y.J., Harries, K.A.: Modeling of timber beams strengthened with various CFRP composites. Eng. Struct. **32**, 3225–3234 (2010). https://doi.org/10.1016/j.engstruct.2010.06.011

22. Vodiannikov, M.A., Kashevarova, G.G.: Analysis of wood structure connections using cylindrical steel and carbon fiber dowel pins. In: IOP Conference Series: Materials Science and Engineering. Institute of Physics Publishing (2017). https://doi.org/10.1088/1757-899X/205/1/012031

23. Kasal, B., Pospisil, S., Jirovsky, I., Heiduschke, A., Drdacky, M., Haller, P.: Seismic performance of laminated timber frames with fiber-reinforced joints. Earthq. Eng. Struct. Dyn. **33**, 633–646 (2004). https://doi.org/10.1002/eqe.368
24. Matveev, R.P., Labudin, B. V., Morozov, V.S., Orlov, A.O.: Numerical analysis of strength and rigidity of the biomechanical system "Bone-Apparatus." Hum. Ecol. (Russian Fed. 0, 58–64 (2017). https://doi.org/10.33396/1728-0869-2017-4-58-64
25. Roschina, S.I., Lisyatnikov, M.S., Koshcheev, A.A.: Technical- and- economic efficiency of reinforced wooden structures. IOP Conf. Ser. Mater. Sci. Eng. **698**, 022005 (2019). https://doi.org/10.1088/1757-899X/698/2/022005
26. Roshchina, S., Lukin, M., Lisyatnikov, M., Koscheev, A.: The phenomenon for the wood creep in the reinforced glued wooden structures. In: MATEC Web of Conferences (2018). https://doi.org/10.1051/matecconf/201824503020
27. Koshcheev, A.A., Roshchina, S.I., Lukin, M. V., Lisyatnikov, M.S.: Wooden beams with reinforcement along a curvilinear trajectory. Mag. Civ. Eng. (2018). https://doi.org/10.18720/MCE.81.19
28. Lukin, M., Prusov, E., Roshchina, S., Karelina, M., Vatin, N.: Multi-span composite timber beams with rational steel reinforcements. Buildings **11**, 11020046 (2021). https://doi.org/10.3390/buildings11020046
29. Telichenko, V.I., Rimshin, V.I., Karelskii, A.V., Kurbatov, B.V.L.A.V.L.: Strengthening technology of timber trusses by patch plates with toothed-plate connectors. J. Ind. Pollut. Control. **33**, 1034–1041 (2017)
30. Karelskiy, A.V., Zhuravleva, T.P., Labudin, B.V.: Load-to-failure bending test of wood composite beams connected by gang nail. Mag. Civ. Eng. **54**, 77–85 (2015). https://doi.org/10.5862/MCE.54.9

Physical and Mechanical Properties of Coniferous Wood After Exposure to Fire

Vladislav Martinov ⓘ, **Mikhail Lisyatnikov** ⓘ, **Svetlana Roshchina** ⓘ, **and Anastasiya Lukina** ⓘ

Abstract The technical qualities of wood are characterized by a significant number of its physical and mechanical properties. The technical qualities of wood are greatly affected by fire. Since there is currently an acute shortage of hardwoods, the issue of maximizing the full use of natural wood resources through wider use where possible is particularly relevant. Thus, one of the main issues of forest research is the question of the technical quality of fire-damaged wood and the possibility of using it as a structural material. In this project, studies were carried out on the structure of raw wood - pine, exposed to fire. At the investigation stage, it can be noted that, based on visual analysis of the samples, no damage caused by insects and fungi was noted within five to seven months after the fire. According to the results of tests of samples for compression along the fibers, tension along the fibers and static bending, with a sufficiently small damage to the tree by fire, it can be recommended that it be partially used as a structural material.

Keywords Fire effect of wood · Wooden beams · Physical properties of wood · Mechanical properties of wood · Rational use

1 Introduction

Wood as a structural material is used in many branches of industry and engineering. The combination of high physical and mechanical characteristics and low specific gravity of wood compared to metal and reinforced concrete determines its high demand in construction [1–6].

Among the main physical properties is the density of wood, and of the mechanical properties, the tensile strength of wood is the most significant [7, 18–20].

At present, the question arises of maximizing the use of natural wood resources through wider use where possible. Thus, one of the main issues of forest research

V. Martinov (✉) · M. Lisyatnikov · S. Roshchina · A. Lukina

Institute of Architecture Construction and Energy Engineering, Vladimir State University named after Alexander and Nikolay Stoletovs, Gorky Street 87, 600000 Vladimir, Russia

e-mail: martinov3369@gmail.com

is the question of the technical quality of fire-damaged wood and the possibility of using it as a structural material. In works [2–6, 17] it is shown that partially charred wood retains sufficiently high physical properties, which makes it possible to use it as a structural material. However, the amount of results obtained, including international studies, is insufficient to form a clear legal framework governing the use of raw wood exposed to fire in building structures [8–12]. It should be noted that the physical and mechanical properties of solid wood have been studied quite deeply [12–16], but studies of raw wood damaged by fire are more than modest. It is necessary to conduct more detailed studies of the mechanical properties of raw wood exposed to fire (namely, the establishment of strength, stability, plasticity, deformability and the determination of the design resistances in tension along the fibers, bending and compression).

The technical qualities of wood exposed to a fire are quite dependent on the type of fire and the felling time that has elapsed since the fire. A ground fire with a flame height of up to 0.5 m, which only scorched tree trunks from below, slightly affects the state of forest stands, and at the same time there is a high probability of their preservation. In the same places where there was a strong ground fire with a flame height of over 1.5 m and a burnt length on tree trunks from 6–8 to 18 m or more, stands are significantly damaged, and, consequently, the quality of wood changes [21–25].

In this work, a study was made of the structure of raw wood - pine, exposed to fire. The main fundamental questions posed in this study are as follows: to establish patterns of the influence of the type (class) of forest fire on changes in the microstructure of pine wood, to establish patterns of the effect of fire on the physical and mechanical properties of pine wood, depending on the degree of wood damage by fire; to form a set of recommendations for standardizing the main structural characteristics of wood (calculated resistance to compression, bending, tension and shearing) for their application in the calculations of design problems. This study will reduce the material consumption of building wooden structures.

2 Methods

Wood degrades when exposed to elevated temperatures. Fire exposure causes the thermal degradation or pyrolysis of wood in which the wood is converted to volatile gases and a char residue. The extent of any thermal degradation depends on both the temperature and the duration of the exposure. At temperatures below 100 °C, the immediate effect of temperature on mechanical properties of wood is essentially reversible, Prolonged exposure to temperatures exceeding 65 °C can result in permanent losses in strength properties. Degradation resulting in weight loss is associated with temperatures exceeding 100 °C. For temperatures less than 200 °C, charring of the wood requires extended exposure. Significant degradation occurs in the temperature range of 200° to 300 °C. A temperature of ≡ 300ºC is commonly associated

Fig. 1 Illustration of the degradation zones in a charred piece of wood
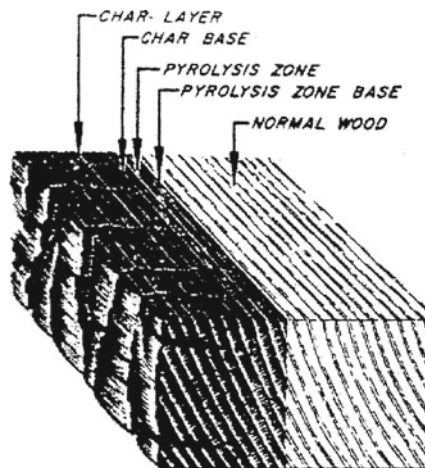
with the base of the char layer for wood subjected to direct fire exposure in the standard fire-resistance test. Vigorous production of flammable volatiles occurs in the temperature range of 300º to 450 ºC., Kinetic parameters are used to model the rate of thermal degradation [4, 5].

Sudden surface heating of a wood member in a fire result in surface charring and a steep temperature gradient. Thus, the stages of thermal wood degradation previously discussed become zones of degradation in a structural wood member exposed to fire. In a broad sense, there is an outer char layer, a pyrolysis zone, a zone of elevated temperatures, and the cool interior (Fig. 1), These zones of degradation reflect the temperature profile through the cross section.

For wood members that have charred, the char layer can be easily scrapped off. Obviously, any charred portion of a fire-exposed wood member has no residual load capacity. The wood beneath the char layer has residual load capacity; but, this residual capacity will be less than the load capacity prior to the fire. Members that have only visual smoke damage or slight browning of the surface also have significant residual load capacity.

To study the density, hardness and strength of wood, several trees (by average diameter) were selected that were exposed to a ground fire. The choice of this type of fire is of certain scientific and practical interest in terms of the further use of wood. The degree of damage to forest stands during these types of fire is different.

From each tree, sections were cut along the height of the trunk from the butt, middle and apical parts. Samples were made from each cut along the radius: in the center, by 0.5 radius (middle) and on the periphery.

The samples were taken in Namskiy Appani, p. Namskiy Yedeytci, p. Namtsy-1 Khomustakh, belonging to the Namsky ulus, the Republic of Yakutia.

The production of samples and testing to determine the tensile strength of wood corresponded to the following methods:

Table 1 Results of determining the density and moisture content of samples from the top part

Sample mark	Sample sizes, mm			Weight, gr	Density, kg/m³	Humidity, %
	a	b	l			
	Tangential direction	Radial direction	Along the fibers			
B-1	20.12	20.39	30.91	5.50	433.73	24.43
B-2	19.71	20.41	30.02	5.32	440.53	26.37
B-3	20.13	20.02	29.22	5.25	445.83	27.43
B-4	20.42	20.01	29.97	5.44	444.23	25.64
B-5	19.51	20.09	30.21	5.12	432.40	24.27
B-6	19.03	19.92	29.62	4.82	429.27	14.49
B-7	20.32	20.54	30.23	5.25	416.10	27.43
B-8	20.23	20.32	30.10	5.72	462.29	35.22
B-9	19.81	20.71	30.74	5.43	430.56	27.76
B-10	19.71	20.38	30.05	5.56	460.62	28.70
Mean	19.90	20.28	30.11	5.34	439.55	26.17

- GOST 16,483.10-73 "Wood. Methods for determining the compressive strength along the fibers";
- GOST 16,483.23-73* "Method for determining the tensile strength along the fibers";
- GOST 16,483.3-84 "Wood. Method for determining the ultimate strength in static bending".

3   Results and Discussion

3.1   Study of Physical Properties

Before studying the mechanical properties, the dimensions and mass of all samples were measured, their density and moisture content were determined. The results showed that the density of wood from the butt is higher than from the middle and apex, this explains the higher strength when tested for compression along the fibers, tension along the fibers and static bending (Tables 1, 2 and 3).

3.2   Results of Mechanical Tests

The results of testing samples for compression along the fibers are shown in Figs. 2, 3 and 4.

Table 2 Results of determining the density and moisture content of samples from the butt part

Sample mark	Sample sizes, mm			Weight, gr	Density, kg/m³	Humidity, %
	a	b	l			
	Tangential direction	radial direction	Along the fibers			
К-1	19.42	20.12	30.62	5.62	469.74	24.61
К-2	19.73	19.68	30.55	5.63	474.62	27.38
К-3	19.55	20.01	31.13	5.72	469.70	26.27
К-4	19.42	20.04	30.42	5.61	473.87	27.21
К-5	19.83	20.11	31.03	5.62	454.17	24.61
К-6	19.54	20.52	30.34	5.65	464.44	27.83
К-7	20.21	19.02	30.52	5.83	496.94	35.27
К-8	19.52	20.31	30.25	5.85	487.80	28.85
К-9	20.32	20.85	30.44	5.92	459.04	28.42
К-10	19.61	20.32	30.45	5.65	465.65	23.36
Mean	19.72	20.10	30.58	5.71	471.60	27.38

Table 3 Results of determining the density and moisture content of samples from the middle part

Sample mark	Sample sizes, mm			Weight, gr	Density, kg/m³	Humidity, %
	a	b	l			
	Tangential direction	radial direction	Along the fibers			
С-1	20.35	20.34	29.02	5.44	452.88	25.06
С-2	20.12	20.32	30.61	5.42	433.10	25.46
С-3	20.11	20.21	30.53	5.43	437.62	25.12
С-4	20.68	20.43	29.81	5.01	397.79	23.70
С-5	20.34	20.41	30.94	5.52	429.76	25.17
С-6	19.51	20.31	30.68	5.13	421.98	17.93
С-7	19.51	20.32	30.25	5.15	429.44	18.66
С-8	19.02	19.91	30.33	4.89	425.75	15.60
С-9	20.29	19.72	30.11	5.11	424.15	20.24
С-10	20.47	20.51	30.13	5.34	422.14	23.33
Mean	20.04	20.25	30.24	5.24	427.46	22.03

The results of testing samples for static bending are shown in Figs. 5, 6 and 7. The results of the tensile tests along the fibers are shown in Figs. 8, 9 and 10.

According to the results of tests for compression, tension along the fibers and for static bending, it can be concluded that the strength limits of wood from the butt part of the trunk are higher than from the apical and middle ones.
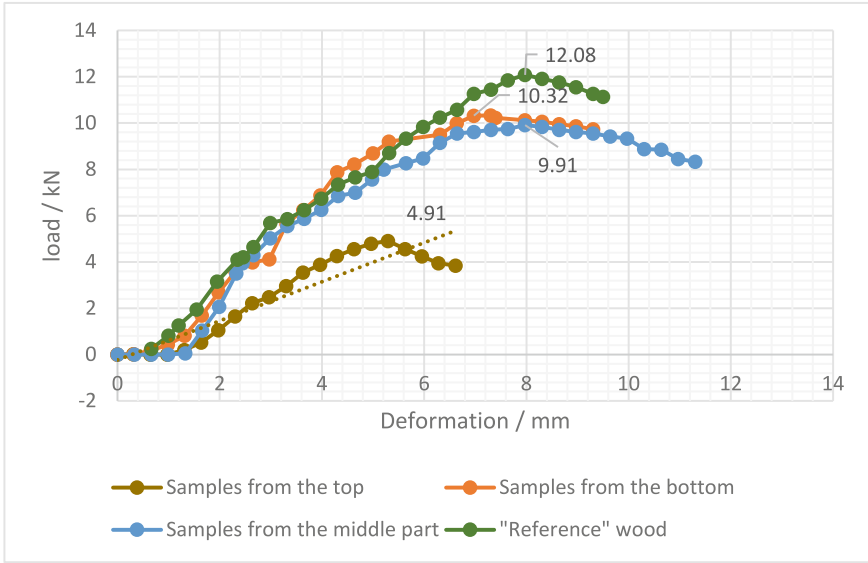
Fig. 2 The results of testing samples for compression along the fibers of the Namskiy Appani
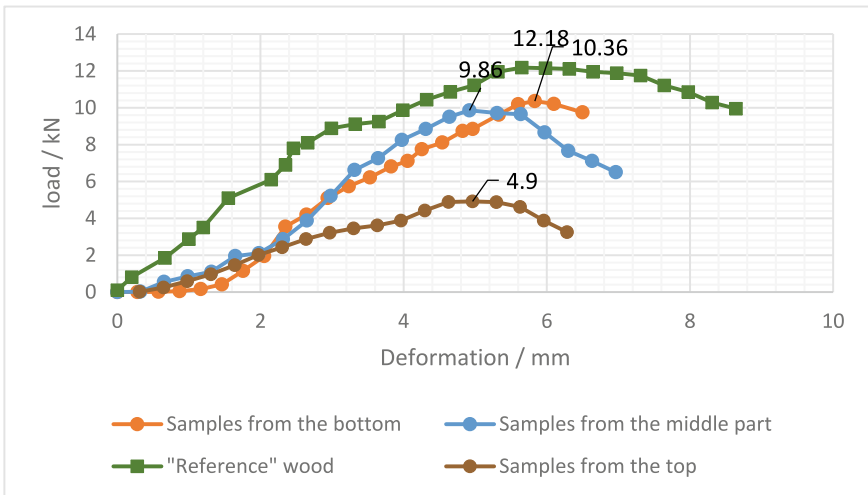
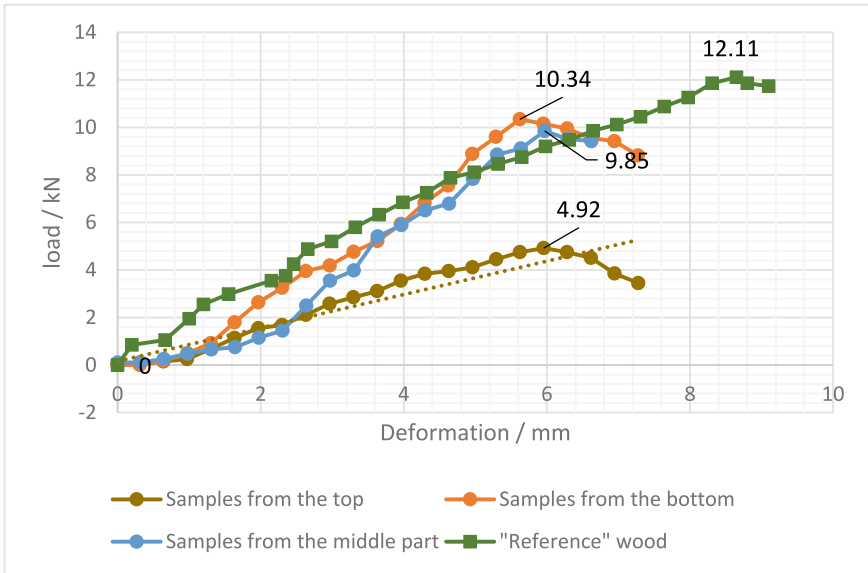**Fig. 3** The results of testing samples for compression along the fibers. Namskiy Yedeytci

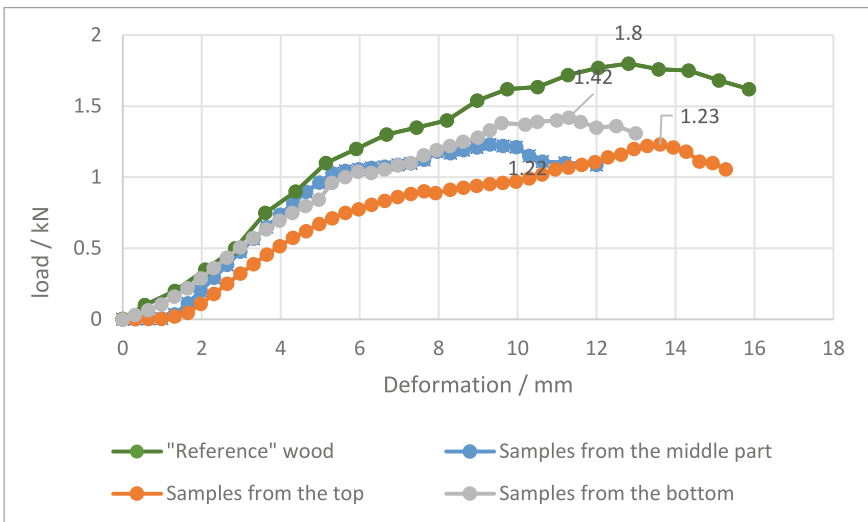**Fig. 4** Results of testing samples for compression along the fibers. Namtsy-1 Khomustakh

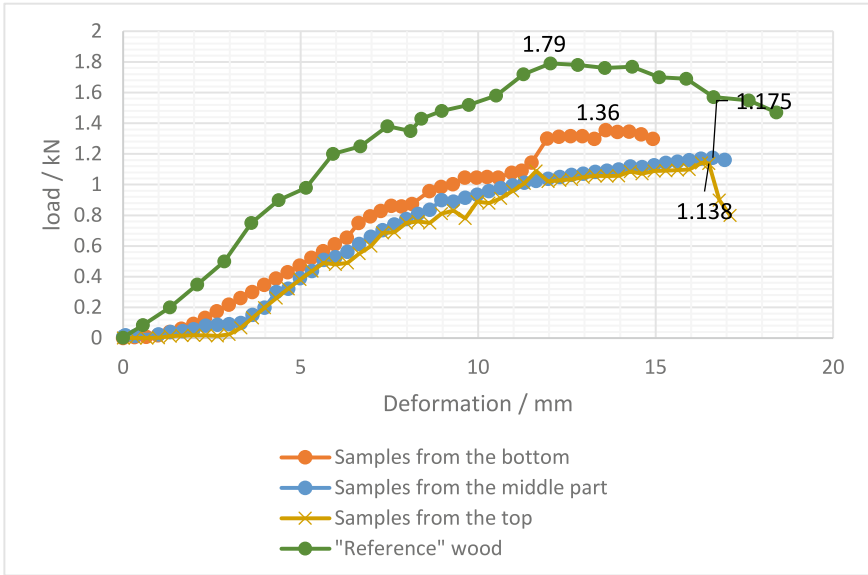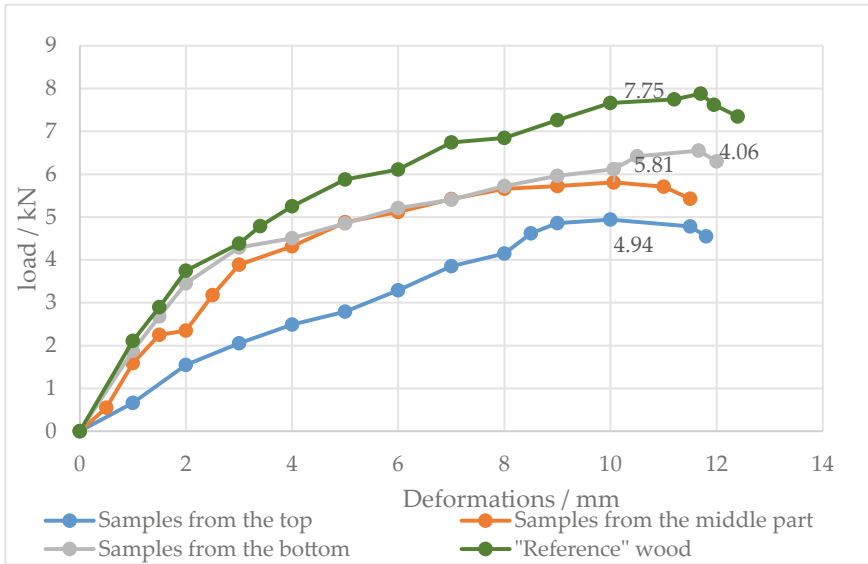**Fig. 5** Results of testing specimens for static bending. Namskiy Appani

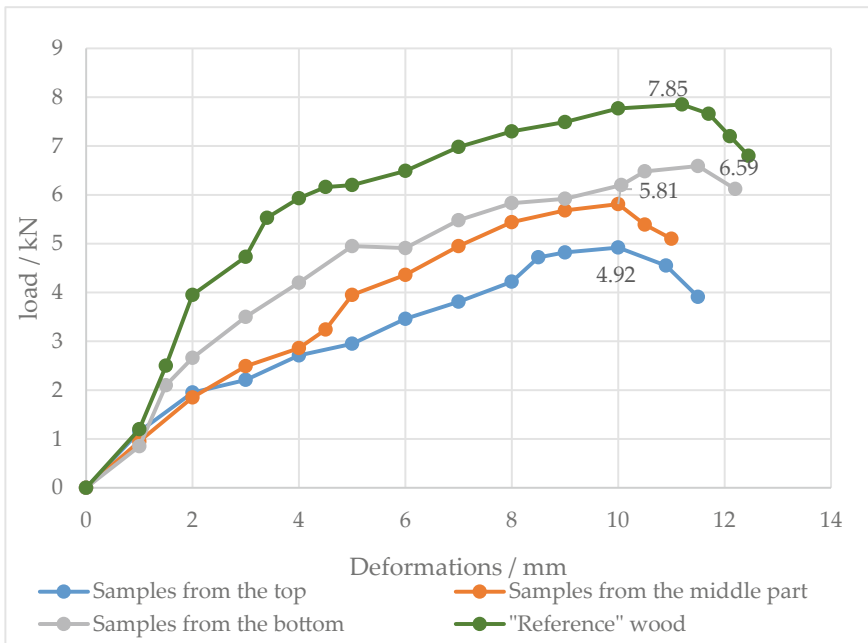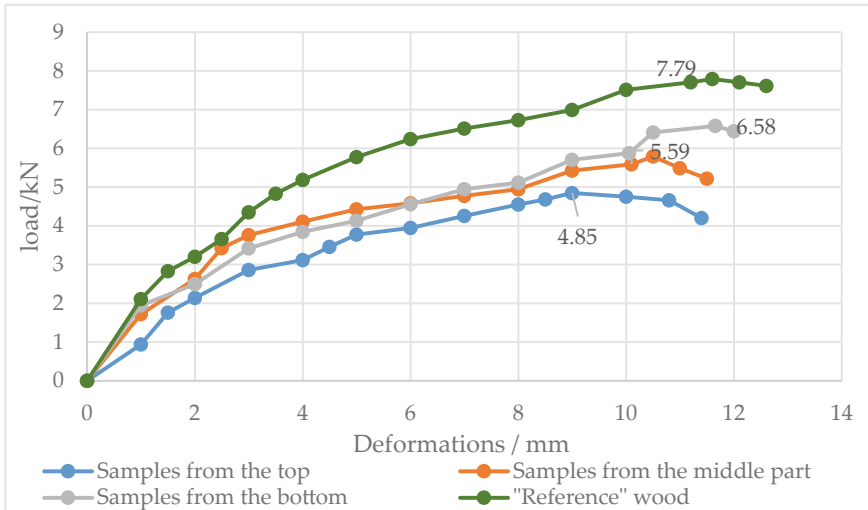**Fig. 6** Results of testing specimens for static bending. Namskiy Yedeytci

Fig. 7 Results of testing specimens for static bending. Namtsy-1 Khomustakh

Fig. 8 Results of tensile testing of samples along the fibers. Namskiy Appani

Fig. 9 Results of testing samples for tension along the fibers. Namskiy Yedeytci

Fig. 10 Tensile test results along the fibers. Namtsy-1 Khomustakh

4 Conclusions

1. During the tests, it was found that during a ground and medium fire, the strength properties of wood are most reduced in the apical part of the trunk, the smallest decrease is in the butt part. A gradual decrease in the density of wood from the butt part of the trunk to the apical part was also noted.

2. It has been determined that with a sufficiently small damage to a tree by a fire, i.e. reduction of the cross-sectional area up to 15%, its partial use as a structural material is possible.

3. The greatest decrease in strength for all types of tests was observed in samples taken from the upper part of the tree trunk. Thus, with static bending relative to the "reference" wood, the decrease is more than 20%, with compression along the fibers - up to 28.81%, with tension - 30.61%.

4. Often the end product of the reaction of wood to fire is a charred outer layer of wood and a relatively intact core of harder wood. In most cases, there is a clear boundary between the charred layer and the intact core. After laboratory testing, the core is suitable for use as an independent element or as part of a glued structure, after removing the charred layer by scraping or sandblasting.

References

1. Roshchina, S., Lukin, M., Lisyatnikov, M.: Compressed-bent reinforced wooden elements with long-term load. In: Anatolijs, B., Nikolai, V., Vitalii, S. (eds) Proceedings of EECE 2019, pp. 81–91. Springer International Publishing, Cham (2020)
2. Wimmers, G.: Wood: a construction material for tall buildings. Nat. Rev. Mater. **2**, 17051 (2017)
3. Júnior, G., Moreschi, J.: Physical-mechanical properties and chemical composition of Pinus taeda mature wood following a forest fire. Bioresour. Technol. **87**, 231–238 (2003)
4. Kukay, B., Barr, P., Friel, L., et al.: Post-fire assessments, methodology, and equations for directly determining wood's residual flexural properties. For. Prod. J. **58**, 40–46 (2008)
5. Suzuki, J., Mizukami, T., Naruse, T., Araki, Y.: Fire resistance of timber panel structures under standard fire exposure. Fire Technol. **52**, 1015–1034 (2016)
6. Sergeev, M., Rimshin, V., Lukin, M., Zdralovic, N.: Multi-span composite beam. IOP Conf. Ser. Mater. Sci. Eng. **896**, 12058 (2020)
7. Gribanov, A., Strekalkin, A., Kudryatseva, A., Zdralovic, N.: CFRP composites for strengthening wooden structures. IOP Conf. Ser. Mater. Sci. Eng. **896**, 12114 (2020)
8. Roshchina, S., Lukin, M., Lisyatnikov, M., Koscheev, A.: The phenomenon for the wood creep in the reinforced glued wooden structures. MATEC Web Conf. **245**, 3020 (2018)
9. Sergeev, M., Lukin, M., Strekalkin, A., Roshchina, S.: Mathematical modeling of stress-strain state of the nodal joint of wooden beams. J. Phys. Conf. Ser. **2131**, 32088 (2021)
10. Shishov, I., Lukin, M., Sergeev, M.: Roofing of an industrial building with variable height rafters and wooden decking. In: Vatin, N., Roshchina, S., Serdjuks, D. (eds.) Proceedings of MPCPE 2021, pp. 463–473. Springer International Publishing, Cham (2022)
11. Lukin, M., Prusov, E., Roshchina, S., et al.: Multi-span composite timber beams with rational steel reinforcements. Buildings **11**, 46 (2021)
12. Lisyatnikov, M., Glebova, T., Rusak, K., Ivaniuk, A.: Strength and deformability of reinforced wooden beams of variable stiffness. In: Vatin, N., Roshchina, S., Serdjuks, D. (eds) Proceedings of MPCPE 2021, pp. 549–561. Springer International Publishing, Cham (2022)
13. Lisyatnikov, M., Glebova, T., Ageev, S., Ivaniuk, A.: Strength of wood reinforced with a polymer composite for crumpling across the fibers. IOP Conf. Ser. Mater. Sci. Eng. **896**, 12062 (2020)
14. Naychuk, A.: Estimation of load-bearing capacity and stiffness of timber beams with through-thickness cracks. Adv. Mater. Res. **778**, 361–368 (2013)
15. Douglas, B.: Calculating the Fire Resistance of Exposed Wood Members (1999)
16. Bu, R., Zhou, Y., Shi, L., Fan, C.: Experimental study on combustion and flame spread characteristics in horizontal arrays of discrete fuels. Combust. Flame **225**, 136–146 (2021)
17. Ślósarz, S.: Strengthening of the wooden structures. Bud. i Archit. **18**, 17–28 (2020)
18. Labudin, B., Popov, E., Sopilov, V.: Calculation features of wooden-composite ribbed plates with splices in the cover. IOP Conf. Ser. Mater. Sci. Eng. **1079**, 52005 (2021)
19. Gribanov, A., Rimshin, V., Roshchina, S.: Experimental investigations of composite wooden beams with local wood modification. IOP Conf. Ser. Mater. Sci. Eng. **687**, 33039 (2019)
20. Lukin, M., Sergeev, M., Lisyatnikov, M.: Non split wooden beam reinforced with composite reinforcement. In: Vatin, N., Borodinecs, A., Teltayev, B. (eds.) Proceedings of EECE 2020, pp. 115–123. Springer International Publishing, Cham (2021)
21. Zhang, Y., Sun, J., Huang, X., Chen, X.F.: Heat transfer mechanisms in horizontal flame spread over wood and extruded polystyrene surfaces. Int. J. Heat Mass. Transf. **61**, 28–34 (2013)
22. Repin, V., Grinyov, V.: The experience in automating scientific research to identify dangerous zones in the near-support sections of wooden beams. In: Manakov, A., Edigarian, A. (eds.) International Scientific Siberian Transport Forum TransSiberia - 2021, pp. 1230–1238. Springer International Publishing, Cham (2022)
23. Labudin, B., Popov, E., Sopilov, V.: Stability of compressed sheathings of wood composite plate-ribbed structures. IOP Conf. Ser. Mater. Sci. Eng. **687**, 33041 (2019)

24. Sergeev, M., Lukina, A., Zdralovic, N., Reva, D.: Stress–strain state of a wood-glued three-span beam with layer-by-layer modification. In: Vatin, N., Roshchina, S., Serdjuks, D. (eds.) Proceedings of MPCPE 2021, pp. 485–491. Springer International Publishing, Cham (2022)
25. Labudin, B., Popov, E., Oshchepkova, E., Sopilov, V., Ruslanova, A., Fukalov, A.: Influence of cover splices on the stress-strain state of plate-ribbed wood-composite panels. Struct. Mech. Eng. Constr. Build. **16**(6), 439–451 (2021)

Studies of Screw Behavior in Modified Wood

Artem Strekalkin ⓘ **, Anastasiya Lukina** ⓘ **, Mikhail Lisyatnikov** ⓘ **, and Vladislav Martinov** ⓘ

Abstract The article describes the research devoted to the study of the behavior of the screw in solid wood, modified with a composition based on dimeacrylic polyester. Comparative indicators of the value corresponding to the force of pulling out a screw from an array of pure and modified wood are given. The influence of the angle of inclination of the screw on the force of pulling out the screw from an array of modified wood has been studied. The technology of modification of wood samples for testing the screw for pulling out and equipment that allows modifying wood and curing samples for testing are given. A model for the modernization of the testing machine is proposed, which makes it possible to carry out research on pulling out at different angles of inclination of the screw to the axes of wood anisotropy. Comparative results of numerical and experimental studies are presented. On the basis of the experiments carried out, it was found that the modification of wood can significantly increase the bearing capacity of the screw for pulling out of solid wood both at an angle of 90 degrees with the wood anisotropy axes, and at different angles of inclination.

Keywords ANSYS · Construction · Dowel · Finite element · Joint · Simulation · Structure · Timber · Wood · Modification · Buildings

1 Introduction

Since wood is a renewable natural resource, its use as a material for load-bearing structures is always relevant [1–6]. One of the ways to improve the physical and mechanical properties of wood is its modification with various compositions [7–10]. One of the most suitable composition from a technological point of view is a composition based on dimethacrylic polyester [11–14]. The composite obtained as a result of the modification has increased strength and reduced deformability compared to conventional wood [15].

A. Strekalkin (✉) · A. Lukina · M. Lisyatnikov · V. Martinov
Vladimir State University Named After Alexander and Nikolay Stoletovs, Vladimir, Russia
e-mail: a.a.strekalkin@gmail.com

Thus, it is possible to increase, by means of modification, not only the strength of the wood itself, but also its joints. For this, numerical and experimental studies were given, described below. The behavior of the screw in an array of ordinary and modified wood was studied.

2   Methods

Numerical and experimental studies were carried out. Numerical studies were modeled using the ANSYS software package. The model of the studied compound is shown in Fig. 1.

Wood was specified as an orthotropic material, steel as an isotropic one. At the same time, the strength characteristics of the modified wood were specified in the form of dependences obtained earlier when testing specimens for compression and shearing along and across the fibers.

As a result of preliminary mathematical studies and numerical simulation, it was found that the pull-out bearing capacity of screws with a diameter of less than 6 mm and a length of less than 80 mm is too low for their use in bearing joints of the type under study. Thus, the following set of simulated compounds was defined, consisting of two groups:

Group 1 (assessment of the degree of influence of wood modification of the contact zones on the bearing capacity of the screw for pulling out of solid wood):

1. Screw diameter - 6 mm, length - 100 mm, wood of the second grade;
2. Screw diameter - 6 mm, length - 100 mm, wood of the second grade modified;
3. Screw diameter - 8 mm, length - 100 mm, wood of the second grade;
4. Screw diameter - 8 mm, length - 100 mm, wood of the second grade modified;

Group 2 (assessment of the degree of influence of the geometric parameters of the screw connection on pulling out of the modified wood mass):

1. Screw diameter - 6 mm, length - 100 mm, wood of the second grade modified, the angle of deviation of the force from the wood anisotropy axes is 90º;

Fig. 1 General view of the sample for research on screw retention in solid wood
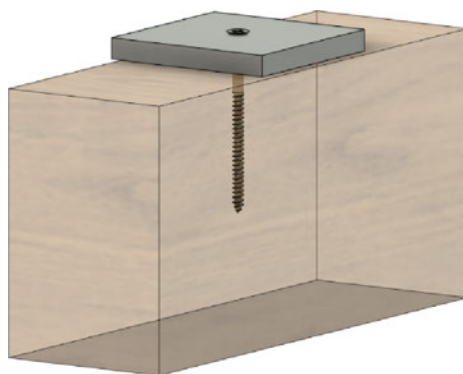
2. Screw diameter - 6 mm, length - 100 mm, wood of the second grade modified, angle of deviation of the force from the wood anisotropy axes 45º;
3. Screw diameter - 8 mm, length - 80 mm, wood of the second grade modified, the angle of deviation of the force from the wood anisotropy axes is 90º;
4. Screw diameter - 8 mm, length - 80 mm, wood of the second grade modified, the angle of deviation of the force from the wood anisotropy axes is 45º.

The REM-100-A-1 electromechanical tensile testing machine was used for experimental studies. The main function of the tensile testing machine is to determine the normalized value of the force during physical and mechanical testing of samples from various materials. The general view of the machine is shown in Fig. 2(a).

A mobile vacuum effusion unit was used to modify the samples (Fig. 2(b)). The curing of the images took place in a specialized oven, which allows maintaining the temperature up to 130˚C.

To test screws for pulling out from solid wood four series of samples of 3 pieces were made. Dimensions of wooden elements 150 × 150 × 400 mm. For testing, a REM-100-A-1 tensile testing machine was used. Similar to the numerical study, two groups were selected.

For ease of identification, the following marking was chosen for 1 group:

1) Marking "D-6-90", Series No. 1 - wood of the second grade, breed - pine, screw with a diameter of 6 mm, length - 100 mm.

(a)   (b)
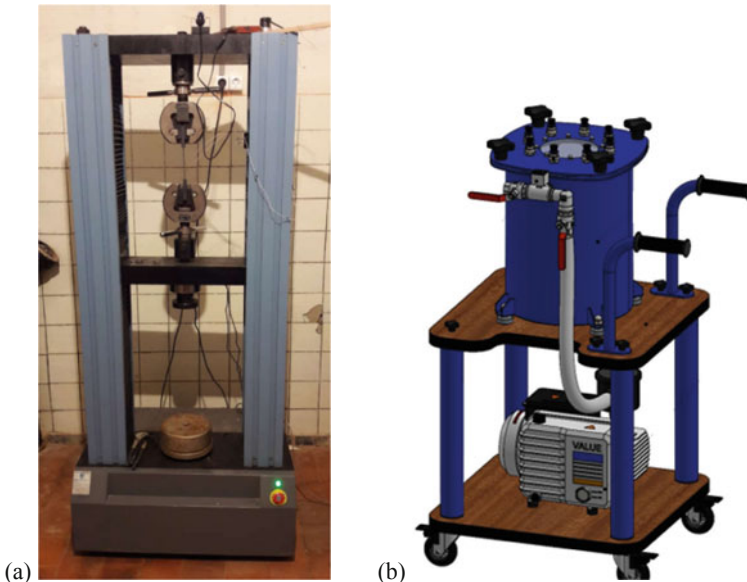
Fig. 2 a Explosive machine REM-100-A-1, **b** Mobile vacuum infusion unit.

2) Marking "DM-6-90", Series No. 1 - wood of the second grade, modified with a solution of dimethacrylic polyester, species - pine, screw with a diameter of 6 mm, length - 100 mm.

3) Marking "D-8-90", Series No. 1 - wood of the second grade, breed - pine, screw with a diameter of 6 mm, length - 80 mm.

4) Marking "DM-8-90", Series No. 1 - wood of the second grade, modified with a solution of dimethacrylic polyester, species - pine, screw with a diameter of 8 mm, length - 80 mm.

For the 2 group, the following identification was chosen:

5) Marking "D-6-45", Series No. 2 - wood of the second grade, species - pine, screw with a diameter of 6 mm, length - 100 mm, the angle of application of force to the main axes of wood anisotropy - 45°;

6) Marking "DM-6-45", Series No. 2 - wood of the second grade, modified with a solution of dimethacrylic polyester, species - pine, screw with a diameter of 6 mm, length - 100 mm, the angle of application of force to the main axes of wood anisotropy - 45°;

7) Marking "D-8-45", Series No. 2 - wood of the second grade, species - pine, screw with a diameter of 6 mm, length - 80 mm, the angle of inclination of the force to the main axes of wood anisotropy - 45°;

8) Marking "DM-8-45", Series No. 2 - wood of the second grade, modified with a solution of dimethacrylic polyester, species - pine, screw with a diameter of 8 mm, length - 80 mm, the angle of application of force to the main axes of wood anisotropy - 45°.

Fig. 3 Deformed scheme based on the results of numerical studies
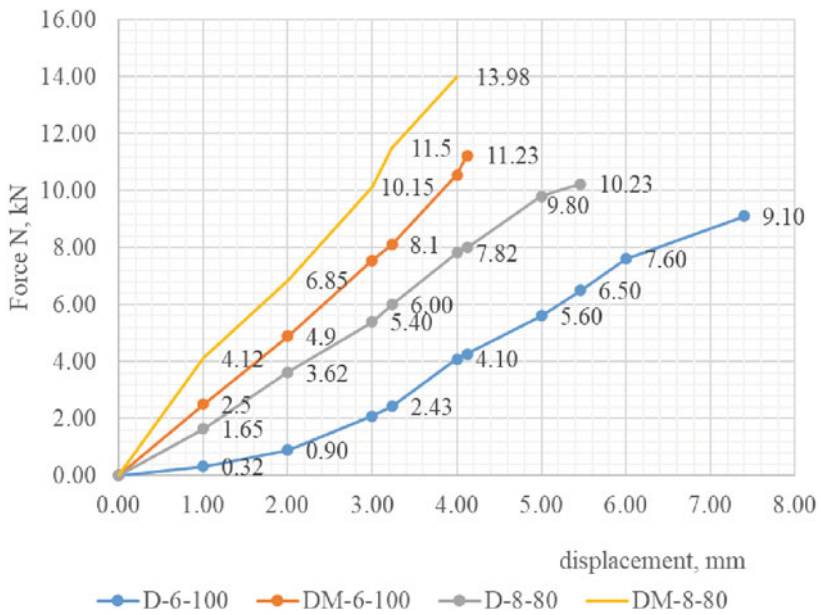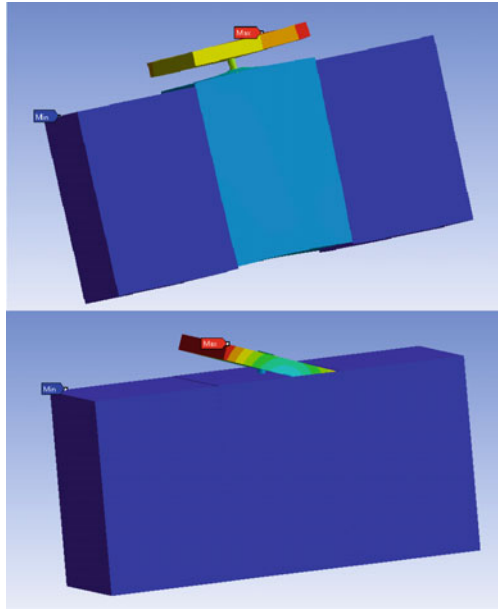
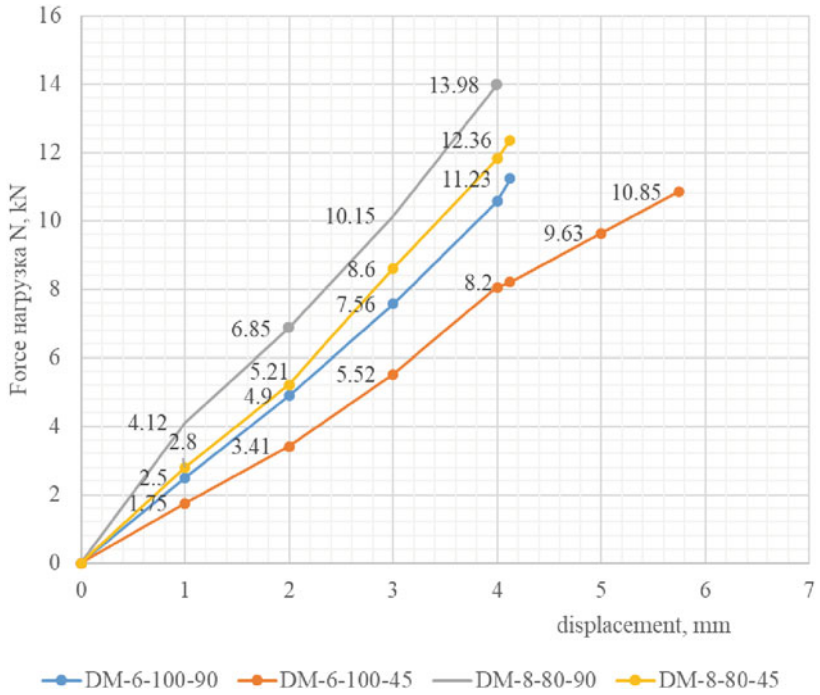**Fig. 4** Dependences of displacements, mm on the applied load, kN

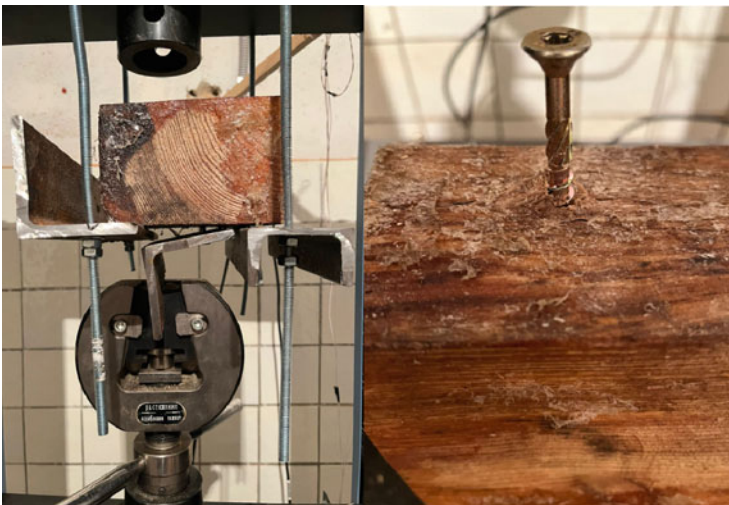**Fig. 5** Dependences of displacements, mm on the applied load,kN

Fig. 6 The process of testing samples for holding screws in a modified wood array

3   Results and Discussion

The numerical studies carried out made it possible to establish the values of the breaking loads given in Table 1. The deformed test schemes are shown in Fig. 3.

The results of numerical studies are shown in Table 1.

Figures 4 and 5 show the dependence of displacements on the applied load.

The general view of the pull-out tests is shown in Fig. 6. The nature of the deformation of the wood when the screw is pulled out of its array is visible.

The results of experimental studies are shown in Table 2 and 3, Figs. 7 and 8.

Table 1 The results of numerical studies of screws for pulling out from an array of ordinary and modified wood

Parameter	Destruction load, kN
Screw d = 6 mm, l = 100 mm	9.10
Screw d = 6 mm, l = 100 mm, mod	11.23
Screw d = 8 mm, l = 80 mm	10.23
Screw d = 8 mm, l = 80 mm, mod	12.36
Screw d = 6 mm, l = 100 mm, 90°, mod	11.23
Screw d = 6, l = 100, 45°, mod	10.85
Screw d = 8 mm, l = 80 mm, 90°, mod	13.98
Screw d = 8 mm, l = 80 mm, 45°, mod	12.36

Table 2 Pull-out test results for solid wood screws (Group 1)

Parameter	D-6	DM-6	D-8	DM-8
Average breaking force N, kN	7.56	9.93	8.46	11.2
Average deformation δ, mm	6.2	4.56	5.12	3.23
Test duration t, sec	113	126	124	139
Type of destruction	Screw pulling, wood crushing	Screw pulling, wood crushing	Screw pulling, wood crushing	Screw pulling, wood crushing

Table 3 Pull-out test results for solid wood screws (Group 2)

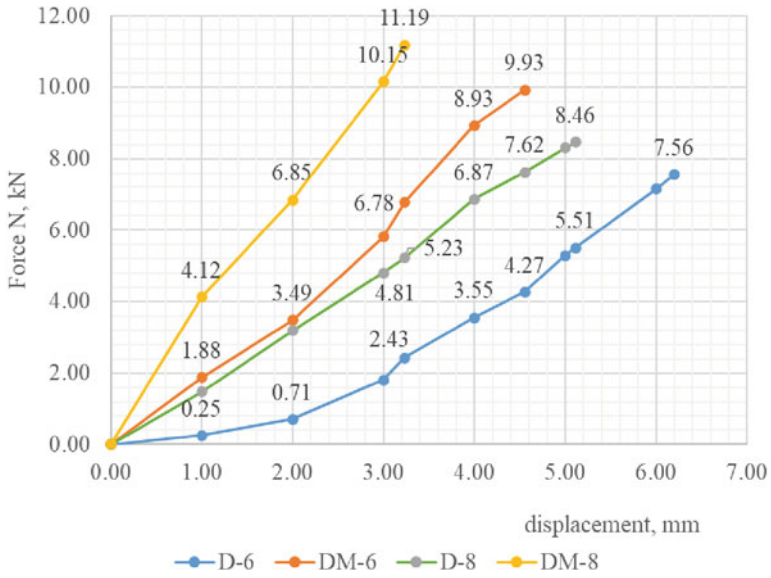| Parameter	D-6-45	DM-6-45	D-8-45	DM-8-45
Average breaking force N, kN	5.96	8.46	6.81	9.58
Average deformation δ, mm	7.21	5.10	5.97	4.12
Test duration t, sec	98	121	109	135
Type of destruction	Screw pulling, wood crushing	Screw pulling, wood crushing	Screw pulling, wood crushing	Screw pulling, wood crushing

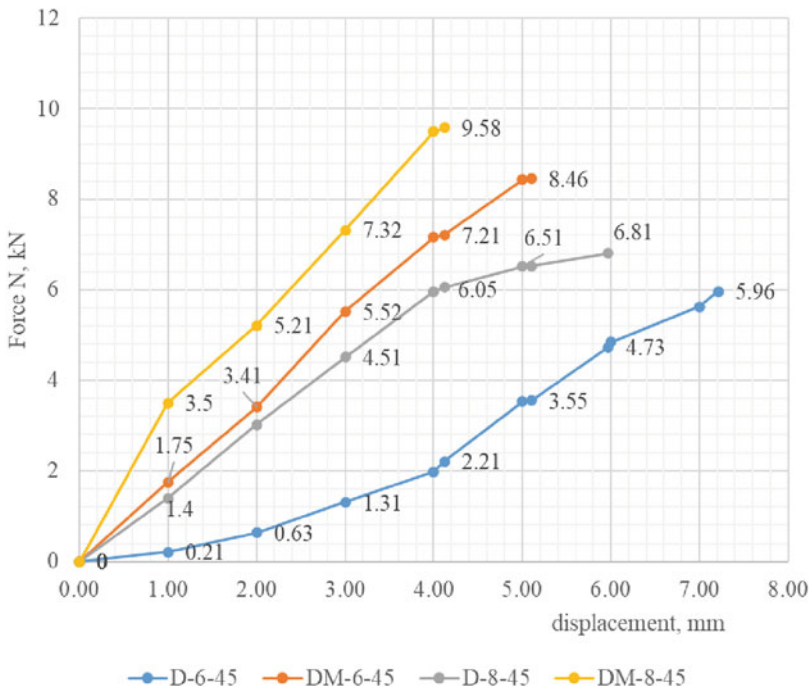**Fig. 7** Dependences of displacements, mm on the applied load, kN

Fig. 8 Dependences of displacements, mm on the applied load, kN

4 Conclusions

As a result of preliminary calculations, the degree of influence of wood modification and the geometric parameters of the screw connection on its bearing capacity to resist pulling out of the solid wood was established. Based on the results of preliminary calculations, it was decided to conduct tests on local samples in order to establish the comparative nature of the loss in the bearing capacity of the screw connection due to pulling out of the massif of ordinary and modified wood. The hypothesis about the effectiveness of wood modification in order to increase the bearing capacity of the joint was also confirmed.

As a result of the research carried out, the following conclusions were drawn:

– Modification of wood allows to increase the breaking load when testing the screw for pulling out of solid wood by an average of 36%;
– The bearing capacity of the screw for pulling out when a force is applied without deviation from the main axes of the anisotropy of wood is on average 24% higher for solid wood and 16% for modified wood.

References

1. Buka-Vaivade, K., Serdjuks, D., Goremikins, V., Pakrastins, L., Vatin, N.I.: Suspension structure with cross-laminated timber deck panels. Mag. Civ. Eng. **83**, 126–135 (2018). https://doi.org/10.18720/MCE.83.12.
2. Yao, Z., Wu, D., Chen, C., Zhang, M.: Creep behavior of polyurethane nanocomposites with carbon nanotubes. Compos. Part A Appl. Sci. Manuf. **50**, 65–72 (2013). https://doi.org/10.1016/j.compositesa.2013.03.015
3. Yahyaei-Moayyed, M., Taheri, F.: Experimental and computational investigations into creep response of AFRP reinforced timber beams. Compos. Struct. **93**, 616–628 (2011). https://doi.org/10.1016/j.compstruct.2010.08.017
4. Fossetti, M., Minafò, G., Papia, M.: Flexural behaviour of glulam timber beams reinforced with FRP cords. Constr. Build. Mater. **95**, 54–64 (2015). https://doi.org/10.1016/j.conbuildmat.2015.07.116
5. Ruslantsev, A.N., Portnova, Y.M., Tairova, L.P., Dumansky, A.M.: Analysis of mechanical properties anisotropy of nanomodified carbon fibre-reinforced woven composites. IOP Conf. Ser. Mater. Sci. Eng. **153**, 012003 (2016). https://doi.org/10.1088/1757-899X/153/1/012003
6. Telichenko, V.I., Rimshin, V.I., Karelskii, A.V., Labudin, B.V., Kurbatov, L.: Strengthening technology of timber trusses by patch plates with toothed-plate connectors. J. Ind. Pollut. Control. **33**, 1034–1041 (2017)
7. Popov, E., Ruslanova, A., Sopilov, V., Zdralovic, N., Mamedov, S., Labudin, B.: Contact interaction of a claw washer with wood at limiting shear. Lesnoy Zhurnal (For. J.) **4**, 178–189 (2020). https://doi.org/10.37482/0536-1036-2020-4-178-189

8. Khelifa, M., Celzard, A.: Numerical analysis of flexural strengthening of timber beams reinforced with CFRP strips. Compos. Struct. **111**, 393–400 (2014). https://doi.org/10.1016/j.compstruct.2014.01.011

9. D'Ambrisi, A., Focacci, F., Luciano, R.: Experimental investigation on flexural behavior of timber beams repaired with CFRP plates. Compos. Struct. **108**, 720–728 (2014). https://doi.org/10.1016/j.compstruct.2013.10.005

10. Basterra, L.A., Balmori, J.A., Morillas, L., Acuña, L., Casado, M.: Internal reinforcement of laminated duo beams of low-grade timber with GFRP sheets. Constr. Build. Mater. **154**, 914–920 (2017). https://doi.org/10.1016/j.conbuildmat.2017.08.007

11. Kim, Y.J., Harries, K.A.: Modeling of timber beams strengthened with various CFRP composites. Eng. Struct. **32**, 3225–3234 (2010). https://doi.org/10.1016/j.engstruct.2010.06.011

12. Vodiannikov, M.A., Kashevarova, G.G.: Analysis of wood structure connections using cylindrical steel and carbon fiber dowel pins. IOP Conf. Ser. Mater. Sci. Eng. **205**, 012031 (2017). https://doi.org/10.1088/1757-899X/205/1/012031

13. Kasal, B., Pospisil, S., Jirovsky, I., Heiduschke, A., Drdacky, M., Haller, P.: Seismic performance of laminated timber frames with fiber-reinforced joints. Earthq. Eng. Struct. Dyn. **33**, 633–646 (2004). https://doi.org/10.1002/eqe.368

14. Matveev, R.P., Labudin, B.V., Morozov, V.S., Orlov, A.O.: Numerical analysis of strength and rigidity of the biomechanical system «bone-apparatus». Ekologiya cheloveka (Hum. Ecol.) **24**(4), 58–64 (2017). https://doi.org/10.33396/1728-0869-2017-4-58-64

15. Karelskiy, A.V., Zhuravleva, T.P., Labudin, B.V.: Load-to-failure bending test of wood composite beams connected by gang nail. Mag. Civ. Eng. **54**, 77–85 (2015). https://doi.org/10.5862/MCE.54.9

Numerical Study of a Wood-Composite Beam Structure

Anastasiya Lukina ⬛, **Artem Koshcheev** ⬛, **Anatoliy Naichuk** ⬛, **and Svetlana Roshchina** ⬛

Abstract The article carried out a numerical study of a wood-composite beam using lamellas (planks) made of fire-prone wood. The percentage of replacement of healthy wood with wood weakened by fire was determined along the height of the section. The studies were carried out in linear and non-linear formulation of problems. It has been established that the maximum percentage of replacing healthy wood with wood weakened by fire should not exceed 47% in terms of the height of the section for wood-composite beams 9 m long.

Evaluating structural and technological indicators, such as cross-sectional dimensions, span and saving resources, it is possible to evaluate the effectiveness of such load-bearing building structures, as well as technical and economic indicators, expressed in the level of consumption of basic materials, factory cost, reduced costs and serviceability.

Keywords Wood · Building wooden structures · Strength · Fire · Beam · Composite

1 Introduction

In modern conditions, the problem of saving resources is of particular importance [1]. In the field of construction, the solution to this problem can be achieved by improving the structure of the materials used, reducing losses, deepening processing, and by using progressive products and designs [2–4].

The successful solution of the problem of resource saving will be facilitated by the introduction of progressive structures made of laminated wood and plywood [5–9].

A. Lukina (✉) · A. Koshcheev · S. Roshchina
Institute of Architecture Construction and Energy Engineering, Vladimir State University Named After Alexander and Nikolay Stoletovs, Gorky Street 87, Vladimir 600000, Russia
e-mail: pismo.33@yandex.ru

A. Naichuk
Brest Technical University, Brest, Belarus

One of the types of progressive structures are wood-glued structures (beams, columns, etc.), in which blanks of wood and wood-based board materials are joined by gluing. The rational placement of different materials in the cross section makes it possible to obtain composite structures with a sufficiently large bearing capacity with a small material capacity. The issues of wood resource saving and reduction of material consumption of building structures are described and substantiated in the works [10–12]. The authors [13, 14] offer new ways to restore the strength of wooden structures with polymer compositions without changing its appearance.

The authors [15–19] explore the stress–strain state of wood-glued structures. It has been determined that it is possible to rationally place boards of different quality in height in board beams. Layers of boards of the first or second grade are laid in the most stressed areas of the beam, and layers of boards of the second or third grade are placed in less stressed places. Undersized lumber can also be used in glulam beams.

In recent years, there have been many fires of varying degrees of intensity [20, 21]. This natural disaster is widespread in the world. The question arises, is it possible to use a tree that has been exposed to fire? If fire damage to a tree is partial, can it be used for structural purposes?

The current study is aimed at solving this problem: to establish the percentage of replacement of healthy wood with wood weakened by fire exposure from the condition of ensuring the bearing capacity and limiting deflections using the example of a wood-composite beam.

2   Methods

The most well-known numerical method that allows studying the complex stress–strain state of anisotropic bodies [22, 23], which is wood, is the finite element method (FEM). This method is used in various computational software systems. In this study, software systems "LIRA 10.10" are used.

The main concept of the FEM is the division of the analysis area into a finite number of subdomains, called finite elements [24, 25]. Each element is defined by a finite number of points, i.e. nodes. The system of nodes and elements forms a so-called grid. For the physical quantities with respect to which the solution is determined, a piecewise continuous approximation is assumed within each element. The computational procedure of the finite element method (FEM) is based on solving a system of algebraic equations that minimizes the functional associated with the desired physical quantity. It can be expected that the discrete approximation of the solution will converge to the exact solution as the number of finite elements increases [26–28]. However, this process also depends on the characteristics of the elements and the accuracy of the piecewise continuous function. The convergence criterion should be used to select valid elements.

For a reasonable calculation of the elements of wooden structures, it is necessary to know the strength of wood under various types of stress state [29, 30]. Typical

stress–strain states in building wooden structures are: compression and tension along the fibers, bending.

Preliminary studies were carried out on samples (pine) of the residual strength of wood in tension and compression along the fibers, chipping and static bending. It was established that the greatest decrease in strength for all types of tests was observed in samples taken from the upper part of the tree trunk. Thus, with static bending of relatively healthy wood, the decrease is more than 20%, with compression along the fibers - up to 28.81%, with tension - 30.61%.

Therefore, with a sufficiently small damage to the tree by fire, i.e. reduction of the cross-sectional area up to 15%, its partial use as a structural material is possible. The results obtained were used to determine the Modulus of elasticity, shear modulus, Poisson's ratio of weakened wood by fire exposure.

Both linear and non-linear calculations of an ordinary beam without reinforcement were performed, taking into account the real (actual) work of the structure. Nonlinearity in the software package is taken into account when stiffnesses are assigned to the finite elements (plates). In each calculation, 4 series of beams were examined. The beams were loaded with concentrated loads, the points of application of which are located at a distance of 0.5 m from each other. The load was applied in steps, the values of which were taken equal to l/10 of the breaking load.

A numerical study of wood-laminated beams (pine) with a cross-section of 140 × 300 mm, a length (l0) of 9 m with a different percentage of the replacement of healthy wood with wood weakened by the fire effect along the height of the section was carried out. The following notation has been introduced:

1. Beam - section from standard wood (B-1);
2. Beams with an insert 140 × 100 mm in the middle of the section: 33% fire wood (B-2);
3. Beams with an insert 140 × 140 mm in the middle of the section: 47% firewood (B-3);
4. Beams with an insert 140 × 180 mm in the middle of the section: 60% fire wood (B-4).

Beam loading is a load uniformly distributed over the area with a value of 1 t/m^2. Table 1 gives the following parameters for calculation.

3 Linear Calculation

A traditional solid wood beam with similar parameters was chosen as a reference (Fig. 1).

Table 1 Characteristics of wood

	Description	Symbol	Options	Number of Finite Elements	Total volume (m³)
1	healthy wood (fire-damaged wood)		ρ=500(kg/m³); E_1=400(MPa); E_2=1E+04(MPa); E_3=400(MPa) G_{12}=1.2E+03(MPa); G_{13}=500(MPa); G_{23}=50(MPa) Nu_{12}=0.5; Nu_{21}=0.02; Nu_{13}=0.5; $Nu23$=0.02; $Nu31$=0.5; $Nu32$=0.5 α_{12}=1E-05; α_{21}=1E-05; α_{13}=1E-05	122850	0.98
2	Tree after fire		ρ=400(kg/m³); E_1=320(MPa); E_2=6.4E+03(MPa); E_3=320(MPa) G_{12}=1.2E+03(MPa); G_{13}=500(MPa); G_{23}=50(MPa); Nu_{12}=0.5;Nu_{21}=0.025; Nu_{13}=0.5; Nu_{23}=0.025; $Nu31$=0.5; $Nu32$=0.5 α_{12}=1E-05; α_{21}=1E-05; α_{13}=1E-05	66150	0.53
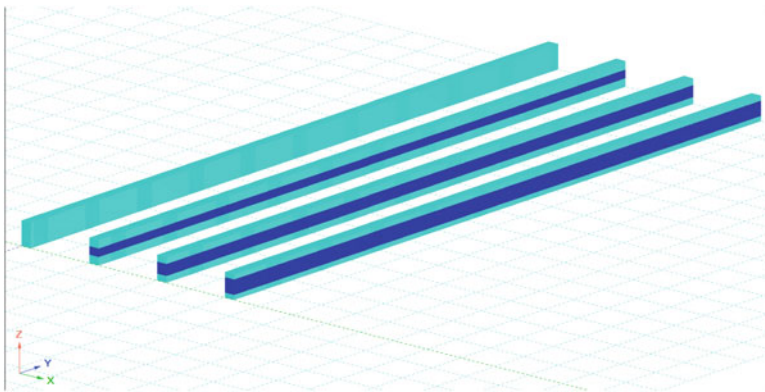
Fig. 1 General view in the materials of beams B-1, B-2, B-3, B-4 (numbering from left to right)

4 Results and Discussion

According to the building structure design standards, the vertical limit deflections are determined as:

$$\Delta \leq [\Delta], \tag{1}$$

where Δ is reversible deformations or deflections, $[\Delta]$ is irreversible deformations or limit deflections. Limit deflections for beam structures are determined by formula 2.
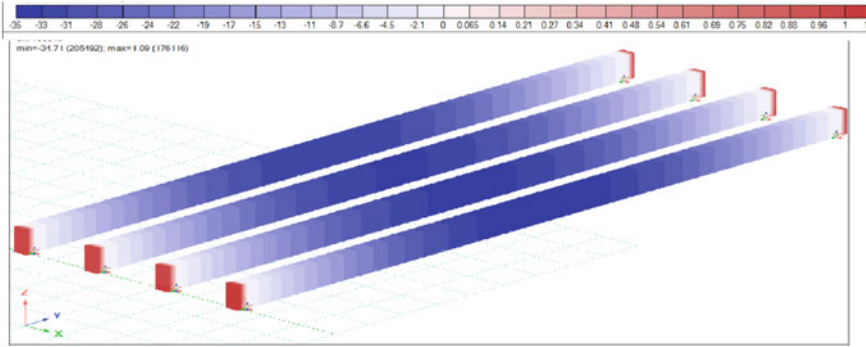
Fig. 2 Movements in system nodes (with a load of 10 kN per beam) in beams B-1, B-2, B-3, B-4

$$l_0/250 = [\Delta] \tag{2}$$

Then, the ultimate deflection for the structure under study is:

$$l_0/250 = 9000/250 = 36\,\text{mm}$$

Figure 2 shows a general view of the deformation of beams under a load of 10 kN per beam.

In the course of a numerical study in the linear formulation of the problem, it was established that the movement of the system along the nodes in the middle of the span with a load of 10 kN on the beam with a replacement for weakened wood up to 33% of wood in the middle of the section, there is a movement along the Z axis up to 33 mm. When healthy wood is replaced with a weakened one up to 47% in cross section, a displacement occurs along the Z axis up to 34 mm, which is the ultimate deflection. The movement of the system along the nodes in the middle of the span (deflection) at a load of 10 kN occurs up to 35 mm per beam with a replacement for weakened wood up to 60% of the cross section. This deflection value exceeds the ultimate deflection.

Figures 3 and 4 show normal and shear stresses in beams B-1, B-2, B-3, B-4.

The numerical study showed that in all four beams under a load of 10 kN they show the same shear stresses equal to 0.34 MPa. Normal stresses increase depending on the increase in the percentage of replacement of healthy wood with wood weakened by fire. Normal stresses in the middle of the span for a solid wood beam B-1 are 4.74 MPa. The normal stresses in the middle of the span for the B-2 beam are 4.79 MPa, for the B-3 beam they are 4.91 MPa, for the B-4 beam they are 5.11 MPa.

Thus, in a linear calculation, it was determined that the maximum percentage of replacing healthy wood with wood weakened by fire is possible up to 47% relative to the section height for beams l = 9 m. Since the calculations were carried out in the elastic stage of wood work, conclusions about the strength indicators of beams at this stage would be premature. Based on the foregoing, it was decided to conduct
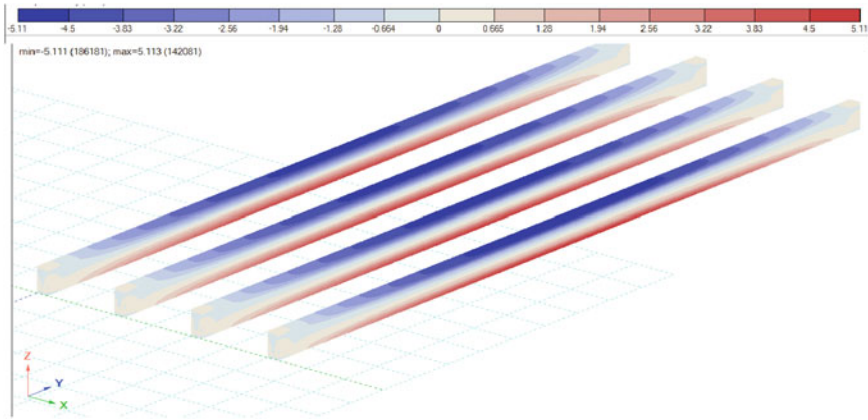
Fig. 3 Strain Ny in beams B-1, B-2, B-3, B-4
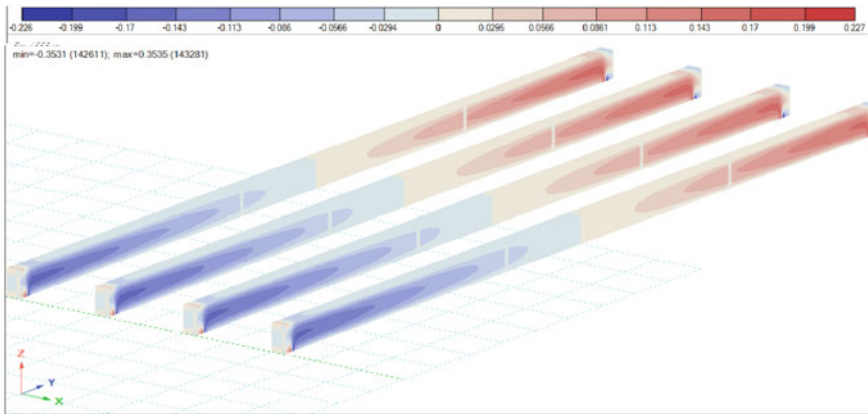
Fig. 4 Tangential stresses in plane ZoY in beams B-1, B-2, B-3, B-4 (numbering from left to right)

a study in a nonlinear formulation of the problem, reflecting the real work of the B-3 wood-composite structure.

5 Nonlinear Calculation

The purpose of the non-linear calculation is to determine the actual work of a wood-composite beam (B-3) with 47% replacement of healthy wood with fire-weakened wood along the height of the section. The results of the calculation were compared with the work of the all-wood beam B-1 (Figs. 5 and 6).
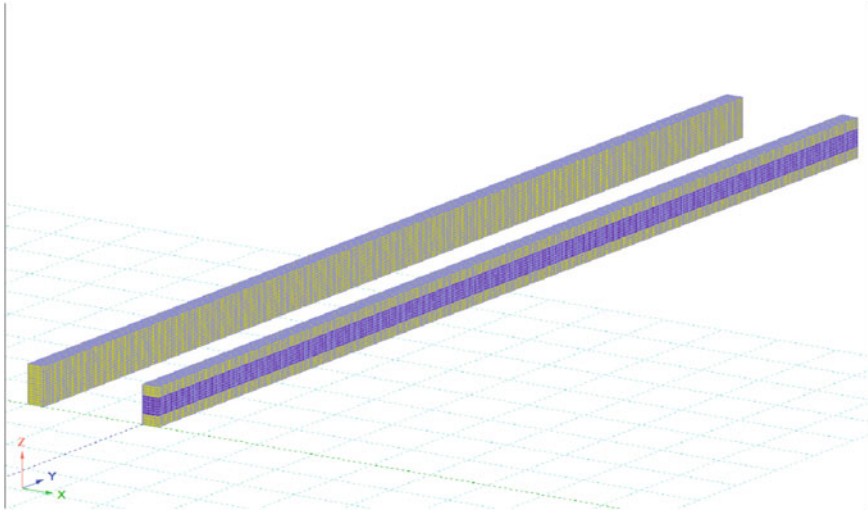
Fig. 5 General view of beams B-1 and B-3 in materials (numbering from left to right)
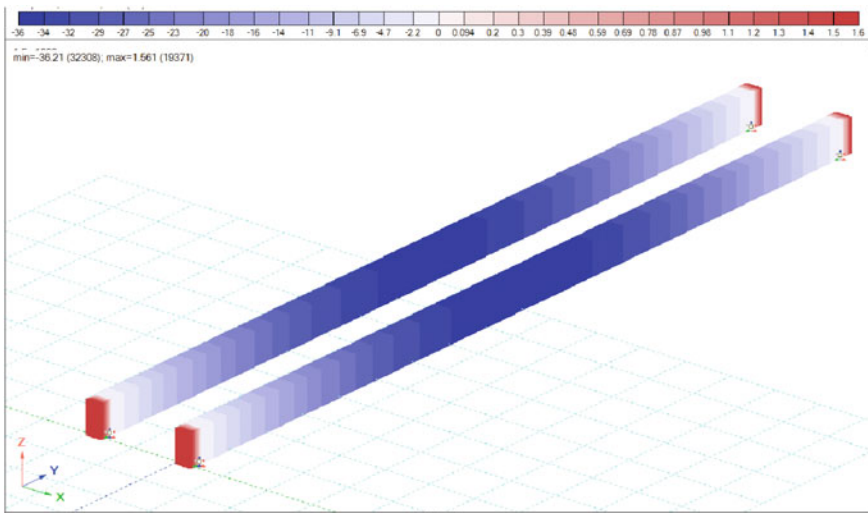
Fig. 6 Vertical displacements in the nodes of the system of beams B-1 and B-3

When healthy wood is replaced with a weakened one up to 47% in cross section, there is a movement along the Z axis up to 36 mm, which is the ultimate deflection. Figures 7 and 8 show the normal and shear stresses in beams B-1 and B-3.

In the course of the research, it was determined that the normal stresses in the middle of the span into the beams B-3 amounted to 12.89 MPa. This indicator is 2.6 times greater than in the linear formulation of the problem. Shear stresses in the
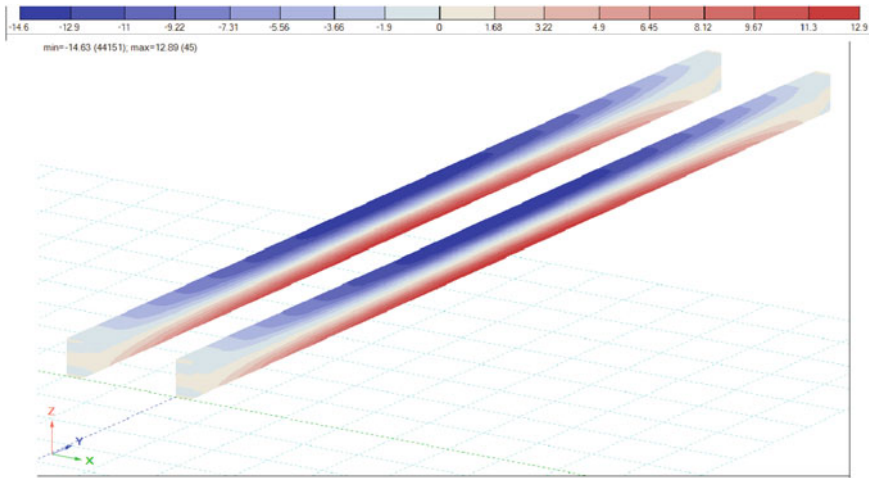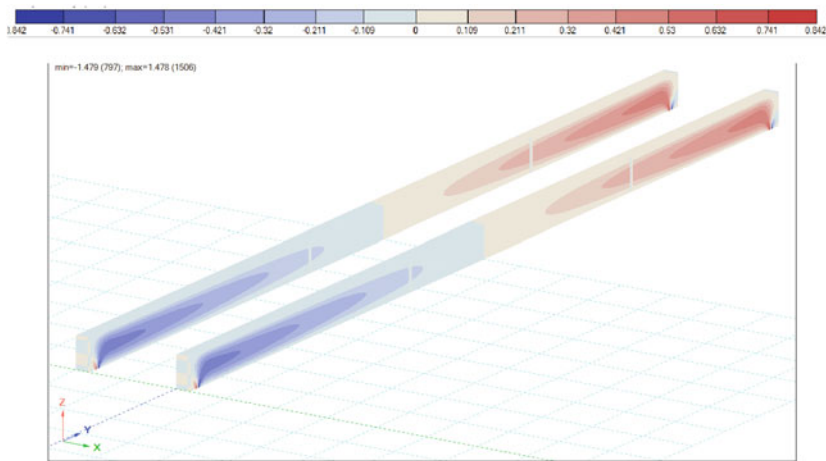
Fig. 7 Stress Ny in beams B-1 and B-3

Fig. 8 Shear stresses Tyz beams B-1 and B-3

non-linear formulation of the B-3 beam problem are 1.4 MPa. Such a difference in the values of linear and non-linear calculations is explained by the large margin of safety provided by the designers. Wood is an anisotropic material that has various knots, cross layers and other defects. It is known that it is precisely these defects that often lead to the destruction of a wooden structure [31–33]. A wood-composite structure excludes such a nature of destruction.

Numerical calculations by the finite element method in the Lira software package made it possible to determine the rational parameters for constructing a wood-composite beam with the replacement of healthy wood with weakened wood and to identify possible problem areas where maximum stresses occur.

6   Conclusions

In the process of analyzing the calculation results, a number of issues were identified for this type of beam design, the main of which boiled down to the emergence of local zones with increased compressive and tensile stresses, which increased with an increase in the percentage of replacement of healthy wood with wood weakened by fire.

1. For wooden beams in the elastic stage of design, the limiter is the calculation for the 2nd group of limit states (in terms of stiffness), for composite beams, the calculation for the 1st group of limit states (in terms of strength).
2. It has been established that the maximum percentage of replacement of healthy wood with wood weakened by fire should not exceed 47% of the height of the section for beams 9 m long.
3. It is determined that the normal stresses in the middle of the span in the B-3 beams are 2.6 times greater than in the linear formulation of the problem. The tangential stresses in the non-linear formulation of the problem are 4 times greater than in the linear calculation. The values obtained in the non-linear analysis of a wood-composite beam reflect the actual work of the structure.
4. The deformability of wood-glued beams is reduced by 1.8 … 2.1 times compared to traditional wooden beams.

The effectiveness of wood-composite structures, which partially consist of weakened wood, namely, the proposed structure can be attributed to them, in comparison with traditional solid wood structures, is beyond doubt. Based on the results obtained in the course of a numerical study, it can be argued that the considered method of constructing wooden beams is expedient and economical.

References

1. Gałka, M., Obremska, M., Feurdean, A.: Forest ecosystem development in European nemoreal-boreal forest (NE Poland) over the last 2200 years: Impact of human activity and climate change. Holocene **32**, 650–663 (2022). https://doi.org/10.1177/09596836221088249

2. Gonshakov, A., Gonshakov, N., Popova, M., Medvedev, E., Popova, O.: Lightweight construction formed on the basis of a typical reinforced concrete lattice beam, pp. 1450–1458 (2022). https://doi.org/10.1007/978-3-030-96383-5_162

3. Lukin, M., Popova, M., Reva, D., Abdikarimov, R.: Reinforced concrete shallow shell of negative double gaussian curvature built on the basis of a four-lobed hyperbolic paraboloid. Lect. Notes Civ. Eng. **182**, 563–576 (2022). https://doi.org/10.1007/978-3-030-85236-8_49

4. Lisyatnikov, M.S., Glebova, T.O., Ageev, S.P., Ivaniuk, A.M.: Strength of wood reinforced with a polymer composite for crumpling across the fibers. IOP Conf. Ser. Mater. Sci. Eng. **896**(1), 012062 (2020). https://doi.org/10.1088/1757-899X/896/1/012062

5. Dziurka, D., Derkowski, A., Dukarska, D., Kawalerczyk, J., Mirski, R.: The effect of periodic loading of glued laminated beams on their static bending strength. Materials **15**(11), 3928 (2022). https://doi.org/10.3390/ma15113928

6. Romanovich, A., Lisyatnikov, M., Vlasov, A., Aleksiievets, V.: Geodesic domes with installing floor using a cable stay system, pp. 1459–1466 (2022). https://doi.org/10.1007/978-3-030-96383-5_163.

7. Xu, G., Tian, H., Xi, X., Song, J., Lei, H., Du, G.: Preparation and characterization of urea–formaldehyde adhesives modified with glyoxalated tannin. Eur. J. Wood Wood Prod. (2022). https://doi.org/10.1007/s00107-022-01819-1

8. Lukin, M., Sergeev, M., Lisyatnikov, M.: Non split wooden beam reinforced with composite reinforcement (2021). https://doi.org/10.1007/978-3-030-72404-7_12

9. Estévez-Cimadevila, J., Martín-Gutiérrez, E., Suárez-Riestra, F., Otero-Chans, D., Vázquez-Rodríguez, J.A.: Timber-concrete composite structural flooring system. J. Build. Eng. **49**, 104078 (2022). https://doi.org/10.1016/j.jobe.2022.104078

10. Wang, Y.: Research on the revival application of wooden building with the properties of anti-seismic energy-saving and environment protection. Adv. Mater. Res. **255**, 1551–1557 (2011). https://doi.org/10.4028/www.scientific.net/AMR.255-260.1551

11. Morkovina, S.S., Panyavina, E.A., Platonov, A.D., Kolesnichenko, E.A.: Economic aspects of organizing high-technology resource saving production in the Forest Sector of Russia. Int. J. Econ. Bus. Adm. **7**, 395–402 (2019)

12. Chu, D., Mu, J., Kang, L., Lai, Z.: Three-dimensional optical deformation measurement of laminated veneer lumber and the finite element simulation analysis of the pallets∣单板层积材的三维光学检测及其托盘的有限元仿真分析. Beijing Linye Daxue Xuebao/J. Beijing For. Univ. **41**, 147–155 (2019). https://doi.org/10.13332/j.1000-1522.20190056

13. Lukina, A., Roshchina, S., Lisyatnikov, M., Zdralovic, N., Popova, O.: Technology for the restoration of wooden beams by surface repair and local modification (2022).https://doi.org/10.1007/978-3-030-96383-5_153

14. Descamps, T., Monhonval, M., Latteur, P.: An assessment methodology for timber beams in a restoration context, based on a dimensionless formulation of EC5 design criteria. Int. J. Archit. Herit. **12**, 726–733 (2018). https://doi.org/10.1080/15583058.2018.1442527

15. Wang, K., et al.: Shape-reconfigurable transparent wood based on solid-state plasticity of polythiourethane for smart building materials with tunable light guiding, energy saving, and fire alarm actuating functions. Compos. Part B Eng. **246**, 110260 (2022). https://doi.org/10.1016/j.compositesb.2022.110260

16. Tambi, A.A., et al.: A Study of Wood Glued Joints Formed by Urea Melamine Formaldehyde Binders. Polym. Sci. Ser. D **12**(1), 51–57 (2019). https://doi.org/10.1134/S1995421219010209

17. Roshchina, S.I., Lukin, M.V., Shokhin, P.B., Sergeev, M.S., Lisyatnikov, M.S.: Allowance for creep in the study of the reinforced wood-based constructions. Life Sci. J. **11**, 192–195 (2014)

18. Sedliačik, J., Šmidriaková, M.: Heat resistance of adhesive joints for wood constructions ∣ Tepelná odolnost' lepených spojov pre drevné konštrukcie. Acta Fac. Xylologiae. **54**, 79–94 (2012)

19. Kelleci, O., et al.: Wood flour-reinforced green composites: parameter optimization via multi-criteria decision-making methods. J. Polym. Environ. **30**, 3091–3106 (2022). https://doi.org/10.1007/s10924-022-02415-3

20. EU-ECE Forest Health Inventory (IDF) in Spain: European Level I Network monitoring of forest health damage sampling of results of 2006 survey | Inventario UE-ECE de Daños Forestales (IDF) en España. Red Europea de seguimiento de daños en los bosques. Nive. Ecologia, pp. 303–337 (2007)
21. Eriksson, L.: Risk perception and responses among private forest owners in Sweden. Small-scale For. **13**, 483–500 (2014). https://doi.org/10.1007/s11842-014-9266-6
22. Gribanov, A.S., Roshchina, S.I., Naichuk, A.Y., Melekhov, V.I.: Wooden beams with local wood modification. IOP Conf. Ser. Mater. Sci. Eng. **896**(1), 012067 (2020). https://doi.org/10.1088/1757-899X/896/1/012067
23. Koshcheev, A.A., Roshchina, S.I., Naichuk, A.Y., Vatin, N.I.: The effect of eccentricity on the strength characteristics of glued rods made of steel cable reinforcement in solid wood. IOP Conf. Ser. Mater. Sci. Eng. **896**(1), 012059 (2020). https://doi.org/10.1088/1757-899X/896/1/012059
24. Vanalli, L., Scoaris, M.R., Romera, G.F.S., Mascia, N.T.: Analysis of the mechanical behavior of composite beams. Civil-Comp Proc. **102** (2013)
25. Lisyatnikov, M., Glebova, T., Rusak, K., Ivaniuk, A.: Strength and deformability of reinforced wooden beams of variable stiffness. Lect. Notes Civ. Eng. **182**, 549–561 (2022). https://doi.org/10.1007/978-3-030-85236-8_48
26. Lukin, M., Martynov, V., Rimshin, V., Aleksiievets, I.: Reinforced concrete vertical structures under a gently sloping shell of double curvature under the influence of progressive collapse. Lect. Notes Civ. Eng. **182**, 577–587 (2022). https://doi.org/10.1007/978-3-030-85236-8_50
27. Sergeev, M., Rimshin, V., Lukin, M., Zdralovic, N.: Multi-span composite beam. IOP Conf. Ser. Mater. Sci. Eng. **896**(1), 012058 (2020). https://doi.org/10.1088/1757-899X/896/1/012058
28. Kang, C.-W., Wen, M.-Y., Park, H.-J., Kang, H.-Y., Kang, S.-G., Matsumura, J.: Changes in some mechanical and physical properties and anatomical structure of spruce and larch wood after fire-retardant treatment. BioResources **12**(1), 1358–1368 (2017). https://doi.org/10.15376/biores.12.1.1358-1368
29. Lukin, M., Prusov, E., Roshchina, S., Karelina, M., Vatin, N.: Multi-Span Composite Timber Beams with Rational Steel Reinforcements. Buildings **11**, 46 (2021). https://doi.org/10.3390/buildings11020046
30. Yang, X., Sun, C., Huo, F., Gong, Y., Sun, Y.: Shear property and uniform vertical load capacity of bamboo i-beams. Forests **13**(6), 826 (2022). https://doi.org/10.3390/f13060826
31. Karinkanta, P., Illikainen, M., Niinimäki, J.: The effect of anisotropicity of Norway spruce (Picea abies) during two-body abrasion. Wear **272**, 38–42 (2011). https://doi.org/10.1016/j.wear.2011.07.004
32. Zhivotov, D., Tilinin, Y.: Experimental studies of nodal joints of wooden elements in trusses and geodesic domes. Architect. Eng. **7**(2), 96–105 (2022). https://doi.org/10.23968/2500-0055-2022-7-2-96-105
33. Nemirovsky, Y.V., Boltaev, A.I.: Calculation and design of hybrid wooden beams. PNRPU Mech. Bull. **15**, 129–152 (2017). https://doi.org/10.15593/perm.mech/2017.3.08.

Determination of Local Stresses in Places Where the Stiffness of Reinforced Wooden Beams Changes

Mikhail Lisyatnikov (ID)**, Svetlana Roshchina** (ID)**, Vladislav Martynov** (ID)**, and Rustamkhan Abdikarimov** (ID)

Abstract The problem of local stresses arising in the wood of reinforced beams in the process of loading structures is considered. The calculation of local stresses arising in places of change in the stiffness of reinforced beams should be carried out according to three expressions, taking into account the main factors affecting the stress state of the point of the section under consideration: the placement of reinforcement in the cross section from the breakage of the reinforcement, the action of a uniformly distributed load and support reactions. An analysis of these stresses shows that their development is significantly affected by the intensity of the normal stresses of the reinforcement that occurs in the process of loading the beams. The obtained solution shows that the section height has the greatest influence on the strength and stiffness of reinforced beams. An increase in the height of the section leads to a decrease in the clip effect, i.e. reducing the influence of reinforced zones on each other. At the same time, the uneven distribution of shear stresses along the section height increases, which leads to premature destruction of structures of variable stiffness in the zone of tensile reinforcement breakage. A further direction of research is indicated, which consists in determining the influence of other factors on the strength and stiffness of reinforced beams: the distribution of reinforcement over the section width, the compliance of the steel-wood adhesive joint, the difference in the moduli of elasticity of wood in compression and tension, etc. Their influence can be established by a predictive method for calculating the strength and stiffness of reinforced beams, based on rational planning of the experiment.

Keywords Timber · Building · Beams · Reinforcement of wooden beams

M. Lisyatnikov (✉) · S. Roshchina · V. Martynov
Vladimir State University Named After Alexander and Nikolay Stoletovs, Vladimir, Russian Federation
e-mail: mlisyatnikov@gmail.com

R. Abdikarimov
Tashkent Institute of Finance, Tashkent, Uzbekistan

235

1 Introduction

The article [1] outlined a design technique for reinforced wooden beams of variable stiffness with group reinforcement. Such reinforcement is used to save materials of steel and epoxy compound [2–8].

At the previous stage of research, a theoretical determination was made of the optimal location for the breakage of reinforcement in the span of beams of variable stiffness [9–12]. The breakage point of the reinforcement takes into account the introduction of the reinforcement beyond the theoretical breakage point by the anchoring length from 0.0018 to 0.025 of the design span of the beams. The anchoring length was obtained under the condition that during the operation of the beams in the zone of action of the maximum bending moment, the calculated strength characteristics of the materials: steel and wood are fully used [13]. In this case, several factors influence the anchoring zone and the place of reinforcement breakage: reinforcement coefficient, reinforcement diameter and span of beams.

Also, the influence of the reinforcement coefficient on the place of reinforcement breakage in the span of beams was determined. The dependence of anchoring on the diameter of the reinforcement and the coefficient of reinforcement of complex structures is revealed. The influence of the span of beams on the relative length of the embedment of the rods has been established. The influence of a change in the rigidity of a reinforced structure on the deformability is considered.

It was found that in beams with broken reinforcement in the span, the redistribution of stresses from wood to steel leads first to an increase in local stresses in wood, and then to a decrease in them due to a change in the modulus of elasticity of wood over time. Hence, it became necessary to determine local stresses in the zones of changes in the stiffness of beams, often leading to premature failure of structures.

The magnitude of such local stresses can be determined by applying the plane problem of elasticity theory [14–17].

2 Methods

Consider the problem of local stresses arising in the wood of reinforced beams in the process of loading structures.

Let us consider the general case of determining local stresses on a beam reinforced in a sloped zone and loaded with a uniformly distributed load. The connection of reinforcement with wood is assumed to be continuous along the entire length.

The problem is solved within the framework of the following assumptions:

1. Wood is assumed to be equal in tension and compression along the fibers [18].
2. The anisotropy of wood is not taken into account, since its influence is insignificant on the distribution of stresses when the direction of the largest modulus of elasticity coincides with the axis of the beam.

3. Materials of a complex design work within the limits of elastic deformations and obey the generalized Hooke's law [19–21].
4. Deformations of reinforcement and wood are equal and joint.
5. The main material of the beams - wood is considered to be an idealized solid, i.e. a continuous, solid deformable body endowed with a property that takes into account only the basic qualities of a real body.

It is known that when loading reinforced wooden beams with external loads, normal stresses arise in steel rods that are approximately 20 times greater in absolute value than in wood. The area of the reinforcement compared to the area of the main material of the beam - wood is in the range of 1.5–3.5%, and the ratio of the diameter of the reinforcement to the height of the beam is less than 5%. Therefore, we will consider a reinforcing bar as a fiber, but with a relatively greater rigidity, since the modulus of elasticity of steel reinforcement is 20 times higher. Therefore, reinforcing bars are the main stress concentrators in wood, because prevent the beam from bending. The reaction from the action of normal stresses in the opposite direction leads to the destruction of the main material of wood, and in places where the stiffness of the beams changes, to the concentration of stresses. The intensity of the reaction, as shown by the analysis of experimental data, obeys the law of distribution of transverse forces [22].

The absolute value of the reaction from the reinforcement in any section of the beam is proposed to be determined by the formula:

$$q_n = \frac{q}{200}(l_a - 2y) \tag{1}$$

where q – uniformly distributed load acting on the main beam;
y – current coordinate;
l_a– reinforced section length;
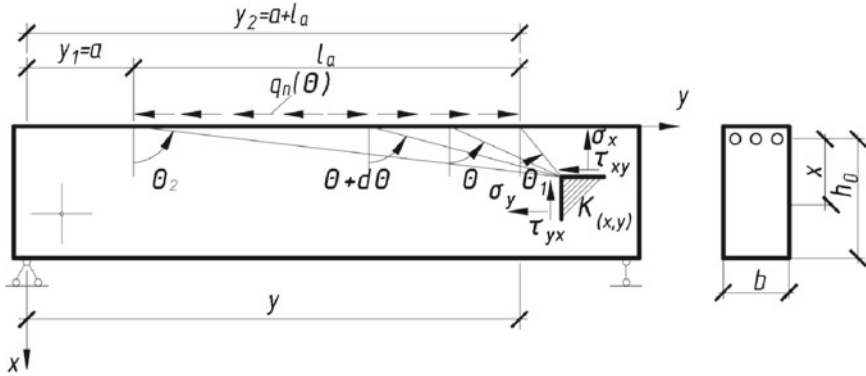200 – approximation factor.

Since the ratio of the sum of the diameters of the rods of the compressed and tensioned zones to the width of the beam is a commensurate value, the reactions arising from them in wood can be considered a band uniformly distributed load applied tangentially to the surface of the beam (Fig. 1).

The solution of problems in this formulation reduces to the well-known solution [23].

Stresses σ_x, σ_y and τ_{xy} will be determined by the following dependencies:

$$\sigma_x = \int_{\theta_1}^{\theta_2} -\frac{2q_n(\theta)}{\pi} \sin\theta \cos\theta d\theta \tag{2}$$

$$\sigma_y = \int_{\theta_1}^{\theta_2} -\frac{2}{\pi}q_n(\theta)\frac{\sin^3\theta}{\cos\theta}d\theta \tag{3}$$

Fig. 1 Design diagram of a beam adopted to determine the concentration of stresses arising in wood from the influence of reinforcement

$$\tau_{xy} = \int_{\theta_1}^{\theta_2} -\frac{2}{\pi} q_n(\theta) \sin^2 \theta d\theta \tag{4}$$

Since the absolute value and direction of the strip load (1) depends on the current coordinate – y, then to further solve the problem, it is necessary to write down the intensity of the strip load depending on the current angle θ [24–26]. The positive value of which is redistributed when counted from the vertical axis counterclockwise and negative when counted in the opposite direction.

The intensity of the strip load depending on the angle θ should be determined by the formula::

$$q_n = \frac{q}{200}(l_a - 2xtg\theta) \tag{5}$$

Substituting the found expression for the band load (5) into formulas (2)–(4), we obtain:

$$\sigma_x = \frac{q}{100\pi} \int_{\theta_1}^{\theta_2} (2xtg\theta - l_a) \sin \theta \cos \theta d\theta$$

$$\sigma_y = \frac{q}{100\pi} \int_{\theta_1}^{\theta_2} (2xtg\theta - l_a) \frac{\sin^3 \theta}{\cos \theta} d\theta$$

$$\tau_{xy} = \frac{q}{100\pi} \int_{\theta_1}^{\theta_2} (2xtg\theta - l_a) \sin^2 \theta d\theta$$

After integration:

$$\sigma_x = \frac{q}{200\pi}[2x(\theta_2 - \theta_1 - \sin\theta_2 cos\theta_2 + \sin\theta_1 cos\theta_1) - \\ -l_a(\sin^2\theta_2 - \sin^2\theta_1)] \tag{6}$$

$$\sigma_y = \frac{q}{200\pi}\{[2x(\sin\theta_2 cos\theta_2 - \sin\theta_1 cos\theta_1) + 2(tg\theta_2 - tg\theta_1) - \\ -3(\theta_2 - \theta_1)] + l_a\left(\sin^2\theta_2 - \sin^2\theta_1 + 2\ln\frac{cos\theta_2}{cos\theta_1}\right)]\} \tag{7}$$

$$\tau_{xy} = \frac{q}{200\pi}[2x\left(\sin^2\theta_2 - \sin^2\theta_1 - 2\ln\frac{cos\theta_2}{cos\theta_1}\right) - \\ -l_a(\theta_2 - \theta_1 - \sin\theta_2 cos\theta_2 + \sin\theta_1 cos\theta_1)] \tag{8}$$

Let us express the stresses in terms of the coordinate of the point k. According to Fig. 1 we have:

$$tg\theta_1 = \frac{y - y_2}{x}; \quad tg\theta_2 = \frac{y - y_1}{x};$$

$$\sin\theta_1 = \frac{y - y_2}{\sqrt{x^2 + (y - y_2)^2}}; \quad \sin\theta_2 = \frac{y - y_1}{\sqrt{x^2 + (y - y_1)^2}};$$

$$\cos\theta_1 = \frac{x}{\sqrt{x^2 + (y - y_2)^2}}; \quad \cos\theta_2 = \frac{x}{\sqrt{x^2 + (y - y_1)^2}};$$

$$\theta_1 = arctg\frac{y - y_2}{x}; \quad \theta_2 = arctg\frac{y - y_1}{x};$$

We substitute the found expressions into formulas (5)–(7), we obtain:

$$\sigma_x = \frac{q}{200\pi}\{2x[\frac{x(y - y_2)}{x^2 + (y - y_2)^2} - \frac{x(y - y_1)}{x^2 + (y - y_1)^2} + \\ +arctg\frac{x(y_2 - y_1)}{x^2(y - y_1)(y - y_2)}] - l_a(\frac{(y - y_1)^2}{x^2 + (y - y_1)^2} - \\ -\frac{(y - y_2)^2}{x^2 + (y - y_2)^2})]\} \tag{9}$$

$$\sigma_y = \frac{q}{200\pi}\{2x[\frac{x(y - y_1)}{x^2 + (y - y_1)^2} - \frac{x(y - y_2)}{x^2 + (y - y_2)^2} + \frac{2(y_2 - y_1)}{x} - \\ -3arctg\frac{x(y_2 - y_1)}{x^2(y - y_1)(y - y_2)}] + l_a[\frac{(y - y_1)^2}{x^2 + (y - y_1)^2} - \\ -\frac{(y - y_2)^2}{x^2 + (y - y_2)^2}) + \ln\frac{x^2 + (y - y_2)^2}{x^2 + (y - y_1)^2}]\} \tag{10}$$

$$\tau_{xy} = \frac{q}{200\pi} \{2x[\frac{(y-y_2)^2}{x^2+(y-y_2)^2} - \frac{(y-y_1)^2}{x^2+(y-y_1)^2}) -$$
$$-\ln\frac{x^2+(y-y_2)^2}{x^2+(y-y_1)^2}] - l_a[\frac{x(y-y_2)}{x^2+(y-y_2)^2} -$$
$$-\frac{x(y-y_1)}{x^2+(y-y_1)^2} + arctg\frac{x(y_2-y_1)}{x^2(y-y_1)(y-y_2)}]\} \tag{11}$$

3 Results and Discussion

The obtained dependences (9)-(11) allow us to evaluate the effect of reinforcement on the stress state of wood and to determine the magnitude of local stresses arising in the zones of change in stiffness from the action of an external uniformly distributed load.

In turn, this makes it possible to determine local stresses in the zone of change in stiffness of a symmetrically reinforced beam loaded with a uniformly distributed load.

According to Fig. 2, the effect of reinforcement on the stress state of the point of the section under study is generally equal to:

$$\sigma_{xa} = \sigma_{xac} + \sigma_{xas} \tag{12}$$

$$\sigma_{ya} = \sigma_{yac} + \sigma_{yas} \tag{13}$$

$$\tau_{xya} = \tau_{xyac} + \tau_{xyas} \tag{14}$$

Let us substitute into the obtained Eqs. (12)–(14) expressions (9)–(11), describing the point stresses depending on the influence of the reinforcement of the compressed zone and with the opposite sign from the tension zone, then:

$$\sigma_{xa} = \frac{q}{200\pi}\{\{2x[\frac{x(y-a_c-l_{ac})}{x^2+(y-a_c-l_{ac})^2} - \frac{x(y-a_c)}{x^2+(y-a_c)^2} +$$
$$+arctg\frac{xl_{ac}}{x^2+(y-a_c)(y-a_c-l_{ac})}] - l_{ac}[(\frac{(y-a_c)^2}{x^2+(y-a_c)^2} -$$
$$-\frac{(y-a_c-l_{ac})^2}{x^2+(y-a_c-l_{ac})^2}]\} - \{2(h-x)[\frac{(h-x)(y-a_s-l_{as})}{(h-x)^2+(y-a_s-l_{as})^2} -$$
$$-\frac{(h-x)(y-a_s)}{(h-x)^2+(y-a_s)^2} + arctg\frac{(h-x)l_{as}}{(h-x)^2+(y-a_s)(y-a_s-l_{as})}] -$$
$$-l_{as}[(\frac{(y-a_s)^2}{(h-x)^2+(y-a_s)^2} - \frac{(y-a_s-l_{as})^2}{(h-x)^2+(y-a_s-l_{as})^2}]\}\} \tag{15}$$
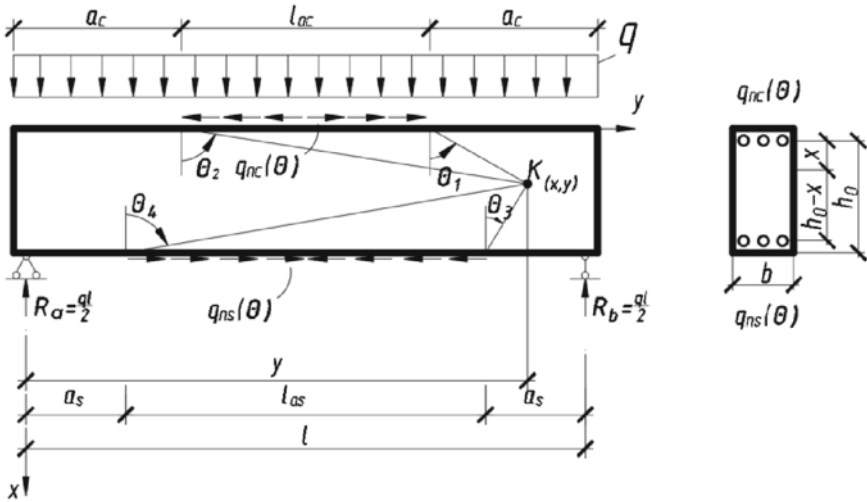
Fig. 2 Design scheme of the beam, taking into account all external factors affecting the development of local stresses

$$\sigma_{ya} = \frac{q}{200\pi}\{\{2x[\frac{x(y-a_c)}{x^2+(y-a_c)^2} - \frac{x(y-a_c-l_{ac})}{x^2+(y-a_c-l_{ac})^2} + \frac{2l_{ac}}{x}$$

$$+3arctg\frac{xl_{ac}}{x^2+(y-a_c)(y-a_c-l_{ac})}] + l_{ac}[(\frac{(y-a_c)^2}{x^2+(y-a_c)^2} -$$

$$-\frac{(y-a_c-l_{ac})^2}{x^2+(y-a_c-l_{ac})^2} + \ln\frac{x^2+(y-a_c-l_{ac})^2}{x^2+(y-a_c)^2}]\} -$$

$$\{2(h-x)[\frac{(h-x)(y-a_s)}{(h-x)^2+(y-a_s)^2} - \frac{(h-x)(y-a_s-l_{as})}{(h-x)^2+(y-a_s-l_{as})^2} + \qquad (16)$$

$$+\frac{2-l_{as}}{(h-x)} + 3arctg\frac{(h-x)l_{as}}{(h-x)^2+(y-a_s)(y-a_s-l_{as})}] -$$

$$-l_{as}[\frac{(y-a_s)^2}{(h-x)^2+(y-a_s)^2} - \frac{(y-a_s-l_{as})^2}{x^2+(y-a_s-l_{as})^2} +$$

$$+\ln\frac{(h-x)^2+(y-a_s-l_{as})^2}{(h-x)^2+(y-a_s)^2}]\}\}$$

$$\tau_{xya} = \frac{q}{200\pi}\{\{2x[\frac{(y-a_c-l_{ac})^2}{x^2+(y-a_c-l_{ac})^2} - \frac{(y-a_c)^2}{x^2+(y-a_c)^2} -$$

$$-\ln\frac{x^2+(y-a_c-l_{ac})^2}{x^2+(y-a_c)^2}] - l_{ac}[\frac{x(y-a_c-l_{ac})^2}{x^2+(y-a_c-l_{ac})^2} -$$

$$-\frac{x(y-a_c)}{x^2+(y-a_c)^2} + arctg\frac{xl_{ac}}{x^2+(y-a_c)(y-a_c-l_{ac})}]\}-$$

$$-\{2(h-x)[\frac{(y-a_s-l_{as})^2}{(h-x)^2+(y-a_s-l_{as})^2} - \frac{(y-a_s)^2}{(h-x)^2+(y-a_s)^2} -$$

$$-\ln\frac{(h-x)^2+(y-a_s-l_{as})^2}{(h-x)^2+(y-a_s)^2}] - l_{as}[\frac{(h-x)(y-a_s-l_{as})^2}{(h-x)^2+(y-a_s-l_{as})^2} -$$

$$-\frac{(h-x)(y-a_s)^2}{x^2+(y-a_s)^2} + arctg\frac{(h-x)l_{as}}{(h-x)^2+(y-a_s)(y-a_s-l_{as})}]\}\}$$

(17)

Let us assume that in beams of variable stiffness, the length of the reinforcement [27] of the compressed zone is equal to the stretched one, i.e. $l_{ac} = l_{as}$, and therefore $a_c = a_s$. Then the stress state, depending on the influence of the reinforcement, will be determined by the following formulas:

$$\sigma_{xa} = \frac{q}{200\pi}\{\frac{(y-a-l_a)[2x^2+l_a(y-a-l_a)]}{x^2+(y-a-l_a)^2} -$$

$$-\frac{(y-a-l_a)[2(h-x)^2+l_a(y-a-l_a)]}{(h-x)^2+(y-a-l_a)^2} - \frac{(y-a)[2x^2-l_a(y-a)]}{x^2+(y-a)^2} +$$

$$+\frac{(y-a)[2(h-x)^2-l_a(y-a)]}{(h-x)^2+(y-a)^2} + 2[x \cdot arctg\frac{xl_a}{x^2+(y-a)(y-a-l_a)} -$$

$$-(h-x)arctg\frac{(h-x)l_a}{(h-x)^2+(y-a)(y-a-l_a)}]\}$$

(18)

$$\sigma_{ya} = \frac{q}{200\pi}\{\frac{(y-a)[2x^2+l_a(y-a)]}{x^2+(y-a)^2} - \frac{(y-a)[2(h-x)^2+l_a(y-a)]}{(h-x)^2+(y-a)^2} -$$

$$-\frac{(y-a-l_a)[2x^2-l_a(y-a-l_a)]}{x^2+(y-a-l_a)^2} + \frac{(y-a-l_a)[2(h-x)^2-l_a(y-a-l_a)]}{(h-x)^2+(y-a-l_a)^2} -$$

$$-6[x \cdot arctg\frac{xl_a}{x^2+(y-a)(y-a-l_a)} - (h-x)\times$$

$$\times arctg\frac{(h-x)l_a}{(h-x)^2+(y-a)(y-a-l_a)} +$$

$$+l_a\ln\frac{[x^2+(y-a-l_a)^2][(h-x)(y-a)(2y-2a-3l_a)]}{[x^2+(y-a)^2][(h-x)^2(y-a-l_a)^2]}]\}$$

(19)

$$\tau_{xya} = \frac{q}{200\pi}\{\frac{x(y - a - l_a)(2y - 2a - 3l_a)]}{x^2 + (y - a - l_a)^2} -$$

$$-\frac{(x - h)(y - a - l_a)(2y - 2a - 3l_a)}{(h - x)^2 + (y - a - l_a)^2} - \frac{x(y - a)(2y - 2a - 3l_a)}{x^2 + (y - a)^2} +$$

$$+\frac{(x - h)(y - a)(2y - 2a - 3l_a)}{(h - x)^2 + (y - a)^2} - 2[x \ln \frac{x^2 + (y - a)(y - a - l_a)^2}{x^2 + (y - a)^2} -$$

$$-(h - x) \ln \frac{(h - x)l_a}{(h - x)^2 + (y - a)(y - a - l_a)}]\}$$

(20)

In addition to the reaction from the action of the normal forces of the reinforcement, the development of local stresses in the zone of change in the stiffness of the beams is also affected by external forces, such as a uniformly distributed load and support reactions (see Fig. 2).

The action of an external uniformly distributed load on the stress state of the section under consideration can be determined by three formulas describing the stress state at the point:

$$\sigma_{xq} = -\frac{q}{\pi}\left[arctg\frac{xl}{x^2 + y(y - l)} + \frac{xy}{x^2 + y^2} - \frac{x(y - l)}{x^2 + (y - l)^2}\right]$$

(21)

$$\sigma_{yq} = -\frac{q}{\pi}\left[arctg\frac{xl}{x^2 + y(y - l)} - \frac{xy}{x^2 + y^2} + \frac{x(y - l)}{x^2 + (y - l)^2}\right]$$

(22)

$$\tau_{xyq} = -\frac{q}{\pi}\left[\frac{y^2}{x^2 + y^2} - \frac{(y - l)^2}{x^2 + (y - l)^2}\right]$$

(23)

The influence of support reactions on the stress state of the considered section can also be determined by three equations that determine the stress state at the point:

$$\sigma_{xR} = -\frac{ql}{b\pi}\left\{\frac{(h - x)^3}{[(h - x)^2 + y^2]} + \frac{(h - x)^3}{[(h - x)^2 + (l - y)^2]^2}\right\}$$

(24)

$$\sigma_{yR} = -\frac{ql}{b\pi}\left\{\frac{(h - x)y^2}{[(h - x)^2 + y^2]} + \frac{(h - x)(l - y)^2}{[(h - x)^2 + (l - y)^2]^2}\right\}$$

(25)

$$\tau_{xyR} = -\frac{ql}{b\pi}\left\{\frac{(h - x)y^2}{[(h - x)^2 + y^2]^2} + \frac{(h - x)^2(l - y)}{[(h - x)^2 + (l - y)^2]^2}\right\}$$

(26)

The calculation of local stresses arising in places of change in the stiffness of reinforced beams should be carried out according to three expressions, taking into account the main factors affecting the stress state of the point of the considered section, written in general form:

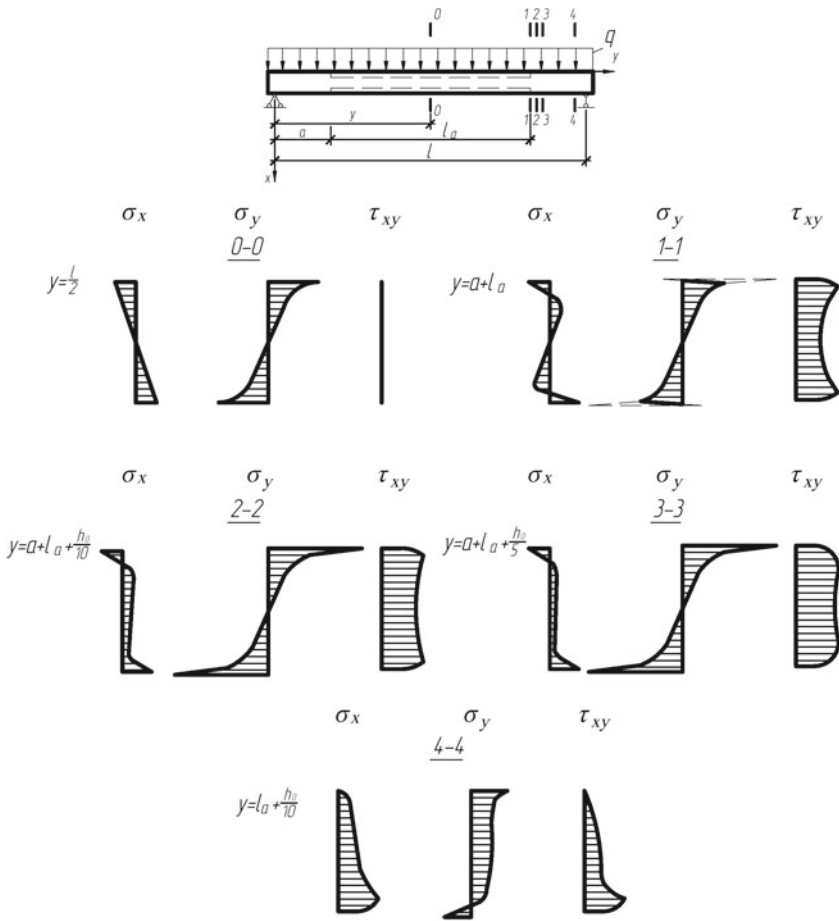$$\sigma_x = \sigma_{xa} + \sigma_{xq} + \sigma_{xR}$$

(27)

Fig. 3 Distribution of local stresses along the section height in reinforced beams of variable stiffness

$$\sigma_y = \sigma_{ya} + \sigma_{yq} + \sigma_{yR} \tag{28}$$

$$\tau_{xy} = \tau_{xya} + \tau_{xyq} + \tau_{xyR} \tag{29}$$

where $\sigma_x, \sigma_y, \tau_{xy}$ – the stresses created in the reinforcement are determined depending on the placement of the reinforcement in the cross section from the breakage of the reinforcement. So for symmetrically reinforced beams of variable stiffness with reinforcement breakage only in the compressed zone, it should be determined by formulas (15)–(17) for beams with reinforcement breakage in one section, i.e. in compressed and stretched zones are determined by formulas (18)–(20);

$\sigma_{xq}, \sigma_{yq}, \tau_{xyq}$ – stresses from the action of a uniformly distributed load are determined by formulas (21)–(23);

$\sigma_{xR}, \sigma_{yR}, \tau_{xyR}$ – stresses arising from support reactions are determined by formulas (24)–(26).

Distribution of local stresses σ_x, σ_y, τ_{xy} along the height of the section of symmetrically reinforced beams is determined by formulas (27)–(29) and is shown in Fig. 3.

4   Conclusions

An analysis of these stresses shows that their development is significantly affected by the intensity of the normal stresses of the reinforcement that occurs in the process of loading the beams. Thus, an increase in normal stresses in reinforcement leads to an increase in local stresses in wood, especially in places where stiffness changes. In turn, the development of normal stresses in the reinforcement depends, in addition to the external load, on the geometric and structural characteristics of the beams, i.e. relative height, reinforcement ratio, reinforcement location both along the span length and section width.

The obtained solution shows that the section height has the greatest influence on the strength and stiffness of reinforced beams. An increase in the height of the section leads to a decrease in the clip effect, i.e. reducing the influence of reinforced zones on each other. At the same time, the uneven distribution of shear stresses along the height of the section increases, which leads to premature destruction of structures of variable stiffness, in the zone of breakage of tensile reinforcement.

The influence of other factors: the distribution of reinforcement over the section width, the ductility of the adhesive joint steel-wood, the difference in the moduli of elasticity of wood in compression and tension, etc., can be taken into account by a predictive method for calculating the strength and stiffness of reinforced beams, based on rational planning of the experiment, which is the next research priority.

References

1. Lisyatnikov, M., Glebova, T., Rusak, K., Ivaniuk, A.: Strength and deformability of reinforced wooden beams of variable stiffness. Lect. Notes Civ. Eng. **182**, 549–561 (2022). https://doi.org/10.1007/978-3-030-85236-8_48
2. Turkovskij, S.B., Pogorel'tsev, A.A.: Wooden structures with rigid joints in structures with corrosive medium. Promyshlennoe i Grazhdanskoe Stroit. 10–13 (2001)

3. Buka-Vaivade, K., Serdjuks, D., Goremikins, V., Pakrastins, L., Vatin, N.I.: Suspension structure with cross-laminated timber deck panels. Mag. Civ. Eng. **83**, 126–135 (2018). https://doi.org/10.18720/MCE.83.12

4. Lukin, M., Prusov, E., Roshchina, S., Karelina, M., Vatin, N.: Multi-span composite timber beams with rational steel reinforcements. Buildings (2021). https://doi.org/10.3390/buildings11020046

5. Göldi, M., Sell, J., Strässler, H.: Scherfestigkeit der Klebverbindung von vorimprägniertem Holz—Beitrag zur Entwicklung wetterbeständigen Brettschichtholzes. Holz als Roh- und Werkstoff **37**(7), 241–250 (1979). https://doi.org/10.1007/BF02607422

6. Roshchina, S., Lukin, M., Lisyatnikov, M.: Compressed-bent reinforced wooden elements with long-term load. In: Lecture Notes in Civil Engineering (2020). https://doi.org/10.1007/978-3-030-42351-3_7.

7. Gravit, M.V., Serdjuks, D., Bardin, A.V., Prusakov, V., Buka-Vaivade, K.: Fire design methods for structures with timber framework. Mag. Civ. Eng. **85**, 92–106 (2019). https://doi.org/10.18720/MCE.85.8

8. Sergeev, M., Lukina, A., Zdralovic, N., Reva, D.: Stress-strain state of a wood-glued three-span beam with layer-by-layer modification. Lect. Notes Civ. Eng. **182**, 485–491 (2022). https://doi.org/10.1007/978-3-030-85236-8_43

9. Gorpinchenko, V.M., Pogorel'tsev, A.A., Ecknadosyan, I.L.: Large-scale tests provided for a block, consisting of two wooden lens-type roof trusses of the sports complex "Strogino". Promyshlennoe i Grazhdanskoe Stroit. **38** (2005)

10. Shishov, I., Lukin, M.V., Sergeev, M.S.: Roofing of an industrial building with variable height rafters and wooden decking. Lect. Notes Civ. Eng. **182**, 463–473 (2022). https://doi.org/10.1007/978-3-030-85236-8_41

11. Haghani, R., Al-Emrani, M.: A new design model for adhesive joints used to bond FRP laminates to steel beams - Part A: background and theory. Constr. Build. Mater. **34**, 486–493 (2012). https://doi.org/10.1016/j.conbuildmat.2012.02.051

12. Repin, V., Grinyov, V.: The experience in automating scientific research to identify dangerous zones in the near-support sections of wooden beams, pp. 1230–1238 (2022). https://doi.org/10.1007/978-3-030-96383-5_137

13. Ando, D., Umemura, K.: Bond structures between wood components and citric acid in wood-based molding. Polymers (Basel). **13**, 1–9 (2021). https://doi.org/10.3390/polym13010058

14. Parida, G., Johnsson, H., Fragiacomo, M.: Provisions for ductile behavior of timber-to-steel connections with multiple glued-in rods. J. Struct. Eng. (U.S.) **139**, 1468–1477 (2013). https://doi.org/10.1061/(ASCE)ST.1943-541X.0000735

15. Sergeev, M., Lukina, A., Shunqi, M., Glebova, T., Kryukov, A.: Work of wood-composite beams in panel floors of prefabricated buildings. Lect. Notes Civ. Eng. **182**, 493–499 (2022). https://doi.org/10.1007/978-3-030-85236-8_44

16. Turkovskij, S.B., Pogorel'tsev, A.A., Eknados'yan, I.L.: Selection of design scheme of lens-shaped trusses from adhesive wood. Stroit. Mater. 18–20 (2003)

17. Roschina, S., Gribanov, A., Lukin, M., Lisyatnikov, M., Strekalkin, A.: Calculation of wooden beams reinforced with polymeric composites with modification of the wood compression area. MATEC Web Conf. **251**, 04029 (2018). https://doi.org/10.1051/matecconf/201825104029

18. De Luca, V., Marano, C.: Prestressed glulam timbers reinforced with steel bars. Constr. Build. Mater. **30**, 206–217 (2012). https://doi.org/10.1016/j.conbuildmat.2011.11.016

19. Koshcheev, A.A., Roshchina, S.I., Lukin, M.V., Lisyatnikov, M.S.: Wooden beams with reinforcement along a curvilinear trajectory. Mag. Civ. Eng. **81**, 193–201 (2018). https://doi.org/10.18720/MCE.81.19

20. Babiak, M., Gaff, M., Sikora, A., Hysek, Š: Modulus of elasticity in three- and four-point bending of wood. Compos. Struct. **204**, 454–465 (2018). https://doi.org/10.1016/j.compstruct.2018.07.113

21. Gribanov, A.S., Strekalkin, A.A., Kudryatseva, A.A., Zdralovic, N.: CFRP composites for strengthening wooden structures. IOP Conf. Ser. Mater. Sci. Eng. **896**(1), 012114 (2020). https://doi.org/10.1088/1757-899X/896/1/012114

22. Steiger, R., Gehri, E., Widmann, R.: Pull-out strength of axially loaded steel rods bonded in glulam parallel to the grain. Mater. Struct. Constr. **40**, 69–78 (2007). https://doi.org/10.1617/s11527-006-9111-2
23. Riberholt, H.: Glued Bolts in Glulam (1986)
24. Popova, M., Sergeev, M., Lukina, A., Shunqi, Mei: Strength and deformability of lightweight metal trusses with elements from cut I-beams. IOP Conf. Ser. Mater. Sci. Eng. **896**(1), 012061 (2020). https://doi.org/10.1088/1757-899X/896/1/012061
25. Preobrazhenskaya, I.P., Pogorel'tsev, A.A., Turkovskij, S.B.: Development of design and construction of potassium chloride storehouse with framework from prefabricated wood frames with size of 63 m. Stroit. Mater. 14–16 (2003)
26. Ling, Z., Liu, W., Yang, H., Chen, X.: Modelling of glued laminated timber joints with glued-in rod considering bond-slip location function. Eng. Struct. **176**, 90–102 (2018). https://doi.org/10.1016/j.engstruct.2018.08.098
27. Tlustochowicz, G., Serrano, E., Steiger, R.: State-of-the-art review on timber connections with glued-in steel rods. Mater. Struct. Constr. **44**, 997–1020 (2011). https://doi.org/10.1617/s11527-010-9682-9

Compressive Strength Along and Across Wood Fibers Modified by a Polymer Composition with a Nanostructured Filler

Mikhail Lukin , **Marina Popova** , **and Tatyana Glebova**

Abstract Today, the main materials for the construction of buildings and structures are concrete, brick, wood, and metal. Improving their strength and operational characteristics is a priority task of modern scientific research. The use of thermochemical modification of wood makes it possible to improve its physical and mechanical characteristics. The paper presents a method of thermochemical modification of wood with polymer compositions based on dimethacrylic polyester and based on dimethacrylic polyester with the introduction of carboxylated CNTs. The method of testing samples for compression along and across fibers is shown, as well as the dependences of "load and strain" are shown, the strength values of samples and so on are found, and the results are statistically processed.

An increase in strength has been established an increase in the compressive strength of the modified scaffold along the fibers - 43%, across the fibers - 58% compared to the reference one was found.

Keywords Wood · Polymer · Nanostructured fillers · Strength

1 Introduction

Wood is one of the most important materials used in construction and other areas of the national economy [1, 2]. Along with its advantages - high strength, hardness, low thermal conductivity, chemical resistance, wood also has significant disadvantages - anisotropy, high porosity and hygroscopicity, and a tendency to bio-damage, which significantly reduces the service life of wooden structures and products [3–10].

To reduce the impact of wood присcavenging during itsи use, the modification process is used [11–14]. Modification is understood as the process of directed changes

M. Lukin · M. Popova (✉) · T. Glebova
Vladimir State University named after Alexander and Nikolay Stoletovs, Vladimir,
Russian Federation
e-mail: popovamv@bk.ru

in the physicomechanical, thermophysical, tribotechnical, and biochemical properties of wood in relation to the operating conditions of wood products [15–17]. Modified wood has increased strength, durability, biostability, lower moisture and water resistance, as well as higher resistance to aggressive environments and other improved properties compared to natural wood [18–21].

The optimal method of wood modification is its thermo-chemical modification - under the influence of temperature using polymer materials [22–24]. ΠPolymers, including those that do not have protective properties, when introduced into wood, increaseт its chemical and biological resistance, strength, hardness, and durability. Polymer compositions can act both on the surface and completely or partially penetrate the wood structure, they help to increase the resistance of modified wood to water, ultraviolet radiation and biological pests.

Polymers used for wood modification should have a number of properties - low viscosity, low evaporation, and polarity for better penetration into the capillary structure of wood and physical and chemical interaction with wood components. After curing, the modifier must have high resistance to water, acids, and alkalis, be strong under static and dynamic loads, and be environmentally friendly. Polyester resins and compositions based on them have all these properties.

A number of studies have been conducted on the introduction of nanostructured fillers into the polymer matrix and the use of the resulting compositions for wood modification [25–27]. The introduction of nanomaterials into wood improves its properties, due to their unique characteristics. [28–31]. Due to their size, nanostructured fillers penetrate deeply into the wood, helping to improve its properties.

2   Methods

In the framework of the presented study, an enlarged technique for modifying wood with a polymer composition and a comparative analysis of the results of testing standard samples for compression along and across fibers are presented.

For each of the corresponding series of tests, the research methodology proposed in the current norms of the Russian Federation was used.

For compression tests three series of five samples in each were formed for testing on the raw material. Series 1 – samples from "reference" wood (samples #1–5), series 2-samples from wood modified with dimethacrylic polyester (samples #6–10), series 3 – wood modified with dimethacrylic polyester with carboxylated carbon nanotubes (samples # 11–15).

Preparation for testing includes the following tasks:

1. Production set of samples of "reference" wood is made. For compression tests along and across fibers, samples are made in the form of a rectangular prism with a base of 20×20 mm and a length along the fibers of 30 mm.
2. Production set of samples of modified wood was made (fritters No. 6–15)

A low-viscosity polymer composition based on hot-cured polyester resins is used as the matrix. Samples No. 6–10 are modified with a polymer composition based on dimethacrylic polyester and dry hardener (0.25 mass parts). Samples No. 11–15 are modified with the following composition: liquid resin based on a new dimethacrylic polyester, dry hardener (0.25 parts by weight), surfactant (OP – 10) in the amount of 0.5 parts by weight), carboxylated carbon nanotubes (CNTsof the Taunit-M series) (0.5 parts by weight). The structural elements are evenly dispersed over the volume of the composition for 15 min by an ultrasonic dispersant with an ultrasonic wave frequency of 30 kHz.

Samples of reference wood in a bathой with a polymer composition are placed in a mobile unit for vacuum infusion. The sample impregnation time is 30 min, and the vacuum pressure is 90 kPa.

After impregnation, the samples are transferred to a drying laboratory шshelf, where they are cured at t = 1–00 °C for 60 min.

3. Before testing, the images are conditioned at a temperature of (20 ± 2) °C and relative humidity of (65 ± 5)% for 24 h.

The samples were tested on an electromechanical bursting machine REM-100-A-1. To perform the test, the fritter is placed in a compression testing device. The sample is loaded evenly with a constant loading speed or a constant speed of movement of the loading head of the machine 4 mm/min.
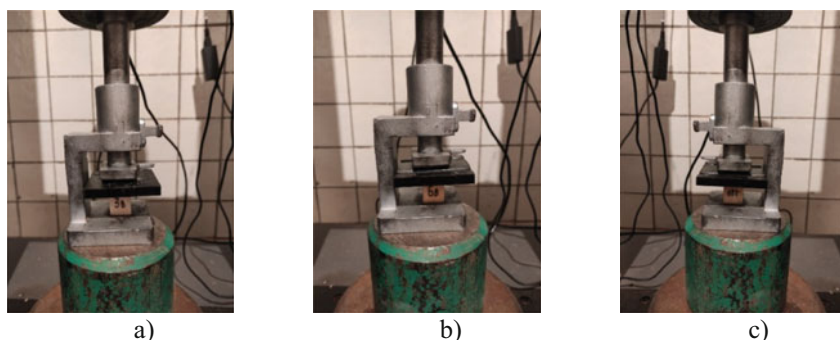
A general view of the samples during the crumple test along the fibers is shown in Fig. 1. A general view of the samples during the crumple test along the fibers is shown in Fig. 2.

A general view of the samples during the cross-fiber crease test is shown in Fig. 2.

a)   b)   c)
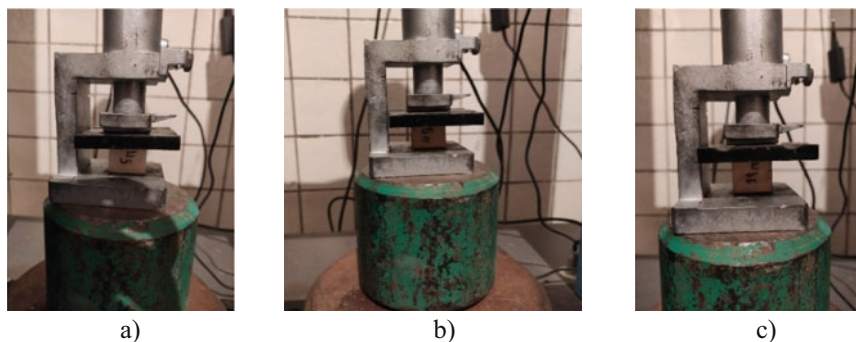
Fig. 1 Samples of wood when tested for compression across fibers: a) series 1; b) series 2; c) series 3

Fig. 2 Wood samples tested for compression along the fibers: a) series 1; b) series 2; c) series 3

3 Results and Discussion

The results of testing samples at compression and across the fibers and compression and along the fibers of the samples are shown in Figs. 3, 4, respectively.

The destruction of the samples during compression along the fibers was plastic in nature with the formation of a characteristic "fold" in the form of individual wood fibers that lost their stability.

The results obtained from the results of destructive studies wood samples have a significant spread of values due primarily to the anisotropy of wood. The value of wood strength is found by the formula 1

$$\sigma = \frac{P_{\max}}{a \cdot b} \tag{1}$$

where P_{max} is the maximum load, kN;

a and b are the cross-sectional dimensions of the sample, see.

The lowest values of the wood strength limits of series 1,2,3 were obtained by statistical processing of tests based on probability theory and are shown in Table 1.

Based on the data obtained, it can be concluded that the increase in compressive strength along the fibers of wood modified with a polymer composition is 23%, and wood modified with a polymer composition with carboxylated carbon nanotubes is 43%. The increase in the conditional compressive strength along the fibers of wood modified with a polymer composition was 3.5%, and wood modified with a polymer composition with carboxylated carbon nanotubes was 58%.
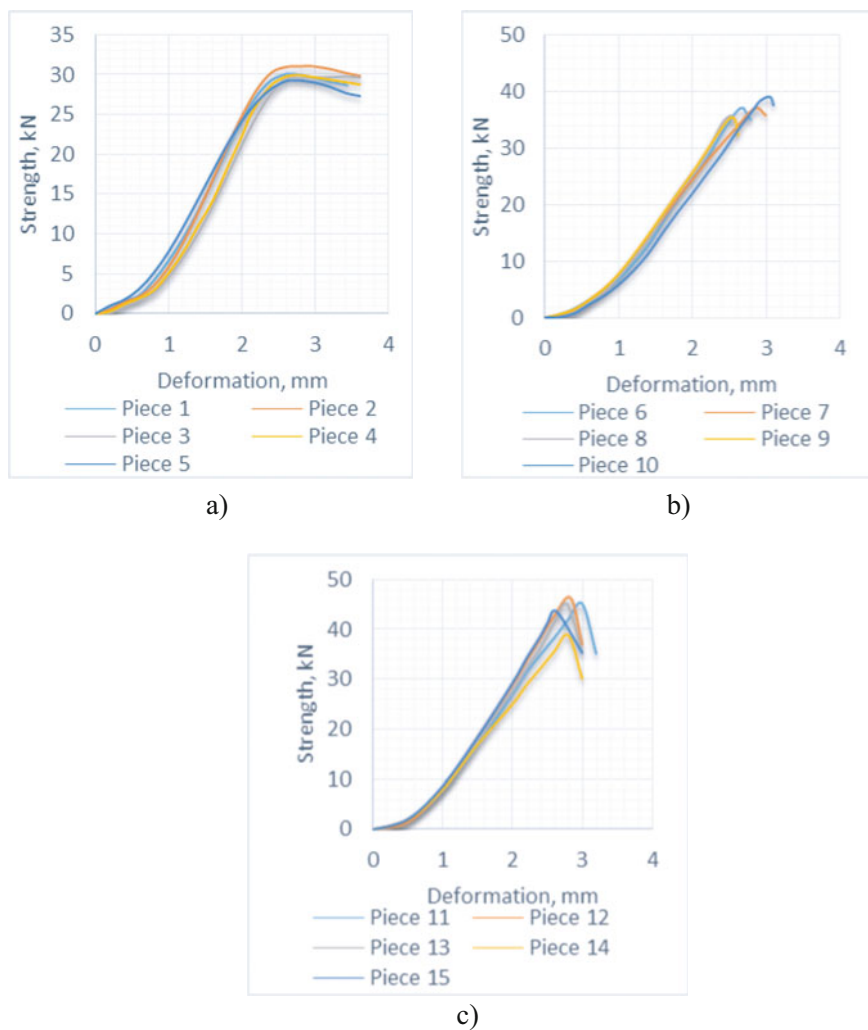
Fig. 3 Changes in the strength of pine wood during compression testing along the fibers: a) series 1; b) series 2 c) series 3
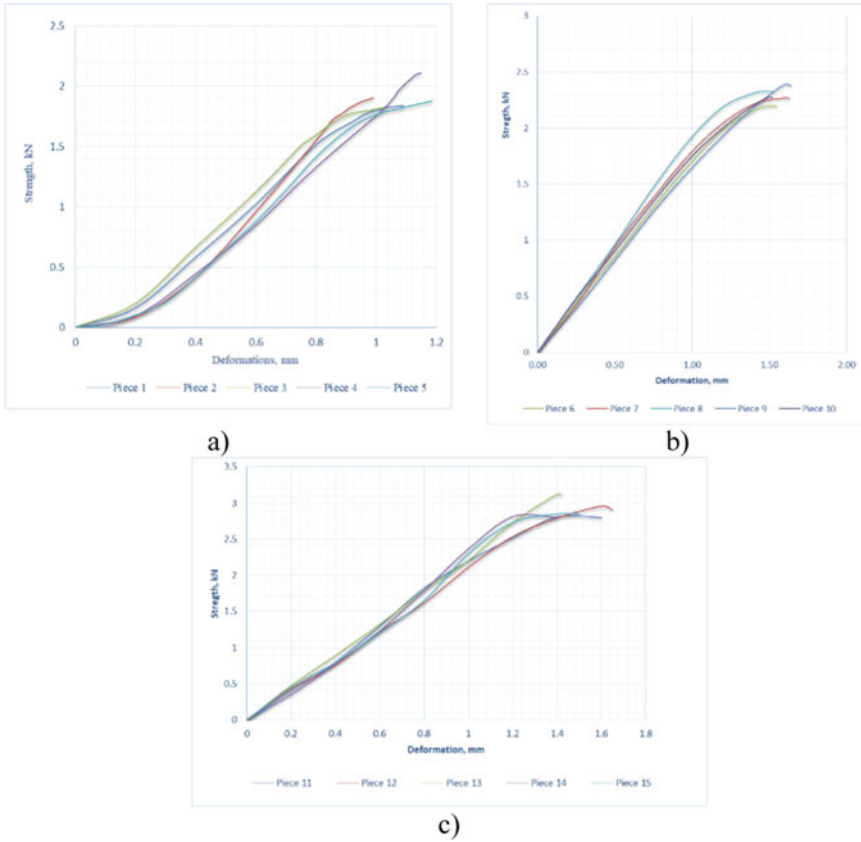
Fig. 4 Change in the conditional tensile strength of pine wood when tested for compression across fibers: a) series 1; b) series 2; c) series 3

Table 1 The lowest value of the wood strength limits of series 1, 2, 3

	Compression along the fibers		Compression across the fibers	
	The lowest strength value, kgf /^{cm2}	Accuracy indicator of the obtained cf. value	The lowest strength value, kgf /^{cm2}	is an indicator of the accuracy of the obtained cf. value mean value
Series 1	611.93	2.27%	26.41	4.67%
Series 2	752.24	2.35%	35.63	2.88%
Series 3	878.01	1.50%	41.70	3.94%

4 Conclusions

Based on the results of the presented study, the following conclusions can be drawn:

1. The proposed method of wood modification can significantly improve its physical and mechanical properties. The increase in compressive strength along the fibers reaches 23%, across the fibers-35%. By introducing carboxylated carbon nanotubes into the polymer compositions нанотрубок, it is possible to achieve an increase in compressive strength along the fibers-43%, and across the fibers-5–8%.
2. The optimal composition for wood modification is a composition of liquid resins based on dimethacrylic polyester, dry hardener (0.25 mass parts), surfactants (OP-10) in the amount of 0.5 mass parts), carboxylated carbon nanotubes (CNT of the Taunit-M series) (0.5 mass parts).
3. Modified wood has improved operational parameters, namely, increased resistance to biological pests, chemical influences, and moisture.

References

1. Chen, C., et al.: Structure–property–function relationships of natural and engineered wood. Nat. Rev. Mater. **5**, 642–666 (2020). https://doi.org/10.1038/s41578-020-0195-z
2. Lukin, M., Prusov, E., Roshchina, S., Karelina, M., Vatin, N.: Multi-span composite timber beams with rational steel reinforcements. Buildings (2021). https://doi.org/10.3390/buildings11020046
3. Labudin, B.V., Nikitina, T.A., Popov, E.V., Varenik, K.A., Novoselova, V.I.: Assessment of the anisotropic wood strength on local crushing. In: IOP Conference Series: Materials Science and Engineering (2020). https://doi.org/10.1088/1757-899X/939/1/012039
4. Gribanov, A.S., Roshchina, S.I., Popova, M.V., Sergeev, M.S.: Laminar polymer composites for wooden structures. Mag. Civ. Eng. (2018). https://doi.org/10.18720/MCE.83.1
5. Lisyatnikov, M.S., Glebova, T.O., Ageev, S.P., Ivaniuk, A.M.: Strength of wood reinforced with a polymer composite for crumpling across the fibers. In: IOP Conference Series: Materials Science and Engineering (2020). https://doi.org/10.1088/1757-899X/896/1/012062
6. Roschina, S.I., Lisyatnikov, M.S., Koshcheev, A.A.: Technical- and- economic efficiency of reinforced wooden structures. IOP Conf. Ser. Mater. Sci. Eng. **698**, 022005 (2019). https://doi.org/10.1088/1757-899X/698/2/022005
7. Sergeev, M.S., Gribanov, A.S., Roschina, S.I.: The stress strain state of composite multi-span beams. In: IOP Conference Series: Materials Science and Engineering (2020). https://doi.org/10.1088/1757-899X/753/3/032068
8. Sergeev, M., Lukina, A., Zdralovic, N., Reva, D.: Stress-strain state of a wood-glued three-span beam with layer-by-layer modification. Lect. Notes Civ. Eng. **182**, 485–491 (2022). https://doi.org/10.1007/978-3-030-85236-8_43

9. Repin, V., Grinyov, V.: The experience in automating scientific research to identify dangerous zones in the near-support sections of wooden beams, pp. 1230–1238 (2022). https://doi.org/10.1007/978-3-030-96383-5_137

10. Kuzina, E., Cherkas, A., Rimshin, V.: Technical aspects of using composite materials for strengthening constructions. In: IOP Conference Series: Materials Science and Engineering (2018). https://doi.org/10.1088/1757-899X/365/3/032053

11. Gribanov, A., Glebova, T., Roschina, S.: Restoration of destructive wood in supporting zones of wooden beams. In: Lecture Notes in Civil Engineering (2020). https://doi.org/10.1007/978-3-030-42351-3_14

12. Roschina, S.I., Lukina, A. V., Sergeev, M.S., Vlasov, A. V., Gribanov, A.S.: Restoration of wooden constructions by impregnation of polymer composition on the example of industrial buildings of light and textile industry. Izv. Vyss. Uchebnykh Zaved. Seriya Teknol. Tekst. Promyshlennosti (2016)

13. Lukina, A., Roshchina, S., Gribanov, A.: Method for restoring destructed wooden structures with polymer composites. Presented at the (2021). https://doi.org/10.1007/978-3-030-72404-7_45

14. Walsh-Korbs, Z., Avérous, L.: Recent developments in the conservation of materials properties of historical wood. Prog. Mater. Sci. **102**, 167–221 (2019). https://doi.org/10.1016/j.pmatsci.2018.12.001

15. Qiu, H., Han, Y., Fan, D., Li, G., Chu, F.: Progress in chemical modification of fast-growing wood | 化学法改良速生木材研究进展. Cailiao Daobao/Mater. Rev. **32**, 2701–2708 (2018). https://doi.org/10.11896/j.issn.1005-023X.2018.15.023

16. Sandberg, D., Kutnar, A., Mantanis, G.: Wood modification technologies - a review. IForest. **10**, 895–908 (2017). https://doi.org/10.3832/ifor2380-010

17. Hill, C.A.S.: Wood modification: chemical. Thermal Other Processes. (2006). https://doi.org/10.1002/0470021748

18. Roschina, S., Gribanov, A., Lukin, M., Lisyatnikov, M., Strekalkin, A.: Calculation of wooden beams reinforced with polymeric composites with modification of the wood compression area. In: MATEC Web of Conferences (2018). https://doi.org/10.1051/matecconf/201825104029

19. Gribanov, A.S., Roshchina, S.I., Naichuk, A.Y., Melekhov, V.I.: Wooden beams with local wood modification. In: IOP Conference Series: Materials Science and Engineering (2020). https://doi.org/10.1088/1757-899X/896/1/012067

20. Lisyatnikov, M.S., Roshchina, S.I., Chukhlanov, V.Y., Ivaniuk, A.M.: Repair compositions based on methyl methacrylate modified with polyphenylsiloxane resin for concrete and reinforced concrete structures. In: IOP Conference Series: Materials Science and Engineering (2020). https://doi.org/10.1088/1757-899X/896/1/012113

21. Gribanov, A.S., Rimshin, V.I., Roshchina, S.I.: Experimental investigations of composite wooden beams with local wood modification. In: IOP Conference Series: Materials Science and Engineering (2019). https://doi.org/10.1088/1757-899X/687/3/033039

22. Lee, S.H., et al.: Thermal treatment of wood using vegetable oils: a review. Constr. Build. Mater. **181**, 408–419 (2018). https://doi.org/10.1016/j.conbuildmat.2018.06.058

23. Gérardin, P.: New alternatives for wood preservation based on thermal and chemical modification of wood— a review. Ann. For. Sci. **73**, 559–570 (2016). https://doi.org/10.1007/s13595-015-0531-4

24. Sandberg, D., Kutnar, A.: Thermally modified timber: recent developments in Europe and north America. Wood Fiber Sci. **48**, 28–39 (2016)

25. Roschina, S.I., Lisyatnikov, M.S., Lukin, M.V., Popova, M.V.: Technology of strengthening the supporting zones of the glued-wood beaming structure with the application of nanomodified prepregs. Mater. Sci. Forum. **931**, 226–231 (2018). https://doi.org/10.4028/www.scientific.net/MSF.931.226

26. Lisyatnikov, M.S., Roshchina, S.I., Chukhlanov, V.Y.: The use of cenospheres for the production of spheroplastics with high dielectric characteristics, obtained from ash of thermal power plant operating on solid fuel. In: IOP Conference Series: Earth and Environmental Science (2020). https://doi.org/10.1088/1755-1315/421/7/072005

27. Łukawski, D., Lekawa-Raus, A., Lisiecki, F., Koziol, K., Dudkowiak, A.: Towards the development of superhydrophobic carbon nanomaterial coatings on wood. Prog. Org. Coatings. **125**, 23–31 (2018). https://doi.org/10.1016/j.porgcoat.2018.08.025
28. Papadopoulos, A.N., Bikiaris, D.N., Mitropoulos, A.C., Kyzas, G.Z.: Nanomaterials and chemical modifications for enhanced key wood properties: a review. Nanomaterials **9** (2019). https://doi.org/10.3390/nano9040607
29. Teng, T.-J., et al.: Conventional technology and nanotechnology in wood preservation: a review. BioResources. **13**, 9220–9252 (2018). https://doi.org/10.15376/biores.13.4.Teng
30. Bi, W., et al.: Effects of chemical modification and nanotechnology on wood properties. Nanotechnol. Rev. **10**, 978–1008 (2021). https://doi.org/10.1515/ntrev-2021-0065
31. Cai, X., Riedl, B., Zhang, S.Y., Wan, H.: The impact of the nature of nanofillers on the performance of wood polymer nanocomposites. Compos. Part A Appl. Sci. Manuf. **39**, 727–737 (2008). https://doi.org/10.1016/j.compositesa.2008.02.004

Strength Properties of Wood for Cleavage on Tangential and Radial Planes Impregnated with a Polymer Composition Based on Dimethacrylic Polyester

Mikhail Sergeev , **Mikhail Lukin** , **and Marina Popova**

Abstract To create new types of wooden structures, new or modified wood-based materials are required. Of interest are the elements of wooden structures made with the use of modern polymer materials with the inclusion of carbon nanotubes, which leads to an increase in strength and rigidity, a decrease in material consumption and installation weight of structures, reduces the effect of anisotropy of properties and defects of wood on the bearing capacity.

The article presents the results of testing samples impregnated with dimethacrylic polyester with nanostructured filler for tangential and radial cleavage. The increase in strength properties during the modification of wood was 21–23%, and with the addition of carbon nanotubes – 28–32%. Experimental studies have proved the promising possibility of using a polymer composition to modify wood in order to increase its strength properties.

Keywords Cleavage · Testing · Polymer composition · Modification · Carbon nanotubes

1   Introduction

Wood is a relatively hard and durable fibrous material that has its advantages as a building material. It consists of countless tube-shaped cells with shells mainly of cellulose, firmly cemented with calcium and magnesium pectates into an almost homogeneous mass [1–3].

The chemical composition of wood includes such chemical elements as carbon C (49.5%), oxygen O (44.1%), hydrogen H (6.3%) and nitrogen N (0.12%). Chemical elements form complex organic substances. The main ones – cellulose, lignin and

M. . Sergeev (✉) · M. Lukin · M. Popova
Vladimir State University named after Alexander and Nikolay Stoletovs, 87 Gorky ul.,
Vladimir 600005, Russian Federation
e-mail: sergeevmichael@inbox.ru

hemicellulose – form the cell wall and make up 95–99% of the mass of absolutely dry wood. The rest include tannins and resins. The location of wood fibers along the axis of the tree causes a sharp difference in the mechanical properties of wood along and across the trunk. The elastic modulus of pine for the direction along the fibers is almost 40 times greater than across, and the compressive strength is 10 times, and the tensile strength is 20–30 times [4–7].

One of the ways to improve the physical and mechanical properties of wood is its modification. Modification of wood should be considered as a process of directed change of physico-mechanical, thermophysical, tribotechnical, biochemical properties of wood in relation to the operating conditions of products made of it [8–10].

Thermochemical modification is based on impregnation of wood with synthetic monomers and oligomers followed by polymerization and curing by thermocatalytic method [11–13]. The technological process of impregnating wood with a modifier based on monomers, oligomers or polycondensation resins is carried out according to the vacuum-pressure or vacuum-pressure-vacuum method at a temperature of 20–30° C. The amount of the absorbed impregnating composition is assumed to be equal to 30–80% of the mass of the original wood. Phenol alcohols, furan-, acetate, methyl methacrylate, styrene methylmethacrylate, styrene vinyl acetate, polyester resins, styrene polyester resins, phenol-formaldehyde, epoxy, furan, urea-formaldehyde, etc. are used as modifiers, the conditional viscosity of which according to the VZ-4 vis-cometer should be 11–14 c at a temperature of 20 °C [14–17]. The viability of the modifier should ensure a complete technological cycle of wood impregnation. The composition can be cured by radiation and thermocatalytic method [18–20].

The purpose of the study is to study the strength properties of wood impregnated with a polymer composition for chipping.

2 Methods

The impregnation composition for wood modification is a polymer composition based on dimethacrylic polyester with a nanostructured filler. The main components that make up the polymer composition are: liquid resin, dry hardener (0.25 mass parts), surfactant (OP–10) in an amount (0.5 mass parts), carbon nanotubes (CNTs of the Taunit-M series) (0.5 mass parts). Mixing of the components was carried out using a PE-8300 top-drive agitator equipped with a built-in control unit [20–23].

The modification was carried out in the following order:

1. Drying of workpieces to a humidity of 5–7% for 2 h at $(110 + 5)$ °C in a standard drying cabinet (SHS-100-1) at atmospheric pressure.
2. Checking the moisture content of each workpiece with a wood moisture meter (Testo-616). If the tests are not breaded immediately after drying, then they should be stored for no more than 3 days in a tightly closed container, for example, in a desiccator) at a temperature of (18–25) °C and humidity control.
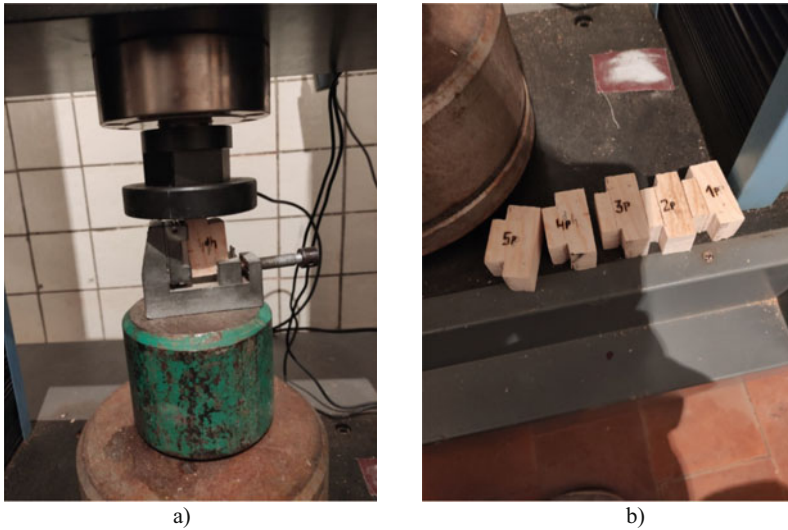
a)　　　　　　　　　　　　　　　　　　b)
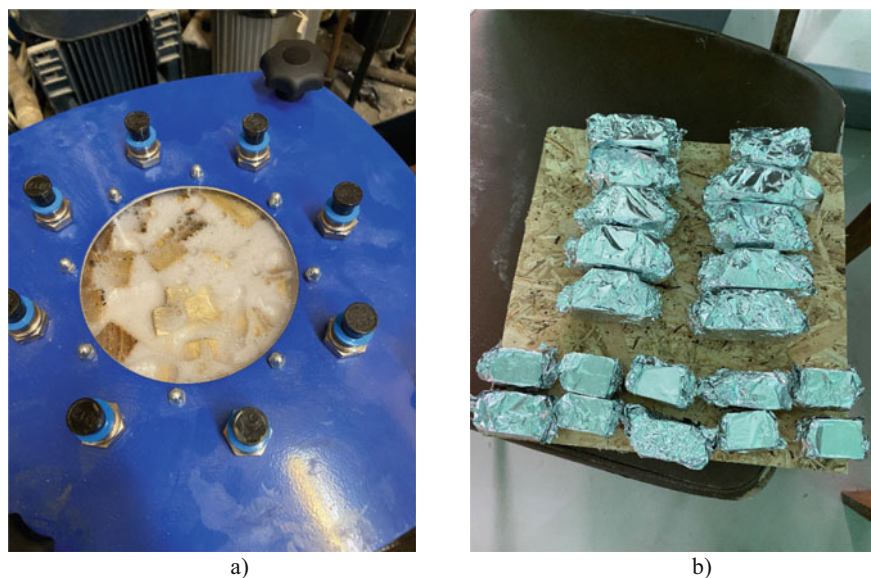
Fig. 1 Technology of wood modification: a) vacuuming of samples; b) preparation of samples for polymerization

3. The blanks are placed in a container for impregnation, fixed with a plate from floating the blanks and filled with an impregnating compound 5 cm above the plate. The container is transferred to a mobile unit for vacuum infusion MVS-20 (−01). Slowly, preventing rapid foaming of the impregnating composition from the air available in the blanks, the air is pumped out to a residual pressure of minus (0.8–0.9) atm. The blanks are kept under vacuum until there is no visible release of even the smallest air bubbles in the layer of the impregnation composition above the blanks, then the vacuum is discharged (see Fig. 1a).

4. To achieve the effect of modification for full volume impregnation, it is recommended to carry out additional exposure (soaking) already impregnated billets in the impregnating composition for up to 15 days.

5. Visually control the degree of filling with the composition of the workpiece. At the end of impregnation, the workpiece should sink in the impregnating composition, and not float. The completeness of the impregnation of the workpiece is controlled visually by a cross-section.

6. The samples are wrapped in aluminum foil and placed at atmospheric pressure in a drying cabinet with forced internal ventilation. The curing temperature is (95–105) °C. The holding time is determined by the type of wood, it is selected for the dimensions of the workpiece and is usually at least 1 h (see Fig. 1b).

The research was carried out on a RM-50 M bursting machine. The bursting machine with a pulsator is equipped with an electrohydraulic automated control system for the loading process based on a computer, which provides static and dynamic

a) b)

Fig. 2 Testing of samples of modified wood for radial cleavage. a) a sample during testing in a press; b) samples after destruction

tensile tests of metal and alloy samples, concrete samples, wood and polymer materials in manual and semi-automatic modes. Loading of standard samples was carried out uniformly with a constant speed of movement of the loading head of the ma-chine – 4 mm/min [24–33].

Cleavage tests were performed on standard samples (Fig. 2, 3).

15 samples were subjected to the radial cleavage test – 3 series of samples of 5 pieces each. 1 series – samples without modification, 2 series – images with modification by polymer composite and 3 series with modification by polymer composition with nanostructured filler. According to the test results, statistical processing of experimental data was carried out.

15 samples were subjected to the tangential cleavage test – 3 series of samples of 5 pieces each. 1 series – samples without modification, 2 series – images with modification by polymer composite and 3 series with modification by polymer composition with nanostructured filler. According to the test results, statistical processing of experimental data was carried out.

a)   b)
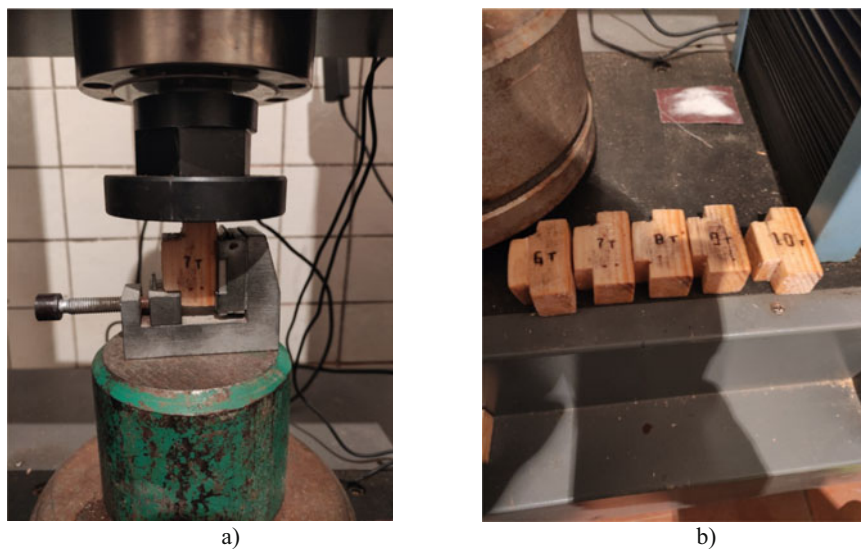
Fig. 3 Testing of samples of modified wood for chipping tangential. a) sample during the test in the press; b) samples after destruction

3   Results and Discussions

Figure 4a shows the results of mechanical tests for radial cleavage of standard wood samples without polymerization, Fig. 4b – wood samples with a modified polymer composition, Fig. 4b – wood samples with a modified polymer composition with a nanostructured filler.

The ultimate strength during cleavage of the samples was determined by the formula:

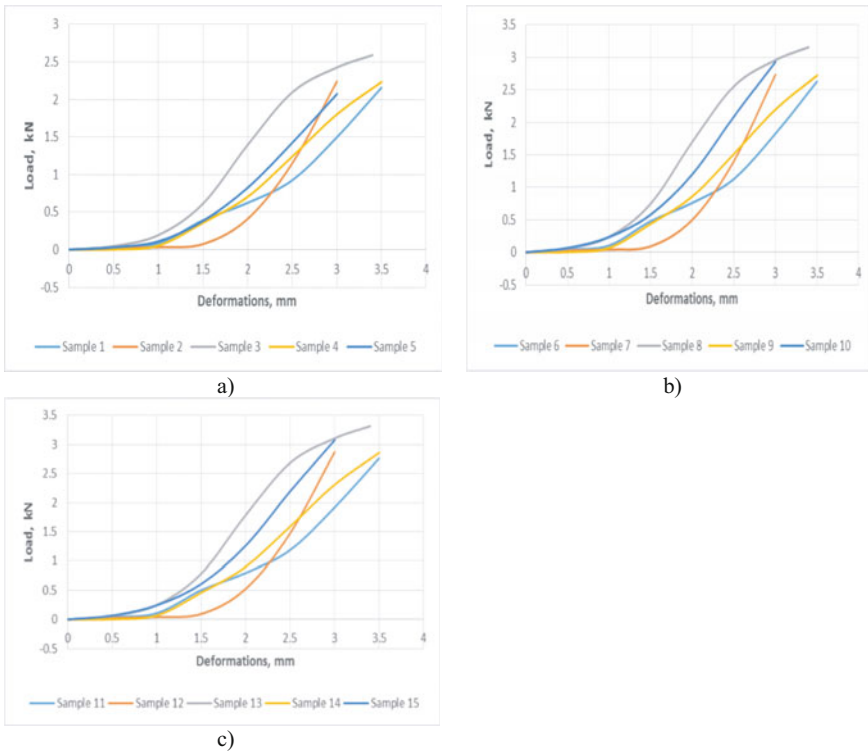$$\sigma_w = \frac{P_{max}}{a \cdot b} \tag{1}$$

where P_{max} – is the maximum load, kN; a, b – the cross-sectional dimensions of the working part of the sample, mm.

According to the test results, statistical processing of experimental data was carried out.

The lowest strength value was determined by the formula:

$$R_s = \overline{x} - \sigma \tag{2}$$

where σ – is the average strength value; x – is the standard deviation.

a)

b)

c)

Fig. 4 Load –strain diagram for wood samples for radial cleavage: a) samples without modification; b) samples with modified polymer composition; c) samples modified with a polymer composition with a nanostructured filler

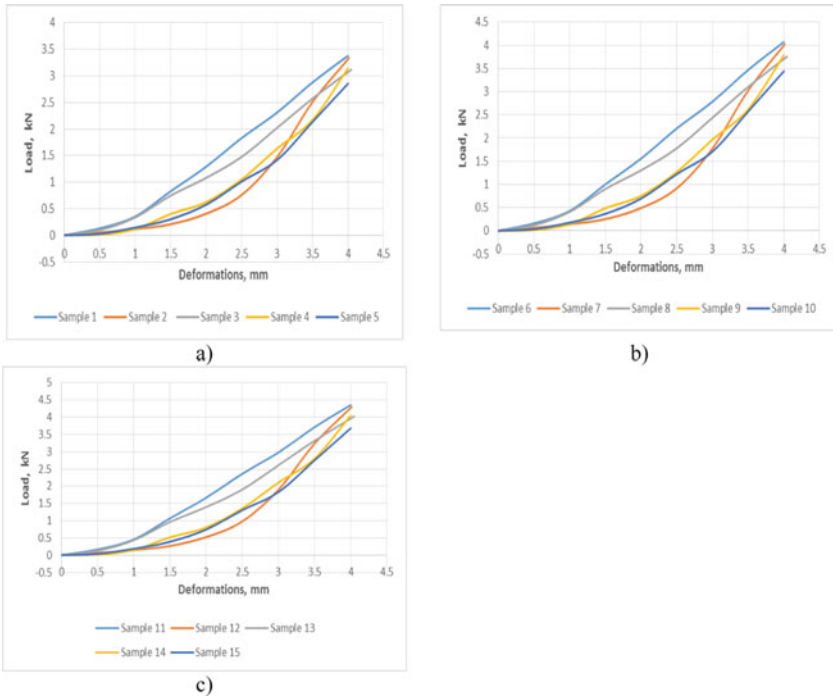The accuracy index of the obtained average value is determined by the formula:

$$\xi = \sigma_x / \overline{x} \tag{3}$$

where σ_x – is the average error of the average value.

To summarize the test results obtained, Table 1 has been compiled.

Table 1 Comparative data on the mechanical properties of samples during radial cleavage

Type of test samples Indicators	Without modification	With modification by polymer composition	With modification by polymer composition with nanostructured filler
Destructive load P$_{max}$,kN Accuracy index P,%	2.33 ±4.35	2.83 ±4.16	2.98 ±4.26
Voltage σ,MPa Strength gain, %	30.27 –	37.0 22.2	38.8 28.2

Fig. 5 Load – strain diagram for wood samples for tangential cleavage: a) samples without modification; b) samples with modified polymer composition; c) samples modified with a polymer composition with a nanostructured filler

Figure 5a shows the results of mechanical tests for tangential cleavage of standard wood samples without polymerization, Fig. 5b – wood samples with a modified polymer composition, Fig. 5b – wood samples with a modified polymer composition with a nanostructured filler.

The calculation of the mechanical properties of the tested samples was carried out according to the formulas (1), (2), (3). To summarize the test results obtained, Table 2 has been compiled.

Table 2 Comparative data of mechanical properties of samples during tangential cleavage

Type of test samples Indicators	Without modification	With modification by polymer composition	With modification by polymer composition with nanostructured filler
Destructive load P_{max},kN Accuracy index P,%	3.17 ±4.66	3.82 ±4.69	4.08 ±4.37
Voltage σ,MPa Strength gain, %	41.12 −	49.44 20.2	53.59 30.3

4   Conclusions

Thus, according to the results of studies on the cleavage of wood with a modified polymer composition with a carbon nanotube filler, the following conclusions can be drawn:

1. Modification of wood with impregnations based on polymer compositions has great prospects and can significantly increase the efficiency of the use of structural solutions of wooden structures.
2. At the stage of destruction of samples during radial cleavage, the stress level in wood is equal to 22–23% of the temporary strength during radial cleavage for wood modified with composite, and 28–29% – with the addition of carbon nanotube filler to the composite.
3. At the stage of destruction of samples during tangential cleavage, the stress level in wood is equal to 21–22% of the temporary strength during tangential cleavage for wood modified with composite, and 31–32% – with the addition of carbon nanotube filler to the composite.
4. A polymer composition based on dimethacrylic polyester with a nanostructured filler was used as a modifier. The main components that make up the polymer composition: liquid resin, dry hardener (0.25 mass parts), surfactant (OP–10) in an amount (0.5 mass parts), carbon nanotubes (CNT series "Taunit-M") (0.5 mass parts).
5. The study contributes to the knowledge base on the use of polymer composites with CNTs for thermochemical modification of wood, which will give development to composite building structures.

References

1. Roschina, S.I., Lisyatnikov, M.S., Koshcheev, A.A.: Technical- and- economic efficiency of reinforced wooden structures. IOP Conf. Ser. Mater. Sci. Eng. **698**, 022005 (2019). https://doi.org/10.1088/1757-899X/698/2/022005
2. Lisyatnikov, M.S., Glebova, T.O., Ageev, S.P., Ivaniuk, A.M.: Strength of wood reinforced with a polymer composite for crumpling across the fibers. In: IOP Conference Series: Materials Science and Engineering (2020). https://doi.org/10.1088/1757-899X/896/1/012062
3. Koshcheev, A.A., Roshchina, S.I., Naichuk, A.Y., Vatin, N.I.: The effect of eccentricity on the strength characteristics of glued rods made of steel cable reinforcement in solid wood. In: IOP Conference Series: Materials Science and Engineering (2020). https://doi.org/10.1088/1757-899X/896/1/012059.
4. Gribanov, A.S., Rimshin, V.I., Roshchina, S.I.: Experimental investigations of composite wooden beams with local wood modification. In: IOP Conference Series: Materials Science and Engineering (2019). https://doi.org/10.1088/1757-899X/687/3/033039

5. Lisyatnikov, M.S., Roshchina, S.I., Chukhlanov, V.Y.: The use of cenospheres for the prodution of spheroplastics with high dielectric characteristics, obtained from ash of thermal power plant operating on solid fuel. In: IOP Conference Series: Earth and Environmental Science (2020). https://doi.org/10.1088/1755-1315/421/7/072005

6. Lukina, A., Roshchina, S., Lisyatnikov, M., Zdralovic, N., Popova, O.: Technology for the restoration of wooden beams by surface repair and local modification. Lect. Notes Networks Syst. **403**, 1371–1379 (2022). https://doi.org/10.1007/978-3-030-96383-5_153

7. Mirsaidov, M., Abdikarimov, R., Khodzhaev, D., Normuminov, B., Roshchina, S., Vatin, N.: Nonlinear vibrations of an orthotropic viscoelastic rectangular plate under periodic loads. Lect. Notes Civ. Eng. **182**, 139–147 (2022). https://doi.org/10.1007/978-3-030-85236-8_11

8. Naichuk, A., Pogoreltsev, A., Demchuk, I., Ivaniuk, A., Roshchina, S.: Rigid joint of bent glued laminated timber structures using inclined glued-in rods. Lect. Notes Civ. Eng. **182**, 501–521 (2022). https://doi.org/10.1007/978-3-030-85236-8_45

9. Lisyatnikov, M.S., Chukhlanov, V.Y., Korshakov, A.V.: Composition based on one-component polyurethane modified with tetrapropoxysilane. J. Phys. Conf. Ser. **2131** (2021). https://doi.org/10.1088/1742-6596/2131/4/042038

10. Lukin, M., Prusov, E., Roshchina, S., Karelina, M., Vatin, N.: Multi-span composite timber beams with rational steel reinforcements. Buildings (2021). https://doi.org/10.3390/buildings11020046

11. Roschina, S.I., Lisyatnikov, M.S., Lukin, M.V., Popova, M.V.: Technology of strengthening the supporting zones of the glued-wood beaming structure with the application of nanomodified prepregs. Mater. Sci. Forum. **931**, 226–231 (2018). https://doi.org/10.4028/www.scientific.net/MSF.931.226

12. Gribanov, A.S., Roschina, S.I., Popova, M.V., Sergeev, M.S.: Laminar polymer compo-sites for wooden structures. Mag. Civ. Eng. (2018). https://doi.org/10.18720/MCE.83.1

13. Roschina, S., Gribanov, A., Lukin, M., Lisyatnikov, M., Strekalkin, A.: Calculation of wooden beams reinforced with polymeric composites with modification of the wood compression area. In: MATEC Web of Conferences (2018). https://doi.org/10.1051/matecconf/201825104029

14. Sergeev, M., Rimshin, V., Lukin, M., Zdralovic, N.: Multi-span composite beam. In: IOP Conference Series: Materials Science and Engineering (2020). https://doi.org/10.1088/1757-899X/896/1/012058

15. Roshchina, S., Lukin, M., Lisyatnikov, M.: Compressed-bent reinforced wooden elements with long-term load. In: Lecture Notes in Civil Engineering (2020). https://doi.org/10.1007/978-3-030-42351-3_7

16. Wang, H., Zhao, Y.: Studies on pre-treatment by compression for wood impregnation III: effects of the solid content of low-molecular-weight phenol formaldehyde resin on the impregnation. J. Wood Sci. **68** (2022). https://doi.org/10.1186/s10086-022-02034-5

17. Feng, X., Chen, J., Yu, S., Wu, Z., Huang, Q.: Mild hydrothermal modification of beech wood (Zelkova schneideriana Hand-Mzt): its physical, structural, and mechanical properties. Eur. J. Wood Wood Prod. (2022). https://doi.org/10.1007/s00107-022-01805-7

18. Gao, Y., Li, Y., Ren, R., Li, L., Gao, J., Chen, Y.: Enhancing the mechanical properties and hydrophobicity of heat-treated wood by migrating and relocating sulfonated lignin. Holzforschung. (2022). https://doi.org/10.1515/hf-2021-0207

19. Novák, I., et al.: The effect of thermal treatment with saturated water steam on the properties of birch wood. Acta Fac. Xylologiae Zvolen. **64**, 5–14 (2022). https://doi.org/10.17423/afx.2022.64.1.01

20. Wu, Y., Cai, Y., Yang, F., Gan, J., Zhang, J.: Chemical modification of poplar wood featuring compressible rebound 3D structure as water treatment absorbents. J. Clean. Prod. **331** (2022). https://doi.org/10.1016/j.jclepro.2021.129952

21. Ermeydan, M.A., Cambazoğlu, M., D. Tomak, E.: A methodological approach to ε-caprolactone modification of wood. J. Wood Chem. Technol. (2022). https://doi.org/10.1080/02773813.2022.2085747

22. Chabert, A.J., Fredon, E., Rémond, R.: Improving the stability of beech wood with polyester treatment based on malic acid. Holzforschung **76**, 268–275 (2022). https://doi.org/10.1515/hf-2021-0030

23. Julian, T.C., Fukuda, H., Novianto, D.: The influence of high-temperature and -pressure treatment on physical properties of Albizia falcataria board. Forests. **13** (2022). https://doi.org/10.3390/f13020239
24. Sargent, R.: Evaluating dimensional stability in modified wood: an experimental comparison of test methods. Forests. **13** (2022). https://doi.org/10.3390/f13040613
25. Younesi-Kordkheili, H., Pizzi, A.: Preparation and properties of a modified corn flour-lignin-glyoxal as a green wood adhesive. Int. Wood Prod. J. **13**, 119–126 (2022). https://doi.org/10.1080/20426445.2022.2048338
26. Wang, X., Wang, M., Cao, J.: Dimensional stability of Scots pine modified by in-situ polymerization esterification | 原位聚合酯化改性欧洲赤松的尺寸稳定性. Beijing Linye Daxue Xuebao/J. Beijing sUniv. **44**, 129–139 (2022). https://doi.org/10.12171/j.1000-1522.20210271
27. Yang, H., Wang, D., Han, Y., Tian, P., Gao, C., Yang, X., Mu, H., Zhang, M.: Preparation and properties of modified poplar impregnated with PVA-nano silica sol composite dispersion system. J. Wood Chem. Technol. (2022). https://doi.org/10.1080/02773813.2022.2064875
28. Yasniy, P., Homon, S., Iasnii, V., Gomon, S.S., Gomon, P., Savitskiy, V.: Strength proper-ties of chemically modified solid woods. In: Procedia Structural Integrity, pp. 211–216 (2022). https://doi.org/10.1016/j.prostr.2022.01.026
29. De Angelis, M., Humar, M., Kržišnik, D., Tamantini, S., Romagnoli, M.: Influence of thermal modification and impregnation with biocides on physical properties of Italian stone pine wood (Pinus pinea L.). Appl. Sci. **12** (2022). https://doi.org/10.3390/app12083801
30. De Ligne, L., et al.: Studying the spatio-temporal dynamics of wood decay with X-ray CT scanning. Holzforschung. **76**, 408–420 (2022). https://doi.org/10.1515/hf-2021-0167
31. He, Z., et al.: Mechanical properties and dimensional stability of poplar wood modified by pre-compression and post-vacuum-thermo treatments. Polymers (Basel). **14** (2022). https://doi.org/10.3390/polym14081571
32. Thang, N.H., Huyen, N.T.B.: Fabrication of transparent composites from pinaceae wood packaging residues. Period. Polytech. Chem. Eng. **66**, 135–146 (2022). https://doi.org/10.3311/PPch.18011
33. Xu, Y., et al.: Constructing SiO2 nanohybrid to develop a strong soy protein adhesive with excellent flame-retardant and coating ability. Chem. Eng. J. **446** (2022). https://doi.org/10.1016/j.cej.2022.137065

Investigation of the Bending Bearing Capacity for Wood Modified with Polymers with Nanoparticle Filler

Svetlana Roschina , **Mikhail Sergeev** , **and Danila Chibrikin**

Abstract The issues of resource conservation are relevant in our time as never before. The study suggests a way to modify wood by vacuum infusion methods using a polymer composition. This method is relevant in the manufacture of new types of wooden structures, reinforcement of nodes and interfaces. Of the greatest interest are structural elements and manufacturing technologies of wooden structures using modern composite polymer materials with the inclusion of carbon nano-tubes (CNTs) in their composition, which leads to increased strength and rigidity, reduced mate-rial consumption and mounting weight of structures, reduces the effect of anisotropy of proper-ties and defects of wood on the bearing capacity.

The wood was impregnated with a polymer composition based on dimethacrylic polyester with a nanostructured filler. At the stage of destruction of samples, during bending tests, the stress level in wood is equal to 25–26% of the temporary bending strength for wood modified with compo-site, and 36–37% - with the addition of carbon nanotube filler to the composite. Experiments on samples have shown the prospects of using a polymer composition to modify wood in order to increase its strength properties.

Keywords Bending · Testing · Polyester · Modification · Carbon nanotubes

1 Introduction

Wood is an environmentally friendly material, it resists static and dynamic loads well, it is very light and at the same time durable. Wood, as a product of plant origin, is a layered-fibrous porous material in its structure and consists of numerous fused elementary cells, diverse in shape, size, and elongated mainly along the trunk. All of them are strongly connected with each other. The cell cavities can be filled with res-ins, gums (resinous secretions), tiles, and water. Vessels, core rays, and wood pulp

S. Roschina · M. Sergeev (✉) · D. Chibrikin
Vladimir State University named After Alexander and Nikolay Stoletovs, 87 Gorky ul.,
Vladimir 600005, Russian Federation
e-mail: sergeevmichael@inbox.ru

are formed from the cells. Each cell has its own shell (wall). The cell walls are 99% com-posed of organic compounds: carbohydrates (70–80%) and lignin (about 30%). The carbohydrate part of wood includes cellulose, glucose, sugar, hemicellulose. Carbo-hydrates and lignin are natural high-molecular compounds (polymers).

The location of wood fibers along the axis of the tree causes a sharp difference in the mechanical properties of wood along and across the trunk. The elastic modulus of pine for the direction along the fibers is almost 40 times greater than across, and the compressive strength is 10 times, and the tensile strength is 20–30 times [1–7].

One of the ways to improve the physical and mechanical properties of wood is its modification. Modification of wood should be considered as a process of directed change of physico-mechanical, thermophysical, tribotechnical, biochemical proper-ties of wood in relation to the operating conditions of products made of it [8–10].

Thermochemical modification is based on the impregnation of wood with syn-thetic monomers and oligomers, followed by polymerization and curing by a thermo-catalytic method [11–13]. The technological process of impregnating wood with a modifier based on monomers, oligomers or polycondensation resins is carried out according to the vacuum-pressure or vacuum-pressure-vacuum method at a temper-ature of 20–30 °C. The amount of absorbed impregnation composition is assumed to be equal to 30–80% of the mass of the original wood. Phenol alcohols, furan-, ace-tate, methyl methacrylate, styrene methylmethacrylate, styrene vinyl acetate, polyes-ter resins, styrene polyester resins, phenol-formaldehyde, epoxy, furan, urea-formaldehyde, etc. are used as modifiers, the conditional viscosity of which accord-ing to the VZ-4 viscometer should be 11–14 c at a temperature of 20 °C [14–17]. The viability of the modifier should ensure a complete technolog-ical cycle of wood impregnation. The composition can be cured by radiation and thermocatalytic meth-od [18–20].

The study is carried out in order to study the strength properties of wood impreg-nated with a polymer composition when working on bending standard samples.

2   Methods

The impregnation composition for wood modification is a polymer composition based on dimethacrylic polyester with a nanostructured filler. The main components that make up the polymer composition are: liquid resin, dry hardener (0.25 mass parts), surfactant (OP–10) in an amount (0.5 mass parts), carbon nanotubes (CNTs of the Taunit-M series) (0.5 mass parts). Mixing of the components was carried out using a PE-8300 top-drive agitator equipped with a built-in control unit [20–23].

The modification was carried out in the following order:

1. Drying of workpieces to a humidity of 5–7% for 2 h at $(110 + 5)$ °C in a standard drying cabinet (SHS-100–01) at atmospheric pressure.
2. Checking the moisture content of each workpiece with a wood moisture meter (Testo-616). If the tests are not breaded immediately after drying, then they should

be stored for no more than 3 days in a tightly closed container, for example, in a desiccator) at a temperature of (18–25) °C and humidity control.

3. The blanks are placed in a container for impregnation, fixed with a plate from floating the blanks and filled with an impregnating compound 5 cm above the plate. The container is transferred to a mobile unit for vacuum infusion MVS-20 (−01). Slowly, preventing rapid foaming of the impregnating composition from the air available in the blanks, the air is pumped out to a residual pressure of minus (0.8–0.9) atm. The blanks are kept under vacuum until there is no visible release of even the smallest air bubbles in the layer of the impregnation composition above the blanks, then the vacuum is discharged (see Fig. 1a).

4. To achieve the effect of modification for full volume impregnation, it is recommended to carry out additional exposure (soaking) already impregnated billets in the impregnating composition for up to 15 days.

5. Visually control the degree of filling with the composition of the workpiece. At the end of impregnation, the workpiece should sink in the impregnating composition, and not float. The completeness of the impregnation of the workpiece is controlled visually by a cross-section.

6. The samples are wrapped in aluminum foil and placed at atmospheric pressure in a drying cabinet with forced internal ventilation. The curing temperature is (95–105) °C. The holding time is determined by the type of wood, it is selected for the dimensions of the workpiece and is usually at least 1 h (see Fig. 1b).

The research was carried out on a RM-50 M bursting machine. The bursting machine with a pulsator is equipped with an electrohydraulic automated control system for the loading process based on a computer, which provides static and dynamic
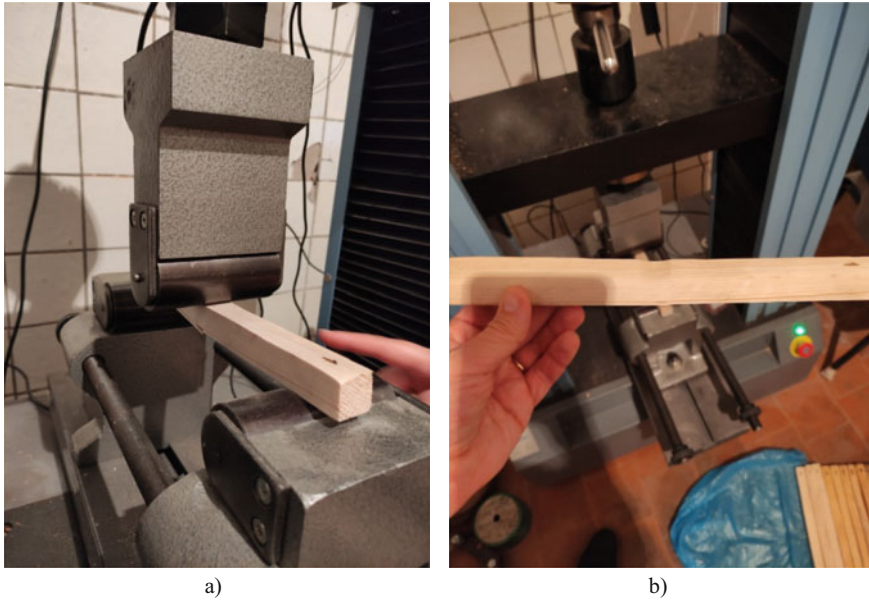

Fig. 1 Technology of wood modification: a) vacuuming of samples; b) samples before testing

Fig. 2 Testing of modified wood samples for bending. a) a sample during the test in the press; b) samples after destruction

tensile tests of metal and alloy samples, concrete samples, wood and polymer materials in manual and semi-automatic modes. Loading of standard samples was carried out uniformly with a constant speed of movement of the loading head of the ma-chine - 4 mm/min [24–31].

15 samples were subjected to the radial cleavage test - 3 series of samples of 5 pieces each. 1 series - samples without modification, 2 series - images with modification by polymer composite and 3 series with modification by polymer composition with nanostructured filler. According to the test results, statistical processing of experimental data was carried out.

Cleavage tests were performed on standard samples (Fig. 2).

3 Results and Discussions

Figure 3a shows the results of mechanical bending tests of standard wood samples without polymerization, Fig. 3b – wood samples with a modified polymer composition, Fig. 3b - wood samples with a modified polymer composition with a nanostructured filler.

The bending strength of the samples was determined by the formula:

a)

b)

c)
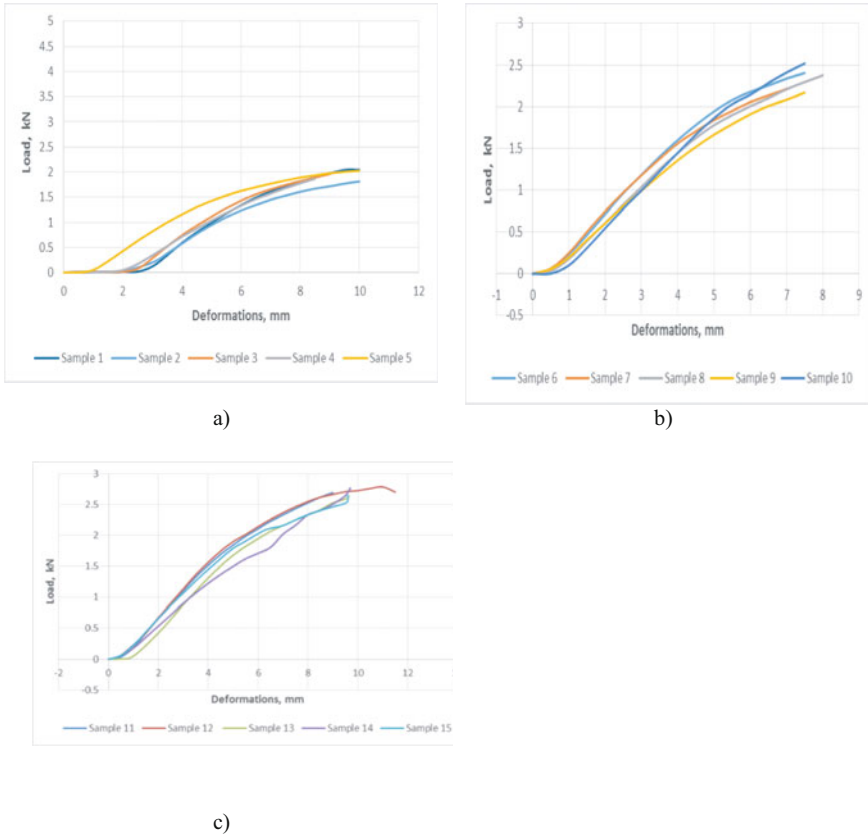
Fig.3 Load –strain diagram for tensile wood samples: a) samples without modification; b) samples with modified polymer composition; c) samples modified with a polymer composition with a nanostructured filler

$$\sigma_w = \frac{P_{max}}{a \cdot b} \qquad (1)$$

where P_{max} - is the maximum load, kN; a,b - the cross-sectional dimensions of the working part of the sample, mm.

According to the test results, statistical processing of experimental data was carried out.

The lowest strength value was determined by the formula:

$$R_s = \bar{x} - \sigma \qquad (2)$$

where σ - is the average strength value; x – is the standard deviation.

The accuracy index of the obtained average value is determined by the formula:

Table 1 Comparative data on the mechanical properties of samples during radial cleavage

Type of test samples Indicators	Without modification	With modification by polymer composition	With modification by polymer composition with nanostructured filler
Destructive load P$_{max}$,kN Accuracy index P,%	2.03 ±4.7	2.31 ±3.58	2.74 ±4.63
Voltage σ,MPa Strength gain, %	34.96 —	43.56 25.7	47.58 36.1

$$\xi = \sigma_x/\overline{x} \tag{3}$$

where σ_x – is the average error of the average value.

To summarize the test results obtained, Table 1 has been compiled.

4 Conclusions

Based on the conducted studies of prismatic bending wood samples modified with a polymer composition with a carbon nanotube filler, the following conclusions can be drawn:

1. Modification of wood by means of its impregnation with polymer compositions has prospects and is relevant for further use. This solution makes it possible to significantly increase the efficiency of the use of various structures and compositions made of wood.
2. At the stage of destruction of samples, during bending tests, the stress level in wood is equal to 25–26% of the temporary bending strength for wood modified with composite, and 36–37% - with the addition of carbon nanotube filler to the compo-site. The limiting state occurs at the moment of rupture of the stretched fibers or by weakening in the form of various defects of the stretched zone.
3. As a modifier, in the above series of tests, a polymer composition based on di-methacrylic polyester with a nanostructured filler was used. The main components that make up the polymer composition are: liquid resin, dry hardener (0.25 mass parts), surfactant (OP–10) in an amount (0.5 mass parts), carbon nanotubes (CNTs of the Taunit-M series) (0.5 mass parts).
4. The conducted research contributes to the knowledge base on the use of polymer composites with CNTs for thermochemical modification of wood, which will give development to composite building structures.

References

1. Lisyatnikov, M.S., Shishov, I.I., Sergeev, M.S., Hisham, E.: Precast monolithic coating of an industrial building based on variable-height beam-slabs. In: IOP Conference Series: Materials Science and Engineering (2020). https://doi.org/10.1088/1757-899X/896/1/012064
2. Sergeev, M., Rimshin, V., Lukin, M., Zdralovic, N.: Multi-span composite beam. In: IOP Conference Series: Materials Science and Engineering (2020). https://doi.org/10.1088/1757-899X/896/1/012058
3. Roshchina, S., Lukin, M., Lisyatnikov, M.: Compressed-bent reinforced wooden elements with long-term load. In: Lecture Notes in Civil Engineering (2020). https://doi.org/10.1007/978-3-030-42351-3_7
4. Lukin, M., Prusov, E., Roshchina, S., Karelina, M., Vatin, N.: Multi-span composite timber beams with rational steel reinforcements.Buildings (2021). https://doi.org/10.3390/buildings11020046
5. Koshcheev, A.A., Roshchina, S.I., Lukin, M.V., Lisyatnikov, M.S.: Wooden beams with reinforcement along a curvilinear trajectory. Mag. Civ. Eng. (2018). https://doi.org/10.18720/MCE.81.19
6. Roshchina, S., Sergeev, M., Lukin, M., Strekalkin, A.: Reconstruction of fixed fertilizer folders in the Vladimir region. In: IOP Conference Series: Materials Science and Engineering (2018). https://doi.org/10.1088/1757-899X/463/4/042011
7. Wang, H., Zhao, Y.: Studies on pre-treatment by compression for wood impregnation III: effects of the solid content of low-molecular-weight phenol formaldehyde resin on the impregnation. J. Wood Sci. **68** (2022). https://doi.org/10.1186/s10086-022-02034-5
8. Feng, X., Chen, J., Yu, S., Wu, Z., Huang, Q.: Mild hydrothermal modification of beech wood (Zelkova schneideriana Hand-Mzt): its physical, structural, and mechanical properties. Eur. J. Wood Wood Prod. (2022). https://doi.org/10.1007/s00107-022-01805-7
9. Gao, Y., Li, Y., Ren, R., Li, L., Gao, J., Chen, Y.: Enhancing the mechanical properties and hydrophobicity of heat-treated wood by migrating and relocating sulfonated lignin.Holzforschung. (2022). https://doi.org/10.1515/hf-2021-0207
10. Wu, Y., Cai, Y., Yang, F., Gan, J., Zhang, J.: Chemical modification of poplar wood featuring compressible rebound 3D structure as water treatment absorbents. J. Clean. Prod. **331** (2022). https://doi.org/10.1016/j.jclepro.2021.129952
11. Ermeydan, M.A., Cambazoğlu, M., D. Tomak, E.: A methodological approach to ε-caprolactone modification of wood. J. Wood Chem. Technol. (2022). https://doi.org/10.1080/02773813.2022.2085747
12. Lisyatnikov, M.S., Glebova, T.O., Ageev, S.P., Ivaniuk, A.M.: Strength of wood reinforced with a polymer composite for crumpling across the fibers. In: IOP Conference Series: Materials Science and Engineering (2020). https://doi.org/10.1088/1757-899X/896/1/012062
13. Repin, V., Grinyov, V.: The experience in automating scientific research to identify dangerous zones in the near-support sections of wooden beams, pp. 1230–1238 (2022). https://doi.org/10.1007/978-3-030-96383-5_137
14. Lukin, M., Popova, M., Reva, D., Abdikarimov, R.: Reinforced concrete shallow shell of negative double Gaussian curvature built on the basis of a four-lobed hyperbolic paraboloid. Lect. Notes Civ. Eng. **182**, 563–576 (2022). https://doi.org/10.1007/978-3-030-85236-8_49
15. Gonshakov, A., Gonshakov, N., Popova, M., Medvedev, E., Popova, O.: Lightweight construction formed on the basis of a typical reinforced concrete lattice beam, pp. 1450–1458 (2022). https://doi.org/10.1007/978-3-030-96383-5_162
16. Romanovich, A., Lisyatnikov, M., Vlasov, A., Aleksiievets, V.: Geodesic domes with installing floor using a cable stay system, pp. 1459–1466 (2022). https://doi.org/10.1007/978-3-030-96383-5_163
17. Lisyatnikov, M., Glebova, T., Rusak, K., Ivaniuk, A.: Strength and deformability of reinforced wooden beams of variable stiffness. Lect. Notes Civ. Eng. **182**, 549–561 (2022). https://doi.org/10.1007/978-3-030-85236-8_48

18. Lisyatnikov, M.S., Chukhlanov, V.Y., Korshakov, A.V.: Composition based on one-component polyurethane modified with tetrapropoxysilane. J. Phys. Conf. Ser. **2131** (2021). https://doi.org/10.1088/1742-6596/2131/4/042038

19. Modin, A., Lukin, M., Vlasov, A., Hisham, E.: Energy-efficient indicators of panel housing mass construction in the climatic conditions of central Russia. In: IOP Conference Series: Materials Science and Engineering (2020). https://doi.org/10.1088/1757-899X/896/1/012063

20. Gribanov, A.S., Strekalkin, A.A., Kudryatseva, A.A., Zdralovic, N.: CFRP composites for strengthening wooden structures. In: IOP Conference Series: Materials Science and Engineering (2020). https://doi.org/10.1088/1757-899X/896/1/012114

21. Julian, T.C., Fukuda, H., Novianto, D.: The Influence of high-temperature and -pressure treatment on physical properties of Albizia falcataria board. Forests. **13** (2022). https://doi.org/10.3390/f13020239

22. Sargent, R.: Evaluating dimensional stability in modified wood: an experimental comparison of test methods. Forests. **13** (2022). https://doi.org/10.3390/f13040613

23. Younesi-Kordkheili, H., Pizzi, A.: Preparation and properties of a modified corn flour-lignin-glyoxal as a Green wood adhesive. Int. Wood Prod. J. **13**, 119–126 (2022). https://doi.org/10.1080/20426445.2022.2048338

24. Wang, X., Wang, M., Cao, J.: Dimensional stability of Scots pine modified by in-situ polymerization esterification | 原位聚合酯化改性欧洲赤松的尺寸稳定性. Beijing Linye Daxue Xuebao/J. Beijing Univ. **44**, 129–139 (2022). https://doi.org/10.12171/j.1000-1522.20210271

25. Yang, H., Wang, D., Han, Y., Tian, P., Gao, C., Yang, X., Mu, H., Zhang, M.: Preparation and properties of modified poplar impregnated with PVA-nano silica sol composite dispersion system. J. Wood Chem. Technol. (2022). https://doi.org/10.1080/02773813.2022.2064875

26. Yasniy, P., Homon, S., Iasnii, V., Gomon, S.S., Gomon, P., Savitskiy, V.: Strength properties of chemically modified solid woods. In: Procedia Structural Integrity, pp. 211–216 (2022). https://doi.org/10.1016/j.prostr.2022.01.026

27. De Angelis, M., Humar, M., Kržišnik, D., Tamantini, S., Romagnoli, M.: Influence of thermal modification and impregnation with biocides on physical properties of Italian stone pine wood (Pinus pinea L.). Appl. Sci. **12** (2022). https://doi.org/10.3390/app12083801

28. De Ligne, L., et al.: Studying the spatio-temporal dynamics of wood decay with X-ray CT scanning.Holzforschung. **76**, 408–420 (2022). https://doi.org/10.1515/hf-2021-0167

29. He, Z., et al.: Mechanical properties and dimensional stability of poplar wood modified by pre-compression and post-vacuum-thermo treatments. Polymers (Basel). **14** (2022). https://doi.org/10.3390/polym14081571

30. Thang, N.H., Huyen, N.T.B.: Fabrication of transparent composites from pinaceae wood packaging residues. Period. Polytech. Chem. Eng. **66**, 135–146 (2022). https://doi.org/10.3311/PPch.18011

31. Xu, Y., et al.: Constructing SiO2 nanohybrid to develop a strong soy protein adhesive with excellent flame-retardant and coating ability. Chem. Eng. J. **446** (2022). https://doi.org/10.1016/j.cej.2022.137065

Mechanical Properties of Polymer Composition Based on Dimethacrylic Polyester with Nanostructured Filler for Wood Modification

Mikhail Lukin (ID)**, Roschina Svetlana** (ID)**, and Vladimir Rimshin** (ID)

Abstract Polymer materials are used in a variety of sectors of the national economy, including in construction. Due to the development of science and technology, higher and higher requirements are being imposed on them, which conventional polymers no longer satisfy. Significantly improve the performance properties of polymers allows the creation of polymer composite materials based on them. One of the promising areas of research in the field of composite materials is the creation of polymer composites based on carbon nanotubes (CNTs). The effectiveness of the use of wooden structures can be increased by modifying wood. Modification is proposed to be carried out using a polymer composition based on dimethacrylic polyester with a nanostructured filler. The solution of this problem will allow, with an increase in strength and rigidity, to reduce the material consumption and installation weight of structures, to reduce the influence of anisotropy of properties and defects of wood on the bearing capacity. In order to establish the mechanical properties of wood, experimental tests were carried out with a polymer composition without filler and with a nanostructured filler. The increase in strength properties with the introduction of filler was 27.7% in compression tests and 23.49% in tensile tests. Studies have proved the promising possibility of using a polymer composition for wood modification.

Keywords Polymer composition · Modification · Strength · Microstructure · Nanotubes

M. Lukin (✉) · R. Svetlana
Vladimir State University named after Alexander and Nikolay Stoletovs, 87 Gorky ul., Vladimir 600005, Russian Federation
e-mail: lukin_mihail_22@mail.ru

V. Rimshin
National Research Moscow State University of Civil Engineering, Yaroslavskoe Shosse, 26, Moscow 129337, Russian Federation

1 Introduction

Wood, as a material used in construction, along with its advantages, has major disadvantages [1]. Improving the properties of natural wood not only increases the time and reliability of its service in buildings, products, but also expands the scope of its application and allows more extensive use of wood [2, 3].

One of the methods that comprehensively improves the properties of wood is its modification with synthetic resins [4, 5].

Modification of wood in a broad sense should be understood as directed improvement of its properties, giving it new positive qualities, elimination of natural disadvantages for wider and full use in construction [6–8].

A very promising method of wood modification is its impregnation with polymers, followed by their curing in wood under the influence of heat treatment [9–12].

An important issue is the definition of the scientific principles of the choice of monomers and oligomers for the modification of wood and the action of various additives (catalysts, plasticizers) and the choice of optimal different ratios of resin components at different stages of their polymerization and condensation [13–16].

It was found that resins with low viscosity and polarity, easily penetrating into wood and curing at temperatures up to 100–150 °C are most suitable for modification purposes [17–19]. Resins that give wood high water and moisture resistance and good dimensional stability and shape of products should have a relatively low molecular weight and be located in the intermolecular spaces of cell walls. High-molecular and relatively more viscous resins are placed mainly in the cavities of cells and do not impart significant hydrophobicity to wood.

The polymer protects wood from internal and external destruction and is chemically resistant to the operational effects of petroleum products, gas and fuel–air mixtures, water and steam, organic solvents, acid and alkali solutions. The operating temperature of cured sealants is from minus 70 °C to plus 220 °C and up to plus 250 °C for (1–4) h without oxygen access [20, 21].

Impregnation compositions are mobile liquids with high capillary fluidity based on methacrylic monomers and oligomers that do not contain solvents and plasticizers [22, 23].

The aim of the study is to experimentally substantiate the mechanical characteristics of the impregnation composition for wood modification based on methacrylic monomers and oligomers that do not contain solvents and plasticizers.

2 Methods

Impregnation formulations are supplied with a set of two components: liquid resin and dry hardener, which are mixed together before use in a ratio of 0.25 g of hardener per 100 g of resin.

a)   b)
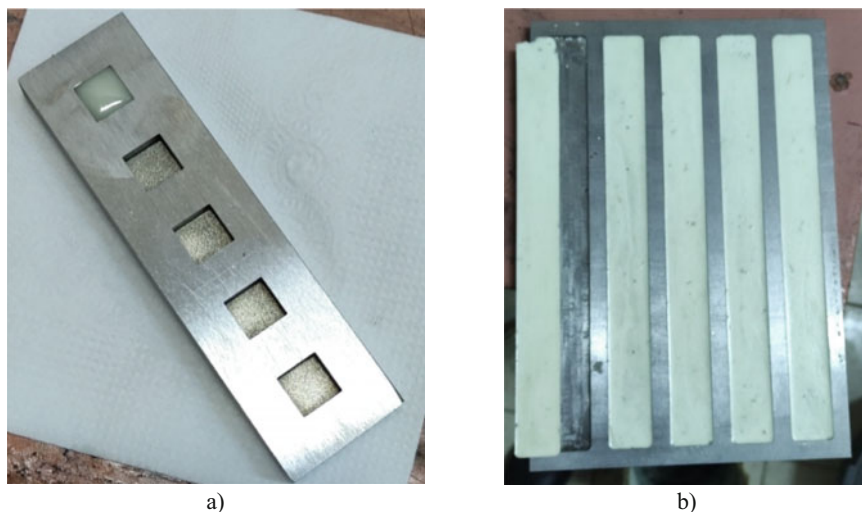
Fig. 1 Special molds for casting polymer samples: **a** compression; **b** tensile

Special steel molds with specified geometric dimensions were developed for casting samples (Fig. 1).

Compression test samples had dimensions of $10 \times 10 \times 4$ mm, tensile $250 \times 25 \times 2$ mm. The tests were carried out on a series of 5 samples each. Destructive testing methods were adopted as a method of studying the physical and mechanical properties of a polymer composition. To fully study the strength properties of the composition, it is necessary to conduct compression and tensile tests [24, 25].

As an additive, carbon nanotubes (CNTs) of the Taunit-M series were adopted, which are quasi-one-dimensional, nanoscale, filamentous formations of polycrystalline graphite, mainly cylindrical in shape with an internal channel in the amount of 0.5%.

In order to exclude the settling of nanotubes, surfactants (surfactants) were added to the liquid phase of the polymer composite. The OP-10 wetting agent was used as a surfactant in an amount of 0.5%. The introduction of surfactants also contributed to an increase in the adhesive strength of the composition with wood. OP-10 wetting agents are a product of processing a mixture of mono- and dialkylphenols with ethylene oxide, have a slightly alkaline or slightly acidic reaction and are well soluble in water.

The introduction of additives was carried out in the following sequence: a hardener is introduced into the resin, then a surfactant and only then CNT [26, 27]. Mixing was carried out using a PE-8300 top-drive agitator equipped with a built-in control unit (see Fig. 2).

For curing, the samples were wrapped in aluminum foil and placed at atmospheric pressure in a drying cabinet with forced internal ventilation. Smoothly, in (5–10) min,

Fig. 2 Mixing of the solution for the preparation of the polymer composition
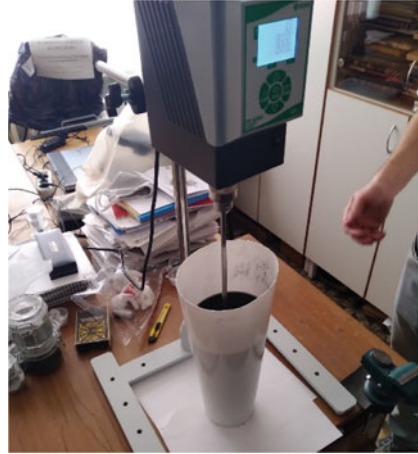
the temperature reached (95–105) °C. The exposure time was usually at least 1 h (see Fig. 3).

The strength properties of a polymer composite depend on the microscopic structure of the material. In order to clarify and confirm the results of mechanical tests, optical microscopy of samples was carried out [28, 29].

Optical microscopy was performed on a Raztek MRX9-D digital optical microscope (Russia), which allows visual observation of the microstructure of opaque objects. Microscopic studies were carried out on samples that were selected for mechanical testing prior to their compression experiment.

Before the start of the tests, the samples were weighed and their density was determined. The average density value for the samples of the polymer composition is 1030 kg/m^3, and the polymer composition with a nanostructured filler is

Fig. 3 Curing of the composition in the drying cabinet

a) b)

Fig. 4 Destruction of polymer composition samples: **a** for compression; **b** for stretching

1080 kg/m^3. This fact can also be explained by the change in the structure of the polymer matrix itself under the influence of CNT.

The research was carried out on the REM-100-A-1 testing machine. The universal testing machine REM-100-A-1 meets the requirements and is designed for mechanical tests in the mode of stretching, compression and bending of samples and products made of materials for which the destructive load does not exceed 100 kN. Loading of samples uniformly with a constant speed of movement of the loading head of the machine. The speed of movement of the loading head of the test machine was 4 mm/min.

Compression and tensile tests were performed on standard samples (Fig. 4).

According to the test results, statistical processing of experimental data was carried out.

3 Results and Discussions

Figure 5 shows the results of mechanical tests of samples for compression and stretching of standard samples of a polymer composition, Fig. 6 shows samples of a composition with a nanostructured filler.

The compressive and tensile strength of the samples was determined by the formula:
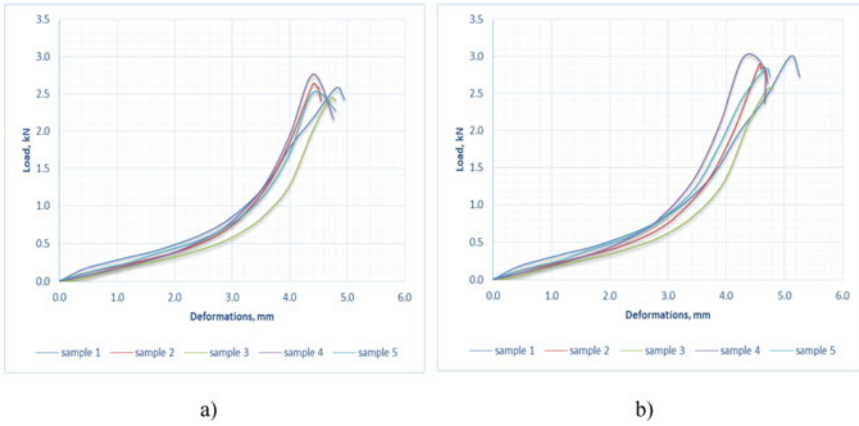
Fig. 5 Load–strain diagram for compression samples: **a** polymer composition **b** polymer composition with nanostructured filler
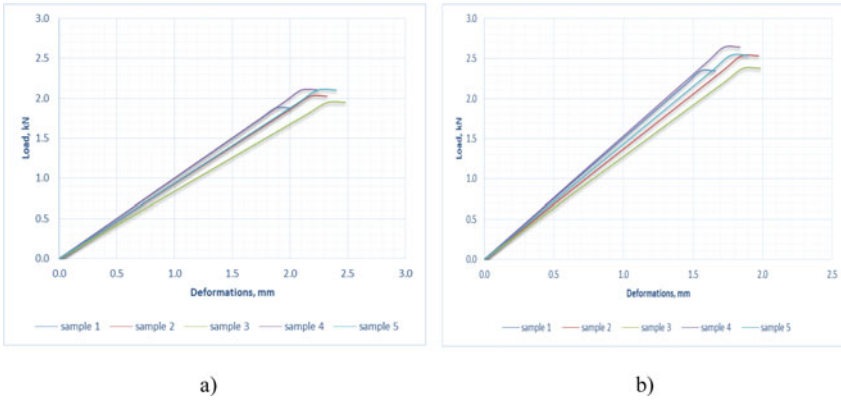
Fig. 6 Load–strain diagram for tensile samples: **a** polymer composition **b** polymer composition with nano-structural filler

$$\sigma_w = \frac{P_{max}}{a \cdot b} \tag{1}$$

where P_{max}—is the maximum load, kN; $a \cdot b$—re the cross-sectional dimensions of the working part of the sample, mm.

According to the test results, statistical processing of experimental data was carried out.

The lowest strength value was determined by the formula:

$$R_s = \overline{x} - \sigma \tag{2}$$

where $\overline{x}$—is the average strength value; σ—is the standard deviation.

The accuracy index of the obtained average value is determined by the formula:

$$\xi = \sigma_x / \overline{x} \tag{3}$$

where σ_x—is the average error of the average value.

To summarize the test results obtained, Table 1 has been compiled.

Figure 7 shows the results of studies of samples by optical microscopy in the longitudinal section.

Optical microscopy illustrates the distribution of nanostructured filler in a polymer composition.

Nanotubes, being distributed in the volume of the polymer matrix, cause the processes of molecular ordering in the amorphous phase of the polymer [30–34]. The resulting local ordering regions cause the effect of compaction of the composite structure [35–38]. It was found that an increase in the concentration of CNTs of more than 0.5% practically does not affect the size of their clusters, but only the number of these sites.

Table 1 Comparative data on the mechanical properties of a polymer composition and a composition with a nanostructured filler

Type of tests	Destructive load P_{max},kN / Accuracy index P,%		Voltage σ,MPa / Strength gain,%	
	Polymer composition	Polymer composition with nanostructured filler	Polymer composition	Polymer composition with nanostructured filler
Compression	$\frac{2.19}{+3.89}$	$\frac{2.54}{+4,99}$	$\frac{49.86}{-}$	$\frac{63,68}{27,72}$
Stretching	$\frac{1.83}{+3.95}$	$\frac{2.26}{+4.10}$	$\frac{36,65}{-}$	$\frac{45.26}{23.49}$

a)   b)
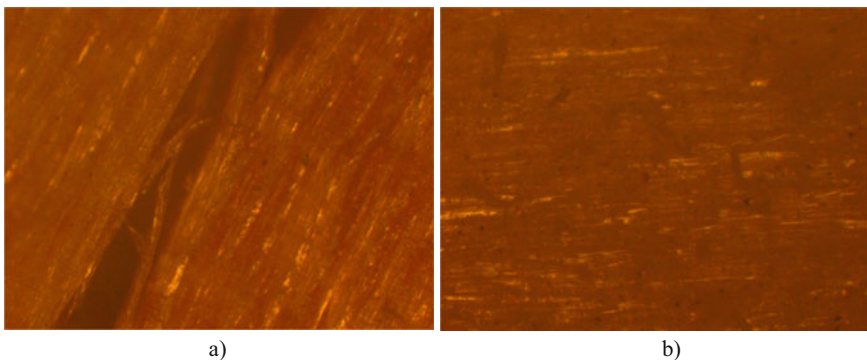
Fig. 7 Examination of samples by optical microscopy: **a** polymer composition; **b** polymer composition with nanostructured filler

The micrographs shown in Fig. 7 can be interpreted as follows: samples with a content of 0.05 CNT mass fraction in the polymer composition in the polymer composition are characterized by the greatest uniformity of structure; carbon nanotubes form clusters of individual bundles that are differently oriented in the matrix. At a concentration of 0.05 of the mass part of CNT, clusters obviously fill the free space. At lower concentrations of CNTs, the concentration of bundles is insufficient to fill the free volume, therefore, they are mainly located on the surface.

All these factors make it possible to explain the changes in the macro properties of composites, namely the greatest value of density and strength at concentrations of 0.05 mass fraction.

4   Conclusions

Thus, based on the results of studies of the mechanical properties of a polymer composition based on dimethacrylic polyester with a nanostructured filler for wood modification, the following conclusions can be drawn:

1. A polymer composition based on dimethacrylic polyester with a nanostructured filler for wood modification was obtained. Carbon nanotubes (CNTs) of the Taunit-M series were adopted as an additive.
2. The optimal amount of filler, established as a result of strength experimental studies, as well as optical microscopy, is 0.05 mass parts.
3. In order to exclude the settling of nanotubes, surfactants (surfactants) must be added to the liquid phase of the polymer composition, for example, OP–10 in an amount of 0.05 mass parts.
4. The strength of the thermally cured polymer composition according to the test results is 49.86 and 36.65 MPa, respectively, for compression and tensile samples.
5. The strength of the composition when carbon nanotubes are introduced into its composition increases by 27.72 and 23.49%, respectively, during compression and tensile tests.
6. Taking into account the strength properties of the polymer compositions under study, allows us to conclude that they can be used for thermochemical modification of wood.
7. This study substantiates the theoretical possibility of using a composition with CNT for thermochemical modification of wood, which ultimately contributes to the development of composite building structures.

References

1. Roshchina, S., Sergeev, M., Lukin, M., Strekalkin, A.: Reconstruction of fixed fertilizer folders in the vladimir region. In: IOP Conference Series: Materials Science and Engineering (2018). https://doi.org/10.1088/1757-899X/463/4/042011

2. Roshchina, S.I., Lukin, M.V., Lukina, A.V., Sergeyev, M.S., Lisyatnikov, M.S.: Experimental research on pressed-bending reinforced timberwork. Int. J. Appl. Eng. Res. **10**, 45307–45312 (2015)

3. Romanovich, A., Lisyatnikov, M., Vlasov, A., Aleksiievets, V.: Geodesic Domes with Installing Floor Using a Cable Stay System, pp. 1459–1466 (2022). https://doi.org/10.1007/978-3-030-96383-5_163

4. Zhou, T., Liu, H.: Research progress of wood cell wall modification and functional improvement: a review. Materials **15** (2022). https://doi.org/10.3390/ma15041598

5. Zhang, E., Tu, Y., Ye, M., Zhu, Z., Chen, N.: Preparation and performance of tannin and Nano SiO<inf>2</inf> modified soy-based adhesives | 单宁和纳米SiO<inf>2</inf>改性大豆基胶黏剂的制备及其性能. Chem. Ind. For. Prod. **42**, 36–42 (2022). https://doi.org/10.3969/j.issn.0253-2417.2022.01.005

6. Klébert, S., Mohai, M., Csiszár, E.: Can plasma surface treatment replace traditional wood modification methods? Coatings **12** (2022). https://doi.org/10.3390/coatings12040487

7. Xu, K., Zhang, X., Li, Z., Zhou, C., Lyu, J., Li, X., Wu, Y.: Research progress of wood low molecular weight resin impregnation modification and its drying | 木材低分子量树脂浸渍改性与干燥研究进展. Cailiao Daobao/Mater. Rep. **36** (2022). https://doi.org/10.11896/cldb.20110248

8. David, M.E., Ion, R.-M., Grigorescu, R.M., Iancu, L., Constantin, M., Stirbescu, R.M., Gheboianu, A.I.: Wood surface modification with hybrid materials based on multi-walled carbon nanotubes. Nanomaterials **12** (2022). https://doi.org/10.3390/nano12121990

9. Bytner, O., Drożdżek, M., Laskowska, A., Zawadzki, J.: Temperature, time, and interactions between them in relation to colour parameters of black poplar (Populus nigra L.) thermally modified in nitrogen atmosphere. Materials **15** (2022). https://doi.org/10.3390/ma15030824

10. Lisyatnikov, M., Lukina, A., Chibrikin, D., Labudin, B.: The strength of wood-reinforced polymer composites in tension at an angle to the fibers. Lecture Notes in Civil Engineering, vol. 182, pp. 523–533 (2022). https://doi.org/10.1007/978-3-030-85236-8_46

11. Sergeev, M., Lukina, A., Zdralovic, N., Reva, D.: Stress–strain state of a wood-glued three-span beam with layer-by-layer modification. Lecture Notes in Civil Engineering, vol. 182, pp. 485–491 (2022). https://doi.org/10.1007/978-3-030-85236-8_43

12. Lisyatnikov, M.S., Glebova, T.O., Ageev, S.P., Ivaniuk, A.M.: Strength of wood reinforced with a polymer composite for crumpling across the fibers. In: IOP Conference Series: Materials Science and Engineering (2020). https://doi.org/10.1088/1757-899X/896/1/012062

13. Goswami, N., Kumar, T., Sodhi, P.K.: Fabrication of nanowoods and nanopapers (2022). https://doi.org/10.1016/B978-0-323-85835-9.00010-6

14. Gong, X., Meng, Y., Lu, J., Tao, Y., Cheng, Y., Wang, H.: A review on lignin-based phenolic resin adhesive. Macromol. Chem. Phys. **223** (2022). https://doi.org/10.1002/macp.202100434

15. Tsoi, Y.I., Blinov, A.K., Ugryumov, S.A., Birman, A.R.: Features of gluing a wood-polymer material. Polym. Sci. Ser. D. **15**, 229–231 (2022). https://doi.org/10.1134/S1995421222020290

16. Tenorio-Alfonso, A., Sánchez, M.C., Franco, J.M.: Impact of the processing method on the properties of castor oil/cellulose acetate polyurethane adhesives for bonding wood. Int. J. Adhes. Adhes. **116** (2022). https://doi.org/10.1016/j.ijadhadh.2022.103153

17. Borah, N., Karak, N.: Tannic acid based bio-based epoxy thermosets: evaluation of thermal, mechanical, and biodegradable behaviors. J. Appl. Polym. Sci. **139** (2022). https://doi.org/10.1002/app.51792

18. Luo, H., Yin, Y., Wang, Y., Li, Q., Tang, A., Liu, Y.: Enhanced properties of a soybean adhesive by modification with a cycloaliphatic epoxy resin. Int. J. Adhes. Adhes. **114** (2022). https://doi.org/10.1016/j.ijadhadh.2021.103026

19. Gan, W., Liu, J., Zhang, J., Fang, J., Hou, Z., Zhang, Y.: Research progress on utilizing lique-faction of lignin to modify phenolic resin丨木质素液化改性酚醛树脂研究进展. J. For. Eng. **7**, 11–19 (2022). https://doi.org/10.13360/j.issn.2096-1359.202107042

20. Cermák, P., Baar, J., Dömény, J., Výbohová, E., Rousek, R., Pařil, P., Oberle, A., Cabalová, I., Hess, D., Vodák, M., Vodák, M., Brabec, M.: Wood-water interactions of thermally modified, acetylated and melamine formaldehyde resin impregnated beech wood. Holzforschung **76**, 437–450 (2022). https://doi.org/10.1515/hf-2021-0164

21. Yuan, S., Wang, H., Li, X., Du, Z., Cheng, X., Du, X.: Flame retardant and form-stable phase change composites based on phytic acid/dopamine-decorated delignified wood for efficient solar-thermal energy conversion and storage. Compos. Part A Appl. Sci. Manuf. **160** (2022). https://doi.org/10.1016/j.compositesa.2022.107048

22. Xu, L., Zhang, H., Xu, F., Zheng, C., Wu, J.: Study on the constructions of special wettability surface of earlywood and latewood丨利用早材和晚材构筑木材不均匀润湿性表面研究. J. For. Eng. **7**, 35–42 (2022). https://doi.org/10.13360/j.issn.2096-1359.202106004

23. Bisht, P., Pandey, K.K., Srinivas, G.: Physiochemical characterization and thermal behaviour of transparent wood composite. Mater. Today Commun. **31** (2022). https://doi.org/10.1016/j.mtcomm.2022.103767

24. Lukin, M., Prusov, E., Roshchina, S., Karelina, M., Vatin, N.: Multi-span composite timber beams with rational steel reinforcements. Buildings (2021). https://doi.org/10.3390/buildings11020046

25. Koshcheev, A.A., Roshchina, S.I., Lukin, M. V., Lisyatnikov, M.S.: Wooden beams with rein-forcement along a curvilinear trajectory. Mag. Civ. Eng. (2018). https://doi.org/10.18720/MCE.81.19

26. Song, P., Chen, C., Shen, X., Zeng, S., Premlatha, S., Ji, Z., Zhai, L., Yuan, A., Liu, Q.: Metal-organic frameworks-derived carbon modified wood carbon monoliths as three-dimensional self-supported electrodes with boosted electrochemical energy storage performance. J. Colloid Interface Sci. **620**, 376–387 (2022). https://doi.org/10.1016/j.jcis.2022.04.048

27. Chen, G., Gupta, A., Mekonnen, T.H.: Silane-modified wood fiber filled EPDM bio-composites with improved thermomechanical properties. Compos. Part A Appl. Sci. Manuf. **159** (2022). https://doi.org/10.1016/j.compositesa.2022.107029

28. Roshchina, S., Lukin, M., Lisyatnikov, M., Koscheev, A.: The phenomenon for the wood creep in the reinforced glued wooden structures. In: MATEC Web of Conferences (2018). https://doi.org/10.1051/matecconf/201824503020

29. Roschina, S., Gribanov, A., Lukin, M., Lisyatnikov, M., Strekalkin, A.: Calculation of wooden beams reinforced with polymeric composites with modification of the wood compression area. In: MATEC Web of Conferences (2018). https://doi.org/10.1051/matecconf/201825104029

30. Plaza, N.Z., Pingali, S.V., Ibach, R.E.: Nanostructural changes correlated to decay resistance of chemically modified wood fibers. Fibers **10** (2022). https://doi.org/10.3390/fib10050040

31. Zhou, J., Wang, B., Xu, C., Xu, Y., Tan, H., Zhang, X., Zhang, Y.: Performance of composite materials by wood fiber/polydopamine/silver modified PLA and the antibacterial property. J. Mater. Res. Technol. **18**, 428–438 (2022). https://doi.org/10.1016/j.jmrt.2022.02.113

32. Li, M., Wang, L., Zhang, J., Zhan, R., An, N., Sun, Y., Wu, F., Yang, J., Su, H.: Single-walled carbon nanotubes promotes wood formation in Populus davidiana × P.bolleana. Plant Physiol. Biochem. **184**, 137–143 (2022). https://doi.org/10.1016/j.plaphy.2022.05.015

33. Adibaskoro, T., Sołowski, W., Hostikka, S.: Multi-surfaced elasto-plastic wood material model in material point method. Int. J. Solids Struct. 236–237 (2022). https://doi.org/10.1016/j.ijsolstr.2021.111333

34. Sergeev, M., Lukina, A., Shunqi, M., Glebova, T., Kryukov, A.: Work of wood-composite beams in panel floors of prefabricated buildings. Lecture Notes in Civil Engineering, vol. 182, pp. 493–499 (2022). https://doi.org/10.1007/978-3-030-85236-8_44

35. Popova, M., Sergeev, M., Lukina, A., Shunqi, M.: Strength and deformability of lightweight metal trusses with elements from cut I-beams. In: IOP Conference Series: Materials Science and Engineering (2020). https://doi.org/10.1088/1757-899X/896/1/012061

36. Gribanov, A.S., Strekalkin, A.A., Kudryatseva, A.A., Zdralovic, N.: CFRP composites for strengthening wooden structures. In: IOP Conference Series: Materials Science and Engineering (2020). https://doi.org/10.1088/1757-899X/896/1/012114
37. Repin, V., Grinyov, V.: The Experience in Automating Scientific Research to Identify Dangerous Zones in the Near-Support Sections of Wooden Beams, pp. 1230–1238 (2022). https://doi.org/10.1007/978-3-030-96383-5_137
38. Lisyatnikov, M., Glebova, T., Rusak, K., Ivaniuk, A.: Strength and deformability of reinforced wooden beams of variable stiffness. Lecture Notes in Civil Engineering, vol. 182, pp. 549–561 (2022). https://doi.org/10.1007/978-3-030-85236-8_48

Tensile Strength of Wood Modified Polymer Composition with Carbon Nanotube Filler

Mikhail Lukin , **Tatyana Glebova** , **and Anatoly Naichuk**

Abstract For the rational use of wood in the manufacture of new types of wooden structures, strengthening of nodes and interfaces, it is currently advisable to use new materials and technical solutions using polymer compositions. Of the greatest interest are structural elements and manufacturing technologies of wooden structures using modern composite polymer materials with the inclusion of carbon nanotubes (CNTs) in their composition, which leads to increased strength and rigidity, reduced material consumption and mounting weight of structures, reduces the effect of anisotropy of properties and defects of wood on the bearing capacity.

Modification is carried out using a polymer composition based on dimethacrylic polyester with a nanostructured filler. In order to establish the mechanical properties of wood, experimental tests were carried out with a polymer composition without filler and with a nanostructured filler. The increase in strength properties during the modification of wood was 23.55%, and with the addition of carbon nanotubes— 37.15%. Experimental studies have proved the promising possibility of using a polymer composition to modify wood in order to increase its strength properties.

Keywords Stretching · Testing · Polymer composition · Modification · Microstructure · Nanotubes

1 Introduction

Wood as a structural material is used in many industries and engineering. The combination of high physical and mechanical characteristics and low specific gravity of wood in comparison with metal and reinforced concrete determines its high demand in construction [1–3].

M. Lukin (✉) · T. Glebova
Vladimir State University named after Alexander and Nikolay Stoletovs, 87 Gorky ul., Vladimir 600005, Russian Federation
e-mail: lukin_mihail_22@mail.ru

A. Naichuk
Brest State Technical University, 267 Moskovskaya str., 224017 Brest, Belarus

Coniferous and deciduous wood consists of a different set of anatomical elements, for which their ordered fibrous structure is common. The mechanical function in coniferous wood is performed by tracheids, which are located mainly vertically in the growing tree and make up 90% of the volume of wood. The location of wood fibers along the axis of the tree causes a sharp difference in the mechanical properties of wood along and across the trunk. The elastic modulus of pine for the direction along the fibers is almost 40 times greater than across, and the compressive strength is 10 times, and the tensile strength is 20–30 times [4, 5].

One of the ways to increase the physical and mechanical properties of wood is its modification. Modification of wood should be considered as a process of directed change of physico-mechanical, thermophysical, tribotechnical, biochemical properties of wood in relation to the operating conditions of products made of it [6–8].

Thermochemical modification is based on the impregnation of wood with synthetic monomers and oligomers, followed by polymerization and curing by a thermocatalytic method [9–12]. The technological process of saturation of wood with a modifying composition is similar to impregnation with antiseptics and flame retardants, carried out according to the vacuum-pressure or vacuum-pressure-vacuum method at a temperature of 20–30 °C. The amount of the absorbed impregnation composition is assumed to be equal to 30–80% of the mass of the original wood. The compositions of monomers and oligomers (phenol alcohols, furan-, acetate, methyl methacrylate, styrene methylmethacrylate, styrene vinyl acetate, polyester resins, styrene polyester resins, etc.) and polycondensation resins (phenol–formaldehyde, epoxy, furan, urea–formaldehyde, etc.) are used as modifiers, the conditional viscosity of which according to the viscometer VZ-4 should be 11–14 c at a temperature of 20 °C [13–16]. The viability of the modifier should ensure a complete technological cycle of wood impregnation. The composition can be cured by radiation and thermocatalytic method [17–19].

The purpose of the study is to study the tensile strength properties of wood impregnated with a polymer composition.

2 Methods

The impregnation composition for wood modification is a polymer composition based on dimethacrylic polyester with a nanostructured filler. The main components that make up the polymer composition are: liquid resin, dry hardener (0.25 mass parts), surfactant (OP–10) in an amount (0.5 mass parts), carbon nanotubes (CNTs of the Taunit-M series) (0.5 mass parts). Mixing of the components was carried out using a PE-8300 top-drive agitator equipped with a built-in control unit.

The modification was carried out in the following order:

1. Drying of workpieces to a humidity of 5–7% for 2 h at $(110 + 5)$ °C in a standard drying cabinet (SHS-100-01) at atmospheric pressure.

2. Checking the moisture content of each workpiece with a wood moisture meter (Testo-616). If the tests are not breaded immediately after drying, then they should be stored for no more than 3 days in a tightly closed container, for example, in a desiccator) at a temperature of (18–25) °C and humidity control.

3. The blanks are placed in a container for impregnation, fixed with a plate from floating the blanks and filled with an impregnating compound 5 cm above the plate. The container is transferred to a mobile unit for vacuum infusion MVS-20 (−01). Slowly, preventing rapid foaming of the impregnating composition from the air available in the blanks, the air is pumped out to a residual pressure of minus (0.8–0.9) atm. The blanks are kept under vacuum until there is no visible release of even the smallest air bubbles in the layer of the impregnation composition above the blanks, then the vacuum is discharged (Fig. 1a).

4. To achieve the effect of modification for full volume impregnation, it is recommended to carry out additional exposure (soaking) already impregnated billets in the impregnation composition for up to 15 days.

5. Visually control the degree of filling with the composition of the workpiece. At the end of impregnation, the workpiece should sink in the impregnation composition, and not float. The completeness of the impregnation of the workpiece is controlled visually by a cross-section.

6. The samples are wrapped in aluminum foil and placed at atmospheric pressure in a drying cabinet with forced internal ventilation. The curing temperature is (95–105) °C. The holding time is determined by the type of wood, it is selected for the dimensions of the workpiece and is usually at least 1 h (Fig. 1b).


a)	b)

Fig. 1 Technology of wood modification: **a** vacuuming of samples; **b** polymerization of samples

The research was carried out on a RM-50 M bursting machine. The bursting machine with a pulsator is equipped with an electrohydraulic automated control system for the loading process based on a computer, which provides static and dynamic tensile tests of metal and alloy samples, concrete samples, wood and polymer materials in manual and semi-automatic modes. Loading of standard samples was carried out uniformly with a constant speed of movement of the loading head of the machine—4 mm/min [20–23].

Tensile tests were performed on standard samples (Fig. 2).

15 samples were tested—3 series of samples of 5 pieces each. 1 series—samples without modification, 2 series—images with modification by polymer composite and 3 series with modification by polymer composition with nanostructured filler. According to the test results, statistical processing of experimental data was carried out.

In order to clarify and confirm the mechanical properties of wood modified with polymer composites, optical and scanning microscopy of samples was performed [24–26].

a)   b)
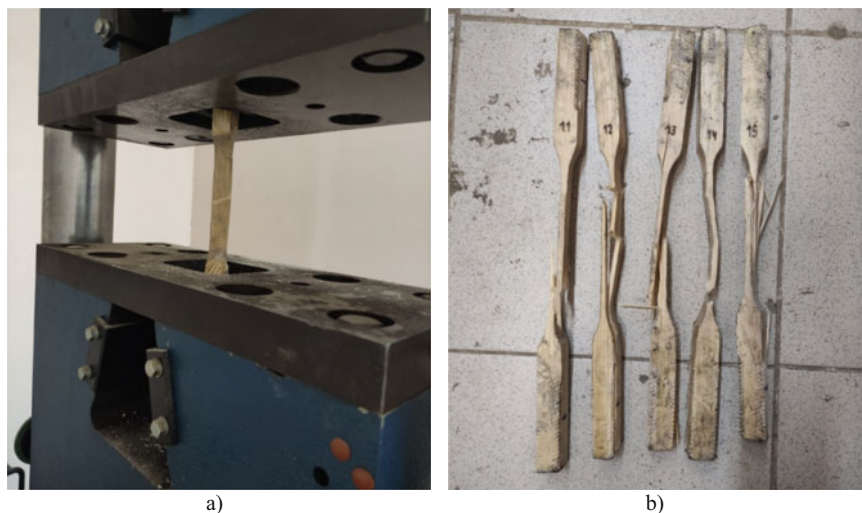
Fig. 2 Tensile testing of modified wood samples: **a** a sample during testing in a bursting machine; **b** samples after destruction

3 Results and Discussions

Optical microscopy was performed on a Raztek MRX9-D digital optical microscope (Russia), which allows visual observation of the microstructure of opaque objects (see Fig. 3). The results of optical microscopy, presented in Fig. 4, illustrate the distribution of the polymer composition in the micropores of wood.

Figure 4b shows that the tracheids of wood, when modified with a polymer composition, are systematically filled with it. The introduction of carbon nanotubes into the composition contributes to an even deeper filling of the tracheids (Fig. 4c). Eventually, wood turns into a composite with a more ordered structure at the cellular level, the anisotropy of properties decreases [27–30].

a)   b)
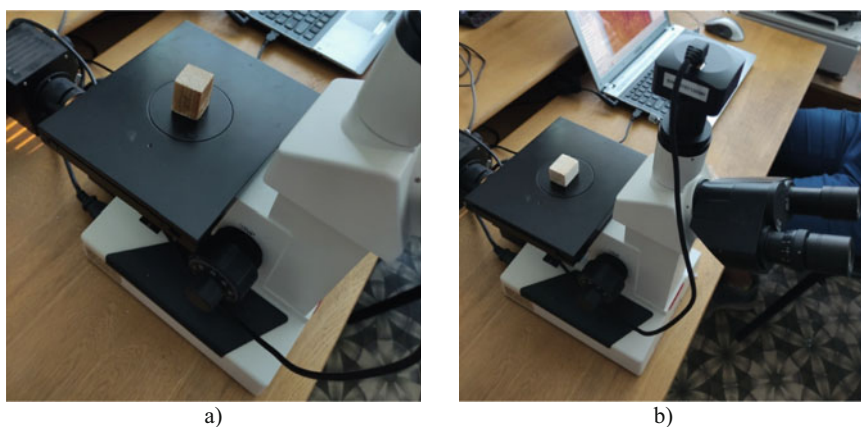
Fig. 3 Microscopy of wood samples: **a** along the fibers; **b** across the fibers

a)   b)   c)
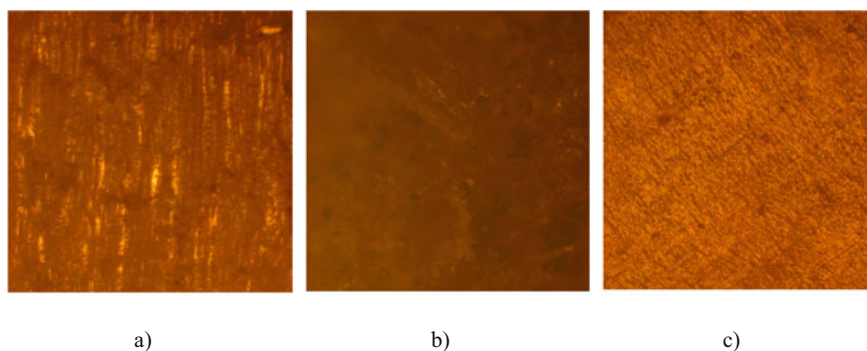
Fig. 4 Results of microscopy of wood samples across fibers: **a** sample without modification; **b** sample with modification of polymer composition; **c** a sample with a modified polymer composition with a carbon nanotube filler

The microstructure of wood was determined using scanning electron microscopy on a Quanta 200 3D microscope. At the molecular level, this method is the most suitable for determining the structure of wood [31–33]. The results of this study contribute to a better understanding of changes in the microstructure of wood when modifying the mechanism of changes in the strength properties of wood (Fig. 5 and 6).

The micrographs shown in Figs. 5 and 6 can be interpreted as follows: with the introduction of a polymer composition into the wood, the pores between the strands of the tracheids are filled. The introduction of nanotubes into the composition contributes to a more complete filling of all the pores present in the cells of wood. As a result of polymerization, the density of wood increases [34–38]. Before the start of the tests, the samples were weighed and their density was determined. The average density value for wood samples without modification was 482 kg/m^3, and the polymer composition with nanostructured filler was 646 kg/m^3. Thus, the density of wood during its polymerization increases by an average of 34%. The introduction

a)　　　　　　　　　　b)　　　　　　　　　　c)
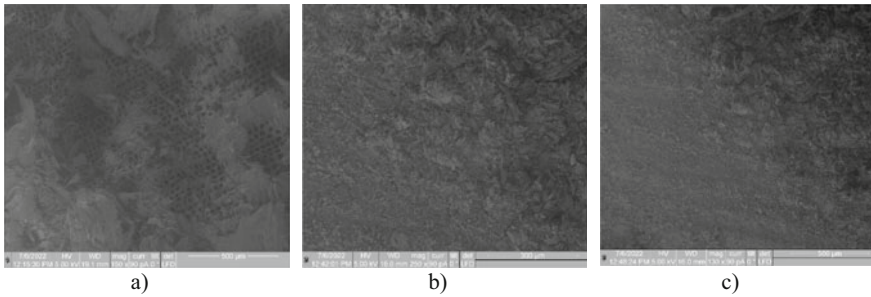
Fig. 5 Examination of samples along fibers by scanning microscopy: **a** sample without modification; **b** sample with modification by polymer composition; **c** a sample with a modified polymer composition with a carbon nanotube filler

a)　　　　　　　　　　b)　　　　　　　　　　c)
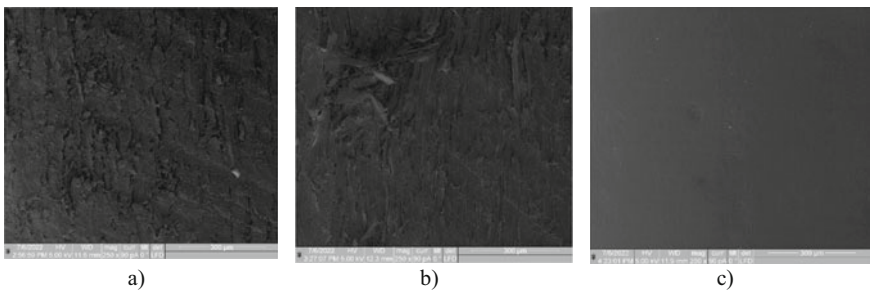
Fig. 6 Examination of samples across fibers by scanning microscopy: **a** sample without modification; **b** sample with modification by polymer composition; **c** a sample with a modified polymer composition with a carbon nanotube filler
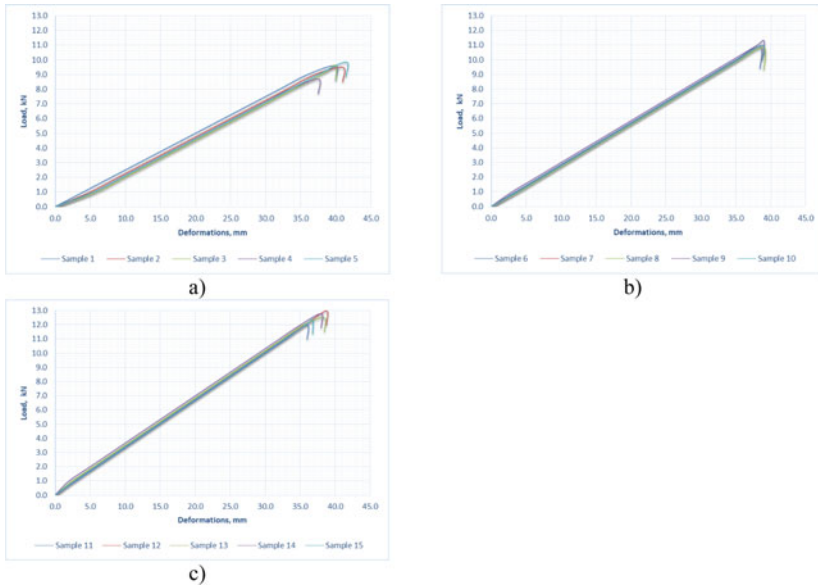
Fig.7 Diagram of "Load-strain" for tensile wood samples: **a** samples without modification; **b** samples with modified polymer composition; **c** samples modified with a polymer composition with a nanostructured filler

of nanotubes into the polymer composition practically does not increase the density of wood.

Figure 7a shows the results of mechanical tensile tests of standard wood samples without polymerization, Fig. 7b—wood samples with a modified polymer composition, Fig. 7c—wood samples with a modified polymer composition with a nanostructured filler.

The compressive and tensile strength of the samples was determined by the formula:

$$\sigma_w = \frac{P_{max}}{a \cdot b} \tag{1}$$

where P_{max}—is the maximum load, kN; $a \cdot b$—re the cross-sectional dimensions of the working part of the sample, mm.

According to the test results, statistical processing of experimental data was carried out.

The lowest strength value was determined by the formula:

$$R_s = \overline{x} - \sigma \tag{2}$$

where $\overline{x}$—is the average strength value; σ—is the standard deviation.

The accuracy index of the obtained average value is determined by the formula:

Table 1 Comparative data on the mechanical properties of a polymer composition and a composition with a nanostructured filler

Type of test samples	Indicators		
	Without modification	With modification by polymer composition	With modification by polymer composition with nanostructured filler
Destructive load P_{max}, kN Accuracy index P, %	8.64 +3.84	10.68 +1.39	11.85 +2.36
Voltage σ, MPa Strength gain, %	43.23 —	53.41 23.55	59.29 37.15

$$\xi = \sigma_x / \overline{x} \qquad (3)$$

where σ_x—is the average error of the average value.

To summarize the test results obtained, Table 1 has been compiled.

4 Conclusions

Thus, based on the results of studies of the tensile strength of wood with a modified polymer composition with a carbon nanotube filler, the following conclusions can be drawn:

1. Modification of wood with polymer composites has great prospects and can significantly increase the efficiency of the use of structural solutions of wooden structures.
2. At the stage of destruction of samples, the stress level in wood is equal to 23–24% of the temporary tensile strength along the fibers for wood modified with composite, and 37–38%—with the addition of carbon nanotube filler to the composite. The limiting state occurs at the moment of rupture of stretched fibers or by weakening in the form of various defects of the stretched zone.
3. As a composite, it is recommended to use the so-called impregnating composition, which is a polymer composition based on dimethacrylic polyester with a nanostructured filler. The main components that make up the polymer composition are: liquid resin, dry hardener (0.25 mass parts), surfactant (OP–10) in an amount (0.5 mass parts), carbon nanotubes (CNTs of the Taunit-M series) (0.5 mass parts).
4. At the cellular level, the tracheids of wood, when modified with a polymer composition, are systematically filled with it. The introduction of carbon nanotubes into the composition contributes to an even deeper filling of the tracheids. A composite with an ordered structure is formed at the cellular level, which ultimately leads to a decrease in the anisotropy of mechanical properties.

5. This study substantiates the theoretical possibility of using polymer composites with CNTs for thermochemical modification of wood, which gives a strong impetus to the development of composite building structures and their further promising implementation.

References

1. Roschina, S.I., Lukina, A. V., Sergeev, M.S., Vlasov, A. V., Gribanov, A.S.: Restoration of wooden constructions by impregnation of polymer composition on the example of industrial buildings of light and textile industry. Izv. Vyss. Uchebnykh Zaved. Seriya Teknol. Tekst. Promyshlennosti. (2016)
2. Roschina, S.I., Lisyatnikov, M.S., Koshcheev, A.A.: Technical- and- economic efficiency of reinforced wooden structures. IOP Conf. Ser. Mater. Sci. Eng. **698**, 022005 (2019). https://doi.org/10.1088/1757-899X/698/2/022005
3. Lukin, M., Prusov, E., Roschina, S., Karelina, M., Vatin, N.: Multi-span composite timber beams with rational steel reinforcements. Buildings (2021). https://doi.org/10.3390/buildings11020046
4. Sergeev, M.S., Gribanov, A.S., Roschina, S.I.: The stress strain state of composite multi-span beams. In: IOP Conference Series: Materials Science and Engineering (2020). https://doi.org/10.1088/1757-899X/753/3/032068
5. Lisyatnikov, M., Lukina, A., Chibrikin, D., Labudin, B.: The strength of wood-reinforced polymer composites in tension at an angle to the fibers. Lecture Notes in Civil Engineering, vol. 182, pp. 523–533 (2022). https://doi.org/10.1007/978-3-030-85236-8_46
6. Wang, H., Zhao, Y.: Studies on pre-treatment by compression for wood impregnation III: effects of the solid content of low-molecular-weight phenol formaldehyde resin on the impregnation. J. Wood Sci. **68** (2022). https://doi.org/10.1186/s10086-022-02034-5
7. Feng, X., Chen, J., Yu, S., Wu, Z., Huang, Q.: Mild hydrothermal modification of beech wood (Zelkova schneideriana Hand-Mzt): its physical, structural, and mechanical properties. Eur. J. Wood Wood Prod. (2022). https://doi.org/10.1007/s00107-022-01805-7
8. Gao, Y., Li, Y., Ren, R., Li, L., Gao, J., Chen, Y.: Enhancing the mechanical properties and hydrophobicity of heat-treated wood by migrating and relocating sulfonated lignin. Holzforschung (2022). https://doi.org/10.1515/hf-2021-0207
9. Gribanov, A.S., Rimshin, V.I., Roshchina, S.I.: Experimental investigations of composite wooden beams with local wood modification. In: IOP Conference Series: Materials Science and Engineering (2019). https://doi.org/10.1088/1757-899X/687/3/033039
10. Novák, I., Sedliačik, J., Kleinová, A., Janigová, I., Mičušík, M., Bekhta, P., Šlouf, M., Matyašovský, J., Jurkovič, P.: The effect of thermal treatment with saturated water steam on the properties of birch wood. Acta Fac. Xylologiae Zvolen. **64**, 5–14 (2022). https://doi.org/10.17423/afx.2022.64.1.01
11. Wu, Y., Cai, Y., Yang, F., Gan, J., Zhang, J.: Chemical modification of poplar wood featuring compressible rebound 3D structure as water treatment absorbents. J. Clean. Prod. **331** (2022). https://doi.org/10.1016/j.jclepro.2021.129952
12. Ermeydan, M.A., Cambazoğlu, M.D., Tomak, E.: A methodological approach to ε-caprolactone modification of wood. J. Wood Chem. Technol. (2022). https://doi.org/10.1080/02773813.2022.2085747

13. Chabert, A.J., Fredon, E., Rémond, R.: Improving the stability of beech wood with polyester treatment based on malic acid. Holzforschung **76**, 268–275 (2022). https://doi.org/10.1515/hf-2021-0030

14. Julian, T.C., Fukuda, H., Novianto, D.: The influence of high-temperature and -pressure treatment on physical properties of Albizia falcataria board. Forests **13** (2022). https://doi.org/10.3390/f13020239

15. Sargent, R.: Evaluating dimensional stability in modified wood: an experimental comparison of test methods. Forests **13** (2022). https://doi.org/10.3390/f13040613

16. Du, H., Lü, W., Liu, Q., Kong, J., Wang, X.: Properties and mechanism of poplar wood modified by melamine-urea-glucose (MUG) biomass resin and sodium silicate compound丨三聚氰胺-尿素-葡萄糖(MUG)生物质树脂/硅酸钠复合改性杨木的性能与机理研究. Beijing Linye Daxue Xuebao/Journal Beijing For. Univ. **44**, 124–131 (2022). https://doi.org/10.12171/j.1000-1522.20210535

17. Younesi-Kordkheili, H., Pizzi, A.: Preparation and properties of a modified corn flour-lignin-glyoxal as a Green wood adhesive. Int. Wood Prod. J. **13**, 119–126 (2022). https://doi.org/10.1080/20426445.2022.2048338

18. de Oliveira Lopes, J., Cáceres, C.B., Hernández, R.E., Garcia, R.A.: Effect of the thermal treatment on the chemical components, sorption, and shrinkage properties of tectona grandis juvenile wood. Maderas Cienc. y Tecnol. **24**, 1–16 (2022). https://doi.org/10.4067/S0718-221X2022000100418

19. Wang, X., Wang, M., Cao, J.: Dimensional stability of Scots pine modified by in-situ polymerization esterification丨原位聚酯化改性欧洲赤松的尺寸稳定性. Beijing Linye Daxue Xuebao/Journal Beijing For. Univ. **44**, 129–139 (2022). https://doi.org/10.12171/j.1000-1522.20210271

20. Roschina, S.I., Lisyatnikov, M.S., Lukin, M.V., Popova, M.V.: Technology of strengthening the supporting zones of the glued-wood beaming structure with the application of nanomodified prepregs. Mater. Sci. Forum. **931**, 226–231 (2018). https://doi.org/10.4028/www.scientific.net/MSF.931.226

21. Roshchina, S., Lukin, M., Lisyatnikov, M.: Compressed-bent reinforced wooden elements with long-term load. In: Lecture Notes in Civil Engineering (2020). https://doi.org/10.1007/978-3-030-42351-3_7

22. Lisyatnikov, M.S., Roshchina, S.I., Chukhlanov, V.Y.: The use of cenospheres for the production of spheroplastics with high dielectric characteristics, obtained from ash of thermal power plant operating on solid fuel. In: IOP Conference Series: Earth and Environmental Science (2020). https://doi.org/10.1088/1755-1315/421/7/072005

23. Yang, H., et al.: Preparation and properties of modified poplar impregnated with PVA-nano silica sol composite dispersion system. J. Wood Chem. Technol. (2022). https://doi.org/10.1080/02773813.2022.2064875

24. Gribanov, A.S., Roshchina, S.I., Popova, M. V., Sergeev, M.S.: Laminar polymer composites for wooden structures. Mag. Civ. Eng. (2018). https://doi.org/10.18720/MCE.83.1

25. Yasniy, P., Homon, S., Iasnii, V., Gomon, S.S., Gomon, P., Savitskiy, V.: Strength properties of chemically modified solid woods. In: Procedia Structural Integrity, pp. 211–216 (2022). https://doi.org/10.1016/j.prostr.2022.01.026

26. Zhou, K., Luo, L., Na, B.: Study on flame retardant leach resistant of modified poplar wood. Wood Res. **67**, 268–279 (2022). https://doi.org/10.37763/wr.1336-4561/67.2.268279

27. De Angelis, M., Humar, M., Kržišnik, D., Tamantini, S., Romagnoli, M.: Influence of thermal modification and impregnation with biocides on physical properties of italian stone pine wood (Pinus pinea L.). Appl. Sci. **12** (2022). https://doi.org/10.3390/app12083801

28. De Ligne, L., De Muynck, A., Caes, J., Baetens, J.M., De Baets, B., Van Hoorebeke, L., Van Acker, J., Van Den Bulcke, J.: Studying the spatio-temporal dynamics of wood decay with X-ray CT scanning. Holzforschung **76**, 408–420 (2022). https://doi.org/10.1515/hf-2021-0167

29. He, Z., et al.: Mechanical properties and dimensional stability of poplar wood modified by pre-compression and post-vacuum-thermo treatments. Polymers **14** (2022). https://doi.org/10.3390/polym14081571

30. Thang, N.H., Huyen, N.T.B.: Fabrication of transparent composites from pinaceae wood packaging residues. Period. Polytech. Chem. Eng. **66**, 135–146 (2022). https://doi.org/10.3311/PPch.18011

31. Shi, J., Chen, H., Ye, J., Zhang, Y., Wu, Z., Zhan, X.: Properties of poplar veneer and plywood modified by in-situ synthesis of CaC0<inf>3</inf>|碳酸钙原位合成改性杨木单板及胶合板性能研究. J. For. Eng. **7**, 43–51 (2022). https://doi.org/10.13360/j.issn.2096-1359.202107002

32. Möttönen, V., Helama, S., Pranovich, A., Korotkova, E., Xu, C., Herva, H., Heräjärvi, H., Mäkinen, H., Nöjd, P., Jyske, T.: Subfossil scots pine (Pinus sylvestris L.) Wood from Northern Finland—physical, mechanical, and chemical properties and suitability for specialty products. Forests **13** (2022). https://doi.org/10.3390/f13050704

33. Xu, Y., Zhang, X., Liu, Z., Zhang, X., Luo, J., Li, J., Shi, S.Q., Li, J., Gao, Q.: Constructing SiO<inf>2</inf> nanohybrid to develop a strong soy protein adhesive with excellent flame-retardant and coating ability. Chem. Eng. J. **446** (2022). https://doi.org/10.1016/j.cej.2022.137065

34. Sergeev, M., Rimshin, V., Lukin, M., Zdralovic, N.: Multi-span composite beam. In: IOP Conference Series: Materials Science and Engineering (2020). https://doi.org/10.1088/1757-899X/896/1/012058

35. Lukin, M. V., Roshchina, S.I., Smirnov, E.A., Shunqi, M.: Strengthening of the operated wooden floor beams with external rigid reinforcement. In: IOP Conference Series: Materials Science and Engineering (2020). https://doi.org/10.1088/1757-899X/896/1/012065

36. Merkulov, S., Rimshin, V., Akimov, E., Kurbatov, V., Roschina, S.: Regulatory support for the use of composite rod reinforcement in concrete structures. In: IOP Conference Series: Materials Science and Engineering (2020). https://doi.org/10.1088/1757-899X/896/1/012022

37. Roschina, S.I., Lisyatnikov, M.S., Melekhov, V.I., Labudin, B.V., Lukin, M.V.: Application of high glued wooden beams in the ceiling of buildings textile plants. Izv. Vyss. Uchebnykh Zaved. Seriya Teknol. Tekst. Promyshlennosti. (2016)

38. Lukina, A., Roshchina, S., Gribanov, A.: Method for restoring destructed wooden structures with polymer composites. Presented at the (2021). https://doi.org/10.1007/978-3-030-72404-7_45

Strength and Stability of a Double Curvature Vaulted Shell

Marina Popova [ORCID]**, Mei Shunqi** [ORCID]**, and Dmitry Reva** [ORCID]

Abstract In the course of the study, an analysis of the basics and the beginning of the operation of the shells was carried out; the calculation of the structure was carried out taking into account the dimensions of the section due to deformations. During the review of the literature, it was found that the principle of operation of the United Nations depends on their Gaussian curvature, since the size differs significantly from the bearing capacity of the system; They actively begin to work as structural elements around the world, they begin to act as a shaping element of a building fence or protection of its cover; the double curvature configuration is exceptional as its shape is close to a parabola or pressure curve consumed as a result of loading; lattice shells of double curvature are self-supporting and allow covering a large area without the use of additional non-existent structures. In the shell of double curvature, there is a uniform distribution of loads on all elements, which virtually eliminates brittle fracture, and also helps to optimize the mass of the coating and increase the efficiency of the structure for payloads. As part of the work, the stress–strain state of a shell with double curvature was studied. Based on the data obtained, it can be concluded that the operation of the shell is limited due to corrosion of the elements. When replacing the lost elements, the shell is able to perceive the required standard load. The margin of safety and stability, taking into account the flexibility of the elements, is 35%. The reliability of the data obtained for the analysis of the model under study is ensured by the accuracy of the finite element method. The practical significance of the work lies in the development of a methodology for calculating and building a model of a unique structure.

Keywords Double curvature shell · Strength · Spatial structures · Displacements · Stability

M. Popova (✉) · D. Reva
Vladimir State University named after Alexander and Nikolay Stoletovs, Gorky Street, 87, 600000 Vladimir, Russian Federation
e-mail: popovamv@bk.ru

M. Shunqi
Wuhan Textile University, Wuhan, China

1 Introduction

In modern design, the use of shells of double curvature allows you to create unique architectural objects. Due to their bearing capacity and lightness, the shells make it possible to cover large spaces without the use of internal supports, which has great prospects for the future [1–3].

Modern achievements in the use of shells are based on the developments of V.G. Shukhov, who became the founder of design and their application. From the point of view of nature, the shell is a shell or a curved outer durable coating [4].

In engineering, a shell is a spatial structure formed by two curved surfaces, the distance between which (thickness) is small compared to the other two dimensions [5].

Shells are used in industrial and civil construction—as load-bearing surfaces and ceilings, canopies, etc.; in tunneling, in particular—in the subway; in shipbuilding, rocket and aircraft construction—ship hulls, docks, fuselages and aircraft wings; in mechanical engineering—car bodies, tanks for transporting liquids, bunkers, etc. [6]. As a rule, they are used to cover large areas without intermediate supports, which allows the design to increase rationality and economy, as well as to achieve reliability, elegance and increased attention, thanks to the self-supporting properties of the structure [7]. Types of shell surfaces are classified according to their Gaussian curvature [8]. The Gaussian curvature of the shell surface is the measure of the curvature of the surface in the vicinity of any of its points [9]. These surfaces can be formed by the rotation and translation of the shell when some generatrix curve moves along an arbitrary guide so that the planes in which the generatrix lies remain parallel to each other at every moment [10].

Shell theory is used to calculate structures [11]. The methods for calculating thin and very thin shells are based on the assumptions that the shell material is isotropic and follows Hooke's law, and that when the shell is deformed, the normals at each point of the middle surface are straight and do not shorten (the Kirchhoff–Love hypothesis) [12]. Based on these hypotheses, two groups of shell theories have been built:

– linear, or the theory of small displacements;
– non-linear, or the theory of shells, taking into account finite displacements.

Based on the magnitude of the bending and torque moments, the theory of shells is divided into moment and momentless. In momentless theories, the magnitude of bending and torsional moments is small and practically does not affect the accuracy of the calculation [13].

Shells are made from a variety of materials: reinforced concrete, wood, metal, glass, composite materials, etc. [14–17].

Let us dwell in more detail on metal structures. The following advantages can be distinguished [18]:

– high bearing capacity, that is, they can perceive significant forces with relatively small cross sections due to the high strength of the metal [19];

– high reliability is ensured due to the uniformity of the metal structure and its elastic properties;
– relatively small weight and portability [20];
– equal strength of welded joints with the base metal of the structure;
– high industrialization ensures their increased quality due to prefabrication [21];
– are convenient in operation, as they have a sufficiently high maintainability and can be strengthened, for example, with an increase in loads in emergency situations [22].

The disadvantages of metal structures include:

– subject to corrosion, which requires special measures to protect them;
– low fire resistance (at temperatures above 400 °C for steels and temperatures above 200 °C for aluminum alloys, the material begins to creep, i.e. its destruction).

Shells allow you to:

– significantly increase the range of spans of coatings of buildings and structures for various purposes;
– block the premises with any configuration of the plan;
– significantly lighten the mass of the coating, thereby increasing the efficiency of the structure for payloads [23–27];
– transform designs, give them uniqueness.

Thanks to all the properties of objects, they are promising areas in architecture [28, 29].

The aim of the work is to study the application of double curvature, to determine the possibilities and conditions for its use, to determine design solutions in the application of the structure.

To achieve the goal:

– to analyze the foundations and riches of the work of shells;
– agreed analysis of the constitution and basic definitions of geometric parameters and design features;
– calculations of hull calculations;
– Prepared recommendations for its further application.

The object of study is a metal mesh shell of double curvature.

The subject of the study is the strength characteristics of a shell of double curvature and the conditions for its application.

2 Methods

The methodology of the study is to review the current experience in the calculation and design of biconvex shells, the choice of the optimal design scheme, computer calculation and analysis of the data obtained [30]. Machine calculation involves the

following steps: 1) calculation of a shell with various options for loading with a live load; 2) study of shell flexibility; 3) calculation of the control finite element model of the shell [31].

In this study, a finite element model is adopted for calculation, in which the shell is specified by rod finite elements of the 5th type (spatial rod). The use of the 5th type element is due to the fact that the Z-shaped profiles are made continuous along the length.

As a research model, a metal mesh vault of double curvature with a plan size of 14.6 × 38.4 m was chosen. In the cross section in the longitudinal and transverse directions, the vaults form circular segments with a bowing arrow equal to 1/6 of the span. The supporting base of the vaults is made up of curved Z-shaped rolled profiles connected to the arches through gussets. Z-shaped profiles, crossing at two levels and connected by means of rivets, form a rigid, unchanging shell. This shell of double curvature is a translation shell. Surface type—barrel vault. On rise—gentle, on execution—mesh with a rhombic pattern. The thrust that occurs in the mesh vault is perceived by horizontal puffs made of round steel and adjacent to the upper belt of arches in every second supporting node of the mesh vault. Each arch is a rectangular (14.63 × 38.4 m) flat shell of positive Gaussian curvature, consisting of 54 continuous bent (rolled) Z-shaped runs (profiles), 27 of which are located at a positive angle to the x-axis, and the remaining 27 form the opposite angle and are displaced by the size of the section.

The result is an intersecting network in the form of arches or a paired structure of two parallel flat systems connected at the junction with rivets and horizontal ties (along the upper chords, this is just a continuous sheet tie). The general scheme of the shell is shown in Fig. 1.
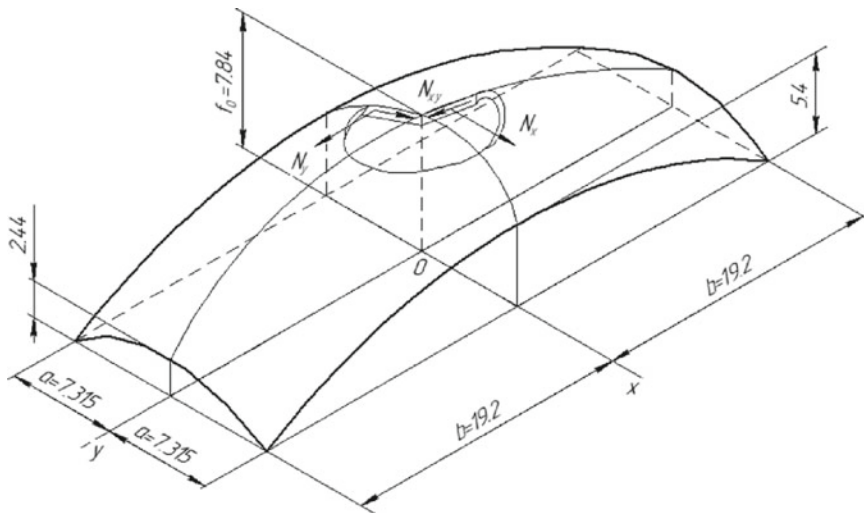
Fig. 1 General shell scheme
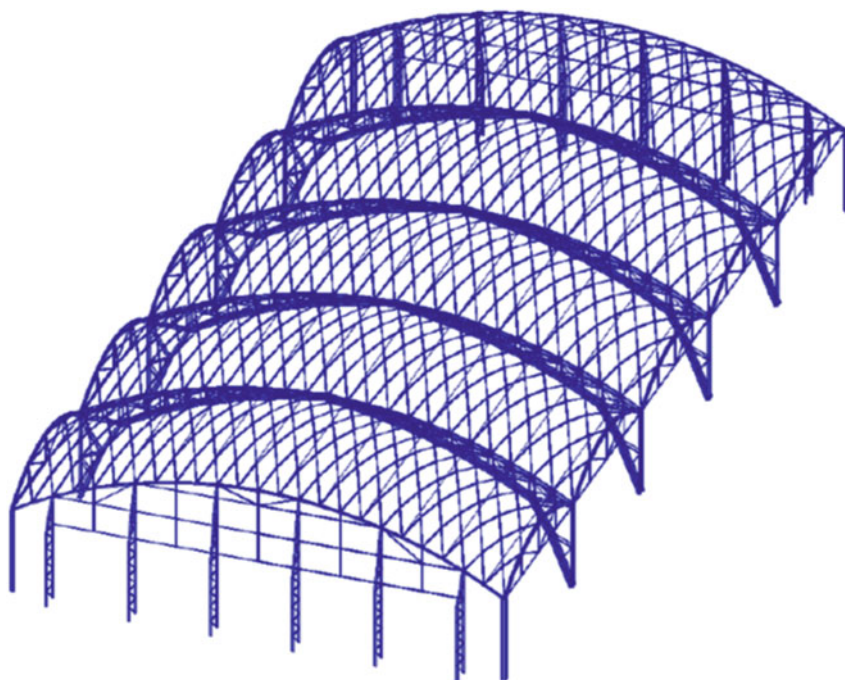
Fig. 2 Spatial finite element rod model of the shell

The automated technological chain of creating a design model based on a linear processor in SP LIRA-SAPR is as follows: design model—static analysis—DCF (design combination of forces)—DCF (design load combination)—design system—output of results.

The spatial finite element model of the object under study is displayed in Fig. 2.

In the course of the calculation, 8 loadings were formed: self-weight of the shell and cover frame; wind load in two loaded places (wind in Y, wind in X); ice load; snow load; pulsating component of the wind load. Estimated values of the weight of the snow cover and the standard value of wind pressure for the conditions of the city of Vyksa of the Russian Federation.

In accordance with building codes, the selection and verification of metal sections are carried out in accordance with the most dangerous coverage conditions. The calculation of the calculated combinations of outcomes was carried out according to the criterion of increased values of significant diseases at the characteristic points of the sections of the elements on the basis of the rules selected by the regulatory documents. Calculation stages: received calculation, calculated events (hereinafter referred to as DCS), calculated arrivals of loads (hereinafter referred to as RCL), cases according to RCL.

3 Results and Discussion

As a result of the static calculation, the forces in the rod finite elements of the shell are determined. The calculation and analysis of design combinations of loads was carried out, and the most unfavorable design combination of loads was determined. For the convenience of reading the results, the maximum forces in the characteristic groups of finite elements, simulating the main metal structures of the workshop, were selected based on the design combinations of loads. According to the maximum efforts, the percentages of the depletion of the bearing capacity of the structural elements of the shop are determined.

The maximum displacement of the upper point of the workshop according to the calculation carried out according to the RCL from the snow load is:

– along the horizontal axis X: 20 mm;
– along the vertical Z-axis: −41.3 mm.

The resulting values of the maximum displacements in the shell satisfy the current standards, according to which the vertical limit deflections of the elements of this design should not exceed l/300. For l we take the largest span width of 38.4 m.

One of the main reasons for the destruction of shell structures is the loss of stability of the original form of equilibrium. Destruction in this case occurs almost instantly.

Oscillations are one of the most common forms of motion. As a result of the dynamic calculation, thirteen vibration modes and characteristics for each of the modes were obtained. The calculation and analysis of the design combination of loads was carried out. The results of dynamic analysis for load cases containing wind pulsation are converted into loads and stored in new static load cases (static wind along the Y axis, taking into account the pulsation component, and static wind along the X axis, taking into account the pulsation component).

Natural frequencies of certain modes of vibration are given in Table 1.

For the convenience of analyzing the results, the vibration modes that have the greatest impact on the calculation scheme are given (Fig. 3a, b, c).

As a result of the stability calculation, three forms of buckling were obtained (Fig. 3d, i, f).

As a result of the calculation, taking into account the geometric nonlinearity, the forces in the rod finite elements of the workshop and the maximum displacement of the nodes were determined. The calculation and analysis of design combinations

Table 1 Natural frequencies of certain vibration modes

Form No.	Eigenvalues	Frequencies		Period, s
		Circular frequency, rad/s	Frequency, Hz	
1	0.059	17.022	2.709	0.369
2	0.054	18.405	2.929	0.341
3	0.052	19.302	3.072	0.326
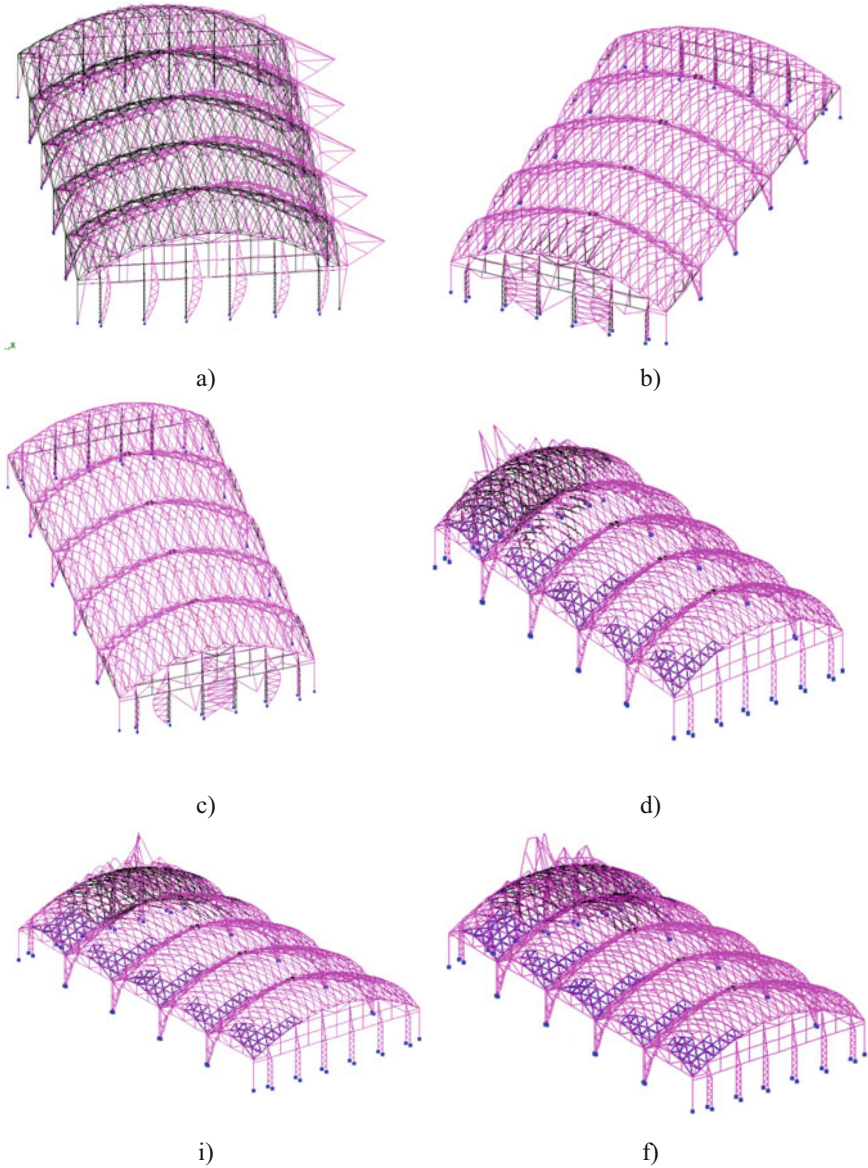
Fig. 3 Forms of oscillations and buckling of the shell: **a** the first form of oscillations (wind pulsation Y, waveform 1); **b** second waveform (wind pulsation Y, waveform 2); **c** third waveform (wind pulsation Y, waveform 3); **d** first form of buckling (buckling form, factor 1.4278); **i** second form of buckling (buckling form, factor 1.45696); **f** third form of buckling (buckling form, factor 1.49788)

of loads was carried out, and the most unfavorable design combination of loads was determined. For the convenience of reading the results, the maximum forces in the characteristic groups of finite elements simulating the main metal structures of the shop were selected based on the design combinations of loads. Based on the maximum efforts, the percentage of depletion of the bearing capacity of the structural elements of the shop is determined.

The safety factors of the general stability are determined (they correspond to the minimum safety factor for individual rods). For the most unfavorable design combination of loads (DCL 2), the safety factor for the first form of buckling is 1.4178, for the second form of buckling—1.4570, for the third form of buckling—1.4979.

4 Conclusions

1. The most loaded structures are the corner posts of the building and elements of the upper and lower chords of three-hinged arches.
2. After the destruction of the brick walls, the flexibility of the corner posts increased, which caused the formation of additional forces from an eccentric load transfer. The lower section of the corner posts is the most loaded, and at the same time is highly susceptible to corrosion.
3. Due to the fact that some nodes of the supports of the girders of the roof vaults on the three-hinged arch, as well as some of the elements of the lattice of arches, were removed from the design scheme, due to their almost complete destruction, the distribution of loads occurs unevenly and individual elements of the upper and lower chords of three-hinged arches perceive additional forces.
4. The percentage of depletion of the bearing capacity in the elements of the workshop does not exceed 94% according to the calculation for the first group of limit states. The calculation for the second group of limit states showed that in all elements of the workshop, except for the corner posts and elements of the upper chords of the end trusses, the necessary conditions are met. The percentage of bearing capacity depletion in all elements of the shop does not exceed 71% according to the local stability calculation.
5. The smallest stability factor of the frame was K = 1.4178.
6. The strength and stability of the workshop, taking into account the removal of heavily damaged nodes and sections of structural elements of the workshop building from the design scheme, is sufficient to absorb the existing loads from its own weight, snow, ice and wind loads, and temperature effects.

References

1. Koshcheev, A.A., Roshchina, S.I., Aleksiievets, V., Labudin, B. V.: Local deformation and strength characteristics of S-shaped reinforcement in wood. In: IOP Conference Series: Materials Science and Engineering (2020). https://doi.org/10.1088/1757-899X/896/1/012060
2. Lukin, M.V., Popov, M.V., Lisyatnikov, M.S.: Short-term and long-term deformations of the lightweight concrete. IOP Conf. Ser. Mater. Sci. Eng. **753**, 032071 (2020). https://doi.org/10.1088/1757-899X/753/3/032071
3. Sergeev, M.S., Gribanov, A.S., Roschina, S.I.: The stress strain state of composite multi-span beams. In: IOP Conference Series: Materials Science and Engineering (2020). https://doi.org/10.1088/1757-899X/753/3/032068
4. Vatin, N., Sinelnikov, A., Garifullin, M., Trubina, D.: Simulation of cold-formed steel beams in global and distortional buckling (2014). https://doi.org/10.4028/www.scientific.net/AMM.633-634.1037
5. Kuzina, E., Rimshin, V., Kurbatov, V.: The reliability of building structures against power and environmental degradation effects. In: IOP Conference Series: Materials Science and Engineering (2018). https://doi.org/10.1088/1757-899X/463/4/042009
6. Modin, A., Lukin, M., Vlasov, A., Hisham, E.: Energy-efficient indicators of panel housing mass construction in the climatic conditions of central Russia. In: IOP Conference Series: Materials Science and Engineering (2020). https://doi.org/10.1088/1757-899X/896/1/012063
7. Kaveh, A., Talatahari, S.: Geometry and topology optimization of geodesic domes using charged system search. Struct. Multidiscip. Optim. **43**, 215–229 (2011). https://doi.org/10.1007/s00158-010-0566-y
8. Carlini, A., Tedeschini Lalli, L.: A metallic 1928 geodesic dome in Rome. In: 18th Conference on Applied Mathematics, APLIMAT 2019, pp. 182–189 (2019)
9. Zabojszcza, P., Radon, U.: Effect of increased density of nodes in geodesic dome on its critical load capacity. In: IOP Conference Series: Materials Science and Engineering (2019). https://doi.org/10.1088/1757-899X/471/5/052051
10. Nieboer, M., McCormack, C.W.: Under geodesic skies; a cultural perspective on the former South Pole Dome and geodesic domes in outer space. Polar J. **7**, 351–373 (2017). https://doi.org/10.1080/2154896X.2017.1373914
11. Marimuthu, V., Seetharaman, S., Arul Jayachandran, S., Chellappan, A., Bandyopadhyay, T.K., Dutta, D.: Experimental studies on composite deck slabs to determine the shear-bond characteristic (m - k) values of the embossed profiled sheet. J. Constr. Steel Res. **63**, 791–803 (2007). https://doi.org/10.1016/j.jcsr.2006.07.009
12. Campian, C., Chira, N., Iuhos, V., Pop, M., Vatin, N.: Structural upgrading of steel columns for overhead power lines. Procedia Eng. 876–882 (2016). https://doi.org/10.1016/j.proeng.2016.11.787
13. Popova, M., Sergeev, M., Lukina, A., Shunqi, M.: Strength and deformability of lightweight metal trusses with elements from cut I-beams. In: IOP Conference Series: Materials Science and Engineering (2020). https://doi.org/10.1088/1757-899X/896/1/012061
14. Roschina, S.I., Lukina, A. V., Sergeev, M.S., Vlasov, A. V., Gribanov, A.S.: Restoration of wooden constructions by impregnation of polymer composition on the example of industrial buildings of light and textile industry. Izv. Vyss. Uchebnykh Zaved. Seriya Teknol. Tekst. Promyshlennosti (2016)
15. Lukin, M., Prusov, E., Roshchina, S., Karelina, M., Vatin, N.: Multi-span composite timber beams with rational steel reinforcements. Buildings (2021). https://doi.org/10.3390/buildings11020046
16. Lukin, M. V., Roshchina, S.I., Smirnov, E.A., Shunqi, M.: Strengthening of the operated wooden floor beams with external rigid reinforcement. In: IOP Conference Series: Materials Science and Engineering (2020). https://doi.org/10.1088/1757-899X/896/1/012065
17. Lukin, M. V., Roshchina, S.I., Gribanov, A.S., Naychuk, A.Y.: Stress-strain state of wooden beams with external reinforcement. In: IOP Conference Series: Materials Science and Engineering (2020). https://doi.org/10.1088/1757-899X/896/1/012066

18. Graver, J.E.: Encoding fullerenes and geodesic domes. SIAM J. Discret. Math. **17**, 596–614 (2004). https://doi.org/10.1137/S0895480101391041
19. Romanovich, A., Kleshcunov, Y., Vlasov, A.: On potentiality and practicability of installing flooring suspended in geodesic domes by means of cable system. In: IOP Conference Series: Materials Science and Engineering (2019). https://doi.org/10.1088/1757-899X/687/3/033025
20. Sergeev, M., Lukina, A., Zdralovic, N., Reva, D.: Stress–strain state of a wood-glued three-span beam with layer-by-layer modification. In: Lecture Notes in Civil Engineering, vol. 182, pp. 485–491 (2022). https://doi.org/10.1007/978-3-030-85236-8_43
21. Gonshakov, A., Gonshakov, N., Popova, M., Medvedev, E., Popova, O.: Lightweight Construction Formed on the Basis of a Typical Reinforced Concrete Lattice Beam, pp. 1450–1458 (2022). https://doi.org/10.1007/978-3-030-96383-5_162
22. Gribanov, A.S., Roshchina, S.I., Popova, M. V., Sergeev, M.S.: Laminar polymer composites for wooden structures. Mag. Civ. Eng. (2018). https://doi.org/10.18720/MCE.83.1
23. Lukin, M., Popova, M., Reva, D., Abdikarimov, R.: Reinforced concrete shallow shell of negative double gaussian curvature built on the basis of a four-lobed hyperbolic paraboloid. In: Lecture Notes in Civil Engineering, vol. 182, pp. 563–576 (2022). https://doi.org/10.1007/978-3-030-85236-8_49
24. Roshchina, S.I., Gonshakov, A.G., Gonshakov, N.G.: Taking into consideration the work of monolithic reinforced concrete floor with shaped steel profiles in two directions. In: IOP Conference Series: Materials Science and Engineering (2020). https://doi.org/10.1088/1757-899X/753/4/042084
25. Lisyatnikov, M.S., Shishov, I.I., Sergeev, M.S., Hisham, E.: Precast monolithic coating of an industrial building based on variable-height beam-slabs. In: IOP Conference Series: Materials Science and Engineering (2020). https://doi.org/10.1088/1757-899X/896/1/012064
26. Roshchina, S., Ezzi, H., Shishov, I., Lukin, M., Sergeev, M.: Evaluation of the deflected mode of the monolithic span pieces and preassembled slabs combined action. In: IOP Conference Series: Earth and Environmental Science (2017). https://doi.org/10.1088/1755-1315/90/1/012075
27. Gonshakov, N.G., Gonshakov, A.G., Aleksiievets, I.I.: Reinforcement of brick structures with carbon fiber. In: IOP Conference Series: Materials Science and Engineering (2020). https://doi.org/10.1088/1757-899X/896/1/012032
28. Roshchina, S., Sergeev, M., Lukin, M., Strekalkin, A.: Reconstruction of fixed fertilizer folders in the vladimir region. In: IOP Conference Series: Materials Science and Engineering (2018). https://doi.org/10.1088/1757-899X/463/4/042011
29. Lukin, M., Martynov, V., Rimshin, V., Aleksiievets, I.: Reinforced concrete vertical structures under a gently sloping shell of double curvature under the influence of progressive collapse. In: Lecture Notes in Civil Engineering, vol. 182, pp. 577–587 (2022). https://doi.org/10.1007/978-3-030-85236-8_50
30. Roschina, S.I., Lukin, M. V., Lisyatnikov, M.S., Sergeyev, M.S.: Reconstruction of coating by a single-stage adjustment of a lind-fitting factory in the city of Vyazniki (2017)
31. Romanovich, A., Lisyatnikov, M., Vlasov, A., Aleksiievets, V.: Geodesic Domes with Installing Floor Using a Cable Stay System, pp. 1459–1466 (2022). https://doi.org/10.1007/978-3-030-96383-5_163

Comparative Evaluation of Aluminum Alloys for the Manufacture of Connecting Systems in Building Structures

Dmitriy Reva [ID]**, Alexey Usov** [ID]**, and Mikhail Lukin** [ID]

Abstract This paper discusses industrial aluminum alloys that are most suitable for manufacturing small-sized parts for the construction industry using the example of timber connecting systems. A reasonable choice of the most suitable alloys was made, then the product designs were developed and their mechanical behavior was simulated in the LIRA software package with the condition of rigid fastening, considering loading conditions. It is shown that the designed products as part of the building structure, withstand the maximum load under the accepted operating conditions for each type of size, while connectors do not deform, which allows the use of less expensive alloys while maintaining the required bearing capacity.

Keywords Industrial aluminum alloys · Connecting systems · Building structures · Evaluation of the alloys effectiveness

1 Introduction

Aluminum alloys are most widely used as decorative building materials in products such as building cladding, doors, glass curtain wall support systems, and aluminum alloy curtain wall framing. Spatial structures made of aluminum alloys actually appeared as early as the 1940s. However, today they are increasingly being used as a critical material for small parts that can operate in aggressive environments. For example, for pre-fabricated wooden structures, which at the same time can be hidden from the eyes so as not to spoil the overall look. Aluminum can work well in many structures, especially wood, because of its corrosion resistance. It lends itself well to processing and electric arc welding. As a material, it is quite common and has a low cost in all its many variations of alloys. It also has a low density, therefore, low weight. The above properties significantly distinguish this material from the usual steel products.

D. Reva (✉) · A. Usov · M. Lukin
Vladimir State University named after Alexander and Nikolay Stoletovs, 87 Gorky St., Vladimir 600006, Russian Federation
e-mail: reva-dima@mail.ru

311

According to GrandView Research, the global wood connector market was valued at $753.0 million in 2020 and is expected to grow at a compound annual growth rate (CAGR) of 13.9% between 2021 and 2028. Solid wood, cross-laminated wood, wood panels, reinforced wood beams [1–3], composite beams [4–6], and other wood products [7–10] are widely used in construction projects [11, 12], which will continue to drive demand for specialized connectors. The Austrian company "SHERPA" manufactures aluminum connectors, which comprise two parts, forming a rigid connection "Dovetail" [13]. This type of connection provides good transmission of horizontal and vertical forces, and performs well in compression and tension.

To date, there are many options for connecting wooden structures, using corners, plates, pins [14–16], in small-sized structures, such as furniture, with screws, confirmations, furniture eccentrics. All the proposed methods after fixing remain visible on the finished structure, which spoils the overall appearance, and sometimes breaks faster than fixed objects. The proposed option by the manufacturer is quite expensive for customers. Therefore, for the production of analogues, it is necessary to identify which alloys are most suitable.

The analysis of domestic and foreign literature in the field of the use of aluminum alloys in construction indicates significant progress in the search for suitable alloys and the development of technologies for obtaining promising materials [17–19] that are widely in demand in the construction industry. Aluminum alloys are a promising material for manufacturing monolithic and composite beams and bearing supports, especially in those areas that are associated with the design of light prefabricated structures and engineering structures. In this regard, the purpose of the work is to identify and justify the most appropriate grades of industrial aluminum alloys for manufacturing small building products.

2   Materials and Research Methods

The object of study in this paper is the connecting elements (connectors) for wooden, concrete, and metal structures. Aluminum alloys, which are most often used in construction, and their characteristics are investigated. To select among the tested alloys, it is necessary to know not only the physical and mechanical characteristics but also economic indicators, such as the market price. The price is determined by calculating the average value of the selling price of one kilogram of the alloy of each of the grades under consideration according to the data provided by suppliers as of May 31, 2022, translated at the official rate. Each given value of the price of 1 kg of the alloy is an arithmetic average value determined from the data of at least five different suppliers.

Three alloys must be selected for further study of the models. Since we need the optimal combination of strength and price, also the average elongation percentage. To evaluate the indicators available in the table, the logical formula (1) was proposed

$$\frac{UTS}{\text{Price}} - \frac{|\text{Mean Elongation} - \text{Elongation}|}{10} \tag{1}$$

The design of small-sized building products was carried out using the Solid Works 2017 software package (Dassault Systèmes SolidWorks Corporation, Waltham, MA, USA). The simulation of the mechanical behavior of the developed samples was carried out in the LIRA 10.10 software package (LIRA soft, Moscow).

3 Selection and Justification of Grades of Aluminum Alloys for Modeling

Having selected the most commonly used alloys in construction, having learned their mechanical characteristics, an assessment was made of the coefficients of efficiency of use for manufacturing small-sized parts [20–22]. The results of calculations according to the proposed formula (1) are given and sorted in descending order of the coefficients of efficiency of use in Table 1.

Using the table data, a visual graph was constructed in descending order of the efficiency of use according to our criteria (Fig. 1).

Alloys AA2024 (D16), EN 46,100 (AK9M2), AA3004 (D12) can be considered the most rational for the conditions under consideration, because they are very common, the strength is sufficient, and relatively cheap.

It was decided to offer our own version of the connector design. The Austrian analogue SHERPA was taken as a basis. The manufacturer claims that SHERPA wood connectors allow efficient and competitive planning and execution of complex tasks in the construction industry. From connections in timber structures through roof and wall elements to mixed and special steel and concrete structures, everything is possible. For a general analysis, 3 variants of our own product design were selected. In particular, a small connector, with dimensions of $40 \times 25 \times 10$ mm, suitable for the safe construction of winter gardens, assembling furniture, sheds for parking lots, stairs, landings, and so forth. Medium, with dimensions of $120 \times 70 \times 14$ mm, and large, $300 \times 120 \times 22$ mm, they can be used in various areas of construction, the choice is wide: from the installation of wooden structures in the construction of roofs and walls to the erection of building structures (Fig. 2).

According to the developed solid models, the approximate mass of each designed part was estimated, taking into account the grade of the aluminum alloy used. The evaluation results are shown in Table 2.

Table 1 Comparative evaluation of the efficiency coefficients for the use of various grades of aluminum alloys

Alloy grade	UTS, MPa	Elongation, %	Average market price of the material, $/kg	Evaluation of the efficiency coefficients
AA2024	420	7	3.2	1.9375
AA2219	440	8	3.33	1.8536
EN 46,100	274	1.5	2.04	1.7157
AA7075	490	4	4.3	1.6498
AA3004	220	3	2.08	1.4211
A13600	235	3	2.36	1.3295
7005	375	8	3.88	1.2889
ZL201	333	4	4.31	1.0659
A03280	284	2	3.33	0.9940
AA6351	315	8	4.09	0.9793
UNI 7369	260	1.5	210	0.8298
A03600	245	1	3.33	0.7083
A04130	157	2	2.36	0.7025
312	265	2	4.09	0.6688
A03550	235	1	3.33	0.6607
AA6060	195	13	2.31	0.5939
AA5005	175	10	2.85	0.5306
A25140	167	1	2.92	0.4493
518.0	225	6	7.69	0.4223
A03560	235	1	4.31	0.4056
AA6061	265	15	3.38	0.3025
AA7049	660	8	21.08	0.2546
A95154	185	12	3.65	0.1627
A05200	314	12	9.48	-0.1166

4   Simulation Results

A real example for modeling connectors from the considered alloys in the Lira software package was the connection of two beams at an angle of 90°. In the selected program, there is no possibility of detailed display, but this does not affect the quality of modeling, since it is possible to set object connections. For the EN 46,100 alloy, the modulus of elasticity is 70000 MPa, the density is 2720 kg/m^3. Set a hard anchor for the connector as if it is attached to another beam and give a load for the large 100 kg/m^2. We carried out the calculation; we are interested in the results for the connector itself. Figures 3, 4 and 5 show normal stress calculations for a large connector.

We set the modulus of elasticity of the alloy AA2024 as 72,000 MPa, density 2670 kg/m^3. Figures 6, 7 and 8 show normal stress calculations for a large connector.
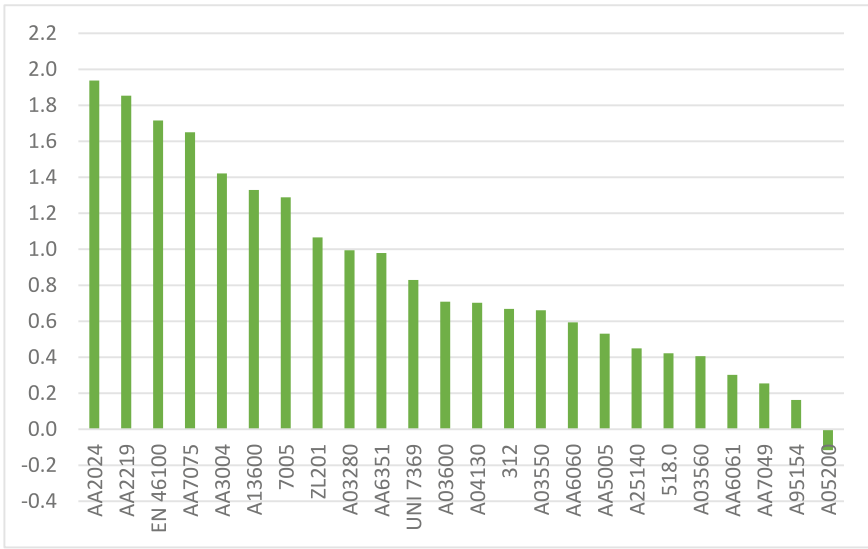
Fig. 1 Graph of a comparative assessment of the efficiency coefficients for the use of various grades of industrial aluminum alloys
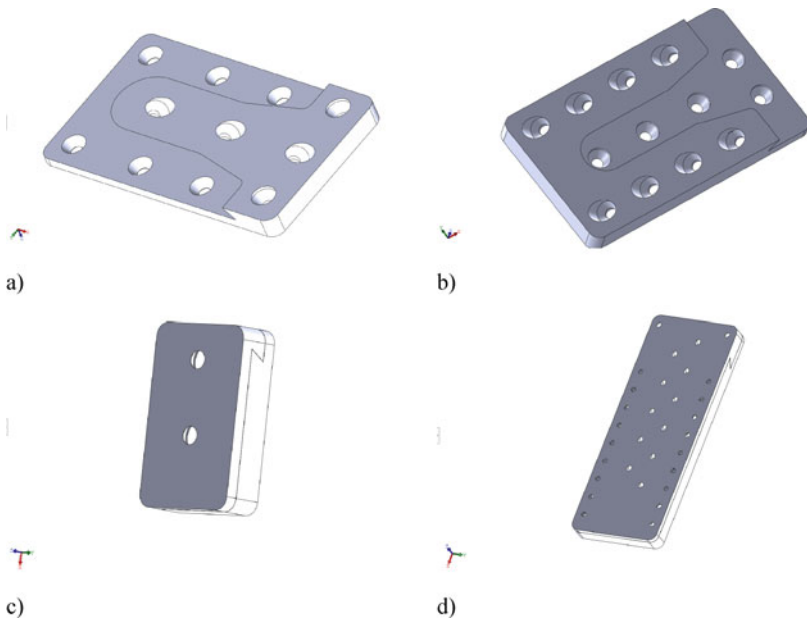
Fig. 2 Type of connector design: **a** 1st half of the middle connector; **b** 2nd half of the middle connector; **c** small connector assembly; **d** large connector assembly

Table 2 Weight of designed connectors, g

| Type of connector	EN 46,100	AA2024	AA3004
small	25.4	24.9	25.4
medium	287	282	287
large	1991.5	1954.9	1991.5
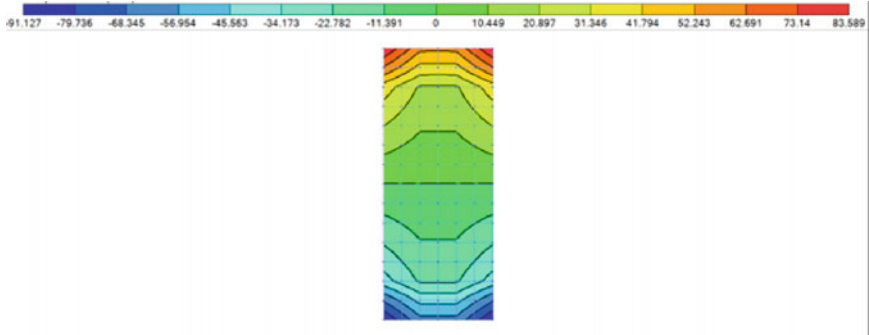
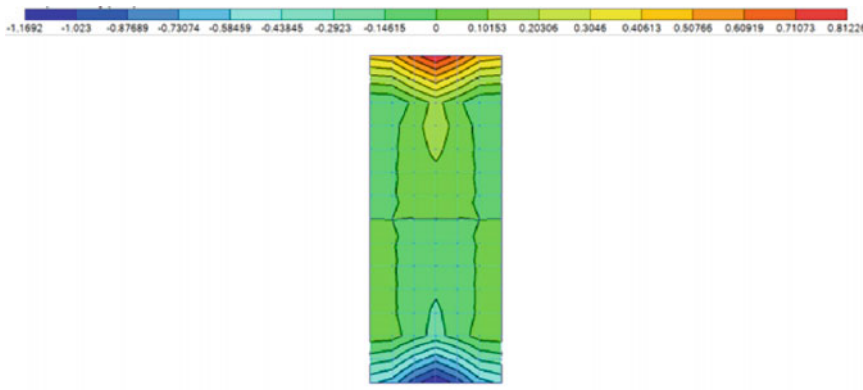**Fig. 3** Calculation of the normal x-axis stress of a large connector in LIRA (Nx stress, MPa)
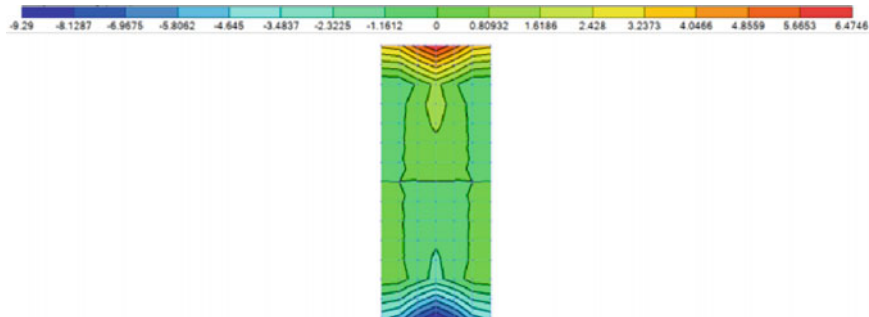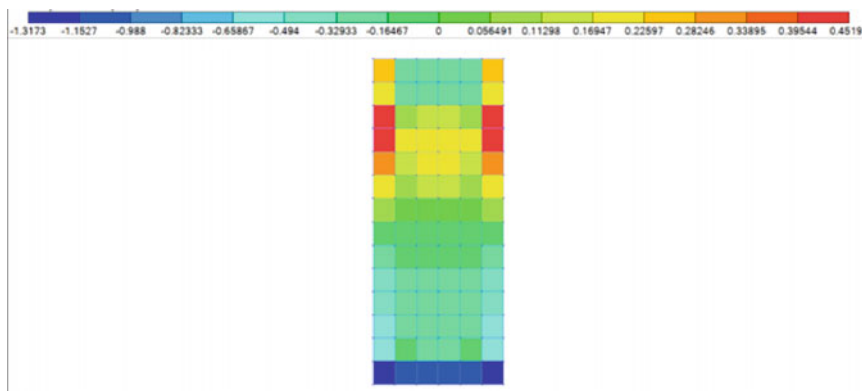

Fig. 4 Calculation of the normal stress along the y-axis of a large connector in LIRA (Ny stress, MPa)
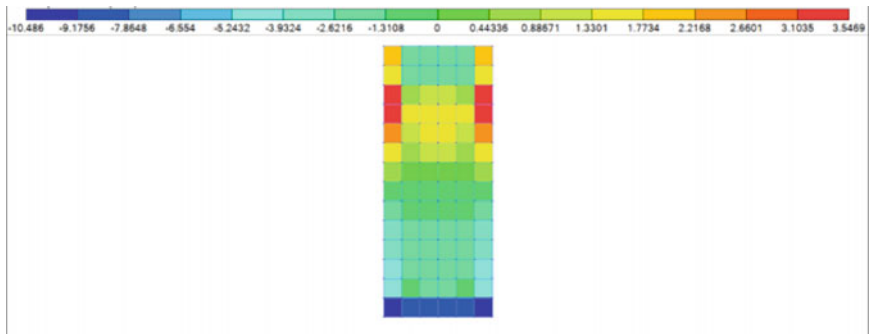
Fig. 5 Calculation of the normal z-stress of a large connector in LIRA (Nz stress, MPa)
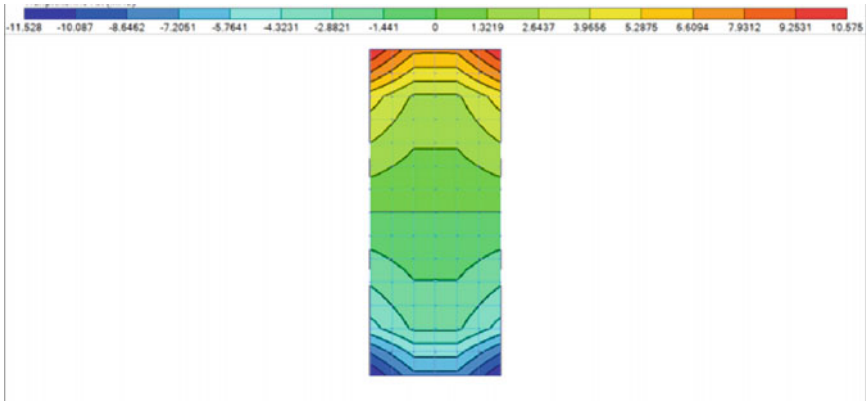
Fig. 6 Calculation of the normal x-axis stress of a large connector in LIRA (Nx stress, MPa)
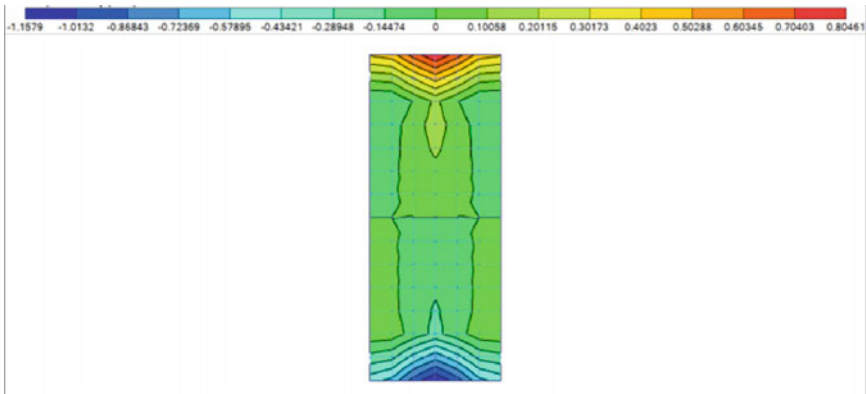
Fig. 7 Calculation of the normal stress along the y-axis of a large connector in LIRA (Ny stress, MPa)
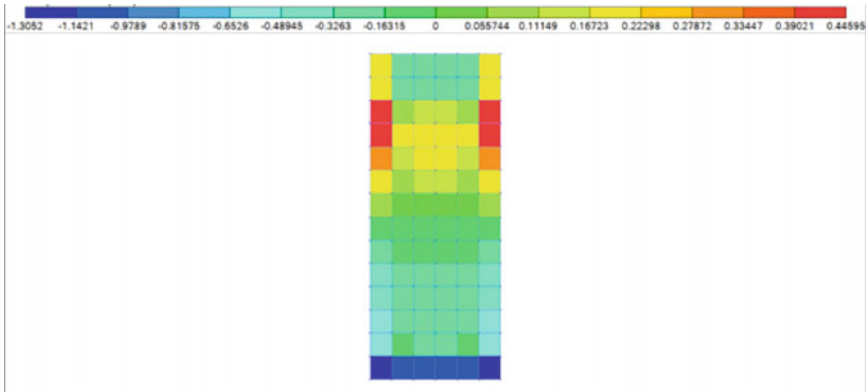
Fig. 8 Calculation of the normal z-stress of a large connector in LIRA (Nz stress, MPa)

We set the modulus of elasticity of the alloy AA3004 (D12) as 68,000 MPa, density 2720 kg/m^3. Figures 9, 10 and 11 show normal stress calculations for a large connector.

The performed calculations show that the products can withstand the maximum load under the accepted operating conditions. The results shown indicate that there is no deformation in the connectors. The conducted studies were carried out with the assumption of a rigid fastening of the connector in the beam's body. In fact, the connectors will be fastened with screws, which will lead to the plastic nature of the destruction, which will begin with the screws being pulled out of the body of the beams, due to which the wood will collapse, while the connectors will not deform at the time of destruction even with rigid termination. Thus, it is possible to use less expensive alloys, such as EN 46,100, for manufacturing connectors, in this case, the use of alloy AA3004 is not appropriate, since it is similar in properties to EN
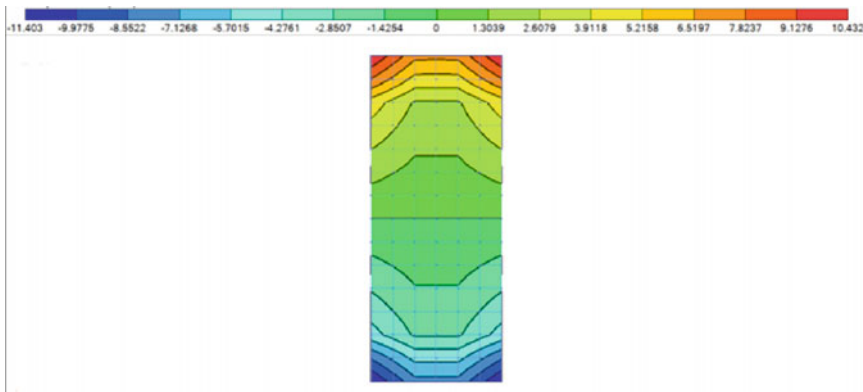
Fig. 9 Calculation of the normal x-axis stress of a large connector in LIRA (Nx stress, MPa)

Fig. 10 Calculation of the normal stress along the y-axis of a large connector in LIRA (Ny stress, MPa)

Fig. 11 Calculation of the normal stress along the z-axis of a large connector in LIRA (Nz stress, MPa)

46,100, but more expensive, and less common on the market, which may lead to supply instability.

5 Conclusions

Based on the analysis of cost indicators and mechanical characteristics, we made a choice of the range of aluminum alloys and composites for manufacturing shaped small-sized building products. A comparative assessment of the use of various grades of alloys by the values of the coefficient of efficiency of use is given. It is shown that, in terms of the combination of technical, economic, and mechanical characteristics, the use of EN 46,100 and AA2024 alloys is promising. Calculations show that the designed products withstand the maximum load under the accepted operating conditions for each type of size, while connectors do not deform, which allows the use of less expensive alloys while maintaining the required bearing capacity.

References

1. Lukin, M., Prusov, E., Roshchina, S., Karelina, M., Vatin, N.: Multi-span composite timber beams with rational steel reinforcements. Buildings (2021). https://doi.org/10.3390/buildings11020046

2. Roschina, S.I., Lisyatnikov, M.S., Lukin, M.V., Popova, M.V.: Technology of strengthening the supporting zones of the glued-wood beaming structure with the application of nanomodified prepregs. Mater. Sci. Forum. **931**, 226–231 (2018). https://doi.org/10.4028/www.scientific.net/MSF.931.226

3. Roshchina, S., Sergeev, M., Lukin, M., Strekalkin, A.: Reconstruction of fixed fertilizer folders in the vladimir region. In: IOP Conference Series: Materials Science and Engineering (2018). https://doi.org/10.1088/1757-899X/463/4/042011

4. Lisyatnikov, M.S., Glebova, T.O., Ageev, S.P., Ivaniuk, A.M.: Strength of wood reinforced with a polymer composite for crumpling across the fibers. In: IOP Conference Series: Materials Science and Engineering (2020). https://doi.org/10.1088/1757-899X/896/1/012062

5. Gonshakov, A., Gonshakov, N., Popova, M., Medvedev, E., Popova, O.: Lightweight Construction Formed on the Basis of a Typical Reinforced Concrete Lattice Beam, pp. 1450–1458 (2022). https://doi.org/10.1007/978-3-030-96383-5_162

6. Lisyatnikov, M., Lukina, A., Chibrikin, D., Labudin, B.: The strength of wood-reinforced polymer composites in tension at an angle to the fibers. In: Lecture Notes in Civil Engineering, vol. 182, pp. 523–533 (2022). https://doi.org/10.1007/978-3-030-85236-8_46

7. Roschina, S.I., Lisyatnikov, M.S., Koshcheev, A.A.: Technical- and- economic efficiency of reinforced wooden structures. IOP Conf. Ser. Mater. Sci. Eng. **698**, 022005 (2019). https://doi.org/10.1088/1757-899X/698/2/022005

8. Roschina, S., Gribanov, A., Lukin, M., Lisyatnikov, M., Strekalkin, A.: Calculation of wooden beams reinforced with polymeric composites with modification of the wood compression area. In: MATEC Web of Conferences (2018). https://doi.org/10.1051/matecconf/201825104029

9. Koscheev, A.A., Lukin, M. V., Roshchina, S.I.: Investigation of glued in bars strength and deformability indexes within framework of research of wood reinforcement with cable reinforcement. In: IOP Conference Series: Materials Science and Engineering (2019). https://doi.org/10.1088/1757-899X/687/3/033023

10. Lisyatnikov, M.S., Shishov, I.I., Sergeev, M.S., Hisham, E.: Precast monolithic coating of an industrial building based on variable-height beam-slabs. In: IOP Conference Series: Materials Science and Engineering (2020). https://doi.org/10.1088/1757-899X/896/1/012064

11. Repin, V., Grinyov, V.: The Experience in Automating Scientific Research to Identify Dangerous Zones in the Near-Support Sections of Wooden Beams, pp. 1230–1238 (2022). https://doi.org/10.1007/978-3-030-96383-5_137

12. Lisyatnikov, M., Glebova, T., Rusak, K., Ivaniuk, A.: Strength and deformability of reinforced wooden beams of variable stiffness. In: Lecture Notes in Civil Engineering, vol. 182, pp. 549–561 (2022). https://doi.org/10.1007/978-3-030-85236-8_48

13. Strekalkin, A., Koshcheev, A., Roshchina, S., Naichuk, A.: Dowel connections with local wood modification. In: Lecture Notes in Civil Engineering, vol. 182, pp. 385–392 (2022). https://doi.org/10.1007/978-3-030-85236-8_35/TABLES/2

14. Naka, T., Odani, R., Aoki, K., Inayama, M.: Study on assurance design method of connections at the bottom of columns in wooden wall structure (part 1): proposal of design flow for connections and experimental and analytical study on the modeling of vertical structural plane. J. Struct. Constr. Eng. **87**, 116–127 (2022). https://doi.org/10.3130/AIJS.87.116

15. Naka, T., Odani, R., Murakami, M., Kamachi, K., Aoki, K., Inayama, M.: Study on assurance design method of connections at the bottom of columns in wooden wall structure (part 2): proposal of a classification method of connection and a calculation method of rocking behavior. J. Struct. Constr. Eng. **87**, 622–633 (2022). https://doi.org/10.3130/AIJS.87.622

16. Bian, Z.H., Wang, T.C., Zhao, S.Y., Li, X.G.: A study on node connection technology of wood structure. Appl. Mech. Mater. **405–408**, 3094–3098 (2013). https://doi.org/10.4028/WWW.SCIENTIFIC.NET/AMM.405-408.3094

17. Sergeev, M., Lukina, A., Shunqi, M., Glebova, T., Kryukov, A.: Work of wood-composite beams in panel floors of prefabricated buildings. In: Lecture Notes in Civil Engineering, vol. 182, pp. 493–499 (2022). https://doi.org/10.1007/978-3-030-85236-8_44

18. Mirsaidov, M., Abdikarimov, R., Khodzhaev, D., Normuminov, B., Roshchina, S., Vatin, N.: Nonlinear vibrations of an orthotropic viscoelastic rectangular plate under periodic loads. In:

Lecture Notes in Civil Engineering, vol. 182, pp. 139–147 (2022). https://doi.org/10.1007/978-3-030-85236-8_11

19. Romanovich, A., Lisyatnikov, M., Vlasov, A., Aleksiievets, V.: Geodesic Domes with Installing Floor Using a Cable Stay System, pp. 1459–1466 (2022). https://doi.org/10.1007/978-3-030-96383-5_163

20. Davis J. R.: Aluminum and Aluminum Alloys Introduction and Overview, pp. 351–416 (2001). https://doi.org/10.1361/autb2001p351.

21. Aluminum Properties and Chemical Composition of Alloys. https://unitedaluminum.com/aluminum-technical-data-alloy-chmeistry-and-mechanical/. Accessed 16 May 2022

22. Grade Steel and Alloys. http://www.splav-kharkov.com/main.php. Accessed 16 May 2022

Mechanical Behavior of Aluminum Matrix Composites in the Elements of Building Structures

Dmitriy Reva , **Mikhail Lisyatnikov** , **and Evgeny Prusov**

Abstract Prospects for the application of aluminum matrix composites as a material for building structure are considered and analyzed in the context of current trends in the development of the construction industry. The possibility of replacing standard aluminum alloys with aluminum matrix composites in the manufacture of small-sized parts for building structures is considered, using the example of connectors. The selection of a composite for modeling was carried out, three-dimensional models were developed, and the stress–strain state was calculated in the LIRA software package under the condition of rigid fastening, taking into account the loading conditions. Analysis of the results of computer simulation of the mechanical behavior of aluminum matrix composites as part of a real building structure confirms that they perceive the applied load without deformation and destruction.

Keywords Aluminum matrix composites · Building structures · Mechanical behavior · Stress–strain state · Computer modeling of structures

1 Introduction

In recent years, one of the pronounced trends in the development of the construction industry around the world is the development and implementation into production of new lightweight and durable structural materials [1–3]. Using aluminum alloys in the elements of building structures allows to significantly reduce the weight of structures and their parts as compared to the steel or reinforced concrete, as well as reduce the total material consumption of structures [4, 5]. Among other things, it contributes to improved transportability and simplicity of installation of structural elements and, as a consequence, reduces the overall construction time. In many cases, the use of aluminum alloys can improve the corrosion resistance of building structures and extend their service life, as well as reduce operating costs [6–8]. In

D. Reva (✉) · M. Lisyatnikov · E. Prusov

Vladimir State University named after Alexander and Nikolay Stoletovs, 87 Gorky St., Vladimir 600000, Russian Federation

e-mail: reva-dima@mail.ru

a number of areas of industrial and civil engineering, aluminum alloys have long been successfully competing with steel, primarily in various marine structures and waterworks, bridges, earthquake resistant structures [9–12].

At the same time, aluminum products cannot always meet the strength and stiffness requirements for building structures, so their use in many areas is limited, despite the many potential advantages. In addition, the strength and stiffness of non-reinforced aluminum alloys decrease very quickly at elevated temperatures, for example, under fire conditions [13–15]. In this regard, it is of considerable interest to assess the possibility of using aluminum matrix composites for elements of light building structures, in comparison with aluminum alloys, which provide an increase in stiffness and damping characteristics, an increase in resistance to elevated temperatures, a decrease in the thermal expansion coefficient and the overall material consumption of products [16–18].

However, aluminum matrix composites, despite their obvious advantages, have a relatively high price in comparison with traditional materials. This is due to the high cost of the reinforcing components used, the more complex and multistage technological process for obtaining products, as well as the difficulties in subsequent processing. These aspects are among of the reasons for the limited use of these promising materials. Improvement of technological processes of production of aluminum matrix composites and the selection of cost-effective reinforcing components will contribute to the expansion of their use in various fields. At the same time, one of the questions requiring the decision for the reasonable use of aluminum matrix composites at manufacturing of elements of building structures is the study of their mechanical behavior in the structure's composition.

Thus, considering the identified trends and problematic issues, priority should be given to assessing the potential possibility of replacing traditional materials with aluminum matrix composites, which are characterized by low weight, increased strength and thermal resistance compared to many standard materials, including non-reinforced alloys. The production of small-sized building parts from aluminum matrix composites, included in the work in the wooden structures, has significant potential. To create competitive products from aluminum matrix composites, it is required to simulate and analyze their mechanical behavior in the calculation systems. The present work is devoted to the solution of this issue using the example of connectors for wooden structures.

2   Materials and Methods

Figure 1 compares the tensile strength of aluminum matrix composites of various compositions with standard grade A04130 aluminum alloy used as the matrix material. The given values were systematized by one of the authors of this paper based on the results of searches in specialized databases, reviews and scientific papers, as well as considering information provided by various manufacturers. The collected data
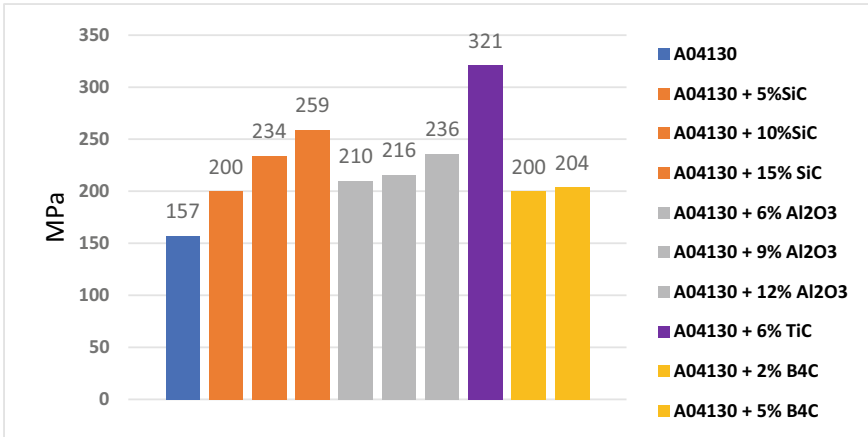
Fig. 1 Comparison of tensile strength of aluminum matrix composites with standard grade aluminum alloy A04130

were compared and critically analyzed; in the case of discrepancies in the reported values for the same position, the average value of the strength is given.

The accumulated experience in obtaining aluminum matrix composites with various reinforcements indicates that the addition of dispersed reinforcing particles increases the strength by 30% or more of the same indicator of the standard A04130 alloy. SiC powdered particles are the most widespread as a reinforcing component in obtaining aluminum matrix composites, largely due to the fact that with a sufficiently good reinforcing effect they are widely used in industry and have a low cost. In this work, the composition A04130 + 10 vol.% SiC was set to analyze the mechanical behavior of aluminum matrix composites. We considered small-sized building products in the form of connectors used in the assembly of wooden structures. In our previous exploratory tests, aluminum connector designs have been developed for various types of structures. A three-dimensional model of the connectors of the proposed design was developed in SolidWorks software, Fig. 2 shows the models of a small, medium and large connector, the latter is shown separately in halves.

The estimated weight of the connectors is shown in Table 1.

The simulation of the mechanical behavior of the developed aluminum matrix composite connectors was carried out in the LIRA 10.10 software package (LIRA soft, Moscow).

3   Results and Discussion

A real example for simulation was the connection of two wooden beams at an angle of 90° using the considered types of aluminum matrix composite connectors. In the selected software, there is no possibility of detailed imaging, but this does not
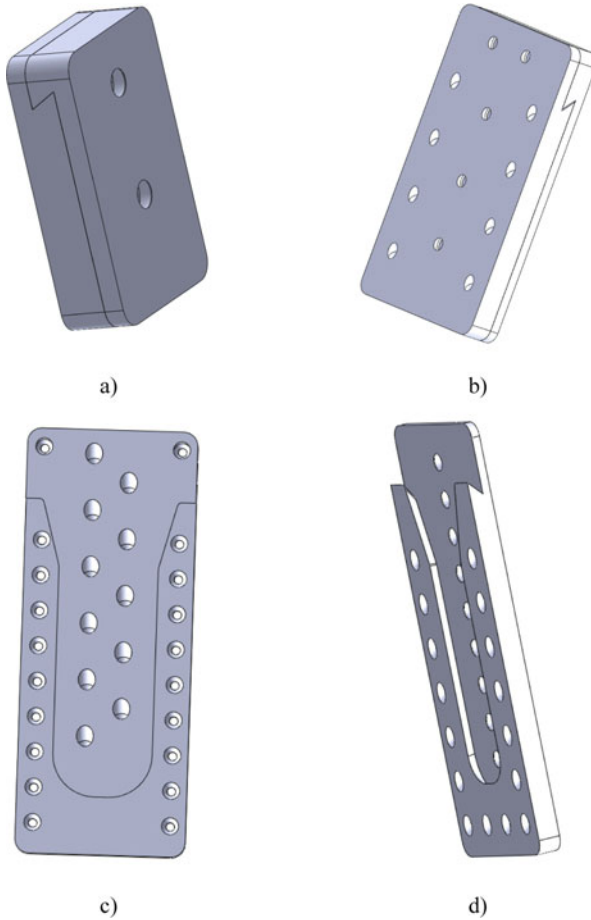
Fig. 2. 3D models of connectors: a) small connector; b) medium connector; c) 1st half of the large; d) 2nd half of the large connector

Table 1 Weight of aluminum matrix composite connectors

Connector model	R small	R medium	R large
Weight, g	26.6	300.7	2086.7

affect the overall simulation results, since it is possible to set and analyze object relationships. The connectors were depicted according to the dimensions: small $40 \times 25 \times 10$ mm, medium $120 \times 70 \times 14$ mm, and large $300 \times 120 \times 22$ mm. The calculated modulus of elasticity of the aluminum matrix composite (A04130 + 10 vol.% SiC) was set to 103,000 MPa, and density was set to 2850 kg/m^3. The following loading parameters were set: 50 MPa for a small connector, 75 MPa for a medium connector, and 100 MPa for a large connector. Figures 3, 4, 5, 6, 7, 8, 9,

10 and 11 show the calculated shift relative to the initial fixation and normal stress calculations for the considered types of connectors.

Analysis of the results of computer simulation of the mechanical behavior of aluminum matrix composites as part of a real building structure confirms that they perceive the applied load without deformation and destruction. Thus, the use of aluminum matrix composites instead of traditional aluminum alloys opens up additional opportunities for improving the performance characteristics of architectural and building structures, as well as engineering structures for various functional purposes, primarily as a material for small-sized building products. At the same time, it is assumed that such an approach will make it possible to overcome the main disadvantages that limit the use of aluminum structures, in particular, insufficient stiffness and mechanical characteristics, a high coefficient of thermal expansion, as well as increased material consumption (due to the selection of reinforcing components from among non-deficient materials and the widespread use secondary raw materials). The reasonable use of aluminum matrix composites to solve the identified problems requires the development of a set of technical, economic and engineering
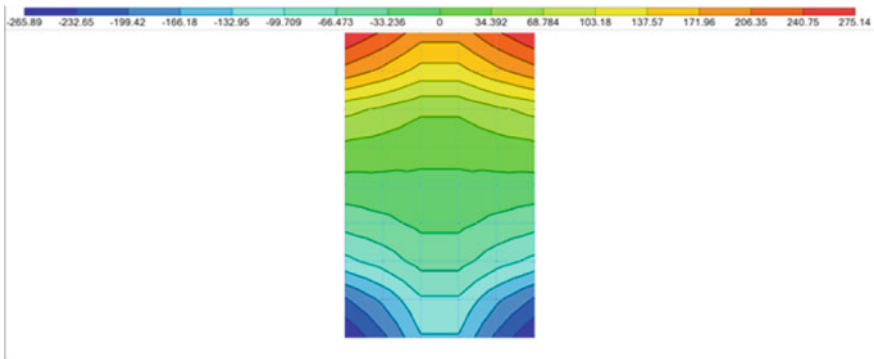
Fig. 3 Calculation of the normal x-axis stress of a small connector in LIRA (Nx stress, MPa)
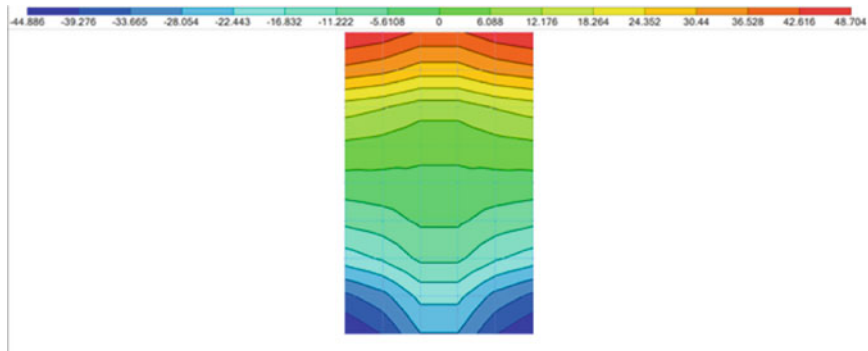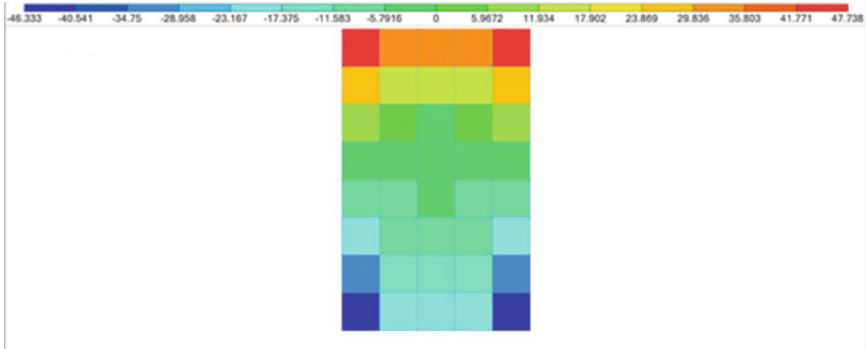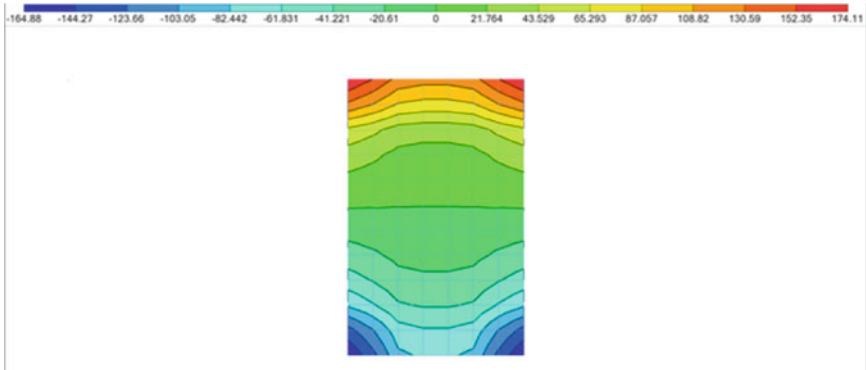

Fig. 4 Calculation of the normal y-axis stress of a small connector in LIRA (Ny stress, MPa)
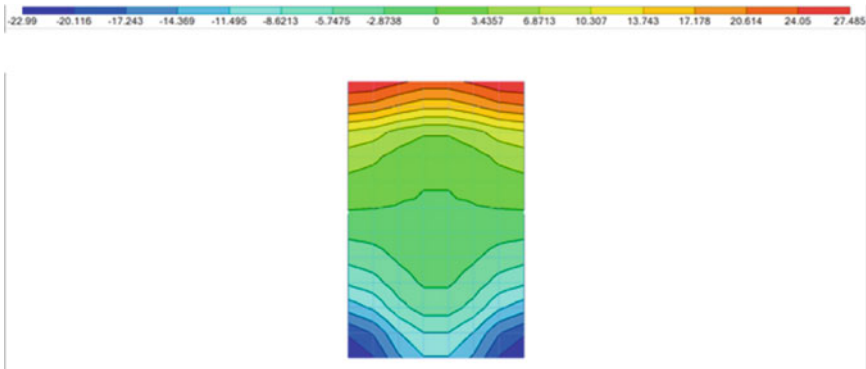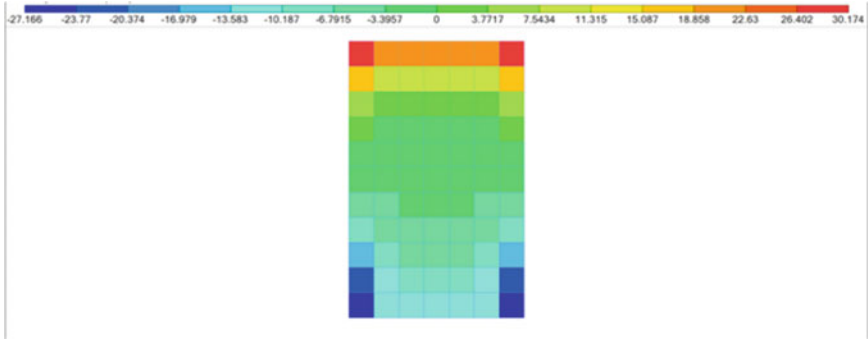
Fig. 5 Calculation of the normal z-axis stress of a small connector in LIRA (Nz stress, MPa)
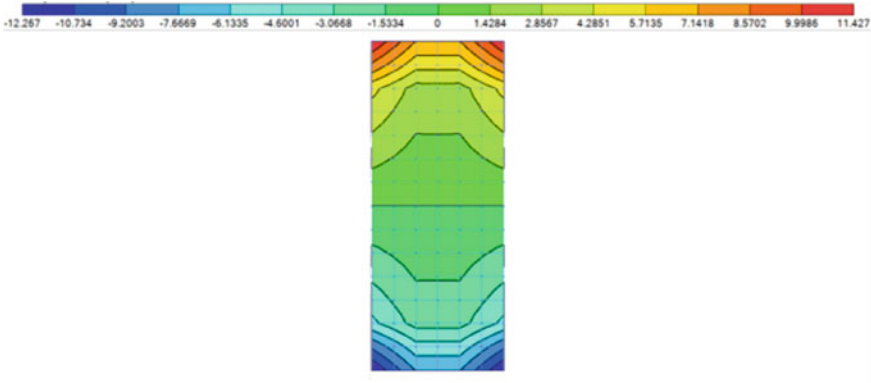

Fig. 6 Calculation of the normal x-axis stress of a medium connector in LIRA (Nx stress, MPa)
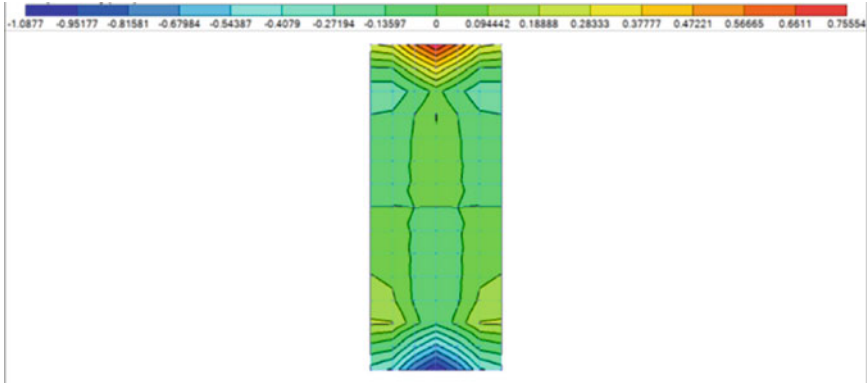

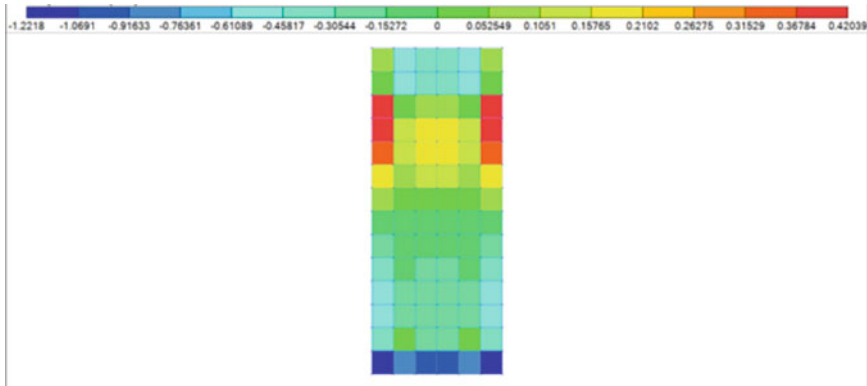**Fig. 7** Calculation of the normal y-axis stress of a medium connector in LIRA (Ny stress, MPa)

Fig. 8 Calculation of the normal z-axis stress of a medium connector in LIRA (Nz stress, MPa)

Fig. 9 Calculation of the normal x-axis stress of a large connector in LIRA (Nx stress, MPa)

Fig. 10 Calculation of the normal y-axis stress of a large connector in LIRA (Ny stress, MPa)

Fig. 11 Calculation of the normal z-axis stress of a large connector in LIRA (Nz stress, MPa)

criteria for the selection of components and optimization of technological solutions for the production of parts from composite materials for the manufacture of elements of building structures.

4 Conclusions

The performed calculations show that aluminum matrix composite connectors can be used as an effective alternative to standard aluminum alloys in the manufacture of connectors for building structures, since they can carry a large load without deforming even at maximum loads in the accepted operating modes.

References

1. Khedari, J., Suttisonk, B., Pratinthong, N., Hirunlabh, J.: New lightweight composite construction materials with low thermal conductivity. Cement Concr. Compos. **23**(1), 65–70 (2001)
2. Czarnecki, L., Hager, I., Tracz, T.: Material problems in civil engineering: ideas-driving forces-research arena. Procedia Eng. **108**, 3–12 (2015)
3. Ha, N.S., Lu, G.: A review of recent research on bio-inspired structures and materials for energy absorption applications. Compos. B Eng. **181**, 107496 (2020)
4. Sharp, M.L.: Behaviour and Design of Aluminium Structures. McGraw-Hill, New York (1992)
5. Mazzolani, F.M.: Aluminium Structural Design. Springer, Wien (2003)

6. Strąk, A., Małek, M., Chlanda, A., Sudoł, E.: The impact of temperature and mechanical load on corrosion resistance of anodized aluminum EN AW-6063 (T6 temper) alloy for potential architectonic application. J. Build. Eng. **50**, 104128 (2022)

7. Rong, B., Guo, Y., Li, Z.: Study on the stability behavior of 7A04-T6 aluminum alloy square and rectangular hollow section columns under axial compression. J. Build. Eng. **45**, 103652 (2022)

8. Rong, B., Zhang, S., Zhang, Y., Liu, H., Li, Z.: Study on the ultimate bearing capacity of 7A04-T6 CFAT columns under eccentric compression. J. Build. Eng. **46**, 103654 (2022)

9. Okura, I.: Application of aluminium alloys to bridges and joining technologies. Weld. Int. **17**, 781–785 (2003)

10. Soetens, F.: Aluminium structures in building and civil engineering applications. Struct. Eng. Int. **20**(4), 430–435 (2010)

11. Siwowski, T.: Aluminium bridges – past, present and future. Struct. Eng. Int. **16**(4), 319–326 (2006)

12. Wang, Z., Wang, Y., Li, B., Zhang, Y.: Experimental and numerical study on seismic behaviour of aluminium alloy frames. J. Build. Eng. **50**, 104231 (2022)

13. Maljaars, J., Soetens, F., Katgerman, L.: Constitutive model for aluminium alloys exposed to fire conditions. Metall. Mater. Trans. A **39**, 778–789 (2008)

14. Maljaars, J., Twilt, L., Soetens, F.: Flexural buckling of fire exposed aluminium columns. Fire Saf. J. **44**, 711–717 (2009)

15. Maljaars, J., Soetens, F., Snijder, H.H.: Local buckling of fire exposed aluminium members – a new design model. J. Struct. Eng. **136**, 66–75 (2010)

16. Panfilov, A., Prusov, E.: Current state and trends of development of aluminum matrix composite alloys. In: Proceedings of METAL 2013 – 22nd International Conference on Metallurgy and Materials, pp. 1195–1199. Tanger Ltd., Brno (2013)

17. Prusov, E., Deev, V., Rakhuba, E.: Effect of superheat melt treatment on structure and mechanical properties of in-situ aluminum matrix composites. In: Proceedings of METAL 2018 – 27th International Conference on Metallurgy and Materials, pp. 1358–1362. Tanger Ltd., Brno (2018)

18. Garg, P., Jamwal, A., Kumar, D., Sadasivuni, K.K., Hussain, C.M., Gupta, P.: Advance research progresses in aluminium matrix composites: manufacturing & applications. J. Mater. Res. Technol. **8**(5), 4924–4939 (2019)

Composites for Bricklaying and Decorative Elements

Lubov Zakrevskaya and **Ksenia Nikolaeva**

Abstract The object of the study is the building materials of a building that is subject to restoration. Laboratory studies were carried out, during which the physical and mechanical properties of the studied materials were determined: density, compressive strength, humidity. X-ray phase analysis and scanning electron microscopy give an idea of the chemical composition and microstructure of materials. During the work, the compositions of restoration compositions for bricks and decorative concrete elements (balusters, cornices) were developed. In the course of laboratory studies, a composite for the restoration of brickwork and a composition of fiber concrete for the restoration of architectural elements of a building with the addition of asbestos fibers was obtained, which has the following characteristics: dry matter density of 1.83 g/cm^3, compressive strength of 45.2 MPa, elastic modulus of 0.95 MPa, thermal conductivity of 0.65 W/(m · C), frost resistance F75. Asbestos fibers are the optimal reinforcing element of fiber concrete, composites with the addition of chrysotile have a strong energy bond along the fibers, which provides greater tensile strength. The resulting material is resistant to chemical influences, since chrysotile, unlike many other fillers, does not dissolve in an alkaline environment. Surfactant P-17 in the compositions of the obtained composites contributes to the optimization of their physical, mechanical and operational properties, and also meets modern requirements for environmental safety.

Keywords Restoration · Brickwork · Mineral mortar · Fiber concrete · Chrysotile-asbestos · Physical and mechanical characteristics · Surfactants

1 Introduction

There are many studies in the field of masonry restoration, which describe in detail various methods of its restoration [1–5]. One of the most effective methods is the method of recoveries brickwork. It is well known that when restoring architectural

L. Zakrevskaya (✉) · K. Nikolaeva
Vladimir State University, Gorky Str., 87, Vladimir 600000, Russian Federation
e-mail: lvzak@mail.ru

monuments, materials should be used that are similar in composition, physical and mechanical properties to the original materials. Also, during the restoration, it is important to preserve the masonry technique that was used during the construction of the reconstructed structure. According to studies [6, 7], the method of bricklaying allows to preserve the original materials in their original form, since special modified mineral solutions are used to restore the bricklaying, which correspond to the original material in composition and physical and mechanical properties.

The study [8] describes the technology of restoration of brickwork, and what materials are needed to perform a particular technological operation. Also, there are no compositions of modified mineral solutions for restoration in the work. In the study [9], the injection method is considered in the most detail. However, with many advantages of this method, it is quite problematic to reproduce the technique of old masonry when using it. For the correct organization and execution of works on the reconstruction of brickwork, it is necessary to know the main factors leading to its destruction. Thanks to the research [8–10], factors affecting the durability and suitability of brickwork have been formed. The aggressive impact of the urban environment, the vital activity of living organisms and temperature changes caused by the influence of solar radiation negatively affect the condition of the masonry. It is also important to remember that when water penetrates into the joints of the masonry in the structure, there is a violation of the integrity due to freezing and thawing [9].

Facade decor made of concrete has been used in construction for a long time, but facade decorative elements are destroyed over time. When restoring decorative elements from concrete, the most effective solution is the use of architectural fiber concrete, this material is modern and quite common in construction [11]. Fiber-reinforced concrete has a number of features, thanks to which this material is effective and durable. Fiber-reinforced concrete facades have higher strength characteristics compared to traditional concrete, as well as greater opportunities for creating decorative elements of complex shape and resistance to external influences for a long time [12, 13].

The appearance of decorative elements made of fiber-reinforced concrete does not depend on weather conditions. This is largely due to the fact that the coefficient of linear expansion of fiber concrete practically does not differ from the similar indicator of the material of the external walls to which the decor or decoration is attached. This is an important quality for facade elements made of fiber concrete, since all types of loads that a building experiences are equally distributed between all its parts, including decorative elements.

Almost any type of material can act as a micro-reinforcing element. In this paper, it is proposed to use asbestos fiber as a reinforcing element. In studies [14–17, 20], chrysotile fibers are considered as an optimal reinforcing element, and the mechanism of interaction of the components of fiber concrete is also described. At the same time, the compositions of fiber concrete with chrysotile fibers as a reinforcing element are not presented. One of the important properties of chrysotile is its resistance to aggressive alkaline environment.

2   Materials and Methods

The object of the study is the construction materials selected at the restoration object – Voronov's dacha. The studied samples are ceramic bricks, concrete balusters. The samples selected for the study are shown in Figs. 1 and 2.

Table 1 shows the physical and mechanical properties of the materials under study: concrete balusters and ceramic bricks.

Physical and technical properties were studied according to standard methods. The density of the samples was measured by the hygrostatic method, the strength was measured by the non-destructive method using the strength meter of building materials IPS-MG4. 036. The humidity of the samples was obtained by using the Protymeter MMS Plus moisture meter (manufacturer "GE Protimeter", Ireland).

The chemical composition and microstructure of the starting materials were studied using X-ray phase analysis and electron microscopy on a Bruker AXS D8 ADVANCE powder diffractometer (model D8, manufacturer: Bruker Optik GmbH,

Fig. 1 Samples selected for the stud concrete balusters
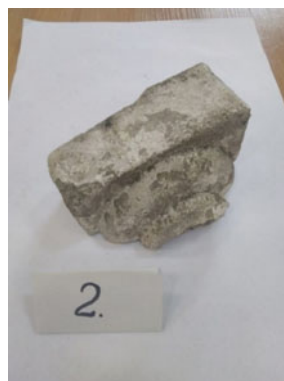
Fig. 2 Samples selected for the study ceramic bricks

**Table 1** Physical and mechanical characteristics of the materials under study

Sample name	Name of properties			Notes, explanations
	Density, g/cm^3	Compressive strength, MPa	Humidity, % by weight	
Concrete balusters	2.06	37	2.2	The material is in working condition, suitable for further use, taking into account the restoration
Ceramic brick	1.73	15.8	2.5	The material is in working condition, suitable for further use, taking into account the restoration

Germany) and a FEI Quanta 200 3D scanning electron microscope (manufacturer: FEI, United States of America).
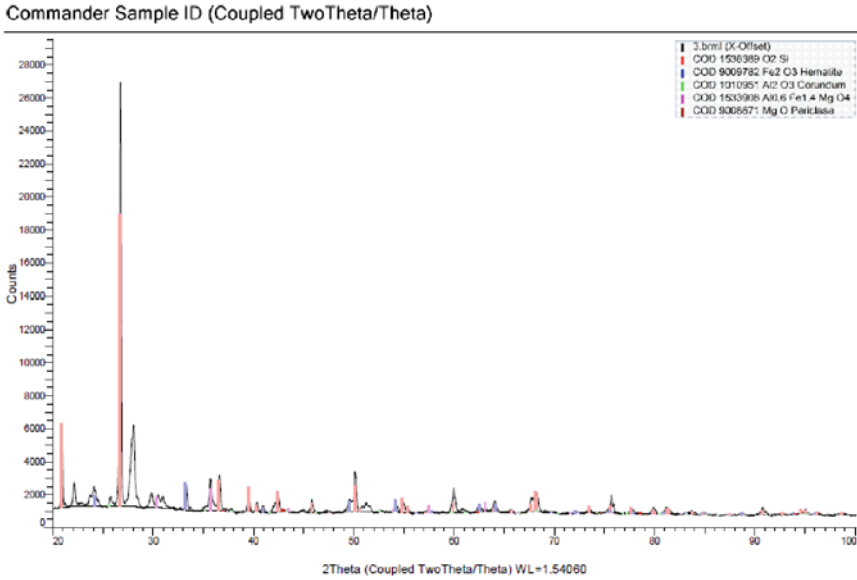
3 Results and Discussions

The results of the X-ray phase analysis are presented in Figs. 3 and 4.
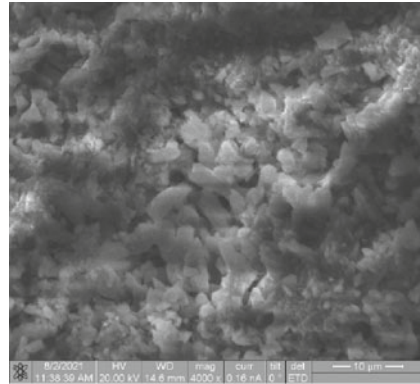
Figures 5 and 6 shows the results of electron microscopy.
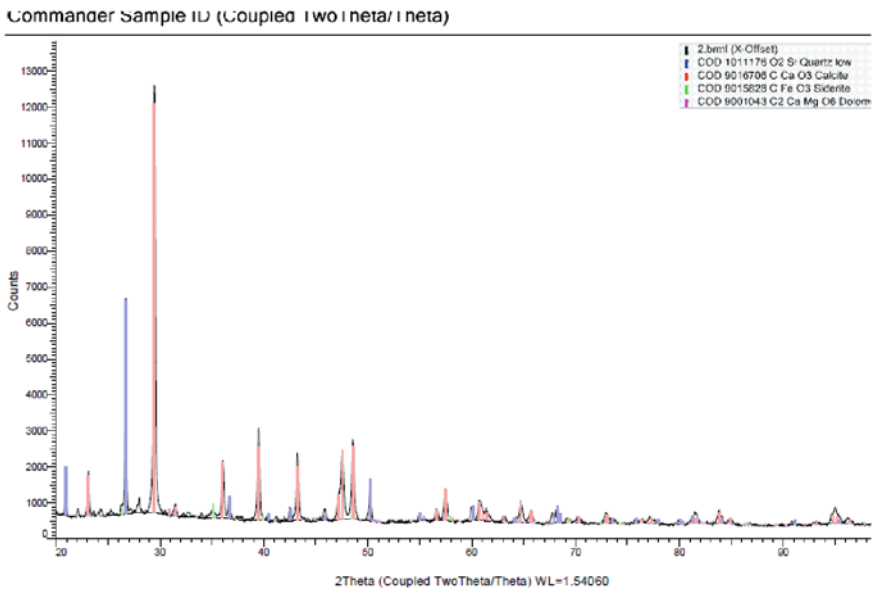
Fig. 3 Results of X-ray phase analysis of sample No. 1 – concrete balusters

Commander Sample ID (Coupled TwoTheta/Theta)

Fig. 4 Results of X-ray phase analysis of sample No. 2 – ceramic brick

Fig. 5 The results of electron microscopy of the selected samples concrete balusters


The following materials are used for the restoration of brickwork: gray portland cement; brick chips (0.01–0.25 mm, 0.5–1 mm); superplasticizer P-17; water for sealing; pigment (if the brickwork is not subject to finishing and painting).

According to the results of laboratory studies, the composition of a modified mineral solution was developed, which is used for the restoration of brickwork. The composition of the mineral solution is shown in Table 2.

The technology of restoration and repair of architectural concrete is selected taking into account the purpose and degree of loading of the structure, the degree of damage, environmental conditions, aesthetic requirements for the object. Table 3 shows the

Fig. 6 The results of
electron microscopy of the
selected samples ceramic
bricks
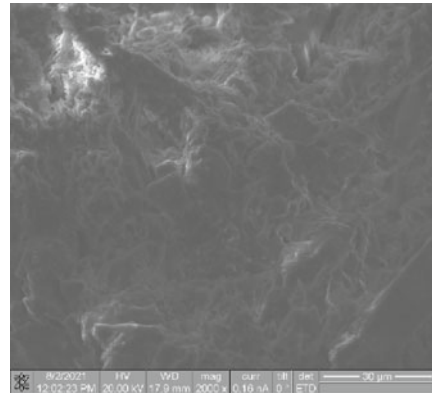
Table 2 Composition of the modified mineral solution for the restoration of brickwork

Serial number	Components	Composition of the composition in weight parts
1	Grey Portland cement M-400	1.0
2	Brick chips of the fraction: 0.01–0.25 mm (60%) 0.5–1.0 mm (40%)	4.0 2.4
3	Superplasticizer P-17	0.01
4	Water	1.0–1.1

composition of fiber concrete, which is used in the restoration of architectural elements of buildings.

Table 4 shows the physical, mechanical and operational properties of the resulting material.

Chrysotile forms micro-reinforcement in the composite due to its structure – the thinnest tubes, which can be attributed to natural nanostructured materials. A characteristic feature of the material with the addition of chrysotile is a powerful bond along the fiber, which is confirmed by high values of the average elastic modulus (about 20 000 MPa) and tensile strength (about 400 kg/mm^2). They are also characterized by high chemical resistance and low thermal conductivity and favorably differ from CNTs by a well-defined orientation [15, 18–20].

Table 3 Composition of fibro concrete on asbestos fiber

Composition	The content of components, masses.%				
	Portland Cement	Silica component	Fiber (asbestos fiber)	Superplasticizer P-17	Water
FBA-1	49	23	8	0.55	19.45
FBA-2	50	20	10	0.5	19.5
FBA-3	51	19	12	0.65	17.35

Table 4 Physical, mechanical and operational properties of the obtained material

Name of material properties	Composition		
	FBA-1	FBA-2	FBA-3
Dry matter density, g/cm^3	1.75	1.83	1.79
Compressive strength, MPa	35.4	44.8	33.6
Modulus of elasticity, MPa	0,4	0.95	0.88
Thermal conductivity, W/(m · °C)	0.56	0.65	0.62
Frost resistance	F50	F75	F50

The rational choice of surfactants is of great importance in optimizing the properties of the developed composite. A polycarboxylate superplasticizer (PKS) of the Makromer brand was used in the work, since plasticizing additives of the C-3 type do not meet the requirements for environmental safety. The use of PKS contributes to the production of composites with low creep under load. The minimum dosages of PKS ensure a high density of fiber-concrete mixtures and increase their operational characteristics. According to the results of the studies shown in Table 4, the composition of fiber concrete FBA-2 has the best indicators.

4 Conclusions

According to the results of the study, it can be concluded that the material of sample No. 1 (concrete baluster) consists of calcium hydrosilicates, quartz and carbonates in the form of dolomite and siderite. The reactions of silicate formation went through to the end, the material gained the maximum possible strength.

Sample No. 2 (ceramic brick) includes clay minerals and quartz.

According to the results of electron microscopy, the material of sample No. 1-a concrete baluster, at an increase of 4000 times, is represented by a fine-grained structure of cement hydration products, the volume is permeated with pores. According to the results of the research, it can be concluded that the material of sample No. 2 (ceramics) is dense, of a homogeneous structure.

During the research, a modified mineral solution was developed for the restoration of brickwork. To prepare this solution, the following technological operations must be performed: weigh the dry components of the mixture on a technical scale, and then place them in a container for dry mixing; mix the dry components of the mixture thoroughly; weigh the required amount of polycarboxylate superplasticizer, dose the required amount of water into a special container, place the additive (superplasticizer P-17) in it and mix thoroughly.; add the cement and brick chips in portions to the dry mixture, and then add water and mix thoroughly for 15 min until smooth. The mixture should be thoroughly mixed and not contain unevenly mixed parts of cement, brick chips and pigment, the mixture should be plastic during restoration work. The granulometric composition of the mixture should not change during mixing; after

mixing, the composition is discharged into an intermediate container, and it can be used for work. It should not be stored for more than 2 h from the moment of preparation, when stored for two hours, it must be periodically mixed to preserve plasticity.

As a result of the research, the composition of fiber concrete based on asbestos fiber was developed, which is an innovative and durable material that is not prone to cracking, like most modern architectural concretes. Thanks to the chrysotile fibers, this material is frost-and heat-resistant, has low thermal conductivity and has sufficient resistance to aggressive environmental conditions and has high tensile strength.

References

1. Anikanova, L., Dizendorf, T., Loskutov, O., Nikitina, O., Baigulova, I.: Methods of restoration of brickwork of old buildings. Constr. Mater. Equip. Technol. XXI Century **5**, 42–43 (2010)
2. Serikova, L., Lapunova, K.: Technologies of restoration of a bricklaying. Sci. Almanac **4–3**(42), 85–87 (2018)
3. Evseev, E.: The evolution of construction technologies in the context of the history of architecture of the XIX century: restoration aspect. Bulletin of the International Institute of Antiques ASG MIR **3**, 86–92 (2016)
4. Sosenko, A., Kotlyar, V., Cherevkova, Y.: Restoration of buildings made of ceramic bricks. Constr. 2015 Modern Probl. Constr. **2**, 463–465 (2015)
5. Anikanova, L., Volkova, O., Kurmangalieva, A., Volkov, K.: Research of fluoroanhydrite raw materials for obtaining composite binders. Vest. Tomsk. Gos. Arkh. Stroit. Univ. **4**, 160–170 (2015)
6. Riva, G., Zorgno, A.: Old brickwork chimneys: structural features and restoration problems Stremah. Trans. Built Environ. **15**, 23–35 (1995)
7. Ivashko, Y.: Problems of restoration of architectural monuments and restoration technologies. Budmeister **4**, 22–24 (2003)
8. Maltseva, I.: About the use of hydrophobizers in facade finishing materials. Eng. Bull. Don **4**, 21–27 (2017)
9. Belanovskaya, E.: Protection of brickwork of architectural monuments from corrosion. Bull. Cherepovets State Univ. **1**, 7–9 (2013)
10. Klyuev, S., Bratanovsky, C., Trukhanov, S., Manukyan, G.: Strengthening of concrete structures with composite based on carbon fiber. J. Comput. Theor. Nanosci. **7**, 2810–2814 (2019)
11. Shchetkova, E., Sevast'ianov, R.: Chrysotile as optimal reinforcing agent for fiber-reinforced concrete. Perm National Research Polytechnic University **2**, 174–190 (2015)
12. Grigorenko, I., Zakharova, N., Cartel, N., Brichka, A., Oranskaya, B., Gorelov, B., Brichka, S.: Changes in the structure and chemical composition of Chryso fibersrear asbestos under the influence of technological factors of production izvestkovo-silica thermal insulation products. Chem. Phys. Surf. Technol. **3**, 349–357 (2014)
13. Friday-Gorpinchenko, N.: Asbestos and fibrous carcinogenesis. Environ. Health **1**, 4–9 (2014)

14. Shchetkova, E., Sevastyanov, R.: The processes of structure and phase formation in the system "binder (cement) - water- filler" and their influence on the properties of concrete. Bulletin of the Perm National Research Polytechnic University. Appl. Ecol. Urban Stud. **4**, 48–58 (2014)
15. Kalashnikov, V., Tarakanov, O.: Application of complex additives in new generation concrete. Constr. Mater. **1–2**, 62–67 (2017)
16. Zotov, A.: Research and forecasting of technological properties of concrete mixtures with polypropylene fiber. Bull. Civil Eng. **1**(42), 79–83 (2014)
17. Korovkin, M., Eroshkina, M., Yanbukova, A.: Investigation of the effectiveness of polymer fiber in fine-grained concrete. Eng. Bull. Don **2**, 22–25 (2017)
18. Cherepanova, E., Molemaeva, E.: Innovations in construction: fiber concrete. Traditions Innov. Constr. Archit. **2**, 42–46 (2013)
19. Loshak, V., Cherkasov, S., Vlasov, V.: The influence of the granulometric composition of the aggregate on the aesthetic and operational properties of decorative concrete. Sci. Bull. VGASU **3–4**, 61–65 (2011)
20. Falikman, V., Sorokin, Y., Deniskin, V., Bashlykov, N.: Architectural concrete: new approaches to quality assurance. Concr. Reinforced Concr. **5**, 10–14 (2002)

Soil Compositions Based on Binders from Carbonate Waste Rocks

Lubov Zakrevskaya and **Ksenia Nikolaeva**

Abstract The object of the study is a weak water-saturated soil. It is well known that soils with a high degree of humidity are difficult to compact and loosen. Natural drying of waterlogged clay soils occurs very slowly, and artificial methods are ineffective. At the same time, such soils are characterized by thixotropy of properties. Due to the above-mentioned features of water-saturated clay soil, a method of using complex mineral binders was chosen. The dependence of density and strength on the consumption of a complex binder is established: the density of the soil being fixed is inversely proportional to the content of slaked lime. The maximum compressive strength of the soil to be fixed is achieved with a lime content in the range of 26–32 wt.%. The optimal amount of lime is 28.3 wt.%, dolomite is sufficient in the amount of 30 wt.%, chrysotile asbestos − 7 wt.%. At the same time, strong crystals of hydrosilicates and hydroaluminates are formed in the soil fixed with chrysotile asbestos. Based on the conducted studies, it was concluded that the complex fixation of clay soil with chrysotile asbestos, polycarboxylates leads to an increase in the calculated resistance of the soil, improving its operational characteristics.

Keywords Fixed soil · Strength characteristics · Binders · Moisture resistance · Thixotropy · Carbonate rocks · Surfactants · Chrysotile-asbestos

1 Introduction

For clay-type soils, thixotropy is characteristic, due to the mobile equilibrium under mechanical action [1–4]. The optimal amount of lime added to them can vary depending on the humidity of the soil being fixed and its structure. There is a large amount of research in the field of fixing weak soils with mineral binders [5–12].

L. Zakrevskaya (✉) · K. Nikolaeva
Vladimir State University, Gorky Str., 87, Vladimir 600000, Russian Federation
e-mail: lvzak@mail.ru

In the course of studies [2, 6, 13], it was found that to stabilize and compact the water-saturated soil, it is enough to introduce lime in an amount of 2–4% of the total mass of the soil. The possibility of using such a soil composition in the conditions of modern construction was proved experimentally. At the same time, the addition of lime in the amount proposed in [9] cannot significantly affect the increase in the strength of the soil and the change in its degree of humidity. When using the methods of soil consolidation described in the studies [9, 10], it is impossible to carry out mass processing of industrial waste. In this regard, there is a need to increase the content of lime waste in the fixed array.

A similar situation is observed in [5, 6]: a description of the effect of the interaction of a binder with a water-saturated clay soil is presented. There is no development and study of the compositions of soil compositions modified with binders based on mining waste. The results of the interaction of the binder with the finely dispersed part of the clay soil are presented in the form of graphs, which does not give a complete idea of the properties of the material based on the fixed clay soil. The maximum lime content does not exceed 10% of the soil mass. The addition of a binder in the amount proposed by the authors in the study [6] allows to achieve an increase in strength to a small extent, while the low content of lime waste reduces the volume of processing of mining industry waste.

In the studies [13–15], the goal is to select the minimum amount of binder for modifying and optimizing the properties of water-saturated soil, this allows to improve its properties and characteristics to some extent. The material presented in [14] has low strength, is rather heterogeneous, and loses the obtained properties when the soil mass is watered.

The world practice has a rich experience in fixing soils using various modifying additives. Basically, stabilizers are used, which, due to the activation of physico-chemical processes, contribute to the optimization of the strength characteristics of the soil base. The most well-known and generally accepted stabilizers of clay soils are: EN-1, Roadbond, Gonsolid, Perma-Zume, ECOroads, M10+50, Under-bold, SPP, Nanostab, Nikoflok, T-RRP, RRP-235 Special, Terrastone, Consodolid, Status, Dorzin, NiCoflok, ANT, EI-GI-1. The existing publications do not contain a sufficiently evidence-based experimental base, which does not allow us to qualitatively assess the physical and mechanical characteristics of the material obtained on the basis of soil fixed with mineral binders.

It is well known that in order to improve the characteristics and form a more solid and monolithic structure of the fixed soil, complex stabilization methods are used. Complex soil fixing is the treatment of soil with a combination of several components at once: organic and inorganic binders, surfactants. This allows us to obtain a qualitatively new material with improved performance and characteristics by optimizing the amount of chemical additives.

2 Materials and Methods

2.1 *Materials*

Table 1 show the chemical compositions of the clay soil being fixed.

Table 2 present the chemical composition of lime waste.

In the course of the study, a binder from dolomite waste was used, which is magnesia lime, which in turn provides low porosity and high strength indicators of soils, is characterized by high adhesion (up to 3 MPa) with various soil bases.

Table 3 show the chemical compositions of dolomite waste from the Melekhosky deposit.

Polycarboxylate superplasticizers "Macromer" (PKS), in particular the P-16, P-17 brands, consist of polycarboxylate acid and alkylene oxide branches from the main chain of various molecular weights. This structure provides the particles of the soil composite with electrostatic and spatial repulsion. Table 4 shows the properties of polycarboxylates used in the work.

The rational choice of surfactants and the optimal content of carbonate rock waste is of great importance in optimizing the properties of the soil being fixed. A polycarboxylate superplasticizer (PKS) of the Makromer brand was used in the work, since plasticizing additives of the C-3 type do not meet the requirements for environmental safety. The use of PKS contributes to the production of soil-concrete mixtures with low shrinkage deformation and creep under load. Minimum dosages of PKS ensure high dispersion of soil-concrete mixtures and increase their operational characteristics. P16 and P17 grade PCS at concentrations from 0.3 to 0.6 mass percent allow the use of soil-concrete mixtures in the construction of foundations of residential buildings [16–18].

Table 1 Chemical composition of clay soil

Oxides	SiO_2	Al_2O_3	Fe_2O_3	TiO_2	CaO
Quantity, mass.%	56.0–69.3	26.9–35.6	0.45	1.01	0.51

Table 2 Chemical composition of lime waste

Oxides	$Ca(OH)_2$	$CaCO_3$	MgO	SiO_2
Quantity Mass, %	68.35	25.24	4.12	2.29

Table 3 Chemical composition of dolomite waste

Oxides	CaO	MgO	CO_2	$Al_2O_3+Fe_2O_3$	SiO_2
Quantity, Mass., %	29.4–30.6	19.8–20.2	44.9–45.9	0.3–1.8	0.5–4.2

Table 4 Properties of polycarboxylates

Name of the indicator	Macrometer P-11	Macrometer P-13	Macrometer P-15	Macrometer P-16	Macrometer P-17
Appearance	Liquid—from colorless to yellow color without mechanical impurities				
Indicator of the activity of hydrogen ions, pH of units, within the limits	6–8	6–8	6–8	6,5–8	6,5–8
Density at 25 °C, g/cm^3	1.07 ± 0.01	1.092 ± 0.003	1.110 ± 0.006	1.110 ± 0.005	1.110 ± 0.005
Dry matter content, %	25	30	40	40	40
Dynamic viscosity at 25 °C, MPa*s, within	20–40	30–90	110–250	140–280	130–250

Table 5 Content of surfactants and lime for various clay soils

Type of clay soil and its humidity characteristics	Additives of surfactants and lime waste	
	SURFACTANT	Lime waste
Loam	0.2–0.5	5–7
Clay	0.3–0.7	7–12
Sandy loam	0.15–0.18	8–9

Table 5 shows the ranges of surfactant and lime content for various clay soils when optimizing their properties.

2.2 Methods

The physical and mechanical properties of the initial materials and the resulting soil-concrete compositions were studied according to standard methods. The samples were subjected to a strength test (for uniaxial compression). To obtain a quantitative characteristic, the strength of the samples was measured by the method of destruction under the PGM-1500M4 press.

The samples were tested for frost resistance by an accelerated method using a 5% sodium chloride solution. The pre-tested samples were saturated with a solution, then subjected to freezing in air at a temperature of minus 18–20 °C for 2.5 h and subsequent thawing in a solution of sodium chloride for 3.5 h at a temperature of plus 20 °C.

After the required number of freezing and thawing cycles, the samples were subjected to a compression test. The remaining samples were tested for water resistance: they were saturated with water, after which they were subjected to a compression test. The water resistance of the obtained material was evaluated using the softening coefficient.

The microstructure of the initial materials was studied using X-ray phase analysis and electron microscopy on a Bruker AXS D8 ADVANCE powder diffractometer and a FEI Quanta 200 3D scanning electron microscope, which allows observations on secondary and reflected electrons. The test samples were examined in a vacuum medium with a resolution of 1000 and 2000 times, which made it possible to study the micro-uniformity of the test sample.

3 Results

3.1 Research Results

The results of X-ray phase analysis are shown in Figs. 1, 2 and 3.

The results of electron microscopic examination of lime, dolomite and chrysotile asbestos waste are presented in Figs. 4 and 5.
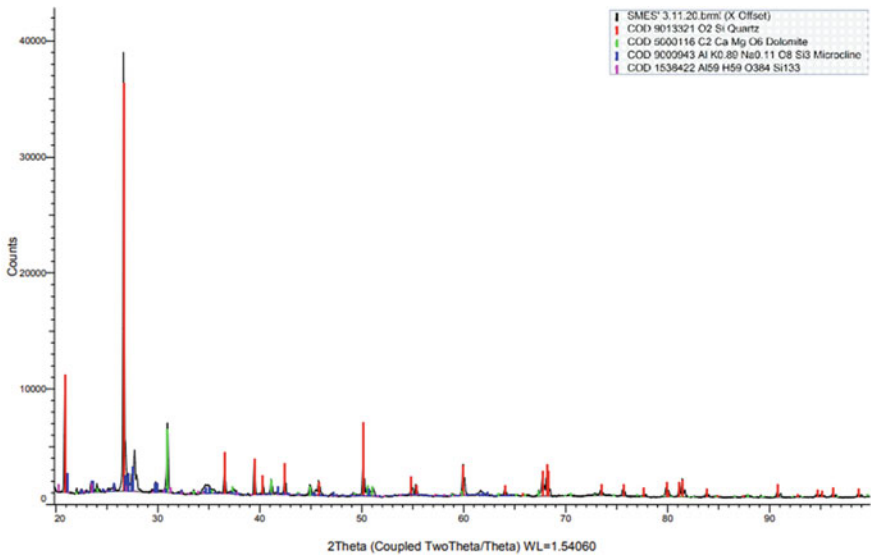

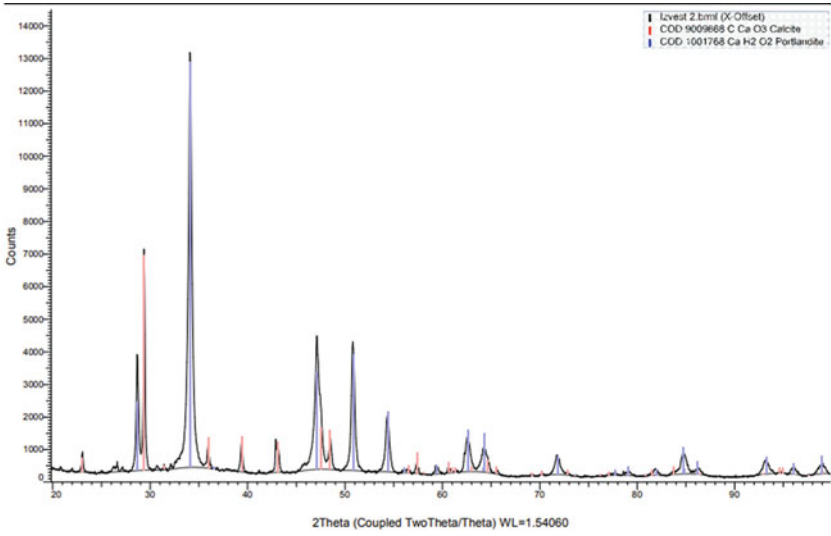**Fig. 1** The result of X-ray phase analysis of clay soil

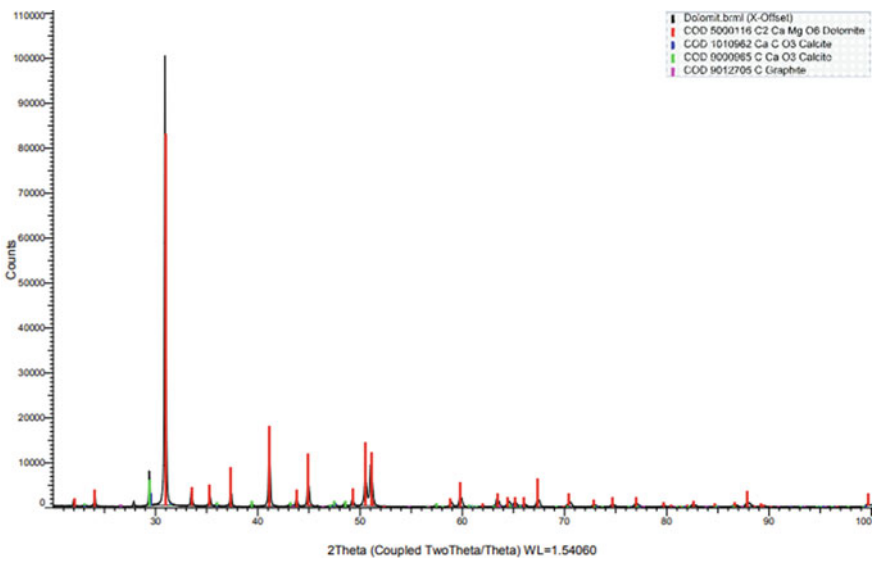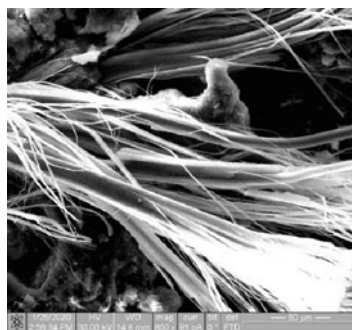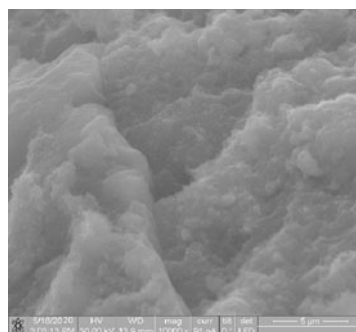**Fig. 2** The result of X-ray phase analysis of lime waste

Fig. 3 The result of X-ray phase analysis of dolomite waste

Fig. 4 The result of electron microscopic examination of chrysotile asbestos

Fig. 5 The result of electron microscopic examination of lime waste

3.2 Compositions of the Obtained Soil-Concrete Compositions

Table 6 shows the sections of developed soil compositions with the addition of binders from lime waste.

Tables 7 and 8 present the results of studying the physical and mechanical properties of synthesized soil-concrete compositions.

Table 6 Compositions of ground-concrete compositions with the addition of lime waste

Brand of the train	Components, mass. %		
	Clay soil	Waste lime	Surfactant (polycarboxylate P-17)
GBI-1	56.60	37.74	0.3
GBI-2	61.32	33.02	0.5
GBI-3	66.04	28.30	0.6
GBI-4	70.76	23.58	0.7
GBI-5	75.46	18.88	0.8

Table 7 Density of ground-concrete compositions

Brand of composition	GBI-1	GBI-2	GBI-3	GBI-4	GBI-5
Density, g/cm^3	1.591	1.686	1.670	1.765	1.779

**Table 8** Physical and mechanical characteristics of soil-concrete compositions

| Brand of the train	Compressive strength, MPa		Frost resistance, number of cycles	Water resistance, %	
	28 days	60 days	60 days	28 days	60 days
GBI-1	2.7	4	20	0.58	0.58
GBI-2	2.5	4.4	25	0.61	0.61
GBI-3	2.8	4.7	35	0.64	0.64
GBI-4	1.9	4.5	45	0.73	0.73
GBI-5	2.2	4.4	45	0.75	0.75

Based on the results of measuring the density of samples, statistical processing of experimental data was performed and a graph of the density dependence on the content of lime waste was constructed.

From the graph shown in Fig. 6, it can be seen that with an increase in the amount of lime waste, the density of the soil-concrete composition decreases, but this does not significantly affect the decrease in strength, as evidenced by the graph of the dependence of strength on the lime content shown in Fig. 7: an increase in the lime concentration from 19 to 38% by weight leads to a decrease in strength by 10%.

The maximum strength of the synthesized material is achieved at a lime concentration of 28.3% by weight for 60 days. The increase in the strength of the soil fixed with mineral binders is due to the theory of hardening of the aluminosilicate matrix under the influence of slaked lime [19, 20].

To create a structural material based on ground concrete, waste dolomite (see Tables 5 and 6) and bischofite were used. In this case, dolomite acts as a binding
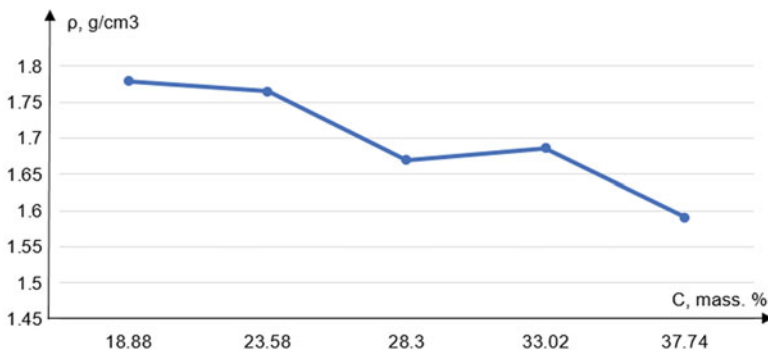
Fig. 6 Dependence of the density of the soil-concrete composition on the lime concentration
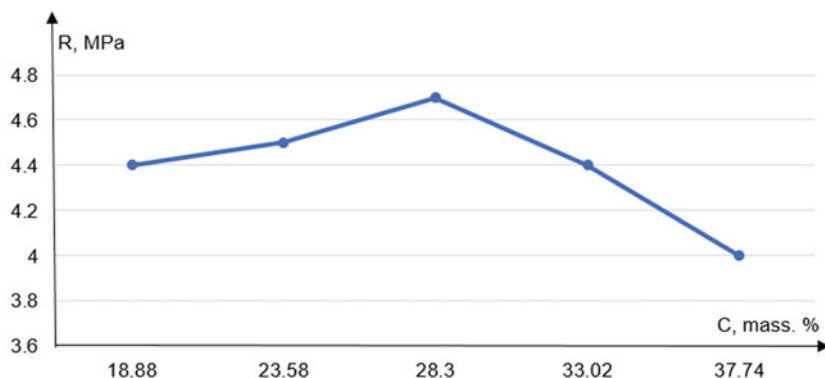
Fig. 7 Graph of strength versus lime concentration

component that increases the strength of the material. Bischofite is a recluse for magnesia cement and binds soil particles, as a result of which the soil dusts less and becomes less porous over time, this ensures a decrease in water absorption of the material. Table 9 shows the compositions of the obtained ground concrete materials.

Table 10 presents the results of laboratory studies of the physical and mechanical properties of the resulting structural soil-concrete material.

Table 9 Compositions of clay-concrete construction material

Brand of the train	Clay soil	Components, wt %		
		Dolomite waste	Bischofite dolomite waste	Water
GBK-1	56.2	21.6	15.8	6.4
GBK-2	51.5	25.1	17.0	6.4
GBK-3	42.1	23.4	28.1	6.4
GBK-4	37.5	32.8	23.3	6.4
GBK-5	32.8	42.1	18.7	6.4

Table 10 Physical and mechanical characteristics of ground concrete compositions with the addition of a binder based on dolomite waste

Brand of the train	Compressive strength, MPa		Frost resistance, number of cycles	Water resistance, %	
	28 days	60 days	60 days	28 days	60 days
GBK-1	8.9	15.8	40	0.78	0.79
GBK-2	9.4	17.7	45	0.83	0.83
GBK-3	7.3	13.6	40	0.87	0.87
GBK-4	10.6	18.1	50	0.95	0.95
GBK-5	9.6	18.3	50	0.93	0.93

In addition to the compositions of soil concrete compositions with the addition of a binder based on lime and dolomite waste, presented in Tables 12, soil compositions with the addition of chrysotile asbestos were developed. Chrysotile forms micro-reinforcement in the soil due to its structure—the thinnest tubes, which can be attributed to natural nanostructured materials. Microscopic examination of chrysotile-asbestos waste, presented in Fig. 5, gives the most complete and visual representation of the chrysotile-asbestos nanostructure. A characteristic feature of the material with the addition of chrysotile is a powerful energy bond along the fiber, which confirms a high tensile strength of about 400 kg/mm^2 and an average elastic modulus of about 20,000 MPa. They are also characterized by high chemical resistance and low thermal conductivity and differ favorably from CNTs (carbon nanotubes) by a clearly defined orientation.

The chemical formula of chrysotile asbestos has the following form: $3MgO \cdot 2SiO_2 \cdot 2H2O$, that is, these are crystals related to dolomite ($MgCO_3 \cdot CaCO_3$), and semi-burnt dolomite contains pure MgO (30% of the total content), which helps to reduce the humidity of water-saturated soil.

Table 11 shows the compositions of soils with the addition of chrysotile asbestos waste. According to previous studies, the optimal amount of chrysotile asbestos was 7% [21–23].

Table 12 shows the results of studying the physical and mechanical properties of soil-concrete compositions modified with chrysotile-asbestos waste.

According to the data given in Table 12, the GBIAs - 3 sample has the highest strength indicators. When adding chrysotile asbestos waste, it was possible to achieve an increase in water resistance and strength.

Table 11 Compositions of ground-concrete compositions with chrysotile-asbestos

Brand of the train	Components, mass %			
	Clay soil	Dolomite waste	Polycarboxylate	Waste of chrysotile asbestos
GBIAs - 1	49.6	37.74	0.3	7
GBIAs - 2	54.32	33.02	0.5	7
GBIAs - 3	59.04	28.30	0.6	7

Table 12 Physical and mechanical characteristics of ground-concrete compositions with the addition of chrysotile-asbestos waste

Brand of the train	Compressive strength, MPa		Frost resistance, number of cycles	Water resistance, %	
	28 days	60 days	60 days	28 days	60 days
GBIAs - 1	10.1	18.2	50	0.84	0.85
GBIAs - 2	9.3	14.8	45	0.85	0.85
GBIAs - 3	9.7	19.0	50	0.81	0.81

3.3 Results of the Conducted Research

The analysis of the obtained results allows us to conclude that it is advisable to use the compositions of ground concrete compositions modified with mineral binders and polycarboxylates proposed in this work. Dolomite, like lime, is an affordable and common material. On the basis of their waste, it is possible to obtain a binder that can be comparable in strength to some brands of cement. The content of dolomite waste in the range of 30% allows to increase the strength of the resulting material, as well as to reduce the water absorption of the material, its porosity, which allows avoiding soil heaving [24, 25]. During the study, it was possible to increase the amount of lime added by 20% compared to the results of previous studies [26] without reducing the strength characteristics.

The study of the microstructure of the fixed soil proves the formation of strong crystalline formations (hydrosilicates, hydroaluminates) in it, which have cementing properties in the massif. Polycarboxylates in the composition of the fixed soil indirectly contribute to an increase in the reaction surface between the soils and the fixing components and make it possible to exclude the operation of mechanical activation from the technological process. The synergistic effect of the interaction of dolomite and chrysotile with clay soil gives it the ability to quickly gain strength in a short time.

4 Conclusions

1. In the course of the study, compositions of fixed soils based on waste of carbonate rocks and chrysotile asbestos were developed. The obtained results of the study confirmed the possibility of using in construction and obtaining soil compositions fixed with binders based on waste from the mining industry in the construction industry.
2. The soil fixed with various mineral binders can be used as a natural foundation for buildings and structures during the construction of foundations of low-rise buildings. After fixing the waterlogged clay soils with slaked lime, the soils become more durable.
3. The chemical and mineralogical compositions of mining waste have been established. It has been experimentally established that the samples of fixed soil with the content of lime waste 28.3 wt.%, dolomite waste—32.8–42.1%, chrysotile-asbestos waste—7 wt.% have the greatest strength.
4. Polycarboxylates in an amount from 0.3 to 0.8 wt.% favorably affect the increase in reactivity between clay soil and fixing components, and they can be confidently called stabilizing components, since they contribute to the creation of high-strength crystallization structures of the soil.

References

1. Firoozi, A., Olgun, G., Firoozi, A., Baghini, M.: Fundamentals of soil stabilization. Int. J. Geo-Eng. **8**(1), 8–26 (2017)
2. Bessiam, M., Bessiam, A., Missuom, H., Bendani, K.: Effect of quick lime on physicochemical properties of clay soil. In: MATEC Web of Conferences CMSS-2017, vol. 149, pp. 1–5 (2018)
3. Lofler, M., Slobodchikova, N.: Methods of selecting soil compositions reinforced with lime for road construction. Izvestiya vuzov: Investment. Construction. Real Estate - Irkutsk: INITU 2 (25), vol. 8, pp. 141–147 (2018)
4. Slobodchikova, N.: Nauchnye osnovy podbora sostava gruntov, fortified with lime. Vestnik nauki i obrazovaniya Severo-Zapad Rossii. Kaliningrad **4**(25), vol. 3, pp. 62–68 (2017)
5. Tarasov, V., Lebedev, V.: The Domestic polycarboxylate superplasticizers production of NPP Macromer of concrete, plaster and stroitelnyy mixtures. Withoncrete Technol. **2**, 1–12 (2015)
6. Vatin, N., Chechevichkin, A., Chechevichkin, V., Shilova, E.: Ecological problems of construction and prirodopolzovaniya. Mag. Civ. Eng. **39**(7), 16–23 (2011)
7. Fauzi, A., Nazmi, W., Abdul-Rahman, W., Jauhari, Z.: Utilization waste material as stabilizer on Kuantan clayey soil stabilization. Procedia Eng. **53**, 42–47 (2013)
8. Halsted, G., Adaska, W., McConnell W.: Guide to Cement-Modified Soil (CMS), T.: EB242 Portland Cement Association. Illinois, USA: Skokie (2008)
9. Faizi, K., Armaghani, D.J., Sohai, H., Rashid, A.S.A., Nazir, R.: Deformation model of sand around short piles under pullout test. Measurement **63**, 110–119 (2015)
10. Szybilski, M., Nocuń-Wcz, W.: The effect of dolomite additive on cement hydration. Procedia Eng. **108**, 193–198 (2015)
11. Dinakar, K., Prasad, S.: Behaviour of tie back sheet pile wall for deep excavation using plaxis. Int. J. Res. Eng. Technol. **3**, 97–103 (2014)
12. Osipov, V.I., Sokolov V.N.: Clays and Their Properties. Composition, Structure and Formation of Properties, T.: GEOS, Moskau (2013)
13. Lehmann, S.: Resource recovery and materials flow in the city: zero waste and sustainable consumption as paradigm in urban development. J. Green Build. **6**(3), 88–105 (2011)
14. Jayalath, N., Mosley, L., Fitzpatrick, R., Marschner, P.: Addition of organic matter influences pH changes in reduced and oxidised acid sulfate soils. Geoderma **262**, 125–132 (2016)
15. Khemissa, M., Mahamedi, A.: Cement and lime mixture stabilization of an expansive over consolidated clay. Characterization Probl. Soils Stabilization **95**, 104–110 (2014)
16. Kalinkin, A., Belogurova, T.: Constructional materials from mining-and-metallurgical waste and natural minerals of the kola region. Gornyi Zhurnal **12**, 9–15 (2019)
17. Fomina, N., Pavlova, I., Kochergina, M.: Industrial waste as components of building materials. In: E3S Web of Conferences, vol. 1, pp. 216–222 (2020)
18. Oza, J., Gundaliya, P.: Study of black cotton soil characteristics with cement waste dust and lime. Procedia Eng. **51**, 110–118 (2013)
19. Vatalis, K., Manoliadis, O., Charalampides, G.: Sustainability components affecting decisions for green building projects. Econ. Financ. **2**, 747–756 (2013)
20. Ahmed, A.: Compressive strength and microstructure of soft clay soil stabilized with recycled basanite. Appl. Clay Sci. **104**, 27–35 (2015)
21. Chim-oye, W., Marumdee, N.: Estimation of uplift pile capacity in the sand layers. Int. Trans. J. Eng. Manag. Appl. Sci. Technol. **4**, 57–65 (2013)

22. Tejinder, S., Navjot, R.: Strengthening of subgrade by using RBI grade-81 a case study. IOSR J. Mech. Civil Eng. **8**(101–106), 2013 (2013)
23. Zezin, A., Mikheikin, S., Rogacheva, V., Zansokhova, M.: Polymeric stabilizers for protection of soil and ground against wind and water erosion. In: Advances in Transportation Geotechnics II. Proceedings of the 2nd International Conference on Transportation Geotechnics, ICTG, vol. 4, pp. 23–34 (2012)
24. Obuzor, G., Kinuthia, J., Robinson, R.: Soil stabilization with lime activated GGBS-a mitigation to flooding effects on road structural layers embankments constructed on floodplains. Eng. Geol. **151**(29), 112–119 (2012)
25. Dobrescu, C.: Assessment of soil bearing capacity for mixtures with construction wastes and eco-materials. In: International Multidisciplinary Scientific GeoConference Surveying Geology and Mining Ecology Management, vol. 18(12), pp. 115–120 (2018)
26. Ter-Martirosyan, Z., Ter-Martirosyan, A.: Experimental and theoretical bases of transformation of weak water-saturated clay soils under surface and deep compaction. Eng. Geol. **4**, 16–25 (2015)

Utilization of Dolomite Waste from the Vladimir Region for the Synthesis of Concrete

Ilya Kapush ⬤, Lubov Zakrevskaya ⬤, Viktor Ilyin ⬤, and Sergey Prokhorov ⬤

Abstract The article considers options for introducing waste from the mining industry of the Vladimir region into the production of construction products. Experimental data on the operational characteristics of materials have been obtained and their use in various types of concrete has been substantiated. The following operational characteristics of concrete have been achieved: thermal insulation concretes: strength 1.2–1.3 MPa, density 392–404 g/cm^3, thermal conductivity 0.076–0.08 W/m*K, frost resistance 27–30 cycle; structural and thermal insulation concretes: strength 5–5.8 MPa, density 714–720 g/cm^3, thermal conductivity 0.094–0.1 W/m*K, frost resistance 35–37 cycle, allowing the use of synthesized composites in the construction of buildings and structures with improved properties.

Keywords Concrete · Magnesia binder · Industrial waste · Synthesis

1 Introduction

The modern construction industry is subject to a number of technological, economic and environmental trends [1]. This applies both to the construction process as a whole, and to building structures and materials. Classic types of concrete made of a simple binder – Portland cement and classic aggregate are less and less relevant in the era of "green construction" [2]. To solve this problem, the study suggests using local industrial waste, from which concrete synthesis is possible, and at the same time the possibility of recycling by-products is considered.

One of the main industries in our country, rich in minerals and underground resources, is the mining industry [3]. Figure 1 shows a graph of changes in the volume of financing of the mining industry and a graph of changes in the number of mining facilities. Based on the figure, we can conclude that this industry is very promising and is developing quite rapidly.

I. Kapush (✉) · L. Zakrevskaya · V. Ilyin · S. Prokhorov
Vladimir State University named after Alexander and Nikolay Stoletovs, 600000 Vladimir, Russia
e-mail: ilya.kapush@gmail.com
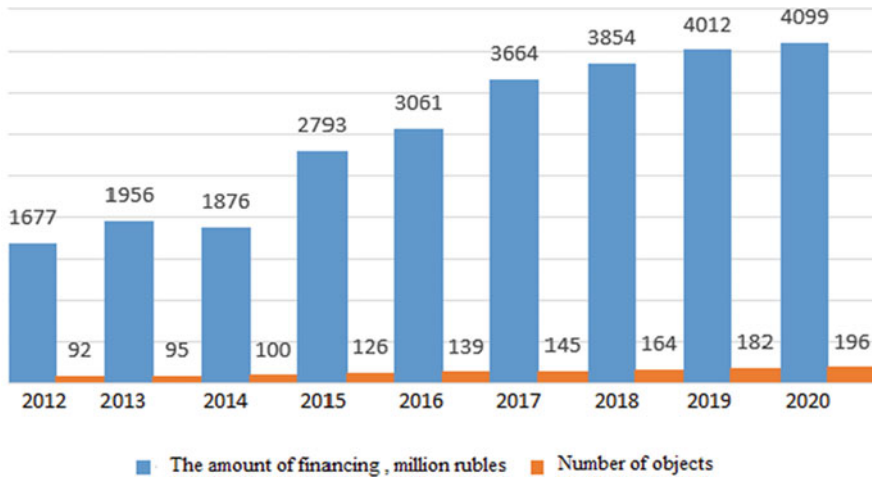
Fig. 1 The amount of financing and the number of mining facilities

But any technological process is imperfect, and has its disadvantages. This industry is no exception, which, according to ROSSTAT, allocates a multimillion-dollar amount of by-product. In the period from 2012 to 2020, the increase in the volume of recyclable materials of the mining industry amounted to 48%, from 3334.6 to 6386.2 million tons.

Analyzing the above data, it can be concluded that the problem of waste disposal is quite acute in every region [4] where mining is carried out. There are many different mineral deposits in the Vladimir region, and almost every one is mined and, as a result, waste is generated [5].

Of particular interest are deposits of dolomite and brucite, which are available in the Vladimir region (Murom district, Melenkovsky district), where there is an urgent need to dispose of waste accumulated in dumps in the form of flour, which makes the tasks of processing this material urgent [6].

2   Materials and Methods

To implement this task, the properties and structure of dolomite, which acts as a binder in the experiment, were studied.

Table 1 shows the mineralogical composition of dolomite waste.

Dolomite is a magnesia binder based on magnesium oxide, sealed with a solution of magnesium salts, usually magnesium chloride and/or magnesium sulfate [7].

Setting time: the beginning is not earlier than 20 min, the end is not later than 6 h from the moment of closing the test of normal density. It is characterized by increased adhesion strength, especially with wood materials. A bonfire of technical

Table 1 Mineralogical composition of dolomite waste

Mineral	Mass content of mineral, %
Dolomite	95.22
Quartz	0.62
Calcite	4.16

Table 2 Compositions of synthesized concrete

Mass component, %	Appointment					
	Thermal insulation			Structural and thermal insulation		
	T1	T2	T3	К1	К2	К3
Shutter	15	20	25	15	20	25
Hemp shives	65	60	55	20	20	20
Dolomite waste	20	20	20	65	60	55

hemp from the Vyaznikovsky district, also a by-product of the textile industry, was used as wood materials [8–10].

The selection of the basic composition of concrete was made based on the average level of strength, thermal conductivity and density of concrete [11].

Several compositions were created for the synthesis of lightweight concrete acting as heat-insulating plates, and several compositions for structural and heat-insulating concrete capable of taking a load.

The fundamental difference in the composition of concrete was the amount of wood aggregate [12]—the greater its proportion in the composition, the lower the coefficient of thermal conductivity, and the more energy-intensive the material [13–15].

For the synthesis of structural and heat-insulating concrete, a minimum amount of filler was used, since it is necessary to create concrete with high strength, which depends directly on the binder.

A solution of magnesium salts was chosen as a recluse, which increases the bonding ability of dolomite [16] and hemp shives. Based on the above, the concrete compositions presented in Table 2 were synthesized.

3   Results and Discussion

After mixing and mixing to a homogeneous raw material mass, the samples were placed in special molds for strength gain and subsequent study of operational characteristics [17].

The obtained results of studying the operational characteristics of synthesized composites are shown in Table 3.

Table 3 Performance characteristics of composites

Brands of concrete	Characteristics			
	Density, g/cm^3	Compressive strength, MPa	Thermal conductivity λ, W/m·K	Frost resistance grade, cycle
T1	392	1.2	0.08	27
T2	401,5	1.3	0.076	29
T3	404	1.3	0.079	30
К1	720	5.8	0.1	35
К2	714	5.3	0.096	37
К3	715	5	0.094	36

To compare the operational properties of the obtained composites with the normative values, GOST 25820–2014 "Light concretes. Technical conditions", which are indicated in Table 4.

After receiving the data, the structure of the material was studied. The microstructure of the building material was studied at two levels [18]: macrostructure—the structure of the material visible to the naked eye; microstructure—the structure visible through a microscope [19, 20].

During visual inspection, the presence of defects, namely chips, cracks, traces of delamination, air voids was not established. To study the microstructure, a scanning electron microscope provided by the Engineering Center within the framework of the program of the Ministry of Education and Science of the Russian Federation "Promotion of employment of graduates in 2022 for research positions in educational institutions of higher education and scientific organizations" was used.

Figure 2 shows the results of electron microscopy, which show that the composite is a complex structure.

Analyzing Tables 3 and 4, as well as the microstructure of synthesized lightweight concrete shown in Fig. 2, it can be concluded that the resulting material fully meets the regulatory requirements for strength, density, thermal conductivity and frost resistance. The explanation of the results obtained lies in the synergistic effect of all

Table 4 Properties of light concrete in accordance with GOST 25820–2014

Concrete	Characteristics			
	Grade of medium density, g/cm^3	Compressive strength, Mpa (min)	Thermal conductivity λ, W/m·K	Frost resistance grade, cycle (min)
Thermal insulation	≤500	≥0,3	0.05–0,14	Not standardized
Structural and thermal insulation	≥500	≥1	0.14–0,3	≥25
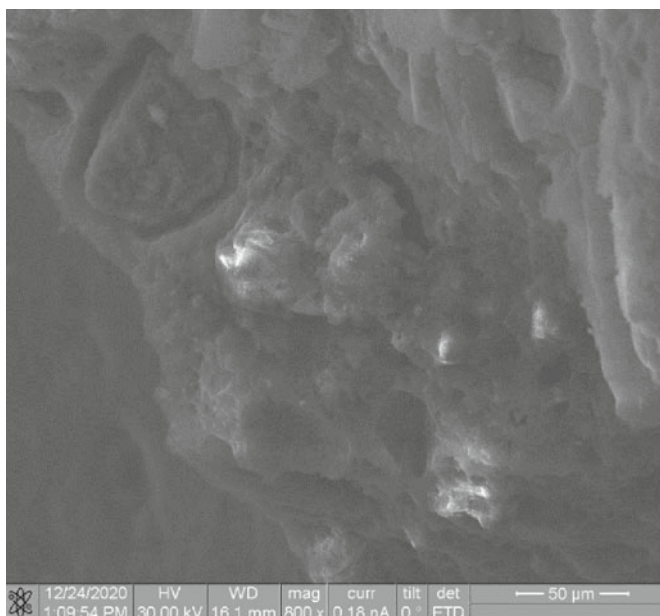
Fig. 2 Microstructure of the synthesized material

the components of the composite, namely, in the interaction of the magnesia binder and filler, their correctly selected ratio for thermal insulation and structural-thermal insulation concrete.

4 Conclusions

Thus, the possibility of recycling mining waste, which is dolomite flour, for the creation of concretes of various application ranges has been studied. This allows not only to reduce the cost of the product, but also to improve the environmental situation by recycling waste in the Vladimir region. The presented compositions can be used both for the creation of thermal insulation boards and panels with a low coefficient of thermal conductivity, and in the form of individual elements or pazogreb-neevyh blocks with high strength for frame private housing construction. Synthesized composites have the following characteristics: thermal insulation concretes: strength 1.2–1.3 MPa, density 392–404 g/cm^3, thermal conductivity 0.076–0.08 W/m·K, frost resistance 27–30 cycle; structural and thermal insulation concretes: strength 5–5.8 MPa, density 714–720 g/cm^3, thermal conductivity 0.094–0.1 W/m·K, frost resistance 35–37 cycle.

References

1. Sakir, S.: Utilization of by-products and wastes as supplementary cementitious materials in structural mortar for sustainable construction. Sustainability (Switzerland) 14–20 (2020). T. 12. № 9. https://doi.org/10.3390/su12093888
2. Jannat, N.: Application of agro and non-agro waste materials for unfired earth blocks construction: a review. Constr. Build. Mater., 314–320 (2020). T. 254. https://doi.org/10.1016/j.conbuildmat.2020.119346
3. Srivastava, A., Singh, S.K.: Utilization of alternative sand for preparation of sustainable mortar: a review. J. Cleaner Prod. (2020). T. 253
4. Magar, J.: Application of industrial and agricultural waste for sustainable construction. Int. J. Res. Appl. Sci. Eng. Technol. (2020). № 7 (8). https://doi.org/10.22214/ijraset.2020.30699
5. Gavali, H.R.: Development of sustainable alkali-activated bricks using industrial wastes. Constr. Build. Mater. (2019). T. 215. https://doi.org/10.1016/j.conbuildmat.2019.04.152
6. Jin Y.: A government value compensation model of waste recycling in an industrial park: a game theory approach. J. Clean. Prod. (2020). (275). https://doi.org/10.1016/j.jclepro.2020.122976
7. Chen, Y.X.: Bio-based ultra-lightweight concrete applying miscanthus fibers: acoustic absorption and thermal insulation. Cem. Concr. Compos. (2020). https://doi.org/10.1016/j.cemconcomp.2020.103829
8. Elrahman, M.A., Chung, S.Y., Stephan, D.: Effect of different expanded aggregates on the properties of lightweight concrete. Mag. Concr. Res. (2019). № 2 (71). https://doi.org/10.1680/jmacr.17.00465
9. Bremner, T.W.: Lightweight concrete (2019). https://doi.org/10.1016/B978-0-08-102616-8.00013-7
10. Maletaškić, J.: Acid leaching of natural chrysotile asbestos to mesoporous silica fibers. Phys. Chem. Miner. (2018). № 4 (45). https://doi.org/10.1007/s00269-017-0924-z
11. Kuzmin, S.A.: Durability of construction materials modified by polymeric additives (2019). https://doi.org/10.1016/j.prostr.2019.12.152
12. Aruova, L.B.: Manufacturing arbolitic building products using solar energy. J. Mech. Eng. Res. Dev. (2018). № 2 (41). https://doi.org/10.26480/jmerd.02.2018.49.55
13. Isakulov, B.R.: Formation of strength and phases of sequence of destruction of arbolite composites at various long loads. News Natl. Acad. Sci. Repub. Kazakhstan Ser. Geol. Tech. Sci. (2020). № 442 (4). https://doi.org/10.32014/2020.2518-170X.81
14. Zakrevskaya, L.V.: Wall materials based on complex binders and organic aggregate (2020). https://doi.org/10.1088/1757-899X/896/1/012083
15. Ramsheva, Y.K., Moalem, R.M., Milios L.: Realizing a circular concrete industry in Denmark through an integrated product, service and system perspective. Sustainability (Switzerland) (2020). № 22 (12). https://doi.org/10.3390/su12229423
16. Tolstoy, A.D., Lesovik, V.S., Milkina, A.S.: Improving New Generation Concretes (NGCs) by Introducing Technogenic Materials (2018). https://doi.org/10.1088/1757-899X/463/2/022095
17. Balčiūnas, G.: Ecological, thermal and acoustical insulating composite from hemp shives and sapropel binder. Ind. Crops Prod. (2016). https://doi.org/10.1016/j.indcrop.2016.06.034
18. Członka, S., Strąkowska, A., Kairytė, A.: The impact of hemp shives impregnated with selected plant oils on mechanical, thermal, and insulating properties of polyurethane composite foams. Materials (2020). № 21 (13). https://doi.org/10.3390/ma13214709

19. Brzyski, P.: Influence of hemp shives size on hygro-thermal and mechanical properties of a hemp-lime composite. Materials (2020). № 23 (13). https://doi.org/10.3390/ma13235383
20. Kleijer, A.L., Lasvaux, S., Citherlet, S., Viviani, M.: Product-specific life cycle assessment of ready mix concrete: comparison between a recycled and an ordinary concrete, pp. 210–218 (2017). https://doi.org/10.1016/J.RESCONREC.2017.02.004

Magnesia Cements Based on Trepel and Diatomite of the Vladimir Region

Ilya Kapush , **Vladislav Bitkov** , **Sergey Bulakhtin** ,
Aleksandr Semenov , and **Lubov Zakrevskaya**

Abstract The article discusses options for the introduction of silicon-containing natural materials in the production of magnesia binders. Experimental data on the performance characteristics of materials have been obtained and their application in various types of concrete has been substantiated. A technology for the production of pellets for diapene has been developed, including the following sequential actions:

– Granulated trepel is ground to a powder state
– Mixing of the resulting powder and alkali
– Mixing of the resulting mixture until a plastic mass is formed
– Then the resulting powder is wetted and mixed until a plastic mass is formed
– The pellets are then granulated and sintered in a rotary kiln

Keywords Light concrete · Magnesia binder · Trepel · Diatomite · Synthesis

1   Introduction

The production of various types of concrete on magnesia cements occupies a small share in Russia, which is completely unjustified by the arguments of the quality of the material, since this type of cement has excellent performance properties, whether it is abrasion, density and strength, and the history of production and examples of use go back centuries [1]. Works [2–4] are devoted to the problems of using this type of binder in the production of concrete.

The main difference between cement concretes and mortars, in contrast to magnesia, is delayed hardening, up to several tens of hours, as well as heterogeneous composition and conglomerate structure [5]. Therefore, the existing traditional concretes do not meet modern standards for durability and resistance to destruction of the visual structure and cracking. Crystalline and colloidal neoplasms formed during

I. Kapush (✉) · V. Bitkov · S. Bulakhtin · A. Semenov · L. Zakrevskaya
Vladimir State University named after Alexander and Nikolay Stoletovs, 600000 Vladimir, Russia
e-mail: ilya.kapush@gmail.com

hydration dry out and condense over time, which is accompanied by shrinkage of the cement stone. When using a magnesia binder in the raw material composition of concrete in building mixes, a dense material without pores with high wear resistance is obtained [6].

Materials based on magnesia binder also have high adhesion not only to minerals, but also to organic substances [7]. Due to the high density of the material, low alkalinity and the presence of the mineral bischofite in the composition of magnesia cements, organic fillers in them do not rot, which allows us to conclude that they are bactericidal and resistant to mold and mildew formation [8].

When using solutions of magnesium salts in concrete as a sealer, the hardening structure changes slightly—complex salts of various compositions are created: $MgCl_2$-5MgO-17H_2O (Sorel, 1867), $MgCl_2$-5MgO-8H_2O (Bender, 1871), and so on. Due to this, magnesium hydroxide is removed from the solution, and new portions of magnesium oxide enter into the hydration reaction [9].

Table 1 presents a comparative analysis of the characteristics of cements.

A distinctive feature of magnesia cement is the creation of a slightly alkaline environment (pH ~ 8.5), which prevents the development of microorganisms that can destroy the material from the inside. The sealing of such a binder with water leads to slow hardening of the material and low strength, therefore, this material is sealed with a solution of magnesium chloride, which is a good flame retardant impregnation, as well as resistant to biological destruction. In this case, the closed magnesia mixture is a rapidly hardening white viscous product. After hardening, solutions prepared on the basis of magnesia cement and magnesium chloride solution at an early stage are characterized by good bending, compressive and tensile strength.

Table 1 Comparative characteristics of magnesia cement and Portland cement

Characteristics	Cement	
	Magnesium	Portlandcement
Grosscomposition	$3MgO \cdot MgCl_2 \cdot 11H_2O$	$12CaO \cdot 6SiO_2 \cdot 7H_2O$
Structuralformula	$[Mg_{42} + (OH)_6{}^- (H_2O)_6]_2 + Cl_2{}^- \cdot 2H_2O$	$Ca[Si_6O_{17}](OH)_{14}$ (hillebrandite)
Crystalstructure	Sharp anisodesmic, formed by twin chains of $Mg(OH, H_2O)_6$ and water molecules	Quasi-coordinate, represented by alternating xonotlite and portlandite elements: $Ca[Si_6O_{17}](OH)_2 \cdot 6Ca(OH)_2$
Macrostructure	A multitude of tangled fibers enclosed in a volume	Massive single element
Density ρ, g/m^3	1.8– 2.0	2.5– 2.7
Brittle HV (GPa)/K1c	0.45–0.55	3.8–4.2
Thermal conductivity λ, W/(m–K)	0.51–1.51	1.4–1.9
Compressivestrength, c_w, MPa	3–100	3–80

2 Materials and Methods

For the first time, Stanton described the topic of alkali-silicate reactions in the world. Hydroxide- react with certain types of silica in the filler, which leads to internal stresses that can cause destruction or cracking [10]. This fact will negatively affect the material, as it can occur both instant cracking, during the hardening period, and only after a few years already in the finished exploited material. In stressed concrete, cracks, as a rule, are formed parallel to the reinforcement, in turn, splits show cracks passing through the filler [11]. The task was set to synthesize light concrete based on both traditional foam glass and light aggregate from silica-containing natural materials such as trepel and diatomite.

The rocks described above are called siliceous because of the high silica content (SiO_2 from 50 to 90%) [12–15], also the second necessarily present oxide is Al_2O_3_a finely porous structured powder consisting of cristobalite, as well as clay minerals. In the Vladimir region, trepels are common in the Kolchuginsky district, as well as along the banks of the Belaya, Seraya and Peksha rivers. Table 2 shows the compositions of trepels.

In this study we synthesized lightweight aggregates in the form of granules based on trepel and diatomite. "Diapen" is a new generation building material synthesized from quartz rocks with a porous chemically resistant structure and a raw material component for lightweight concrete.

A technology for the production of pellets for diapene has been developed, including the following sequential actions:

– Granulated trepel is ground to a powder state
– Mixing of the resulting powder and alkali
– Mixing of the resulting mixture until a plastic mass is formed
– Then the resulting powder is wetted and mixed until a plastic mass is formed
– The pellets are then granulated and sintered in a rotary kiln

The pellets we obtained were tested for strength, thermal conductivity and water absorption. The results are presented in Table 3.

Table 2 Chemical composition of trepels

Chemicalcompound	SiO_2, %	Al_2O_3, %	Fe_2O_3, %	CaO, %	MgO, %	SO_3, %
Quantity	72–88	3.5–15.5	0.3–5.0	0.5–2.5	0.4–1.8	0 –1.5

Table 3 Physical and technical properties of diapene

Density, kg/m^3	Strength, MPa	Thermal conductivity coefficient, W/(m·°K)	Water absorption, %ob	Fire safety
250–500	1.5–3.0	0.07–0.09	11–13	Non-combustible

One of the advantages of the production of trepel is its cost, and, as a result, the low cost of "Diapen". Among the closest analogues, it is twice cheaper than expanded clay, and 5 times cheaper than foamed stone. To select the optimal fractional composition with high performance characteristics while maintaining strength, the Eq. (1)—Andreassen-Andersen formula was used [15].

$$P(D) = \frac{D^q - D_{min}^q}{D_{max}^q - D_{min}^q} \tag{1}$$

where P(D) is the total fraction of solid matter with particles smaller than D, D is the particle size (μm), D_{max} and D_{min} are the largest and smallest particle size (μm) in the mixture, respectively, q is the distribution module.

Table 4 shows the fractional composition of aggregate when selecting the optimal packing density for concrete.

After the tests, it was found that the optimal fractional ratio has the composition of C-1.

In the course of the study, light concrete was synthesized on the basis of a magnesia binder and filler. The basic composition of concrete was chosen based on the average level of strength, thermal conductivity and density of concrete. To further study the operational characteristics, several compositions for synthesis were created. The principal difference in the composition of concrete was the amount of half-baked dolomite waste with the addition of 30% MgO. The compositions of light concrete based on diamine and the investigated binder are presented in Table 5.

Table 4 Fractional composition of lightweight aggregate to achieve maximum packing density

Fraction, mm	C-1	C-2	C-3	C-4	C-5	C-6	C-7
0–1.25	24	22	35	20	22	21	22
1.25–2.5	11	9	9	17	22	9	10
2.5–5.0	15	13	13	17	13	13	25
5.0–10.0	18	28	15	18	15	15	15
>10.0	32	28	28	30	28	42	28

Table 5 Compositions of lightweight concrete

| Mark	Components, %			
	Semi-burned dolomite waste with the addition of 30% MgO	Diapen	Bischofit	Water
M-1	45	15	40	The rest
M-2	50	15	25	The rest
M-3	55	15	20	The rest
M-4	60	15	25	The rest

3 Results

The obtained compositions were tested for mechanical and thermal-physical properties the main indicators of quality of the developed concrete are strength and thermal conductivity [16–18]. The strength was studied in accordance with GOST 10180-2012 after 7 and 28 days after formation of concrete. To study the strength was used non-destructive method of control, namely, the method of impact pulse with the device IPS 1 mg. Thermal conductivity was studied in accordance with GOST 7076-99 probe method using the device MIT-1. The obtained results of the study of the performance characteristics of the synthesized composites are given in Table 6.

Table 6 shows that the composition of M-4 has optimal performance characteristics.

Table 6 Mechanical and thermal-physical properties of lightweight concrete

Brand	Specifications		
	Strength, MPa	Thermal conductivity, W/(m·°K)	Density, kg/m³
M-1	2.1	0.43	850
M-2	2.3	0.38	830
M-3	2.0	0.37	745
M-4	2.5	0.34	780
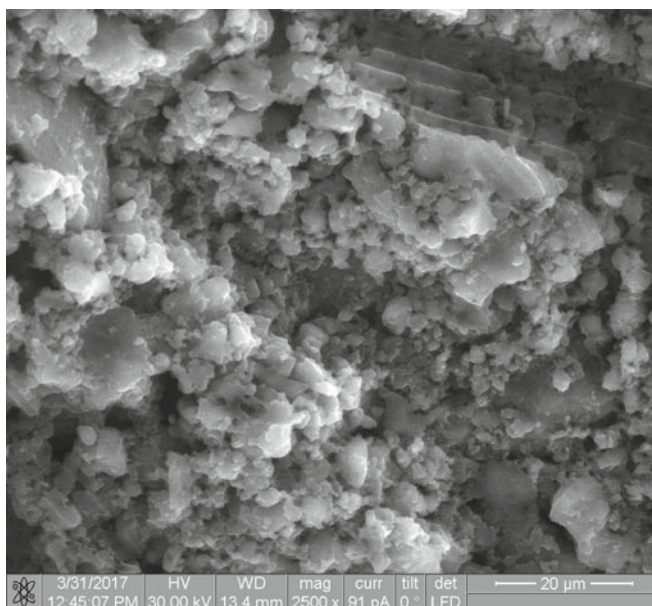
Fig. 1 Microphotograph of a magnesia composition with a "diapene" filler

Commander Sample ID (Coupled TwoTheta/Theta)
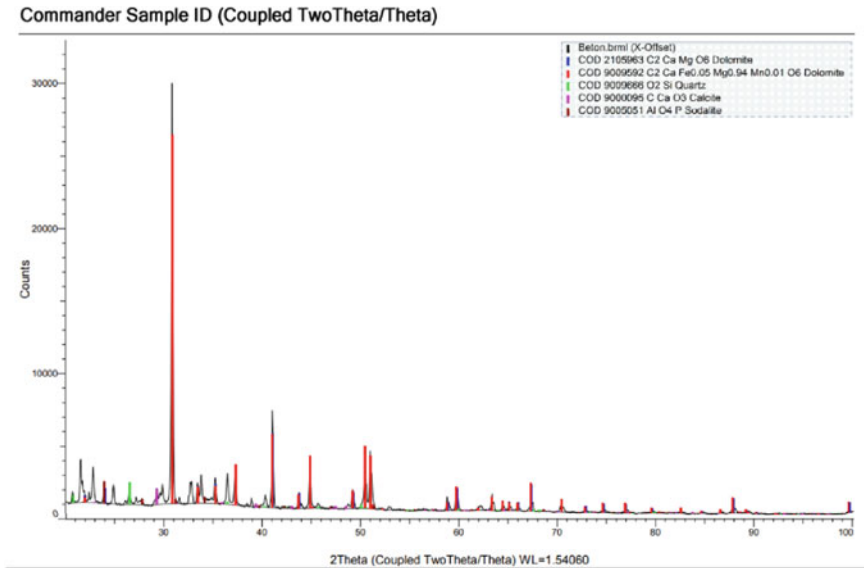
Fig. 2 X-ray phase analysis of the sample

4 Discussion of the Results

The study of physical and mechanical properties of concrete (Table 6) showed that the most optimal composition is M-4 on the basis of the largest soda-lime dolomite waste with the addition of 30% MgO. The results of the study of the microstructure of the synthesized concrete shown in Fig. 1 indicate that the main crystalline phase is periclase [18–20]. X-ray phase analysis of the sample is shown in Fig. 2.

5 Conclusions

1. The compositions of energy-efficient building compositions based on the integrated use of waste dolomite and local silica rocks have been developed.
2. The calculation and selection of the composition of lightweight concrete with the highest packing density in accordance with the Andreassen-Andersen formula;
3. The comparative characteristic of different types of concrete is presented;
4. The study of the microstructure of lightweight magnesia concrete showed that the main crystalline phase is periclase;
5. Theoretical justification of technology of new kind of lightweight concrete excluding alkali-silicate interaction is given.

References

1. Arianit, A.: Effect of thermal treatment of trepel at temperature range 800–1200˚C (2019). https://doi.org/10.1515/chem-2019-0132
2. Ahmet, M.: Cakal expanded perlite aggregate characterization for use as a lightweight construction raw material (2013). https://doi.org/10.5277/ppmp130227
3. Filiz, K.: Effect of expanded perlite on the mechanical properties and thermal conductivity of lightweight concrete (2011). https://doi.org/10.1016/j.enbuild.2010.11.008
4. Nalan, T.: Adsorption of cationic polyacrylamide (C-PAM) on expanded perlite (2010). https://doi.org/10.1016/j.clay.2010.07.014
5. Arianit, R., Lisichkov, K.: Chemical, mineralogical and structural features of native and expanded perlite from Macedonia (2019). https://doi.org/10.4154/gc.2019.18
6. Shinkevich, G.: Analysis of properties of modified fine-grained polyfunctional concrete and information model of decision support system (2019). https://doi.org/10.35579/2076-6033-2019-11-19
7. Erofeev, V., Rodin, A., Bikbaev, R.: Investigation of the properties of Portland cement with an active mineral additive based on Trepel (2019). https://doi.org/10.25686/2542-114X.2019.3.7
8. N.A. Belkova, N.: The influence of critical technology parameters on the properties of composites based on Portland and tova matrix (2020). https://doi.org/10.24866/2227-6858/2020-4-12
9. Aidana, B.: Lightweight structural concrete with the use of a diatomite-based aggregate (2022). https://doi.org/10.32743/26870142.2022.19.242.339297
10. Neha, S., Prashant, S., Sujit, V.: Influence of Diatomite on the properties of mortar and concrete: a review (2021). https://doi.org/10.1088/1757-899X/1116/1/012174
11. Amanda, R.: Study of the effect of diatomite on physico-mechanical properties of concrete (2020). https://doi.org/10.1590/0366-69132020663772561
12. Patcharapol, P., Surasit, L.: Pressed lightweight concrete containing calcined diatomite aggregate (2013). https://doi.org/10.1016/j.conbuildmat.2013.05.094
13. Nguyen, N.: Immobilized in micropores of diatomite for using in self-healing concrete (2017). https://doi.org/10.1016/j.proeng.2017.01.385
14. Mustafa, S., Ahmet, Y.: Effect of elevated temperatures on properties of high strength mortars containing ground calcined diatomite with limestone sand (2022). https://doi.org/10.1016/j.jobe.2022.104748
15. Posi, P.: Investigation of properties of lightweight concrete with calcined diatomite aggregate (2014). https://doi.org/10.1007/s12205-014-0637-5
16. Taoukil, D., Lahlaouti, M.: Effect of the use of diatomite as partial replacement of sand on thermal and mechanical properties of mortars (2021). https://doi.org/10.1016/j.jobe.2021.103038
17. Du, W.: Study on preparation of ultra-high strength and high performance concrete from diatomite and its mechanical properties (2019). https://doi.org/10.1088/1755-1315/376/1/012054
18. Jiang, F., Shi, Y., Zhang, H.: Effect of the pre-wetted diatomite on the cracking resistance of high-strength concrete at early-age (2018). https://doi.org/10.11896/j.issn.1005-023X.2018.20.009
19. Elrahman, M., Chung, S.: Effect of different expanded aggregates on the properties of lightweight concrete. Mag. Concr. Res. (2019). № 2 (71). https://doi.org/10.1680/jmacr.17.00465
20. Srivastava, A., Singh, S.: Utilization of alternative sand for preparation of sustainable mortar: a review. J. Clean. Prod. **253**, 119706 (2020)

Author Index